komunikácie

COMMUNICATIONS

SCIENTIFIC LETTERS OF THE UNIVERSITY OF ŽILINA

Volume 25

UNIVERSITY
OF ŽILINA

ISSN 1335-4205

1953 70 2023

2/2023

UNIVERSITY OF ŽILINA
EDIS-Publishing House
UNIZA

1953 70 2023

EDIS-Publishing House of the University of Žilina (UZ) is one of the University of Žilina's consituents. The beginning of its existence dates back to 1990. In the course of its work, the publishing house has published more than 4 900 titles of book publications, especially university textbooks, scientific monographs, scripts, prose, but also enriched the book market with titles of regional, children's and popular literature.
Students and professional public have the opportunity to purchase published titles in the „Selling Study Literature" directly on the premises of the University of Žilina, in the EDIS shop or upon order on a „cash on delivery" basis. All published titles are available at: www.edis.uniza.sk.

EDIS-Publishing House of the University of Žilina offers book titles in English

Lenka Černá, Jozef Daniš
APPLICATION OF COST ALCULATIONS IN THE TARIFF POLICY FORMATION IN RAILWAY TRANSPORT
ISBN 978-80-554-1391-4 Price 7.61 €

Jozef Gašparík et al.
RAILWAY TRAFFIC OPERATION
ISBN 978-80-554-1281-8 Price 15.80 €

Eva Nedeliaková, Jana Sekulová
EVALUATION OF QUALITY IN RAILWAY TRANSPORT
ISBN 978-554-1272-6 Price 8.00 €

Anna Tomová
ECONOMICS OF AIR NAVIGATION SERVICES
ISBN 978-80-554-0905-4 Price 14.30 €

Jozef Melcer
Dynamics of structures
ISBN 978-80-554-1698-4 Price 19.00 €

Felix Fedorovič Rybakov, Alexander Nikolaevič Lyakin, Štefan Cisko et.al.
GLOBALIZATION AND DEVELOPMENT OF INFRASTRUCTURE
ISBN 978-80-554-0719-7 Price 19.80 €

Marica Mazurek
MODELS OF BRANDING AND THEIR APPLICATION
ISBN 978-80-554-1705-9 Price 9.00 €

Michal Kvet, Karol Matiaško, Marek Kvet
USB - BECOME EXPERT IN MYSQL PRACTICES FOR DATABASE SYSTEMS IN MYSQL
ISBN 978-80-554-1786-8 Price 13.50 €

Ján Bujňák, Ružica Nikolić, Jelena Djoković
STEEL STRUCTURES COLLECTION OF SOLVED PROBLEMS WITH EXCERPTS FROM THEORY
ISBN 978-80554-0404-2 Price 9.34 €

Martin Bugaj
Aeromechanics 1
ISBN 978-80-554-1675-5 Price 14.50 €

Tetiana Hovorushchenko et.al.
CD - INTELLIGENT INFORMATION-ANALYTICAL TECHNOLOGIES...
ISBN 978-80-554-1729-5 Price 3.50 €

Karol Matiaško, Michal Kvet, Marek Kvet
CD - Practices for database systems
ISBN 978-80-554-1397-6 Price 2.20 €

Michal Kvet, Karol Matiaško, Štefan Toth
USB - Practical SQL for Oracle Cloud
ISBN 978-80-554-1880-3 Price: 11,30 €

Veronika Valašková, Daniela Kucharová
USB - Statics of structures 3
ISBN 978-80-554-1826-1 Price: 8,90 €

EDIS-Publishing House UNIZA
Univerzitná 8215/1,
010 26 Žilina,
Slovakia

e-mail: edis_objednavky@uniza.sk, edis@uniza.sk
www.edis.uniza.sk

A - OPERATION AND ECONOMICS

B - MECHANICAL ENGINEERING

C - ELECTRICAL ENGINEERING IN TRANSPORT

D - CIVIL ENGINEERING IN TRANSPORT

E - MANAGEMENT SCIENCE AND INFORMATICS IN TRANSPORT

F - SAFETY AND SECURITY ENGINEERING IN TRANSPORT

ERRATA

Errata: Communications - Scientific letters of the University of Zilina, 2022, 24(3), p. B228-B238, https://doi.org/10.26552/com.C.2022.3.B228-B238, Prediction of the ultra-large container ships' propulsion power at the initial design stage
P. K. Korlak

THE 15-MINUTE CITY MODEL: THE CASE OF SICILY DURING AND AFTER COVID-19

Socrates Basbas[1], Tiziana Campisi[2], Thomas Papas[1], Mirto Trouva[1], Giovanni Tesoriere[2]

[1]School of Rural and Surveying Engineering, Faculty of Engineering, Aristotle University of Thessaloniki, Thessaloniki, Greece
[2]Faculty of Engineering and Architecture, Kore University of Enna, Enna, Italy

*E-mail of corresponding author: tiziana.campisi@unikore.it

Socrates Basbas 0000-0002-3706-8530,
Thomas Papas 0000-0001-5469-7817,
Giovanni Tesoriere 0000-0001-5201-9887
Tiziana Campisi 0000-0003-4251-4838,
Mirto Trouva 0000-0002-3644-9761,

Resume
Travel restrictions due to COVID-19 initiated a radical rethink of the urban planning process, focussing on a concept initially proposed by Carlos Moreno in 2016; the "15-Minute City" model, aiming at the improvement of quality of life by creating or rearranging cities so that residents' needs can be reached within 15-minutes on foot or by bicycle or by public transit. In continuation to a research in 2020, this paper quantifies the attractiveness of the model to residents in nine regions of Sicily in 2022. Based on statistical analysis concerning the respondents' opinion, the model examined promotes walking as an anti-stress method and improves the overall health conditions at a community level. Therefore, policy makers can revalue the existing planning process and create a blueprint for a healthier and car-free lifestyle.

Article info
Received 12 October 2022
Accepted 22 December 2022
Online 31 January 2023

Keywords:
COVID-19
urban planning
Sicily
15-minute city model
sustainable transport

Available online: https://doi.org/10.26552/com.C.2023.021

ISSN 1335-4205 (print version)
ISSN 2585-7878 (online version)

1 Introduction

The concept of the safe travelling has radically changed due to the COVID-19 pandemic. Fear of contagion and restrictions, imposed by governments in an attempt to mitigate the disease, have contributed to a significant drop in travel frequency [1]. At the same time an increase in private vehicle use and non-motorized modes of transport has been observed [2]. The travel behaviours of citizens differ before and after the pandemic and they are highly affected by gender, car ownership, employment status, distance travelled, purpose of travelling and infection-related factors, such as use of face masks, cleanliness, social distance. Travel distances tend to become shorter and trips less frequent [2]. In areas with sufficient and proper pedestrian and bicycle infrastructure people might tend to use more sustainable modes of transport (walking, e-scooters, e-bikes).

Realising and quantifying these changes is crucial for optimisation of urban spaces. The current demand in terms of city planning shifts towards safer, sustainable and more inclusive cities, independent of private vehicles that increase social inequalities [3]. Many kinds of tools can be used in order to observe citizens' daily practices and mobility can definitely be considered as one, so to construct policies coherent with the emerging demands being made by populations using the city and its service [4]. One of the most promising concepts that satisfies the world's recent needs is the 15-minute city model [5-6].

The 15-minute city model derives from the "neighbourhood unity" concept, first developed in 1923 in a national architectural competition in Chicago, as a proposal to build new compact residential neighbourhoods. The proximity of services, public facilities and housing could create communities with a recognisable social and cultural identity on a local scale, counteracting the anonymity of large cities [7]. As an alternative, the concept of "city region" was developed, first explained in the Regional Plan of New York and its surroundings, published in 1929 [3].

The dissemination of planning tools, such as the SUMP (Sustainable Urban Mobility Plan), provides a set of medium- and long-term strategies by defining different components of individual actions and guidelines for all the parties involved. These urban and mobility planning tools:

- discourage high concentrations of settlement in the city centre through housing programmes in the suburban area, especially with low-density detached and semi-detached houses [8];
- promote the return of productive activities to the city (e.g. handicrafts, commercial activities) [9].
- advocate the construction of new, "compact" residential neighbourhoods, according to the dimensional and spatial criteria of the neighbourhood unit [10]

The new residential neighbourhoods, developed in the last twenty years outside the city centre, often lack services and require the use of transport to reach daily destinations. In order to create residential neighbourhoods, integrated with services, greenery, offices, it is necessary to rethink the location of certain public and collective functions.

Typically, these functions are located in the city centre, making the heart of the city a convenient place to live [10].

The first data recorded after the lockdown in Italy (end of May 2020) show a diversification in modal choice, where walking or cycling is preferred for short distances and private transport is favoured in other cases [11]. In fact, Italy was the first European country to register positive cases of COVID-19 from 8 March 2020 and to implement travel restrictions by adopting the national lockdown until mid-May 2020. Users preferred to travel alone, with individual means of transport, such as electric scooters and regular and pedal-assisted bicycles [12].

Mainly due to fear of contagion, the use of shared and public transport was abandoned. Considering this, local administrations are responding with the proposal of the "15-minute city", i.e. a city in which all the daily activities can be reached within fifteen minutes, either on foot or by bicycle [13].

The mobility concept associated with this urban planning model is characterised by walking and cycling. It is therefore emphasised that there is a different pyramid hierarchy between different modal choices that place the use of private vehicles at the base, compared to the pyramid hierarchy of the 15min city model that places walking at the base

The 15-minute city concept, aiming to maximise each user's time, was implemented before the pandemic in European and non-European cities such as Paris, Helsinki, Los Angeles and Singapore. In those cities, digital platforms or Mobility as a Service (MaaS) were developed by service operators to facilitate the user in multimodal choice [14].

In this sense, digital platforms have been developed to make end-to-end planning, booking and ticketing services interact for all the modes of transport, public or private, while reducing waiting times for users [15]. The 15-minute city concept can be successfully implemented if the presence of services (such as supermarkets, banks, offices) and public spaces for socialising (such as squares or playgrounds for children) are located near the workplace and residence.

This would allow citizens to carry out daily activities without wasting too much time on transport. At the same time, it would discourage the use of private vehicles in an attempt to tackle the problem of traffic congestion (especially during rush hours).

The increase in pedestrian accessibility to services aims to provide residents with a rational distribution of services that facilitates daily travel at a distance of between 200 and 800 meters, with respect to the location of the residences [16].

2 Literature review

The recent pandemic imposed many restrictions and showed that some cities were not ready for the generated impacts, especially in the health and mobility sectors. After the lockdown, it was advised to use single-user mobility options. In particular, in several European cities there has been an increase in the use of bicycles. Actions to improve mobility post COVID-19 include the implementation of new or temporary (pop-up) infrastructure, which in some cases has led to less spread of infections, for example in Germany [17] and Copenhagen [18].

Several parameters characterise 15-minute cities and can be the basis for highlighting the development benefits in different urban contexts worldwide.

In particular:

- easy accessibility
- optimisation of the location of services
- socio-economically equity
- reduction of the use of private vehicles
- strong pedestrianisation.

Most urban areas, built before the overwhelming proliferation of automobiles (1960s-1970s), had a 15-minute urban structure, so restoring the goal can be relatively easy. This will depend on the estimate of the damage produced by urban renewal, for example by the spread of limited traffic areas, the presence of motorways adjacent to the city and the population trend.

There are a lot of alternative and innovative transport modes that can be implemented in order to improve and make more efficient the existing (traditional) urban mobility system and thus, has started to be included within the policy agendas of many modern smart cities [19]. Development of the 15-minute city model allows for development of more infrastructure and pedestrian areas, making cities more liveable, walkable,

healthier, sustainable and economically productive [3]. Increased liveability is linked not only to the functional geometric improvement of streets but also to the better development of neighbourhoods, which also means that people are more likely to meet each other, increase sociality and build a sense of community.

These benefits are particularly relevant for the elderly, as creating spaces and opportunities for accidental social contact throughout the city can reduce the experiences of loneliness in old age [20]. This model provides an equitable socio-economic scenario - those without cars could easily access all their needs. Regarding inclusivity, developing neighbourhood planning can help address urban inequalities by considering those who cannot access urban services [21]. Among the Italian regions, Sicily was the most affected by the pandemic, where the public transport (i.e. trains and metro) is still very limited in terms of infrastructure and there is also a tendency to avoid the use [12], However, there are several parts of the existing infrastructure in which people can safely move on foot. To investigate the travelling habits in the pre-pandemic and the post-pandemic period an initial questionnaire was distributed to a specific sample, which consisted of Sicilian citizens, concerning the perception of walking not only as an alternative means of transport but as an anti-stress method, as well. In addition, the usefulness of implementing the 15-minute city model was assessed in order to make the short distance movement (<1km) more comfortable and quicker [22-23].

2.1 Development of city of proximity in Italy and in Sicily before and after COVID-19

"The "15-minute city" model, represents a city that offers to the citizens all the services they need on a daily basis by reaching the relevant destinations within fifteen minutes (in maximum) of walking from where they live. The evolution of cities and implementation of the 15-minute city model must comply with the technological and socio-economic evolution and the needs of the population [24].

Additionally, a study conducted by [25], highlights the characteristics of climate change and the ongoing pandemic, pointing out the main effects and consequences of these phenomena in cities and the vulnerabilities of the urban system. The dissemination of the 15-minute city model could create a climate-proof adaptive city in the post pandemic period.

The concept of "urban proximity", cannot be associated with the concept of physical proximity to the essential activities of daily life but must be about strengthening the social interactions that some places are more able to activate than others [26].

Over the years some cities, such as Milan, have already started efforts in order to adopt the concept of 15 minute-city model, without neglecting the goal of upgrading the neighbourhoods into attractive places of social aggregation for communities [27].

The above-mentioned research highlights the importance of correlation between the concept of spatial node to the node of local capacities and resources, recognizing the local community as the bearer, which is capable to guide and prefigure the process of regeneration in the post-COVID city.

Regarding Southern Italy, a study conducted by [28], identifies the urban characteristics in the city of Naples that define a 15-minute city, by emphasising to processes that urban, geomorphological, physical (regarding both spaces and routes, such as the geometry of pedestrian and bicycle networks), functional (distribution and location of services), socio-economical (of the population) and settlement characteristics, are taken into account.

Sicily is an island area, characterised by the presence of 3 metropolitan cities facing the sea namely Catania, Messina and Palermo. The rest of the cities can be classified as medium or small cities in terms of number of inhabitants, especially inland. Implementation of proximity city models would allow different contexts to be implemented in order to increase the sustainable urban mobility and help citizens to become more familiar with the daily routine under a 15-minute neighbourhood.

Moreover, based on research published in 2022 by [29], the outbreak of the COVID-19 pandemic had as affect to change the mobility of Polish resident in cities with a significant use of public transport and many residents started to prefer using their private vehicles. In addition, similar research has also shown that around 8% of citizens in Poland are using car-sharing. However, after the COVID-19 pandemic, more than 30% of the examined sample stop using it because of health concerns [30].

Another study, conducted in 2019 by [31], explores that urban sprawl has several negative impacts on the environment, economy and human health. Total of 110 municipalities in Sicily were considered. In addition, principal component analysis was adopted to create the Sicilian dispersion/compactness index and linear regression analysis was used to evaluate the association between the dispersion index and health outcomes.

It was shown that the public transportation has an inverse relationship with increasing sprawl while private transportation is directly related. Attention was also focused on the relationship between the evolution of urbanisation and its relationship with health outcomes, such as cardiovascular mortality.

The recent COVID-19 pandemic has disrupted travel choices for several months, as explained in the following section. Resulting in the desertification of some areas and the closure of businesses due to the rise of e-commerce and online activities [11-32].

Table 1 *Distribution of respondents based on gender (2020)*

Gender	Frequency	Relative Frequency (%)	Cumulative Relative Frequency (%)
Male	306	43.7	43.7
Female	394	56.3	100.0

Table 2 *Distribution of respondents based on age group (2020)*

Age	Frequency	Relative Frequency (%)	Cumulative Relative Frequency (%)
18-25	38	5.4	5.4
26-40	242	34.6	40.0
41-55	276	39.4	79.4
56-70	121	17.3	96.7
>70	23	3.3	100.0
Total	700	100	

2.2 The residents of Sicily during the COVID-19 era

A series of studies have been conducted from 2020 to 2022 to examine the travel behaviour of the Sicilian population. Different segments of population have been considered as well as psycho-social and displacement aspects, such as frequency of movement, preferable means of transport, vehicle ownership etc. The majority of relevant studies in Italy examine different regions of the north and does not focus on the whole country [33].

The region of Sicily has several problems related to the urban mobility, such as poor rail infrastructure in the central southern areas, the absence of highways connecting the westernmost part of the region and several critical issues related to multimodality (in different contexts switching from one mode of transport to another implies very long waiting times). Additionally, Sicily needs travelling connections by ship and airplanes, as all the islands do. The transportation problems, which were presented during the pandemic period, led a number of researchers to investigate regional and local travel dynamics.

A preliminary analysis was conducted on mobility choices [34], considering citizens' opinion regarding the mobility choices in two Italian cities, Palermo and Catania, before and during the pandemic. A series of studies conducted in the Sicilian context, revealed a propensity on the part of islanders to travel shorter distances, respecting social distance and other safety precautions during the COVID-19 therefore preferring to travel by foot or car. The Sicilian context was also the subject of investigations related to the use of public transportation during the different pandemic phases and the evaluation of sentiments that reduced the use of public transportation and travel in general during the various pandemic phases. Different segments of the population were investigated, emphasising on the modal choices of commuters such as workers and college students [35-36].

The present study stands as the first descriptive statistical analysis that instead investigated the propensity to consider walking as a stress-relieving antidote and also considered the view of the spread of proximity city models as useful to be able to popularise greater sustainable mobility and disseminate urban planning strategies that can lift contexts from the critical issues that emerged during the pandemic phase.

3 Descriptive statistics

3.1 Design of the survey

This research focuses on the qualitative evaluation of judgements of a randomly selected sample of users and made use of the CAWI (Computer Assisted Web Interviewing) methodology. The latter is a data collection methodology based on the completion of a web-based questionnaire provided through a link, panel or website. In particular, the study was conducted through the drafting of a closed form questionnaire, distributed online through the Google platform. The sample of users examined refers to a section of members of a social Facebook group of Sicilian inhabitants who generally walk daily for both work and leisure. The sample investigated was composed of 700 users and it was disseminated from February to March 2020 and repeated in March 2022 in order to compare the same date from two different periods.

3.2 Data analysis through the use of descriptive statistics

This study involves a questionnaire distributed in nine cities of Sicily, Italy and consists of two parts. In the first part, the basic socio-demographic data were collected such as gender, age and level of studies. As shown in Tables 1 and 2, 43.7 % of the respondents were male, almost 40 % of them were 41-55 years old. and 40 % of them were 18-40 years old.

Table 3 *Distribution of respondents based on groups of cities in 2020*

Groups of cities	Frequency	Relative Frequency (%)	Cumulative Relative Frequency (%)
metropolitan	157	22.4	22.4
medium	330	47.1	69.6
small	213	30.4	100.0
Total	700	100	

Table 4 *Distribution of respondents based on groups of cities in 2022*

Groups of cities	Frequency	Relative Frequency (%)	Cumulative Relative Frequency (%)
metropolitan	130	18.6	18.6
medium	309	44.1	62.7
small	261	37.3	100.0
Total	700	100	

Table 5 *Distribution of respondents based on car driving*

Car ownership	Relative Frequency 2020	Relative Frequency 2022
I have and I drive	90.7	94.7
I have and I don't use it	6.4	3.9
I do not have	2.9	1.4
Total	100	100

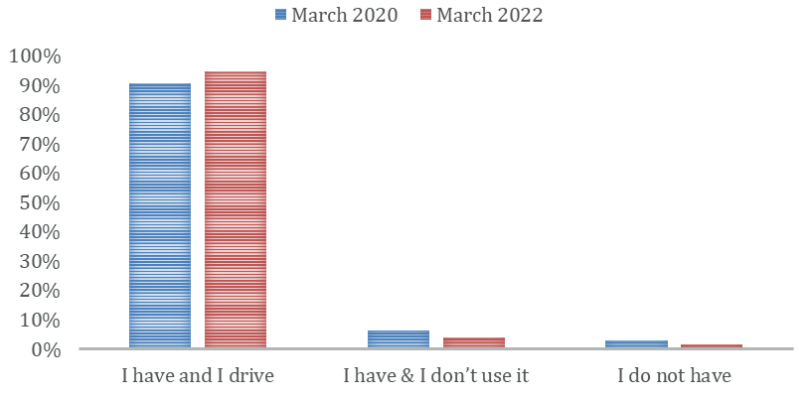

Figure 1 *Car ownership and use (period March 2020-March 2022)*

It is also important to mention that the percentages of gender and age groups for the respondents of the questionnaire in 2022 are very close and almost the same as the above of 2020.

Additionally, the sample of the respondents is divided in three groups based on the population of the nine cities of the research (Tables 3 and 4). The first group consists of small towns with population less than 60.000 (Agrigento, Enna), the second group includes cities with population more than 60.000 habitants and less than 300.000 (Syracuse, Ragusa, Trapani, Caltanissetta) and the third group consists of cities (metropolitan areas) with population ranging from 300.000 to 700.000 (Catania, Palermo, Messina). Almost half of the sample, 47.1% in 2020 and 44.1% in2020), live in medium cities and more than three of ten of the respondents are habitants of Agrigento or Emma (small cities).

In the second part of the questionnaire, the respondents were asked if they possess a car. Based on the results of 2020 and 2020 presented in Table 4, the vast majority of the sample (more than 90%) owns and uses a car.

As shown in Table 4, there was a further increase in use of vehicles in March 2022. This could be linked with the fact that there was a reduction in the frequency of use of the public transport. Additionally, based on Table 5 and as shown in Figure 1, the majority of the respondents, in both time periods (2020 and 2022) possess and drive their own car.

Moreover, citizens were asked if they consider walking an anti-stress method. Figure 2 shows that 90% of the respondents (in 2020 and in 2022) agree or strongly agree with the statement. The percentage of the sample that disagree or strongly disagree with this fact is extremely low and equal to 2.3% in 2020 and less than 1% in 2022.

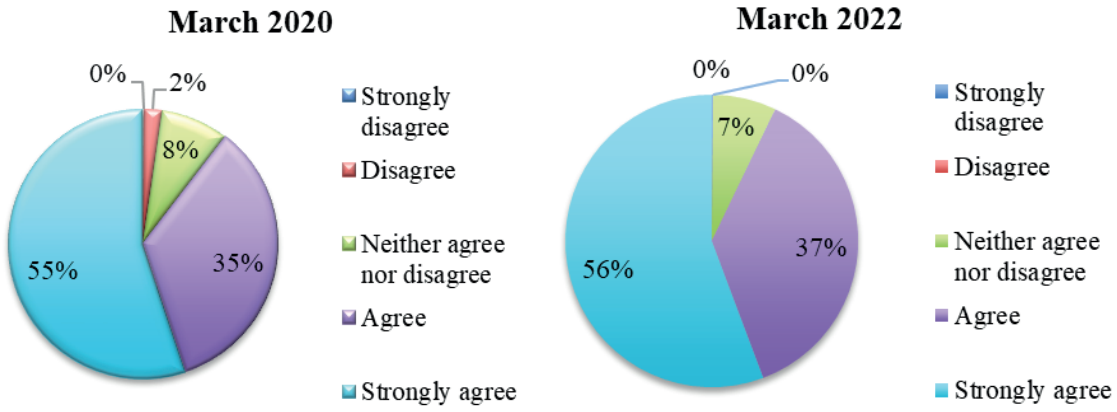

Figure 2 *Walking like antistress concept trend (period March 2020-March 2022)*

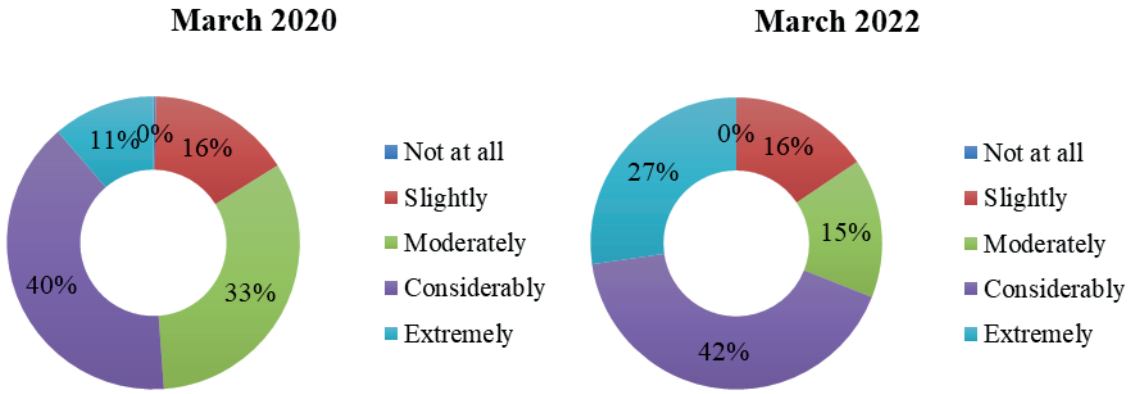

Figure 3 *Usefulness of the 15-minute city model during the monitored periods (March 2020-March 2022)*

It is critical to understand that despite the fact that more than 90 % of the respondents use to drive a car, the same percentage of the sample characterize walking as an anti-stress method.

Finally, they were asked how useful they think it would be to see their cities under the 15-minute city model. More than half of the sample in both examined periods believes that the 15-minute city model would be useful in their city. However, 32.7 % of them neither agree or disagree like described on Figure 3 below.

A series of questions pertaining to the third section of the survey emphasises the need to include 8 services as priorities in the planning of a neighbourhood city.

Some of these services are related to health and education (such as hospitals and schools and libraries), others are related to a socioeconomical aspect (such as local markets, stores) and other to community centres and green spaces; in particular importance was also given to the investigation of improving the road network. In particular, as health services are defined those primary services connected with health care or support.

Then, there are the social centres, which must be open, above all, to young people and families and be the scene of new collaborations with other realities and subjects in the area. Neighbourhood libraries and surrounding areas, understood as places to be enhanced by virtue of their cultural, aggregative and educational role, as well as social presidium in territories that are often peripheral and crossed by social fragility. Oratories, identifiable in places of community gathering, capable of playing an essential role in building cultural exchange, including the interethnic world. Neighbourhood markets, which offer forms of meeting and presiding over the territory with spin-offs in terms of social cohesion in daily life. Schools, understood as places where gathering spaces provide stimuli for the construction and transmission of knowledge. Green spaces, which for neighbourhood residents, represent the spaces for meeting and socialising and which should be more open, accessible and attractive. The road system, which, in addition to being the subject of discussion on mobility policies, is the public space where the needs of the weakest (of the homeless, immigrants ...) are manifested and it is there that it is easiest to intercept the needs of fragile individuals. Commercial activities, which from large shopping centres in the suburbs prospect (in some cities have already been realised) types of businesses that straddle the line between the large supermarket and the post-war "grocery" store.

The research investigated which user choice trends,

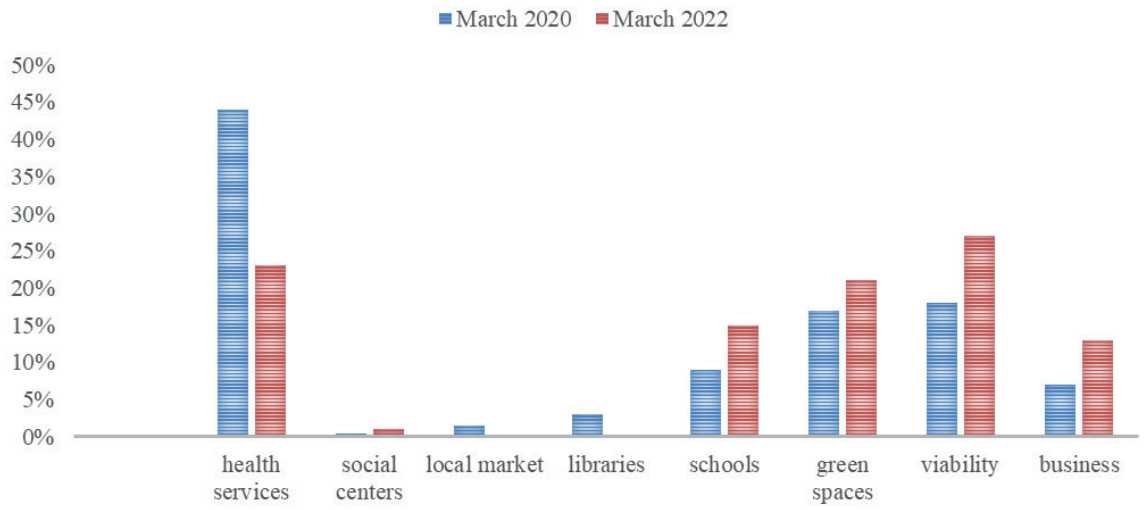

Figure 4 *Comparison of the main services necessary for the definition of a proximity city (period March 2020-March 2022)*

could define priority among those in light of the spread of the virus and strategies to mitigate the spread. Therefore, Figure 4 shows the comparison between years 2020 and 2022.

4 Discussion

The recent pandemic has underlined the importance of respecting the social distancing and encouraging short journeys by making everything easily accessible. The future that cities are preparing for in the post-pandemic phase is linked to a revision of city models, introducing in metropolises, such as London, Paris, Milan or Madrid, the possibility of guaranteeing their inhabitants a sustainable standard of living by ensuring that citizens can travel as little as possible to obtain goods and services. Metropolises have thus begun to rethink themselves, imagining a future similar to that of cities such as Barcelona, famous for its self-sufficient neighbourhoods called "superblocks". The most recent example is Paris and it is a model that Milan now seems to want to take inspiration from. Future surveys can be conducted taking into account the updated transportation habits of citizens after the pandemic period and focus on specific modifications for the existing urban mobility systems in the European Union, so as to create new alternative models of transport such as the 15-minute city model. Implementing a 15-minute city model means guaranteeing citizens all the primary services within a quarter of an hour on foot or by bicycle. To achieve this, it is necessary to lengthen the metro route, reserve a portion of social housing for social housing and work on the spread of IoT technologies, as well as promoting the concept of smart cities. In order to implement useful actions for the population, it is necessary to introduce the concept of participatory planning by promoting the active participation of population in urban planning and mobility choices, participating in surveys/interviews and disseminating awareness campaigns. This can bring out the criticalities of each city at different levels of society and allow the better choice of actions to be taken.

5 Conclusions

The concept of proximity, which is the basis of the city's function, was challenged in the last century when the decision makers (re)thought cities around an idea of efficiency placed on specialization and economy of scale. In deference to efficiency, specialized portions of cities were built (industrial zones, business centres, university citadels, sports centres, residential-dormitory districts etc.). In each of those zones, specific functions of activity and services were concentrated.

The data analysed showed an increase in the use of the private vehicle over the two years monitored, as well as a slight increase in the propensity to implement proximity city strategies and models. In addition, the improvement of services, both related to health, as well as related to the road system and the creation and maintenance of green spaces, will have to be taken into account by local administrators to improve the urban liveability starting from the neighbourhoods. Based on the research results from both time periods (2020, 2022), the 15-minute city model can be very useful for Sicilian residents with its significance to be increased a lot after the pandemic experience.

Useful references are the best practices, where governance has initiated particularly relevant social and urban innovation experiences: think of Paris, Barcelona, Milan. The 15-minute city model is a model of urban development that does not follow the common trends in urban planning. It outlines a scenario where everyone has access to all the services needed at a maximum distance of 15 minutes on foot or by bicycle. A city of this type re-evaluates the concept of the neighbourhood,

which becomes a complete cell of urban life. This concept aims to optimise space, conveying a reflection on the resources available and how they are used. It promotes the presence of green areas to cool down in summer and replace busy streets.

This city model allows for implementation of the majority of the restrictions and strategies developed for restarting activities in urban settings post COVID-19, demonstrating and reducing displacement

The spread of online education and teleworking on a larger scale, the search for services as close as possible to home, the temporary reduction in urban traffic flows and rediscovery of the urban dimension of the neighbourhood, inevitably raise the question of whether an alternative to the frenetic rhythms, traffic and long distances is actually feasible in the near future.

The spread of this good planning practice must therefore ensure that those who live in the centre and those who live in the suburbs have access to all the essential services nearby. The city thus maintains its role as a social, economic and cultural reference point and every citizen can enjoy every advantage of city life without too much difficulty.

Author contribution

Research planning, data analysis and final draft prepared by Tiziana Campisi and Socrates Basbas, initial draft, analysis was done by Thomas Papas and Mirto Trouva, data collection was done by Tiziana Campisi and Giovanni Tesoriere and paper writing modification was done by Tiziana Campisi and Giovanni Tesoriere.

Grants and funding

The authors received no financial support for the research, authorship and/or publication of this article.

Conflicts of interest

The authors declare that they have no known competing financial interests or personal relationships that could have appeared to influence the work reported in this paper.

References

[1] KIM, CH., CHEON, S. H., CHOI, K., JOH, CH.-H., LEE, H.-J. Exposure to fear: changes in travel behavior during MERS outbreak in Seoul. *KSCE Journal of Civil Engineering* [online]. 2017, **21**(7), p. 2888-2895. ISSN 1226-7988, eISSN 1976-3808. Available from: https://doi.org/10.1007/s12205-017-0821-5

[2] ABDULLAH, M., DIAS, C., MULEY, D., SHAHIN, M. Exploring the impacts of COVID-19 on travel behavior and mode preferences. *Transportation Research Interdisciplinary Perspectives* [online]. 2020, **8**, 100255. eISSN 2590-1982. Available from: https://doi.org/10.1016/j.trip.2020.100255

[3] MORENO, C., ALLAM, Z., CHABAUD, D., GALL, C., PRATLONG, F. Introducing the "15-minute city": sustainability, resilience and place identity in future post-pandemic cities. *Smart Cities* [online]. 2021, **4**(1), p. 93-111. eISSN 2624-6511. Available from: https://doi.org/10.3390/smartcities4010006

[4] WANG, R., ZHANG, X., LI, N. Zooming into mobility to understand cities: a review of mobility-driven urban studies. *Cities* [online], 2022, **130**, 103939. ISSN 0264-2751, eISSN 1873-6084.Available from: https://doi.org/10.1016/j.cities.2022.103939

[5] GUZMAN, L. A., ARELLANA, J., OVIEDO, D., ARISTIZABAL, C. A. M. COVID-19, activity and mobility patterns in Bogota. Are we ready for a '15-minute city'? *Travel Behaviour and Society* [online]. 2021, **24**, p. 245-256. ISSN 2214-367X, eISSN 2214-3688. Available from: https://doi.org/10.1016/j.tbs.2021.04.008

[6] BALLETTO, G., LADU, M., MILESI, A., BORRUSO, G. A Methodological approach on disused public properties in the 15-minute city perspective. *Sustainability* [online]. 2021, **13**(2), 593. eISSN 2071-1050. Available from: https://doi.org/10.3390/su13020593

[7] GRAELLS-GARRIDO, E., SERRA-BURRIEL, F., ROWE, F., CUCCHIETTI, F. M., REYES, P. A city of cities: measuring how 15-minutes urban accessibility shapes human mobility in Barcelona. *Plos ONE* [online]. 2021, **16**(5), e0250080. eISSN 1932-6203. Available from: https://doi.org/10.1371/journal.pone.0250080

[8] MARKATOU, M. Planning and sustainable urban mobility plans: parallel orbits or incompatible paths? *Journal of Traffic and Transportation Engineering* [online]. 2020, **8**, p. 63-72. ISSN 2095-7564. Available from: https://doi.org/10.17265/2328-2142/2020.02.003

[9] BANDARIN, F., CICIOTTI, E., CREMASCHI, M., MADERA, G., PERULLI, P., SHENDRIKOVA, D. Which future for cities after COVID-19 an international survey. Reports. Milan, Fondazione Eni Enrico Mattei, 2020.

[10] POZOUKIDOU, G., CHATZIYIANNAKI, Z. 15-minute city: decomposing the new urban planning Eutopia. *Sustainability* [online]. 2021, **13**(2), 928. eISSN 2071-1050. Available from: https://doi.org/10.3390/su13020928

[11] MOSLEM, S., CAMPISI, T., SZMELTER-JAROSZ, A., DULEBA, S., NAHIDUZZAMAN, K. M., TESORIERE, G. Best-worst method for modelling mobility choice after COVID-19: evidence from Italy. *Sustainability* [online]. 2020, **12**(17), 6824. eISSN 2071-1050. Available from: https://doi.org/10.3390/su12176824

[12] CAMPISI, T., BASBAS, S., SKOUFAS, A., AKGUN, N., TICALI, D., TESORIERE, G. The impact of COVID-19 pandemic on the resilience of sustainable mobility in Sicily. *Sustainability* [online]. 2020, **12**(21),8829. eISSN 2071-1050. Available from: https://doi.org/10.3390/su12218829

[13] ABBAS, A. M., YOUSSEF, K. Y., MAHMOUD, I. I., ZEKRY, A. NB-IoT optimization for smart meters networks of smart cities: case study. *Alexandria Engineering Journal* [online]. 2020, **59**(6), p. 4267-4281. ISSN 1110-0168, eISSN 2090-2670. Available from: https://doi.org/10.1016/j.aej.2020.07.030

[14] HENSHER, D. A. What might COVID-19 mean for mobility as a service (MaaS)? *Transport Reviews* [online]. 2020, **40**(5), p. 551-556. ISSN 0144-1647, eISSN 1464-5327. Available from: https://doi.org/10.1080/01441647.2020.1770487

[15] DE VALDERRAMA, N. M. F., LUQUE-VALDIVIA, J., ASEGUINOLAZA-BRAGA, I. The 15 minutes-city, a sustainable solution for postCOVID19 cities? (in Spanish). *Ciudad y Territorio Estudios Territoriales* [online]. 2020, 52(205), p. 653-664. eISSN 2659-3254. Available from: https://doi.org/10.37230/CyTET.2020.205.13.1

[16] GRAELLS-GARRIDO, E., SERRA-BURRIEL, F., ROWE, F., CUCCHIETTI, F. M., REYES, P. A city of cities: measuring how 15-minutes urban accessibility shapes human mobility in Barcelona. *Plos ONE* [online]. 2021, **16**(5), e0250080. eISSN 1932-6203. Available from: https://doi.org/10.1371/journal.pone.0250080

[17] KRAUS, S., KOCH, N. Provisional COVID-19 infrastructure induces large, rapid increases in cycling. *Proceedings of the National Academy of Sciences* [online]. 2021, **118**(15), e2024399118. ISSN 0027-8424. Available from: https://doi.org/10.1073/pnas.2024399118

[18] SCHWEDHELM, A., LI, W., HARMS, L., ADRIAZOLA-STEIL, C. Biking provides a critical lifeline during the coronavirus crisis. Word Resources Institute, 2020.

[19] SAVASTANO, M., SUCIU, M. C., GORELOVA, I., STATIVA, G. A. How smart is mobility in smart cities? An analysis of citizens' value perceptions through ICT applications. *Cities* [online]. 2023, **132**, 104071. ISSN 0264-2751, eISSN 1873-6084. Available from: https://doi.org/10.1016/j.cities.2022.104071

[20] WENG, M., DING, N., LI, J., JIN, X., XIAO, H., HE, Z., SU, S. The 15-minute walkable neighbourhoods: measurement, social inequalities and implications for building healthy communities in urban China. *Journal of Transport and Health* [online]. 2019, **13**, p. 259-273. ISSN 2214-1405, eISSN 2214-1413. Available from: https://doi.org/10.1016/j.jth.2019.05.005

[21] ALLAM, Z. *Surveying the COVID-19 pandemic and its implications: urban health, data technology and political economy*. Amsterdam, The Netherlands: Elsevier Science, 2020. ISBN 9780128243138, eISBN 9780128243145.

[22] PAPAS, T., BASBAS, S., CAMPISI, T. Urban mobility evolution and the 15-minute city model: from holistic to bottom-up approach. In: AIIT 3rd International Conference on Transport Infrastructure and Systems TIS ROMA 2022: proceedings. 2022.

[23] CAMPISI, T., NAHIDUZZAMAN, K. M. *Beyond COVID-19: planning the mobility and cities following "city in 15 minutes" paradigm*. ICCASU Springer Book, in press.

[24] PINTO, F., AKHAVAN, M. Scenarios for a post-pandemic city: urban planning strategies and challenges of making "Milan 15-minutes city. *Transportation Research Procedia* [online]. 2022, **60**, p. 370-377. ISSN 2352-1457, eISSN 2352-1465. Available from: https://doi.org/10.1016/j.trpro.2021.12.048

[25] MORACI, F., ERRIGO, M. F., FAZIA, C., CAMPISI, T., CASTELLI, F. Cities under pressure: strategies and tools to face climate change and pandemic. *Sustainability* [online]. 2020, **12**(18), 7743. eISSN 2071-1050. Available from: https://doi.org/10.3390/su12187743

[26] D'ONOFRIO, R., TRUSIANI, E. The future of the city in the name of proximity: a new perspective for the urban regeneration of council housing suburbs in Italy after the pandemic. *Sustainability* [online]. 2022, **14**(3), 1252. eISSN 2071-1050. Available from: https://doi.org/10.3390/su14031252

[27] ABDELFATTAH, L., DEPONTE, D., FOSSA, G. The 15-minute city: interpreting the model to bring out urban resiliencies. *Transportation Research Procedia* [online]. 2022, **60**, p. 330-337. ISSN 2352-1457, eISSN 2352-1465. Available from: https://doi.org/10.1016/j.trpro.2021.12.043

[28] GAGLIONE, F., GARGIULO, C., ZUCARO, F., COTTRILL, C. Urban accessibility in a 15-minute city: a measure in the city of Naples, Italy. *Transportation Research Procedia* [online]. 2022, **60**, p. 378-385. ISSN 2352-1457, eISSN 2352-1465. Available from: https://doi.org/10.1016/j.trpro.2021.12.049;

[29] GORZELANCZYK, P. Change in the mobility of Polish residents during the COVID-19 pandemic. *Communications - Scientific Letters of the University of Zilina* [online]. 2022, **24**(3), p. A100-A111. ISSN 1335-4205, eISSN 2585-7878. Available from: https://doi.org/10.26552/com.C.2022.3.A100-A111

[30] GORZELANCZYK, P., KALINA, T., JURKOVIC., M. Impact of the COVID-19 pandemic on car-sharing in Poland. *Communications - Scientific Letters of the University of Zilina* [online]. 2022, **24**(4), p. A172-A186. ISSN 1335-4205, eISSN 2585-7878. Available from: https://doi.org/10.26552/com.C.2022.4.A172-A186

[31] RESTIVO, V., CERNIGLIARO, A., CASUCCIO, A. Urban sprawl and health outcome associations in Sicily. *International Journal of Environmental Research and Public Health* [online]. 2019, **16**(8), 1350. eISSN 1660-4601. Available from: https://doi.org/10.3390/ijerph16081350

[32] DEL CHIAPPA, G., BREGOLI, I., ATZENI, M. Uncovering knowledge on travel behaviour during COVID-19: a convergent parallel mixed-methods study in the context of Italy. *Italian Journal of Marketing* [online] 2021, **2021**(4), p. 393-419. ISSN 2662-3323, eISSN 2662-3331. Available from: https://doi.org/10.1007/s43039-021-00036-7

[33] MURGANTE, B., BORRUSO, G., BALLETTO, G., CASTIGLIA, P., DETTORI, M. Why Italy first? Health, geographical and planning aspects of the COVID-19 outbreak. *Sustainability* [online]. 2020, **12**(12), 5064. eISSN 2071-1050. Available from: https://doi.org/10.3390/su12125064

[34] CAMPISI, T., BASBAS, S., AL-RASHID, M. A., TESORIERE, G., GEORGIADIS, G. A region-wide survey on emotional and psychological impacts of COVID-19 on public transport choices in Sicily, Italy. *Transactions on Transport Sciences* [online]. 2021, **12**(3), p. 34-43. Available from: https://doi.org/10.5507/tots.2021.010

[35] CAMPISI, T., TESORIERE, G., TROUVA, M., PAPAS, T., BASBAS, S. Impact of teleworking on travel behaviour during the COVID-19 era: the case of Sicily, Italy. *Transportation Research Procedia* [online]. 2022, **60**, p. 251-258. ISSN 2352-1457, eISSN 2352-1465. Available from: https://doi.org/10.1016/j.trpro.2021.12.033

[36] OLAYODE, I. O., SEVERINO, A. G., CAMPISI, T., TARTIBU, L. K. Comprehensive literature review on the impacts of COVID-19 pandemic on public road transportation system: challenges and solutions. *Sustainability* [online]. 2022, **14**(15), 9586. eISSN 2071-1050. Available from: https://doi.org/10.3390/su14159586

ANALYSIS OF THE IMPACT OF THE POLISH RESIDENTS' MOBILITY ON THE ENVIRONMENT

Piotr Gorzelańczyk*, Aleksandra Śniecikowska

Stanislaw Staszic State University of Applied Sciences in Pila, Pila, Poland

*E-mail of corresponding author: piotr.gorzelanczyk@ans.pila.pl

Piotr Gorzelańczyk 0000-0001-9662-400X

Resume

Environmental protection is a major task for countries around the world in the 21st century. One of the sources of pollution is the road transport. Therefore, an analysis of the impact of the mobility of Polish residents on the environment was carried out. To this end, a survey was conducted, asking questions such as: the frequency of switching from cars to public transportation, the way of moving in and out of built-up areas, the impact of transportation on the environment, the EURO standard, the purchase of an alternative-powered car and eco-driving. This research was carried out on a group of residents, taking into account: age, gender, place of residence and occupational status. Based on the research, it can be concluded that under the influence of Covid-19. the population is trying to protect itself from contagion, so it chooses individual means of transportation.

Article info

Received 13 October 2022
Accepted 17 January 2023
Online 7 February 2023

Keywords:

mobility
environment
Poland
EURO
eco-driving
Covid-19

Available online: https://doi.org/10.26552/com.C.2023.024

ISSN 1335-4205 (print version)
ISSN 2585-7878 (online version)

1 Introduction

The main task for countries around the world is to protect the environment. Increasing amounts of harmful chemicals in soil, water and air will reduce the Earth's natural resources in the future. For this reason, the European Union is encouraging member countries to introduce a policy of sustainable development. This term refers to development that will meet the needs of the population, while at the same time protect the ecosystem for future generations [1].

One source of pollution is the road transport. It is the one that emits large amounts of harmful components into the environment from fuel combustion. It is a source of vibrations and human disease. The creation of linear and point infrastructure from cleared land contributes to the disruption of the proper functioning of plants and animals. The road transport is developing rapidly, so its impact on the environment is changing dynamically. Therefore, there is a need to address the issue of assessing the impact of the mobility of Polish residents on the environment [2].

Mobility is defined differently by authors of publications. Szoltysek [13], treats mobility as daily, routine movement and activities resulting from the reorganization of personal life, which may include a change of residence or place of work. We can equate this with movement and any activities of people performed by means of transportation outside of their place of residence [4-5]. Menes [6], on the other hand, depicts mobility as mobility associated with the daily movement of residents, most often to work or school.

According to the Treaty on the Functioning of the European Union [7] and the resulting EU transport policy, mobility, understood as an element of human activity, depends on the person making the trip, the infrastructure manager and other users of the transport system for that mobility [8-9]. Closely related to mobility issues is the concept of sustainable development, which includes economic, environmental and social issues [10-13].

When analyzing the mobility of residents, it is important to keep in mind the transportation challenges, which are included in the 2011 White Paper [14] and the Urban Mobility Action Plan [15], among others. Taking into account the behavior of urban residents, a policy for sustainable transportation development in urban areas should be developed. These policies create plans for development of sustainable transportation in cities, in which the most important element is sustainable

urban mobility. This is the main goal of the 21st century transportation policy [12-13, 16-17]. Among other things, the sustainable transportation plan calls for a reduction in the daily use of cars in favor of greater use of public transportation, cycling and walking [18]. Behavior of the Polish public, in terms of choosing a mode of transportation, was also analyzed by the author of [19]. In addition, the problem of the mobility of residents was addressed in the works [20-25]. The pandemic has affected the mobility of residents [26-27].

2 Research

2.1 Subject and conditions of the study

The subject of the study was to analyze the impact of the mobility of Polish residents on the environment, in 2000-2020. The results of the survey will show the behavior of citizens in the context of the choice of means of transport versus its impact on the ecosystem. The survey is designed to determine the transport preferences of Poles and test their knowledge of environmentally friendly activities.

2.2 Methods and measures for assessing the impact of road transport on the environment

The survey was conducted in 2021 among Polish residents. Due to the limitations of the then prevailing Covid-19 pandemic, the survey was conducted via the Internet. The electronic survey was created using the Google Forms application. The link assigned to it was distributed on social networks, transportation portals and among friends. The survey was fully anonymous and consisted of 18 closed-ended questions, but with the option to enter your own answer. At the beginning of the form was a metric on gender, age, labor market status and place of residence. This was followed by questions about respondents' travel patterns in cities and outside the built-up areas, both before and during the pandemic. Respondents were asked about public transportation problems and their environmentally friendly behavior related to their choice of individual transportation. The last question asked about solutions to reduce the negative impact of road transportation on the environment. The answer to this question was partly imposed by the survey author, but respondents also had the opportunity to introduce their own ideas. Before conducting the target survey, a pilot study was conducted, which consisted of sending a form with survey questions to a selected group of people.

An important step during the implementation of the survey was the calculation of the survey sample. For Poland (population of 38151,000), assuming a confidence level of 95% and a maximum error of 5%, the required number of people taking part in the survey was 384 respondents. The survey on changes in mobility versus its impact on the environment was completed by 414 respondents [28].

The respondents' answers were also analyzed for metric questions, namely: gender, age, labor market status, place of residence and possession of a driver's license. In addition, two analyses (by gender and driver's license) were considered in the context of the Chi-square statistics. This statistical test is used to test hypotheses for random variables. One can test whether the variables are related by the common pattern of the results obtained. If the Chi-square has a greater value than the theoretical Chi-square, then there is no relationship between the variables [29]. The formula for the Chi-square test of concordance is of the form:

$$\chi^2 = \sum_{r}^{i=1} \frac{(f_i - np_i)^2}{np_i}, \tag{1}$$

where:
χ^2 - Chi-square test;
f_i - number of values in a given range;
np_i - the number of units that are in a given range.

2.3 Results

The survey included 414 participants: 211 women and 203 men. Respondents were divided into six age groups: under 18 (those without a driver's license), 18 to 25 (mainly students), 26 to 35, 36 to 45, 46 to 55 and over 55 (especially retirees). The smallest group is made up of people under the age of 18, as the questions are specifically aimed at those authorized to drive. The chart below shows the percentage distribution of respondents' ages (Figure 1).

Almost half of the respondents are employed (55.1 %). The second largest group is students, 26.8%, but 2.6% both study and work. The 55+ age bracket includes 10.3% of respondents with retired status. The remaining respondents are students (3.9%) and unemployed (3.9%) (Figure 2).

Figure 3 shows a graph of the respondents' place of residence. The survey was addressed to residents of each settlement unit. The responses of respondents from different areas of permanent residence are relatively equal to each other. Respondents were then asked about having the authority to drive a vehicle with a gross vehicle weight of up to 3.5 tons. Of the 414 people who took part in the survey, as many as 349 have a Cat B driver's license and only 65 do not have driving privileges.

The next question was addressed to those with driving privileges. It should be noted that it was not mandatory for respondents to complete. The question "How long have you held a driver's license?" was answered by 316 people. The length of time that respondents have held a driver's license starts at one year and for some it is already 45 years (Figure 4).

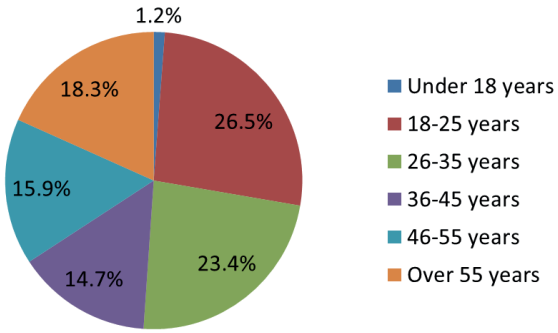

Figure 1 *Age of respondents*

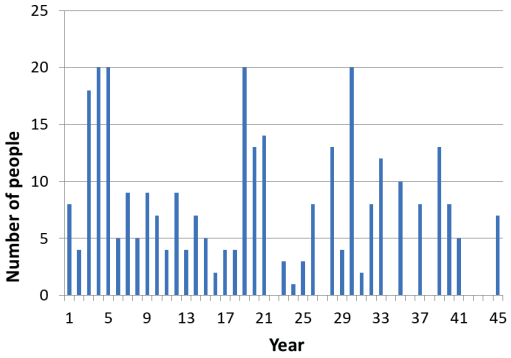

Figure 4 *Length of ownership of a driver's license by respondents*

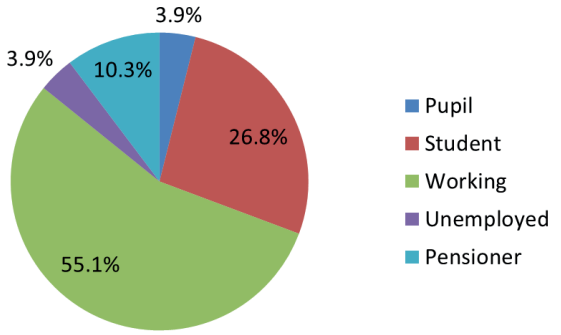

Figure 2 *Respondents' labor market status*

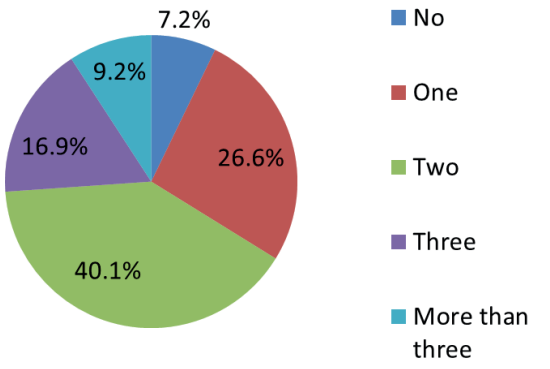

Figure 5 *Number of vehicles in respondents' households*

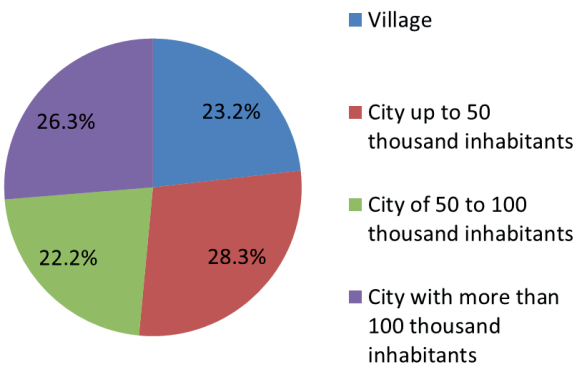

Figure 3 *Respondents' place of residence*

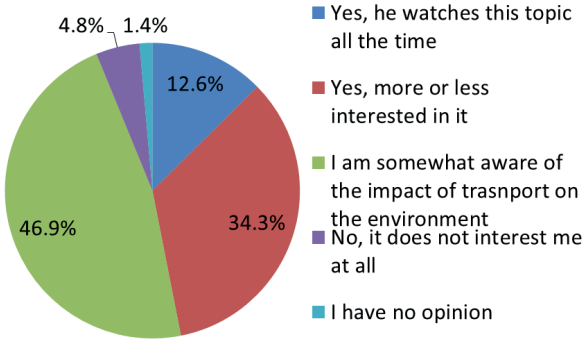

Figure 6 *Awareness of Poles regarding the impact of transportation on the environment*

For 40.1% of respondents, there are two vehicles in the household. The second group is made up of families with only one passenger car (26.6 %). Ownership of three means of transportation was declared by 16.9% of respondents, while more than three motor vehicles were marked by 9.2% of respondents. Only 7.2% of respondents have no vehicle in their household (Figure 5).

The survey asked respondents about their general knowledge of the environmental impact of road transportation. 12.6% of people observe and analyze environmental changes caused by transportation all the time, while 34.3% of respondents are more interested in the issue. Nearly half of respondents said they are somewhat aware of how the way they travel and operate their vehicle affects the ecosystem. 4.8% said they were not interested in the topic related to the impact of transportation on the biosphere and 6 people expressed no opinion (Figure 6).

The next step assessed Poles' awareness according to gender, age, labor market status and place of residence. In this case, taking into account gender, age and driver's license held, there are no significant differences between the responses of men and women. The Chi square test shows that there is no correlation between the responses of men and women, as the Chi^2 is 10.47, where the theoretical Chi^2 is 9.49. Moreover, it can be concluded that Poles are interested in this topic regardless of where they live (Table 1).

With environmental protection in mind, respondents were asked how they travel around the city most often, as well as outside the built-up area. The question was

Table 1 *Awareness of Poles related to the impact of transportation on the environment (%)*

	I don't have an opinion	No. it doesn't interest me at all	Yes. I watch this topic all the time	Yes. more or less interested in this	Somewhat. I am aware of the impact of transportation on the environment
Sex					
Women	2.84	3.32	11.37	31.75	50.72
Men	0.00	5.91	13.79	37.44	42.86
Age					
Under 18 years	0.00	0.00	20.00	40.00	40.00
18-25	2.41	4.35	10.63	28.99	53.62
26-35	1.69	6.78	16.95	25.42	49.16
36-45	0.00	10.87	6.52	47.83	34.78
46-55	0.00	4.08	14.28	36.73	44.91
Over 55	0.00	0.00	18.75	52.08	29.17
Status in the labor market					
Pupil	0.00	6.25	6.25	31.25	56.25
Student	1.80	3.60	13.51	31.54	49.55
Working	1.75	6.58	12.28	34.65	44.74
Unemployed	0.00	0.00	6.25	37.50	56.25
Pensioner	0.00	0.00	16.28	39.53	44.19
Place of residence					
Village	3.13	3.13	11.46	34.38	47.90
City of up to 50.000 residents	0.85	4.27	11.97	34.19	48.72
City of 50.000 to 100.000 residents	2.17	8.70	8.70	39.13	41.30
City >100.000 residents	0.00	3.67	17.43	30.28	48.62
Driver's license					
Yes	1.43	5.16	11.75	35.53	46.13
No	1.54	3.08	16.92%	27.69	50.77

Table 2 *Most common way respondents travel around the city (%) - part 1*

		Car	Public transport	On foot	Bike. scooter	Other (e.g.cab)
Sex						
Before the pandemic	Women	41.23	45.97	10.43	2.37	0.00
	Men	63.55	27.59	6.90	1.96	0.00
During the pandemic	Women	56.40	25.59	14.22	3.32	0.47
	Men	83.74	7.39	8.38	0.49	0.00
Age						
Before the pandemic	Under 18 years	20.00	20.00	40.00	20.00	0.00
	18-25	40.58	43.96	13.05	2.41	0.00
	26-35	64.41	28.82	5.08	1.69	0.00
	36-45	82.61	10.87	2.17	4.35	0.00
	46-55	71.53	28.47	0.00	0.00	0.00
	Over 55	41.67	52.08	6.25	0.00	0.00
During the pandemic	Under 18 years	0.00	60.00	0.00	40.00	0.00
	18-25	58.45	24.64	14.98	1.93	0.00
	26-35	74.58	13.56	8.48	1.69	1.69
	36-45	89.13	2.17	6.53	2.17	0.00
	46-55	93.88	6.12	0.00	0.00	0.00
	Over 55	77.08	6.25	16.67	0.00	0.00

Table 3 *Most common way respondents travel around the city (%) - part 2*

		Car	Public transport	On foot	Bike. scooter	Other (e.g.cab)
Status in the labor market						
Before the pandemic	Pupil	18.75	12.50	56.25	12.50	0.00
	Student	33.34	54.05	11.71	0.90	0.00
	Working	67.54	26.32	3.95	2.19	0.00
	Unemployed	68.75	25.00	6.25	0.00	0.00
	Pensioner	25.58	62.79	9.30	2.33	0.00
During the pandemic	Pupil	37.50	18.75	25.00	18.75	0.00
	Student	55.86	27.93	16.21	0.00	0.00
	Working	82.89	8.78	5.70	2.19	0.44
	Unemployed	75.00	18.75	6.25	0.00	0.00
	Pensioner	46.51	27.91	25.58	0.00	0.00
Place of residence						
During the pandemic	Village	69.79	21.88	8.33	0.00	0.00
	City of up to 50.000 residents	56.41	30.77	8.55	4.27	0.00
	City of 50.000 to 100.000 residents	54.35	33.69	10.87	1.09	0.00
	City >100.000 residents	30.28	59.63	7.34	2.75	0.00
During the pandemic	Village	85.42	7.29	6.25	1.04	0.00
	City of up to 50.000 residents	79.48	8.55	8.55	3.42	0.00
	City of 50.000 to 100.000 residents	68.48	17.39	14.13	0.00	0.00
	City >100.000 residents	46.79	33.03	16.51	2.75	0.92
Driver's license						
Before the pandemic	Yes	59.31	33.24	6.02	1.43	0.00
	No	77.36	12.32	8.60	1.43	0.29
During the pandemic	Yes	56.92	13.85	23.08	6.15	0.00
	No	40.00	29.23	26.15	4.62	0.00

divided into the time before and during the Covid-19 pandemic, as the restrictions introduced contributed to changes in residents' lives. By 2019, 216 respondents were using a personal car to get around the city. Another very popular mode of travel was the use of public transportation. Only 9 people indicated that they used bicycles and scooters and 36 people moved around the city on foot. The breakthrough comes as the Covid-19 pandemic continues, with as many as 289 people indicating that they mostly move around the city by individual means of transportation. The number of people traveling by public transportation decreased (by 84 people), but more respondents chose to cover urban routes on foot (by 11 people). Among all the survey participants, no one uses the services of cab companies (Figure 7).

In the next step, the way respondents get around the city was analyzed according to gender, age, labor market statute and place of residence, as well as the driver's license held, according to pandemic. It is men who are most likely to travel by car in built-up areas, while women choose public transportation for travel. During the pandemic, many people switched from the public transportation to personal transportation. The chi-square test shows that there is no relationship between the way of urban travel and gender, as the Chi^2 is 20.9, where the theoretical Chi^2 is 7.81. In addition, people in the 36-45 and 46-55 age groups are most likely to use a personal car when traveling in a built-up area. Public transportation is mainly used by people over 55 and those in the 18-25 age group. In terms of choice of mode of transportation before the pandemic, students were the most likely to walk, students chose public transportation, employed and unemployed people used a personal car and retirees and pensioners traveled by public transportation. During the Covid-19 period, the share of passenger cars increased in each group of respondents. In the built-up area, the passenger car is mainly used by residents of rural areas and cities with up to 50,000 and 50-100,000 residents. The public living in larger metropolitan areas uses public transportation for this purpose. However, during the pandemic, many respondents substituted public transportation in favor of individual means of transportation. Respondents most often use a personal car to travel in built-up areas. During the Covid-19 pandemic, many people switched

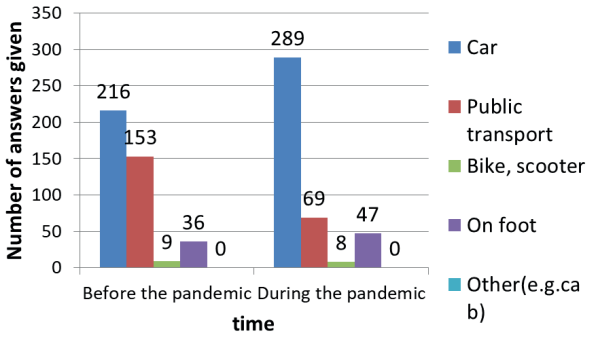

Figure 7 *The most common way respondents move around the city*

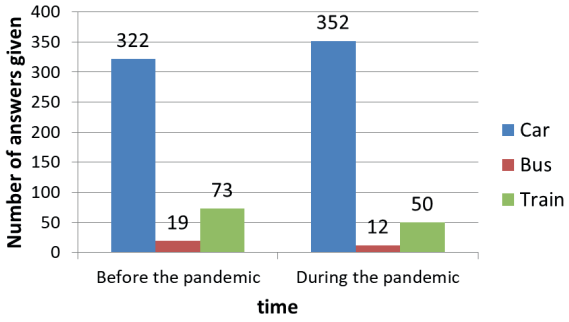

Figure 8 *Respondents' responses regarding the mode of travel outside the built-up area*

from the road transportation to traveling on foot (Table 2 and 3).

The timing of the Covid-19 pandemic has not drastically changed the way Poles travel outside built-up areas. Most respondents use a personal car outside urban zones. Respondents who do not have a driver's license prefer to choose the train over the bus. However, the pandemic has contributed to the public's reduction in the use of public transportation in favor of the personal car (Figure 8).

In addition, respondents were asked about the frequency of switching from cars to public transportation. Before the Covid-19 pandemic, a very large number of respondents were willing to travel by public transportation. The distribution of responses to this question is as follows: 80 respondents travel by bus/tram daily, 120 respondents several times a week, 60 respondents several times a month and as many as 83 respondents always choose personal transportation.

One of the effects of the pandemic is that the public is using public transportation less. As many as 131 people declared that they do not substitute their personal car for public transportation at all. Sixty-three respondents choose public transportation several times a month and 54 people only occasionally during the year. There was a decrease in the number of people who, before the pandemic, declared that they take public transportation every day. The above responses of respondents are shown in Figure 9.

Before the Covid-19 pandemic, the public was more likely to travel by public transportation. During this infectious disease, the percentage of people who do not substitute a personal car at all has increased. Daily passengers on public transportation are mainly people under the age of 18 and respondents in the 18-25 age range. The answer "does not replace at all" was marked by the largest number of respondents in the 26-35 and 46-55 age brackets. In addition, daily passengers of public transportation are mainly students, schoolchildren and unemployed people. Working people prefer to choose a personal car over public transportation for work-related travel. In contrast, residents of metropolitan areas travel by bus/tram. In addition, daily trips by public transportation are made mainly by people without a driver's license for motor vehicles. Among respondents who choose only a personal car is the public who own their own means of transportation (Table 4 and 5).

Public transportation is more environmentally

Table 4 *Frequency of switching from personal car to public transportation among respondents (%) - part 1*

		Everyday	2-3 times a week	Once a week	Several times a month	Several times a year	It does not replace at all	Not applicable
				Sex				
Before the pandemic	Women	27.01	17.06	5.69	9.00	10.43	20.85	9.96
	Men	11.33	16.75	18.72	20.69	10.34	19.21	2.96
During the pandemic	Women	20.38	10.43	9.95	12.32	9.95	27.49	9.48
	Men	5.42	9.85	11.33	18.23	16.26	35.96	2.95
				Age				
Before the pandemic	Under 18 years	40.00	0.00	0.00	0.00	0.00	20.00	40.00
	18-25	25.12	19.81	5.80	10.14	12.56	15.94	10.63
	26-35	18.65	18.65	8.47	11.86	10.17	28.81	3.39
	36-45	15.22	6.52	45.65	8.70	2.17	21.74	0.00
	46-55	8.16	10.21	12.25	30.61	8.16	30.61	0.00
	Over 55	8.33	20.83	12.50	29.17	12.50	14.58	2.09

Table 5 *Frequency of switching from personal car to public transportation among respondents (%) - part 2*

		Everyday	2-3 times a week	Once a week	Several times a month	Several times a year	It does not replace at all	Not applicable
Status in the labor market								
Before the pandemic	Pupil	25.00	12.50	0.00	6.25	12.50	18.75	25.00
	Student	26.12	27.03	7.21	9.01	9.01	11.71	9.91
	Working	14.91	11.40	16.23	17.11	10.53	25.44	4.38
	Unemployed	31.25	0.00	0.00	25.00	12.50	25.00	6.25
	Pensioner	18.60	27.90	11.63	16.28	11.63	11.63	2.33
During the pandemic	Pupil	25.00	18.75	0.00	6.25	12.50	18.75	18.75
	Student	18.92	13.51	13.51	16.22	8.11	19.82	9.91
	Working	8.77	7.89	10.96	14.04	14.47	39.92	3.95
	Unemployed	18.50	6.25	0.00	12.50	6.25	44	12.50
	Pensioner	13.95	11.63	9.30	23.26	20.93	18.60	2.33
Place of residence								
During the pandemic	Village	11.46	10.42	4.17	6.25	19.79	41.66	6.25
	City of up to 50.000 residents	11.12	15.38	17.95	25.64	9.40	16.24	4.27
	City of 50.000 to 100.000 residents	16.30	21.74	23.91	13.04	5.43	13.04	6.54
	City >100.000 residents	37.61	20.18	2.75	11.93	7.34	11.02	9.17
During the pandemic	Village	6.25	6.25	6.25	8.33	13.54	54.17	5.21
	City of up to 50.000 residents	5.98	5.98	11.12	21.37	17.09	33.33	5.13
	City of 50.000 to 100.000 residents	10.87	14.13	19.57	15.22	9.78	23.91	6.52
	City >100.000 residents	28.44	14.68	6.42	14.68	11.01	16.51	8.26
Driver's license								
Before the pandemic	Yes	16.91	15.47	12.61	16.33	11.75	22.64	4.29
	No	32.31	24.62	9.23	6.15	3.08	6.15	18.46
During the pandemic	Yes	10.32	8.31	10.03	15.76	14.61	36.68	4.29
	No	27.69	20.00	13.85	12.31	4.62	4.62	16.91

friendly than using individual transportation. As the survey above shows, it is not the most popular choice among respondents. For this reason, Poles were asked what discourages them from using public transportation. Most people declared the lack of direct connections as a problem. Travel time and delays that occur are other factors. Respondents do not pay attention to the price and possible danger. For some people, discouraging factors are the quality of public transportation, fear of contracting coronavirus, crowding and lack of seats, lack of personal hygiene of other travelers. Respondents' responses are shown in Figure 10.

Behaviors that can be considered pro- or anti-environmental are those related to actions in the context of used car parts. The survey asked drivers what they do with used batteries and tires. 23.7% of respondents indicated that this question does not apply to them, as they do not own a passenger car. More than half of the respondents present environmentally friendly behaviors in terms of used car parts, which include: leaving them at a store (17.1 %), giving them to a recycling center (26.3%) and leaving them at a workshop (17.6 %). Only 15% of people declared actions that could endanger the environment. Among activities that do not threaten the environment, storing them in the garage or basement (10.6%) dominates, as their future fate should be decided. 3.9% use used tires or batteries for other purposes and only two people threw them in the

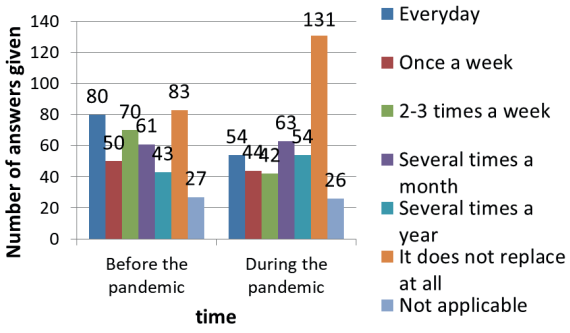

Figure 9 *Frequency of switching from personal cars to public transportation among respondents*

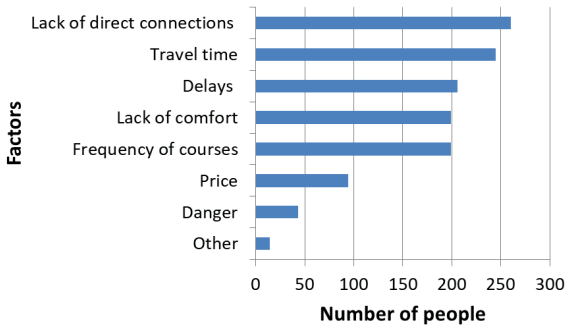

Figure 10 *Distribution of respondents' answers on factors that discourage them from choosing public transportation*

garbage. The percentage distribution of the number of respondents' answers is shown in Figure 11.

The next question asked about respondents' actions in the context of used car parts. Most respondents marked the answer that they give them to a recycling center. Among non-environmental behaviors among men, using batteries and tires for other purposes dominated, while women's responses included throwing them in the garbage. Among ecological behaviors in the context of used car parts, two responses dominated: leaving them at the store and giving them to a recycling point. Among those aged 18-25 and 26-35, there are respondents who throw them in the garbage. As many as 17.39 % of those in the 36-46 age bracket use used

Table 6 *Drivers' behavior toward used car parts (%)*

	I leave in the store when I buy new	I leave in the workshop	Surrenders to a point accepting waste tires/ batteries	Stores in garage/ basement	Uses for other purposes	I throw in the garbage	Not applicable
Sex							
Women	14.22	16.10	23.70	9.48	0.95	0.95	34.60
Men	20.69	19.21	29.06	11.82	6.90	0.00	12.32
Age							
Under 18 years	0.00	0.00	0.00	0.00	0.00	0.00	100.00
18-25	13.53	13.53	22.71	12.07	1.93	0.48	35.75
26-35	37.29	15.25	27.12	3.39	3.39	1.69	11.87
36-45	26.09	6.52	30.44	13.04	17.39	0.00	6.52
46-55	16.33	24.49	36.74	12.24	2.04	0.00	8.16
Over 55	4.17	43.75	29.16	10.42	2.08	0.00	10.42
Status in the labor market							
Pupil	6.25	6.25	6.25	6.25	6.25	0.00	68.75
Student	9.92	11.71	22.52	13.51	1.80	0.00	40.54
Working	24.12	19.74	28.51	10.53	5.70	0.87	10.53
Unemployed	12.50	25.00	43.75	0.00	0.00	0.00	18.75
Pensioner	6.98	23.26	25.58	9.30	0.00	0.00	34.88
Place of residence							
Village	20.83	20.83	25.00	16.67	5.21	0.00	11.46
City of up to 50.000 residents	20.51	23.93	25.64	9.40	0.85	0.00	19.67
City of 50.000 to 100.000 residents	20.65	9.78	26.09	9.78	9.78	2.18	21.74
City >100.000 residents	8.25	14.68	28.44	7.34	0.92	0.00	40.37
Driver's license							
Yes	19.48	20.34	29.51	12.32	4.30	0.29	13.76
No	6.16	3.07	9.23	1.54	1.54	1.54	76.92

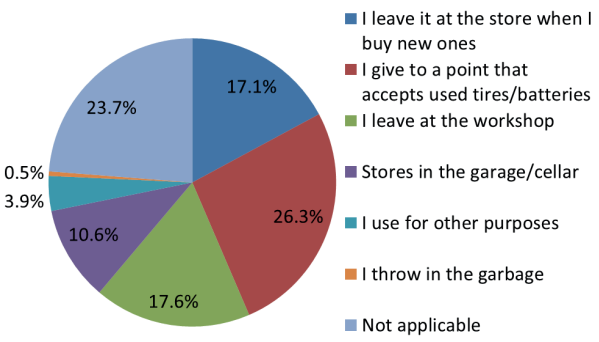

Figure 11 *Drivers' behavior toward used auto parts*

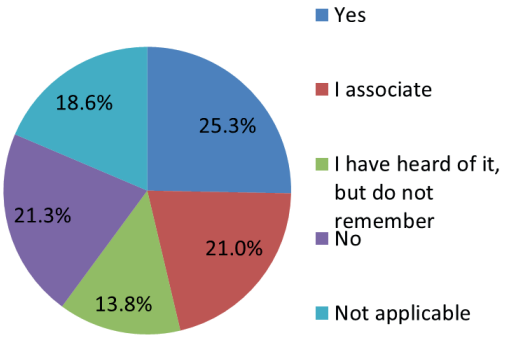

Figure 12 *Drivers' knowledge of EURO standards*

car parts for other purposes. In addition, there are two predominant responses: leaving them at the store and giving them to a recycling center. Among working people, there are respondents who throw them in the garbage and use them for other purposes. Respondents' place of residence has no influence on the further fate of used car parts. The answers to this question are very close to each other. Those with a driver's license have the largest share of used car parts, as they are the ones who own their own means of transportation (Table 6).

The next questions were aimed at those with a driver's license and a passenger car. Respondents' knowledge of the European emission standard was tested. 25.4% of respondents know what the EURO standard defines. Among the 34.8% of respondents are those who associate or once heard, but cannot fully describe the meaning of the European exhaust gas standard. As many as 21.3% of respondents do not know the meaning of the EURO standards (Figure 12).

In the case of European exhaust gas standards, it is 37.44% of men and 13.74% of women who know what EURO stands for. According to the chi-square test,

Table 7 *Drivers' knowledge of knowledge of EURO standards (%)*

	Yes	I have heard of it. but I do not remember	I associate	No	Not applicable
Sex					
Women	13.74	17.06	14.69	27.01	27.50
Men	37.44	10.34	27.59	15.27	9.36
Age					
Under 18 years	0.00	0.00	0.00	0.00	100.00
18-25	21.26	12.07	12.56	26.09	28.02
26-35	38.98	15.25	18.64	16.95	10.18
36-45	30.43	21.74	28.26	15.22	4.35
46-55	42.86	10.20	20.41	24.49	2.04
Over 55	6.25	16.66	56.25	10.42	10.42
Status in the labor market					
Pupil	12.50	0.00	12.50	12.50	62.50
Student	12.61	16.22	9.01	30.63	31.53
Working	36.41	14.47	25.00	17.54	6.58
Unemployed	12.50	0.00	37.50	31.25	18.75
Pensioner	9.30	13.95	27.91	16.28	32.56
Place of residence					
Village	25.00	11.45	22.92	30.21	10.42
City of up to 50.000 residents	35.05	8.55	19.66	23.08	13.66
City of 50.000 to 100.000 residents	22.81	18.48	30.43	8.70	19.58
City >100.000 residents	17.43	17.43	12.84	22.02	30.28
Driver's license					
Yes	28.37	15.47	24.07	24.64	7.45
No	9.23	4.62	4.62	3.08	78.45

there is no correlation between knowledge and gender, as the Chi^2 is 59.47, where the theoretical Chi^2 is 9.49. Those in the age range of 26-35 and 46-55 have the greatest knowledge on the subject. As many as 30.21% of rural residents do not know what the EURO standard defines. In contrast, residents of cities up to 50,000 have the most knowledge and those who have successfully passed the state driving test have some knowledge on the subject. The group of people with knowledge of the meaning of the abbreviation "EURO norm" includes: 36.41% of working people, 12.61% of students, 9.3% of pensioners and 12.5% of student unemployed respondents. A large number of people cannot identify the assumptions of European emission standards. The Chi-square test shows that there is no relationship between the purchase of a car regarding the EURO standard and knowledge of the subject and possession of a driver's license. In this case, the Chi^2 is equal to 183.02 and the theoretical Chi^2 is equal to 9.49 (Table 7).

Air quality is affected by the amount of exhaust fumes emitted by personal vehicles. Respondents were asked whether they pay attention to the level of pollutants emitted by a vehicle when buying an individual means of transportation. The survey found that 35.5% paid no attention to this issue and for 15.6% of people it is not important when choosing a vehicle. For only 12.1% of respondents, the EURO standard is an important criterion when acquiring a new means of transportation. Due to the fact that many people do not have knowledge of European exhaust gas standards, 14.3% of those questioned did not know that this is a factor worth considering when choosing a passenger car (Figure 13).

It is men who do not weigh the emission standard when choosing an individual means of transportation. For 13.74% of women, it is an important criterion when choosing a personal vehicle. The chi-square test shows that there is no relationship between the purchase of a car with a certain standard and gender, as the Chi^2 is 27.93, where the theoretical Chi^2 is 9.49. When purchasing a vehicle, as many as 20.34% of

Table 8 *EURO standard as a criterion for buying a new vehicle (%)*

	This is an important criterion when purchasing a vehicle	It matters little to me	I didn't know it was something to pay attention to	I wasn't paying attention	Not applicable
Sex					
Women	13.74	11.85	10.43	31.75	32.23
Men	10.34	19.21	18.23	39.41	12.81
Age					
Under 18 years	0.00	0.00	0.00	0.00	100.00
18-25	11.59	12.56	8.70	33.82	33.33
26-35	20.34	16.95	10.17	37.29	15.25
36-45	6.52	15.22	17.39	54.35	6.52
46-55	18.38	8.16	24.49	42.85	6.12
Over 55	4.17	35.42	31.25	18.75	10.41
Status in the labor market					
Pupil	0.00	6.25	0.00	25.00	68.75
Student	12.61	12.61	10.81	26.13	37.84
Working	14.03	15.79	16.23	44.30	9.65
Unemployed	18.75	18.75	0.00	43.75	18.75
Pensioner	2.32	23.26	23.26	13.95	37.21
Place of residence					
Village	9.38	21.88	11.46	43.74	13.54
City of up to 50.000 residents	12.82	13.68	19.66	35.89	17.95
City of 50.000 to 100.000 residents	16.30	17.39	15.22	30.44	20.65
City >100.000 residents	10.09	10.09	10.09	32.12	37.61
Driver's license					
Yes	12.89	17.76	16.91	40.69	11.75
No	7.69	3.08	0.00	7.69	81.54

those in the 26-35 age group and 18.38% of those in the 46-55 age group consider the EURO standard as an important criterion. In contrast, more than half of respondents in the 36-45 age group have never paid attention to the emission standard. In addition, when buying a vehicle, as many as 18.75% of the unemployed and 12.61% of students consider the EURO standard as an important criterion. In contrast, almost half (44.3%) of the working respondents and (43.75%) of the unemployed did not pay attention to this aspect. Among those with knowledge of the meaning of the abbreviation "EURO standard" are: 36.41% of working, 12.61% of students, 9.3% of pensioners and 12.5% of unemployed respondents. A large number of people cannot identify the assumptions of European emission standards. In addition, the respondents' place of residence does not affect the answers in the context of purchasing a vehicle, the main criterion of which is the Euro standard. Most people indicated that they do not pay attention to the level of pollution emitted by the car they are looking for. The situation was similar in the questions about the Euro standard, as they were aimed at those with a cat. B driver's license. 40.69% of people never paid attention to the level of pollution emitted by the vehicle. The chi-square test shows that there is no correlation between the purchase of a car regarding the Euro standard and knowledge of the subject and having a driver's license. For the first question, the Chi^2 is 153.73 and the theoretical Chi^2 is 9.49 (Table 8).

The amount of exhaust fumes emitted by a vehicle depends on fuel consumption. Of great importance is the driving style of drivers. Smooth acceleration, braking or the way gears are changed, are characterized by the fact that driving is more efficient and as a result, the driver reduces the vehicle's production of harmful exhaust components. The European Union has begun to promote and support the new economical driving style. Half of those surveyed drive according to the principles of Eco-driving. 20% know what the method is about, but do not use it and only 12.6% have never heard of the economic driving technique (Figure 14). Thus, drivers who apply eco-driving principles individually affect the environmental protection caused by road transportation.

An important issue, related to the environmental impact of transportation, is the driving style of drivers. Definitions of eco-driving have been created and for this reason respondents were asked whether they use it in their daily driving of passenger cars. As many as 59.61% of men and 40.28% of women use this driving technique. According to the Chi-square test, there is no

Table 7 *Use of Eco-driving technique (%)*

	Yes	No. but I know the rules	No. I don't know what eco-driving is	Not applicable
Sex				
Women	40.28	19.43	13.74	26.55
Men	59.61	20.69	11.33	8.37
Age				
Under 18 years	0.00	0.00	0.00	100.00
18-25	42.52	20.77	12.56	24.15
26-35	52.54	25.42	10.18	11.86
36-45	60.87	28.26	0.00	10.87
46-55	65.31	12.24	20.41	2.04
Over 55	56.25	12.50	20.83	10.42
Status in the labor market				
Pupil	18.75	12.50	6.25	62.50
Student	44.14	15.32	16.22	24.32
Working	57.02	23.25	10.96	8.77
Unemployed	50.00	31.25	0.00	18.75
Pensioner	37.22	13.95	18.60	30.23
Place of residence				
Village	42.71	30.21	17.71	9.37
City of up to 50.000 residents	56.41	18.80	12.82	11.97
City of 50.000 to 100.000 residents	54.35	16.30	9.78	19.57
City >100.000 residents	44.95	15.60	10.09	29.36
Driver's license				
Yes	57.88	22.06	14.04	6.02
No	6.15	9.23	4.62	80.00

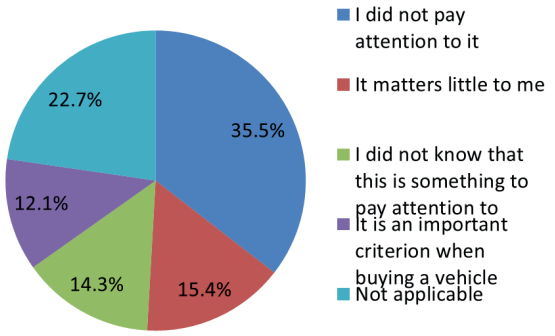

Figure 13 *EURO standard as a criterion for buying a new vehicle*

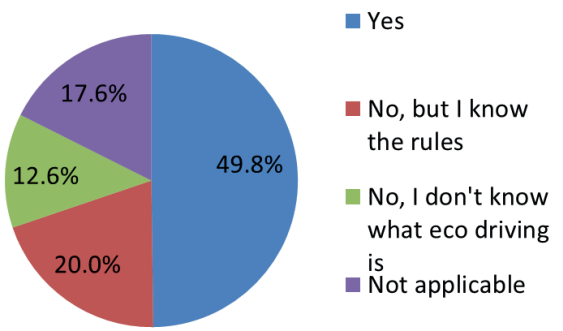

Figure 14 *Use of Eco-driving technique by respondents*

relationship between the use of eco-driving and gender, as the Chi^2 is 27.69, where the theoretical Chi^2 is 7.81. The economical driving technique is used by more than half of the respondents in each age bracket who have reached the appropriate age to take the driving test. The eco-driving style is used by students (44.14 %), working people (57.02%) and the unemployed (50 %). The eco-driving technique is used by almost half of the respondents in each group of localities. An interesting phenomenon is that as many as 30.21% of respondents from rural areas know the eco-driving method, but do not use it. More than half of the people (57.88%) use the eco-driving. The Chi-square test shows that there is no correlation between the use of eco-driving and having a driver's license, as the Chi^2 is 39.16, where the theoretical Chi^2 is 7.8 (Table 9).

Many car brands are producing and releasing more and more cars with alternative powertrains, such as hybrids and electrics. Their registration and popularity in Poland are growing. Respondents with

Table 9 *Use of Eco-driving technique (%)*

	Yes	No. but I know the rules	No. I don't know what eco-driving is	Not applicable
		Sex		
Women	40.28	19.43	13.74	26.55
Men	59.61	20.69	11.33	8.37
		Age		
Under 18 years	0.00	0.00	0.00	100.00
18-25	42.52	20.77	12.56	24.15
26-35	52.54	25.42	10.18	11.86
36-45	60.87	28.26	0.00	10.87
46-55	65.31	12.24	20.41	2.04
Over 55	56.25	12.50	20.83	10.42
		Status in the labor market		
Pupil	18.75	12.50	6.25	62.50
Student	44.14	15.32	16.22	24.32
Working	57.02	23.25	10.96	8.77
Unemployed	50.00	31.25	0.00	18.75
Pensioner	37.22	13.95	18.60	30.23
		Place of residence		
Village	42.71	30.21	17.71	9.37
City of up to 50.000 residents	56.41	18.80	12.82	11.97
City of 50.000 to 100.000 residents	54.35	16.30	9.78	19.57
City >100.000 residents	44.95	15.60	10.09	29.36
		Driver's license		
Yes	57.88	22.06	14.04	6.02
No	6.15	9.23	4.62	80.00

Table 10 *Respondents' willingness to purchase an alternatively powered vehicle (%)*

	Yes	No	Not applicable
Sex			
Women	38.39	38.86	22.75
Men	54.68	38.42	6.90
Age			
Under 18 years	0.00	0.00	100.00
18-25	38.65	39.13	22.22
26-35	49.16	38.98	11.86
36-45	54.35	45.65	0.00
46-55	65.31	34.69	0.00
Over 55	54.17	37.50	8.33
Status in the labor market			
Pupil	18.75	18.75	62.50
Student	39.64	36.04	24.32
Working	53.07	41.23	5.70
Unemployed	25.00	50.00	25.00
Pensioner	46.52	34.88	18.60
Place of residence			
Village	37.50	53.13	9.37
City of up to 50.000 residents	47.86	41.03	11.11
City of 50.000 to 100.000 residents	54.35	25.00	20.65
City >100.000 residents	45.87	34.86	19.27
Driver's license			
Yes	51.86	42.98	5.16
No	16.92	15.39	67.69

internal combustion cars were asked if they had ever considered buying an alternatively powered car. 46.4% of respondents said they had been able to switch from gasoline or diesel modes of transportation to environmentally friendly cars. Only 38.6% had never thought about buying a hybrid or electric vehicle (Figure 15).

More often it is men who are willing to purchase an electric or hybrid vehicle. According to the Chi square test, there is no relationship between vehicle purchase and gender, as the Chi^2 is 23.29, where the theoretical Chi^2 is 5.99. Nearly half of respondents aged 26 to over 55 are willing to switch from an internal combustion vehicle to an electric or hybrid vehicle. Readiness to purchase such a car indicated: 39.64% of students, 53.07% of working people and 46.52% of retirees. Nearly half of respondents living in cities are willing to switch from a combustion vehicle to an electric or hybrid car. 53.13% of respondents from small towns and cities have not considered buying an environmentally friendly vehicle. Those without a driver's license also considered buying an alternatively powered car. 42.98% of respondents with driving skills had never considered buying an electric or hybrid car. The chi-square test shows that there is no relationship between the willingness to purchase an alternatively-powered vehicle and having a driver's license, as the Chi^2 is 168.30, where the theoretical Chi^2 is 5.99 (Table 10).

The European Union is seeking and constantly studying possible solutions to reduce the negative impact of road transport on the environment. The European Commission is urging member countries to implement a policy of sustainable development by supporting and funding research into environmentally friendly transportation activities. For this reason, respondents were asked what solutions they think would minimize the negative environmental impact of road transportation. Most would like to see those in power allocate more resources to properly functioning public transportation. In the second place was the idea of more electric vehicles on Polish roads. As many as 179 people marked the solution of introducing green zones in cities. Respondents do not want to eliminate all internal combustion vehicles from the roads, but would prefer more restrictive diagnostic testing of older cars (Figure 16.). Respondents typed in their own ideas such as:

- limiting the production of new vehicles,
- greater subsidies for electric means of transportation,
- building a nuclear power plant in Poland to generate electricity to power electric vehicles,
- the invention of alternative fuel,

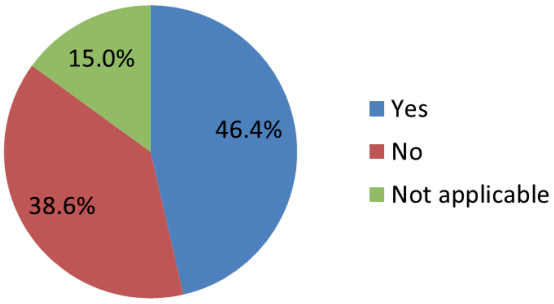

Figure 15 *Willingness of respondents to purchase an alternatively-powered vehicle*

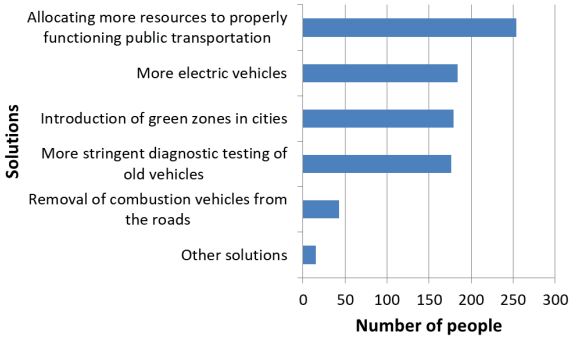

Figure 16 *Summary of solutions to reduce the negative impact of road transport on the environment*

- popularizing the use of alternative means of transportation,
- modernization of roads,
- increasing parking fees in cities and introducing a 30-mph speed limit in built-up areas.

The next step presents a summary of correlations between Poles' awareness of the impact of transportation on the environment, the way respondents drive in and out of built-up areas, drivers' knowledge of EURO standards, purchase of a car with the applicable exhaust gas standard, Eco-driving and purchase of an alternatively powered vehicle. As can be seen, there is no correlation

Table 9 *Correlation of answers given*

Criterion	*df*	α	χ^2	χ^2_d	Conclusion
Awareness of Poles related to the impact of transportation on the environment	4	0.05	10.47	9.49	No correlation between the responses of men and women
Manner of movement of respondents in a built-up area	4	0.05	20.9	7.81	No correlation between the way of movement in the city and gender
The way respondents travel outside built-up areas	2	0.05	18.43	5.99	No correlation between mode of movement in the city and gender
Drivers' knowledge of knowledge of EURO standards	4	0.05	59.47	9.49	No correlation between knowledge and gender
Drivers' knowledge of knowledge of EURO standards	4	0.05	183.02	9.49	No correlation between buying a car regarding the EURO standard and knowledge about it and having a driver's license
Purchase of a car	4	0.05	27.93	9.49	No correlation between buying a car with a particular standard and gender
Purchase of a car	4	0.05	153.73	9.49	No correlation between buying a car regarding the EURO standard and knowledge about it and having a driver's license
Eco-driving	3	0.05	27.69	7.81	No correlation between the use of Eco-driving and gender
Eco-driving	3	0.05	39.16	7.81	No correlation between using eco-driving and having a driver's license
Purchase of an alternatively powered vehicle	2	0.05	23.29	5.99	No correlation between buying a vehicle and gender
Purchase of an alternatively powered vehicle	2	0.05	168.30	5.99	No correlation between buying a vehicle and having a driver's license.

where:
df - the degrees of freedom,
α - the significance level,
χ^2 - the Chi-square statistic,
χ^2_d - the critical Chi-square value.

between the answers given among respondents to the question by gender and driver's license held (Table 11)

Summarizing the survey results, rural residents cannot imagine daily life without a personal car. It turns out that rural households usually own three or more vehicles. It can be concluded that every person with a driver's license owns a personal car. The reason for this phenomenon is that public transportation to small towns is poorly developed. Therefore, rural residents are forced to have their own car for each family member. Official errands, professional work and education are the main activities for which the rural residents must travel to larger settlements. In smaller settlements, on the other hand, there are usually one to two means of transportation per household, while residents of metropolitan areas mainly own one personal car or no vehicle at all. This is due to the fact that public transportation in larger cities is well-developed, so the urban population prefers to use public transportation such as buses, streetcars, light rail, among others.

The Covid-19 pandemic has changed transportation behavior in Polish cities. It was enforced by government-imposed restrictions, such as limits on the number of passengers in public transportation vehicles. In addition, fear of contracting the coronavirus was widespread among the public. During the pandemic, the population abandoned public transportation in cities shifting mainly to the personal car. Many respondents declared that they walk in urban areas. Respondents who declared that they were switching from public transportation to a personal car were those with a driver's license. In contrast, respondents who did not have driving privileges were forced to use the bus or streetcar. Summarizing urban mobility, the pandemic is the result and the main factor that changed the public's choice of mode of transportation in the urban area. In addition, outside the built-up area, respondents are most likely to choose a passenger car. On the other hand, for longer routes, passengers prefer to choose rail transportation (train) rather than bus.

Public transportation is not so popular among respondents that they choose it for longer routes. Respondents were asked what discourages them from using the public transportation. The main factor is the offerings of transportation companies and their shortcomings in performing transportation services. For this reason, carriers should work together to create consistency in schedules and the frequency of courses that occur. Reaching a destination even with a change, but without unnecessary waiting, is the biggest advantage of choosing the public transportation. This will minimize the travel time, which a very large number of people pay attention to when planning a trip and choosing a mode of transportation. In addition to schedules, public transportation passengers point to the comfort found in public transportation as a deterrent. In addition, carriers should provide more funding for modern vehicles, which will change the vision regarding the quality and safety of travel. Respondents' answers, about the problems they face in public transportation, are the best way for carriers to see the bad sides of company management. As a result of changes in creation of transportation offers suggested by the public, more people will choose to travel by public transportation than by individual means.

The public most often uses the passenger car for travel, which is an emitter of a large amounts of harmful components into the air, from fuel combustion. The largest number of combustion vehicles travel on Polish roads. However, the number of passenger cars with an alternative source of propulsion is steadily increasing. Nearly a half of the survey's respondents are considering purchasing an electric or hybrid vehicle. There are people in every age group who are willing to swap their gasoline or internal combustion vehicle for an environmentally friendly means of personal transportation. In addition to the choice of means of transportation, driving technique is important for environmental protection in the context of the road transport. Eco-driving style is now popular and since 2015 it has been one of the tasks tested on the driving test. Half of the respondents use Eco-driving as a result of their individual commitment to minimizing the amount of harmful exhaust components in the air. Those who marked the answer "no, I don't know what Eco-driving is" are mostly young people who are licensed to drive a vehicle with a maximum permissible weight of up to 3.5 tons, having acquired it after 2015. It can be inferred that they drive according to certain principles of economical driving, but do not realize it. On the other hand, there are many people who have knowledge of Eco-Driving, but do not apply this method in their daily driving of passenger cars.

The survey also tested knowledge of the European emissions standard. More than a half of the respondents do not know or only somewhat associate the meaning of EURO standards. One in five has full knowledge of permissible emission limits. Another question concerned those who own an individual means of transportation. A very large number of people, that took part in the survey, do not pay attention to which EURO standard their vehicle has. For only 50 people, this is an important criterion when buying a personal vehicle. The responses of those surveyed show that knowledge of the introduced exhaust gas standards is low among the Polish public. Thus, on this topic, more education should be introduced for the future applicants to drive motor vehicles. In this way, the nation's awareness of the negative impact of vehicles' engines combustion on the environment can be increased.

The public's awareness of the environmental impact of the road transportation is improving. A very large number of respondents are interested in environmental protection to some extent. This is a positive result of the survey, as the future population will deeply analyze their behavior and choices to act in accordance with the principles of sustainable development. Pro-

environmental actions can be encouraged through various social campaigns, subsidies and increased fees for those who will negatively impact the ecosystem. Respondents also identified environmentally friendly transportation solutions that should be introduced in Poland. More than a half believe that the state should allocate more money for properly functioning public transportation. Create it according to the public's expectations, which will result in more people being able to replace individual means of transportation with public transportation. In the second place was the idea of electric vehicles, to increase their number and increase subsidies for purchase of an alternatively powered car. However, to power such a vehicle, electricity is needed, which in Poland is generated from a coal-fired power plant. Therefore, there is a need to change the way electricity is produced, which will be less invasive to the environment. Only one person indicated that a nuclear power plant should be built as a source of energy to power electric vehicles. Respondents pointed to solutions that should be introduced in cities, such as green zones, a 30km/h speed limit in built-up areas and higher parking fees. This would result in less congestion on the roads and, in part, encourage the public to use public transportation.

3 Conclusion

The survey of the Polish public revealed their transportation preferences and knowledge of the negative impact of the road transport on the environment. The respondents' responses were influenced by the current situation of the infectious disease Covid-19. The population is trying to protect itself from contagion, so it chooses individual means of transportation. Before the outbreak of the pandemic, they were able to swap the personal car in favor of public transportation. However, there are many factors that influence the decision to choose the public transportation. The public is willing to travel more often by public transport when carriers create transportation offers that are in line with citizens' needs. As a result, there will be fewer passenger cars on the roads, thus reducing the negative components from the fuel combustion.

Public interest in environmental protection in the context of road transportation, is growing all the time. Many people are basing their activities on environmental solutions. Drivers, in addition to the proper operation of the vehicle, are interested in the technologies used in their vehicles to reduce exhaust fumes and are prudent in deciding the fate of used car parts. Respondents want the Polish state to function in accordance with the principles of sustainable development. For this reason, green innovations should be introduced, such as development of public transportation, elimination of old combustion vehicles and more electric cars. Those measures will affect the environment to some extent, but will not minimize the negative impact of the road transport on the ecosystem.

The road transport plays a very important role for the proper functioning of the country's economy. It is also growing very rapidly and is the most popular mode of transport chosen for transporting people and cargo. In an uncontrolled way, road passenger transport has begun to dominate in the form of individual transport. The public seeks to move as quickly as possible between designated points than to travel according to public transportation schedules. Road transportation has a significant impact on the environment. Currently, transportation means are powered by gasoline or diesel fuel, which emit large amounts of harmful products of their combustion into the environment. The highest concentration of pollutants is shown by use of the passenger car. Their registrations are increasing every year, resulting in increased traffic caused by personal travel vehicles. Road transportation also affects the health and life of the public. This is influenced by noise and air, soil and groundwater pollution.

There is a growing awareness in Polish society of the negative impact of individual road transport on the environment. For environmental action is to use buses or streetcars to get around cities. A better way is to choose a bicycle or cover routes on foot. This is ideal for the environment and for human health and fitness. Even such small measures can, to some extent, reduce the negative impact of transportation on the ecosystem.

The aim is to make residents think about the planet and the environment when choosing a means of transportation and actions in the context of operating their own vehicle. All the time, it is necessary to educate the public and increase their knowledge about the drastic development and impact of the road transport on the ecosystem.

Grants and funding

The authors received no financial support for the research, authorship and/or publication of this article.

Conflicts of interest

The authors declare that they have no known competing financial interests or personal relationships that could have appeared to influence the work reported in this paper.

References

[1] Poland on the path of sustainable development - Central Statistical Office [online] [accessed 2022-02-21]. Report. 2020. Available from: https://raportsdg.stat.gov.pl/2020/

[2] Environmental impact of transport [online] [accessed 2020-02-21]. Available from: https://redakcjabb.pl/17209/wplyw-transportu-na-srodowisko

[3] SZOLTYSEK, J. *Creating mobility of city residents*. Warsaw: Wolters Kluwer, 2011. ISBN 978-83-264-1549-4.

[4] ZALOGA, E., DUDEK, E. Selected problems of mobility of European society. *Problems of Transport and Logistics*. 2009, **9**, p. 99-109. ISSN 1644-275X, eISSN 2353-3005.

[5] FLEJTERSKI, S., PANASIUK, A., PERENC, J., ROSA, G. *Contemporary economics of services*. Warsaw: Polish Scientific Publishers PWN, 2008. ISBN 83-01-14488-2.

[6] MENES, E. Socio-economic aspects of the development of individual motorization in Poland. *Communication Review*. 2001, **01**, p 1-6. ISSN 0033-2232, eISSN 2544-6037.

[7] Treaty on the functioning of the European Union. Official Journal of the European Union [online]. C 326/49. TFEU, 2012. Available from: https://eur-lex.europa.eu/legal-content/EN/TXT/?uri=CELEX%3A12012E%2FTXT

[8] KRUSZYNA, M. Traffic engineering and mobility shaping. *Communication Review*. 2010, **11-12**, p. 52-53. ISSN 0033-2232, eISSN 2544-6037.

[9] KRUSZYNA, M. Railway station as a mobility hub. *Communication Review*. 2012, **10**, p. 34-37. ISSN 0033-2232, eISSN 2544-6037.

[10] BORYS, T. *Measuring sustainable development of transport, in ecological problems of sustainable development*. KIELCZEWSKI, D., DOBRZANSKA, B. (EDS.). Bialystok: Publishing House of the Higher School of Economics in Bialystok, 2009. ISBN 978-83-61247-07-4.

[11] LITMAN, T. Developing indicators for comprehensive and sustainable transport planning. *Transportation Research Record: Journal of the Transportation Research Board* [online]. 2007, **2017**(1), p. 10-15. ISSN 0361-1981, eISSN 2169-4052. Available from: https://doi.org/10.3141/2017-02

[12] CHAMIER-GLISZCZYNSKI, N. Sustainable urban mobility as an element of the transportation plan Koszalin University of Technology. *Logistics*. 2015, **4**, p.107-116. ISSN 1231-5478.

[13] BANISTER, D. The paradigm of sustainable mobility. *Transport Policy* [online]. 2008, **15**(2), p. 73-80. ISSN 0967-070X, eISSN 1879-310X. Available from: https://doi.org/10.1016/j.tranpol.2007.10.005

[14] Transport White Paper - Roadmap to a single European transport area - towards a competitive and resource-efficient transport system. European Commission, Directorate-General for Mobility and Transport. 2011.

[15] European parliament resolution of April 23, 2009 on the action plan on urban mobility 2008/2217 (INI).

[16] CERVARO, R. Paradigm shift: from automobility to accessibility planning. Working Paper No. 677. Berkeley CA, 1996.

[17] KOMSTA H., DROZDZIEL, P., OPIELAK, M. The role of urban public transport in creating mobility of residents. *Buses: Technology, Operation, Transportation Systems* [online]. 2019, **1-2**, p. 393-397. ISSN 1509-5878, eISSN 2450-7725. Available from: https://doi.org/10.24136/atest.2019.073

[18] KLOS-ADAMKIEWICZ, Z. Mobility plan as a tool for implementing sustainable transport development in cities. *Logistics*. 2014, **2**, p. 124-129. ISSN 1231-5478.

[19] KRAEMER, M. U., YANG, C. H., GUTIERREZ B., WU, C. H., KLEIN, B., PIGOTT, D. M., DU PLESSIS, L., FARIA, N. R., LI, R., HANAGE, W. P., BROWNSTEIN, J. S. The effect of human mobility and control measures on the COVID-19 epidemic in China. *Science* [online]. 2020, **368**(6490), p. 493-497. ISSN 0036-8075, eISSN 1095-9203. Available from: https://doi.org/10.1126/science.abb4218

[20] STAVRINOS, D., MCMANUS, B., MRUG, S., HE, H., GRESHAM, B., ALBRIGHT, M. G., SVANCARA, A. M., WHITTINGTON, C., UNDERHILL, A., WHITE, D. M. Adolescent driving behavior before and during restrictions related to COVID-19. *Accident Analysis and Prevention* [online]. 2020, **144**,105686. ISSN 0001-4575, eISSN 1879-2057. Available from: https://doi.org/10.1016/j.aap.2020.105686

[21] DE VOS, J. The effect of COVID-19 and subsequent social distancing on travel behavior. *Transportation Research Interdisciplinary Perspectives* [online]. 2020, **5**, 100121. eISSN 2590-1982. Available from: https://doi.org/10.1016/j.trip.2020.100121

[22] OLIVER, N., LEPRI, B., STERLY, H., LAMBIOTTE, R., DELETAILLE, S., DE NADAI, M., LETOUZE, E., SALAH, A. A., BENJAMINS, R., CATTUTO, C., COLIZZA, V. (2020). Mobile phone data for informing public health actions across the COVID-19 pandemic life cycle. *Science Advances* [online]. 2020, **6**(23), eabc0764. eISSN 2375-2548. Available from: https://doi.org/10.1126/sciadv.abc0764

[23] ZHANG, L., GHADER, S., PACK, M., DARZI, A., XIONG, C., YANG, M., SUN, Q., KABIRI, A., HU, S. An interactive COVID-19 mobility impact and social distancing analysis platform. *Transportation Research Record: Journal of the Transportation Research Board* [online]. 2021, online first. ISSN 0361-1981, eISSN 2169-4052. Available from: https://doi.org/10.1177/036119812110438

[24] ZUO, F., WANG, J., GAO, J., OZBAY, K., BAN, X. J., SHEN, Y., YANG, H., IYER, S. An interactive data visualization and analytics tool to evaluate mobility and sociability trends during COVID-19. *arXiv* [online]. 2020, 14882. Available from: https://doi.org/10.48550/arXiv.2006.14882

[25] GORZELANCZYK, P. Change in the mobility of Polish Residents during the Covid-19 pandemic. *Communications - Scientific letters of the University of Zilina* [online]. 2022, **24**(3), p. A100-A111. ISSN 1335-4205, eISSN 2585-7878. Available from: https://doi.org/10.26552/com.C.2022.3.A100-A111

[26] JURKOVIC, M., GORZELANCZYK, P., KALINA, T., JAROS, J., MOHANTY, M. Impact of the COVID-19 pandemic on road traffic accident forecasting in Poland and Slovakia. *Open Engineering* [online]. 2020, **12**(1), p. 578-589. ISSN 2391-5439. Available from: https://doi.org/10.1515/eng-2022-0370

[27] GORZELANCZYK, P. Mobility of Polish residents. In: *Research and the future of telematics*. MIKULSKI, J. (Ed.). Springer, 2020, p. 3-15. ISBN 978-3-030-59269-1.

[28] Population structure by age in 1970-2050 [online] [accessed 2020-02-21]. Available from: https://stat.gov.pl/obszary-tematyczne/ludnosc/ludnosc/struktura-ludnosci,16,1.html

[29] WEGNER, T. *Applied business statistics. Excel-based methods and applications*. 3. ed. Claremont: Juta Academic, 2013. ISBN 978 0 7021 7774 3.

UNIZA

12th International Conference on Air Transport

INAIR 2023

„THE FUTURE OF AVIATION - IS THE SKY THE LIMIT?“

Tartu, Estonia
November 15 – 17, 2023

INAIR 2023 represents a forum in which industry and academia meet to exchange their ideas, to share best practices and to set up common challenges. The interaction between researchers and industry representatives is significant in order to come up with innovative solutions for the challenges of the future in air transport.

IMPORTANT DATES

- August 13, 2023
  FULL PAPERS SUBMISSION
- September 22, 2023
  NOTIFICATION OF ACCEPTANCE
- September 29, 2023
  CAMERA-READY PAPER SUBMISSION
- October 31, 2023
  FINAL CONFERENCE PROGRAMME
- November 15 – 17, 2023
  CONFERENCE DATES

TOPICS

- Airport Operation and Design
- Airline Operation
- Flight Trainings
- Safety and Security
- Air Traffic Management
- Human Performance
- Air Transportation Governance, Economics and Policy
- Education and Training
- UAS: Development, Design, Protection and Regulation
- Aerospace Engineering
- Urban Air Mobility; Innovative Air Mobility
- Communication Navigation Surveillance

CONTACT

University of Zilina, Air Transport Department
Univerzitná 8215/1, 010 26 Zilina, Slovakia
e-mail: inair@fpedas.uniza.sk
https://www.inairportal.uniza.sk

DEVELOPMENT OF THE UNIVERSAL WORKING EQUIPMENT OF THE EXCAVATOR FOR PREPARATION OF MATERIALS BASED ON WASTE DURING THE ROAD BUILDING

Ivan Georgiadi[1], Adil Kadyrov[1], Vyacheslav Kunaev[2,*]

[1]Abylkas Saginov Karaganda Technical University, Karaganda, Kazakhstan
[2]Karaganda Industrial University, Temirtau, Kazakhstan

*E-mail of corresponding author: kunaev91@list.ru

Ivan Georgiadi 0000-0001-5996-2595,
Adil Kadyrov 0000-0001-7071-2300,
Vyacheslav Kunaev 0000-0001-8283-7186

Resume

The article proposes a technological line for recycling the blast-furnace slag. This line makes it possible to obtain the crushed stone for road building, which has high water and frost resistance. The design of replaceable working equipment of a single-bucket excavator, with replaceable working tools for loosening frozen slag in dumps and preparing it for use in road building, is proposed. The results of testing the manufactured replacement working equipment are presented. The results of mathematical processing of experimental data using the approximation method are presented, as well.

Article info

Received 8 November 2022
Accepted 9 January 2023
Online 27 January 2023

Keywords:

loosening of frozen grounds
waste recycling
blast-furnace slag
single-bucket excavator
working equipment
working tool
excavation machines

Available online: https://doi.org/10.26552/com.C.2023.022

ISSN 1335-4205 (print version)
ISSN 2585-7878 (online version)

1 Introduction

Development of the road infrastructure and, in particular, the construction and reconstruction of highways, bridges and overpasses, is one of the most pressing issues in the field of transportation [1-8]. At the same time, one of the most material-intensive, financial and energy-consuming operations in the road construction, is the production of building materials and its transportation to the place of road building. This fact determines the relevance of the development of new cheaper materials for road building [9-25].

Organizations involved in the road building widely use artificial materials made on the basis of man-made waste, for example, based on the blast furnace slag, as an alternative to natural materials [9-11].

Blast furnace slag is one of the wastes of ferrous metallurgy, which is formed in a liquid state during the smelting of pig iron and solidifies when it is cooled. Blast-furnace slag consists mainly of gangue iron ore. There are about 500 kg of blast-furnace slag per each 1 ton of cast iron, which needs to be processed. About 1.1 billion tons of pig iron are produced annually in the world, therefore, the annual global production of the blast furnace slag is about 500-550 million tons [2].

Recycling and further use of solid metallurgical slags, instead of expensive natural materials, reduces the cost of road building, significantly reduces the environmental burden in the regions due to elimination of slag dumps, allows to preserve mining and chemical raw materials, mineral materials [9-11]. All this confirms the need to solve the environmental problem of disposal of solid blast furnace slag accumulated in dumps.

The results of research in the field of processing the blast-furnace slag for use in construction are presented in a large number of scientific papers by both the authors of this article [9-11] and many other authors, [26-38].

A preliminary literature analysis of these articles showed that the most common method of recycling the blast-furnace slag is its granulation. Granulation is a rapid cooling of liquid hot slag in a water jet, leading to formation of a fine-grained (less than 10 mm) bulk

Figure 1 *The blast-furnace slag dump of ArcelorMittal Temirtau JSC on a satellite image*

multicomponent material - granulated blast-furnace slag.

Granulation of the blast-furnace slag is carried out for its further use as an active mineral additive in the production of cement and concrete. Blast-furnace slag is also used for the production of the calcium-containing ferroalloy, paving slabs, curbs, fertilizers, asphalt concrete pavements and heat-insulating materials. Despite this, the demand for blast-furnace slag in regions with ferrous metallurgy enterprises is, as a rule, much lower than the volume of production of this material.

Due to the limited demand for the blast-furnace slag in regions with metallurgical production, despite the processing of most of the material in the ways described above, a significant part of the slag is still sent to dumps that occupy huge areas and require disposal. For example, according to the data for 2022, more than 30 million tons of the blast-furnace slag have been accumulated in the dumps of ArcelorMittal Temirtau JSC (Figure 1).

The main method of recycling the solid blast-furnace slag from dumps is production of the crushed stone for road building. However, today the use of the blast-furnace slag for roads building is limited due to its high water absorption (6 - 8%) and insufficient frost resistance.

The main reason for these disadvantages is the high porosity of a significant part of crushed stone grains made based on the blast furnace slag (Figure 2). The moisture absorbed by the pores of the blast-furnace slag in summer increases in volume when it freezes in winter and destroys crushed stone grains, as well as pavement built on its basis, causing the formation of cracks, subsidence and ruts on the asphalt pavement. [39].

To solve this problem, the work [39] proposes a technology for processing the slag crushed stone, which includes the following steps:

1) mixing pre-moistened crushed stone with a liquid mixture containing cement, microsilica and crushed (to a powder state) blast-furnace slag;
2) filling the pores of the obtained material with a powdered filler of a similar composition;
3) removal of excess powdered filler from the surface of crushed stone grains;
4) moistening the slag crushed stone for better setting of the filler in the pores;
5) drying of the slag crushed stone with filled pores;
6) impregnation of the obtained material with a water-repellent composition.

Kunaev proposed an experimental production line for the practical implementation of this technology (Figure 3), [39]. Let us consider the principle of operation of this production line.

Mixer 1 performs the pre-mixing of the pre-moistened (for better adhesion) crushed stone with a liquid mixture containing cement, silica fume and crushed (to a powder state) blast-furnace slag [9]. Next, the slag crushed stone enters into the mixer 2, which fills pores with a dry mixture of a similar composition.

Figure 2 *External pores on the surfaces of slag crushed stone grains*

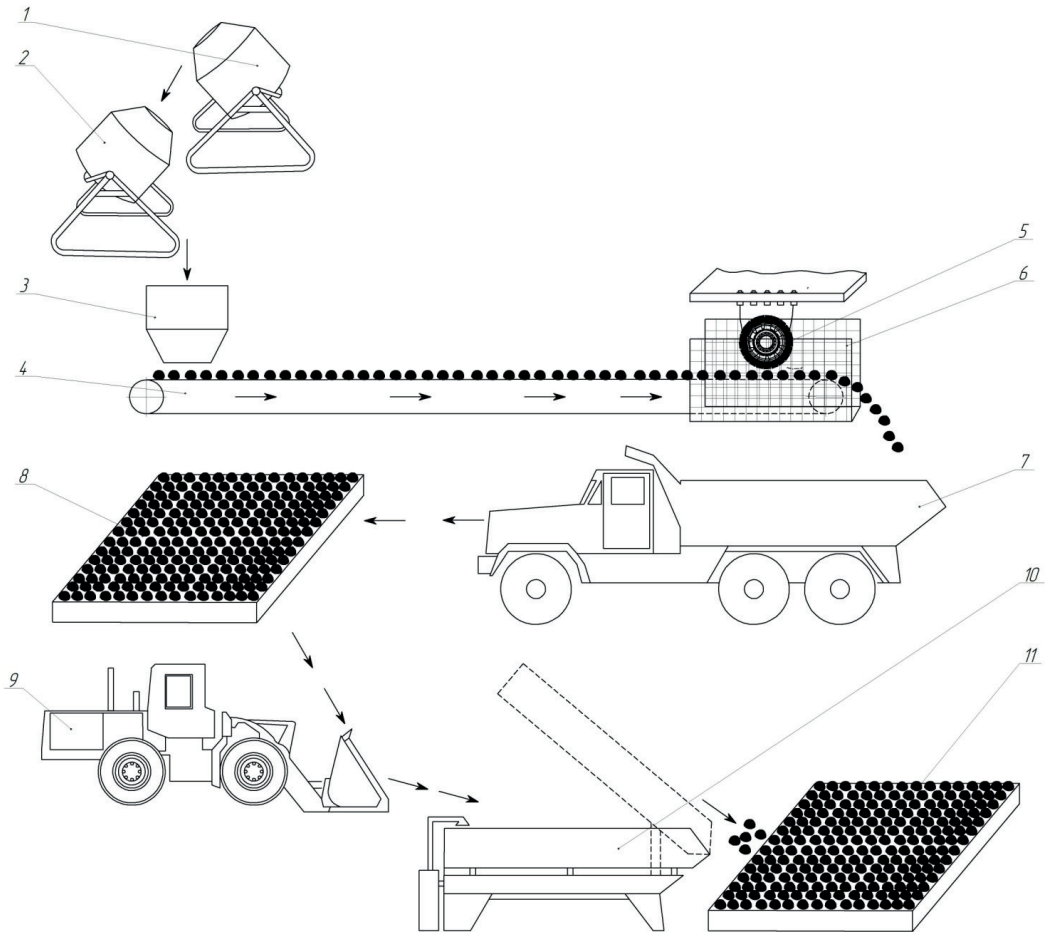

Figure 3 *Experimental technological line for hydrophobization of slag crushed stone: 1, 2 - mixers; 3 - dispenser; 4 - belt conveyor; 5 - rotating brush with synthetic bristles; 6 - metal gratings; 7 - dump truck, 8 section of moistening and pre-drying, 9 - single-bucket loader, 10 - bath for hydrophobization (impregnation with a water-repellent composition), 11 - finished product storage section*

After that, the crushed stone is directed through the dispenser 3 along the conveyor 4, to the rotating brush with synthetic bristles 5. The brush 5 during rotation ensures indentation of the powdered filler deep into the pore space and the removal of excess mixture from the surface of the crushed stone grains. Metal gratings 6, installed on both sides of the conveyor, prevent the crushed stone from spilling over the borders of the conveyor belt when in contact with the brush. The dump truck 7 transports the slag crushed stone with filled pores to the section of moistening and pre-drying 8, where the surface of the material is moistened for setting the powder mixture. The crushed stone is located at this site until the setting the powdery filler in its pores. Then, the single-bucket loader 9 loads the slag crushed stone into the impregnation bath for hydrophobization (impregnation with a water-repellent composition) 10. After impregnation for a predetermined time, the crushed stone is unloaded to the finished product storage section 11. For convenience, this technology of the slag crushed stone recycling is supposed to be used directly near the road under construction [39].

Prior to the delivery of the slag crushed stone to this technological line, the blast furnace slag must be removed from the dumps and crushed to the required fraction size. However, during the long-term (20 - 30 years) storage of slag in dumps, its elements are compressed, fastening together and forming a monolithic material, inconvenient for loading into dump trucks and crushing. This task is especially difficult in winter, when the blast-furnace slag in dumps becomes a frozen material. In conditions of a sharply continental climate, this period can be more than half of a calendar year. In order to avoid stopping the extraction of slag from dumps and further hydrophobization for the winter period, the preparation of this material for crushing into crushed stone and subsequent processing should include preliminary loosening [9]. Based on the foregoing, the purpose of this paper was formulated.

The purpose of research is to develop, manufacture and test equipment with interchangeable working tools for preparation of building materials based on industrial waste during the road infrastructure building, namely loosening frozen dump slag in the winter, as well as pressing powdered filler deep into the pore space of crushed stone grains and removing its excess from the surface of the processed material.

To achieve this purpose, the following tasks were solved:

- analysis of equipment constructions and methods for loosening the hard rocks and frozen soils;
- selection of materials and methods of research;
- development of a 3D model and drawings of a universal working body of a single-bucket excavator with interchangeable working tools;
- manufacturing and testing of a prototype of a universal working body of a single-bucket excavator.

2 Literature review

The first stage of the production of the slag crushed stone for road building is the extraction of raw materials (blast furnace slag) from dumps.

For loosening the blast-furnace slag during its extraction from dumps, it is recommended to use earth-moving machines designed to develop frozen and solid soils.

In order to develop the construction of equipment for loosening the frozen blast-furnace slag in dumps in winter, the existing equipment for loosening the frozen soils was analyzed.

A critical analysis of technologies and equipment for loosening frozen and solid soils, which can be used, among other things, in the loosening of frozen slag in dumps, showed that the most significant results in this area were achieved by authors of [9, 40-50]. The main types of machines used for loosening the frozen soils, discussed in works [40-50], are listed in Figure 4.

Let us consider the main methods and equipment for loosening the frozen soils, which are described in these works and, accordingly, hypothetically can be used for loosening the blast-furnace slag in dumps in winter.

Explosive (slit or hole) method is used in preparation of the frozen soils for further excavation. This method is mainly used in uninhabited areas. It is acceptable in inhabited areas, as well, however, with use of shelters and explosion localizers. Slots are cut at a distance of 0.9-1.2 m from each other by the trencher machines or slot cutters. Next, the slots are loaded through one with concentrated or elongated charges. After that, the slots are filled with sand. When loosening the frozen ground by this method, the site is preliminarily divided into several grips. At the first grip, holes are sequentially drilled, charged and blown up. At the second grip, the work is not carried out according to safety conditions, while at the third grip, the ground excavation is carried out directly.

The method of mechanical loosening of the frozen soils is advisable to apply at a freezing depth of 0.4 to 1.5 m and the excavation of small-sized pits and trenches. This method involves crushing or chipping the frozen layer by static or dynamic action of a special working body mounted on an excavator, tractor or other base machine.

Dynamic impact is provided by shock, vibration or their combined action using a ball or wedge hammer, diesel hammers, wedge tractor rippers and other equipment. It should be noted that the costs of mining by dynamic methods using diesel hammers and hydraulic hammers are 2 to 3 times higher than the costs of mining with rippers, performing mechanical loosening [48-50].

Analysis of the considered methods of loosening the frozen soils showed that the most of them fully meet the requirements for equipment for loosening the frozen dump blast-furnace slag, the replaceable working

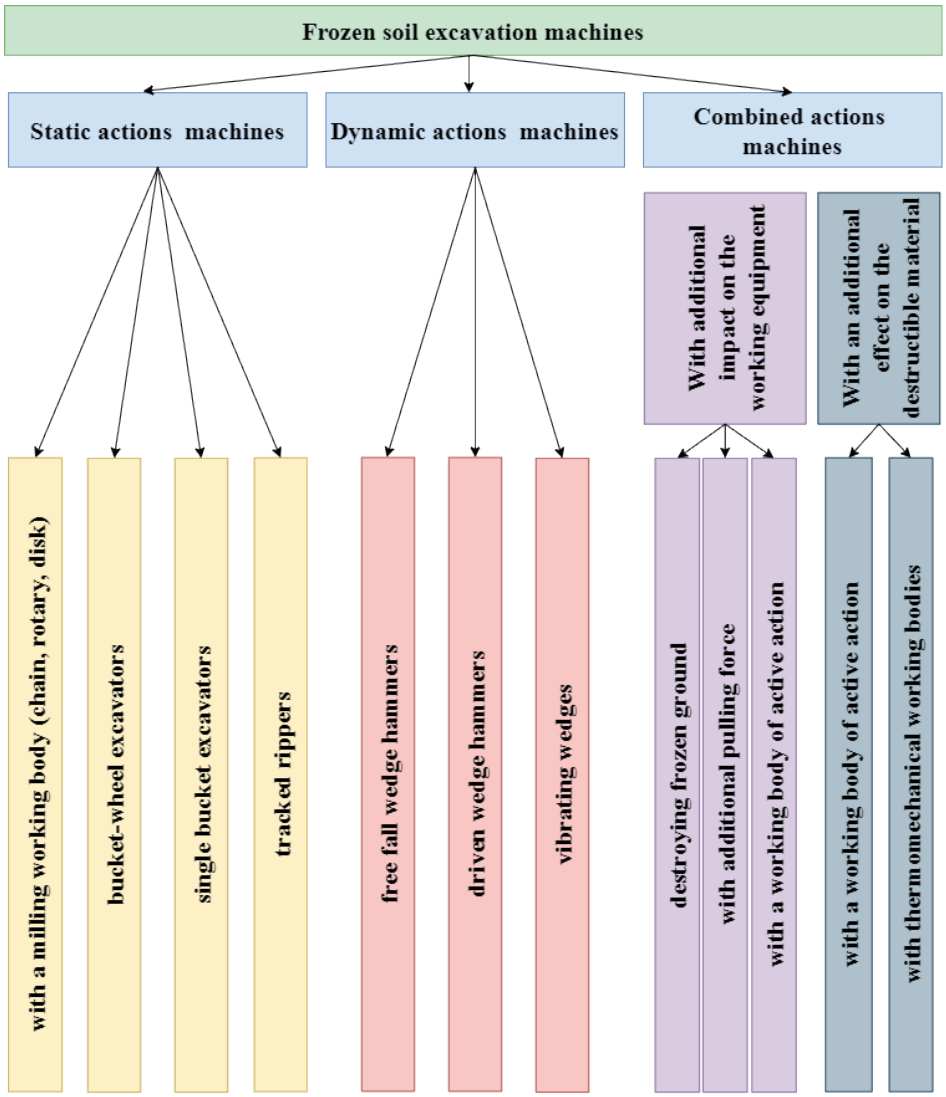

Figure 4 *The main types of machines for loosening the frozen soils*

equipment of a single-bucket excavator, proposed by Letopolsky et al. [50]. Authors proposed to use an excavator bucket combined with a hydraulic hammer as a replaceable working equipment.

In order to optimize the workflow and reduce the time spent on changing work equipment, an improved design of the working body of a single-bucket excavator has been proposed. The design solution combines a bucket and two hydraulic hammers located on the front side of the bucket.

At the first stage, the excavator works with hydraulic hammers, loosening the frozen and hard soil and at the second stage, it works with a bucket, collecting loosened soil and loading it into a dump truck body.

In the course of the theoretical studies, the authors of [50] calculated dependencies that allow to determine the parameters of the installed hydraulic hammers. The proposed design solution increases the performance and operational reliability of the working equipment of the excavator in the development of frozen and solid grounds. Developing their experience, and of other specialists in the field of soil mechanics, as well as based on our own practical experience of the research team, confirmed by analytical studies, our team of authors propose to use cheaper cutterhead ripper for loosening the frozen blast-furnace slag.

3 Materials and methods

To achieve the purpose and objectives of the research, both theoretical (literature review, 3D computer modeling, development of technical specifications for designing of experimental equipment and a flow sheet of the developed processes, approximation of experimental dependencies) and experimental (manufacturing and testing of an experimental construction of the cutterhead ripper, production and testing of an experimental sample of crushed stone based on the blast-furnace slag using the proposed equipment) methods were used.

According to the results of a literature review, the working group of the Karaganda Technical University

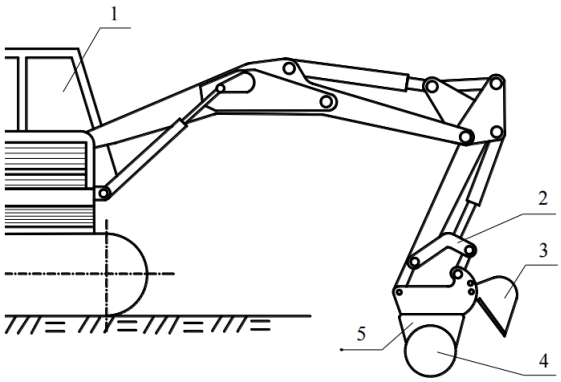

Figure 5 *General view of the cutterhead ripper: 1 - excavator, 2 - bracket, 3 - bucket 3, 4 - cutterheads, 5 - body*

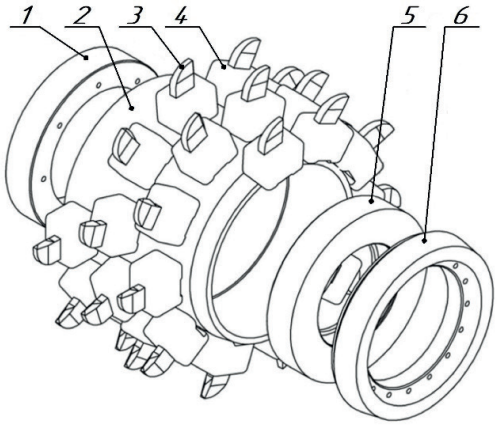

Figure 6 *The construction of the proposed cutterhead (in a disassembled state): 1 - bush, 2 - body, 3 - fist, 4 - cutterhead, 5 - bush, 6 - sidewall*

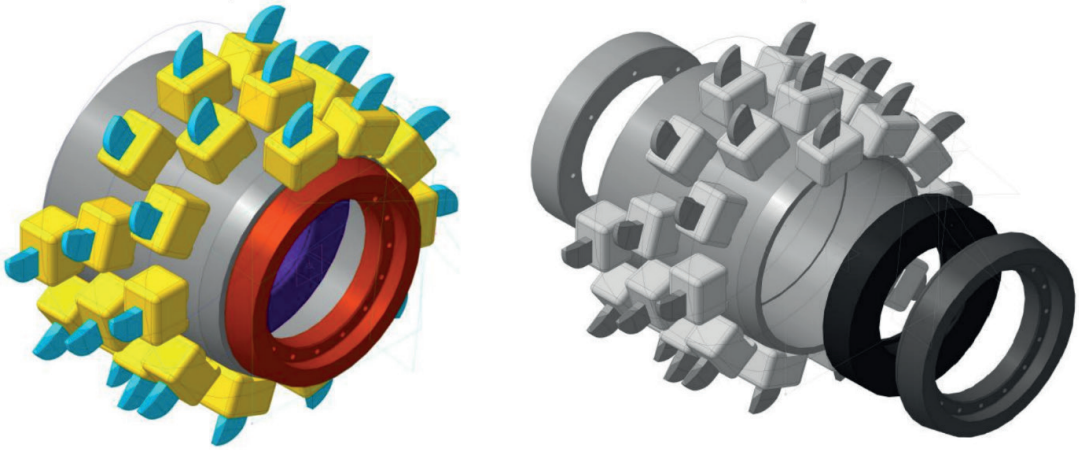

a) *b)*

Figure 7 *The 3D model of the cutterhead: a - cutterhead in the assembled state, b - cutterhead in the disassembled state*

under the leadership of professor Kadyrov (one of the authors of this article) decided to develop the construction of a universal cutterhead ripper with replaceable working tools. The cutters (for loosening frozen grounds) and the synthetic brushes (for pressing powdered filler deep into the pore space of crushed stone grains and removing its excess from the surface of the processed material) were proposed to use as working tools. The proposed construction of the cutterhead ripper is mounted on the basis of a single-bucket excavator and allows to crush and excavate the frozen grounds and rocks of high strength.

The cutterhead ripper is a replaceable working body, which is pivotally mounted on the handle of the base excavator 1 and consists of two coaxially located ground-destroying cutterheads 4, a body 5, a bracket 2, a bucket 3 and a drive (Figure 5). Holders with replaceable cutting elements (cutters) are placed on the surface of the cutterheads along a helical line.

To develop a prototype of a universal cutterhead, 3D models of all parts of this equipment and a general 3D model were preliminarily built. The construction of the cutterhead is shown as a 3D model in Figures 6 and 7.

Structural parameters of the bracket satisfy the condition of interchangeability of the working equipment. A bucket (attached to the bracket) serves to extract the solid blast-furnace slag from the dump. The bucket has two positions relative to the bracket: neutral and working. The transmission of torque to the cutterheads is carried out through a planetary gearbox and a bevel gear from an axial-piston hydraulic motor. The power source of the hydraulic motor is the oil station of the base machine (excavator).

The work of an excavator with a universal cutterhead ripper provides for the layer-by-layer loosening of an array of the dump blast-furnace slag with its further excavation from the dump with a bucket.

Introduction of the working body into the array and its translational movement along the loosening strip located on the slag dump is carried out due to the pressure force of the hydraulic cylinders of the boom and the handle. The main technical characteristics of the universal cutterhead of the proposed construction are presented in Table 1.

Table 1 *Technical parameters of the universal cutterhead of the proposed construction*

Parameter	Value
Loosening depth per pass (m)	0.2
Loosening strip width (m)	1.1
Performance (m^3/hour)	7.0
Hydraulic motor power (kw)	36.9
Torque of the working body (N·m)	6000
Universal cutterhead diameter (by cutters) (m)	0.68
Overall dimensions	
Width (m)	1.1
Height (m)	1.2
Weight (kg)	1000

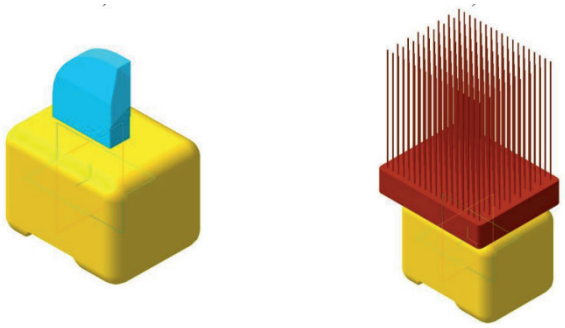

a) *b)*

Figure 8 *Replaceable working tools of a universal cutterhead assembled with a fist: a - cutter, b - brush*

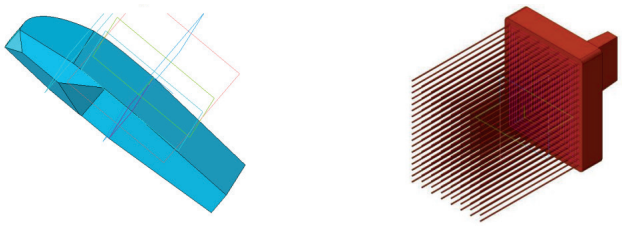

a) *b)*

Figure 9 *Replaceable working tools of a universal cutterhead: a - cutter, b - brush*

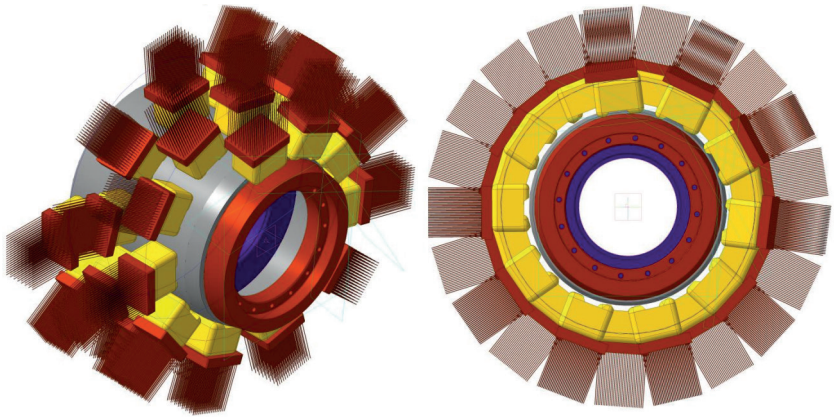

a) *b)*

Figure 10 *The 3D model of the cutterhead with the installed synthetic brushes: a - isometry, b - right side view*

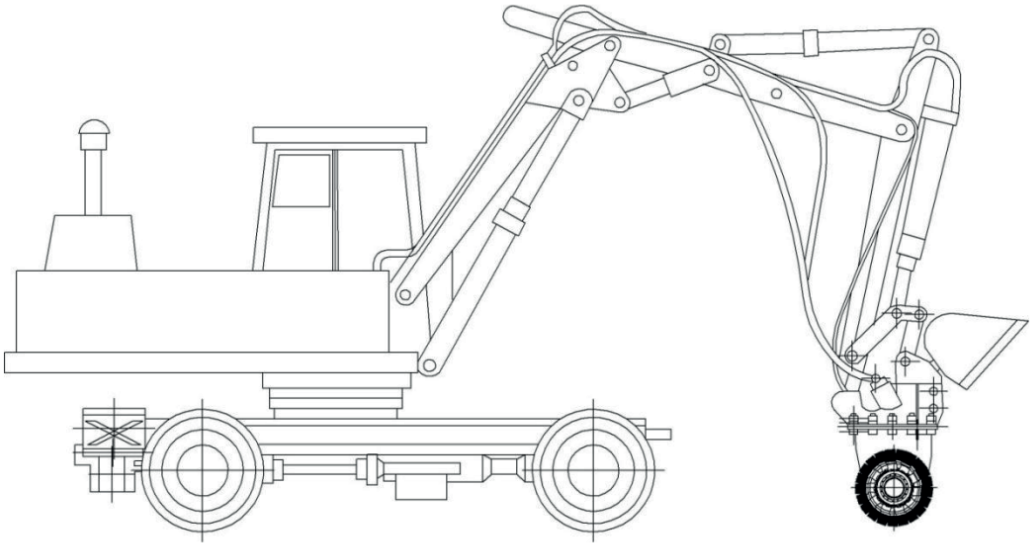

Figure 11 *Cutterhead ripper with replaceable tools - brushes with synthetic bristles*

The peculiarity of the proposed equipment is the presence of a bucket for removing the loosened blast-furnace slag, which allows loosening and moving the material without the involvement of additional machines and ensures the energy efficiency of this equipment [51].

Taking into account the seasonality of work on loosening the frozen ground and blast-furnace slag in dumps, in order to avoid downtime of the cutterhead ripper in the summer, the authors of this paper propose to use it as part of an experimental technological line for hydrophobization of the slag crushed stone, namely, for compacting the powdered filler in the pores of crushed stone grains and removing its excess from the material surface. To solve this problem, the replaceable working tools of a universal cutterhead ripper were developed. These replaceable working tools are the brushes with synthetic bristles (Figures 8, 9). Figure 8 shows two versions of the replaceable working tools of the cutterhead ripper assembly with a fist, for fixing in which a Morse cone connection is used (the cone angle is 3°).

This connection type is chosen as the most quickly detachable. Welding is used to attach the fists to the cutter body. Figure 9 shows the same working tools (cutter and brush), but separated from the fist. A 3D model of a universal cutterhead with installed brushes is shown in Figure 10.

4 Results and discussions

Based on the constructed 3D models, assembly drawings of a universal cutterhead installed on a basic machine (a single-bucket excavator) were developed. Figure 11 shows a general view of a single-bucket excavator with a universal cutterhead with synthetic brushes used as working tools.

In this case, a universal cutterhead with brushes with synthetic bristles, installed as a working body of a single-bucket excavator, can be used as a part of a mobile technological line for processing the crushed slag stone in road conditions in summer, replacing a rotating brush. This completely eliminates the downtime of the proposed equipment in the summer and saves money for the purchase of a separate rotating brush with a drive.

The technological line for processing the slag crushed stone, containing a single-bucket excavator with a universal cutterhead equipped with brushes (highlighted in green oval), is shown in Figure 12. Otherwise, this technological line operates similarly to the line shown in Figure 3.

Based on the developed drawings, a prototype of a universal cutterhead was made. The manufactured prototype of a universal cutterhead, mounted on a base machine (single-bucket excavator), shown in Figure 13, was tested for suitability for loosening (destruction) of various materials. The results of tests are presented in the diagram in Figure 14.

The second experiment was aimed to evaluate the applicability of a universal cutterhead, equipped with replaceable working tools (brushes), as a replacement for a separate rotating brush when used as a part of an experimental technological line to remove excess powdered filler from the surface of the slag crushed stone grains, as well as to determine the optimal time of processing the slag crushed stone by universal cutterhead, equipped with synthetic brushes.

The main task of this experiment was to assess the effect of the processing time of the slag crushed stone with a universal cutterhead t_{proc} equipped with synthetic brushes on the quality of filling the pores of experimental samples of the crushed stone. The quality of filling the pores was evaluated by reducing the water absorption W_{abs} of the slag crushed stone samples after processing

with a universal cutterhead and impregnating with a hydrophobizer (water repellent). Thus, the objective function looks like:

$$W_{abs} = f(t_{proc}) \rightarrow min. \quad (1)$$

For the experiment, 10 experimental samples of the hydrophobized slag crushed stone were prepared. Each of these samples weighed from 2000 to 2100 g. During the experiments, the developed construction of a universal cutterhead was used to fill the pores of the slag crushed stone with powdered filler and remove its excess from the surface of the material. And the processing time was varied from 30 seconds to 300 seconds in increments of 30 seconds (Table 2).

Each sample was tested for water absorption. The water absorption was determined by comparing the mass of samples of the slag crushed stone in water-saturated condition and after drying. Samples of crushed slag stone were placed in the reservoir with water so that the water level in the reservoir was at least 20 mm higher than the top of the slag crushed stone samples. The samples were kept in the reservoirs with water for 48 hours, after which each sample was taken out of the reservoir and weighed on a scale with an error of no more than 1 g. Water absorption was calculated by the formula:

$$W_{abs} = \frac{m_1 - m_2}{m} * 100\,\%, \quad (2)$$

where:

m_1 - mass of a sample in the water-saturated condition, g;

m - mass of a sample in the dry condition, g.

The results are presented in Table 2.

The Microsoft Excel was used to process the experimental data. The graphic dependence presented in Figure 15 shows the effect of the time of processing

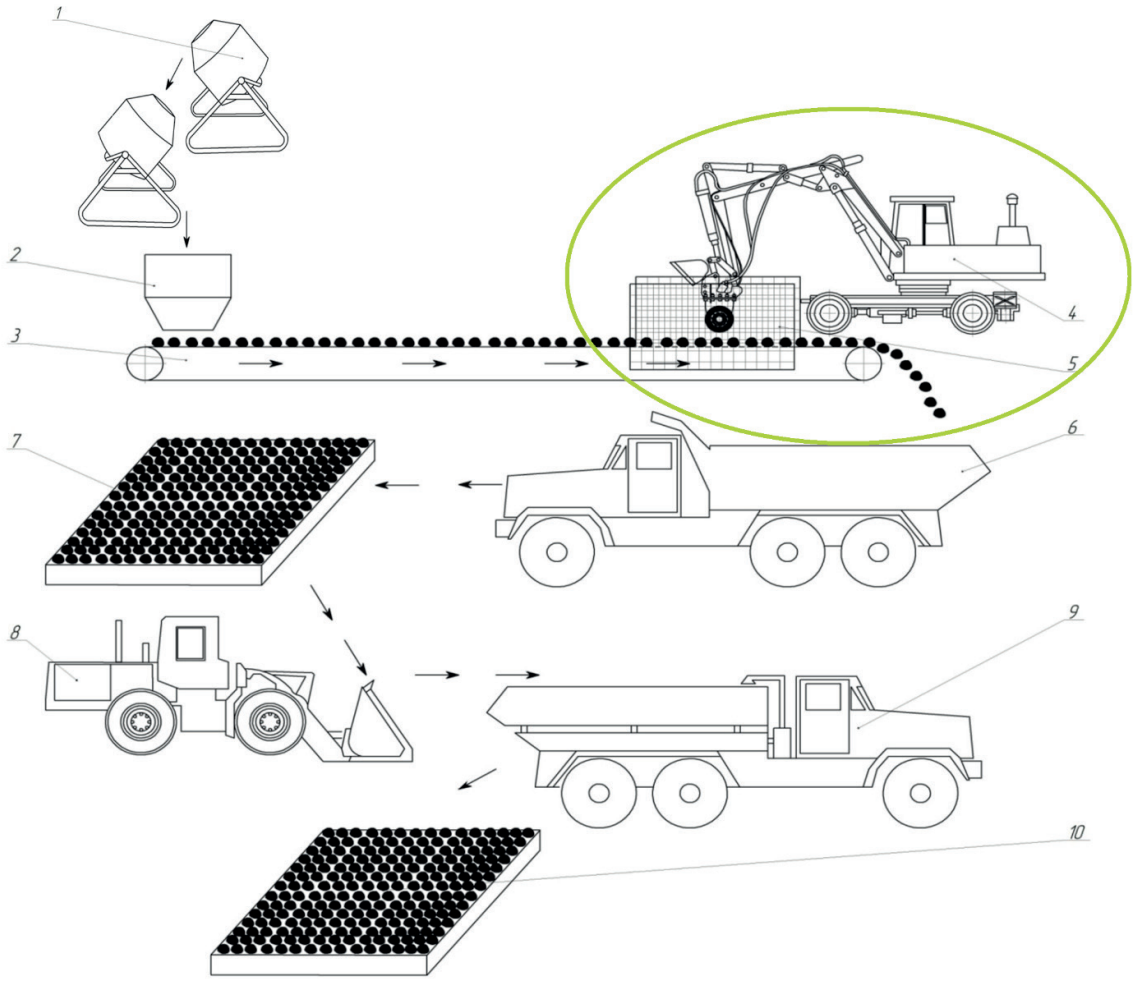

Figure 12 *Experimental technological line for processing the slag crushed stone after modernization: 1 - a complex of 2 mixers; 2 - dispenser; 3 - belt conveyor; 4 - single-bucket excavator with a universal cutterhead, equipped with replaceable brushes with synthetic bristles; 5 - metal gratings; 6 - dump truck, 7 - section for moistening and pre-drying of crushed stone, 8 - single-bucket loader, 9 - mobile equipment for hydrophobization of the slag crushed stone, 10 - section for unloading and storing finished products*

Figure 13 *A prototype of a universal cutterhead with cutters installed on the base machine (single-bucket excavator)*

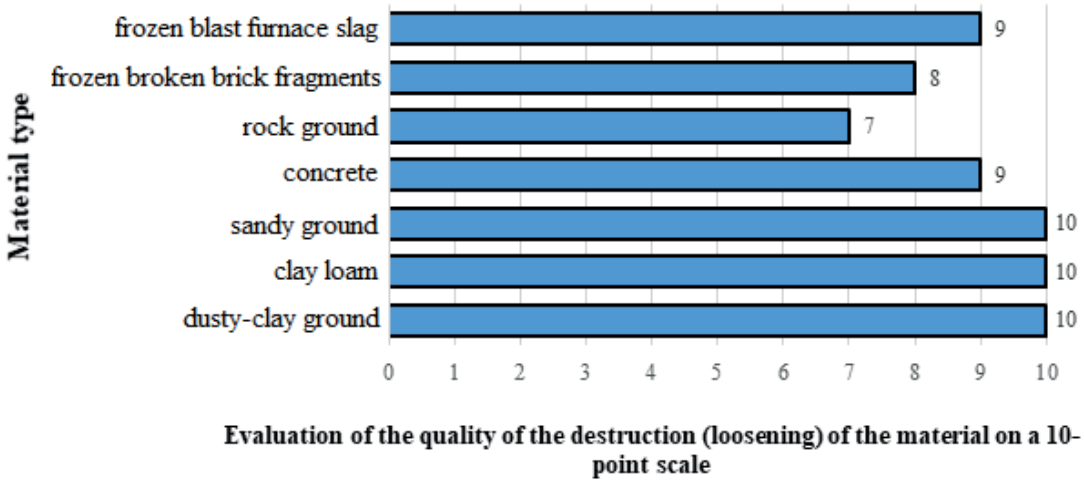

Figure 14 *The results of tests for loosening different materials with a universal cutterhead mounted on a single-bucket excavator*

Table 2 *Calculation of water absorption of the slag crushed stone*

Sample number	Time of processing with universal cutterhead t_{proc} (s)	Mass of a sample in the dry condition m (g)	Mass of a sample in the state water-saturated condition m_1(g)	Water absorption W_{abs} (%)
1	0	2030	2146	5.71
2	30	2085	2176	4.35
3	60	2013	2098	4.20
4	90	2024	2094	3.45
5	120	2006	2053	2.34
6	150	2048	2091	2.09
7	180	2031	2063	1.56
8	210	2044	2071	1.34
9	240	2056	2079	1.11
10	270	2037	2068	1.50

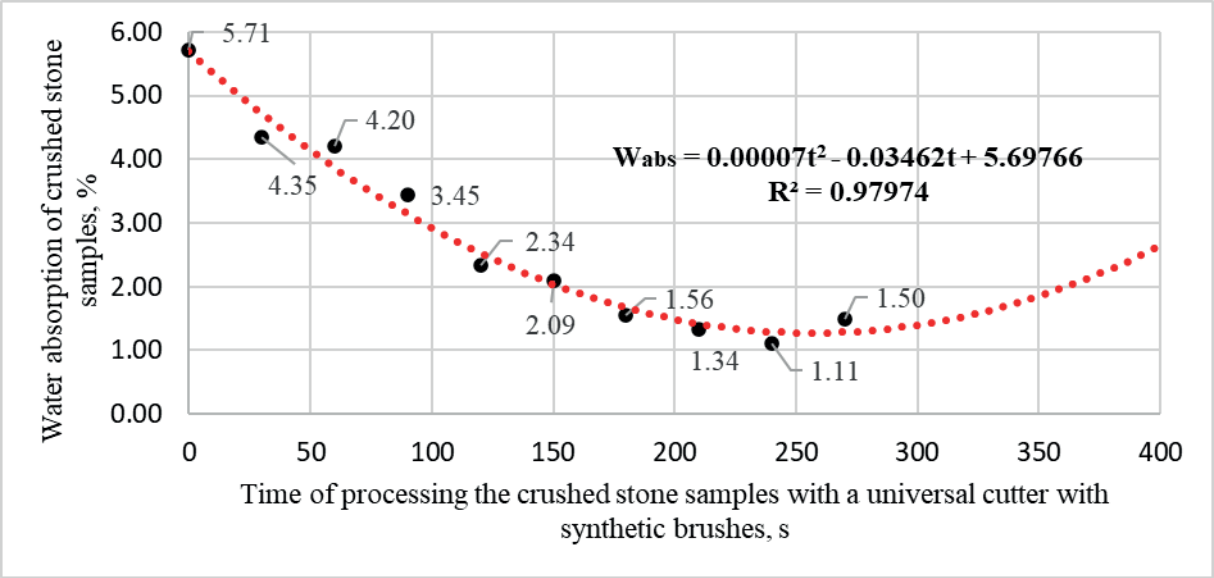

Figure 15 *Influence of the processing time of the slag crushed stone with a universal cutter on its water absorption*

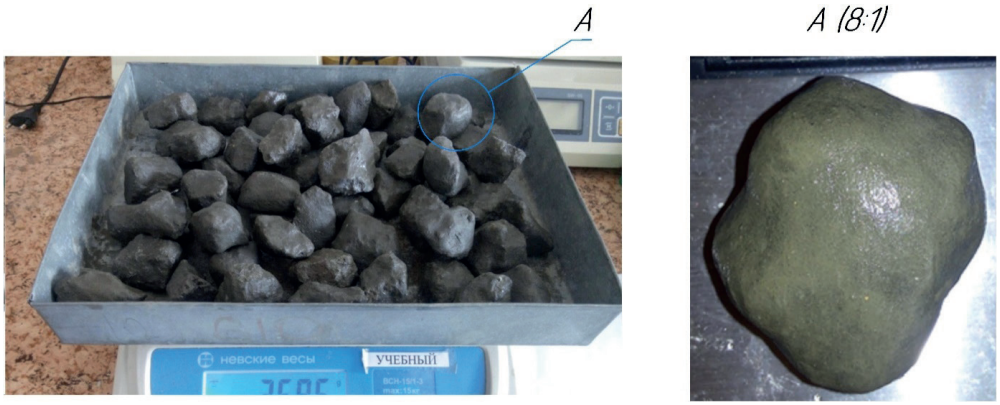

Figure 16 *The samples of the slag crushed stone after processing on the experimental technological line using a single-bucket excavator with a universal cutterhead equipped with replaceable brushes*

the slag crushed stone with a universal cutterhead on the water absorption of the sample.

As readers can see, the water absorption decreases with an increase in the time of processing the crushed stone with a universal cutterhead up to 240 seconds (W_{abs} → min), after which it begins to increase. This is explained by the fact that with an increase in the processing time of the slag crushed stone to 5 minutes or more, a part of the powdered filler is removed from the pore space. This leads to worse filling of the pores and, accordingly, the absorption of more moisture. The Microsoft Excel allowed to obtain a polynomial trend line describing the relationship between the water absorption W_{abs} and the processing time of crushed stone t_{proc}. The obtained polynomial trend line is approximated by the following equation:

$$W_{abs} = f(t_{proc}) = 0.00007\ t_{proc}^{\ 2} - 0.03462\ t_{proc} + 5.69766. \quad (3)$$

This equation has a high reliability coefficient (R^2 = 0.97974). Using the Microsoft Excel functionality, a prediction trend line for graphic dependence in Figure 15 was built. This trend line allows to calculate how the water absorption of the slag crushed stone will change with a further increase in the processing time of this material with a universal cutterhead ripper. It is possible to track (Figure 15) the predicted values of water absorption with a change in the time of processing this material with a universal cutterhead along the trend line in the range t_{proc} = 270-400 s.

Figure 15 shows that with a further increase in the time of processing the slag crushed stone with a universal cutterhead for more than 240 s, the water absorption of the material increases and, for example, at t_{proc} = 400 s it is about 2.7 %.

Based on the foregoing, it can be concluded that the optimal time for processing the slag crushed stone with a universal cutterhead with synthetic brushes is $t_{proc\ opt}$ = 240 s.

As readers can see in Figure 16, including with a significant increase, on the obtained samples of the hydrophobized slag crushed stone (at t_{proc} = 240 s), there are no excess powdered filler and all the existing pores are filled.

Thus, the use of a universal cutterhead equipped with brushes as a part of a mobile technological line for processing the slag crushed stone ensures complete penetration of powdered filler deep into the pore space and removal of excess filler from the surface of crushed stone grains.

5 Conclusions

1. The authors presented the literature review of methods for processing the blast-furnace slag. Based on the literature review, it was concluded that the most appropriate way to process the waste blast-furnace slag is to obtain the slag crushed stone on its basis. The main disadvantages of the resulting material (insufficient water resistance, frost resistance, low strength) are determined.
2. To eliminate these disadvantages, the authors proposed and substantiated the composition of the technological line for filling the pores of the slag crushed stone and impregnating it with a hydrophobizator (water-repellent composition).
3. A critical analysis of machines and equipment that can be used to loosen the frozen blast-furnace slag in dumps in winter showed that cutter equipment is the most suitable. Based on the results of this analysis, the working group of the Karaganda Technical University designed and manufactured the replaceable working equipment of a single-bucket excavator with replaceable working tools (cutters and brushes) for loosening the frozen blast furnace slag in dumps and removing excess powdered pore filler from the surface of the material during its further processing on the proposed technological line.
4. The advantage of using the replaceable working tools of mounted working equipment (in particular, cutters for loosening the blast-furnace slag in dumps and brushes with synthetic bristles) is to save money on purchase of the specialized equipment and prevent downtime of existing machines.
5. Tests of the manufactured equipment showed its high efficiency in loosening the frozen blast-furnace slag and other materials, as well as at use as part of a technological line for processing the slag crushed stone.
6. Further research in the field of mechanization of the obtaining materials for building of the road infrastructure facilities based on metallurgical waste will be aimed at developing an integrated technology for enrichment in strength of the crushed stone from the blast-furnace slag.

Grants and funding

The authors received no financial support for the research, authorship and/or publication of this article.

Conflicts of interest

The authors declare that they have no known competing financial interests or personal relationships that could have appeared to influence the work reported in this paper.

References

[1] BREZINA, I., MACHEL, O., ZAVREL, T. Temperature correction of deflections and backcalculated elasticity moduli determined from falling weight deflectometer measurements on asphalt pavements. *Communications - Scientific Letters of the University of Zilina* [online]. 2022, **24**(1), p. D1-D8. ISSN 1335-4205, eISSN 2585-7878. Available from: https://doi.org/10.26552/COM.C.2022.1.D1-D8

[2] MORAVCIK, M. Dynamic response of a road bridge subjected to passing a heavy vehicle over a standard irregularity - numerical modelling and experimental testing. *Communications - Scientific Letters of the University of Zilina* [online]. 2022, **24**(1), p. D37-D45. ISSN 1335-4205, eISSN 2585-7878. Available from: https://doi.org/10.26552/COM.C.2022.1.D37-D45

[3] SYSYN, M., KOVALCHUK, V., GERBER, U., NABOCHENKO, O., PARNETA, B. Laboratory evaluation of railway ballast consolidation by the non-destructive testing. *Communications - Scientific Letters of the University of Zilina* [online]. 2019, **21**(2), p. 81-88. ISSN 1335-4205, eISSN 2585-7878. Available from: https://doi.org/10.26552/com.C.2019.2.81-88

[4] KADYROV, A., GANYUKOV, A., IMANOV, M., BALABEKOVA, K. Calculation of constructive elements of mobile overpass. *Current Science* [online]. 2019, **116**(9), p. 1544-1550. ISSN 0011-3891. Available from: https://doi.org/10.18520/cs/v116/i9/1544-1550

[5] GANYUKOV, A., KADYROV, A., BALABEKOVA, K., KURMASHEVA, B. Tests and calculations of structural elements of temporary bridges / Badania i obliczenia elementów konstrukcyjnych mostów tymczasowych (in Polish). *Roads and Bridges / Drogi i Mosty* [online]. 2018, **17**(3), p. 215-226. ISSN 1643-1618. Available from: https://doi.org/10.7409/rabdim.018.014

[6] ABDULLAYEV, S. S., BONDAR, I. S., BAKYT, G. B., ASHIRBAYEV, G. K., BUDIUKIN, A. M., BAUBEKOV, Y. Y. Interaction of frame structures with rolling stock. *News of the National Academy of Sciences of the Republic of Kazakhstan, Series of Geology and Technical Sciences* [online]. 2021, **1**(445), p. 22-28. ISSN 2224-5278. Available from: https://doi.org/10.32014/2021.2518-170X.3

[7] KADYROV, A., GANYUKOV, A., BALABEKOVA, K. Development of constructions of mobile road overpasses. *MATEC Web of Conferences* [online]. 2017, **108**, 16002. eISSN 2261-236X. Available from: https://doi.org/10.1051/matecconf/201710816002

[8] KADYROV, A., KUNAEV, V., GEORGIADI, I., KHAIBULLIN, R. Advanced methods for solving the problems of road construction in central Kazakhstan. *Tehnicki Vjesnik* [online]. 2019, **26**(4), p. 1159-1163. ISSN 1330-3651. Available from: https://doi.org/10.17559/TV-20170225144013

[9] BIELIATYNSKYI, A., YANG, S., PERSHAKOV, V., SHAO, M., TA, M. Features of the hot recycling method used to repair asphalt concrete pavements. *Materials Science-Poland* [online]. 2022, **40**(2), p. 181-195. eISSN 2083-134X. Available from: https://doi.org/10.2478/msp-2022-0021

[10] KADYROV, A. S., KUNAEV, V. A., GEORGIADI, I. V. Prospects for processing of ferrous metallurgical waste based on ArcelorMittal Temirtau experience. *Metallurgist* [online]. 2018, **62**(1-2), p. 22-28. ISSN 0026-0894. Available from: https://doi.org/10.1007/s11015-018-0620-3

[11] KADYROV, A. S., KUNAEV, V. A., GEORGIADI, I. V. Ferrous metallurgy waste and waste technical fluids for obtaining the material of road bases. *Ecology and Industry of Russia* [online]. 2017, **21**(12), p. 44-48. ISSN 1816-0395. Available from: https://doi.org/10.18412/1816-0395-2017-12-44-48

[12] KOSTENKO, S. A., PISKUNOV, A. A., GANIN, N. A., EMELIANOVA, G. A. Energy-Saving Thermal Stabilization System and Assessment of Temperature Loadings of a Bridge Deck Pavement. *Communications - Scientific letters of the University of Zilina* [online]. 2022, **24**(3), p. D141-149. ISSN 1335-4205, eISSN 2585-7878. Available from: https://doi.org/10.26552/com.C.2022.3.D141-D149

[13] CHEN, W., LI, Y., CHEN, S., ZHENG, C. Properties and economics evaluation of utilization of oil shale waste as an alternative environmentally-friendly building materials in pavement engineering. *Construction and Building Materials* [online]. 2020, **259**, 119698. ISSN 0950-0618. Available from: https://doi.org/10.1016/j.conbuildmat.2020.119698

[14] ALWETAISHI, M., KAMEL, M., AL-BUSTAMI, N. Sustainable applications of asphalt mixes with reclaimed asphalt pavement (RAP) materials: innovative and new building brick. *International Journal of Low-Carbon Technologies* [online]. 2019, **14**(3), p. 364-374. ISSN 1748-1317. Available from: https://doi.org/10.1093/ijlct/ctz023

[15] CONG, L., YANG, F., GUO, G., REN, M., SHI, J., TAN, L. The use of polyurethane for asphalt pavement engineering applications: a state-of-the-art review. *Construction and Building Materials* [online]. 2019, **225**, p. 1012-1025. ISSN 0950-0618. Available from: https://doi.org/10.1016/j.conbuildmat.2019.07.213

[16] ZHU, J., MA, T., FAN, J., FANG, Z., CHEN, T., ZHOU, Y. Experimental study of high modulus asphalt mixture containing reclaimed asphalt pavement. *Journal of Cleaner Production* [online]. 2020, **263**, 121447. ISSN 0959-6526. Available from: https://doi.org/10.1016/j.jclepro.2020.121447

[17] WU, S., MONTALVO, L. Repurposing waste plastics into cleaner asphalt pavement materials: a critical literature review. *Journal of Cleaner Production* [online]. 2021, **280**, 124355. ISSN 0959-6526. Available from: https://doi.org/10.1016/j.jclepro.2020.124355

[18] BRESSI, S., FIORENTINI, N., HUANG, J., LOSA, M. Crumb rubber modifier in road asphalt pavements: state of the art and statistics. *Coatings* [online]. 2019, 9(6), **384**. ISSN 2079-6412. Available from: https://doi.org/10.3390/COATINGS9060384

[19] SORMUNEN, P., KARKI, T. Recycled construction and demolition waste as a possible source of materials for composite manufacturing. *Journal of Building Engineering* [online]. 2019, **24**, 100742. ISSN 2352-7102. https://doi.org/10.1016/j.jobe.2019.100742

[20] CHEN, S., LIN, W., LIN, K., HUANG, P. A study on the mixed properties of green controlled low strength cementitious. *Materials Science-Poland* [online]. 2021, **39**(1), p. 59-74. eISSN 2083-134X. Available from: https://doi.org/10.2478/msp-2021-0004

[21] MAGBOOL, H., ZEYAD, A. The effect of varied types of steel fibers on the performance of self-compacting concrete modified with volcanic pumice powder. *Materials Science-Poland* [online]. 2021, **39**(2), p. 172-187. eISSN 2083-134X. Available from: https://doi.org/10.2478/msp-2021-0016

[22] HUNG, C., LIN, W., YEIH, W., CHANG, J. Delayed setting time for alkali-activated slag composites using activator containing SiO2 and Na2O. *Materials Science-Poland* [online]. 2021, **39**(4), p. 570-579. eISSN 2083-134X. Available from: https://doi.org/10.2478/msp-2021-0045

[23] LI, W., HUANG, X., ZHAO, J., HUANG, Y., SHUMUYE, E., YANG, X. Effect of sea sand and recycled aggregate replacement on fly ash/slag-based geopolymer concrete. *Materials Science-Poland* [online]. 2021, **39**(4), p. 580-598. eISSN 2083-134X. Available from: https://doi.org/10.2478/msp-2021-0049

[24] WARIS, M., US SAHAR, U., AKMAL, U., KHURRAM, N., ASLAM, F., FATHI, D. Coupled effect of waste tire rubber and steel fibers on the mechanical properties of concrete. *Materials Science-Poland* [online]. 2022, **40**(1), p. 49-59. eISSN 2083-134X. Available from: https://doi.org/10.2478/msp-2022-0009

[25] TCHEKWAGEP, J., ZHAO, P., WANG, S., HUANG, S., CHENG, X. The impact of changes in pore structure on the compressive strength of sulphoaluminate cement concrete at high temperature. *Materials Science-Poland* [online]. 2021, **39**(1), p. 75-85. eISSN 2083-134X. Available from: https://doi.org/10.2478/msp-2021-0006

[26] VAISMAN, Y. I., PUGIN, K. G., RUDAKOVA, L. V., GLUSHANKOVA, I. S., TYURYUKHANOV, K. Y. Production of environmentally safe building materials on the basis of the waste foundry sand. *Theoretical and Applied Ecology* [online]. 2018, **3**, p. 109-115. ISSN 1995-4301. Available from: https://doi.org/10.25750/1995-4301-2018-3-109-115

[27] ROMANOVA, O. A., SIROTIN, D. V. Environmental and economic efficiency of recycling industrial waste in the Urals. *Economy of Region* [online]. 2021, **17**(1), p. 59-71. ISSN 2072-6414. Available from: https://doi.org/10.17059/EKON.REG.2021-1-5

[28] AHN, B., LEE, S., PARK, C. Physical and mechanical properties of rural-road pavement concrete in South Korea containing air-cooled blast-furnace slag aggregates. *Applied Sciences (Switzerland)* [online]. 2021, **11**(12), 5645. ISSN 2076-3417. Available from: https://doi.org/10.3390/app11125645

[29] AMULYA, S., RAVI SHANKAR, A. U. Replacement of conventional base course with stabilized lateritic soil using ground granulated blast furnace slag and alkali solution in the flexible pavement construction. *Indian Geotechnical Journal* [online]. 2020, **50**(2), p. 276-288. ISSN 0971-9555. Available from: https://doi:10.1007/s40098-020-00426-2

[30] LOPEZ-DIAZ, A., OCHOA-DIAZ, R., GRIMALDO-LEON, G. E. Use of BOF slag and blast furnace dust in asphalt concrete: An alternative for the construction of pavements. *DYNA (Colombia)* [online]. 2018, **85**(206), p. 24-30. ISSN 0012-7353. Available from: https://doi:10.15446/dyna.v85n206.70404

[31] GEL'MANOVA, Z. S., FILATOV, A. V. Projects for making efficient use of factory wastes to reduce the load on the environment. *Metallurgist* [online]. 2016, **59**(9-10), p. 747-751. ISSN 0026-0894. Available from: https://doi:10.1007/s11015-016-0169-y

[32] HASAN, U., WHYTE, A., AL JASSMI, H. Life cycle assessment of roadworks in united arab emirates: Recycled construction waste, reclaimed asphalt pavement, warm-mix asphalt and blast furnace slag use against traditional approach. *Journal of Cleaner Production* [online]. 2020, **257**, 120531. ISSN 0959-6526. Available from: https://doi:10.1016/j.jclepro.2020.120531

[33] PASETTO, M., BALIELLO, A., GIACOMELLO, G., PASQUINI, E. Sustainable solutions for road pavements: A multi-scale characterization of warm mix asphalts containing steel slags. *Journal of Cleaner Production* [online]. 2017, **166**, p. 835-843. ISSN 0959-6526. Available from: https://doi:10.1016/j.jclepro.2017.07.212

[34] PHUMMIPHAN, I., HORPIBULSUK, S., RACHAN, R., ARULRAJAH, A., SHEN, S., CHINDAPRASIRT, P. High calcium fly ash geopolymer stabilized lateritic soil and granulated blast furnace slag blends as a pavement base material. *Journal of Hazardous Materials* [online]. 2018, **341**, p. 257-267. ISSN 0304-3894. Available from: https://doi:10.1016/j.jhazmat.2017.07.067

[35] GURUPRASAD, H. C., SRIDHAR, R., RAVI, K. R. Effect of using ground granulated blast furnace slag in rigid pavement overlays. *Materials Science Forum Vols.* [online]. 2022, **1048**. p. 396-402. ISSN 0255-5476. Available from: https://doi:10.4028/www.scientific.net/MSF.1048.396

[36] AKHMETOVA, G. E., ULYEVA, G. A., TUYSKHAN, K. On the issue of alloying and modification of alloys: Using the waste products for creation of novel materials. *Progress in Physics of Met*als [online]. 2021, **22**(2), p. 271-289. ISSN 1608-1021. Available from: https://doi.org/10.15407/ufm.22.02.271

[37] ASAINOVA, D. A., MERKULOV, V. V., AKHMETOVA, G. E., ULYEVA, G. A. Secondary processing of metallurgical production waste to obtain refractory materials. *Inorganic Materials: Applied Research* [online]. 2021, **12**(4), p. 1066-1069. ISSN 2075-1133. Available from: https://doi.org/10.1134/S2075113321040031

[38] AKHMETOVA, G. E., ULYEVA, G. A., DENISSOVA, A. I., TUYSKHAN, K., TULEGENOV, A. B. State-of-the-art and analysis of characteristics, properties, significance and application prospects of metallurgical slags. *Progress in Physics of Metals* [online]. 2021, **23**(1), p. 108-129. ISSN 2075-1133. Available from: https://doi.org/10.15407/ufm.23.01.108

[39] KUNAEV, V. A. Determination of parameters of means of mechanization and technological process of hydrophobization of slag crushed stone: diss. PhD thesis. Karaganda: KarTU, 2018.

[40] BALOVNEV V. I. Analysis of the duration of the workflow when optimizing the parameters of earthmoving machines / Analiz prodolzhitelnosti rabochego processa pri optimizacii parametrov zemlerojnyh mashin (in Russian). *Mechanization of Construction / Mekhanizaciya stroitelstva* [online]. 2011, **10**, p. 17-18. ISSN 0025-8903.

[41] ZHUNUSBEKOVA, Z. Z., KADYROV, A. S. Study of digging machine flat element loading in clay solution. *Scientific Bulletin of National Hirnichoho University*. 2016, **2**, p. 30-33. ISSN 2071-2227.

[42] KADYROV, A., ZHUNUSBEKOVA, Z., GANYUKOV, A., KADYROVA, I., KUKESHEVA, A. General characteristics for loading the working elements of drilling and milling machines when moving in the clay solution. *Communications - Scientific Letters of the University of Zilina* [online]. 2021, **23**(2), p. B97-B105. ISSN 1335-4205, eISSN 2585-7878. Available from: https://doi.org/10.26552/com.C.2021.2.B97-B105

[43] KADYROV, A. S., AMANGELDIYEV, N. E. New specifications of the theory of ground cutting. *Periodico Tche Quimica*. 2019, **16**(31), p. 922-936. ISSN 1806-0374.

[44] KULGILDINOV, M., KAUKAROV, A., KAMZANOV, N., TARAN M., KULGILDINOV, B., ZHAUYT, A. Determination of kinematic and force parameters of the special bucket shovel for the development of large-block soils. *International Journal of Mechanical Engineering and Robotics Research* [online]. 2020, **9**(6), p. 813-824. ISSN 2278-0149. Available from: https://doi.org/10.18178/ijmerr

[45] EGLI, P., GASCHEN, D., KERSCHER, S., JUD, D., HUTTER, M. Soil-adaptive excavation using reinforcement learning. *IEEE Robotics and Automation Letters* [online]. 2022, **7**(4), p. 9778-9785. ISSN 2377-3766. Available from: https://doi.org/10.1109/LRA.2022.3189834

[46] KADYROV A. S., UNAIBAYEV B. Z., KURMASHEVA B. K. *Theory of pre-project designing. On the example of excavation machines*, Karaganda: Sanat, 2008. ISBN 9789965383939.

[47] DYAKOV, I., IVKIN, V., POPOVICH, A. A. Soil loosening machine for winter earth-moving in transport construction. *Transport* [online]. 2007, **22**(4), p. 316-319. ISSN 1648-4142. Available from: https://doi:10.1080/16484142.2007.9638148

[48] ILYUKHIN, A. V., MARSOV, V. I., MARSOVA, E. V., SYETINA, T. A., DZHABRAILOV, K. A. Improving the efficiency of frozen soils excavation using high-frequency vibration. *IOP Conference Series: Materials Science and Engineering* [online]. 2019, **643**(1), 012102. ISSN 1757-8981. Available from: https://doi.org/10.1088/1757-899X/643/1/012102

[49] MARTYUCHENKO, I. G., ZENIN, M. I., KOLESNIKOV, A. Y., IVANOV, S. V. Drilling tool for frozen ground. *Gornyi Zhurnal* [online]. 2022, **3**, p. 49-53. ISSN 0017-2278. Available from: https://doi.org/10.17580/gzh.2022.03.07

[50] LETOPOLSKY, A. B., KORCHAGIN, P. A., TETERINA, I. A. Working equipment of the single-bucket excavator for the development of frozen ground. *IOP Conference Series: Materials Science and Engineering* [online]. 2020, **709**(4), 044027. ISSN 1757-8981. Available from: https://doi.org/10.1088/1757-899X/709/4/044027

[51] GELMANOVA, Z., PAK, O., SIVYAKOVA, G., ZHABALOVA, G., LELIKOVA, O., ONISCHENKO, O. The scenario of development of electric power industry in the Republic of Kazakhstan. *E3S Web of Conferences* [online]. 2019, **124**, 04002. ISBN 2555-0403. Available from: https://doi.org/10.1051/e3sconf/201912404002

STABILITY OF THE TWO-LINK METROBUS

Volodymyr Sakhno[1], Viktor Polyakov[1], Igor Murovany[3], Svitlana Sharai[2], Oleg Lyashuk[4,*], Uliana Plekan[4], Oleg Tson[4], Mariana Sokol[5]

[1]Department of Automobiles, National Transport University, Kyiv, Ukraine
[2]Department of International Transportation and Customs Control, National Transport University, Kyiv, Ukraine
[3]Department of Automobiles and Transport Technologies, Lutsk National Technical University, Lutsk, Ukraine
[4]Department of Automobiles, Ternopil Ivan Puluj National Technical University, Ternopil, Ukraine
[5]Department of Foreign Languages, Ternopil Volodymyr Hnatyuk National Pedagogical University, Ternopil, Ukraine

*E-mail of corresponding author: oleglashuk@ukr.net

Volodymyr Sakhno 0000-0002-5144-7131,
Igor Murovany 0000-0002-9749-980X,
Oleg Lyashuk 0000-0003-4881-8568,
Uliana Plekan 0000-0003-2533-6355,
Viktor Polyakov 0000-0001-7042-3066,
Svitlana Sharai 0000-0001-6568-4990,
Oleg Tson 0000-0003-1056-4697,
Mariana Sokol 0000-0003-3876-026X

Resume

It has been shown that a perspective type of passenger transport is a metro bus, which can be both two- and three-link. Mathematical model of an autotrain has been developed for a two-link metrobus with both an uncontrolled and a controlled trailer, with the help of which it is established that the speed of the metro bus is 10 m/s, the angular speed of links racking, lateral acceleration, the angles of axle wheels' diversion while manoeuvring of "steering wheel jerk" "Shift" and "turn" have a fading nature of oscillation, which ensures the stability of its motion. At the same time, the value of lateral accelerations in the center of masses of metrobus separate links with an uncontrolled trailer at a speed of 15 m/s, while performing various manoeuvres do not exceed 0.45 g, according to this characteristics, such metrobus is stable, instead of a metrobus with a controlled trailer, which at this speed loses its stability. This should be considered when developing the advanced two-link metrobus of increased overall length (24 m).

Available online: https://doi.org/10.26552/com.C.2023.023

Article info

Received 30 October 2022
Accepted 25 November 2022
Online 2 February 2023

Keywords:

metrobus
trailer
controlling wheel module
angular velocity
lateral acceleration
uncontrolled and controlled autotrain trailer

ISSN 1335-4205 (print version)
ISSN 2585-7878 (online version)

1 Introduction

Design of city buses is a topic of interest in current research, both in terms of control [1] and sustainable mobility [2]. As for articulated buses, stability control is an issue of great practical importance, since the onset of unstable oscillations like "jack-knifing" can lead to loss of control and to dangerous accidents. Rapid bus, mainly Metrobus (Eng. Bus rapid transit, BRT) is the way to organize the bus (or trolleybus) connection, which has higher operational characteristics in comparison with regular bus routes (speed, reliability, transportation capacity). According to peculiar parameters (in particular, at speed) the system of high-speed bus transport can be compared to the light rail systems (high-speed tram) [3].

The BRT project involves the bus traffic on dedicated and often enclosed lanes. The main advantage of the metro bus is its complete isolation on the road from other types of transport. As a means of transportation, the next-generation articulated buses, equipped with engines up to 250 kW, have been selected. However, as in the metro and in metrobus salons places for standing are much more preferable. Due to this, only one articulated two-link bus carries up to 200 passengers [4].

The BRT system has a number of undeniable benefits:

- high passenger capacity and efficient payment systems provide low-cost travel;
- high traffic speed allows the metro bus to transport a significant part of passengers, which reduces the number of cars on the city roads and, thereafter, vehicle emissions have been reduced;
- a detailed information system informs passengers about schedules of the routes.

A state of the art study on directional performance

issues in design of articulated heavy vehicles (mainly devoted to trucks) is presented in [5-7], with an overview of the models used in designing controllers. Some studies are specifically devoted to articulated buses (and in particular to pusher articulated buses), however presenting numerical simulations only of particular manoeuvres, using a single-track model [8-10].

Convenience, safety and improved traffic organization are not all that a new system of high-speed bus transport can offer to passengers. At the same time, it is very important to ensure the stability of the hinged-articulated vehicles while driving at high speed. Therefore, the aim of the work is to analyze the influence of mass, power and layout parameters of a two-link metrobus, as with uncontrolled and controlled trailer, on the stability of its traffic.

2 Methodology

The stability of traffic refers to properties of the automatic transport vehicles (ATV), which do not have a strict certainty in terminology, requirements, indicators and methods of assessment [11-16]. In practice, experimental characteristics that determine the stability of the ATV while driving have been used and in theory - direct and indirect indicators and their dependencies, among which the critical speed of traffic is the main one.

In famous nowadays studies the stability and controllability issues have been considered in two aspects [17]:

1. The study concerning the characteristics of all the elements of "driver-vehicle-road" system has been seen as a closed system of automatic control.

2. The study of own stability and controllability of a car (autotrain) in which the driver's influence has been excluded.

To ensure controllability and stability of the system of "driver-autotrain-road", it is necessary, though not sufficiently, to provide its own stability and control of the car and trailer parts, e.g. properties that lie in their design (without driver's motion correction via the instability). Thus, if the stability of the ATV is ensured, then the stability of the driver's system - ATV is also provided, but with a large margin. Therefore, it is enough to consider the traffic in the management of an open scheme, that is, the potential stability of the ATV itself.

Currently, the calculation methods for determining critical speeds are most fully developed for single cars, trailers and two-link sidecar autotrains. Much less studies have been devoted to the critical speed determination of the two-link trailer road trains, which include the two-link metrobus.

In works [18-20], when completing the differential equations of autotrains traffic, the following constraints have been taken into consideration: a flat calculation scheme, autotrain traffic is carried out on an equal supporting surface with constant speed along a linear or curvilinear trajectory set by the angle of rotation of the driven wheels of power unit.

In Equations (1-20) the following notations have been taken:

a - the distance from the front axle to the center of the bus mass;

b - the distance from the middle axis to the center of the bus mass;

bb - the distance from the back axle to the center of the bus mass;

bs - the distance from the center of mass to the axle of the rear suspension of the bus;

c - the distance from the center of the bus mass to the point of coupling with the trailer;

λ -the shift of the front driven wheels of the bus, due to the longitudinal inclination of the kingpin;

c_{o1} - the distance from the coupling point to the bus back position point;

θ - the angle of wheels rotation of the front axle of the bus;

b_1 - the distance from the center of the mass of the trailer to its front axle;

b_{11} - the distance from the center of the mass of the trailer to its back axle;

c_{11} - the distance from the coupling point to bus back overall point;

θ_2, θ_{21} -the rotation angle of the front and back axle of the trailer;

m, J - the mass and central moment of inertia of the bus;

v, u - the longitudinal and transverse speed vector projection of the center of mass on an axle connected with the bus;

ω - the angular speed of the bus according to the vertical axis;

m_1, J_1 - the mass and central moment of inertness of the control wheel module of the bus;

v_1, u_1 - the longitudinal and transverse projections of the speed vector of the center of mass of the control wheel module of the bus;

ω_1 - the angular speed of the control wheel module of the bus;

m_2, J_2 - the *mass and central moment of trailer inertness (second link)*;

v_2, u_2 - the longitudinal and transverse projection of the speed vector of the center of the mass of the trailer;

ω_2 - the angular speed of the trailer;

γ_1 - the angle assembly of the links of the bus;

$X_1, X_2, X_{21}, X_3, X_{31}$ - the longitudinal forces on the axles of the bus and trailer;

$Y_1, Y_2, Y_{21}, Y_3, Y_{31}$ - the transverse forces on the axles of the bus and trailer.

For such restrictions, the equation of two-link metrobus traffic has been written, Figure 1 [21]:

- for the controlling wheel module bus

$$-m_1(\dot{v}_1 - \omega_1 u_1) - XA\cos\theta - X_1 - YA\sin\theta = 0\,, \quad (1)$$

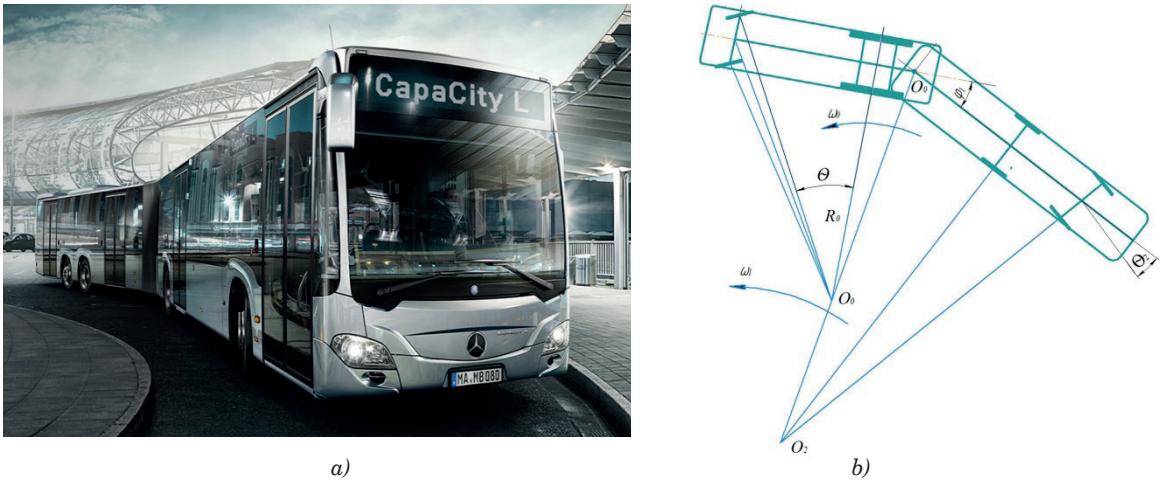

a) *b)*

Figure 1 *Photograph (a) and calculation scheme of a metrobus (b)*

$$-m_1(\dot{u}_1-\omega_1\nu_1)-XA\sin\theta-YA\cos\theta+Y_1=0\,. \quad (2)$$

- for the basic of the bus

$$m(\dot{\nu}-\omega u)+X_2\cos\theta_1+X_{21}\cos\theta_{11}-Y_2\sin\theta_{11}- \\ -XA+XB\cos\gamma_1-YB\sin\gamma_1=0, \quad (3)$$

$$m(\dot{u}-\omega\nu)+Y_2\cos\theta_1+Y_{21}\cos\theta_{11}-X_2\sin\theta_{11}- \\ -YA+YB\cos\gamma_1-XB\sin\gamma_1=0. \quad (4)$$

- for a trailer

$$-m_2(\dot{\nu}-\omega_2u_2)+XB-X_3\cos\theta_2+Y_3\sin\theta_2- \\ -X_{31}\cos\theta_{21}+Y_{31}\sin\theta_{21}=0, \quad (5)$$

$$-m_2(\dot{u}-\omega_2\nu_2)+YB-X_3\sin\theta_2+Y_3\cos\theta_2+ \\ +X_{31}\sin\theta_{21}+Y_{31}\cos\theta_{21}=0. \quad (6)$$

The common solution of Equations (1) - (6) allows to find the reactions at points of connection of the control wheel module with the basic of the bus XA and YA, the basic of the bus and the trailer XB and YB.

$$XB=m_2\dot{\nu}_2-m_2\omega_2u_2+X_3\cos\theta_2-Y_3\sin\theta_2+ \\ +X_{31}\cos\theta_{21}-Y_{31}\sin\theta_{21}, \quad (7)$$

$$YB=m_2\dot{u}_2-m_2\omega_2u_2+X_3\sin\theta_2-Y_3\cos\theta_2+ \\ +X_{31}\sin\theta_{21}-Y_{31}\cos\theta_{21}. \quad (8)$$

$$XA=m_1\dot{u}_1\sin\theta+m_1\omega_1\nu_1\sin\theta-Y_1\sin\theta- \\ -m_1\dot{\nu}_1\cos\theta+m_1\omega_1u_1\cos\theta-X_1\cos\theta; \quad (9)$$

$$YA=-m_1\dot{u}_1\cos\theta-m_1\omega_1\nu_1\cos\theta+Y_1\cos\theta- \\ -m_1\dot{\nu}_1\sin\theta+m_1\omega_1u_1\sin\theta-X_1\sin\theta. \quad (10)$$

After determining the reactions at points of the autotrain links connection, taking into account the equations of the traffic rotation of each link of the autotrain, a system of differential equations has been written in the following form:

$$m(\dot{\nu}-u\omega)=-X_2\cos\theta_1-X_{21}\cos\theta_{11}+ \\ +Y_2\sin\theta_1+XA-XB\cos\gamma_1+YB\sin\gamma_1; \quad (11)$$

$$m(\dot{u}-\nu\omega)=Y_2\cos\theta_1+Y_{21}\cos\theta_{11}+ \\ +X_2\sin\theta_1+YA-YB\cos\gamma_1+XB\sin\gamma_1. \quad (12)$$

$$I\dot{\omega}=aYA-b(Y_2\cos\theta_1+X_2\sin\theta_1)- \\ -bb(Y_{21}\cos\theta_{11}+X_{21}\sin\theta_{11})+ \\ +c(YB\cos\gamma_1+XB\sin\gamma_1)+M_1+M_2; \quad (13)$$

$$I_1\dot{\omega}_1=-YA\lambda\cos\theta+XA\lambda\sin\theta-M_1=0; \quad (14)$$

$$I_2\dot{\omega}_2=d_1YB-b_1(Y_3\cos\theta_2+X_3\sin\theta_2)- \\ -b_{11}(Y_{31}\cos\theta_{21}+X_{31}\sin\theta_{21})+ \\ +c_1(YC\cos\gamma_2+XC\sin\gamma_2)-M_3. \quad (15)$$

After substituting the values of reactions at the points of connection of autotrain individual parts, a system of differential equations relative to the variables $(u,\omega,\theta,\dot{\theta},\gamma_1,\dot{\gamma}_1)$ has been written in the form:

$$m(\dot{\nu}-u\omega)=-\dot{\omega}[m_1\sin\theta\lambda+m_2d_1\sin\varphi_1]- \\ -\ddot{\theta}m_1\sin\theta\times\lambda-\omega^2[m_1\times\lambda\cos\theta+m_2d_1\cos\varphi_1- \\ -m_1a+m_2c]-\dot{\theta}^2m_1\times\lambda\cos-\dot{\varphi}_1^2m_2d_1\sin\gamma_1- \\ -\dot{\omega}_1m_2d_1\sin\varphi_1-2\omega\dot{\theta}m_1\times\lambda\cos\theta+\dot{\varphi}1\omega\times \\ \times[-2m_2d_1\cos\varphi_1]+\omega u(m_1+m_2)-X_1\cos\theta- \\ -Y_1\sin\theta-X_2-X_{21}-X_3\cos(\varphi_1+\theta_2)+ \\ +Y_3\sin(\varphi_1+\theta_2)-X_{31}\cos(\varphi_1+\theta_{21})+ \\ +Y_{31}\sin(\varphi_1+\theta_{21}); \quad (16)$$

$$m(\dot{u}-\omega\nu)=-\dot{u}2m_2\cos^2\varphi_1+\dot{\nu}m_2\sin2\varphi_1-\dot{\omega}\times \\ \times\{m_1(a-\lambda\cos\theta)-m_2[\cos\varphi_1(2c_1+d_1)-c]+ \\ +\cos\varphi_1\times(2c\times\cos\varphi_1+c_1+d_1+c)\}+\ddot{\theta}m_1\times \\ \times\cos\theta-\omega\nu(m_1+m_2)\times(1-2\cos^2\varphi_1)- \\ \omega um_2\sin2\varphi_1-\omega^2[m_1\lambda\sin\theta-m_2\times(d_1\sin\varphi_1+ \\ +c\sin2\varphi_1)]-2\omega\dot{\varphi}_1m_2d_1\sin\varphi_1-\dot{\varphi}_1^2m_2d_1\times \\ \times\sin\varphi_1+m_2d_1\cos\varphi_1+Y_1\cos\theta-X_1\sin\theta+Y_2+ \\ +Y_{21}+Y_3\cos(\varphi_1+\theta_2)-X_3\sin(\varphi_1+\theta_2)+ \\ +Y_{31}\cos(\gamma_1+\theta_{21})-X_{31}\sin(\gamma_1+\theta_{21})]; \quad (17)$$

$$I_1\ddot{\theta} = -\dot{\omega}(I_1 + m_1 a\lambda\cos\theta - m_1\lambda^2) - \dot{v}m_1\lambda\sin\theta - \dot{u}m_1\lambda\cos\theta + \ddot{\theta}m_1\lambda^2 + \omega u m_1\lambda\sin\theta + \omega v m_1\lambda\cos\theta - Y_1\lambda + M_1 + M_2; \quad (18)$$

$$I\dot{\omega} = aYA - b(Y_2\cos\theta_1 + X_2\sin\theta_1) - bb(Y_{21}\cos\theta_{11} + X_{21}\sin\theta_{11}) + c(YB\cos\gamma_1 + XB\sin\gamma_1) + M_1 + M_2; \quad (19)$$

$$I_2\dot{\omega}_1 = -\dot{\omega}[I_2 + m_2 d_1(c\cos\varphi_1 + d_1)] - \dot{\omega}_1 m_2 d_1^2 - \dot{v}m_2 d_1\sin\varphi_1 + \dot{u}m_2 d_1\cos\varphi_1 + \omega v m_2 d_1\cos\varphi_1 + \omega u m_2 d_1\sin\varphi_1 + \omega^2 m_2 c d_1\sin\varphi_1 - Y_3(d_1 + b_1)\times \cos\theta_2 - X_3(d_1 + b_{11})\cos\theta_{21} - X_{31}(d_1 + b_{11})\sin\theta_{21}. \quad (20)$$

To integrate the equations of the metrobus, it is necessary to determine the longitudinal, transverse forces on its axes, as well as the moments of inertia of the metrobus links. Longitudinal forces on the wheels of the autotrain have been determined as:

$$X_1 = f\cdot Z_i, \quad (21)$$

where f - coefficient of autotrain wheels rolling resistance, Z_i - the load on the axis of autotrain individual sections, which have been determined by using the following dependencies:

$$\sum F_Z = 0;\ \sum mom_{oy}F_i = 0,, \quad (22)$$

$$Z_1 = m_1 g + mgbs/l;\ Z_2 0.5mga/l;\ Z_3 = 0.5m_2 g;, \quad (23)$$

where $bs=(b+bb)/2;\ l=a+bs-\lambda$.

The moments of the metrobus links inertia have been determined in accordance with the study of Podrygalo and Volkov [22], where a quite precise probabilistic method for determining the radii of inertia of a car (trailer, semitrailer) has been proposed. It is based on two assumptions: firstly, the moment of inertia of the car (trailer, semitrailer) depends on the law of its mass distribution within the limits of the railway track, base and height; and secondly, the distribution density of the moment of inertia has been subordinated to the normal distribution law.

The most probable values of the radius of inertia relative to the vertical axis have been given by the formula

$$\rho_z = \sqrt{\frac{1}{2}ab + \frac{B^2}{12} \pm \frac{1}{6}ab}, \quad (24)$$

relative to the longitudinal and transverse axes of the formula

$$\rho_x = \sqrt{\frac{1}{2}(H-h)h + \frac{B^2}{12} \pm \frac{1}{6}(H-h)}, \quad (25)$$

$$\rho_y = \sqrt{\frac{1}{2}ab + \frac{1}{3}(H-h)h \pm \frac{1}{6}ab}, \quad (26)$$

where B - the track of the car (trailer), H - the height of the car (trailer), h - the distances from the center of mass to the road's plane.

The moment of inertia of the metrobus links are determined by the known formula

$$I_i = \rho_i m_i. \quad (27)$$

The moment of resistance in the hinge between the links of the metrobus has been determined as [23]

$$M_{0i} = \frac{2}{3}Z_{0i}\mu\frac{R_i^2 - r_i^2}{R_i^2 + r_i^2},, \quad (28)$$

where Z_{0i} - vertical load in the support-coupling device, μ - the coefficient of friction in the support-coupling device, μ=0.15...0.20, R_i, r_i - bigger and smaller radii of the support-coupling device, respectively.

Nowadays, there are several analytical approximations of the dependence of the lateral reaction applied in the spot of the wheel contact, from the angle of lead, namely [24]:

$$Y_i = k_i\times arctg(c_i\delta_i),\quad Y_i = k_i\times th(c_i\delta_i),\quad Y_i = \frac{k_i\delta_i}{\sqrt{1 + k_i\times(\varphi^2 G_i^2)^{-1}\times\delta_i^2}}, \quad (29)$$

where δ_i, Y_i - abduction angles and lateral forces, φ - coefficient of transverse linkage between the tire and the supporting surface (has been considered as a constant value of this study), k_i - coefficient of resistance to lateral withdrawal, G_i - vertical load on the wheel.

The general requirement for all the functions given in the Equation (29) states that, function $f(\delta)$ is the sum of an alternating series

$$Y = k\delta - k'\delta^3 + k''\delta^5 - + \ldots. \quad (30)$$

In the further calculations, in mathematical modelling, the last Y in Equation (29) dependence is used. The need to take into account nonlinearity is explained by the fact that only in a very narrow range the dependence between the forces acting on the axis and the angles of the axis drawdown is close to the linear one, while with other values of the angles of withdrawal, this dependence is nonlinear and the lateral force cannot exceed the Y* adhesion forces. As the lateral force approaches to its maximum value, a partial slip in the lateral direction begins and then a full slide starts. Accordingly, the maximum value of the lateral force $Y = Y^*$ can be found, based on the fact that

$$\lim_{\delta\to\infty} Y(\delta) = \frac{k}{\chi} = Y^*, \Rightarrow \chi = \frac{k}{Y^*}, Y^* = \varphi G. \quad (31)$$

If the coefficient of resistance of the lateral carriage is indicated in the absence of the longitudinal forces acting on the wheel, through k_o, then k is defined as [24]

$$k = k_o\frac{\sqrt{1 - (X/\varphi G)^2}}{1 + 0.375X/G}, \quad (32)$$

where X - the longitudinal force acting on the wheel, the

value of which has been determined by the ratio $X=M/r$, if $M/r < \varphi G$ and $X = \varphi G$, if $M/r \geq \varphi G$.

In the absence of the traction (brake) moment on the wheels of the autotrain axes, the lateral forces on the wheels of its axes have been determined by the dependence [24]

$$Y_i = \frac{k_i \delta_i}{\sqrt{1 + \chi_i^2 \delta_i^2}}, \tag{33}$$

$$\chi_i = \frac{k_i}{\varphi Z_i}. \tag{34}$$

Integration of the equations system in (20) was performed with the software Maple 14. Equation (20) in "the machine form" due to the additional symbols should be written, where:

- v, u - longitudinal, transverse projection of the velocity vector of the center of mass on an axle connected with the tractor;
- *omega* - angular speed of the tractor, relative to the vertical axis;
- *v1*, *u1* - longitudinal and transverse projection of the velocity vector of the center of the masses of the steering wheel module;
- *omega1* - angular speed of the steering wheel module;
- *v2*, *u2* - longitudinal and transverse projection of the velocity vector of the center of the masses of the second link;
- *omega2* - angular velocity of the second link;
- *U* - derivative of the lateral velocity of the center of the masses;
- Ω - derivative of the angular speed of the tractor relative to the vertical axis;
- Θ - the change speed of the rotation angle (θ) of the controlled module;
- *TT* - angular acceleration of the controlled module;
- *Phi1* - the change speed of the rotation angle (φ 1) of the second link;
- *PPT1* - angular acceleration of the second link;
- *V* - acceleration in the longitudinal direction.

Taking into account the accepted symbols of the autotrain motion Equation (6) in the "machine type" for steady motion ($\dot{v} = 0$) has been presented in the form:

- by variable *u*:

e1:=-m(U+omega*v)+Y2+Y21*cos(theta11)+X21*-sin(theta11)-m1*U-X1*sin(theta)+ cos(theta)*Y1+-cos(phi1)*X31*sin(theta21)+sin(phi1)*X31*cos(theta21)+m2*U+*
*cos(phi1)*X3*sin(theta2)-sin(phi1)*Y3*sin(theta2)+-cos(phi1)*Y31*cos(theta21)-2*m2*cos(phi1)^2*U+-cos(theta)*m1*lambda*Omega+m2*omega*v+2*m2*-cos(phi1)^2*c**
*Omega-2*m2*omega*v*cos(phi1)^2-m1*sin(theta)*lambda*Theta^2+cos(theta)*m1*lambda*TT-m1*sin(theta)*lambda*omega^2-m1*omega*v-m1*a*Omega-sin(phi1)*Y31*sin(theta21)+cos(phi1)*m2*d1*PT1+cos(-phi1)*Y3*cos(theta2)-2*cos(phi1)*m2*omega*-sin(phi1)*u-m2*c*Omega+cos(phi1)*m2*d1*Omega+2*cos(phi1)*m2*V*sin(phi1)-+2*cos(phi1)*m2*sin(phi1)*c*omega^2+sin(phi1)*X3*+-sin(phi1)*m2*d1*omega^2+2*sin(phi1)*m2*omega*d1*Phi1+sin(phi1)*m2*d1*Phi1^2;*

- by variable ω:

*e2:=-J*Omega+a*cos(theta)*Y1-c*cos(phi1)*Y31*-cos(theta21)-c*cos(phi1)*X3*sin(theta2)-c*cos(-phi1)*Y3*cos(theta2)-cos(phi1)*X31*sin(theta21)+c*sin(phi1)*X3*cos(theta2)-2*a*m1*sin(theta)*omega*lambda*Theta+a*cos(theta)*m1*lambda*Omega-a*m1*sin(theta)*lambda*omega^2-a*m1*sin(theta)*lambda*Theta^2-a*X1*sin(theta)+a*cos(theta)*m1*lambda*TT+c*sin(phi1)*Y31*sin(theta21)+c*sin(phi1)*X31*cos(theta21)+2*c*sin(phi1)*m2*omega*d1*Phi1+c*sin(phi1)*m2*d1*Phi1^2+*
*c*sin(phi1)*m2*d1*omega^2-c*cos(phi1)*m2*d1*PT1-c*cos(phi1)*m2*d1*Omega-bb*Y21-m2*c^2*Omega-a*m1*U-m1*a^2*Omega+c*m2*U--a*m1*omega*v+c*m2*omega*v+kk1*(theta-theta0)+h1*Theta+kk2*(phi-phi10)+h2*Phi1;*

- by variable θ:

e3:=-J1(Omega+TT)+lambda*(-Y1+cos(theta)*m1*U-m1*lambda*Omega-m1*lambda*TT--m1*sin(theta)*V+m1*sin(theta)*omega*u+cos(theta)*m1*a*Omega+cos(theta)*m1*omega*v+*
*m1*sin(theta)*a*omega^2)-kk1*(theta-theta0)--h1*Theta;*

- by variable φ_1:

e4:=-J2(Omega+PT1)-m2*d1^2*Omega--m2*d1^2*PT1-d1*X31*sin(theta21)-b1*Y3*cos(theta2)-b1*X3*sin(theta2)-b11*Y31*cos(theta21)--b11*X31*sin(theta21)-d1*m2*V*sin(phi1)+d1*m2*cos(phi1)*U+d1*m2*omega*v*cos(phi1)+d1*m2*omega*sin(phi1)*u-d1*Y31*cos(theta21)-d1*X3*sin(theta2)-d1*Y3*cos(theta2)-c*cos(phi1)*m2*d1*Omega-kk2*(phi1-phi10)-h2*Phi1+kk3*(phi2-phi20)+h3*Phi2.*

3 Results

Integration of motion equations has been made by such initial data:

L_a=12 m; L_m=22 m; a =3.9 m; b=1.45 m; bb=2.75 m; c=3.8 m; λ=-0.0023 m; co_1=1.2 m; B=2.0 m; b_1=-0.65 m; b_{11}=0.65 m; DL2=4.8 m; c_{11}=7.8 m; V:=0; X1:=0; X2:=0; X21:=0; X3:=0; X31:=0; m1:=600; m:=17400; kf:=0; m2:=16000; k1:=160000; k2:=252000; k21:=252000; k3:=165000; k31:=165000; kk1:=2600; kk2:=300; h1:=30; h2:=30; kappa1:=0.8; kappa2:=0.8; kappa3:=0.8; kf:=0; v:=10; phi10:=0; theta:=0; theta2:=0; theta21:=0; J1:=12.22; J:=288395; J2:=271189;
Z1:=70000; Z2, Z21:=0.5*m*g*a/l=80000; Z3,

Z31:=0.5*m*g*a/l=55000;
Y1:=k1*delta1/sqrt(1+(k1*delta1/(kappa1*Z1))^2);
Y2:=k2*delta2/sqrt(1+(k2*delta2/(kappa2*Z2))^2);
Y21:=k2*delta21/sqrt(1+(k2*delta21/(kappa2*Z2))^2);
Y3:=k3*delta3/sqrt(1+(k3*delta3/(kappa3*Z3))^2);
Y31:=k3*delta31/sqrt(1+(k3*delta31/(kappa3*Z3))^2).

The results of calculating the angular velocity of the metrobus linkage, lateral acceleration, angles of wheel alignment of axes, the angle of the links folding during the "steering wheel jerk" manoeuvre for a metrobus with an uncontrolled and a controlled trailer for direct control over the axle and gear ratio of about 0.5 has been shown in Figures 2-5.

The fading character of the oscillation of the angular velocity of the bus and the trailer rushing demonstrates the stable character of the metrobus links movement during this manoeuvre (Figure 2). Thus, it should be noted that the absolute values of the rush speed for an uncontrolled and controlled trailer are almost identical, which can lead to a breakdown of stability when increasing the speed of the metrobus.

The stability of motion, to a greater extent, can be judged by the magnitude of lateral accelerations, operating in the center of masses of individual links. According to literary sources, the stability of motion can be considered satisfactory if the transverse accelerations in the center of masses do not exceed 0.45 g. This condition corresponds to the metrobus with a controlled trailer (more unstable in comparison to the uncontrolled one) (Figure 1).

In addition, the fading character of fluctuations also indicates the stability of the metrobus. As in the

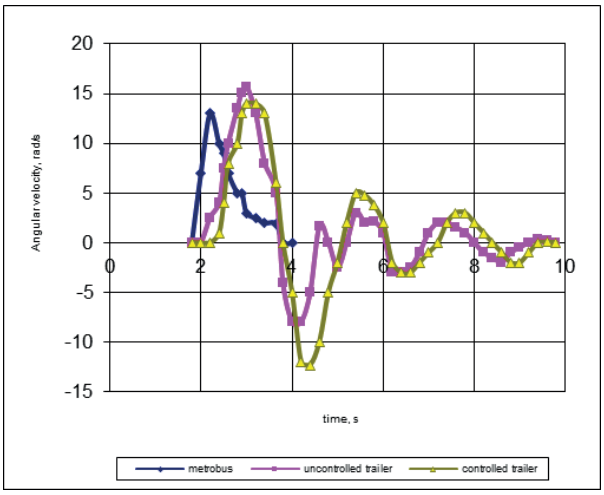

a)

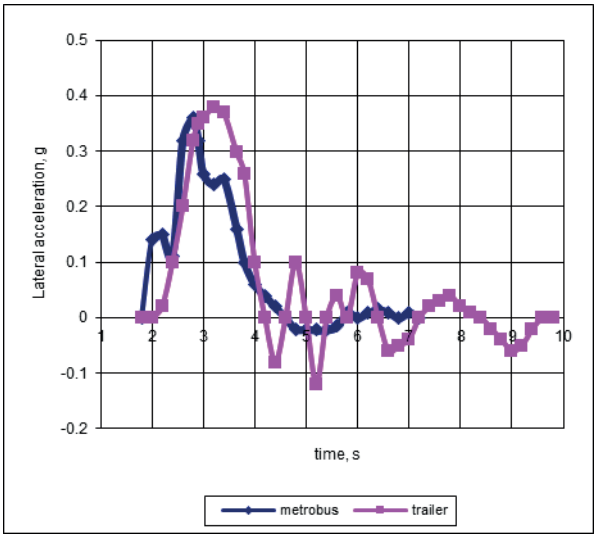

b)

Figure 2 *Angular rushing velocity (a) and lateral acceleration of the metro bus (b) during the manoeuvre "steering wheel jerk"*

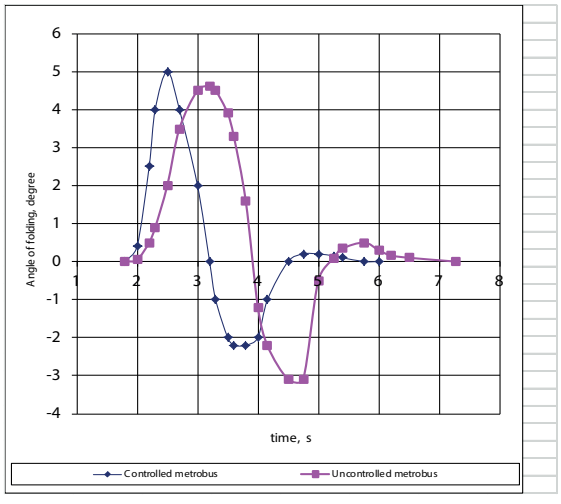

a)

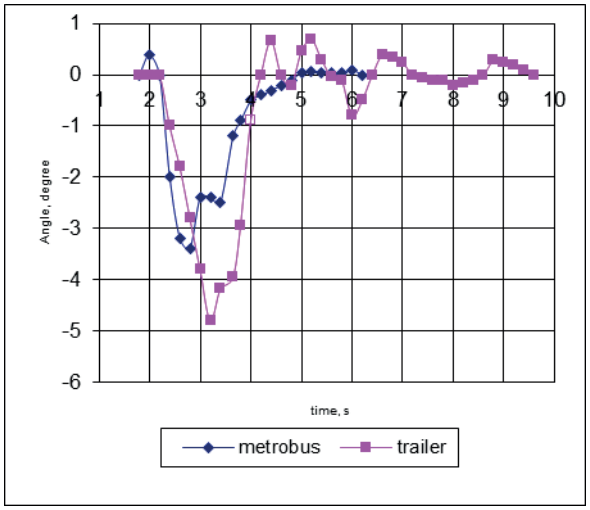

b)

Figure 3 *The* angle of folding *(a) and separation of the centers of the masses links (b) of the metrobus during the manoeuvre of "steering wheel jerk"*

preceding case, the accelerations in the center of the trailer mass are somewhat higher than the acceleration of the bus, so the limiting factor, when performing the manoeuvre of "steering wheel jerk", is either accelerating the center of the mass of the trailer.

According to values of the lateral accelerations, the lateral forces acting in the center of the masses of individual links have been determined and behind them the angle of folding, Figure 3a and the angles of links separation, Figure 3b.

It should be noted that bigger angles of allocations outlets are inherent in the trailer. The variable character of lateral acceleration and lateral forces leads to oscillations of the links lateral displacement angles and the greater amplitude of oscillations takes place at the center of the trailer masses. That can lead to superfluous rotation of the metrobus and the violation of stability when increasing the speed of motion. From this follows an important practical conclusion - the pressure in the trailer tires, as one which largely determines the resistance coefficient of the drive, should be chosen in such a way that does not lead to excessive twist of the metrobus.

While performing a "reset" manoeuvre, similar calculations have been made. The qualitative results of calculating the main parameters of the autotrain motion for the implementation of this manoeuvre, to a large extent, coincide with the results of the previous "steering wheel jerk" manoeuvre, but the absolute values of the parameters are significantly lower.

In addition to the above-discussed manoeuvres of "steering wheel spin" and "reset", other modes of motion

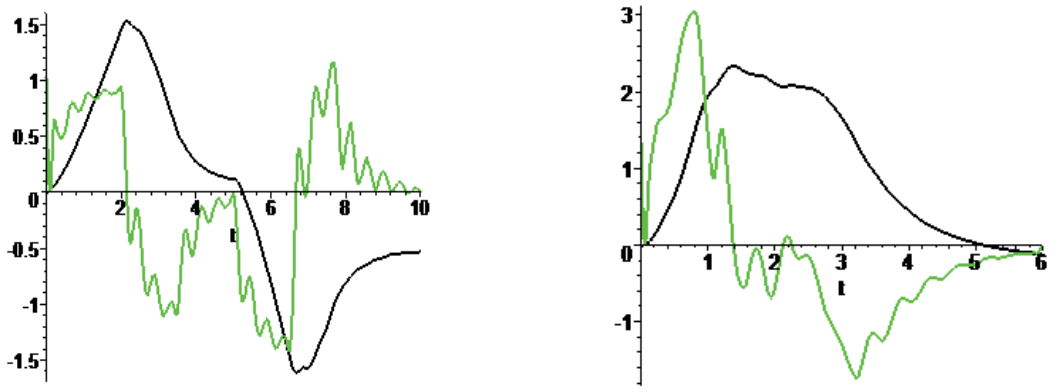

a) lateral speed *b) lateral acceleration*

Figure 4 *Lateral speed and lateral acceleration of the center of the bus with a controlled trailer mass during the manoeuvre "turn" at speeds of 10 m/s (a) and 15 m/s (b)*

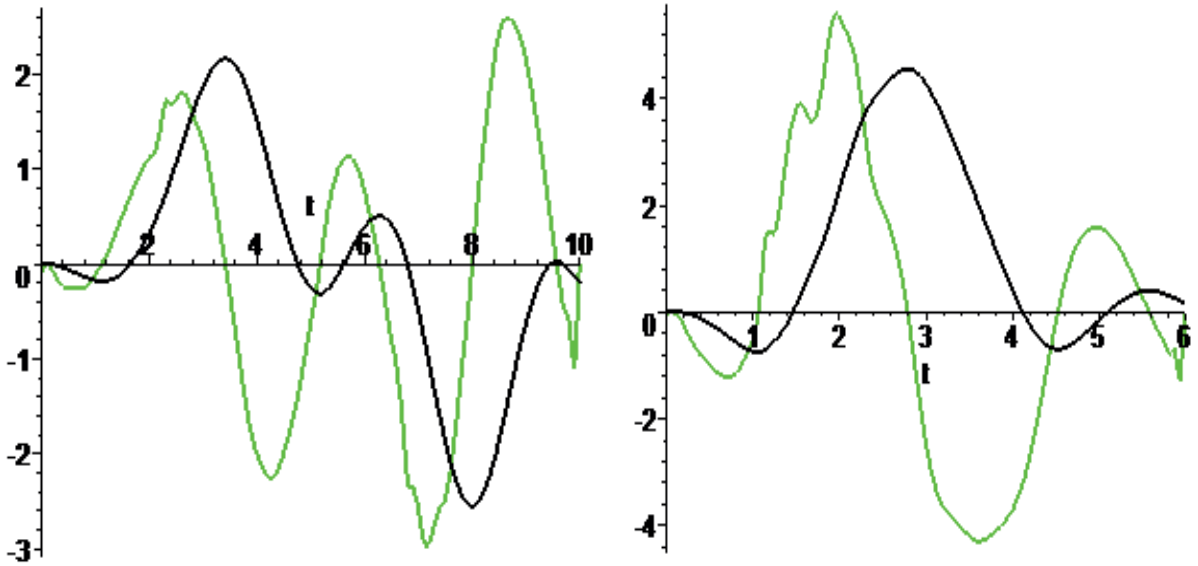

a) lateral speed *b) lateral acceleration*

Figure 5 *Lateral speed and lateral acceleration of the center of the bus with an uncontrolled trailer mass during the manoeuvre "turn" at speeds of 10 m/s (a) and 15 m/s (b)*

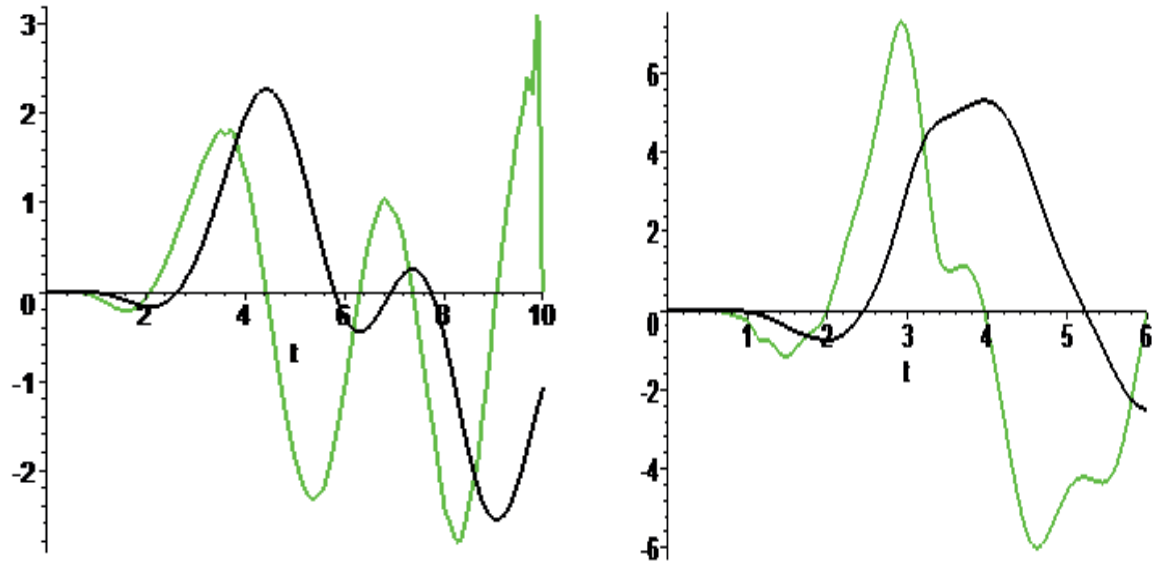

a) lateral speed *b) lateral acceleration*

Figure 6 *Lateral speed and lateral acceleration of the center of the controlled trailer metrobus mass during the manoeuvre "turn" at speed 10 m/s (a) and 15 m/s (b)*

were also considered, namely the 90-degree rotation, S-shaped rotation, ISO manoeuvre, straight-line motion [25].

The results of calculation of the lateral speed and lateral acceleration of uncontrolled and controlled autotrain trailer links during 90-degree rotation manoeuvre are given in Figures 4-6, where a limiting factor in performing various manoeuvres is a controlled metrobus trailer, acceleration of which is 25 to 36 % higher than acceleration of an uncontrolled metrobus trailer.

4 Conclusions

The mathematical model of the metrobus has been developed, both with an uncontrolled and controlled trailer, by means of which it is established, that the speed of the metrobus 10 m/s, the angular velocity of the links, the lateral acceleration, the angles of the wheel axle during the manoeuvre of "steering wheel jerk", "reset" and "turn" have a diminishing character of oscillations. In this case, values of lateral accelerations in the center of the masses of individual links of the metrobus with an uncontrolled trailer when performing various manoeuvres do not exceed 0.45 g. So, according to this characteristic such metrobus is stable, while a metro bus with a controlled trailer at the speed of 15 m/s loses its stability. This should be taken into account when developing the advanced two-link metrobus with increased overall length (24 m).

Grants and funding

The authors received no financial support for the research, authorship and/or publication of this article.

Conflicts of interest

The authors declare that they have no known competing financial interests or personal relationships that could have appeared to influence the work reported in this paper.

References

[1] WEI, L., HONGWEN, H., FENCHUN, S., JIANGYI, L. Integrated chassis control for a three-axle electric bus with distributed driving motors and active rear steering system. *Vehicle System Dynamics* [online]. 2017, **55**(5), p. 601-625. ISSN 0042-3114, eISSN 1744-5159. Available from: https://doi.org/10.1080/00423114.2016.1267368

[2] FRAGASSA, C. Electric city buses with modular platform: a design proposition for sustainable mobility. In: *Sustainable design and manufacturing 2017* [online]. CAMPANA, G., HOWLETT, R. J., SETCHI, R., CIMATTI, B. (Eds.). Vol. 68. Cham: Springer International Publishing, 2017. ISBN 978-3-319-57078-5, p. 789-800. Available from: https://doi.org/10.1007/978-3-319-57078-5

[3] Adrien Arcand - Wikipedia [online]. Available from: https://ru.wikipedia.org/wiki
[4] MetroBus - BRT [online]. Available from: https://bus10.kz/index.php /menu2-brt
[5] FANCHER, P. S., WINKLER, C. Directional performance issues in evaluation and design of articulated heavy vehicles. *Vehicle System Dynamics* [online]. 2007, **45**(7-8), p. 607- 647. ISSN 0042-3114, eISSN 1744-5159. Available from: https://doi.org/10.1080/00423110701422434
[6] ODHAMS, A. C., ROEBUCK, R. L., JUJNOVICH, B. A., CEBON, D. Active steering of a tractor semi-trailer. *Proceedings of the Institution of Mechanical Engineers: Journal of Automobile Engineering* [online]. 2011, **225**(7) p. 847-869. ISSN 0954-4070, eISSN 2041-2991. Available from: https://doi.org/10.1177/0954407010395680
[7] ZHOU, S., ZHANG, S. Jack-knife control on tractor semi-trailer during high speed curve driving. *Sensors and Transducers Journal*. 2012, **16**, p. 277-284. ISSN 1726- 5479.
[8] RUSEV, R., IVANOV, R., STANEVA, G., KADIKYANOV, G. A study of the dynamic parameters influence over the behavior of the two-section articulated vehicle during the lane change manoeuvre. *Transport Problems* [online] 2016, **11**(1), p. 29-40. ISSN 1896-0596, eISSN 2300-861X. Available from: https://doi.org/10.20858/tp.2016.11.1.3
[9] KOLESNIKOVICH, A. N., VYGONNYJ, A. G. Stability of a trailer road train of increased length (25.25m) in straight-line motion. *Actual Problems of Mechanical Engineering.* 2018, **7**, p. 96-100. ISSN 2306-3084.
[10] LUO, R., ZENG, J. Hunting stability analysis of train system and comparison with single vehicle model. *Jixie Gongcheng Xuebao / Chinese Journal of Mechanical Engineering* [online]. 2008, **44**(4), p. 184-188. ISSN 0577-6686. Available from: https://doi.org/10.3901/JME.2008.04.184
[11] ANTONOV, D. A. Calculation of the stability of the movement of multi-axle vehicles. *Moscow: Mechanical Engineering*. 1984, 164 p.
[12] HALES, F. D. *The vertical motion lateral stability of road vehicle trains*. Transport and Road Research Laboratory (TRRL), 1972.
[13] GALLUPPI, O., FORMENTIN, S., NOVARA, C., SAVARESI, S. Nonlinear stability control of autonomous vehicles: a MIMO D2-IBC solution. *IFAC-PapersOnLine* [online]. 2017, **5**(1), p. 3691-3696. ISSN 2405-8963. Available from: https://doi.org/10.1016/j.ifacol.2017.08.563
[14] BARBOSA, H., BARTHELEMY, M., GHOSHAL, G., JAMES, CH. R., LENORMAND, M., LOUAIL, T., MENEZES, R., RAMASCO, J. J., SIMINI, F., TOMASINI, M. Human mobility: models and applications. *Physics Reports* [online]. 2018, **734**, p. 1-74. ISSN 0370-1573, eISSN 1873-6270. Available from: https://doi.org/10.1016/j.physrep.2018.01.001
[15] BERDIYOROV, T. Metrobus in separated corridors as an optimal public transport system. *IOP Conference Series Earth and Environmental Science* [online]. 2020, **614**(1), p. 1-13. ISSN 1755-1307, eISSN 1755-1315. Available from: https://doi.org/10.1088/1755-1315/614/1/012056
[16] MARTINEZ-GONZALEZ, J. U., RIASCOS, A. P. Activity of vehicles in the bus rapid transit system metrobus in Mexico City. *Scientific Reports* [online]. 2022, **12**, 98. eISSN 2045-2322. Available from: https://doi.org/10.1038/s41598-021-04037-6
[17] SAKHNO, V., MUROVANY, I., SHARAI, S., SELEZNEV, V. Comparative evaluation of manoeuvrability of large and extra large class buses. In: International Scientific Conference Mobile Machines: proceedings. 2017. p. 38-47.
[18] CHEN, H.-J., SU, W.-J., WANG, F.-C. Modelling and analyses of a connected multi-car train system employing the inerter. *Advances in Mechanical Engineering* [online]. 2017, **9**(8), p. 1-13. ISSN 1687-8132. Available from: https://doi.org/10.1177/16878140177017
[19] GALLUPPI, O., FORMENTIN, S., NOVARA, C., SAVARESI, S. Nonlinear stability control of autonomous vehicles: a MIMO D2-IBC solution. *IFAC-Papers* [online]. 2017, **50**(1), p. 3691-3696. ISSN 2405-8963.
[20] LUO, R., ZENG J. Hunting stability analysis of train system and comparison with single vehicle model. *Chinese Journal of Mechanical Engineering*. 2008, **44**(4), p. 184-188. ISSN 2192-8258.
[21] SAKHNO, V., POLIAKOV, V., TIMKOV, O., KRAVCHENKO, O. Lorry convoy stability taking into account the skew of semitrailer axes. *Transport Problems* [online]. 2016, **11**(3), p. 69-76. ISSN 1896-0596, eISSN 2300-861X. Available from: https://doi.org/10.20858/tp.2016.11.3.7
[22] PODRIGALO, M. A., VOLKOV, V. P. Determination of the inertia radii of the car at the design stage. *Automotive Industry.* 2003, **6**, p. 19-22. ISSN 0005-2337.
[23] SAKHNO, V., POLJAKOV, V., MYROVANY, I., SELEZNOV, V. Determination of movement stability of especially large class hybrid bus with active trailer. *INMATEN - Agricultural Engineering*. 2016, **49**(2), p. 107-118. ISSN 2068-4215.
[24] PACEJKA, H. B. *Tire and vehicle dynamics* [online]. 3. ed. Butterworth-Heinemann, 2012. ISBN 978-0-08-097016-5. Available from: https://doi.org/10.1016/C2010-0-68548-8
[25] SAKHNO, V. P., YASHCHENKO, D. M., MARCHUK, R. M., MARCHUK, N. M., LYASHUK, O. L. Research of a truck train movement when driving semi-trailer by slow downing wheels of one axis pin on the model. *International Journal of Automotive and Mechanical Engineering*. 2020, **17**(1), p. 7749-7757. ISSN 2229-8649.

IDENTIFICATION OF FLEXSPLINE PARAMETERS AFFECTING THE HARMONIC DRIVE LOST MOTION USING THE GLOBAL SENSITIVITY ANALYSIS

Peter Weis[1,*], Lukáš Smetanka[1], Slavomír Hrček[1], František Brumerčík[1], Jakub Fiačan[1], Muhammad Irfan[2]

[1]Department of Design and Mechanical Elements, Faculty of Mechanical Engineering, University of Zilina, Zilina, Slovakia
[2]Electrical Engineering Department, College of Engineering, Najran University, Najran, Kingdom of Saudi Arabia

*E-mail of corresponding author: peter.weis@fstroj.uniza.sk

Peter Weis 0000-0002-1669-4890,
Slavomír Hrček 0000-0002-8944-3128,
Jakub Fiačan 0000-0001-5171-8467,
Lukáš Smetanka 0000-0001-6583-8128,
František Brumerčík 0000-0001-7475-3724,
Muhammad Irfan 0000-0003-4161-6875

Resume

The aim of this research was to find out the specific geometrical parameters of the harmonic drive with the greatest impact on its lost motion. Harmonic drive units are widely used in production automation, robotics and automated manufacturing systems. Virtual model of Harmonic Drive was examined using the finite element method. The analyses were performed with considering the real test conditions of high precision gearboxes with a lost motion value of 4 % of the nominal output torque. The analyses' results were then used to develop a unique approach to obtain a functional relationship between the input parameters defining the shape of the flexspline and the harmonic drive lost motion value. Subsequently, the global sensitivity analysis was performed to determine the degree of influence of the selected flexspline parameters on the harmonic drive kinematic accuracy.

Article info

Received 8 November 2022
Accepted 9 January 2023
Online 2 February 2023

Keywords:

flexspline
torsional backlash
global sensitivity analysis
harmonic drive

Available online: https://doi.org/10.26552/com.C.2023.025

ISSN 1335-4205 (print version)
ISSN 2585-7878 (online version)

1 Introducion

In 1955, American scientist Clarence Walton Musser published the concept of a new transmission system called „Strain Wave Gearing“. This transmission system was based on a differential transmission with a spur gear, in which the engagement was achieved by periodic elastic deformation of one of the components [1]. Harmonic drives (HD) are distinctive particularly in their compact dimensions, transmission of high torques, small lost motion and high positional accuracy. They retain those properties, especially at steady state at constant speed. Outside the steady state, the mechanisms show a non-linear characteristics, which is manifested by a significant kinematic error in operation of these systems. The application of these transmissions depends on the various advantages of harmonic transmissions. Some applications require zero lost motion and high positional accuracy, others high torque to weight ratio [2]. Experimental measurements of Ghorbel et al. [3] allowed understanding the variation of the kinematic error, depending on the load, the angular velocity and the relative position of certain components of the mechanism. With development of the computer technology, more detailed options enabled examining the properties and dependences of the system characteristics on the mechanical properties of individual components. Further studies have investigated the stress distribution in the flexspline (FS) [4]. Other studies have dealt with the effects of the FS shape on the overall HD properties. Juan et al. [5] have dealt with the optimization of the FS shape using the LSGA program in terms of weight reduction and overall HD size. Zou et al. [6] analyzed the stress and strain of the short FS at different loads.

The harmonic drive consists of three basic components that are essential for the correct operation of the transmission. The wave generator (WG) is designed most often as a thin ball bearing pressed on an elliptical cam. The circular spline (CS) is a rigid

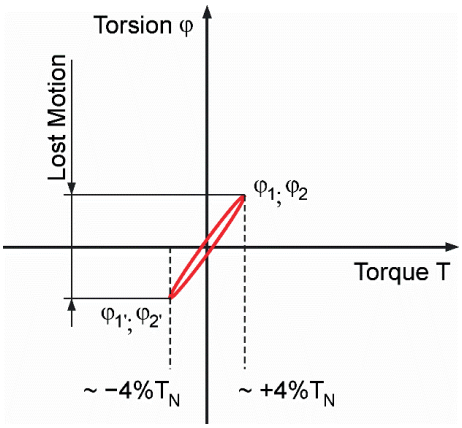

Figure 1 *Torsion characteristics of the HD by applying the ± 4% of the nominal output torque TN*

gear wheel with internal gearing. The flexspline (FS) is the most important part of the HD, which is subject to periodic elastic deformation. It has the shape of a semi-closed cylinder with external gearing at the open end. The overall properties of the HD depend mainly on properties of the WG and FS.

The aim of the presented paper was to determine the influence of selected geometrical FS parameters on the resulting kinematic accuracy, the lost motion. In the case of optimization, several design parameters of the created virtual HD model that contribute to the torsional stiffness and subsequently to the lost motion, are selected. To improve the efficiency of the optimization and design process, the process can be accelerated by eliminating the insignificant input parameters. Identification of the significant and insignificant input parameters is performed using the global sensitivity analysis (GSA), which reduces the number of input variables of the optimization problem as described by Saltelli et al. [7]. The unique method developed by Hrcek et al. [8], which identifies the key parameters of various HD components influencing its lost motion, was already well tested and described.

2 Backlash, lost motion and HD virtual model

The backlash and the lost motion terms are frequently used interchangeably in the technical literature. It is crucial to understand the distinction between the backlash and a lost motion, since the lost motion is one of the most common reasons of the positional inaccuracy in a motion system. Backlash is actually one of the components of the lost motion. It describes the state when the input torque to the mechanism does not bring any corresponding response at the output. Lost motion is a value that is determined by measuring the angular deformation in both directions with the WG fixed and CS blocked and the FS loaded with a certain torque.

Figure 1 shows the hysteresis curve obtained by the HD unit test. It records the torsional stiffness of a harmonic drive with a fixed input. Its value changes depending on the change of the transmitted load. The nonlinear torsion characteristics arises due to the thin-walled construction of the FS. It is important because of the elastic elliptical deformation occurring below the area of the outside FS gearing during the operation of the harmonic transmission system.

With increasing load, an increasing number of teeth engages due to the elastic deformation of the FS and the torsional stiffness increases. The number of engaged teeth changes while the HD gearbox is running. In addition to the torsional characteristics, related to the variable number of teeth, the characteristics in Figure 1 also depends on the elastic deformation of the FS cylindrical thin-walled part by the action of torque. The measurement of the torsional stiffness of the harmonic drive takes place with a fixed WG, using a rotation of FS in both directions with the ± 4% of the nominal output torque T_N.

Calculation of the torsional stiffness constant, which expresses the dependence of the rotation on the value of the applied torque can be expressed as

$$C = \frac{T}{\varphi}, \tag{1}$$

where:
T (Nm) - applied torque;
$\varphi\,(rad)$ - angular displacement.

The lost motion is defined as the angular delay of the output shaft upon changing the direction of rotation of the input shaft, while in the working condition. It follows from the definition that during the measurement, the input shaft is driven by torque and the backlash is measured on the output shaft. Furthermore, the term “in the working condition” means that the output shaft is under the torque load. The analysis of harmonic transmission revealed that the lost motion is caused not only by the backlash, but by elastic deformation, as well [9].

The lost motion of the harmonic transmission is caused by backlash in the gearing between the circular spline and flexspline, as well as by the backlash in the

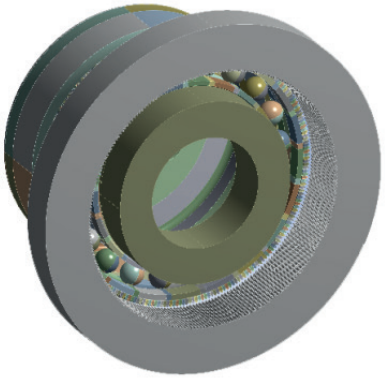

Figure 2 *The geometry of the tested HD unit*

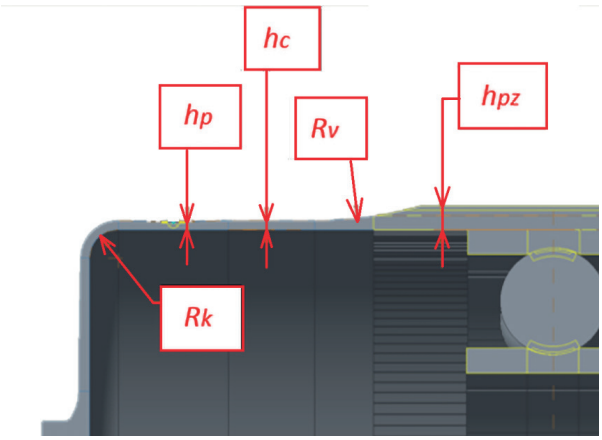

Figure 3 *Selected relevant FS dimensions affecting the HD kinematic accuracy presented on the 3D virtual mode*

Oldham coupling of the Wave generator. The source of backlash caused by elastic deformation is the flexspline under the torque load. The main causes of the backlash in the harmonic drive include [9]:

- Error in machining of the flexspline and circular spline gearing;
- Error in machining of the cam profile;
- Incorrect assembly of the three main components of the harmonic drive;
- Coupling backlash;
- Elasticity of flexspline and other parts.

The lost motion is defined with a nonlinear function that includes the backlash effect as well as the torsional characteristics of the engaging teeth with varying loading torque. This function approximates the real HD torsion characteristics and it is described by the equation [10]

$$f(\delta) = \begin{cases} \delta - b_s, \delta \geq b_s \\ 0, -b_s \leq \delta \leq b_s \\ \delta + b_s, \delta \leq b_s \end{cases}, \quad (2)$$

where the backlash equals to $2\,b_s$.

The loss of contact between the teeth is a phenomenon that occurs especially in systems that are loaded with little or no tor que. Loss of contact and subsequent contact are a source of shocks that cause noise and strong vibrations. These in turn affect the efficiency, wear and reduce the overall life of the mechanism [11]. The kinematic accuracy is defined as the sum of the positive and negative differences between the theoretical and actual rotation output angle. The kinematic accuracy of the examined HD is less than 1 angular minute (arc min) without load and decreases to about 30 angular seconds (arc secs) with loaded gear.

In order to perform the FEM analysis an HD virtual model displayed in the Figure 2 was build following the description published by Majchrak et. al., where the finite element mesh is also described [12-14].

The resulting lost motion is influenced by many geometric parameters of the FS. The selected ones are:

- thickness under teeth $x_1 = h_{pz}$ (mm),
- thickness of cylindrical part of FS $x_2 = h_c$ (mm),
- lead radius of the gearing $x_3 = R_v$ (mm),
- end radius of cylindrical part $x_4 = R_k$ (mm),
- depth of the undercut $x_5 = h_p$ (mm).

The selected relevant FS dimensions are shown in Figure 3.

The lost motion of the HD virtual model was calculated in the ANSYS Workbench software. The material of the harmonic drive components was steel with a Young's modulus of E = 210,000 MPa and a Poisson's ratio of 0.3. Each harmonic driving component must be strained only in the elastic region; therefore, it is enough to use a linear material model where Hooke's law can be employed, as described in [8]. The nonlinear studies were performed since all the contact conditions between the HD components were determined by the Frictionless type of contact. No bonded contact type was considered.

3 Global sensitivity analysis

In order to define the most important parameters from the chosen FS dimension set, which most affect the lost motion, it is necessary to use appropriate techniques for calculating the decision-making values referring to the required variable. The global sensitivity analysis was used in this research to identify the relevant FS dimensions usable by its further optimization with accent on the HD lost motion minimization.

3.1 Functional dependence definition

To be able to express the dependence between individual changing parameters of the FS and the value of the lost motion in more detail using GSA, one first needs to know the functional dependence between the output (HD lost motion) and the input parameters (FS dimensions), $y = f(x_1, x_2, x_3, x_4, x_5)$.

To get a better picture of the dependence between the inputs parameters (iPx - selected dimensional parameters) and the output parameter (oP - lost motion) the linear regression analysis was performed. The red curve in Figure 4 interprets linear interpolation between the lost motion and the spesific dimension parameter. The black curve interprets the exponentional interpolation. The steepness of the red curve defines a sensitivity dependance between the input and the output parameters. The most popular method for solving the task is a simple linear regression. The general form is:

$$oP_{(i)} = b_0 + \sum_{j=1}^{n} b_j iP_j^{(i)}, \tag{3}$$

where the coefficients are b_0, b_j determined by the least square computation, based on the squared differences between the y-values produced by the regression model

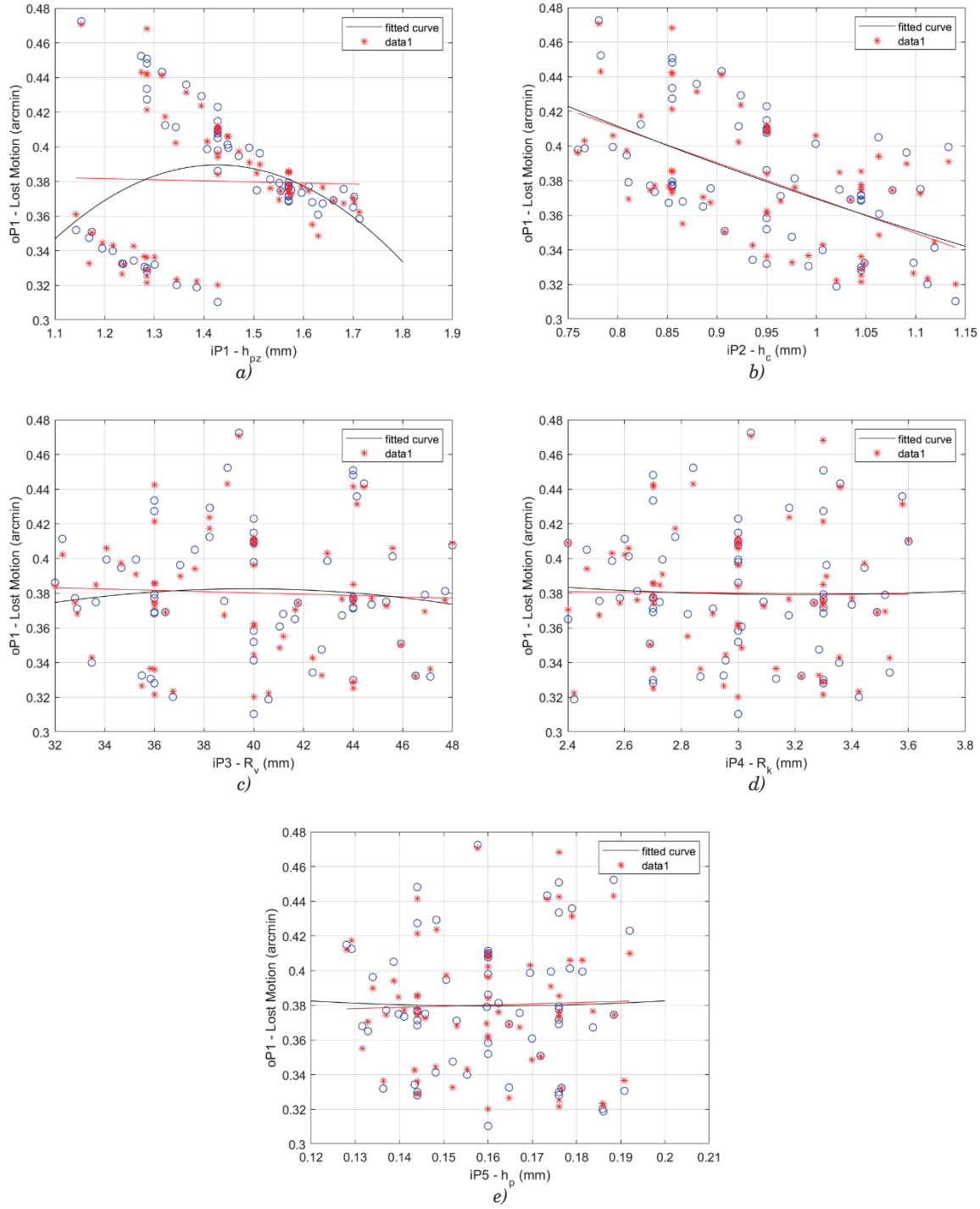

Figure 4 *Comparison of the FEM analysis lost motion results (blue circles) and the lost motion values calculated by the expressed functional dependence (red asterisks): (a) Thickness under gearing; (b) Thickness of the cylindrical part of FS; (c) Lead radius of the gearing; (d) End radius of the cylindrical part; (e) Depth of the undercut*

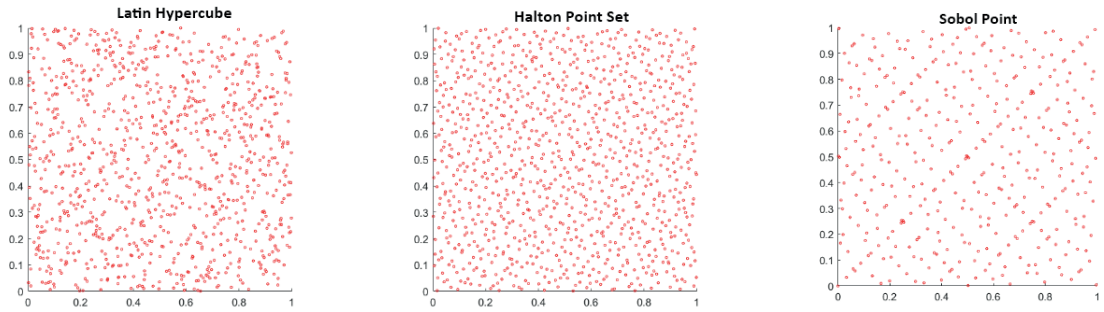

a) *b)* *c)*

Figure 5 *Quasi random variables scatter plots: (a) Latin Hyper Cube; (b) Halton Point Set; (c) Sobol Point*

and the actual model output obtained from the FEM analysis data. For verification, the quadratic coefficient of determination was calculated as well. The calculated value $R^2 = 0.96$ indicates a very good match between the data from the FEM analysis and the calculated data. The FEA results and the fitted curve function results comparison is shown in Figure 4.

3.2 Generating random numbers

After the functional dependence was obtained according to Equation (3) and proved by the quadratic coefficient of determination value, the task of a big set of the input and output variables arised in order to perform the GSA. It would be extremely time consuming to create such a big set of input and output values by the FEM, therefore the generation of the random numbers, based on former calculations, was carried out.

There are many ways to generate as random numbers as possible, but in some cases entire randomness of numbers is actually not desirable. For some types of applications, it is much more important to achieve as even random coverage of the sampled integration domain as possible, than being the numbers truly random. One of the problems with the random sequence of numbers is that the numbers can form clusters in some areas. The overall coverage of the interval may be uneven. On the other hand, the problem of a completely uniform random coverage of the interval is the possible creation of a completely uniform grid of points, which is also undesirable in some cases [15].

Quasi random sequences of numbers represent a compromise between these extremes. These sequences cannot be considered random, as they are deterministic sequences that are designed to provide as even coverage of the sampled interval as possible for a given sample and at the same time to look “sufficiently random”. The individual elements of quasi random sequences deliberately avoid each other in order to avoid the clusters that we observe in random sequences [15]. Several methods for selecting the quasi random numbers are known. In this case, we selected three methods that met the requirements of this research:

- Latin Hypercube;
- Halton Point Set;
- Sobol Point.

The graphical representations of the generated random points (scatter plots) according to these methods are shown in Figure 5.

The calculated values of the lost motion for the individual input parameters from the expressed function, based on the quasi random variables scatter plot by Sobol Point, are shown in Figure 6. The cyclic procedure of their calculation started with a small number of the quasi random variables, which was gradually increased until the convergence was reached. The Sobol Point method was chosen due to the possibility of solving higher order interaction of the input parameters. In order to calculate the Sobol indices, it is necessary to include a large number of data sets in the range of 1000 - 10000 in the analysis. Due to the better comprehensibility of the graphs, only thirteen of them are displayed. The data sets are generated from the detected dependencies of individual input parameters on the output parameter from the FEM analysis.

3.3 Sobol indices calculation

To generate the quasi random data for further GSA, the Sobol Point method was used. The advantage of this method was the speed of data generation. We know several Sobol´s indices [16], but for our calculation the first-order sensitivity index and the total-order index are important. Let the generic model, described in more detail in [7], be used:

$$Y = f(X_1, \ldots, X_p). \tag{4}$$

The output Y is a scalar, while the input elements $X_1, \ldots, X_p$ are independent random variables with known probability distributions. Those distributions reject the system‘s uncertain knowledge. The primary idea behind this strategy is to break down the output variation into contributions from each input factor. Derivation of the

relation for calculation is described by Homma and Saltelli [17]. Using the law of total variance, one can write

$$V(Y) = V_{Xi}(E_{X\sim i}(Y|X_i)) + E_{Xi}(V_{X\sim i}(Y|X_i)), \quad (5)$$

where V is a expected value of process variance and E is a variance of the hypothetical means. The first-order influence of X_i on Y is known as the conditional variance $V_{Xi}(E_{X\sim i}(Y|X_i))$ and the sensitivity measure

$$S_i = \frac{Vx_i(E_{X\sim i}(Y|X_i))}{V(Y)} \quad (6)$$

is known as the first-order sensitivity index of X_i on Y. S_i. S_i is a number always between 0 and 1. The total-order sensitivity index, ST_i described to account for all contributions to output variation owing to factor X_i (i.e. the first-order index plus all its interactions):

$$ST_i = \sum_{k\neq 1} S_k, \quad (7)$$

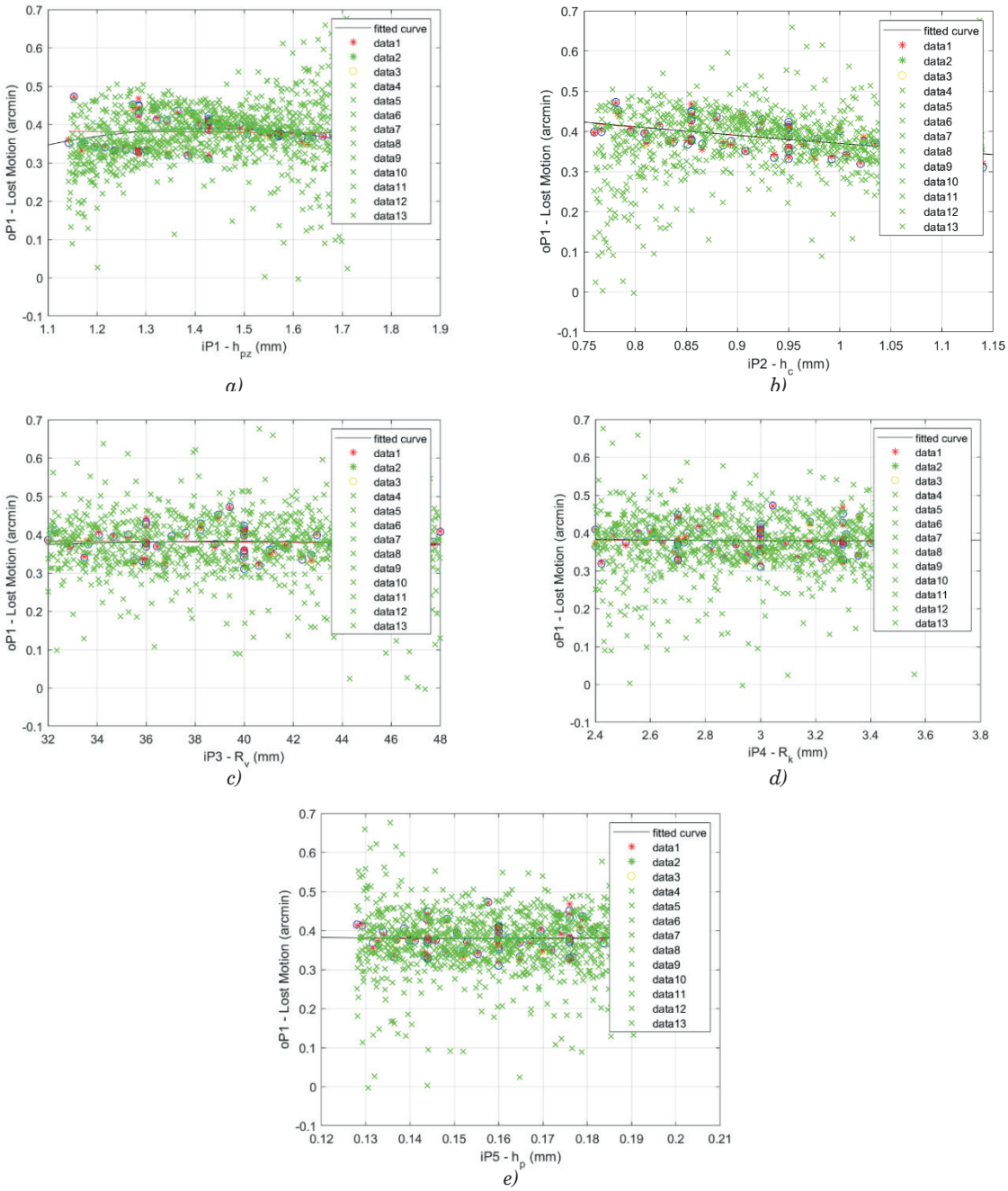

Figure 6 *The lost motion values of the fitted function calculated for the Sobol Point data set: (a) Thickness under gearing; (b) Thickness of the cylindrical part of FS; (c) Lead radius of the gearing; (d) End radius of the cylindrical part; (e) Depth of the undercut*

where $k \neq 1$ indicates all the indices associated to the factor X_i. The total-order index can be expressed as

$$ST_i = 1 - \frac{Vx\sim_i(E_{Xi}(Y|X_{\sim i}))}{V(Y)} \quad (8)$$

and using again the law of total variance and normalizing we get

$$1 = \frac{Vx\sim_i(E_{Xi}(Y|X_{\sim i}))}{V(Y)} + \frac{Ex\sim_i(V_{Xi}(Y|X_{\sim i}))}{V(Y)}. \quad (9)$$

The second term in equation (9) is the total-order index [15]

$$ST_i = \frac{Ex\sim_i(V_{Xi}(Y|X_{\sim i}))}{V(Y)}. \quad (10)$$

The graphically illustrated influence of individual input parameters with respect to the output parameter using GSA can be seen in Figure 7. The First order is represented by the red columns and the Total effect by the blue columns. The resulting values of Sobol's indices are presented in Table 1.

4 Finding and discussion

The presented research dealt with the analysis of the lost motion in a harmonic drive. depending on changing some design parameters of the harmonic drive flexspline. Based on the knowledge from previous research focused on the influence of various HD parameters on its lost motion. The flexspline was selected as the key component of the HD unit. Based on the experience gained, five key geometric parameters, defining the FS geometry with the highest impact on the lost motion, were selected. The examined gearbox was loaded with ± 4 % of the rated output torque, which simulated the real conditions of high precision harmonic drives for robotic and automated manufacturing system applications.

The calculated First-order and Total-effect Sobol's indices in Table 1 indicate that the thickness under the gearing h_{pz} and the thickness of the cylindrical part of FS h_c have the greatest affect to the lost motion. The above mentioned results are consistent with the assumptions based on previous experience with harmonic drive unit design. These identified parameters had the greatest impact on the lost motion even in prototype tests.

The results obtained using the method based on the GSA developed by Hrcek et al. and described in detail in [8] allow to identify unambiguously the relevant parameters affecting the HD kinematic accuracy not only by parameters of various HD components but by various parameters of a the flexpline, as well. The results can help by optimizing the FS and thus the whole HD unit. Based on the results of the used method based on the GSA, the entire optimization process can be accelerated by eliminating irrelevant parameters and thus reducing the number of variants needed for the time consuming finite elements analyses.

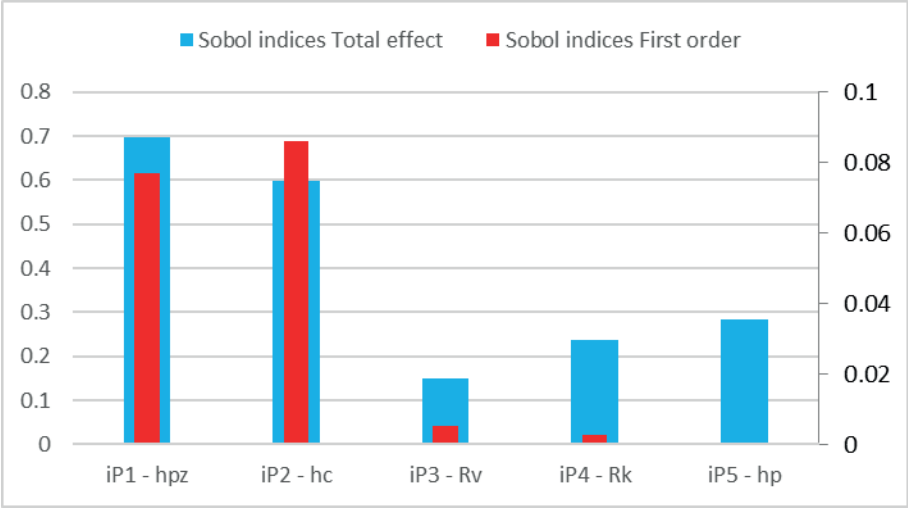

Figure 7 *Results of calculating the Sobol's first-order and total-effect indices*

Table 1 *Values of the calculated Sobol's indices*

FS dimension		iP1 (h_{pz})	iP2 (h_c)	iP3 (R_v)	iP4 (R_k)	iP5 (h_p)
Correlation coefficient	Sobol indices First order	0.0771500	0.0859400	0.0052840	0.0027370	0.0001973
	Sobol indices Total effect	0.6969000	0.5974000	0.1497000	0.2385000	0.2825000

5 Conclusion

The main contribution of the presented research is the clear identification of the input dimensional parameters with the greatest influence on the lost motion. So far, such a precisely quantified dependence has not yet been published in scientific publications. The findings can be used in the design process of harmonic gearboxes. The early stage design process can be directly focused on the specific dimensional parameters with the greatest impact on the lost motion. On the the other hand, less attention can be paid to parameters with less impact. Further research will be focused on investigating the influence of other dimensional parameters on the kinematic properties of harmonic gearboxes. Another goal will be to investigate the torsional properties of individual componets of harmonic gearboxes, as well as the transmission system as a whole unit.

Acknowledgements

This research was funded by Slovak Research and Development Agency, grant number APVV-18-0450 Research of the influence of design parameters of special transmissions with a high gear ratio with respect to kinematic properties.

Conflicts of interest

The authors declare that they have no known competing financial interests or personal relationships that could have appeared to influence the work reported in this paper.

References

[1] MUSSER, C. W. Strain wave gearing. U.S. Patent No. 2,906,143. 29 September 1955.
[2] SHEN, Y. W., YE, Q. T. Theory and design of harmonic drive. Beijing, China Machine Press, 1985.
[3] GHORBEL, F. H., GANDHI, P. S., ALPETER, F. On the kinematic error in harmonic drive gears. *Journal of Mechanical Design* [online]. 2001, **123**, p. 90-97. ISSN 1050-0472, eISSN 1528-9001. Available from: https://doi.org/10.1115/1.1334379
[4] JEONG, H. S., OH, S. H. A study on stress and vibration analysis of a steel and hybrid flexspline for harmonic drive. *Composite Structures* [online]. 1999, **47**(1-4), p. 827-833. ISSN 0263-8223, eISSN 1879-1085. Available from: https://doi.org/10.1016/S0263-8223(00)00060-X
[5] FOLEGA, P., WOJNAR, G., BURDZIK, R., KONIECZNY, L. Dynamic model of a harmonic drive in a toothed gear transmission system. *Journal of Vibroengineering* [online]. 2014, **16**(6), p. 3096-3104. ISSN 1392-8716, eISSN 2538-8460. Available from: https://www.extrica.com/article/15571
[6] LI, S. T. A challenge to design of a new harmonic drive device. *Applied Mechanics and Materials* [online]. 2011, **86**, p. 43-46. ISSN 1662-7482. Available from: https://doi.org/10.4028/www.scientific.net/AMM.86.43
[7] SALTELLI, A., RATTO, M., ANDRES, T., CAPOLONGO, F., CARIBONI, J., GATELLI, D., SAISANA, M., TARANTOLA, S. *Global sensitivity analysis*. The primer. 1. ed. Chichester: John Wiley and Sons, Ltd, 2008. ISBN 978-0-470-05997-5.
[8] HRCEK, S., BRUMERCIK, F., SMETANKA, L., LUKAC, M., PATIN, B., GLOWACZ, A. Global sensitivity analysis of chosen harmonic drive parameters affecting its lost motion. *Materials* [online]. 2021, **14**(17), 5057. eISSN 1996-1944. Available from: https://doi.org/10.3390/ma14175057
[9] WANG, B., LIU, J., WANG, C. Measurement and analysis of backlash on harmonic drive. *IOP Conference Series: Materials Science and Engineering* [online]. 2019, **542**, 012005. ISSN 1757-8981, eISSN 1757-899X. Available from: https://doi.org/10.1088/1757-899x/542/1/012005
[10] SWIC, A., DRACZEW, A., GOLA, A. Method of achieving of thermo-mechanical treatment of low-rigidity shafts. *Advances in Science and Technology - Research Journal* [online]. 2016, **10**(29), p. 62-70. ISSN 2299-8624. Available from: https://doi.org/10.12913/22998624/61934
[11] AMEZKETA, M., IRIARTE, X., ROS, J. Dynamic model of a helical gear pair with backlash and angle-varying mesh stiffness. 2009.
[12] MAJCHRAK, M., KOHAR, R., LUKAC, M., SKYBA, R. The process of creating a computational 3D model of a harmonic transmission. *MM Science Journal* [online]. 2020, **13**, p. 3926-3931. ISSN 1803-1269, eISSN 805-0476. Available from: https://doi.org/10.17973/MMSJ.2020_06_2020009
[13] MAJCHRAK, M., KOHAR, R., KAJAN, J., SKYBA, R. 3D meshing methods of ball-rolling bearings. *Transportation Research Procedia* [online]. 2019, **40**, p. 784-791. ISSN 2352-1457, eISSN 2352-1465. Available from: https://doi.org/10.1016/j.trpro.2019.07.111
[14] MAJCHRAK, M., KOHAR, R., LUKAC, M., SKYBA, R. Creation of a computational 2D model of harmonic gearbox. In: *Current Methods of Construction Design. Lecture Notes in Mechanical Engineering* [online]. MEDVECKY, S., HRCEK, S., KOHAR, R., BRUMERCIK, F., KONSTANTOVA, V. (eds.). Cham: Springer, 2020.

ISBN 978-3-030-33145-0, eISBN 978-3-030-33146-7, p. 95-103, Available from: https://doi.org/10.1007/978-3-030-33146-7_11

[15] KALOS, M. H., WHITLOCK, P. A. Monte Carlo methods. 2. ed. Weinheim: Wiley-VCH, 2008. ISBN 978-3-527-40760-6.

[16] SOBOL, I. M. Sensitivity estimates for nonlinear mathematical models. *Mathematical Modelling and Computational Experiments*. 1993, **4**, p. 407-414. ISSN 1061-7590.

[17] HOMMA, T., SALTELLI, A. Importance measures in global sensitivity analysis of nonlinear models. *Reliability Engineering and System Safety* [online]. 1996, **52**, p. 1-17. ISSN 0951-8320, eISSN 1879-0836. Available from: https://doi.org/10.1016/0951-8320(96)00002-6

METHODOLOGY FOR MAINTAINING THE DYNAMIC CHARACTERISTICS OF PASSENGER CARS

Igor Martynov[1], Juraj Gerlici[2], Alyona Trufanova[1], Vadim Shovkun[1], Vadim Petukhov[1], Oleksandr Safronov[3], Kateryna Kravchenko[2,*]

[1]Ukrainian State University of Railway Transport, Kharkiv, Ukraine
[2]University of Zilina, Zilina, Slovak Republic
[3]State Enterprise Ukrainian Scientific Railway Car Building Research Institute, Kremenchuk, Ukraine

*E-mail of corresponding author: kateryna.kravchenko@fstroj.uniza.sk

Igor Martynov 0000-0002-0481-3514,
Alyona Trufanova 0000-0003-1702-1054,
Vadim Petukhov 0000-0003-4781-9956,
Kateryna Kravchenko 0000-0002-3775-6288
Juraj Gerlici 0000-0003-3928-0567,
Vadim Shovkun 0000-0002-7070-7883,
Oleksandr Safronov 0000-0002-5865-7751,

Resume

The work presents the results of a statistical analysis of random processes of the coefficient of vertical dynamics of a passenger car variation. To determine the dynamic performance of cars the tests were running on the tracks of JSC "Ukrzaliznytsia". The main statistical characteristics of random processes are determined for various modes of car movement along curved and straight sections of the track. As a result of statistical processing of experimental data, correlation functions have been constructed that characterize the degree of connection between different time sections of the process of changing the coefficient of vertical dynamics. The obtained indicators of the law of distribution of the vertical dynamics coefficient values, approximating the models of correlation functions and the numerical values of their parameters, make it possible to further simulate the process of loading a passenger car without carrying out lengthy expensive tests.

Article info

Received 18 October 2022
Accepted 22 December 2022
Online 9 February 2023

Keywords:

passenger car
track section
vertical dynamics coefficient
correlation function

Available online: https://doi.org/10.26552/com.C.2023.027

ISSN 1335-4205 (print version)
ISSN 2585-7878 (online version)

1 Introduction

Facing the growing competition between different kinds of transport one must pay more attention not only to ensure fast transportation of passengers with maximum comfort, but to reliable and coordinated operation of all the parts of railway transport, as well.

In recent years, due to insufficient investment in railways of Ukraine, there has been an increase in physical wear and tear and obsolescence of the operational fleet of passenger cars of JSC "Ukrzaliznytsia".

Most of the passenger car fleet was built in the 70s and 90s of the last century, at the railcar-building plants in Germany (Waggonbau Ammendorf) and the Russian Federation (Kalinin Carriage Plant, nowadays Tver). According to the Passenger Company branch of JSC "Ukrzaliznytsia", most of the cars in the inventory fleet have served their assigned service life. As a result, the current wear of the passenger car fleet is approaching 92 %. Therefore, an urgent issue to increase the competitiveness of rail passenger transport is to overcome the high degree of wear of the passenger cars fleet of JSC "Ukrzaliznytsia".

In recent years, JSC "Ukrzaliznytsia" has been renovating passenger cars in order to extend their service life. That resulted in partial restoration of technical and operational characteristics of the car. However, it is necessary to understand that it is impossible to completely restore cars to the initial condition. Therefore, the analysis of dynamic characteristics of the passenger cars, which have undergone renovation, is an urgent task.

2 Analysis of recent research and publications

The dynamic loading of rail vehicles depends on many factors. Therefore, a significant number of works in different countries of the world are devoted to the study of these issues. A number of scientific studies have

been devoted to the issues of rolling stock dynamics, the determination of vertical and horizontal forces and the study of their influence on stability, strength and traffic safety.

It should be noted that both theoretical and experimental methods for studying dynamics of the rolling stock are constantly being improved with the development of measuring instruments and information processing. The use of modern computer technology makes it possible to obtain results that are important for design of the modern rolling stock.

In article [1], the authors compare the dynamic performance of freight cars equipped with three different types of bogies (models 18-100, Y25, 18-9771). The researchers came to the conclusion that the values of the coefficient of vertical dynamics of the non-sprung part of the car are almost the same for all three models of bogies, on a straight section of the track. The authors also recommend improving the dynamic performance of the car bogies by choosing rational parameters of the spring suspension.

The studies of the specialists of the Faculty of Mechanical Engineering University of Žilina are devoted to issues of dynamic interaction of the rolling stock with the superstructure of the track [2-4]. The authors have developed the solid-state models of passenger cars that allow simulating the real dynamic interactions of the rolling stock, taking into account the rigidity-damping parameters of the railway track. The paper presents simulation calculations for three different models and determines the stiffness-damping parameters of a rail vehicle.

Thus, when modeling the dynamic load of passenger cars, in order to simplify the mathematical model, the authors of papers [5-6] considered the body and bolsters as one inertial element of the car. However, if it was necessary to determine the acceleration of the body capabilities of such models, that turn out to be insufficient. To determine the forces of interaction and mutual displacements of the body and bolsters of the car in studies [7-8], experts considered these structural elements as separate. It is considered that the body rests on the bolsters in four points (slides).

The article [9] shows the results of mathematical modeling of spatial oscillations of passenger cars by determining the forces of dynamic interaction of bodies and bogies, which are used to determine the dynamic running characteristics and strength. The publication [10] evaluates the dynamic qualities of a passenger compartment car model 61-779, constructed by OJSC "Kryukiv Railway Car Building Plant".

Hydraulic vibrations play an important role in ensuring the smooth running of bogies. In the study [11], the authors considered the influence of the parameters of hydraulic vibration dampers of bogies on the dynamics of cars. Numerical analysis has shown that the critical velocity and the stability index increase with an increase in the damping diaphragm and flow area. As the spring stiffness increases, the critical velocity increases and the stability index decreases.

In the rolling stock dynamics, in describing the contact interaction of a wheel with a rail, the theory of creep (elastic sliding) has found application. In [12], a wheel pair is considered as a nonlinear dynamic system. By means of computer simulation, the authors determined the range of the car speeds within which a stable trivial solution and a stable solution of the limit cycle coexist. Their dependence on the car speed is shown.

Issues of the influence analysis of the wheel tread surface taper parameters and the transverse movement of the wheel along the rails are considered in articles [13-15]. The authors show the influence of the geometric parameters of the wheels and the speed of the car on the value of the maximum contact force and its distribution in the contact zone.

The use of analytical methods of the rolling stock dynamics had serious limitations until the middle of the 20th century, since it was based on linear differential equations that do not take into account important features of the design and modes of movement of the rolling stock.

With introduction of the computer technology, there has been a qualitative leap in theoretical studies of dynamics, as well as in processing the results of dynamic tests. The results of computer simulation of the damaged wheels interaction with rails are analyzed in papers [16-19]. The analyzes were focused on evaluating the smoothness of the rail vehicle and its damaging effect on the vehicle. The issues of influence of the vertical static and dynamic loads on the load in the zone of a wheel with a rail, as well as methods of their transmission, are considered in [20].

However, it should be noted that in the scientific literature not much attention is paid to the study of the statistical dynamics of the rolling stock. It is known that the change in time of the dynamic indicators of the car is a random process. However, the characteristics of these processes have not been studied enough and require further in-depth study.

3 Problem statement

The study of loads acting on the rolling stock from the rail track is the most responsible section of the rolling stock dynamics. This is due to the complexity of the interaction of the rolling stock and the track structure.

Conventionally, all the forces of interaction of cars and tracks can be divided into two groups. The first group includes vertical forces acting on the wheelsets of cars, while the second one includes the horizontal loads. They depend on many factors. Therefore, it is advisable to reduce the variety of random factors to one or more equivalents.

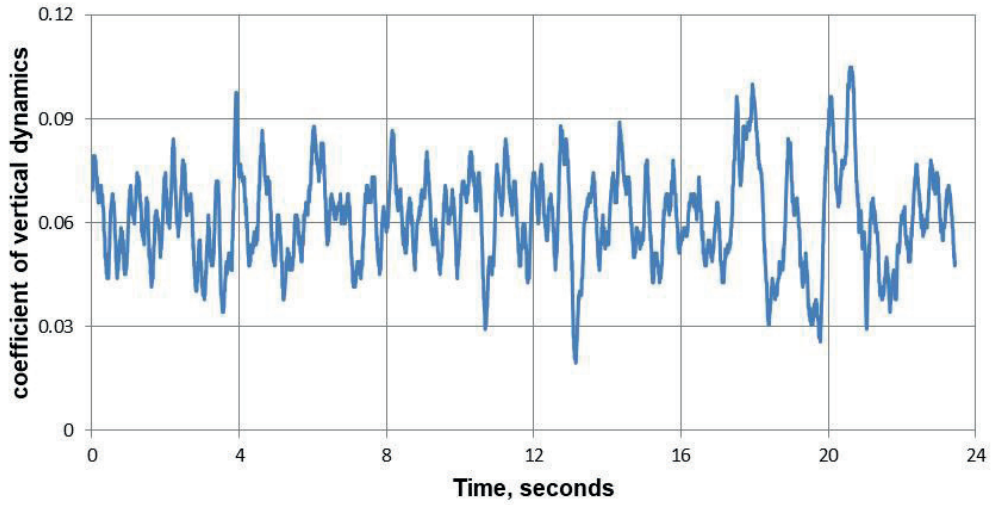

Figure 1 *Change of the coefficient of vertical dynamics at a speed of 40 km/h on a straight track section*

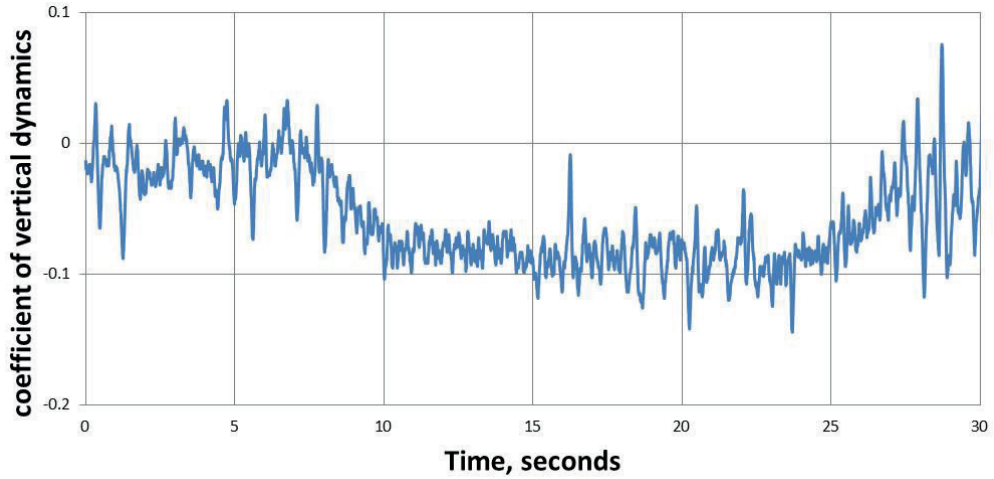

Figure 2 *Change in the coefficient of vertical dynamics at a speed of 110 km/h on the track curved section*

The main indicators that characterize the dynamic qualities of the rail rolling stock in accordance with the requirements of current regulations [21-22] are coefficients of vertical load of bolsters and bogie frames of passenger cars.

To determine the dynamic performance of rigid compartment cars, which were renovated, were running tests on the tracks of JSC "Ukrzaliznytsia". During the tests, the ambient temperature did not exceed 28 °C and the relative humidity was 80 %.

The tests were carried out on straight sections of the track, as well as on curves sections of the track of small ($R \leq 350$ m), medium ($350 < R < \leq 650$ m) and large ($R > 650$ m) radius.

According to the requirements of the JSC Ukrzaliznytsia, one passenger car was subjected to dynamic tests. Since all the passenger cars of this type have the same design and technical characteristics, the results can be extended to the entire fleet of wagons.

Dynamic loading processes of cars, which were registered on magnetic media, were processed by the program for calculating instantaneous values of process amplitudes. Test results were recorded were conducted in both directions of train movement with a total duration of at least 300 s in each speed range. The sampling frequency of records of dynamic processes was chosen more than 128 Hz, which allowed determining the indicators in the required frequency range. For each random process, calculations were performed and the maximum values of the probability of vertical loads were determined. At the first stage, one indicator value was determined within each speed range, starting from a speed of 40 km/h. Some results for speed of 40 km/h and 110 km/h are presented in Figures 1 and 2, respectively.

Analyzing the results, partly shown in Figures 1 and 2, it can be concluded that with increasing the car speed the general amplitude of the vertical dynamic coefficient, considered without the second-order oscillations, becomes more clearly defined with a pronounced cyclicality.

The process the coefficient of vertical dynamics variation in time is a random process.

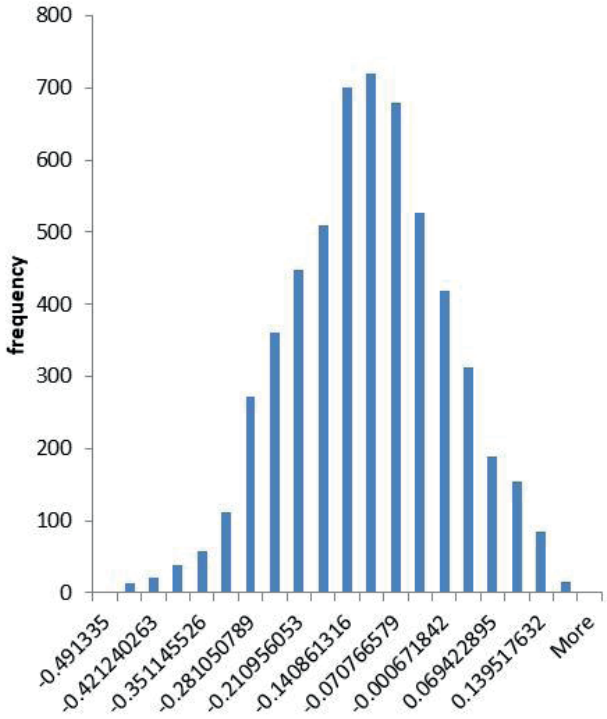

Figure 3 *Distribution of instantaneous values of the vertical dynamics' coefficient at 100 km/h on the track straight section*

It should be noted that when evaluating the driving performance of a car, a check is made to see if the maximum values of the vertical dynamics' coefficient exceed the threshold values regulated by the regulatory document. The influence of high-frequency oscillations on the stress-strain state was not considered in this case.

The second stage determined the following characteristics of a random process, namely mathematical expectation, variance and minimum and maximum efforts values.

The results of statistical processing show that the random processes that characterize the coefficient of vertical dynamics are distributed according to the normal law (Figure 3).

The parameters characterizing this law were obtained and are presented in Table 1.

Testing the hypothesis about the correspondence of the empirical distribution was carried out according to the well-known goodness of fit criteria of mathematical statistics. Thus, for the results of processing the instantaneous values of the coefficient of vertical dynamics, at a speed of 100 km/h on a straight section of the track (Figure 4), at a significance level of 0.05, the value of the coefficient χ^2 was 2.8 at $\chi_{cr} = 6.2$. Therefore, the hypothesis of a normal distribution is not rejected.

Mathematical expectation and variance are important characteristics of a random process, but they do not give a sufficient idea of the nature of individual implementations of a random process.

The correlation function (CF) of a random process is called the non-random function of two arguments, which, for each pair of arbitrarily selected values of arguments (time points), is equal to the mathematical expectation of the product of the two random variables of the corresponding sections of the random process, [23].

Table 1 *The value of the distribution parameters*

Speed (km/h)	Movement mode	Mathematical expectation	Variance
40	straight track section	0.06129	0.00018
	curved track section	0.062302	0.00015
80	straight track section	-0.012078	0.00017
	curved track section	-0.02671	0.00083
110	straight track section	-0.00947	0.00034
	curved track section	-0.00772	0.00056
160	straight track section	-0.09838	0.00076
	curved track section	-0.09804	0.00056

$$K_x(t,t_1) = M[X(t)X(t_1)] = \int_{-\infty}^{\infty}\int_{-\infty}^{\infty} X(t)X(t_1)\times \times\omega_2(X,t,X_1,t_1), \quad (1)$$

where ω_2 (X, t, X_1, t_1) is a two-dimensional probability density.

That is, the CF determines the dependence of the random variable at the next time point x (t_1) on the previous value of $X(t)$ at time tt; i.e. it is a measure of the relationship between them, namely a correlation measure between them.

The need to approximate the CF arises whenever it is necessary to have an analytical description of the experimental correlation function to solve certain problems.

Finding an approximating expression for CF can be done as follows:

- a linear combination of a finite number of functions (approximation by functions of the form $\varphi_x(\tau) = \sigma_x^2 e^{-\alpha_x\tau}\cos\beta_x\tau$);
- a finite series of exponential functions system;
- an infinite series of some definite system of functions (possible partial approximation by step series, orthogonal functions, asymptotic series, etc.).

Denote by $X[i] = X(t_i), t_i = i\Delta t; i = \overline{1,n}$ stationary ergodic random sequence, where Δt is the interval of discreteness of measurements of a stationary random process $X(t)$.

The random processes of change of vertical dynamics coefficients are considered as stationary and ergodic.

The CF estimation of the ergodic stationary random process $X(t)$ can be determined by one of its implementations $x(t)$. From this point on, the sequence $x[i] = x(t_i), i = \overline{1,n}$ is used.

The CF estimation $\hat{K}_x[j] = \hat{K}_x(t_j)$, $(t_j = j\Delta t; j = \overline{1,n})$ is determined by the following formulas:

$$\hat{K}_x[j] = \frac{1}{n-j}\sum_{i=1}^{n-j}[x(i) - \hat{m}_x][x(i+j) - \hat{m}_x], \quad j = \overline{0,m}, \quad (2)$$

where,

$$\hat{m}_x = \frac{1}{n}\sum_{i=1}^{n} x(i). \quad (3)$$

In Equation (3) - $x(i+j); t_{i+j} = (i+j)\Delta t; \hat{m}_x$ is the estimation of the mathematical expectation of the sequence $x(i), i = \overline{1,n}$.

To approximate the obtained estimate of CF in this case, it is advisable to use the analytical dependence in the form of a decaying cosine.

$$\hat{K}_x[j] \approx \sigma_x^2 e^{-\alpha_x\tau}\cos\beta_x j\Delta t, j = \overline{0,m}, \quad (4)$$

where $\sigma_x, \beta_x, \alpha_x$ are the parameters to be determined.

The parameter σ_x is defined as follows:

$$\sigma_x = \sqrt{\hat{K}_x[0]}. \quad (5)$$

If one uses a normalized correlation function, σ_x will be equal to unity.

To obtain the value of the parameter β_x, determine the estimate of the one-sided spectral density $\hat{G}[k] = \hat{G}[f_k], k = \overline{0,m}$ according to the following Equation [24]:

$$\hat{G}[k] = 2\Delta t\left[\hat{K}_x[0] + 2\sum_{r=1}^{m-1}\hat{K}_x[r]\cos\left(\frac{\pi rk}{m}\right) + + (-1)^k\hat{K}_x[m]\right], k = \overline{0,m}, \quad (6)$$

$$\left.\begin{aligned} f_k &= \frac{kf_c}{m} = k\Delta f, k = \overline{0,m},\\ f_c &= \frac{1}{2\Delta t}; \Delta f\frac{f_c}{m}, \end{aligned}\right\} \quad (7)$$

where, $\Delta f = f_{k+1} - f_k, = \overline{0,m-1}$;
f_c is the cutoff frequency, Hz.

Smoothed estimate spectral density $G^*[k], k = \overline{0,m}$ according to [13] is defined as follows:

$$\left.\begin{aligned} G^*(0) &= 0.5\hat{G}(0) + 0.5\hat{G}(1,)\\ G^*(k) &= 0.25\hat{G}(k-1) + 0.5\hat{G}(k) +\\ &+ 0.25\hat{G}(k+1), k = \overline{1,m-1},\\ G^*(m) &= 0.5\hat{G}(m-1) + 0.5\hat{G}(m). \end{aligned}\right\} \quad (8)$$

Further on, it is necessary to find the maximum element in the array $G^*[k], k = \overline{0,m}$ and index of this element $k = k_2^*$. Then the parameter β_x is defined as follows:

$$\beta_x = 2\pi k_2^*\Delta f. \quad (9)$$

The parameter α_x can be determined from the following condition:

$$F(\alpha_x) = \sum_{j=0}^{m1}[\hat{K}_x(j) - \sigma_x^2 e^{-\alpha_x j\Delta t}\cos\beta_x j\Delta t] = \min \quad (10)$$

To find α_x from Equation (10) one obtains the following equation:

$$W(\alpha_x) = \frac{dF(\alpha_x)}{d\alpha_x} = 0 = \sum_{j=0}^{m1}[\hat{K}_x(j) - \sigma_x^2 e^{-\alpha_x j\Delta t}\cos\beta_x j\Delta t]\times \times[j\Delta t]e^{-\alpha_x j\Delta t}\cos\beta_x j\Delta t. \quad (11)$$

To solve the equation, it is advisable to use Newton's method. As a result, one can get:

$$\alpha_x^{(l+1)} = \alpha_x^l - \frac{W(\alpha_x^{(l)})}{W'(\alpha_x^{(l)})}, l = 0,1,2,\ldots, \quad (12)$$

where

$$W'(\alpha_x^{(1)}) = \frac{dW(\alpha_x)}{d\alpha_x} = \sum_{j=0}^{m1}[2\sigma_x^2 e^{-\alpha_x j\Delta t}\cos\beta_x j\Delta t] - - \hat{K}_x(j)[j\Delta t]^2 e^{-\alpha_x j\Delta t}\cos\beta_x j\Delta t.$$

The initial approximation of the parameter $\alpha_X^{(0)}$ of the parameter α_X is determined by the following formula [25]

$$\alpha_X^{(0)} = \frac{1}{T_0}\ln\left(\frac{\hat{K}_x[0]}{\hat{K}_x[1]}\right), \quad (13)$$

$$T_0 = \frac{T}{2}; \quad T = \frac{2\pi}{\beta_x}. \quad (14)$$

The best approximation, which is calculated by Equation (12), will be achieved when realizing the inequality:

$$\left\| \frac{W(\alpha_x^{(l)})}{W'(\alpha_x^{(l)})} \right\|_{l=l^*} < \varepsilon.$$

Then, the parameter α_X is determined as follows:

$$\alpha_X = \alpha_X^{(l^*)}. \quad (15)$$

The values obtained for different speeds on the straight section of the track are given in Table 2.

The corresponding graph of the CF estimation, for changing the vertical dynamics coefficient, at a speed of 40 km/h on a straight section of track and its approximation are shown in Figure 4.

4 Conclusions

1. The work presents the results of a statistical analysis of random processes of changing the coefficient of vertical dynamics of a passenger car. It is confirmed that the distribution law of the vertical dynamics coefficient values is a normal one. It is established that the value of the expectation of the coefficient of vertical dynamics at a speed of 40 km/h is 0.062. As the speed increases to 160 km/h, the expectation value will be 0.09838. Such results are typical for both straight and curved sections of the track.
2. As a result of statistical processing of experimental data, correlation functions have been constructed that characterize the degree of connection between different time sections of the process of changing the vertical dynamics coefficient.
3. To approximate the correlation functions, dependences in the form of a damped cosine curve were used. For each of the motion modes, the parameters α_X and β_x, which characterize them, are obtained.
4. The obtained characteristics of the distribution law of the coefficient of vertical dynamics instantaneous values, approximating the models of correlation functions and the numerical values of its parameters,

Table 2 *Values of the parameters of the approximating CF*

Speed (km/h)	Parameter values		
	σ_x^2	α_X	β_x
40	1	3.23	5.8
80	1	2.8	6.5
110	1	2.6	7.8
160	1	3.1	6.5

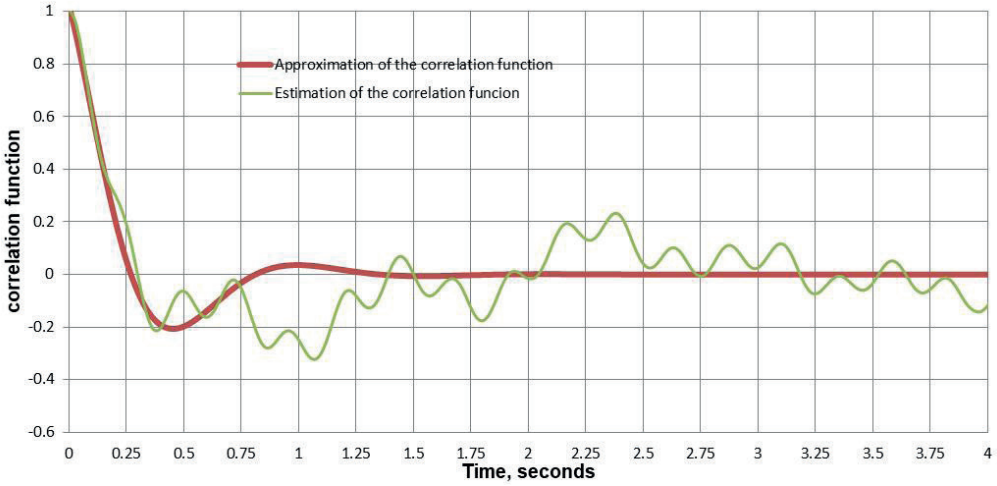

Figure 4 *Correlation function for changing the vertical dynamics coefficient at the speed of 40 km/h on the straight section of the track*

make it possible to further simulate the process of loading a passenger car without carrying out the lengthy expensive tests.

Grants and funding

The authors received no financial support for the research, authorship and/or publication of this article.

Conflicts of interest

The authors declare that they have no known competing financial interests or personal relationships that could have appeared to influence the work reported in this paper.

References

[1] MYAMLIN, S. V., LINGAITIS, L. P., DAILYDKA, S., VAICIUNAS, G., BOGDEVICIUS, M., BUREIKA, G. Determination of the dynamic characteristics of freight wagons with various bogie. *Transport* [online]. 2015, **30**(1), p. 88-92. ISSN 1648-4142, eISSN 1648-3480. Available from: https://doi.org/10.3846/16484142.2015.1020565

[2] DIZO, J., BLATNICKY, M., HARUSINEC, J., SUCHANEK, A. Assessment of dynamics of a rail vehicle in terms of running properties while moving on a real track model. *Symmetry* [online]. 2022, **14**(3), 536. eISSN 2073-8994. Available from: https://doi.org/10.3390/sym14030536

[3] DIZO, J., BLATNICKY, M. Assessment of dynamic properties of a carriage using multibody simulation considering rigid and flexible tracks. *IOP Conference Series: Materials Science and Engineering* [online]. 2019, **659**(1), 012052. ISSN 1757-8981, eISSN 1757-899X. Available from: https://doi.org/10.1088/1757-899X/659/1/012052

[4] STASTNIAK, P. Freight long wagon dynamic analysis in S-curve by means of computer simulation. *Manufacturing Technology* [online]. 2015, **15**(5), p. 930-935. ISSN 1213-2489, eISSN 2787-9402. Available from: https://doi.org/10.21062/ujep/x.2015/a/1213-2489/MT/15/5/930

[5] BLOKHIN, E. P., DANOVICH, V. D., MOROZOV, N. I. *Mathematical model of spatial oscillations of a four-axle rail crew*. Dnipro: Dnepropetrovsk Institute of Railway Transport Engineers, 1986.

[6] MIAMLIN, S. V., PRIKHODKO, V. I. Mathematical model of spatial oscillations of a passenger car. *Bulletin of V. Dahl East Ukrainian National University.* 2006, 8, p. 266-276. ISSN 1998-7927.

[7] MIAMLIN, S. V. *Improvement of dynamic qualities of rail crews by improvement of characteristics of spring suspension* (in Russian). PhD thesis. Dnipro, 2004.

[8] MIAMLIN, S. V. *Modeling of dynamics of rail crews*. Dnipro: Novaya ideologiia, 2002. ISBN 966-8050-04-05.

[9] PRYKHODKO, V. I., MIAMLIN, S. V. Modeling of dynamic interaction of the passenger car body and bogies. *Bulletin of the Dnipropetrovsk National University of Railway Transport named after Academician V. Lazaryan*. 2008, **7**, p. 7-12. ISSN 2222-419X, eISSN 2313-8688.

[10] PSHINKO, A. N., MYAMLIN, S. V., YAGODA, P. A., DONCHENKO, A. V., LOBOIKO, L. M., PRYKHODKO, V. I., IGNATOV, G. S. Estimation of dynamic qualities of a passenger compartment car of model 61-779. *Bulletin of the Dnipropetrovsk National University of Railway Transport named after Academician V. Lazaryan*. 2005, **7**, p. 39-46. ISSN 2222-419X, eISSN 2313-8688.

[11] XIAO, Q., LI, Q., CHANG, C. The influence of lateral shock absorber valve parameters on vehicle dynamic performance. *Journal of Mechanical Science and Technology* [online]. 2015, **29**(5), p. 1907-1911. ISSN 1738-494X, eISSN 1976-3824. Available from: https://doi.org/10.1007/s12206-015-0412-7

[12] VON WAGNER, U. Nonlinear dynamic behaviour of a railway wheelset. *Vehicle System Dynamics: International Journal of Vehicle Mechanics and Mobility* [online]. 2009, **47**(5), p. 627-640. ISSN 0042-3114, eISSN 1744-5159. Available from: ttps://doi.org/10.1080/00423110802331575

[13] BOGDEVICIUS, M., ZYGIENE, R., BUREIKA, G., DAILYDKA, S. An analytical mathematical method for calculation of the dynamic wheel-rail impact force caused by wheel flat. *Vehicle System Dynamics: International Journal of Vehicle Mechanics and Mobility* [online]. 2016, **54**(5), p. 689-705. ISSN 0042-3114, eISSN 1744-5159. Available from: https://doi.org/10.1080/00423114.2016.1153114

[14] KALKER, J. J. A fast algorithm for the simplified theory of rolling contact. *Vehicle System Dynamics: International Journal of Vehicle Mechanics and Mobility* [online]. 1982, **11**(1), p. 1-13. ISSN 0042-3114, eISSN 1744-5159. Available from: https://doi.org/10.1080/00423118208968684

[15] RAJIB, U. A. U. Analysis of a three-dimensional railway vehicle-track system and development of a smart wheelset. Doctoral Disertation Thesis. Montreal, Quebec, Canada: Concordia University, 2012.

[16] DIZO, J., BLATNICKY, M., STEISUNAS, S., VAICIUNAS, G. Evaluation of the influence of a rail vehicle running with wheel-flat on the railway track. *LOGI - Scientific Journal on Transport and Logistics* [online]. 2018, **9**(1), p. 24-31. eISSN 2336-3037. Available from: https://doi.org/10.2478/logi-2018-0004

[17] DIZO, J., STEISUNAS, S., BLATNICKY, M. Simulation analysis of the effects of a rail vehicle running with wheel flat. *Manufacturing Technology* [online]. 2016, **16**(5), p. 889-896. ISSN 1213-2489, eISSN 2787-9402. Available from: https://doi.org/10.21062/ujep/x.2016/a/1213-2489/MT/16/5/889

[18] ZYGIENE, R. Research on dynamic processes of the interaction between the damaged wheels of a railway vehicle and rails. Doctoral Dissertation. Lithuania: Vilnius Gediminas Technical University, 2015.

[19] WU, X., CHI, M. Study on stress states of a wheelset axle due to a defective wheel. *Journal of Mechanical Science and Technology* [online]. 2016, **30**(11), p. 4845-4857. ISSN 1738-494X, eISSN 1976-3824. Available from: https://doi.org/10.1007/s12206-016-1003-y

[20] BOGDEVICIUS, M., ZYGIENE, R., DAILYDKA, S., BARTULIS, V., SKRICKIJ, V., PUKALSKAS, S. The dynamic behaviour of a wheel flat of a railway vehicle and rail irregularities. *Transport* [online]. 2015, **30**(2), p. 217-232. ISSN 1648-4142, eISSN 1648-3480. Available from: https://doi.org/10.3846/16484142.2015.1051108

[21] Passenger main-line locomotive-hauled wagons. General technical standards for the calculation and design of the mechanical part of wagons (in Ukrainian). DSTU 7774: 2015 from 1-st April 2016. Kyiv: Ministry of Economic Development of Ukraine, 2017.

[22] Freight and passenger cars. Test methods for strength and running quality (in Russian). Effective 91-01-01. Moscow: GosNIIV, 1990.

[23] ROSIN, M. F., BULYGIN, V. C. *Statistical dynamics and efficiency theory of the control system* (in Russian). Moscow: Mechanical engineering, 1981.

[24] BENDAUT, J., PIRSOL, A. *Measurement and analysis of random processes* (in Russian). Moscow: Mir. 1974.

[25] POMANENKO, A. F., SERHIEIEV, G. A. *Concerning the application analysis of random processes* (in Russian). Moscow: Soviet radio, 1968.

JUSTIFICATION OF THE CAM ROLLER PARAMETERS FOR DESTRUCTION OF THE ROAD COATINGS FOR OBTAINING THE LUMPY ASPHALT SCRAP

Rustem Kozbagarov[1,*], Nurbol Kamzanov[2], Marzhana Amanova[3], Aigyl Baikenzheyeva[1], Guldariya Naimanova[1]

[1]Academy of Logistics and Transport, Almaty, Republic of Kazakhstan
[2]Satbayev University, Almaty, Republic of Kazakhstan
[3]Kazakh University of Transport Communications, Almaty, Republic of Kazakhstan

*E-mail of corresponding author: ryctem_1968@mail.ru

Rustem Kozbagarov 0000-0002-7258-0775,
Marzhana Amanova 0000-0002-8894-5257,
Guldariya Naimanova 000-0003-4619-7243
Nurbol Kamzanov 0000-0002-2420-8362,
Aigyl Baikenzheyeva 0000-0002-6013-2086,

Resume

Cam rollers can be used to break up cold asphalt pavements. In Kazakhstan, about 70% of roads have such coatings. It is most effective to open at temperatures above 20 °C. To reduce the traction force and uniform movement of the roller, it is necessary to eliminate the resistance of the coating to the exit of the cams, when rolling the drum by pivoting the cams in the roller's direction. The reliability of the theoretical studies' results was confirmed by production tests of the cam rollers during the opening of the asphalt concrete pavement on the Gulshad-Akchatau highway.

Article info

Received 19 November 2022
Accepted 1 February 2023
Online 15 February 2023

Keywords:

highway
cam rollers
asphalt concrete pavement
working bodies
asphalt scrap

Available online: https://doi.org/10.26552/com.C.2023.028

ISSN 1335-4205 (print version)
ISSN 2585-7878 (online version)

1 Introduction

Highways are of a great importance in the socio-economic development of the country. Therefore, much attention is paid to development of the road network in the country. More than 10000 km of paved roads are built and overhauled annually. The development of the country's economy requires an increase in the intensity and carrying capacity of the traffic flow, which is impossible without improving the quality of road construction [1-2].

Currently, more than 70% of highways of republican significance with asphalt concrete pavement are subject to reconstruction and this is over 50000 km of roads, which will require 55 to 65 million tons of asphalt concrete. To restore the working capacity of roads in Kazakhstan, it is mainly necessary to reconstruct the most material-intensive structural element - road pavement, which contains over 150 million tons of asphalt concrete as useless ballast.

The world practice of reusing asphalt scrap of old pavements shows that countries such as the USA, England, Germany and France, reuse all asphalt scrap, Japan, Hungary and Poland - 60% and 50%, respectively and much less in Kazakhstan [3-5].

To restore the entire network of highways in Kazakhstan with a minimum of fuel, energy and material resources, it is necessary to reuse the entire mass of pavement materials, the reserves of which are sufficient. One of the main reasons for the slow implementation of the technology of reusing the old asphalt concrete pavement is the imperfection of the mechanisms used to destroy the pavement [6].

To facilitate the opening of the asphalt concrete pavement, it is proposed to use a cam roller with some improvement of the cams to prevent the resistance of the asphalt pavement when the cams enter and leave the surface [7-9].

At the same time, the use of a cam roller would avoid mixing of coating and base materials, as happens when using a ripper.

Asphalt concrete pavements are destroyed to pieces of a certain size, taking into account the location of the cams at a given distance from each other in a checkerboard pattern. Usually, during

the reconstruction of roads, the "old" coatings are destroyed, which are almost all covered with a network of cracks, so lumpy asphalt scrap should not exceed 500 mm in size.

2 Materials and methods

There are two fundamentally different methods of opening the old asphalt concrete pavement - milling and breaking by scraping. Milling is usually performed to a shallow depth and scarification, mainly, to the full thickness of the coating [10-12].

Milling is carried out by special machines using the milling cutters installed in most cases on a drum. When milling, the so-called cold and hot methods are used. Recently, only the cold milling method has been used, since bitumen does not burn out and liquefied gas, which is a scarce and expensive energy carrier, is not used. However, during the cold milling, cutter cutters wear out 5-10 times more intensively than during the hot milling, which leads to a rapid wear of expensive hard alloys used on cutters [13-14].

The destruction of old asphalt concrete pavements that have lost their operational qualities is still regarded as the simplest technological operation. Destruction is carried out with the help of traditional road machines - medium and heavy type motor graders with scarifies, bulldozers with rippers on tractors weighing 10 tons or more, as well as special hydraulic hammers or concrete breakers of hydraulic or pneumatic action [15-16].

The main disadvantages of machines for opening asphalt concrete pavements are: the accepted principle of loosening and scarifying the asphalt concrete pavement requires significant energy consumption, since the destructive force is directed along the entire length of the asphalt concrete slab; the impossibility of emergency adjustment of the depth of scarification by rippers according to the thickness of the slab being destroyed, as a result of which the coating and base materials are mixed, thereby reducing the quality of the products obtained subsequently; the method of rough and fine milling is the least effective for opening the coating and with fine milling, stone fractions of crushed stone are crushed, which limits the use of the resulting material; lumpy asphalt scrap, obtained as a result of scarification, has different sizes and requires additional costs for breaking them down to the required dimensions acceptable for feeding into the crushing plant.

The most rational way to open the coating slab is the method of pressing a wedge on top of the slab, in which the destruction force will be directed along its smallest size - the thickness of the slab.

In view of the foregoing, it is proposed to use the cam rollers for destruction and opening of asphalt concrete pavements. The specific pressure of medium-type cam rollers ranges from 2 MPa to 6 MPa or more, which is sufficient to press the cams into the old coating, the strength of which is much lower due to cracking from its long-term operation.

The maximum effect can be achieved only with a rational choice of parameters of the rink's working equipment.

The analysis carried out allows to conclude that there is no holistic concept for increasing the efficiency of the road rollers by creating an information bank of their technical parameters, identifying the main trends in development of machines using probabilistic-statistical methods, predicting promising directions in the design of working bodies and developing a methodology for substantiating the main parameters of the cam rollers at the stage of their design. and applications, taking into account the nature of their interaction with destructible material for opening old asphalt concrete pavements during the reconstruction of roads.

The possibility of using the cam rollers for destruction of the old asphalt concrete pavement of roads during their reconstruction, with development of an engineering method for calculating their main parameters (roller weight, dimensions and number of cams) is justified. A cam 2 with a spring-loaded latch 3 is pivotally attached to the roller structure 1 and is accepted as the base for further operation (Figure 1). Depending on the type of the working body, the nature and conditions of its interaction with the destructible material, various types of deformations and their combination take place. The most effective is the vertical introduction of wedges and dies, which is ensured by use of the cam rollers for the destruction of asphalt pavements with production of the lumpy scrap of a given size.

For effective opening of old asphalt concrete pavements during their reconstruction, the most effective is the vertical introduction of wedges and dies, which is ensured by using cam rollers to obtain lumpy scrap of specified sizes, while the following requirements must be met with a roller mass of at least 5 tons: the number of cams in one row should not exceed from 4 to 5 pieces [3-6, 10-12, 16]: the distance between them should not be more than 0.4 m; the number of cams along the perimeter must be at least 15 pcs.; the distance between them is not more than 0.35 m; cams should be staggered; The height of the cams should be 250 to 300 mm, thickness - no more than 40 mm and width - no more than 100 mm at the top.

Consider the case of an elastic-viscous state of asphalt concrete. Let a wedge with side faces under the action of a statically applied vertical force P enter an elastic-viscous medium (Figure 2) and the length of an infinitely small element of the wedge section in the direction perpendicular to the plane of the drawing will be taken as unity. Typically, the depth of penetration or destruction of asphalt concrete is equal

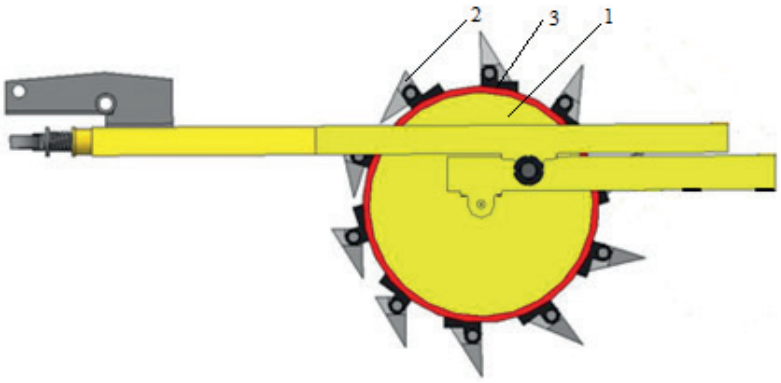

Figure 1 *General view of the cam roller [8]: 1 - road skating rink; 2 - cam; 3 - spring-loaded latch*

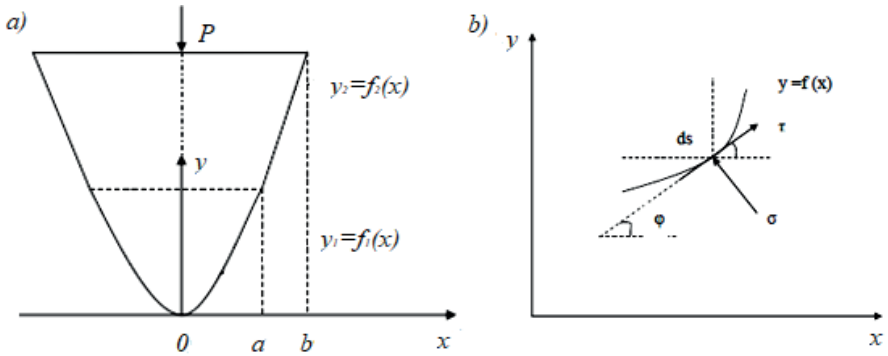

Figure 2 *The introduction of a wedge into an elastic-viscous medium:*
a) a wedge with side faces under the action of a statically applied vertical force P;
b) to the equilibrium condition of an elementary wedge

to the thickness of the pavement layer. We believe that to open the old coating, it is enough to pierce it with the cams of the roller for its entire thickness.

The side faces of the wedge are described by two surfaces (or two functions)

$$y_1 = f_1(x), y_2 = f_2(x)). \tag{1}$$

Let, for example, the function $f_1(x)$ describe the face of the wedge in the interval $0 \le x \le a$ and the function $f_2(x)$ in the interval $0 \le x \le b$. Consider the equilibrium condition for an infinitely small elementary section of the wedge. On the side faces of the wedge, from the side of the elastic-viscous medium, act the normal and shear stresses σ and τ, the resultants of which are the reactive resistance forces of the medium. If μ is the coefficient of viscoelastic friction of the medium on the metal, then

$$\tau = \mu\sigma . \tag{2}$$

As known, the differential of the arc length of a plane curve is determined from the expression

$$ds = \sqrt{1 + y'^2}dx . \tag{3}$$

The pressing force of the wedge is determined by the formula:

$$\int_s \sigma ds\cos\phi + \tau ds\sin\phi = p/2 . \tag{4}$$

We substitute the expression for ds and, taking into account Equation (2), we obtain for an elastic-viscous medium

$$\int_0^b \sigma(\cos\varphi + \mu\sin\varphi)\sqrt{1 + y'^2}dx = p/2; \tag{5}$$

taking into account the geometric meaning of the derivative

$$y' = tg\varphi , \tag{6}$$

we have:

$$\varphi = arctgy' . \tag{7}$$

Using the trigonometric identities of the function $\cos\varphi$ and $\sin\varphi$ Equation (5), it is transformed to the form:

$$\int_0^b (1 + \mu y')\sigma dx = p/2 \tag{8}$$

To use equation (8) in practical calculations, it is necessary, firstly, to have the equation of the curvilinear wedge face $y = f(x)$ and secondly, to know the law of distribution of normal and shear stresses along the wedge faces. Usually, in the theory

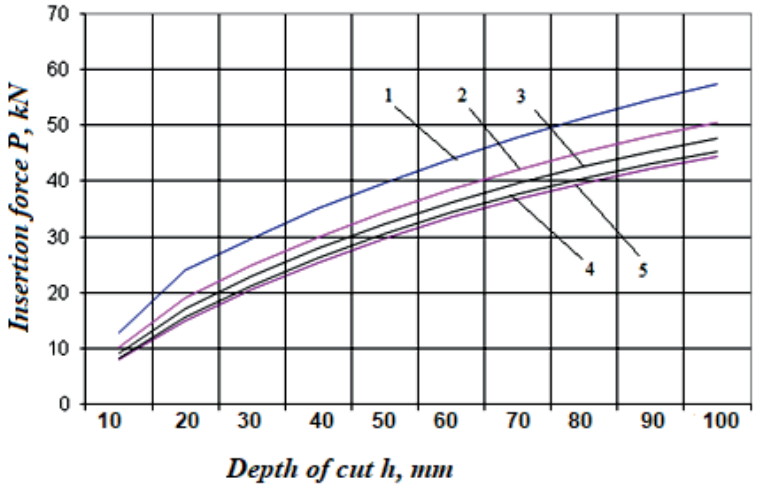

Figure 3 *Dependence of the cam insertion force on the depth at various values of the coefficient* μ *: 1-* μ *=0.72; 2 -* μ *=0.374; 3 - t* μ *=0.232; 4 -* μ *=0.116; 5-* μ *=0.065*

of elasticity and plasticity, the law of distribution of normal and shear stresses is given by the stress functions, which must satisfy the equilibrium equations, boundary conditions and strain continuity equations. Hence, it follows that the problem of equilibrium of a wedge in an elastic or viscoelastic medium is solved ambiguously: the set of suitable stress functions is very extensive.

The stress distribution law can be approximated according to the experimental data of Bocharov [17] function of the form

$$\sigma = Ae^{-Bh}, \tag{9}$$

where h - is the penetration depth of the wedge, A and B are constant coefficients.

As the experience of other researchers shows, recently the most common are cams in the form of: a truncated cone, a truncated pyramid, cams with side surfaces formed by second-order curves (involutes, spirals, cycloids) or complex curves with a trapezoidal shape, [3, 7, 9, 11].

Calculation of penetration forces into an elastic-viscous medium of different variants of cam profiles, with varying coefficient of viscoelastic friction of the medium against metal and penetration depth has been performed. A graphical interpretation of the calculation results for the considered cam profile is shown in Figure 3, where μ is the coefficient of viscous-elastic friction of the medium on the metal in the asphalt concrete layer.

The criterion for the destruction of the asphalt concrete pavement is the ratio

$$\sigma_y \geq R_{compres}, \tag{10}$$

where is σ_y - the vertical compressive stress; $R_{compres}$ - compressive strength of asphalt concrete.

The strength properties of asphalt concrete depend on temperature, with its increase, the pressing force of the wedge decreases. The most intense changes are in the positive temperature range from 10 to 35 °C, when the indentation force is reduced by almost 3 times. This property depends on the amount and viscosity of bitumen in asphalt concrete and bituminous rocks. Comparing the strength indicators of asphalt concrete pavements to the specific pressure created by the cam rollers, we conclude that medium and heavy rollers can be used to open asphalt concrete pavements of highways during their reconstruction to obtain lumpy scrap of given sizes.

3 Results and discussions

The analysis of technical literature showed that cams with concave or convex curvilinear side surfaces formed by second-order curves are the most appropriate for road rollers [1-9].

Studies show that the degree of fulfillment of all the requirements largely depends on the correct choice of the geometric shape of the cam and the design parameters of the working body itself, but there is still no consensus on this issue. This is evidenced by a wide variety of geometric shapes of the cam and a significant discrepancy in the size of the working bodies used on rollers of various companies. It was mainly the shape or profile of the cam that was changed, since they have a significant impact on the compaction parameters, as well as on the degree of loosening of the soil or other material.

As experience of researchers from different countries shows, recently the most common are cams in the form of a truncated cone and a truncated pyramid. Cams with lateral surfaces formed by second-order

Figure 4 *Cam roller with opening of the asphalt concrete pavement*

Figure 5 *General view of the crushed asphalt scrap padfoot roller*

Table 1 *Results of testing crushed scrap when pressed by a press and rollers*

No.	The composition of the crushed scrap (%)	Addition of water (over 100 %) (%)	Density (kg/m^3)	Coefficient seals
1	20-40 mm - 60			
	10-20 mm - 20	5	2320	0.97
	0-10 mm - 20			
2	10-20 mm 50			
	0-10 mm - 50	6	2360	0.98
3	Production composition of crushed asphalt	5.5	2350	0.98-1

curves (involutes, spirals, cycloids) or complex curves are beginning to be widely used.

Cams with involutes side surfaces are more efficient in terms of achieved soil density, self-cleaning and other indicators compared to cams of a different shape.

Experimental tests of a cam roller for destruction of the asphalt concrete pavement were carried out during the reconstruction of the Akchatau-Gulyshad section of the highway, 192 km long.

The existing structure of the pavement consists of a 130 to 140 mm asphalt concrete pavement and a base of crushed stone with a fraction of 200 to 400 from 120 to 180 mm. The width of the pavement is 8 m and the shoulder is 1.5 m each.

The design of the pavement consists of the following layers: pavement of two-layer asphalt concrete, 130 mm thick, of which 40 mm is fine-grained asphalt concrete and 90 mm is coarse-grained asphalt concrete; base made of crushed old asphalt concrete (with the addition of crushed stone of a fraction of 20 to 40 mm, if necessary), with a thickness of 150 to 180 mm; leveling layer of sand-gravel mixture.

The volume of asphalt scrap to be processed was more than 505 thousand tons. To open the old asphalt concrete pavement, up to 140 mm thick and grind asphalt scrap, they used the recommendation of the manufacturer of the DU -94 cam rollers weighing 5 tons (Figure 4).

The opening and grinding of the asphalt concrete pavement was carried out directly on the road in the following technological order. The cam rollers cracked and crushed the coating in several passes, then the resulting material was mixed with a disk mixer. Then, the final grinding of the material was carried out in 2 and 3 passes with cam rollers. A general view of crushed asphalt concrete is shown in Figure 5.

During the first passes of the roller, due to the resistance to the exit of the cams, the movement of the K-700 tractor was slow. After partial destruction of the cover over the entire area, the speed of the K-700 tractor was from 3 to 5 km/h.

To reduce the resistance of the cams when leaving the coating, a technical solution was developed that made it possible to freely exit the coating by means of hinged fastening of the cams.

After the final grinding, the resulting asphalt material presents fractions from 0 to 70 mm, consisting of the sand-crushed stone granules coated with an asphalt binder, i.e. bitumen mixed with mineral powder. According to the grain composition, the crushed material was granules: crushed stone fractions from 5 to 70 mm from 65 to 75 %, sandy from 1.25 to 5 mm from 20 to 30% and less than 1.25 mm about 5 %. Taking into account that the grain composition is close to the required one and when the crushed material is compacted, further crushing of weak granules will occur, it was decided to carry out a test rolling by pressing samples on a press at a load of 20 MPa. The molding of the samples was

carried out at the optimum moisture content of the mixture, while comparing to the structural densities of asphalt concrete (Table 1).

Production tests of compacted pulverized asphalt have shown that the required density is achieved.

4 Conclusions

Based on the experimental tests of the cam rollers during the reconstruction of the Gulshad-Akchatau highway, it seems possible to draw the following conclusions: mathematical dependencies have been obtained that allow calculating the necessary efforts for destruction of the old asphalt concrete pavement by the cam rollers during the reconstruction of roads, taking into account the physical and mechanical properties of the medium and the geometric dimensions of the working body; an engineering method has been developed for calculating the main parameters of a cam roller (mass of the rink, dimensions and number of cams necessary for the destruction of an asphalt concrete pavement with the production of lumpy scrap of a given size) used to open and destroy the old asphalt concrete pavement of reconstructed roads; to reduce the rolling resistance of the roller, the cams are hinged to ensure their free exit from the pavement. The pilot tests of the cam roller, during the destruction of the old asphalt concrete pavement during the reconstruction of the road, confirmed the efficiency and reliability of theoretical calculations and scientific points made in the work.

Grants and funding

The authors received no financial support for the research, authorship and/or publication of this article.

Conflicts of interest

The authors declare that they have no known competing financial interests or personal relationships that could have appeared to influence the work reported in this paper.

References

[1] BAHIA H. U., COENEN, A., TABATABAEE, N. Mixture design and compaction. *Advances in Interlaboratory Testing and Evaluation of Bituminous Materials* [online]. 2012, **9**, p. 85-142. ISSN 2213-2031. Available from: https://doi.org/10.1007/978-94-007-5104-0_3

[2] IMASHEVA, G., ABDULLAYEV, S., TOKMURZINA, N., ADILOVA, N., BAKYT G. Prospects for the use of gondola cars on bogies of model ZK1 in the organization of heavy freight traffic in the Republic of Kazakhstan. *Mechanika International Scientific Journal* [online]. 2018, **24**(1), p. 32-36. ISSN 1392-1207. Available from: https://doi.org/https://doi.org/10.5755/j01.mech.24.1.17710

[3] WHITE, D. J., THOMPSON M. J. Relationships between in situ and roller integrated compaction measurements for granular soils. *Journal of Geotechnical and Geoenvironmental Engineering* [online]. 2008, **134**(12), p. 1763-1770. ISSN 1090-0241. Available from: https://doi.org/10.1061/(ASCE)1090-0241(2008)134:12(1763)

[4] COMMURI, S., MAI, A. T., ZAMAN, M. Neural network-based intelligent compaction analyzer for estimating compaction quality of hot asphalt mixes. *Journal of Construction Engineering and Management* [online]. 2011, **137**(9), p. 634-644. ISSN 07339364 Available from: https://doi.org/10.1061/(ASCE)CO.1943-7862.0000343

[5] ROOHI SEFIDMAZGI, N., TASHMAN, L., BAHIA, H. U. Internal structure characterization of asphalt mixtures for rutting performance using imaging analysis. *Journal of Road Materials and Pavement Design* [online]. 2012, **13**(1), p. 1-17. ISSN 1468-0629. Available from: https://doi.org/10.1080/14680629.2012.657045

[6] TASSYBEKOV, Z., BEKENOV, T., NUSSUPBEK, Z. Assessment of compaction of the road base from repeated exposure to frequently repeated loads of self-propelled road roller. In: Workshop on ICTE in Transportation and Logistics 2019: proceedings [online]. Springer. 2019. ISBN 978-3-030-39688-6, eISBN 978-3-030-39688-6, p. 164-170. Available from: https://doi.org/10.1007/978-3-030-39688-6_22

[7] BALOVNEV, V. I., IVANCHENKO, S. N., DANILOV, R. G., LESHCHINSKY, A. V. *Road rollers: development, design, calculation.* Khabarovsk: Pacific National University, 2016. ISBN 978-5-7389-1930-5.

[8] PUGIN, K. G., BURGONUTDINOV, A. M. *Machines for the construction, repair and maintenance of highways. Part 1. Road rollers and shovel loaders.* Perm: Perm National Research Polytechnic University, 2011. ISBN 978-5-398-00635-3.

[9] BURGONUTDINOV, A. M. *Machines for the construction, repair and maintenance of highways. Part 3: Machinery and equipment for the repair and maintenance of road.* Perm: Perm National Research Polytechnic University, 2011. ISBN 978-5-398-00900-2.

[10] HU, W., SHU, X., HUANG, B., WOODS, M. Field investigation of intelligent compaction for hot mix asphalt resurfacing. *Frontiers of Structural and Civil Engineering* [online]. 2017, **11**, p. 47-55. ISSN 2095-2449. Available from: https://doi.org/10.1007/s11709-016-0362-x

[11] RAMBABU, D., SHARMA, S. K., AKBAR, M. A. A review on suitability of roller-compacted concrete for constructing high traffic resisting pavements. *Innovative Infrastructure Solutions* [online]. 2023, **8**, 20. ISSN 2364-4176. Available from: https://doi.org/10.1007/s41062-022-00989-4

[12] TEBALDI, G., DAVE, E. V., MARSAC, P., MURAYA, P., HUGENER, M., PASETTO, M. Synthesis of standards and procedures for specimen preparation and in-field evaluation of cold-recycled asphalt mixtures. *Road Materials and Pavement Design* [online]. 2014, **15**(2), p. 272-2997. ISSN 14680629. Available from: https://doi.org/10.1080/14680629.2013.866707

[13] KOZBAGAROV, R. A., ZHUSSUPOV, K. A., KALIYEV, Y. B., YESSENGALIYEV, M. N., KOCHETKOV, A. V. Determination of energy consumption of high-speed rock digging. *News of the National Academy of Sciences of the Republic of Kazakhstan, Series of Geology and Technical Sciences* [online]. 2021, **6**(450), p. 85-92. ISSN 2518-170X. Available from: https://doi.org/10.32014/2021.2518-170X.123

[14] KOZBAGAROV, R. A., SHALBAYEV, K. K., ZHIYENKOZHAYEV, M. S., KAMZANOV, N. S., NAIMANOVA, G. T. Design of cutting elements of reusable motor graders in mining. *News of the National Academy of Sciences of the Republic of Kazakhstan, Series of Geology and Technical Sciences* [online]. 2022, **3**(453), p. 128-141. ISSN 2518-170X. Available from: https://doi.org/10.32014/2022.2518-170X.185

[15] KOZBAGAROV, R., AMANOVA, M., KAMZANOV, N., BIMAGAMBETOVA, L., IMANGALIYEVA, A. Investigation of wear of cutting part of polygonal knife car graders in different ground conditions. *Communications - Scientific letters of the University of Zilina* [online]. 2022, **24**(4), p. D229-D238. ISSN 1335-4205, eISSN 2585-7878. Available from: https://doi.org/10.26552/com.C.2022.4.D229-D238

[16] KOZBAGAROV, R. A., KAMZANOV, N. S., AKHMETOVA, S. D., ZHUSSUPOV, K. A., DAINOVA, Z. K. Improving the methods of milling gauge on highways. *News of the National Academy of Sciences of the Republic of Kazakhstan, Series of Geology and Technical Sciences* [online]. 2021, **3**(447), p. 87-93. ISSN 2518-170X. Available from: https://doi.org/10.32014/2021.2518-170X.67

[17] BOCHAROV, V. S. *Interaction of working bodies of machines with bituminous rocks.* Moscow: Transport, 1992. ISBN 5-277-01382-2.

DISCUSSION ABOUT METAL EXPANSION JOINTS MANUFACTURING TECHNOLOGY OF PREVENTING THERMAL DEFORMATION PIPELINES INTENDED FOR THE FLUIDS TRANSPORT

Piotr Kurp[1,*], Hubert Danielewski[1], Bartłomiej Szwed[1], Krzysztof Borkowski[1], Andrej Zrak[2], Oksana P. Gaponova[3]

[1]Kielce University of Technology, Kielce, Poland
[2]University of Zilina, Zilina, Slovakia
[3]Sumy State University, Sumy, Ukraine

*E-mail of corresponding author: pkurp@tu.kielce.pl

Piotr Kurp 0000-0002-1001-5033,
Bartłomiej Szwed 0000-0002-2453-7369,
Andrej Zrak 0000-0003-1883-7047,
Hubert Danielewski 0000-0003-4675-6236,
Krzysztof Borkowski 0000-0003-2869-5425,
Oksana P. Gaponova 0000-0002-4866-0599

Resume

In this paper, the authors discuss the method of deformations compensation (resulting from the impact of variable temperatures and pressure) in pipelines intended for fluids transport (liquids and gases). Classical methods of compensation through the so-called "natural compensation" and using special devices called expansion joints. In this paper authors present research work on a new type of the metal expansion joints, called bellow-lens expansion joints. The mechanically assisted laser forming method, which was used to manufacture the bellow-lens expansion joints, was presented. The method uses CO_2 laser radiation to heat the element from which the expansion joint will be made and the proprietary system consists of an actuator and swivel handle.

Article info

Received 7 November 2022
Accepted 3 February 2023
Online 23 February 2023

Keywords:

metal expansion joints
laser forming
pipelines compensating
pipelines thermal deformation

Available online: https://doi.org/10.26552/com.C.2023.030

ISSN 1335-4205 (print version)
ISSN 2585-7878 (online version)

1 Introduction

Industrial transport systems, commonly called pipelines, are used to move mainly fluids such as, for example: natural gas (gas pipelines), oil (oil pipelines), steam and water (power pipelines) and others. These types of installations operate with various operating parameters, such as temperature and pressure [1]. Inadequate construction of such a pipeline may lead to its damage and, consequently, even to a huge catastrophe and threat to human health and life and the natural environment.

Therefore, the pipeline spools should be designed in such a way that the deformations arising from changing temperatures and changing pressures will be compensated. One of the easiest ways to compensate for this type of deformations are “natural” spool direction changes, implemented on standard fittings, such as elbows or tees. If the route of the pipeline does not assume a change of direction, then the special “loops” should be designed to enable this type of compensation. The method of compensation for “natural” direction changes and “loop” is presented in Figure 1.

This type of solution is applied where there is a lot of space to use a “loop”, mainly on overhead and underground pipelines. However, it is not always possible, e.g. due to lack of space or technological and economic limitations. In such circumstances, specialized devices, called lens compensators or bellows compensators, are used [2]. As the name suggests, on the circumference of the pipe there are bellows or, less often, lenses that can expand and contract under the influence of temperature (similar to the bellows in an instrument called an accordion), thus acting as a compensator (expansion joint). The classic methods of producing these elements are plastic working on sets of rollers, hydroforming, redrawing and welding.

The authors of this paper proposed to produce a new type of metal expansion joint called a bellow-lens expansion joint (combining the advantages of two

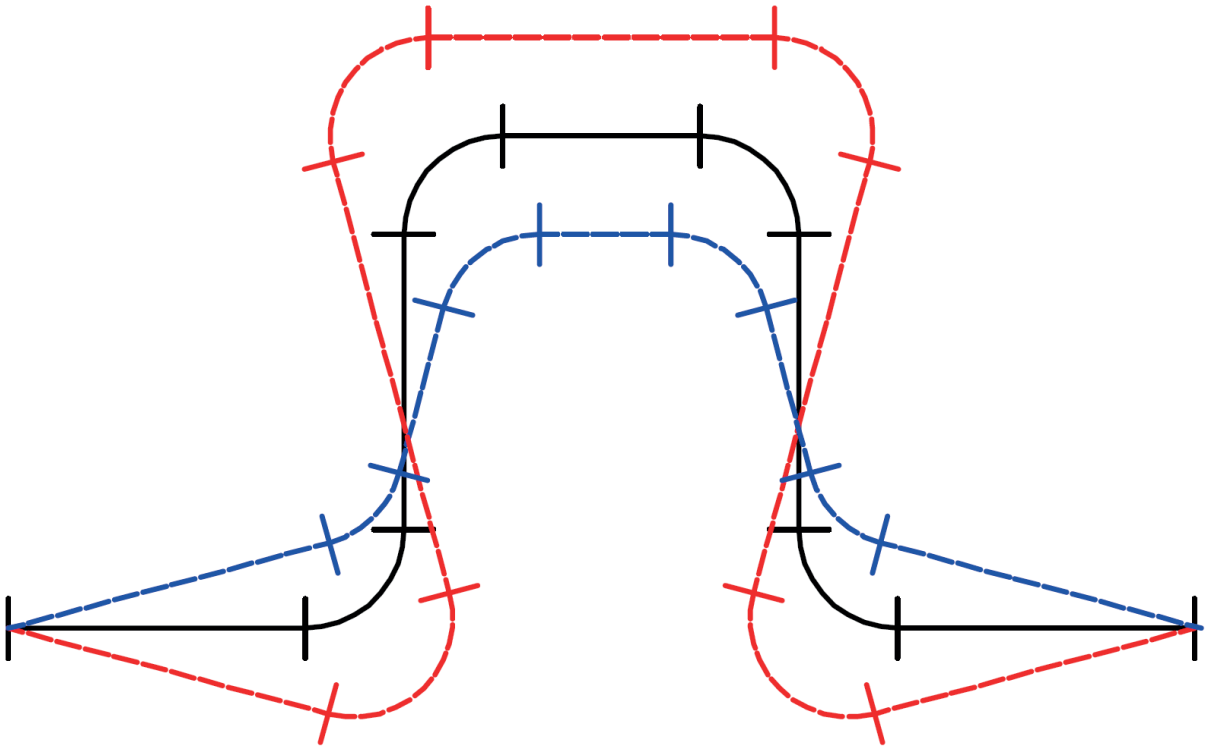

Figure 1 *Pipeline thermal compensation on elbows, the so-called "natural" in the form of a "loop". Schematically showed: black line - nominal pipeline route (designed route), red line - compensation caused by material expansion (temperature rise), blue line - compensation caused by material shrinkage (temperature drop)*

types: a bellow joint with a lens expansion joint) by using laser treatment. Currently, laser technologies are very widespread in industrial practice. They are used to perform such industrial operations as: cutting, welding, industrial coatings applications, creating textures on the material's surface, additive manufacturing etc., [3-8].

In addition to the above-mentioned laser technologies, we also have a laser forming technique. The phenomenon of material deformation as a result of the element's local temperature change is used here. The element is locally heated by the energy of the laser beam acting on it. The appropriate geometry and trajectory of the laser beam led to the desired shape of the element. In this case, the local shape change of the element is achieved due to the difference in thermal expansion of the "cold" and "warm" parts of the material. Plastic deformation is achieved by causing internal thermal stresses in the material without the participation of external forces. Vollertsen [9] distinguished three main mechanisms of laser forming: the temperature gradient mechanism (TGM), the upsetting mechanism (UM) and the buckling mechanism (BM).

The mechanisms presented above apply to laser forming, without the participation of external forces. The disadvantage of this type of technology is its time and energy consumption. According to this fact, to speed up the laser forming process, it was decided to additionally use external forces. Technologies that use a laser beam as a heat source are called laser-assisted forming or mechanically assisted laser forming [10-13].

The concept of the mechanically assisted laser forming method, which technology was used to manufacture expansion joints, are presented below. The results of experimental research are presented, as well.

2 Method concept

The concepts of new metal expansion joints manufacturing process, using a mechanically assisted laser forming hybrid method, are described in paper [13] and the patent [14]. Below is a general description of the metal expansion joints manufacturing concept to introduce the assumptions of the technology to the readers. Figure 2 presents a conceptual stand for expansion joints manufacturing. The description of the method is given below.

The general conception of bellows-lens expansion joints manufacturing is as follows (see Figure 2):

1. The starting element is a pipe (1) with a known diameter and wall thickness, made of a material of an appropriate grade.
2. The pipe (1) is placed between the actuator (5) and the swivel handle (6).
3. The pipe (1) is set into rotation ω.
4. The laser head (2) guiding the laser beam with the power P heats the pipe (1) in the given area to the plasticization temperature T.
5. The plasticization temperature T is monitored in real-time by a pyrometer (3) coupled to the laser

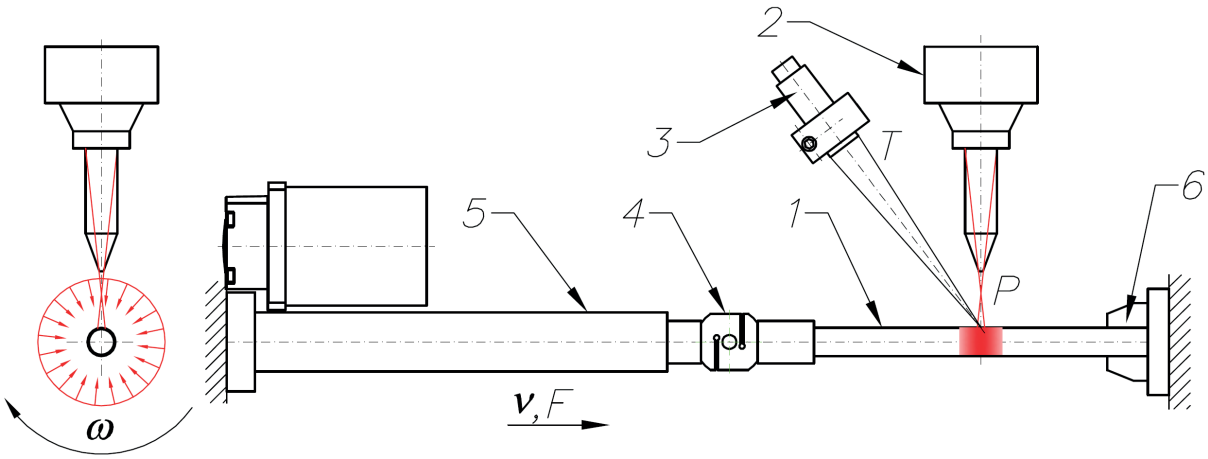

Figure 2 *The execution and measurement stand concept: 1 - pipe quickly rotating around its axis, 2 - laser head (pipe heating), 3 - pyrometer, 4 - force sensor, 5 - axial thrust actuator, 6 - swivel handle*

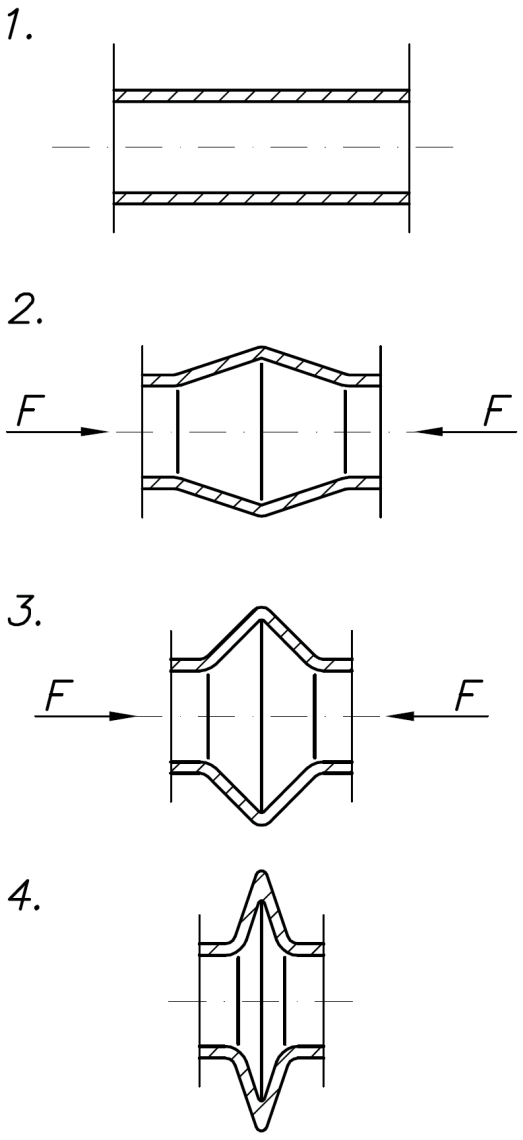

Figure 3 *Individual steps of bellow-lens forming (concept):*
1 - straight output pipe, 2, 3 - pipe upsetting, 4 - the final bellow-lens shape

Table 1 *Chemical composition, main physical properties and mechanical properties of X5CrNi18-10 austenitic stainless steel*

Chemical composition (wt. %)							
C	Cr	Ni	Mn	Si	P	S	N
<0.07	17.5 ÷ 19.5	8.0 ÷ 10.5	<2.0	<1.0	<0.045	<0.015	<0.11

Density	Thermal expansion coefficient	Heat capacity	Thermal conductivity
ρ (kg/m^3)	α (1/K)	C_{p20} (J/kgK)	λ (W/mK)
8020	14.2×10^{-6}	480	15

Proof stress $R_{0,2}$ (MPa)	Tensile strength R_m (MPa)	Elongation at fracture A_{80} (%)	Hardness (HV)
230	540-750	35-45	min. 220

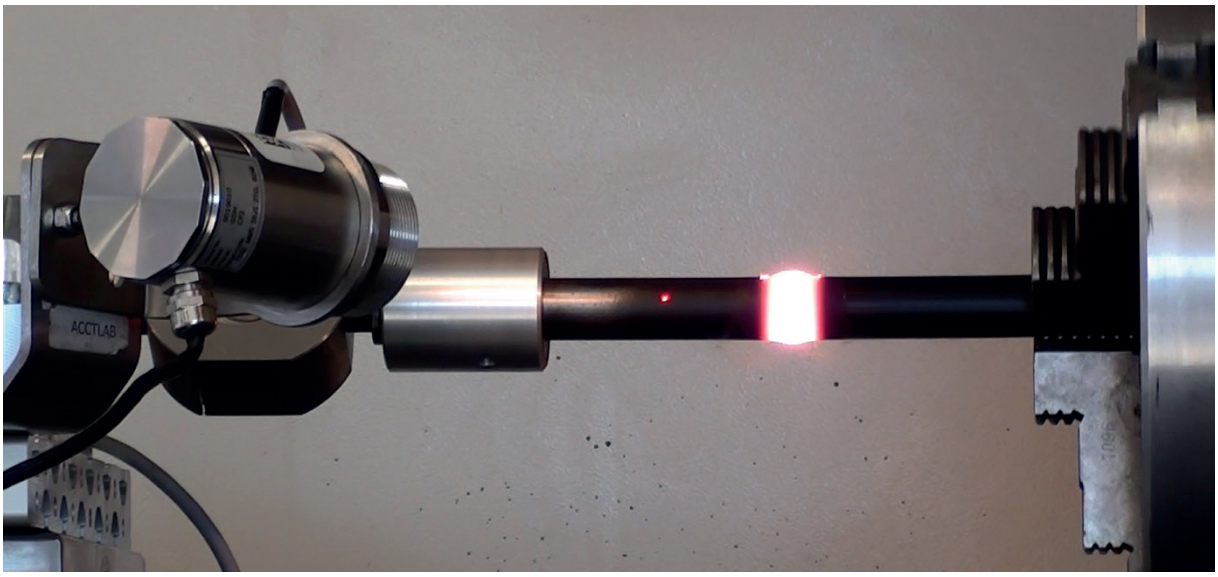

Figure 4 *Pipe in the course of the experiment: heating and compression process*

device. This allows the plasticization temperature to be kept constant.

6. After reaching the appropriate plasticization temperature T, the actuator (5) presses onto the pipe (1) with the force F and the velocity v.
7. The pushing force is recorded by a force sensor (4) installed between the actuator (5) and the pipe (1). The final result is the formation of a bulge, which is a bellows-lens expansion joint. The individual stages of bellows-lens formation are presented in Figure 3.

The concept presented above was verified by experiment. The results of the experiment are presented in the following section.

3 Materials, methods and experimental results

A stainless steel pipes, of dimensions of ϕ20 x 1 mm (DN20) and ϕ50 x 1.5 mm (DN50), were used for the experiment. The elements are made of austenitic steel X5CrNi18-10 grade. The surface of the specimens was covered with a special absorber to increase the laser radiation absorption. The specimens were mounted in the previously described device. The actual view of the test stand is shown in Figure 4. The chemical composition and selected physical properties of this steel are presented in Table 1 [15].

A TRUMPF TruFlow 6000 CO_2 laser with a maximum power of 6kW was used for the experiment. The laser treatment parameters were as follows:

- laser wavelength: λ =10.6 µm,
- CW laser mode,
- laser power (recorded): P = 900-1100 W (for DN20 pipe); P= 1000-1300 W (for DN50 pipe),
- process temperature: approx. T = 1050-1100 °C (directly heated zone),
- compressive length: s = 10 mm (for DN20 pipe); s = 25 mm (for DN50 pipe)
- pipe rotation speed: ω = 10 000 °/min,
- pipe compressive speed: v= 10 mm/s.

The process of mechanically assisted laser forming uses proprietary research equipment, made by the authors especially for this purpose. The device consists of an execution stand and a control cabinet. The execution stand is attached to the frame of the CNC chuck cooperating with the TRUMPF TruFlow 6000 CO_2 laser. It is equipped with a linear actuator with

a stepper motor and a strain gauge force sensor (Figure 2). The Siemens S7-1200 PLC controller was installed in the control cabinet. Its task is to read signals from sensors, generate control signals, manage the process and communicate with the operator's dedicated application on a PC (the application was developed by the authors of this paper).

The way the equipment works is as follows. Based on the parameters set by the operator and readings from the sensors, control signals are generated. The working process starts automatically when the set sample temperature is reached. The actuator moves to the set position with the control of the maximum force compressing the specimen and the maximum feed rate. The temperature at the point of impact of the laser beam is regulated in a closed feedback loop from a monochromatic pyrometer. The plasticizing temperature can be set in any range, for the tested steel it is in the range (1050 °C-1100 °C). Based on the pyrometer indications, the data sent to the laser device regulates the laser power so that the temperature does not exceed the set values. Depending on the pipe diameter, the laser power automatically varies in the ranges mentioned above. For this purpose, the

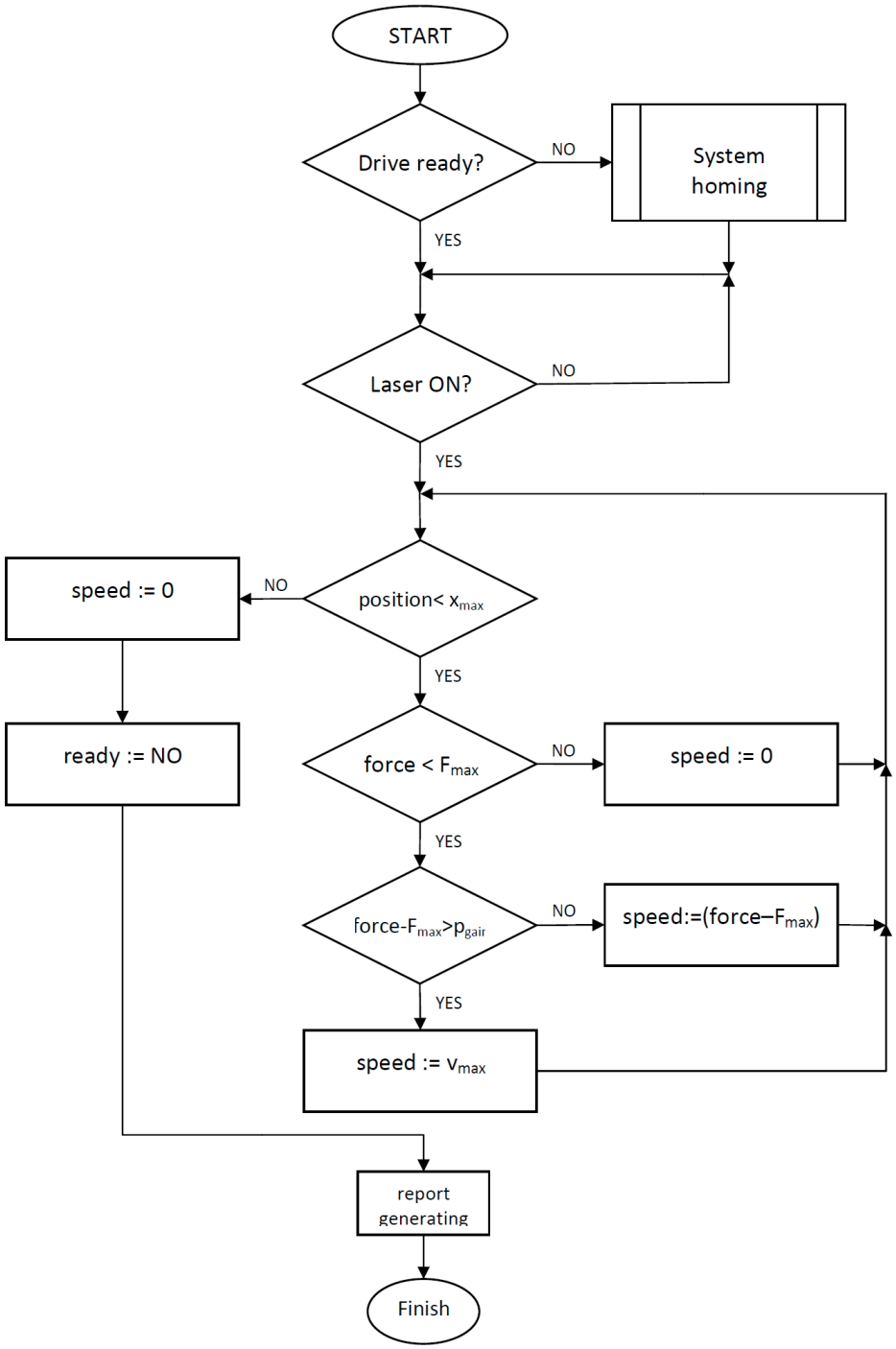

Figure 5 *The block diagram control of the mechanically assisted laser forming process*

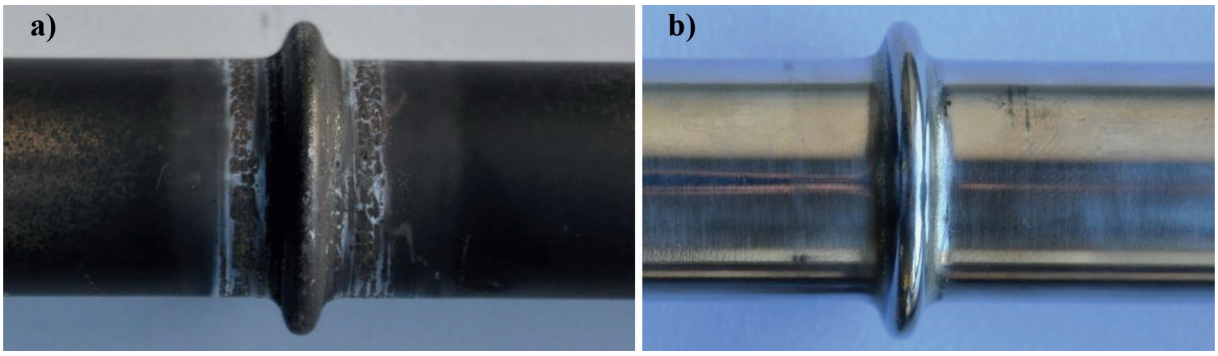

Figure 6 *Example of the final bellow-lens shape: a) just after process with absorber, b) after polishing*

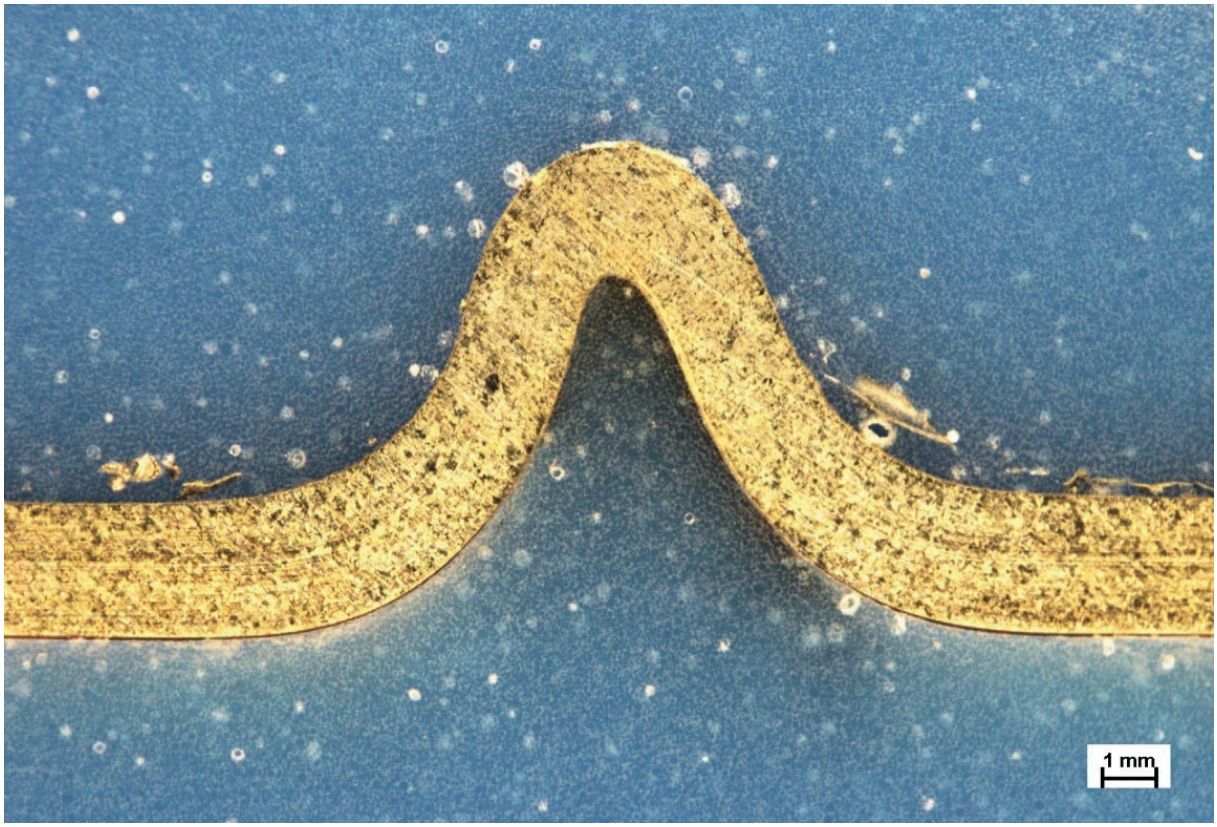

Figure 7 *An exemplary view of the expansion joint bulge formed after the mechanically assisted laser forming process*

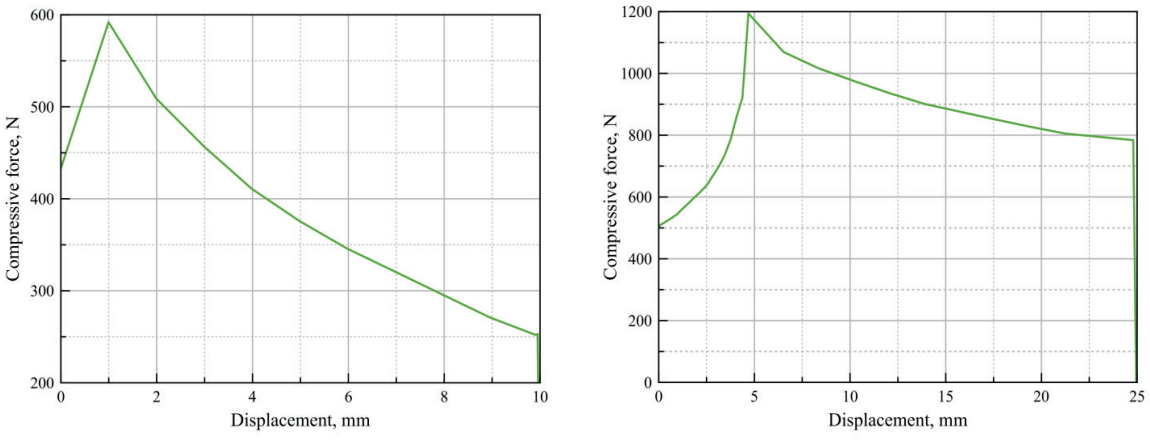

a) *b)*

Figure 8 *Change of the pushing force during the element compression under expansion joint manufacturing process: a) for DN20 pipe, b) for DN50 pipe*

PID SENSORTHERM REGULUS RD00 00 regulator, controlling the CO_2 laser power, was used. Pre-processed measurement data are sent to the application on an ongoing basis for their visualization and archiving in the test report. The implemented actuator control algorithm is shown in the block diagram in Figure 5.

The following were used to build the research equipment:

- Siemens S7-1200 6ES7212-1AE40-0XB0 PLC controller,
- linear actuator Thompson PC-40-PA-999-B05-0250-X-F-1,
- SM86/156-4208B stepper motor - 12.2Nm,
- TB6600 stepper motor driver,
- strain gauge force sensor SPAIS FT - 5306L/±5 kN/M12x1.25/DL/5mb,
- amplifier for strain gauge WObit WDT11-U force sensors.
- SENSORTHERM REGULUS RD00 00 temperature controller with a monochromatic pyrometer.
- PC.

After the experiment performed with the parameters given in the previous chapter, it was possible to obtain the shape of the bellows-lens on the pipe. An exemplary view of the finished element is presented in Figure 6.

The cross-section of the finished element was done to check the internal shape of the created expansion joint. The view of the intersection is shown in Figure 7.

During the process, the pushing force F was also registered, the operation of which led to creation of a bellows-lens metal expansion joint. The registered forces data are presented in Figure 8.

4 Conclusions

The conducted experiment proves that the presented concept of metal expansion joints manufacturing, the so-called bellow-lens, is correct. Obtaining elements with the required geometry was preceded by many empirical tests. The selection of correct parameters of mechanically assisted laser forming, such as: the plasticization temperature of the element, the width of the plasticization zone, the compression length and the compression speed, have a significant impact on the final shape of the bellows-lens. The preliminary studies, mentioned in this paragraph, were not cited in this paper, but they can be traced under [13].

The authors confirmed that the developed technology allows the production of correct elements. The authors are convinced that the appropriate equipment will allow the production of a number of bellow-lenses on the one tubular element. It is impossible at the moment, due to the initial period of research and due to technological limitations.

As shown in Figures 6 and 7, the element geometry is correct. The buckling that forms the bellow-lens has no defects in the form of cracks or discontinuities. The upset is symmetrical and has appropriate fillets, which the authors hope, will be able to work under the correct pressure and temperature.

The diagram of force changes as a function of the piston displacement (during pipe upsetting) is also worth noting. In both cases, a characteristic peak (maximum compression force) is observable, which appears at the beginning of the process. For a DN20 pipe element, the maximum compressive force is approx. 600 N, while for a DN50 pipe element, this force is twice as high and amounts to approx. 1200 N. It should be noted that this force only reaches its maximum value for a while and it decreases. Observations during the tests show that this force reaches its maximum value when the bulge in the shape of a bellow-lens begins forming. After the bellow-lens started forming, this force diminishes. Thus, the onset of upset formation is a critical point in the process when it comes to the need to apply an appropriate force.

In the future, the authors plan to more accurately recognize the element's forming process itself by using, among others, measuring instruments with better resolution. The process temperature is approx. 1100° C and this is the hyper-quenching temperature of the X5CrNi18-10 grade steel. Therefore, the authors suspect that the crystal structure of this steel should remain an austenitic structure (without changes to material properties). Therefore, material tests are planned for the finished element, hardness tests and the distribution of alloying elements, after the laser forming process in the area exposed to the laser beam and crushing zone. In addition, strength tests of the finished element are planned. In the future, an FEM analysis of the mechanically assisted laser forming process is also planned. The results of the above-planned work will be published in the future.

Acknowledgement

The research reported herein was supported by a grant from the National Centre for Research and Development. Program title: Lider XI, grant title: "Development of new type metal expansion joints and their manufacturing technology", contract number: LIDER/44/0164/L-11/19/NCBR/2020.

Conflicts of interest

The authors declare that they have no known competing financial interests or personal relationships that could have appeared to influence the work reported in this paper.

References

[1] ZHAPBASBAYEVA, U. K., RAMAZANOVAA, G. I., BOSSINOVAB, D. Z., KENZHALIYEVAC, B. K. Flow and heat exchange calculation of waxy oil in the industrial pipeline. *Case Studies in Thermal Engineering* [online]. 2021, **26**, 101007. eISSN 2214-157X. Available from: https://doi.org/10.1016/j.csite.2021.101007

[2] Standards of the expansion joint manufacturers association.10th ed. 10th EJMA, 2019.

[3] DANIELEWSKI, H., MESKO, J., NIGROVIC, R., NIKOLIC, R. R., HADZIMA, B., GUBELJAK, N. Laser cutting of ductile cast iron. *Materials Testing* [online]. 2020, **62**, p. 820-826. ISSN 2195-8572. Available from: https://doi.org/10.3139/120.111548

[4] DANIELEWSKI, H., ZRAK, A. Concept of laser welding of concentric peripheral lap joint. *Materials Research Proceedings* [online]. 2022, **24**, p. 227-232. eISSN 2474-395X. Available from: https://doi.org/10.21741/9781644902059-33

[5] RADEK, N., PIETRASZEK, J., BRONCEK, J., GONTARSKI, D., SZCZOTOK, A., PARASKA, O., MULCZYK, K. Laser processing of WC-Co coatings. *Materials Research Proceedings* [online]. 2022, **24**, p. 34-38. eISSN 2474-395X. Available from: https://doi.org/10.21741/9781644902059-6

[6] TOFIL, S., MANOHARAN, M., NATARAJAN, A. Surface laser micropatterning of polyethylene terephthalate (PET) to increase the shearing strength of adhesive joints. *Materials Research Proceedings* [online]. 2022, **24**, p. 27-33. eISSN 2474-395X. Available from: https://doi.org/10.21741/9781644902059-5

[7] DUTKIEWICZ, J., ROGAL, L., KALITA, D., KAWALKO, J., WEGLOWSKI, M. S., KWIECINSKI, K., SLIWINSKI, P., DANIELEWSKI, H., ANTOSZEWSKI, B., CESARI, E. Microstructure, mechanical properties, and martensitic transformation in NiTi shape memory alloy fabricated using electron beam additive manufacturing technique. *Journal of Materials Engineering and Performance* [online]. 2022, **31**, p. 1609-1621. ISSN 1059-9495. Available from: https://doi.org/10.1007/s11665-021-06241-x

[8] SCENDO, M., SPADLO, S., STASZEWSKA-SAMSON, K., MLYNARCZYK, P. Influence of heat treatment on the corrosion resistance of aluminum-copper coating. *Metals* [online]. 2020, **10**, 966. eISSN 2075-4701. Available from: https://doi.org/10.3390/met10070966

[9] VOLLERTSEN, F. Mechanisms and models for laser forming. In: Laser Assisted Net Shape Engineering LANE'94: proceedings.1994. p. 345-360.

[10] REUTZEL, E. W., MARTUKANITZ, R. P., MICHALERIS, P., ZHANG, L., SAVITZ, A.J., MAGNUSEN, J. P., ABURDENE, J. U., GOMBOTZ, K. J. Development of a system for the laser assisted forming of plate. *Journal of Laser Applications* [online]. 2001, **779**. eISSN 1938-1387. Available from: https://doi.org/10.2351/1.5059935

[11] MAGEE, J., DE VIN, L. J. Process planning for laser-assisted forming. *Journal of Materials Processing Technology* [online]. 2002, **120**(1-3), p. 322-326. ISSN 0924-0136, eISSN 1873-4774. Available from: https://doi.org/10.1016/S0924-0136(01)01134-7

[12] GEIGER, M., MERKLEIN, M., PITZ, M. Laser and forming technology - an idea and the way of implementation. *Journal of Materials Processing Technology* [online]. 2004, **151**, p. 3-11. ISSN 0924-0136, eISSN 1873-4774. Available from: https://doi.org/10.1016/j.jmatprotec.2004.04.004

[13] KURP, P., DANIELEWSKI, H. Metal expansion joints manufacturing by a mechanically assisted laser forming hybrid method - concept. *Technical Transactions* [online]. 2022, **119**(1), p. 1-7. eISSN 2353-737X. Available from: https://doi.org/10.37705/TechTrans/e2022008

[14] KURP, P. Method and device for production of metal expansion joints. RP Patent, Pat. 240903, 2022-04-11. Warsaw: The Patent Office of the Republic of Poland, 2022.

[15] MILLS, K.C. *Recommended values of thermophysical properties for selected commercial alloys*. 1st ed. Abington, England: Woodhead Publishing Limited, 2002. ISBN 0-87170-753-5, p. 127-134.

CYCLIC VARIABILITY CORRELATIONS TO OPERATING CONDITIONS FOR SPARK-IGNITION ENGINES

Mohamed I. Amin[1,*], Ali Elmaihy[1], Moatasem Shahin[2]

[1]Mechanical Power Engineering Department, Military Technical College, Cairo, Egypt
[2]Mechanical Engineering Department, School of Engineering, Badr University of Cairo, Cairo, Egypt

*E-mail of corresponding author: mamin@mtc.edu.eg

Mohamed I. Amin 0000-0002-4348-6595, Ali Elmaihy 0000-0002-3917-9533,
Moatasem Shahin 0000-0003-3662-2453

Resume

Variations of successive combustion cycles are associated with power losses, vibration and fluctuations in the engine speed, torque and work done. Previous studies declared that the elimination of cycle-to-cycle variation (CCV) could improve the engine power by 10 %. This work aims at correlating cyclic variability to engine operating conditions to determine the relevant operating conditions that affect the CCV and help designers to predict it. Experimental work was carried out on spark ignition, 4-stroke, 4-cylinder, 2.2 liters, with an 8.85:1 compression ratio and a maximum power of 85 kW at 5,000 rpm. The cyclic variability of many indicators is calculated from the measured in-cylinder pressure data. Results have been used to introduce new correlations considering the effect of normalized speed and load on cyclic variability with acceptable fit. These correlations could be a useful tool in early design calculations, CCV modeling and control.

Article info

Received 11 December 2022
Accepted 10 February 2023
Online 24 March 2023

Keywords:

spark ignition engines
cyclic variability
engine speed
engine load
compression ratio

Available online: https://doi.org/10.26552/com.C.2023.035

ISSN 1335-4205 (print version)
ISSN 2585-7878 (online version)

1 Introduction

Cyclic variability in spark-ignition engines causes a drop in overall engine performance and high emissions [1]. So, the control of Cycle-to-Cycle Variation (CCV) becomes a main target in the research field to improve engine efficiency and diminish their emissions.

Indicators have been developed to quantify the cyclic variability in internal combustion engines [2-5]. Based on these works, the CCV can be characterized by (i) the variation in pressure-related parameters; maximum pressure $(P_{\max})$, crank angle at maximum pressure $(\theta_{P\max})$, maximum rate of pressure rise $\left[\frac{dP}{d\theta}\right]_{\max}$, the crank angle at the maximum rate of pressure rise $\left(\theta_{\left(\frac{dp}{d\theta}\right)\max}\right)$, or coefficient of variance in indicated mean effective pressure (COV_{IMEP}), (ii) the concentration of exhaust gases components; (HC), (CO) or (NO_x), (iii) flame front-related parameters; flame front position (L), crank angle lapse between the flame front arrivals to two pre-specified different locations in the cylinder θ_{L1-2}, displacement of the flame kernel center from the spark gap at different crank angles $\left(\frac{dc}{d\theta}\right)$, or (iv) combustion related parameters; maximum rate of heat release $\left(\frac{dQ}{d\theta}\right)_{\max}$, maximum rate of mass burning $\left(\frac{dX_b}{d\theta}\right)_{\max}$, ignition delay $\Delta\theta_d$, combustion duration $\Delta\theta_b$, or time elapse from ignition to a moment, at which a certain mass fraction is burnt $\Delta\theta_{Xb}$.

Factors that influence the cyclic variability in the SI engines have been extensively studied during the last couple of decades. Authors have identified factors affecting the CCV to include mixture composition factors, cylinder charge factors, spark factors and in-cylinder mixture motion factors. Chemical (combustion-related factors) and physical (operating conditions and engine geometry) factors have also been ascribed to CCV. It is a common opinion [6-8], that the higher the laminar flame propagation velocity for a given type of fuel, the higher is the burning rate and the less is the CCV due to the combustion process. Examination of the overall equivalence ratio reveals [9-11] that minimum CCV occurs at a slightly rich mixture equivalence ratio (1-1.2) [12], which gives the shortest combustion

duration and the highest peak pressure. Fraction of diluent studies, some of them incorporating skip firing to vary scavenging, confirm that the higher the diluent concentration the less is the burning rate and the greater the CCV [13-15]. This observation reveals the criteria for minimizing the NO_x emissions through the exhaust gas recirculation and the criteria for minimizing the CCV conflict. Mixture non-homogeneity as a result of imperfect fuel atomization and evaporation process, or as a result of poor mixing between the fresh charge and residual gases, repeatedly yields the conclusion that as mixture non-homogeneity increases, cyclic variability increases due to lower growth of pressure rate and predominant deceleration of flame propagation speed [16-18]. However, Ozdor [5] declares that the effect of inhomogeneity is still uncertain because its effect depends, to a large extent, on the turbulence intensity and scales.

The factors mentioned in the previous paragraph relate to mixture composition. Ignition-related factors follow. Examination of spark timing results [9, 19-21] yields a common conclusion that the minimum CCV can be achieved when ignition occurs at maximum break torque (MBT). Investigations of spark discharge characteristics, which means spark duration and energy, lead to two conflicting conclusions. First, the quicker the flame kernel reaches a critical size, as affected by the high spark energy, the lower is combustion-related cyclic variability [20, 22]. Second, spark discharge characteristics have been concluded not to affect the CCV, as long as the mixture can be ignited [5, 21, 23-24]. Spark plug design may influence the CCV through the shape and number of electrodes by affecting the flame/plug contact area fraction and thereby affecting flame kernel heat loss and through the spark gap by affecting the flame kernel development [24-26]. Some authors find no effect of electrode geometry on the standard deviations in burning times of the smallest flame kernel [27]; while others confirmed that fewer variations, especially in terms of the CCV_{IMEP} are experienced for cylinders equipped with four electrode plugs. Spark plug number and location have a strong influence on cyclic combustion variations [28]. Any change in these parameters decreases the maximum flame travel distance or increases the rate of mass burning and hence, decreases the flame travel times, resulting in lower cyclic variations [29].

The CCV factors related to in-cylinder mixture motion are described next. Due to the probabilistic nature of in-cylinder turbulence motion, investigators consider in-cylinder mixture motion as the major cause of the CCV that hampers engine performance. The mean flow velocity in the vicinity of the spark gap has a dominant effect on the very early stage of sparking and flame initiation; it affects the flame kernel growth rate through an alteration of spark characteristics and flame kernel convection [30-32]. Investigations of spark plug orientation, concerning the mean velocity vector, result in the observations that the cross-flow orientations produce the lowest levels of cyclic variability in indicated mean effective pressure (IMEP), while an upstream orientation produces the highest [33-34]. It is believed that turbulence intensity and scales affect combustion by wrinkling and corrugating the flame front, thus increasing flame surface area [35]. Nishiyama et al. [36] commented that the level of turbulence intensity near the spark gap should be increased up to a certain limit, depending on operating conditions and engine geometry. Above this limit, excessive flame stretching occurs causing the local flame quenching and increased CCV. Overall, in-cylinder flow pattern affects the CCV through early flame kernel convection and turbulence generation. Authors [37-39] provide different conclusions regarding swirl, tumble and squish motions, but the most common conclusion is that the swirl motion can provide a significant decrease in cyclic variability as measured by CCV in pressure, combustion development, burning rate and IMEP.

Sources of CCV have been hypothesized and discussed by different authors [5, 21, 40]. It is a common opinion that cyclic variability in turbulence intensity, cyclic variability of in-cylinder mixture homogeneity, cycle-to-cycle variation in velocity pattern inside the cylinder, cycle-to-cycle variation of mixture composition and cyclic variability in spark discharge characteristics are the main sources of CCV in combustion cycles.

Previous studies [41-42] show different approaches to model combustion and in-cylinder combustion process CCV. Some authors investigated the effect of displacement of the flame kernel on CCV in combustion. Others studied the turbulence variations, manifold pressure and residual gas effect on cycle-to-cycle variations in flame development using different approaches like the Auto-Regressive Moving Average (ARMA) technique.

It is a very complex and difficult task to quantify and control the cyclic variability phenomena given their dependence on such a large number of factors. To determine the lowest number of relevant independent factors, needed to be controlled to control CCV, it is mandatory to investigate them individually and in a factorial manner. Although most of these factors depend, more or less, on operating parameters, there is no explicit relation that quantifies cyclic variability in terms of operating parameters. This work aims to study the effect of operating parameters (speed, load), rather than one design parameter (compression ratio) on CCV experimentally. Moreover, empirical relations that predict the cyclic variability in terms of operating parameters are introduced. Such investigation could be an important step for engine assessment and cyclic variability phenomena prediction, modelling and control.

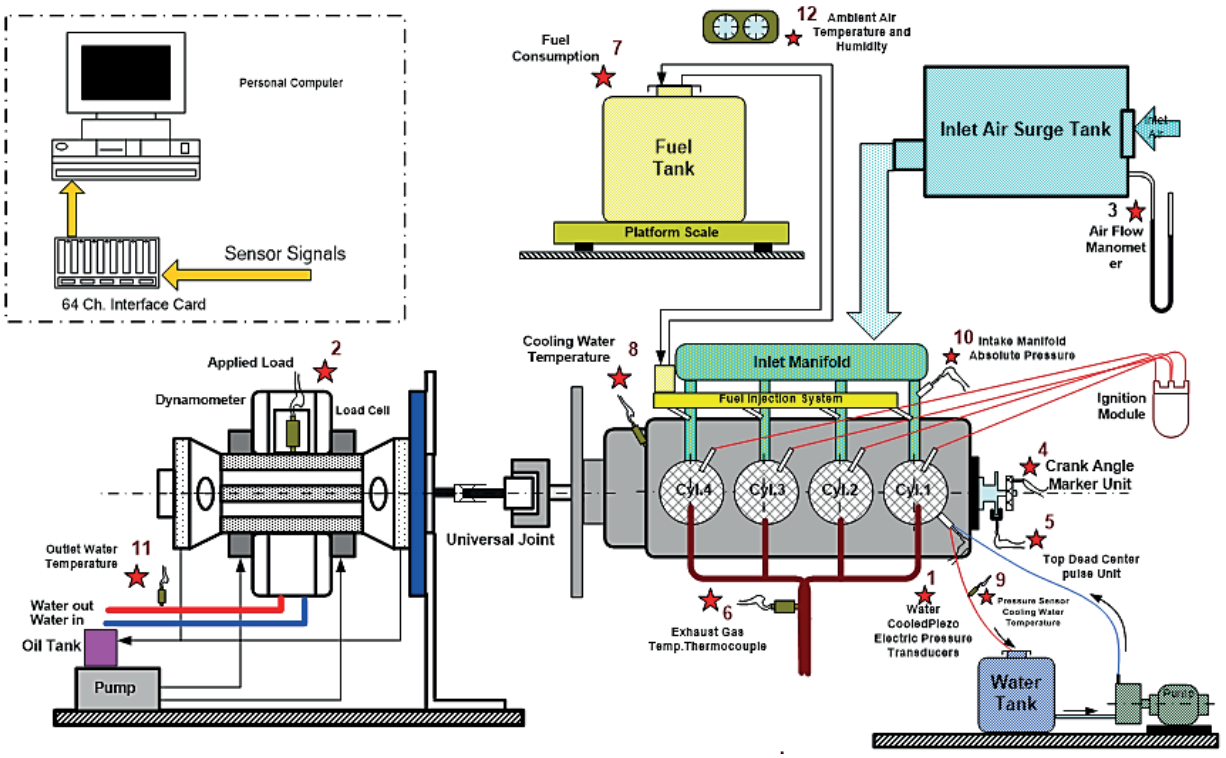

Figure 1 *Schematics of the test rig*

2 Experimental setup and program

The first stage of this research work was to erect a modern test rig for the study of the characteristics of spark-ignition engines. The test rig included an engine and the instrumentation that was necessary for measuring and recording the parameters important to engine performance and combustion. The experimental investigations were conducted on a General Motors four-stroke, four-cylinder water-cooled spark-ignition engine. The engine capacity was 2.2 litres, with an 8.85:1 compression ratio, 115 horsepower maximum power at 5,000 rpm and 183 Nm maximum torque at 3,600 rpm. The engine external load was applied by a Go-Power Systems hydraulic dynamometer; model D-356, with water as the working fluid. The maximum braking torque could reach 690 Nm at 3,000 rpm. Figure (1) gives a general schematic of the complete test rig with the locations of the used sensors and transducers. The positions of measuring transducers and pickups (relevant to Figure 1) with their main specifications are listed in Table 1.

The data acquisition system, which was used in this work, is a 64-input channel online system for recording the slowly and quickly varying parameters. The system operates in a sequence of input channel multiplexing, signal sampling and holding, analogue to digital conversion and finally, storing the digital result. This sequence is controlled, step by step, by a computer, which at the end of each measuring procedure stores the test data. The used card is an NI input-output data acquisition one type PCI-6071E with 64 analogue inputs A/D channels and two outputs D/A channels. The resolution of this card is 12 bits. The sampling rate of the A/D channels is software adjustable with a maximum 1.25 MHz rate. The Lab-View software was used in acquiring and saving the data. The acquisition rate, start and duration of acquisition, number of channels and data storage processes, were controlled through the program. To keep the acquisition process as fast as possible, this program was used for acquiring and saving only; another MATLAB program was written for later data analysis.

At the beginning of this work, 600 to 1,000 successive data cycles were acquired in each test. The resulting data was then divided into batches, each containing the pressure data for 25 successive cycles. The standard deviations and the coefficient of variance of the IMEP were then repeatedly evaluated for the first group of cycles, which contained an increasing multiple of 25 cycles. It is evident that both the coefficient of variance and the standard deviation become almost constant after 300 cycles, as shown in Figure (2). Therefore, it was concluded that it is necessary to investigate the data of at least 300 successive cycles to study the cyclic variability problem.

Steady-state tests were carried out under different operating conditions: namely engine speed and brake load. At each engine speed of 1,000, 1,500, 2,000, 2,500 and 3,000 rpm, data acquisition was performed at specific brake loads, namely 00, 27.1, 54.2, 81.35, 108.35, 135.58 and 162.7 N.m. These values of speed

Table 1 *The measured parameters with their corresponding measuring instruments, accuracies and uncertainties (Measured Point no. is pertinent to Figure 1).*

Meas. Point No	Measured Parameter	Instrument	Range	Accuracy	Uncertainty (%)
1	Cylinder Pressure	6041A Kistler Water-Cooled Pressure Transducer	0 - 250 bar	Th. Sens. < ± 0.5%. Linearity 0.5% OFS. Hysteresis 0.5% OFS	± 0.2%
10	Intake manifold absolute pressure	PX-203 OMEGA Absolute Pressure Transducer	0-206.8 kpa	0.25% FS. Th. effect 0.009% FS/1F	NA
4	Crank Angle and Engine Speed	Encoder (WD GI 58B)	1 pulse/ 0.25 ° CA to 1 pulse/ 1 ° CA.)	Phase Shift 90° ± max. 7. 5% of the period duration. pulse-/pause-ratio ≤ 5000 ppr: 50% ± max. 7%	± 0.6%
2	Load cell reading	Load Cell Central CTD2-300	1334.5 N	< 0.05% OFS. Th. shift < 0.09% FS/C	± 0.1%

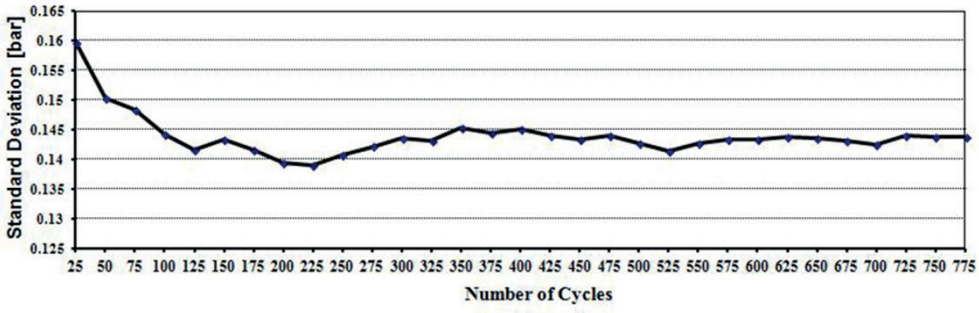

(A) Applied Load = 54.2 Nm, Engine Speed = 1,000 rpm

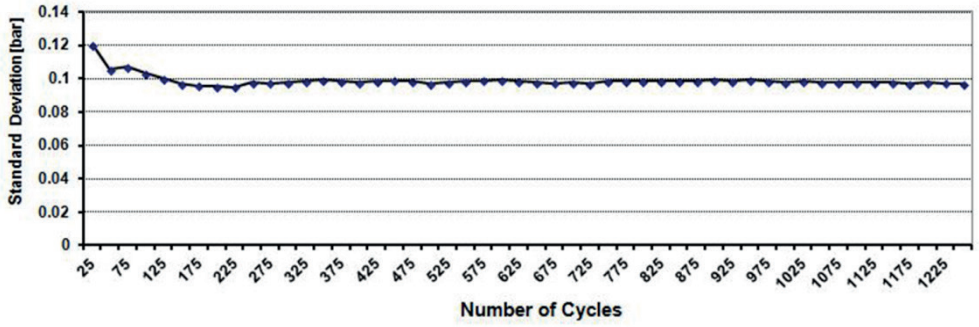

(B) Applied Load = 27.1 Nm, Engine Speed = 1,500 rpm

Figure 2 *Sample of the IMEP standard deviation in terms of number of successive cycles at different operating conditions*

and load were chosen to cover the widest range of engine operation (35 combinations) and thus increase, as much as possible, the range of the cyclic variability investigation. In each test, the in-cylinder pressure, crank angle and TDC marker data were acquired and retained for 300 successive cycles. Engine speed and load, in addition to fuel and air consumption, exhaust temperature and intake manifold absolute pressure, were monitored and recorded, as well.

3 Results and discussion

3.1 Effect of external applied load and engine speed on cyclic variation

Heywood [4] defined the coefficient of variance of indicated mean effective pressure (COV_{IMEP}) as an important indicator of the cyclic variability. This variable is defined as the ratio of the standard deviation

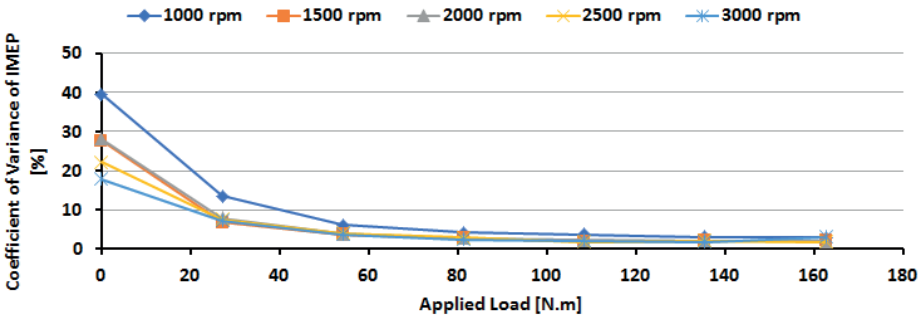

Figure 3 *Dependence of the COV_{IMEP} on applied load at different engine speeds*

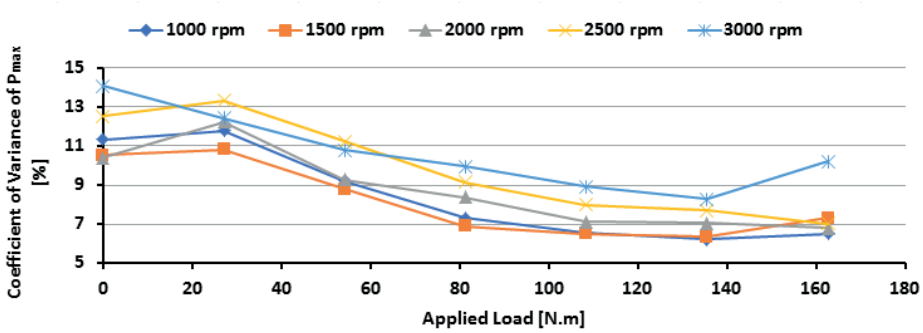

Figure 4 *Dependence of the COV of maximum pressure on applied load at different engine speeds*

in the indicated mean effective pressure (σ_{IMEP}) over many successive cycles divided by its mean value and is usually expressed as a percentage as follows:

$$COV_{IMEP} = \frac{\sigma_{IMEP}}{IMEP} * 100\,\%, \qquad IMEP = \frac{\oint P\,dV}{Swept\ Volume}. \tag{1}$$

Figure 3 indicates the dependence of the COV of the IMEP on the externally applied loads [Nm] at constant speeds. The values of the COV are almost constant at loads higher than 30 Nm, irrespective of engine speed. However, at lower loads, the COV progressively increases, especially at engine speeds below 1500 rpm. The negative effect at low loads can be attributed to the increased amount of residual gases remaining in the combustion chamber at the end of the scavenging period, which leads to lower combustion flame speed. Besides this negative effect, there is the negative effect of the valve overlap at low engine speeds accounts for the increased COV at 1000 rpm. In addition, at near idle conditions (low engine speeds and low loads), the low level of turbulence results in a poor premixing of the fresh charge and higher cyclic variations.

The effect of the engine load on the COV of the maximum value of the cylinder pressure at constant speeds is depicted in Figure 4. It is evident that the COV increases slightly as the loads decrease to lower than 30 Nm, the same trend as the COV_{IMEP}.

Figures 5 to 7 summarize the effects of load on the cylinder pressure history at constant speeds and show that the combustion process is greatly disturbed at low loads. This is manifested in the large relative changes in the timing ($\theta_{P\max}$) of the maximum cylinder pressure, as shown in Figure 5. Consequently, the expansion process, represented by expansion polytropic exponent n_2, is affected, especially at low loads, Figure 7. On the other hand, Figure 6 proves that the compression curve, represented by compression polytropic exponent n_1, is only slightly affected at low loads. It is believed that this is a result of the ignition point changing and the beginning of the combustion process.

The effects of the engine speed on the COV of the various parameters seem to be relatively small at all the loads except close to idle conditions (low speed and low load). This supports the previous analysis and confirms that cyclic variability is practically experienced at speeds below 1,500 rpm and external braking loads less than 30 N.m. This is seen in Figures 5 to 7, where there are no significant changes at different speeds except at low loads.

3.2 Correlating cyclic variations to engine speed and external load

Previous results and discussion show that the cyclic variations are dependent on engine speed and external load. Other design characteristics, such as the compression ratio, valve timing and ignition and fuel system parameters, are expected to contribute to the cyclic variations. Further investigations of these parameters need to be conducted in a factorial manner to provide a complete map of the CCVs.

The IMEP value is affected mainly by the pressure-

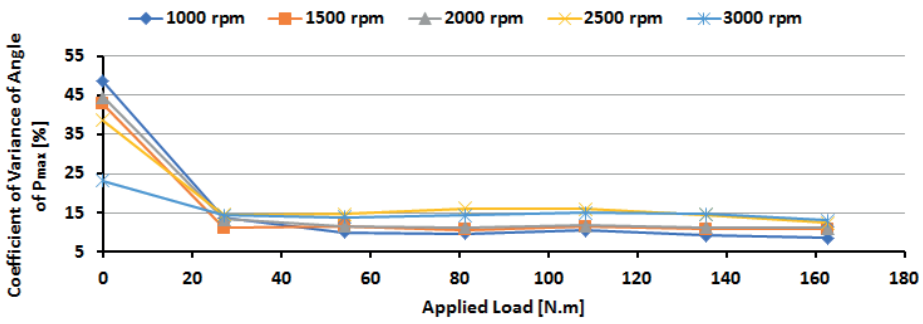

Figure 5 *Dependence of the COV of* θ_{Pmax} *on applied load at different engine speeds*

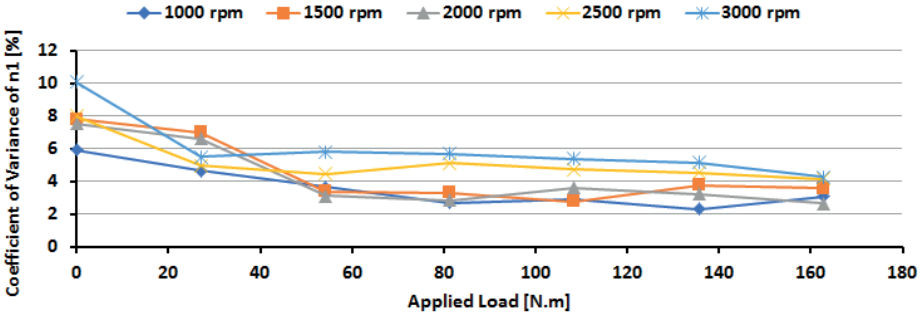

Figure 6 *Dependence of the COV of compression polytropic exponent* (n_1) *on applied load at different engine speeds*

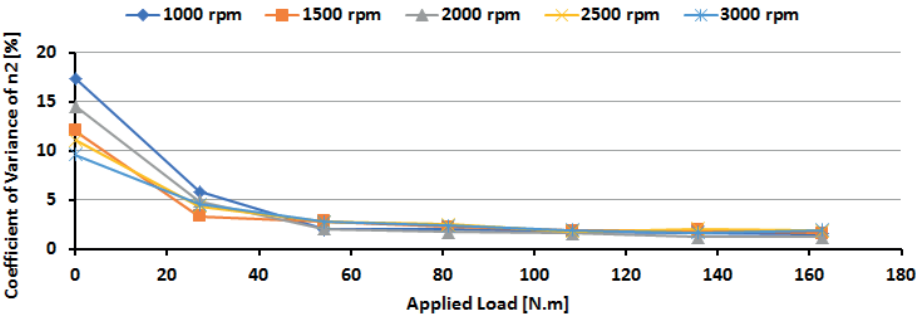

Figure 7 *Dependence of the COV of expansion polytropic exponent* (n_2) *on applied load at different engine speeds*

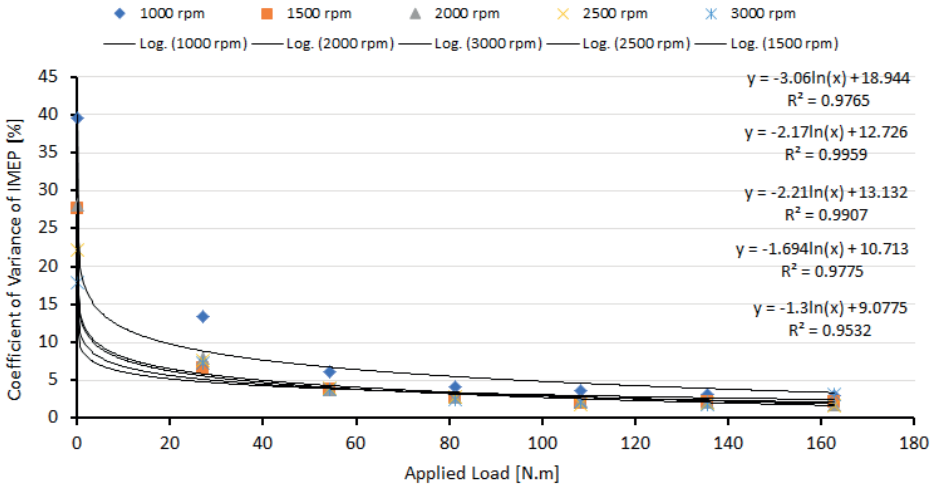

Figure 8 *Trend lines of the* COV_{IMEP} *dependence on applied load at constant speeds*

Table 2 *Correlation formulae of the COV of characterizing parameters*

Correlation Formulae	R^2	Standard Error	Significance F
$COV_{IMEP} = -0.678\frac{\ln(v)}{v} + 7.1436\frac{e^{-9.73\mu}}{v} - 9.311\left(\frac{\mu}{v}\right)^{0.18} + 10.993$	0.987813	1.046008	9.7E-30
$COV_{P_{max}} = -102.33(v) - 81.651(\mu) + 103.287(v)^{1.1} - 7.0551(e^{-12\mu}) + +71.0315(\mu)^{1.25} + 21.191$	0.942634	0.584337	4.33E-17
$COV_{\theta P_{max}} = 256.629(v) + 25.3746(\mu) - 128.94(v)^2 - 55.889\ln(v) + +8.76612\left(\frac{e^{-12\mu}}{v}\right) - 19.025(\mu)^2 - 16.599\left(\frac{\mu}{v}\right)^{0.12} - 113.28$	0.953413	2.516873	2.56E-16
$COV_{n1} = -31.412(v) - 29.104(\mu) + 24.0818(v)^2 + 52.0949(\mu)^2 - -29.125\mu^3 + 0.99789\left(\frac{Ln(v)}{v}\right) - 0.3357\left(\frac{\mu}{v}\right) - 0.6793\left(\frac{e^{-14\mu}}{v}\right) + 20.0566$	0.870005	0.748355	1.15E-09
$COV_{n2} = -0.1108\frac{Ln(v)}{v} + 2.62169\left(\frac{e^{-9\mu}}{v}\right) - 5.5041\left(\frac{\mu}{v}\right)^{0.16} + 7.26$	0.973009	0.694006	2.17E-24

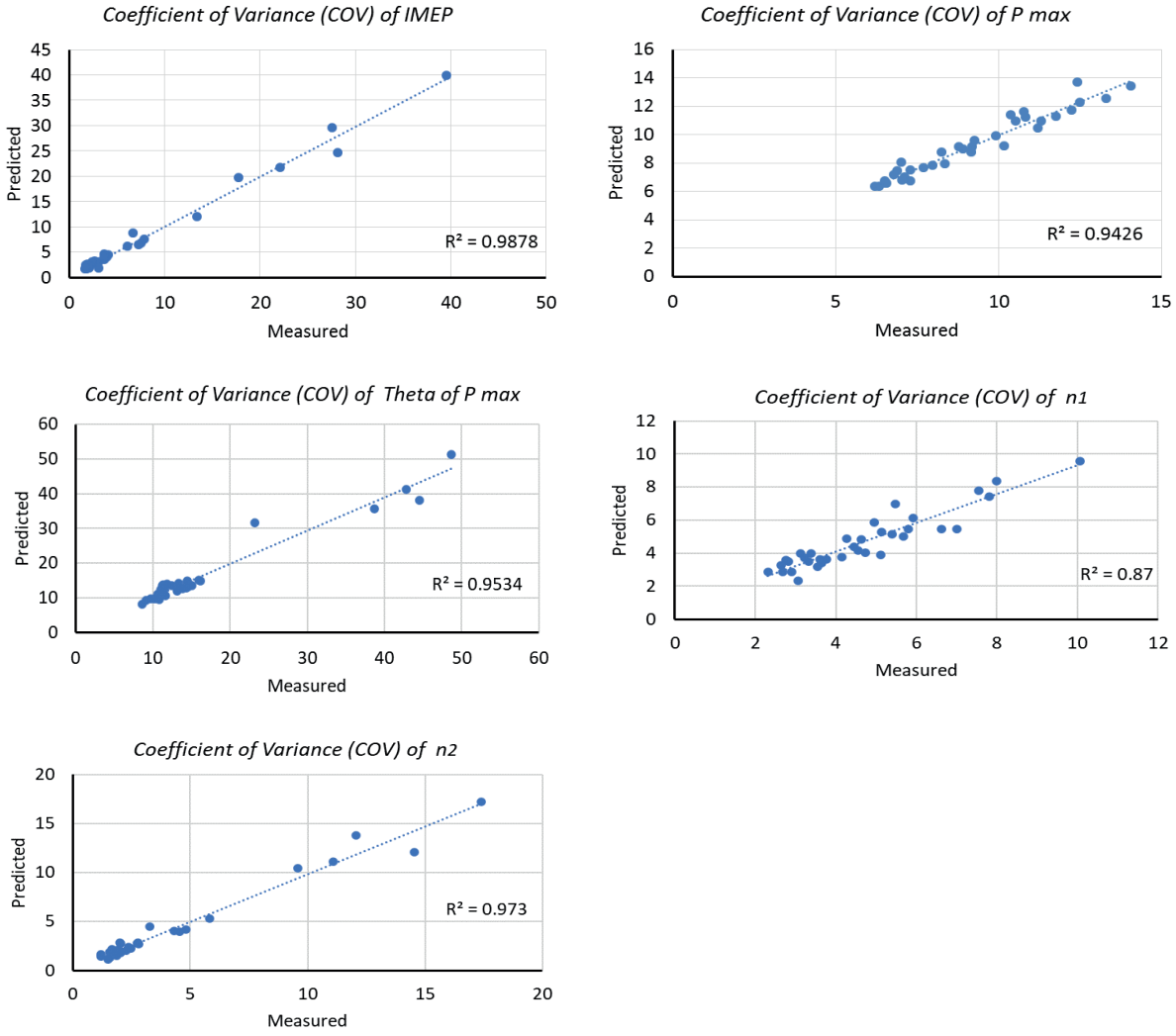

Figure 9 *Measured VS predicted COV of different characterizing parameters*

volume diagram characterizing parameters, such as the maximum pressure P_{max}, the crank angle at which maximum pressure occurs θ_{Pmax}, compression polytropic exponent n_1 and expansion polytropic exponent n_2. So, it is convenient to investigate the effect of operating conditions (speed and load) on these characterizing parameters variation.

Figure 8 displays the dependence of the COV of the IMEP on the externally applied load with the trend lines drawn at constant engine speeds. Several attempts

are made to obtain a sound mathematical dependence of the COV on the engine load, with different degrees of success. The best results are obtained when the dependence is assumed to take a logarithmic form as suggested by the shapes of the trend lines. The least-square curve fitting techniques are used to evaluate the coefficients of the assumed equation, which gives the minimum residuals ($R^2 > 0.95$).

The procedure that was previously followed is repeated to correlate the characterizing parameters variations and operating conditions of the engine. These steps provide guidelines about the nature of relations. Regression techniques are then used to correlate these parameters to both engine speeds and loads.

To normalize the variables and make the empirical relations more applicable to other engines, the following ratios are introduced:

$$v = \frac{Engine\ Speed}{Engine\ Speed\ at\ Maximum\ Torque}, \qquad \mu = \frac{Applied\ External\ Torque}{Maximum\ Engine\ Torque}. \tag{2}$$

These ratios are substituted into the relations and the final shape of the equations describing the COVs of the IMEP, P_{max}, θ_{Pmax} , n_1 and n_2 are provided, as shown in Table 2.

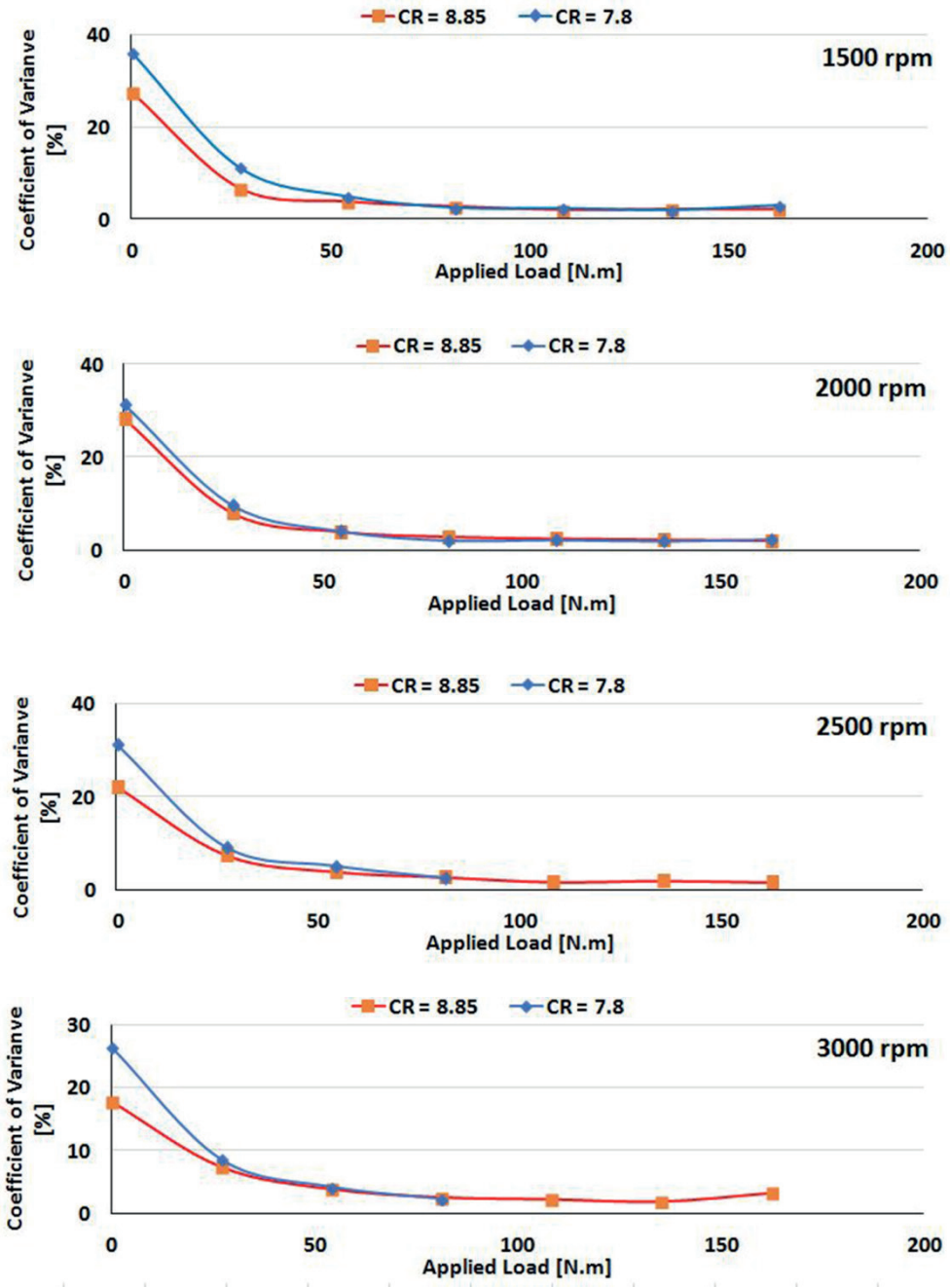

Figure 10 *Coefficient of the IMEP variance at two values of Compression Ratios (CR)*

These equations were used to calculate the COVs under the same measurements' conditions. The calculated results are confirmed by the measured values in Figure 9. For example, the COV_{IMEP} can be predicted within 98 % accuracy, while P_{max} with 94 % and so on as shown in Table 2 and Figure 9. The highest percentage of error is encountered at low load conditions.

3.3 Compression ratio effect on cyclic variability

Figure 10 presents a comparison of the measured COVs of IMEP at the compression ratio of 7.8 to those that were obtained with the initial compression ratio of 8.85. The figure proves that the dependence of the cyclic variability on the engine speed and load generally remains the same. However, with the lower compression ratio, the cyclic variability seems to increase at low loads, irrespective of the engine speed. This is attributed to the lower pressure and temperature at the end of the compression stroke, which eventually leads to longer delay periods and lower flame propagation speeds. The fresh charge, being slightly rich under the conditions of low load and the poor mixing at low speeds, can also increase the cyclic variability. Measurements could not be conducted for all the cases at high loads and speeds, at low compression ratios, as shown in Figure 10 at 2,500 and 3,000 rpm.

4 Conclusions

Extensive experimental work has been conducted to investigate the cyclic variability in spark-ignition engines. Conclusions can be summarized as follows:

1. Calculations of standard deviation of the COV_{IMEP} for different batches of successive cycles show that the optimum number of successive cycles, needed to be acquired to investigate the CCV problem, should be at least 300 cycles, at which the value of standard deviation starts to become constant. Previous works showed wide variations regarding that number starting from 42 up to 1,000 cycles.
2. Experimental results show that the COV are higher at lower loads and speeds (lower than $\mu = 16.5\,\%$ and $\nu = 41\,\%$, corresponding to 30 Nm load and 1,500 rpm speed in this engine respectively), due to low level of turbulence, poor mixing and higher residual gases. Moreover, the applied load has a dominant effect more than the engine speed in the cyclic variability problem, this is clear by checking the coefficients of relations illustrated in Figure (2).
3. By investigating the P-V curves for successive cycles it was found that the variations occur in six characterizing parameters, namely in-cylinder maximum pressure, the crank angle at which the maximum pressure occurs, compression and expansion polytropic indexes and suction and exhaust lines. The first four characterizing parameters exhibit the highest variations.
4. Novel empirical mathematical relations for IMEP and pressure characterizing parameters variation have been introduced (Table 2), as a function of applied load and speed, using an enormous amount of experimental data that were acquired at a high rate of 50 kHz.
5. The empirical relations were normalized to be applicable to any spark ignition engine by using the two dimensionless parameters ν and μ, instead of using absolute engine speed and applied load. Those relations give acceptable errors in predicted results compared to the measured ones.
6. In the case of a lower compression ratio, the cyclic variability seems to increase at low loads, irrespective of the engine speed.

These normalized empirical relations could be a useful tool in the early stages of engine design procedures and could be a guideline for cyclic variability control and assessment. However, other design and operating parameters, such as more compression ratio values, inlet conditions etc. need extensive investigation to introduce a complete map for cyclic variability.

Acknowledgement

The authors would like to thank the Department of Mechanical Power and Energy, Military Technical Collage for continuous support.

Conflicts of interest

The authors declare that they have no known competing financial interests or personal relationships that could have appeared to influence the work reported in this paper.

References

[1] HANUSCHKIN, A., SCHOBER, S., BODE, J., SCHORR, J., BOHM, B., KRUGER, CH., PETERS, S. Machine learning-based analysis of in-cylinder flow fields to predict combustion engine performance. *International Journal of Engine Research* [online]. 2019, **22**(1), p. 257-272. ISSN 1468-0874, eISSN 2041-3149. Available from: https://doi.org/10.1177/1468087419833269

[2] YOUNG, M. Cyclic dispersion in the engine - a literature survey. *SAE Technical Paper* [online]. 1981, 810020. ISSN 0148-7191, eISSN 2688-3627. Available from: https://doi.org/10.4271/810020
[3] MATEKUNAS, F. A. Modes and measures of cyclic combustion variability. *SAE Technical Paper* [online]. 1983, 830337. ISSN 0148-7191, eISSN 2688-3627. Available from: https://doi.org/10.4271/830337
[4] HEYWOOD, J. B. *Internal combustion engine fundamentals*. USA: McGraw-Hill, Inc., 1988. ISBN 0-07-028637-X.
[5] OZDOR, N., DULGER, M., SHER, E. Cyclic variability in spark ignition engines. A literature survey. *SAE Technical Paper* [online]. 1994, 940987. ISSN 0148-7191, eISSN 2688-3627. Available from: https://doi.org/10.4271/940987
[6] BAYRAKTAR, H. Theoretical investigation of flame propagation process in an SI engine running on gasoline-ethanol blends. *Renew. Energy* [online]. 2007, **32**(5), p. 758-771. ISSN 0960-1481, eISSN 1879-0682. Available from: https://doi.org/10.1016/j.renene.2006.03.017
[7] WANG, S., JI, C. Cyclic variation in a hydrogen-enriched spark-ignition gasoline engine under various operating conditions. *International Journal of Hydrogen Energy* [online]. 2012, **37**(1), p. 1112-1119. ISSN 0360-3199, eISSN 1879-3487. Available from: https://doi.org/10.1016/j.ijhydene.2011.02.079
[8] HANUSCHKIN, A., ZUNDORF, S., SCHMIDT, M., WELCH, C., SCHORR, J., PETERS, S., DREIZLER, A., BOHM, B. Investigation of cycle-to-cycle variations in a spark-ignition engine based on a machine learning analysis of the early flame kernel. *Proceedings of the Combustion Institute* [online]. 2020, **38**(4), p. 5751-5759. ISSN 1540-7489, eISSN 1873-2704. Available from: https://doi.org/10.1016/j.proci.2020.05.030
[9] HILL, P. G. Cyclic variations and turbulence structure in spark-ignition engines. *Combustion and Flame* [online]. 1988, **72**(1), p. 73-89. ISSN 0010-2180, eISSN 1556-2921. Available from: https://doi.org/10.1016/0010-2180(88)90098-3
[10] KAZMOUZ, S. J., HAWORTH, D. C., LILLO, P., SICK, V. Large-eddy simulations of a stratified-charge direct-injection spark-ignition engine: comparison with experiment and analysis of cycle-to-cycle variations. *Proceedings of the Combustion Institute* [online]. 2021, **38**(4), p. 5665-5672. ISSN 1540-7489, eISSN 1873-2704. Available from: https://doi.org/10.1016/j.proci.2020.08.035
[11] KAMMERMANN, T., MEROTTO, L., BLEINER, D., SOLTIC, P. Spark-induced breakdown spectroscopy for fuel-air equivalence ratio measurements at internal combustion engine-relevant conditions. *Spectrochimica Acta Part B: Atomic Spectroscopy* [online]. 2019, **155**, p. 79-89, ISSN 0584-8547, eISSN 1873-3565. Available from: https://doi.org/10.1016/j.sab.2019.03.006
[12] BOETTCHER, P. A., MEVEL, R., THOMAS, V., SHEPHERD, J. E. The effect of heating rates on low-temperature hexane air combustion. *Fuel* [online]. 2012, **96**, p. 392-403. ISSN 0016-2361, eISSN 1873-7153. Available from: https://doi.org/10.1016/j.fuel.2011.12.044
[13] ZUO, Z., ZHU, Z., LIANG, K., BAO, X., ZENG, D., KONG, L. Impact of dilution on laminar burning characteristics of premixed methane-dissociated methanol-air mixtures. *Fuel* [online]. 2021, **288**, 119741, ISSN 0016-2361, eISSN 1873-7153. Available from: https://doi.org/10.1016/j.fuel.2020.119741
[14] ZHANG, X., HUANG, Z., ZHANG, Z., ZHENG, J., YU, W., JIANG, D. Measurements of laminar burning velocities and flame stability analysis for dissociated methanol-air-diluent mixtures at elevated temperatures and pressures. *International Journal of Hydrogen Energy* [online]. 2009, **34**(11), p. 4862-4875. ISSN 0360-3199, eISSN 1879-3487. Available from: https://doi.org/10.1016/j.ijhydene.2009.03.046
[15] LIAO, S. Y., JIANG, D. M., HUANG, Z. H., CHENG, Q., GAO, J., HU, Y. Approximation of flammability region for natural gas-air-diluent mixture. *Journal of Hazardous Materials* [online]. 2005, **125**(1-3), p. 23-28. ISSN 0304-3894, eISSN 1873-3336. Available from: https://doi.org/10.1016/j.jhazmat.2005.05.021
[16] PUNDIR, B. P., ZVONOW, V. A., GUPTA, C. P. Effect of charge non-homogeneity on cycle-by-cycle variations in combustion in SI engines. *SAE Technical Paper* [online]. 1981, 810774. ISSN 0148-7191, eISSN 2688-3627. Available from: https://doi.org/10.4271/810774
[17] ZHU, Z., GU, H., ZHUB, Z., WEI, Y., ZENG, K., LIU, S. Investigation on mixture formation and combustion characteristics of a heavy-duty SI methanol engine. *Applied Thermal Engineering* [online]. 2021, **196**, 117258. ISSN 1359-4311, eISSN 1873-5606. Available from: https://doi.org/10.1016/j.applthermaleng.2021.117258
[18] WANG, Y., WEI, H., ZHOU, L., ZHANG, X., ZHONG, L. Effects of reactivity inhomogeneities on knock combustion in a downsized spark-ignition engine. *Fuel* [online]. 2020, **278**, 118317. ISSN 0016-2361, eISSN 1873-7153. Available from: https://doi.org/10.1016/j.fuel.2020.118317
[19] JI, C., WANG, S., ZHANG, B. Effect of spark timing on the performance of a hybrid hydrogen-gasoline engine at lean conditions. *International Journal of Hydrogen Energy* [online]. 2010, **35**(5), p. 2203-2212. ISSN 0360-3199, eISSN 1879-3487. Available from: https://doi.org/10.1016/j.ijhydene.2010.01.003
[20] KARVOUNTZIS-KONTAKIOTIS, A., DIMARATOS, A., NTZIACHRISTOS, L., SAMARAS, Z. Exploring the stochastic and deterministic aspects of cyclic emission variability on a high-speed spark-ignition engine. *Energy* [online]. 2017, **118**, p. 68-76. ISSN 0360-5442, eISSN 1873-6785. Available from: https://doi.org/10.1016/j.energy.2016.12.026

[21] OZDOR, N., DULGER, M., SHER, E. An experimental study of the cyclic variability in spark-ignition engines. *SAE Technical Paper* [online]. 1996, 412. ISSN 0148-7191, eISSN 2688-3627. Available from: https://doi.org/10.4271/960611

[22] ALEIFERIS, P. G., TAYLOR, A. M. K. P., WHITELAW, J. H., ISHII, K., URATA, Y. Cyclic variations of initial flame kernel growth in a Honda VTEC-E lean-burn spark-ignition engine. *SAE Technical Paper* [online]. 2000, 724. ISSN 0148-7191, eISSN 2688-3627. Available from: https://doi.org/10.4271/2000-01-1207

[23] SJERIC, M., KOZARAC, D., TATSCHL, R. Modelling of early flame kernel growth towards a better understanding of cyclic combustion variability in SI engines. *Energy Conversion and Management* [online]. 2015, **103**, p. 895-909. ISSN 0196-8904, eISSN 1879-2227. Available from: https://doi.org/10.1016/j.enconman.2015.07.031

[24] JUNG, D., SASAKI, K., SUGATA, K., MATSUDA, M., YOKOMORI, T., IIDA, N. Combined effects of spark discharge pattern and tumble level on cycle-to-cycle variations of combustion at lean limits of SI engine operation. *SAE Technical Paper* [online]. 2017, 2017-01-0677. ISSN 0148-7191, eISSN 2688-3627. Available from: https://doi.org/10.4271/2017-01-0677

[25] ABDEL-REHIM, A. A. Impact of spark plug number of ground electrodes on engine stability. *Ain Shams Engineering Journal* [online]. 2013, **4**(2), p. 307-316. ISSN 2090-4479, eISSN 2090-4495. Available from: https://doi.org/10.1016/j.asej.2012.09.006

[26] CRAVER, R. J., PODIAK, R. S., MILLER, R. D., CRAVER, R. J., PODIAK, R. S., MILLER, R. D. Spark plug design factors and their effect on engine performance spark plug design factors and their effect on engine performance. *SAE Technical Paper* [online]. 1970, 1970-02-01. ISSN 0148-7191, eISSN 2688-3627. Available from: https://doi.org/10.4271/700081

[27] HILL, P. G., KAPIL, A. The relationship between cyclic variations in spark-ignition engines and the small structure of turbulence. *Combustion and Flame* [online]. 1989, **78**(2), p. 237-247. ISSN 0010-2180, eISSN 1556-2921. Available from: https://doi.org/10.1016/0010-2180(89)90128-4

[28] RAVI, K., KHAN, M. A., BHASKER, J. P., PORPATHAM, E. Effects of spark plug configuration on combustion and emission characteristics of an LPG fuelled lean burn SI engine. *IOP Conference Series: Materials Science and Engineering* [online]. 2017, **263**(6), 062070. ISSN 1757-8981, eISSN 1757-899X. Available from: https://doi.org/10.1088/1757-899X/263/6/062070

[29] CHEN, L., WEI, H., ZHANG, R., PAN, J., ZHOU, L., FENG, D. Effects of spark plug type and ignition energy on combustion performance in an optical SI engine fueled with methane. *Applied Thermal Engineering* [online]. 2019, **148**, p. 188-195. ISSN 1359-4311, eISSN 1873-5606. Available from: https://doi.org/10.1016/j.applthermaleng.2018.11.052

[30] BERTSCH, M., SCHREER, K., DISCH, C., BECK, K. W., SPICHER, U. Investigation of the flow velocity in the spark plug gap of a two-stroke gasoline engine using laser-doppler-anemometry. *SAE Technical Paper* [online]. 2011, 2011-11-08. ISSN 0148-7191, eISSN 2688-3627. Available from: https://doi.org/10.4271/2011-32-0529

[31] SAYAMA, S., KINOSHITA, M., MANDOKORO, Y., FUYUTO, T. Spark ignition and early flame development of lean mixtures under high-velocity flow conditions: An experimental study. *International Journal of Engine Research* [online]. 2019, **20**(2), p. 236-246. ISSN 1468-0874, eISSN 2041-3149. Available from: https://doi.org/10.1177/1468087417748517

[32] GALLONI, E. Analyses about parameters that affect cyclic variation in a spark-ignition engine. *Applied Thermal Engineering* [online]. 2009, **29**(5-6), p. 1131-1137. ISSN 1359-4311, eISSN 1873-5606. Available from: https://doi.org/10.1016/j.applthermaleng.2008.06.001

[33] WANG, Y., ZHANG, J., WANG, X., DICE, P., SHAHBAKHTI, M., NABER, J., CZEKALA, M., QU, Q., GARLAN HUBERTS, G. Investigation of impacts of spark plug orientation on early flame development and combustion in a DI optical engine. *SAE International Journal of Engines* [online]. 2017, **10**(3), p. 995-1010. ISSN 1946-3936, e-ISSN 1946-3944. Available from: https://doi.org/10.4271/2017-01-0680

[34] ZHAO, L., MOIZ, A. A., SOM, S., FOGLA, N., BYBEEM, M., WAHIDUZZAMAN, S., MIRZAEIAN, M., MILLO, F., KODAVASAL, J. Examining the role of flame topologies and in-cylinder flow fields on cyclic variability in spark-ignited engines using large-eddy simulation. *International Journal of Engine Research* [online]. 2018, **19**(8), p. 886-904. ISSN 1468-0874, eISSN 2041-3149. Available from: https://doi.org/10.1177/1468087417732447

[35] TAMADONFAR, P., GULDER, O. L. Effects of mixture composition and turbulence intensity on flame front structure and burning velocities of premixed turbulent hydrocarbon/air Bunsen flames. *Combustion and Flame* [online]. 2015, **162**(12), p. 4417-4441. ISSN 0010-2180, eISSN 1556-2921. Available from: https://doi.org/10.1016/j.combustflame.2015.08.009

[36] NISHIYAMA, A., LE, M. K., FURUI, T., IKEDA, Y. The relationship between in-cylinder flow-field near spark plug areas, the spark behavior and the combustion performance inside an optical S.I. engine. *Applied Sciences* [online]. 2019, **9**(8), p. 1-13. eISSN 2076-3417. Available from: https://doi.org/10.3390/app9081545

[37] URUSHIHARA, T., MURAYAMA, T., TAKAGI, Y., LEE, K. H. Turbulence and cycle-by-cycle variation of mean velocity generated by swirl and tumble flow and their effects on combustion. *SAE Technical Paper* [online]. 1995, 412, ISSN 0148-7191, eISSN 2688-3627. Available from: https://doi.org/10.4271/950813

[38] LE COZ, J. F. Cycle-to-cycle correlations between flow field and combustion initiation in an S.I. engine. *SAE Technical Paper* [online]. 1992, 920517. ISSN 0148-7191, eISSN 2688-3627. Available from: https://doi.org/10.4271/920517

[39] MATSUDA, M., YOKOMORI, T., IIDA, N. Investigation of cycle-to-cycle variation of turbulent flow in a high-tumble SI engine. *SAE Technical Paper* [online]. 2017, 2017-01-2210. ISSN 0148-7191, eISSN 2688-3627. Available from: https://doi.org/10.4271/2017-01-2210

[40] REUSS, D. L. Cyclic variability of large-scale turbulent structures in directed and undirected IC engine flows. *SAE Technical Paper* [online]. 2000, 724. ISSN 0148-7191, eISSN 2688-3627. Available from: https://doi.org/10.4271/2000-01-0246

[41] BADE SHRESTHA, S. O., KARIM, G. A. Considering the effects of cyclic variations when modeling the performance of a spark-ignition engine. *SAE Technical Paper* [online]. 2001, 724. ISSN 0148-7191, eISSN 2688-3627. Available from: https://doi.org/10.4271/2001-01-3600

[42] MANZIE, C., WATSON, H. C., BAKER, P. Modeling the effects of combustion variability for application to idle speed control in SI engines. *SAE Technical Paper* [online]. 2002, 724. ISSN 0148-7191, eISSN 2688-3627. Available from: https://doi.org/10.4271/2002-01-2734

INVESTIGATION OF THE STRENGTH OF A CHAIN BINDER FOR SECURING A WAGON ON THE RAILWAY FERRY DECK

Alyona Lovska[1,2], Juraj Gerlici[2], Oleksij Fomin[3], Pavol Šťastniak[2], Yuliia Fomina[2], Kateryna Kravchenko[2,*]

[1]Ukrainian State University of Railway Transport, Kharkiv, Ukraine
[2]University of Zilina, Zilina, Slovak Republic
[3]State University of Infrastructure and Technology, Kiev, Ukraine

*E-mail of corresponding author: kateryna.kravchenko@fstroj.uniza.sk

Alyona Lovska 0000-0002-8604-1764,
Oleksij Fomin 0000-0003-2387-9946,
Yuliia Fomina 0000-0003-0884-5107,
Juraj Gerlici 0000-0003-3928-0567,
Pavol Šťastniak 0000-0003-1128-7644,
Kateryna Kravchenko 0000-0002-3775-6288

Resume

The article presents the results of the strength analysis of the chain binder components for symmetry fixing a wagon on the railway ferry deck, taking into account the actual hydrometeorological conditions of the navigation area. The simulation of the wagon dynamic load during the railway ferry rolling was carried out to determine the loads acting on the chain binder. The strength of the chain binder hook was analysed. The calculation results showed that the maximum equivalent stresses in the hook occur in the radial part and exceed the allowable ones by 23%. Therefore, to ensure the strength of the chain binder, it is necessary to comply with the appropriate roll angles of the railway ferry or create measures to reduce its load when rolling. The conducted studies will contribute to ensuring the safety of wagon transportation by sea and increasing the efficiency of rail-ferry transportation.

Article info

Received 28 October 2022
Accepted 28 February 2023
Online 30 March 2023

Keywords:

transport mechanics
chain binder
loading
strength
rail and ferry transportation

Available online: https://doi.org/10.26552/com.C.2023.037

ISSN 1335-4205 (print version)
ISSN 2585-7878 (online version)

1 Introduction

Ensuring the efficiency of the functioning of the transport industry leads to the need to introduce intermodal transport systems into operation. One of the most successful among these is rail-ferry transportation [1], which has become used in countries that have access to international traffic through sea areas. A feature of these transportations is the possibility of wagon transport by sea on special ships, which are railway ferries equipped with the appropriate infrastructure.

The wagon is fixed by using chain binders to ensure its stability on the railway ferry deck (Figure 1).

Eight chain binders per wagon are used. A typical design of a chain binder for fastening a wagon on the railway ferry deck is shown in Figure 2 [2].

For fastening, one end of the chain binder using a hook 2 is attached to the wagon structural element 1, and the other end is attached to the deck eye bolt (Figure 3, a). The tension of the chain binder is provided by using a pneumatic gun (Figure 3, b). The tensile force of the chain binder is about 5 tons.

In order to effectively secure the wagon on the deck, chain binders are spatially located relative to the body (Figure 4) [3].

Chain binders must meet strength conditions in order to ensure reliable fastening wagon on the deck. One of the most important components of the binder is the hook for fastening the wagon and the chain. Under the conditions of alternate stresses caused by oscillation of a railway ferry during sea disturbance, damage to the chain binder hook occurs, in particular, deformations and cracks. Mostly cracks occur in the zone of interaction between the hook eye and the shackle (Figure 5) or in the zone of the radial tide. When we speak about the chain, the most common damage is its break.

This circumstance contributes to the violation of the wagon stability on the deck and threatens the safety of the railway ferry movement. It is important to say that the violation of the vehicles fastening has repeatedly become the cause of the sea craft wreck. For example, the wreck of the railway ferry Mercury - 2 in 2002

(a) (b)

Figure 1 *Fastening the wagon on the railway ferry deck: (a) by the bottom rail of the side wall; (b) by the towing shackle*

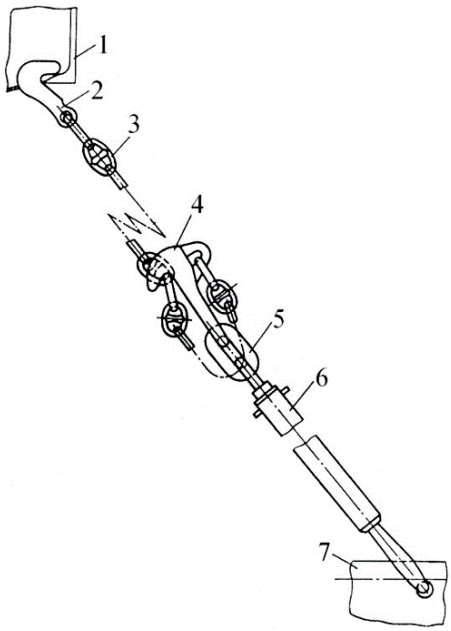

Figure 2 *Chain binder in working position: (1) is a wagon frame; (2) is a hook; (3) is a stud chain; (4) is a claw hook; (5) is an enlarged link; (6) is a turnbuckle; (7) is an eye bolt fixed on the deck*

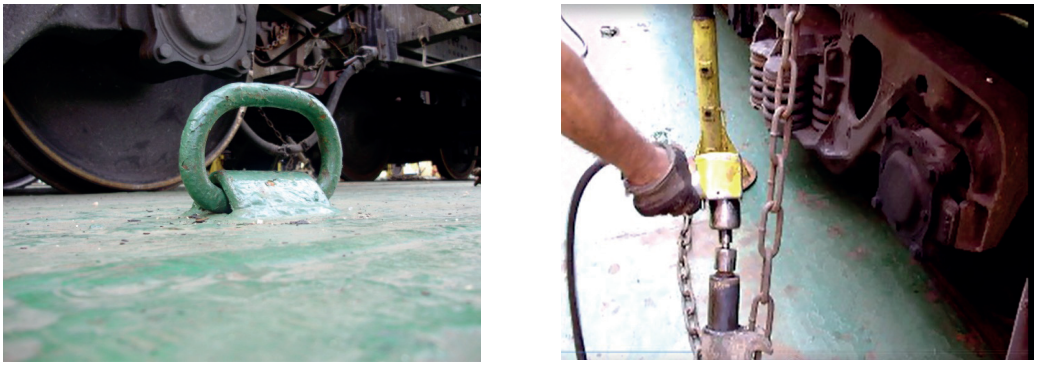

(a) (b)

Figure 3 *Means of fixing the lashing chain: (a) the deck pad-eye; (b) the pneumatic ratchet*

was caused by a violation of the tank wagon stability on the deck during a storm in the Caspian Sea [4]. In prior years, namely, on December 8, 1966, as a result of unreliable fastening on the Greek ferry ship Heraklion, the refrigerator trailer broke off and damaged the ferry gate, through which water began to flow onto the cargo deck. In a matter of minutes, the ship lost its stability, overturned and sank. The tragedy occurred in the Mediterranean Sea during a storm [5].

In this regard, it is important to determine the actual conditions under which the strength of chain binders for securing wagons on railway ferries is ensured. This will help to ensure the safety of carriages by sea and increase the efficiency of rail and ferry transportation.

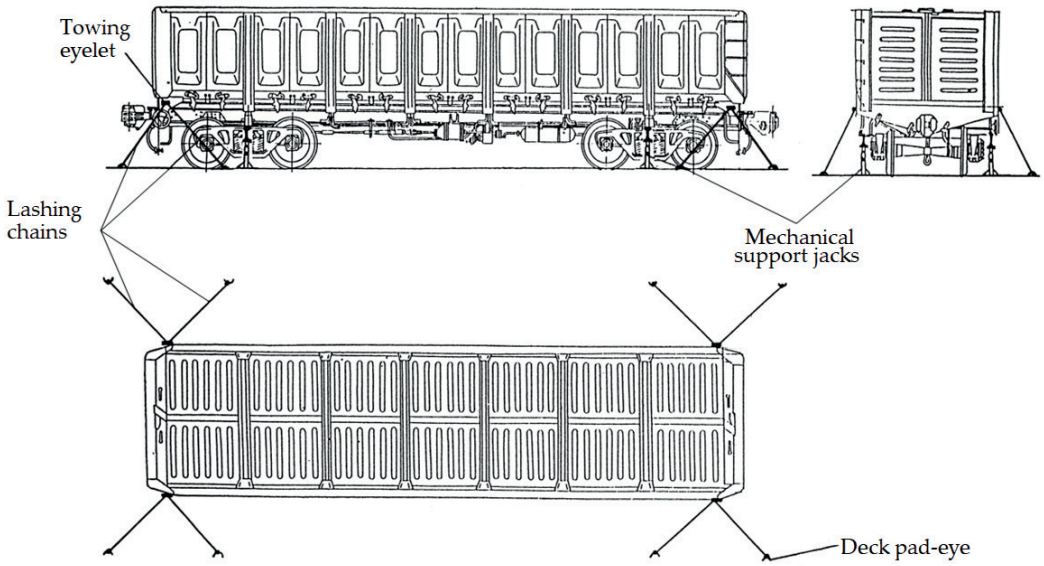

Figure 4 *Scheme of fixing the wagon on the railway ferry desk*

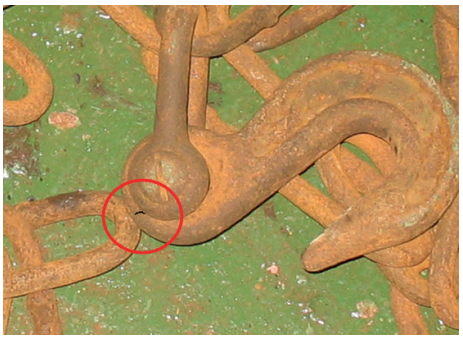

Figure 5 *Crack in chain link hook*

2 Analysis of recent research and publications

The issue of determining the load of reusable fastening means is covered in a book [2]. The author proposed a simplified method for calculating the means of fastening wagons on railway ferries. When determining the chain binder strength, classical formulas of strength of materials, which allow obtaining the stress in an uniaxial stress state, are used. It is important to say that this method is quite simplified and does not allow to investigate stress concentrators in the components of the hook of the chain binder.

In the paper [6] Zemlezin gave a method for calculating the forces acting on the wagon bearing structure during transportation by railway ferry. When doing this, the author considered the disturbing effect in the form of a plane wave, which is described by the harmonic law. However, the paper did not investigate the strength of the means of fixing the wagons on the decks.

The load of vehicle bearing structures during transportation by railway ferries are modelled in publications [7-9]. The specified value of the dynamic load acting on them during the oscillations of the railway ferry was determined. The stability of the vehicles was studied, taking into account the typical interaction with the deck. Along with this, the authors did not make the strength analysis of chain binders for securing vehicles on decks.

The results of mathematical modelling of the load of the rigging lines for containers fastening on the deck are presented in [10]. Forces at the points of their interaction with containers are calculated. Forces and moments are obtained taking into account different schemes for rigging lines. However, the above methodology applies to metal cables and cannot be used to calculate chain binders.

The author proposed elements of calculation models for different methods of fastening cargo placed on semi-trailers in the paper [11-12]. Calculations were made in accordance with the requirements of the XL Code. The results of the analysis of transport security management are given. At the same time, the given method cannot be used to determine the strength of chain ties of railway ferries.

The issue of increasing the level of reliability of fastening military wheeled vehicles on a railway flat wagon by using improved technical means is carried out in a paper [13]. The design features of a reusable tension cable are described. However, when designing this cable, the loads that may act on it during the transportation

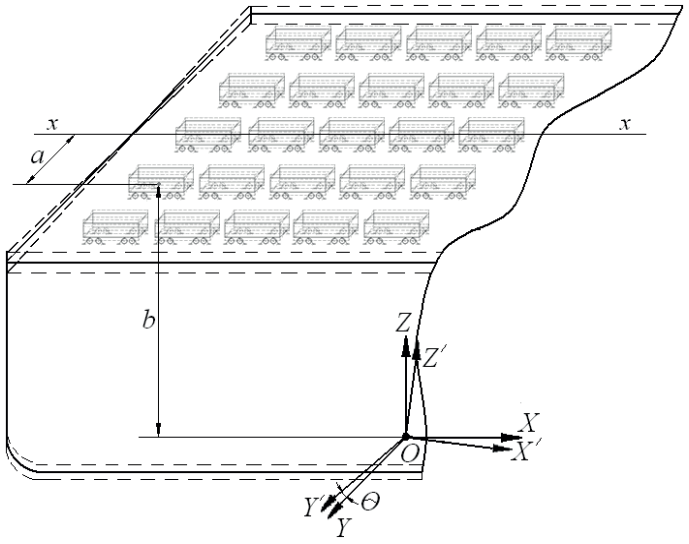

Figure 6 *Movement of a railway ferry with wagons during rolling motion*

of goods by rail are taken into account. That is, it is not suitable for securing cargo on decks during sea transportation.

Calculation of marine fastenings of a container crane for the transportation of heavy cargo is carried out by the authors in [14]. The highest stress fields in the crane structure are determined and, taking this into account, the places of its fastening are chosen. The calculations confirmed the possibility of its fastening, taking into account the proposed scheme. However, the authors focused on determining the strength of the crane, and not the means of its fastening.

The publication [15] presents the results of determining the forces acting on the container and means of securing during maritime transportation. Solutions are proposed for optimal fastening of containers on deck in terms of ensuring the safety of their transportation by sea. At the same time, certain forces are not taken into account for strength calculation of the means of securing containers on the deck during vessel oscillations.

The dynamic load of the wagon bearing structures during transportation on rail ferries was determined in papers [16-17]. The main strength characteristics of wagon bodies are determined in the course of their interaction with the fastening means on the decks. It is proposed to improve the wagon bearing structures to ensure the reliability of their fastening. At the same time, the author did not calculate the strength of the fastening means, taking into account their interaction with improved wagon designs during railway ferry oscillations.

The manuals [18-21] contain features of the placement, fastening and loading of car-goes on the railway ferry decks, which are operated in the Black Sea. Possible schemes of cargo fastenings are given. The strength conditions of reusable fasteners are mentioned. However, these regulatory documents do not provide methods for strength calculation of the fastening means in the conditions of railway ferry rolling.

An analysis of literature sources [2-21] allows us to conclude that the issues of strength calculation of the means of wagon fastening on the railway ferry decks have not been given due attention. Therefore, there is a need for research in this direction.

3 The aim and main objectives of the article

The aim of the article is to determine the strength of the main components of a chain binder for symmetry fastening a wagon on the railway ferry deck, taking into account the actual hydrometeorological conditions of the navigation area. To achieve the goal, the following tasks are defined:

- to investigate the dynamic load of the wagon during transportation by rail ferry to determine the actual loads acting on the chain binder;
- to conduct the strength analysis of the chain binder hook;
- check the strength of the binder chain.

4 Investigation of the dynamic load of a wagon during its transportation by the railway ferry

To determine the actual values of the loads perceived by the chain binder in storm conditions, mathematical modelling of the dynamic load of the wagon during the railway ferry rolling motion has been carried out in the case of the highest load of its structure (Figure 6) [22].

The differential equation, which describes the movement of a wagon placed on the deck of a railway ferry during its roll, has the form in Equation (1)

$$\left(\frac{D}{12\cdot g}(B^2+4z_g^2)\right)\cdot\ddot{q}+\left(\Lambda_\theta\cdot\frac{B}{2}\right)\cdot\dot{q}= p'\cdot\frac{h}{2}+\Lambda_\theta\cdot\frac{B}{2}\cdot\dot{F}(t), \tag{1}$$

where $q=\theta$ is a generalized coordinate corresponding to the angular movement of a railway ferry with wagons around the longitudinal axis. The origin of the coordinate system is located at the mass center of the railway ferry.

D is weight water displacement; B is the width of the railway ferry; h is the height of the railway ferry board; Λ_θ is a coefficient of resistance to of the railway ferry motion; z_g is a coordinate of the railway ferry gravity center; p' is a wind load; and $F(t)$ is the law of action of the force that disturbs the motion of a railway ferry with wagons placed on its deck.

Equation (1) is a second order equation for non-conservative systems.

When doing this, the law of a sea wave motion is considered in the form of a trochoidal curve [23]:

$$F(t) = a + R \cdot e^{kb} \sin \cdot (k \cdot a + \omega \cdot t) + b - \\ - R \cdot e^{kb} \cos \cdot (k \cdot a + \omega \cdot t), \quad (2)$$

where a and b are the horizontal and vertical coordinates of the center of the trajectory along which the particle rotates, which currently has x and z coordinates; R is the radius of the trajectory along which the particle rotates; ω is the sea wave frequency; k is the frequency of the disturbing force trajectory.

When compiling the mathematical model, it was taken into account that the wagon body is rigidly and symmetry fastened on the deck and moves with it. The shock effect of sea waves on the hull of a railway ferry with wagons placed on its board was not taken into account [24].

Input parameters to the mathematical model are geometric characteristics of the railway ferry and hydrometeorological characteristics of the Black Sea water area. The model also took into account different angles on the bow of the wave χ in relation to the railway ferry body [18].

To solve the mathematical model, a calculation program was created in the environment of the Mathcad, for what it was reduced to the Cauchy normal form, and then integrated according to the Runge-Kutta method [25-28]. The initial conditions were assumed to be zero [29-30]. The obtained results are given in Figure 7.

The largest acceleration, which acts relative to the standard place of the wagon on the deck, occurs at χ° and is 0.4 m/s². Accelerations are given for wagons placed on the last track from the bulwark of the railway ferry upper deck.

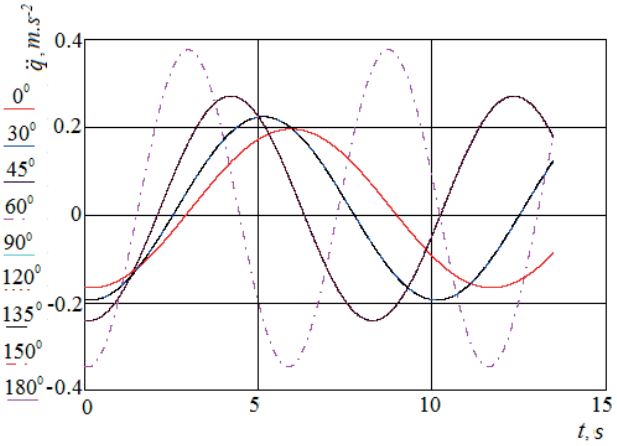

Figure 7 *Acceleration of the wagon during railway ferry rolling motion*

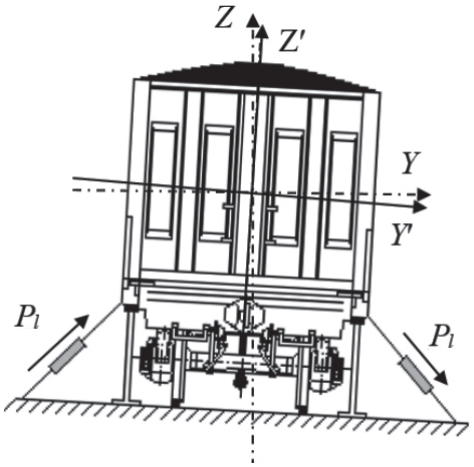

Figure 8 *The scheme of chain binder operation in the case of railway ferry rolling motion*

The total amount of acceleration acting on the wagon is the sum of the accelerations on its regular place on the deck, as well as the horizontal component of the acceleration of free fall due to the railway ferry roll angle. The roll angle was 12.2° based on the manual [3], for the case of static wind action on the surface projection of a railway ferry with wagons placed on its upper deck and the hydrometeorological conditions of the Black Sea water area. Taking this into account, the total acceleration acting on the wagon farthest from the bulwark is equal to 2.47 m/s^2 (0.25g). The obtained acceleration value is considered when determining the dynamic loads acting on the chain binder. The calculation was carried out under the condition of fixing the open wagon model 12-757 with chain binders. The total value of the dynamic load acting on it is equal to 208.96 kN. Therefore, 52.24 kN falls on one binder during the railway ferry rolling motion.

The total load perceived by the binder also takes into account the load from its tension. That is, in the case of rolling motion of the railway ferry, the chain binders will tense on one side of the wagon, and will be destressed on the other side (Figure 8).

Then the total value of the load on the chain binder from the side of its tension is equal to 101.3 kN.

Table 1 *The main technical characteristics of the hook*

Parameter	Value
Allowable load (kN)	80
Material of manufacture	Steel 20MnCr5
Diameter of the hole for the bracket (mm)	25
Mass (kg)	1.3

Table 2 *The main properties of the hook material*

Parameter	Value
Modulus of elasticity (Pa)	$2.1 \cdot 10^{11}$
Poisson's ratio	0.28
Shear modulus (Pa)	$7.9 \cdot 10^{10}$
Mass density (kg.m^{-3})	7800
Tensile strength (Pa)	1100825984
Yield strength (Pa)	750000000

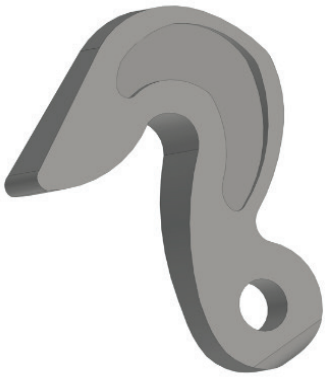

Figure 9 *Spatial model of the chain binder hook*

Figure 10 *Finite element model of the hook*

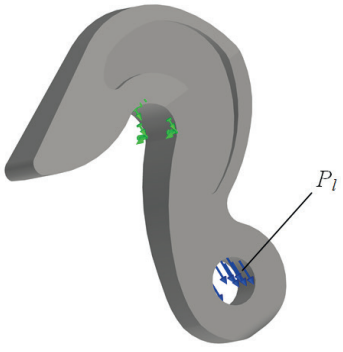

Figure 11 *Calculation scheme of the hook*

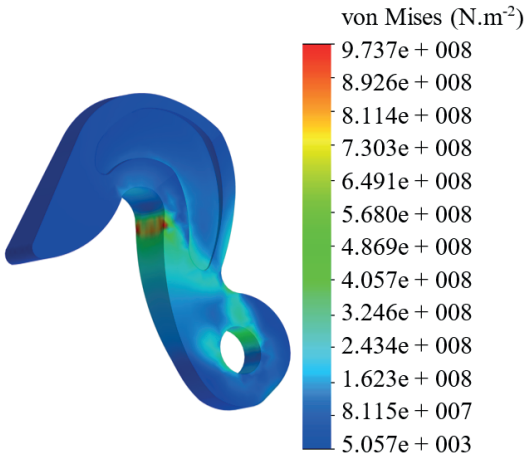

Figure 12 *The stress state of the hook*

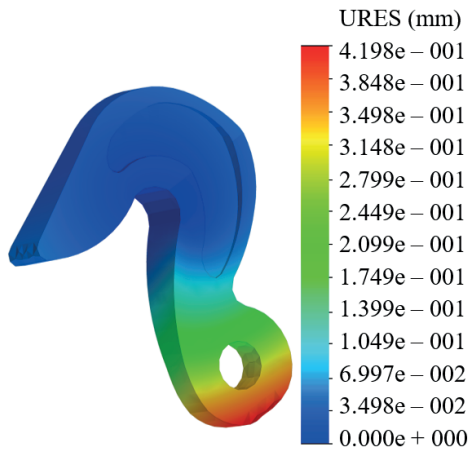

Figure 13 *Displacements in hook nodes*

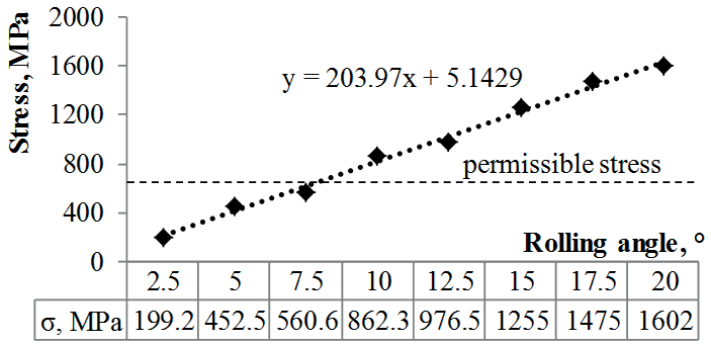

	2.5	5	7.5	10	12.5	15	17.5	20
σ, MPa	199.2	452.5	560.6	862.3	976.5	1255	1475	1602

Figure 14 *Dependence of stresses in the hook of the chain tie on the railway ferry rolling angle*

5 The strength calculation of the chain binder hook

The load obtained in the previous section of the article is considered when calculating the strength of the chain binder hook. The calculation was carried out using the finite element method in the SolidWorks Simulation software.

The spatial model of the hook was built in accordance with the album of drawings of reusable railway ferry fastening means (Figure 9). Solid modeling was made in the SolidWorks software [31-34].

The main technical characteristics of the hook are summarized in the Table 1.

It is important to note that the load on one binder, which is equal to 80 kN, is determined from the strength conditions of the wagon frame items.

Isoparametric tetrahedrons were used in the building of the hook finite element model (Figure 10). The mesh was created based on curvature. The optimal number of tetrahedrons was calculated by using the graphic and analytic method [35-37]. The mesh contained 74647 elements and 14985 nodes. The maximum size of the mesh element is 3.2 mm, and the minimum size is 1.1 mm. The number of elements in the circle was 8. The ratio of the increase in the element size is 1.5.

The calculation scheme of the hook is shown in Figure 11. The longitudinal load P_l was applied to its bridge. Its fastening was carried out behind the work surface. In this case, hard clamping was used. The main properties of the hook material, steel 20MnCr5, are given in Table 2. The material was considered as linear isotropic.

The calculation was made according to the Mises criterion (energy theory of strength). The calculation results are shown in Figures 12 and 13.

The obtained results allow us to conclude that the maximum equivalent stresses in the hook occur in the radial part and amount to about 973.7 MPa. That is, they exceed the allowable ones by 23%. In this case, the allowable stresses for a hook made of 20MnCr5 steel are 750 MPa. This stress value is taken from the technical data sheet for the chain binder.

The maximum displacements in the hook take place in the zone of the bridge and are equal to 0.4 mm.

On the basis of variational calculations, the permissible rolling angle of the railway ferry has been determined from the point of view of ensuring the hook strength (Figure 14). This angle is about 9°.

Table 3 *The main technical characteristics of the binder chain*

Parameter	Value
Diameter of the ring bar (mm)	14
Manufacturing material	Steel 20MnCr5
Total length including hook (m)	2.5
Allowable load (kN)	80
Weight (kg)	11

6 The binder chain strength test

To ensure the strength of the chain, the condition [38] must be satisfied:

$$n = \frac{S_{cr}}{S_c} \geq [n], \tag{3}$$

where S_{cr} is the critical load of the chain, kN; S_c is the calculated chain load, kN; *[n]* is the safety factor of the chain.

The main technical characteristics of the chain are listed in Table 3.

Taking into account the fact that S_c = 101.3 kN and S_{cr} = 80 kN, the safety margin of the chain is less than 1. Therefore, the strength of the binder chain is not provided.

Therefore, in order to ensure the strength of the chain binder, it is necessary to comply the appropriate rolling angles of the railway ferry or to create measures to reduce its load during rolling motion.

The conducted studies will contribute to ensuring the safety of wagon transportation by sea and increasing the efficiency of railway and ferry transportation.

7 Conclusions

1. The dynamic loading of the wagon during its transportation by railway ferry was studied to determine the actual loads acting on the chain binder. It has been established that the total value of the acceleration acting on the wagon furthest from the bulwark is equal to 2.47 m.s^{-2} (0.25g). The obtained acceleration value was taken into account when determining the dynamic loads acting on the chain binder. Taking into account the calculations, the total value of the load acting on the chain binder from the side of its tension is equal to 101.3 kN.
2. The strength of the chain binder hook has been calculated. The maximum equivalent stresses in the hook occur in the radial part and are about 973.7 MPa, which exceed the permissible ones by 23%. The maximum displacements in the hook occur in the zone of the bridge and are equal to 0.4 mm. The admissible railway ferry rolling angle at which the chain binder strength is ensured has been determined. This angle is about 9°.
3. The strength of the binder chain was tested by comparing its critical load with the calculated one. In this case, the safety margin of the chain is less than 1. Therefore, the binder chain strength is not observed.

In order to ensure the strength of the chain binder, it is necessary to comply the appropriate railway ferry rolling angles or to create measures to reduce its load in the case of rolling motion.

Acknowledgements

This contribution was elaborated within execution of the project "New generation of freight railway wagons" (Project code in ITMS2014+: 313010P922), on the basis of support of the operational program Research and innovation financed from the European Regional Development Fund.

Conflicts of interest

The authors declare that they have no known competing financial interests or personal relationships that could have appeared to influence the work reported in this paper.

References

[1] FOMIN, O., LOVSKA, A., MASLIYEV, V., TSYMBALIUK, A., BURLUTSKI, O. Determining strength indicators for the bearing structure of a covered wagon's body made from round pipes when transported by a railroad ferry. *Eastern-European Journal of Enterprise Technologies* [online]. 2019, **1**(7(97)), p. 33-40. ISSN 1729-3774. Available from: https://doi.org/10.15587/1729-4061.2019.154282

[2] SHMAKOV, M. G. *Special ship devices*. Saint Petersburg, Russia: Shipbuilding, 1975.

[3] Cargo securing manual for m/v "Geroi Plevny" No. 2512. 02. Odesa, Ukraine: Ministry Transport of Ukraine. State Department of Sea and River Transport: 1997.

[4] Death of "Mercury - 2". How it was… [online] [accessed 2022-08-11]. Available online: https://www.pravda.ru/accidents/9720-parom/
[5] Marine ferries [online] [accessed 2022-08-11]. Available online: http://www.diveclub.lv
[6] ZEMLEZIN I. N. Methodology for calculating and studying the forces acting on a wagon during transportation by sea ferries. Moscow, Russia: Transport, 1970.
[7] LOVSKA, A., FOMIN, O., PISTEK, V., KUCERA P. Dynamic load modelling within combined transport trains during transportation on a railway ferry. *Applied Sciences* [online]. 2020, **10**(16), 5710. ISSN 2076-3417 Available from: https://doi.org/10.3390/app10165710
[8] LOVSKA, A., FOMIN, O., PISTEK, V., KUCERA, P. Dynamic load and strength determination of carrying structure of wagons transported by ferries. *Journal of Marine Science and Engineering* [online]. 2020, **8**(11), 902. ISSN 2077-1312 Available from: https://doi.org/10.3390/jmse8110902
[9] LOVSKA, A., FOMIN O., SKURIKHIN, D. Special determination of the stress state of the body of a hopper car transported by sea. In: 26th International Scientific Conference Transport Means 2022: proceedings. Part I. 2022. p. 525 - 529.
[10] HYEON-KYU YOON, GYEONG JOONG LEE, YOUNG-HOON YANG. Calculation of securing and lashing loads of containers on the deck of a ship in waves. *Journal of Navigation and Port Research* [online]. 2005, **29**(5), p. 377-382. ISSN 1598-5725, eISSN 2093-8470. Available from: https://doi.org/10.5394/KINPR.2005.29.5.377
[11] SALEK, R., SLABIK, M. The role of fastening loads in the safety management of intermodal transport of truck semi-trailers. *System Safety: Human - Technical Facility - Environment CzOTO* [online]. 2019, **1**(1), p. 978 - 986. eISSN 2657-5450. Available from: https://doi.org/10.2478/czoto-2019-0124
[12] FOMIN, O., LOVSKA, A., KULBOVSKYI, I., HOLUB, H., KOZARCHUK, I., KHARUTA V. Determining the dynamic loading on a semi-wagon when fixing it with a viscous coupling to a ferry deck. *Eastern-European Journal of Enterprise Technologies* [online]. 2019, **8**(2/7(98)), p. 6-12. ISSN 1729-3774. Available from: http://journals.uran.ua/eejet/article/view/160456
[13] KOSTIUK, V. V., RUSILO, P. A., VARVANETS, Y. V., KALININ, A. M. Increase of reliability level of the military wheeled technique fastening. *Bulletin of the National Technical University «KhPI». Series: Transport Engineering Industry*. 2018, **29**(1305), p. 56 - 61.
[14] WARDHANA, W., HADIWIDODO, Y. S., SISWANTO, F. Strength analysis and sea-fastening design of container crane structure for heavy lifting sea transportation. *Applied Mechanics and Materials* [online]. 2018, **874**, p. 147-154. ISSN 1662-7482. Available from: https://doi.org/10.4028/www.scientific.net/AMM.874.147
[15] RADISIC, Z. Necessity of proper lashing of containers on the ship's deck as part of optimization of the sea voyage. *Promet-Traffic-Traffico.* 2004, **16**(2), p. 97-104. ISSN 0353-5320.
[16] LOVSKAYA, A. Assessment of dynamic efforts to bodies of wagons at transportation with railway ferries. *Eastern-European Journal of Enterprise Technologies* [online]. 2014, **3**(4), p. 36-41. ISSN 1729-3774. Available from: https://doi.org/10.15587/1729-4061.2014.24997
[17] PANCHENKO, S., VATULIA, G., LOVSKA, A., RAVLYUK, V., ELYAZOV, I., HUSEYNOV, I. Influence of structural solutions of an improved brake cylinder of a freight car of railway transport on its load in operation. *EUREKA: Physics and Engineering* [online]. 2022, **6**, p. 45-55. ISSN 2461-4254, e ISSN 2461-4262. Available from: https://doi.org/10.21303/2461-4262.2022.002638
[18] Manual on cargo securing for m/v "Petrovsk" PR. No. 002CNF001-LMNL-805. Odesa, Ukraine: MIB, 2005.
[19] Cargo securing manual for m/v "Geroi Shipky" No. 2512. 02. Odesa, Ukraine: Ministry Transport of Ukraine. State Department of Sea and River Transport: 1997.
[20] Cargo secuaring menual m/v "Geroite na Sevastopol". Varna, Bulgaria: LTD, Navigation maritime Bulgaria, 1997.
[21] Cargo secuaring menual transocean line a/s ms "Greifswald". Hamburg, Germany: Germanischer Lloyd, 2001.
[22] PANCHENKO, S., GERLICI, J., VATULIA, G., LOVSKA, A., PAVLIUCHENKOV, M., KRAVCHENKO, K. The analysis of the loading and the strength of the FLAT RACK removable module with viscoelastic bonds in the fittings. *Applied Sciences* [online]. 2023. **13**(1), 79. eISSN 2076-3417. Available from: https://doi.org/10.3390/app13010079
[23] LUGOVSKIJ, V. V. Sea dynamics: selected issues related to the teaching of the seaworthiness of the ship. Textbook for technical universities in the specialty "Hydroaerodynamics". Saint Petersburg, Russia: Shipbuilding, 1976.
[24] MAKOV, Y. L. Pitching of ships. Kalningrad, Russia: Kaliningrad State Technical University, 2007.
[25] OKOROKOV, A., FOMIN, O., LOVSKA, A., VERNIGORA, R., ZHURAVEL, I., FOMIN, V. Research into a possibility to prolong the time of operation of universal open top wagon bodies that have exhausted their standard resource. *Eastern-European Journal of Enterprise Technologies* [online]. 2018, **3**(7(93)), p. 20-26. ISSN 1729-3774. Available from: https://doi.org/10.15587/1729-4061.2018.131309

[26] FOMIN, O., LOVSKA, A., SKURIKHIN, D., NERUBATSKYI, V., SUSHKO, D. Special features of the vertical loading on a flat car transporting containers with elastic-viscous links in their interaction units. In: 26th International Scientific Conference Transport Means 2022: proceedings. Part I. 2022. p. 629 - 633.

[27] KROL, O., PORKUIAN, O., SOKOLOV, V., TSANKOV, P. Vibration stability of spindle nodes in the zone of tool equipment optimal parameters. *Proceedings of the Bulgarian Academy of Sciences: Mathematical and Natural Sciences* [online]. 2019, **72**(11), p. 1546-1556. ISSN 1310-1331. Available from: https://doi.org/10.7546/CRABS.2019.11.12

[28] NALAPKO, O., SHYSHATSKYI, A., OSTAPCHUK, V., MAHDI, Q. A., ZHYVOTOVSKYI, R., PETRUK, S., LEBED, Y., DIACHENKO, S., VELYCHKO, V. and POLIAK, I. Development of a method of adaptive control of military radio network parameters. *Eastern-European Journal of Enterprise Technologies* [online]. 2021, **1**(9(109)), p. 18-32. ISSN 1729-3774. Available from: https://doi.org/10.15587/1729-4061.2021.225331

[29] FOMIN O., GERLICI J., GORBUNOV M., VATULIA G., LOVSKA A., KRAVCHENKO K. Research into the strength of an openwagon with double sidewalls filled with aluminium foam. *Materials* [online]. 2021, **14**(12), 3420. ISSN 1662-7482. Available from: https://doi.org/10.3390/ma14123420

[30] VATULIA, G., LOVSKA, A., PAVLIUCHENKOV, M., NERUBATSKYI, V., OKOROKOV, A., HORDIIENKO, D., VERNIGORA, R., ZHURAVEL, I. Determining patterns of vertical load on the prototype of a removable module for long-size cargoes. *Eastern-European Journal of Enterprise Technologies* [online]. 2022, **6/7**(120), p. 21-29. ISSN 1729-3774. Available from: https://doi.org/10.15587/1729-4061.2022.266855

[31] ALYAMOVSKIJ, A. A. SolidWorks/COSMOSWorks 2006-2007. Engineering finite element analysis. Series "Design". Moscow, Russia: DMK, 2007.

[32] FOMIN, O., GERLICI, J., GORBUNOV, M., VATULIA, G., LOVSKA, A., KRAVCHENKO, K. Research into the strength of an open wagon with double sidewalls filled with aluminium foam. *Materials* [online]. 2021, **14**(12), 3420. ISSN 1662-7482. Available from: https://doi.org/10.3390/ma14123420

[33] FOMIN, O., LOVSKA, A. Determination of dynamic loading of bearing structures of freight wagons with actual dimensions. *Eastern-European Journal of Enterprise Technologies* [online]. 2021, **2/7**(110), p. 6-15. ISSN 1729-3774. Available from: https://doi.org/10.15587/1729-4061.2021.220534

[34] KELRYKH, M. B., FOMIN, O. V. Perspective directions of planning carrying systems of gondolas. *Metallurgical and Mining Industry* [online]. 2014, **6**(6), p. 57-60. ISSN 2076-0507.

[35] VAMBOL, O., KONDRATIEV, A., PURHINA, S., SHEVTSOVA, M. Determining the parameters for a 3D-printing process using the fused deposition modeling in order to manufacture an article with the required structural parameters. *Eastern-European Journal of Enterprise Technologies* [online]. 2021, **2/1**(110), p. 70-80. ISSN 1729-3774. Available from: https://doi.org/10.15587/1729-4061.2021.227075

[36] VATULIA, G., REZUNENKO, M., PETRENKO, D., REZUNENKO, S. Evaluation of the carrying capacity of rectangular steel-concrete columns. *Civil and Environmental Engineering* [online]. 2018, **14**(1), p. 76-83. ISSN 1336-5835, eISSN 2199-6512. Available from: https://doi.org/10.2478/cee-2018-0010

[37] VATULIA, G. L., PETRENKO, D. H., NOVIKOVA, M. A. Experimental estimation of load-carrying capacity of circular, square and rectangular CFTS columns. *Scientific Bulletin of the National Mining University* [online]. 2017, **6**, p. 97-102. ISSN 2071-2227, eISSN 2223-2362.

[38] KUZMIN, A. V., MARON F. L. Handbook on the calculations of the mechanisms of hoisting and transport machines. Minsk, Byelorussia: Higher school, 1983.

DEVELOPMENT OF A PROTOTYPE OF A PROTECTIVE UV-C HALF-FACE MASK WITH IMPLEMENTATION OF ADDITIVE TECHNOLOGY

Daniel Varecha[1,*], Ján Galík[1], František Brumerčík[2], Róbert Kohár[2], Rudolf Madaj[2], Mário Drbúl[3], Adam Glowacz[4], Witold Glowacz[4], Hui Liu[5]

[1]Research and Service Centre, Faculty of Mechanical Engineering, University of Zilina, Zilina, Slovakia
[2]Department of Design and Mechanical Elements, Faculty of Mechanical Engineering, University of Zilina, Zilina, Slovakia
[3]Department of Machining and Production Technology, Faculty of Mechanical Engineering, University of Zilina, Zilina, Slovakia
[4]Department of Automatic Control and Robotics, Faculty of Electrical Engineering, Automatics, Computer Science and Biomedical Engineering, AGH University of Science and Technology, Krakow, Poland
[5]College of Quality and Safety Engineering, China Jiliang University, Hangzhou, China

*E-mail of corresponding author: daniel.varecha@fstroj.uniza.sk

Daniel Varecha 0000-0001-5894-407X,
František Brumerčík 0000-0001-7475-3724,
Rudolf Madaj 0000-0003-2458-2351,
Adam Glowacz 0000-0003-0546-7083,
Hui Liu 0000-0002-4265-7241
Ján Galík 0000-0003-4983-8851,
Róbert Kohár 0000-0001-7872-2829,
Mário Drbúl 0000-0002-8036-1927,
Witold Glowacz 0000-0002-8734-3844,

Resume

The authors of this manuscript present development of a prototype protective UV-C half-face mask. The first stage of this study focuses on proposing a UV-C half-face mask design and the second phase investigates the quality of printings, 3D/2D roughness and porousness of three different printed samples of PA12. Development of the protective half-face mask used the non-destructive technology of 3D scanning of the human body by the Ein Scan scanner. As a part of the experiment, three samples were prepared with Sinterit Lisa, EOS Formiga and HP jet fusion printers. SLS and MJF technology were used during the experiment. The experimental observation of the structure of the surface was secured using the Alicona Infinite focus G5 device. The conclusions present the study's results and the authors' recommendations for other developers dealing with the development of the protective face masks.

Article info

Received 16 February 2023
Accepted 20 March 2023
Online 29 March 2023

Keywords:

rapid prototyping
photogrammetry-3D projection
additive manufacturing, 2D/3D
roughness of PA12
selective laser sintering (SLS)
multi-jet fusion (MJF)

Available online: https://doi.org/10.26552/com.C.2023.038

ISSN 1335-4205 (print version)
ISSN 2585-7878 (online version)

1 Introduction

The human population has been susceptible to new respiratory diseases in the last two years. The emergence of COVID - 19 has sparked a worldwide demand for necessary measures to mitigate the spread of the infection [1]. At the end of 2019, hospitals reported a shortage of personal protective equipment for the frontline health workers [2]. Additive manufacturing brings a unique option to alleviated the lack of these critical medical aids [3]. At this time, the protective half-face masks are essential for masses of people to protect themselves and others from the virus's aerosol. Correct use of protective equipment significantly reduces the risk of virus transmission and protects the medical staff and other patients from infection [4]. It is a common knowledge that respiratory infections are caused mainly by different factors such as bacteria, fungi and viruses. This fact has been known for several tens of years. There are several ways to "fight" against these undesirable factors and keep your health in good condition. Among the primary and best-known methods are a healthy lifestyle, enough sleep, staying in the sun and a vitamin-rich diet. Vitamin D is important, which is essential in strengthening the human immune system [5]. The authors of the qualified manuscript [5] listed that

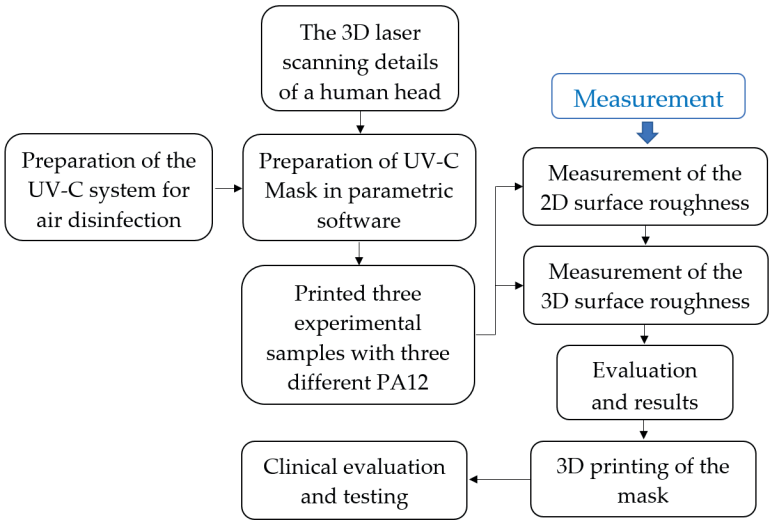

Figure 1 *Flowchart of the experimental setup*

vitamin D has a vital role in enhancing and increasing the immune system's ability. This characteristics of vitamin D prevents the virus's rapid spread in the lungs [5]. It also prohibits the penetration of viruses deep into tissues by maintaining intercellular connections [5]. These aspects contribute favorably to the correct functioning of the immune system, ultimately resulting in a good defense of the human body against these pathogens. However, after breaking through a weakened immune system, pathogens can cause respiratory disease. When an infection occurs, in most cases, medications must be started, which in the current 21st century is evident and effective in the fight against pathogens. Recently, increased number of people are discussing prevention, which is very important. In recent months, the public has used various surgical "no-name" face masks (products without company brand) to protect against respiratory diseases, which is not always quality protection. Wearing the protective face masks is utterly natural in Eastern culture (Asia). The population of Asia uses them not only to protect health but in the case of increased air chemical pollution (smog), as well.

The difference is the case in Europe and America, but the trend has changed and wearing a protective face mask has become a natural part of our lives in recent months. The authors of the manuscript [6] subjected surgical face masks to four simulated cycles of folding, aging with artificial saliva, or sweating and washing. They concluded that folding, saliva and sweat have little effect on the face mask's effectiveness and aging (depreciation). Research has confirmed that one can wear a worn surgical face mask longer than usual, the recommended four hours [6]. The pathogens have lived with us since time immemorial, so it is appropriate to introduce prevention and prevent infection.

The events from the last period have created a space for use of these technologies for disinfection, be it water, air, or surfaces with which a person comes into daily contact. For this reason, the authors of this manuscript began to develop a new type of the protective face mask that would disinfect the air with UV-C light. Value UV-C of the light is moving in the vast range from 100 to 280 nm and is used for disinfection increasingly in everyday life. Many researchers are currently working on the issue of UV-C light disinfection. When developing the protective face masks, information about the shape and features of the human head (face) is crucial. The imprint of the human face can be obtained only scientifically. Anthropology is a scientific field that focuses on measuring the external characteristics of the human body. Anthropology is necessary for developing and producing ergonomically correct workplaces or protective equipment.

Modern 3D scanners are also often used for this. Similar anthropological research took place in the U.S. in 2003 under the leadership of the National Institute for Occupational Safety and Health (NIOSH) [7] to update the respirator testing standards. The measurement was according to the traditional measure of anthropometric techniques on a sample of 3997 subjects, for 947 issues used, a Cyberware 3D Rapid Digitizer. Based on anthropometric data collected during the 2003 NIOSH survey, developed parameters at the National Personal Protective Technology Laboratory (NPPTL) for new digital models of the human head in five categories. The authors of [8] submitted the final report of this research in 2004. The digital head models from the NIOSH survey are symmetrical and represent the shape head-and-face distribution of current U.S. respirator users [9]. In the technical specification standard for protective equipment ISO TC94, upper respiratory protective equipment SC15, WG1 General and PG5 Human factors are also incorporated head forms [9]. The original journal National Library of Medicine [9] and several other highly qualified publications published the NIOSH anthropological data (2D and 3D). Many researchers during the COVID-19 crisis were dedicated to development of protective face masks.

An example can be a manuscript [10] in which authors present the custom-made face masks for pandemic crisis solutions, made using the 3D printing. In addition, the manuscript's authors [11] present a similar issue. The authors' study [12] examined the relationship between the definition of problems related to the COVID-19 pandemics and the characteristics of additive manufacturing solutions.

This study aims to design a protective UV-C half-mask and thus contribute to eliminating infection in society. At the beginning of the development of the protective half-face mask, the researchers established the following attributes as essential:

- The ideal shape designs;
- The high-quality non-porous material PA12;
- The surface structure of the half-face mask should not be enormously rough (the surface of the protective half-face mask will not need additional finishing after being printed out).

The flowchart (Figure1) shows the procedure for developing a prototype and the methods used to investigate the surface roughness of three different materials PA12.

2 Materials and methods

Additive technologies started to develop several decades ago and the development in a few years has grown exponentially. These developing additive technologies are significant and decisive for the fourth industrial revolution. Nowadays, increasing number of people come across devices that work on the principle of additive technologies. The use is very diverse and sometimes it is no longer possible to clearly say what was used in specific additive technology in production. Products realized by the additive technology also bring material and technical limitations that should be discussed more [13-14]. In the final process of the 3D printing, there may be limits, which can be manifested in the size of the printed object or the complex geometry. The current state of matters in the field of 3D printing does not allow fundamental structural changes in the standard design of a 3D printer [14]. The 3D printer forms a definite structure without the possibility of expanding individual parts of the device [14]. In addition, for this reason, a trend in the development of several researchers is a modular 3D printer, which solves these limitations and improves shortcomings. In the future, this would mean that after purchasing and asking for an increase in the construction area, only another block of, for example, the essential construction area would be needed [14]. The research and development details of the modular 3D printer are listed in [14].

In the past, most 3D printers, which worked on the principle of additive technology, used only one material during the printing. The first multi-material 3D printer was presented in 2006 and used a syringe-based system. This experimental study addresses only two specific additive technologies used in developing the protective UV-C mask (SLS, MJF). It should be also mentioned that the 3D printers that work on the principle of fusible link production, Fused Filament Fabrication (FFF), are currently more affordable for the public. In this case, the FPP2 filter housing and internal and external exhalation valves for the prototype protective half-face mask can be 3D printed out of the Fused Filament Fabrication (FFF) technology. The 3D printer, which works on the Fused Filament Fabrication technology (FFF), can simultaneously print a 3D object using several materials [15]. From the knowledge gained from practice, we can conclude that the primary motivation and goal of the 3D printer researchers was the integration of additive technologies into the electronic industry, aviation, bioengineering, robotics, textile industry and development centers, which was achieved [15]. It should also be noted that the ISO/ASTM 529000:2015 standard categorizes the additive technologies into seven main groups [16].

2.1 Three different PA12 powder materials for the experimental samples

At the beginning of 2020, many protective face shields made of polypropylene were used worldwide. Authors of the manuscript [17] verified that the 3D printable extruded material could produce be recycled and reused for 3D printing. However, this experimental study aims to develop and research materials for a prototype protective half-face mask from polyamide 12 (PA12). Within the experimental measurement of the surface roughness 3 test samples were prepared from three different PA12 powder materials (Table 1) of a rectangle shape of 50 mm x 30 mm x 10 mm.

Each sample was printed with another 3D printer. The first sample was printed out with a printer from SINTERIT company, the second sample was with an EOS printer and the third sample was printed out with an HP printer. The 3D printers worked during printing with the powdered material PA12 according to the specific requirements of additive technology (SLS, MJF) and the manufacturer's recommendations.

Table 1 *List of samples used in the experiment*

Samples	AM - No.1	AM - No.2	AM - No.3
Used additive technology	SLS (5W)	SLS (60W)	MJF
The powder material	PA12 Smooth	PA12 PA 2 200	PA12 MJF

Figure 2 *EinScan - SP 3D scanner*

2.2 Photogrammetry - 3D projection

Three-dimensional scanning brings the best choice for obtaining data from physical objects into a digital 3D model. In the 21st century, it is characteristic of the start of the fourth industrial revolution, which presents these technologies. The manuscript [18] states that the 3D scanning systems can work with or without contact. The 3D scanning technology is currently used in the development and research, design, engineering, healthcare, dentistry, or scanning of parts of the human body, as well as in archaeology. Prototyping has become a certain standard in the field of healthcare especially.

Additive manufacturing is used for production of Orthopedic Prosthetics devices, as well. In [19] the authors described the 3D printing and the application of Orthopedic Prosthetics in an industrial area. An example can be the manuscript [20] in which the authors published research results on foot deformation with bearing conditions to improve the design of diabetic footwear. Last but not be least, the authors of [21] used the 3D scanner EinScan-SP to scan the foot deformities.

In addition, dentistry uses 3D scanning; for example, a manuscript [22] confirmed the suitability of intraoral digital scanners for scanning the entire arch for dental patients. The other significant publications of the authors [23-27] present results from their actual medical practice.

The use of photogrammetry is varied. The mentioned authors used the non-contact and non-destructive 3D laser scanning technology during the research and development. The authors [28] stated more information about the technology of 3D scanning in their manuscript.

Technologies of the 3D scanning are just now used in a wide range of various applications. Additionally, photogrammetry use is in scanning museum archaeological objects [29]. Next, in the area of reverse engineering a 3D scan is used for the mechanism's physical parts that lack documentation or have changed from the original CAD design of the element [30]. Scanned 3D objects can be used in further work in virtual assemblies utilizing the CAD system. The EinScan-SP scanner has a fully automatic mode for larger objects with the support of a tripod.

During the development of the protective UV-C mask benefits of the powerful EinScan-SP 3D scanner were used, Figure 2. EinScan features two scanning modes. The first is Fixed Scan (manual control) and the second is Auto Scan. The fully automatic mode is only suitable for up to 5 kg objects with the support of a tripod. The smaller physical objects need a rotary table. When the rotary table is used, it is possible to scan objects with an accuracy of 0.05 mm. In addition to the fixed scanner placement on the tripod, the scanner, even outside the tripod, creates digital 3D objects. EinScan device is recommended in manual mode for objects heavier than 5 kg, of lengths more than 25 cm and for items with complex geometry. In this case, the object to be scanned is placed on a flat surface and gradually rotated manually. The human body is 3D scanned using this manual mode. The advantage of the EinScan-SP scanner is that it provides a new human face and hair scanning mode that works with an invisible infrared light source. It offers a reliable solution even for dark-colored scanning objects and, last but not the least, has high accuracy. The Ein Scan-SP scanner software also adjusts the data coordinates in the post-processing process, which provides spotless 3D data for subsequent applications [31]. Another advantage is that the scanned 3D objects can be used in further work in virtual assemblies utilizing the CAD system [31].

2.3 Selective laser sintering (SLS)

The selective laser sintering (SLS) is a method that creates physical models through the selective solidification of various fine powders and has received much attention in the clinical field [32]. During the 3D printing, tiny powder particles with 18 to 80 μm are sintered. Selective laser sintering (SLS) ranks among a solid freeform fabrication technique developed

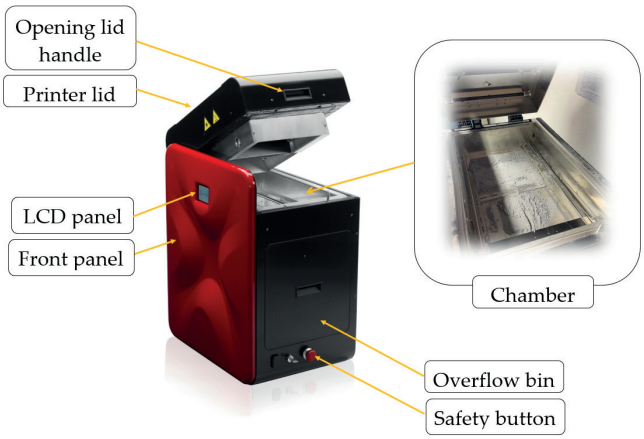

Figure 3 *The 3D printer of the Sinterit Lisa in the laboratory [34]*

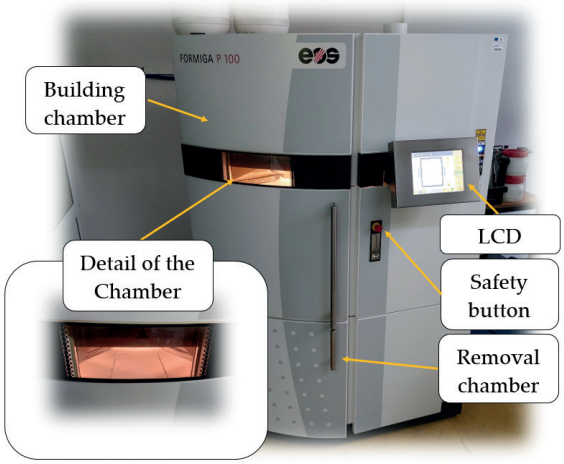

Figure 4 *The 3D printer of the EOS Formiga P100 in the laboratory*

by Deckard for his thesis at the University of Texas, patented in 1989 [32]. The authors of [33] thoroughly addressed the issue of polymers produced using the SLS technology. They developed a transparent production methodology based on research using the desktop printers with selective laser sintering (SLS). The critical aspects described in the manuscript can also apply to developing a protective UV-C half-face mask.

The first used 3D printer Lisa (Figure 3) from Sinterit Lisa, has a laser with a power of 5 - Watts. The working principle of the Lisa 3D printer consists in fusing the powder material with a laser beam. The printer works with the SLS technology, which sinters the powder material layer by layer using a laser emitter. The current market offers several powder materials that apply to Sinterit Lisa. The best known are the PA12 powder material, PA11 and polypropylene (PP) [34].

The Lisa printer can print any shaped object in the printer space. It should be noted that the Sinterit Lisa printer offers the printing of 3D objects without supporting materials, which represents a significant advantage [34]. The Sinterit Lisa can be placed on a worktable thanks to its smaller dimensions, what ultimately brings a practical solution. In general, however, the objects made using the mentioned additive technology (SLS) have a superior surface quality and incomparable mechanical and temperature resistance up to 120 °C. One advantage of the Sinterit Lisa printer is the reuse of unused dust, which is found together with the model in the print cake [34]. The 3D Sinterit Lisa printer can also bake with flex grey powder material - TPU (Thermoplastic Polyurethane Elastomer), which makes it possible to create the 3D prints of high elasticity.

The second 3D printer used, the Formiga P100 from EOS company (Figure 4), uses a 60 - Watt laser to sinter particles of PA12 powder material.

The EOS Formiga P100 printer prints vertical walls of objects with maximum surface quality. For this reason, the printer is ideally suited for small filigree components, precisely like those that make up a protective UV-C face half-mask. The manufacturer states the vertical accuracy at distances of 300 mm ± 0.05 mm. The development of the EOS Formiga P100 printer was primarily aimed for that parameter. Sinterit Lisa (Figure 3) and EOS Formiga P100 (Figure 4)

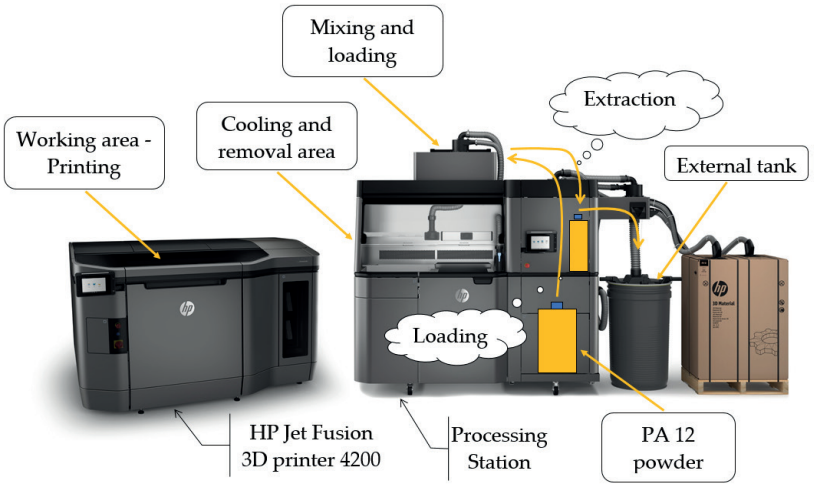

Figure 5 *HP Jet Fusion 3D printer 4200 [35]*

devices offer 3D printing of PA12 using selective laser sintering (SLS). The listed printers differ in dimensions and, above all, sintering performance.

2.4 Multi jet fusion 3D printer

The last 3D printer, used in developing the UV-C protection half-face mask, is the HP Jet Fusion 3D 4200. The device works with Multi-Jet Fusion (MJF) technology. The last sample AM-No. 3, was printed from unique PA 12 powder material, designated for Multi-Jet Fusion sintering technology. The mentioned HP printer can print the PA12 powder material, the polypropylene (PP) and thermoplastic polyurethane (TPU 90A) [35]. After producing three samples from the powder material, visual differences were visible in the surface structure of every experimental sample. Ultimately, the quality of the 3D print depends on the 3D printer technologies. During the development of the protective UV-C face half-mask, emphasis was placed not only on the quality of the surface, which does not let water, viruses and bacteria through the surface of the half-face mask. The EOS Formiga P100 printer produces vertical walls of 3D objects with maximum surface quality.

For this reason, the system is ideally suited for small filigree components, precisely like those that make up a protective UV-C face half-mask. The manufacturer states the vertical accuracy at distances of 300 mm ± 0.05 mm. TThe last sample was made of the PA12 powder material, suitable for multi-jet fusion sintering technology. The research examines several prints' surface quality for the proposed protective half-face mask as a primary goal.

Some medical devices are, at this time, already produced using modern 3D printers with sintering metal powder (SLM) technology. The authors of [36] present experiences with developing medical devices and other applications. In their manuscript, the authors describe attempts to optimize some process properties, such as surface roughness, porosity and mechanical properties of 3D prints. The authors also described the issue in great detail, to understand the existing research gaps. The publication [36] outlines some critical aspects for further development of the technique of selective laser sintering of metal powder, especially in medical applications, which needs consideration. In addition, optimizing process properties, such as surface roughness, porosity and mechanical properties for the 3D prints PA12, printed out with selective laser sintering (SLS) technology, is similarly necessary. Authors of [37] correctly noted one fact. Before achieving more economical production, one must decide on the setup of the 3D printer to economically print parts with good mechanical behavior. They also noted that if the hatch spacing, laser power and scanning speed are selected so that the laser energy density was too high, the powders would burn and the printing process would fail.

2.5 Alicona Infinite Focus G5 and observing 2D and 3D roughness of the samples

The team of researchers defined the essential attributes the protective half-face mask must meet at the beginning of development. The first two important, characteristic primary features that the half-face mask must fulfill are focused on the ideal shape design as well as on the high-quality non-porous material, which is necessary for the correct function of the half-face mask. This second most significant requirement defines the zero penetration of air and liquids through the material's structure of the print-out from PA12 of the powder material. The third condition discusses how the surface of the protective half-face mask will

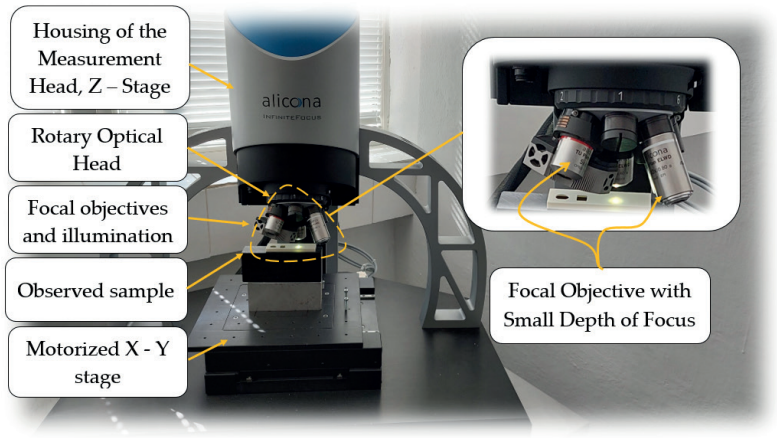

Figure 6 *Alicona Infinite Focus G5*

Figure 7 *3D digital head form-EinScan-SP before digital modification*

Figure 8 *3D digital head form EinScan SP after digital modification*

not be additionally finished after being printed out. It means that the surface structure of the half-face mask should not be enormously rough, but pleasant to the touch after print-out. For this reason, it was necessary to investigate all the samples' roughness, porosity and surface topography. All the samples' surface roughness structures were analyzed using the Alicona Infinite Focus G5 device (Figure 6).

3 Results of the experimental study

The facial features recorded with the 3D EinScan-SP scanner are essential in developing the UV-C protective half-face mask design. The scanned digital model of the head (Figure 7) was subsequently phase modified (Figure 8). The digital model of the human face is used to create the basic parametric model of the protective UV-C face half mask. After printing, the half-face mask should be perfectly sitting on the chin, cheekbones and nose.

The human head's anthropology data was collected using the 3D scanning technology, the so-called photogrammetry-3D projection. The software of the Ein Scan-SP scanner automatically generated a digital file human head, which was subsequently edited by the modeling software Ein Scan-SP scanner. During the scanning, imperfections arose in the digital model in the form of hole shapes. For this reason, using the software Ein Scan the digital model was modified and the holes were filled, smoothed and sharpened. This process aimed to provide the perfect 3D data for the parametric design of the mask in Creo parametric software from PTC company.

3.1 Design of the UV - C half mask

Development of the half-face mask was primarily the parametric 3D model focused, including creating a chamber with an air disinfection system using a UV-C light source. The developers also emphasized the overall appearance and ergonomic shapes of the proposed prototype of the protective half-face mask. In developing the protective UV-C half-face mask the Creo Parametric software was used, with a standard modeling tool and the ISDX (Interactive Surface Design Extension) tool, which allows the modeling of free surfaces (Figure 9).

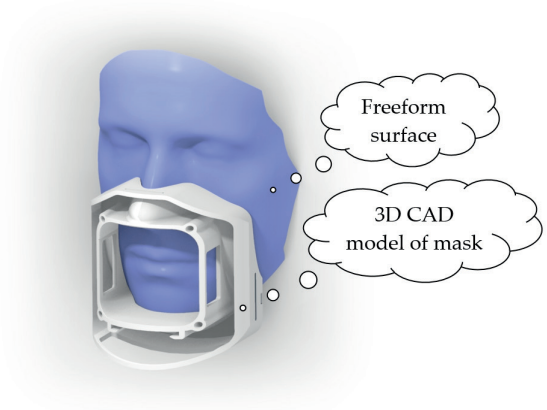

Figure 9 *Enhanced Interactive Head Surface (ISDE)*

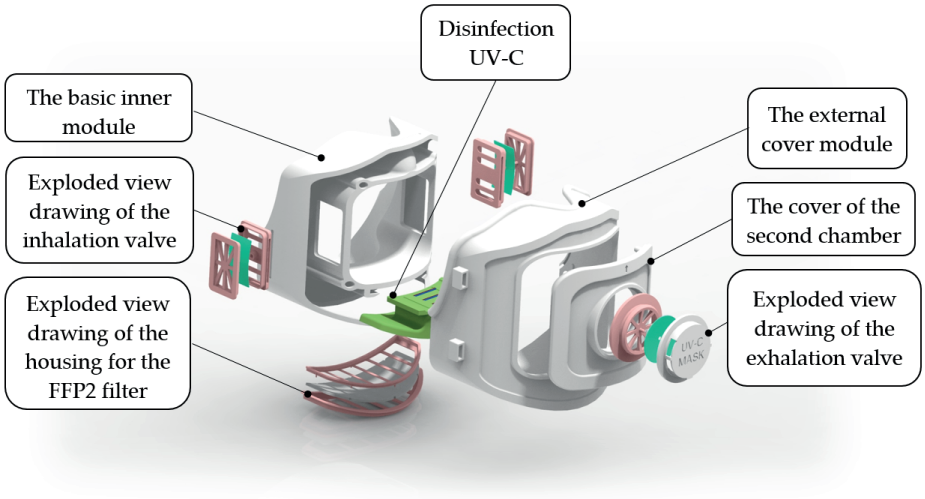

Figure 10 *Protective UV-C half-face mask in the exploded view*

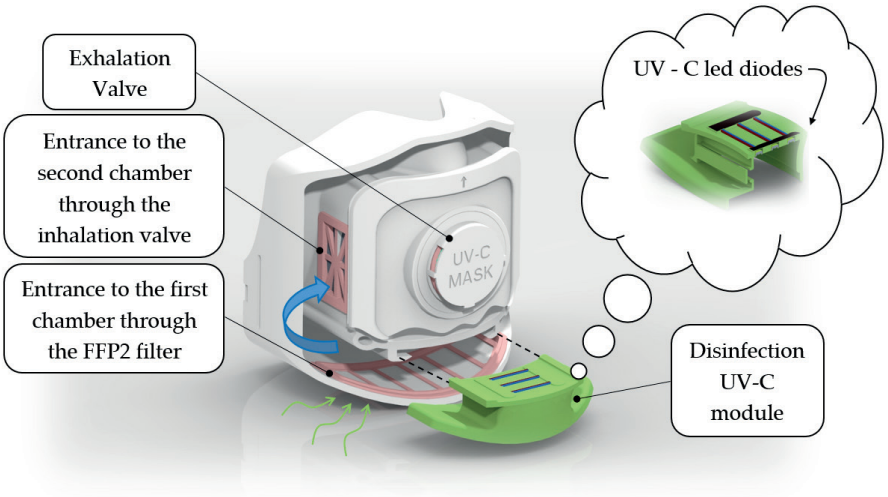

Figure 11 *Construction of the UV-C half-face mask*

In the current era of the 21st century, software tools already handle the demanding requirements of high-quality free characters (class A surfaces), similar to the modeling of structural components using the power of parametric modeling.

The prototype development of the protective UV-C half-face mask used the experience of the researchers from the Rapid Prototyping laboratory. During the development of the mask, the results and experiences of prototyping from publication [38] were applied, as well.

Figure 12 *Inside part of protective UV-C half-face mask*

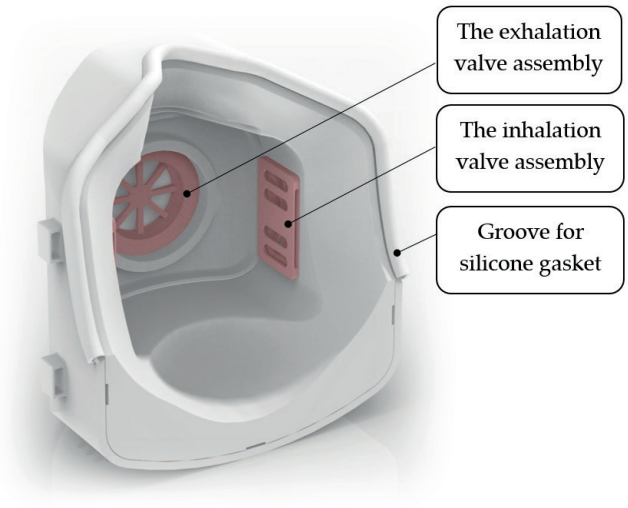

Figure 13 *Inside part of protective UV-C half-face mask*

The parametric 3D model of the protective UV-C half-face mask consists of seven parts. The module for the internal valve the exhalation valve and the FFP2 filter housing comprises two separate parts and the rubber valve together form an assembly. The illustration below shows a parametric 3D prototype of a protective UV-C half-face mask, Figure 10.

The protective half-face mask's working principal rests in disinfecting the air-inhaled using the UV-C light. The inner part of the protective half-face mask has two separate chambers. The first chamber is named the "disinfection module" and forms a separately removable part of the mask. Inhaled air enters the disinfection module with UV-C LED through the FFP2 filter on the bottom of the mask. The air stream slows down in the disinfection module as it passes through the labyrinth-shaped holes. In this case, the slower-flowing air is cleaned effectively of pathogens with UV-C light. The space of the second chamber accumulates the disinfected air, which the person subsequently breathes (Figure 11).

The inside valve design ensures that the airflow direction is always from the accumulation chamber to the other section, never in the opposite direction. During inhaling, the person breathes disinfected air, passing through the two side valves into the second chamber. During exhalation, the consumed air is enriched with CO_2 and exhaled through the exhalation valve into the surrounding space. The external exhalation valve works on a similar principle. However, the air fluxed is the opposite, as in the case of the two internal valves. The air flows from the exhalation valve only to the surrounding area, never back inside.

The protective half-mask is removable for more accessible cleaning of all corners and inaccessible crevices. An outer part of the mask covers the space where the disinfected air is maintained. The figure below illustrates four slots integrated into the outer part of the mask, respectively, the outer cover (Figure 12).

The 3D model of the prototype protective half-face mask contains two side valves on both the right-hand

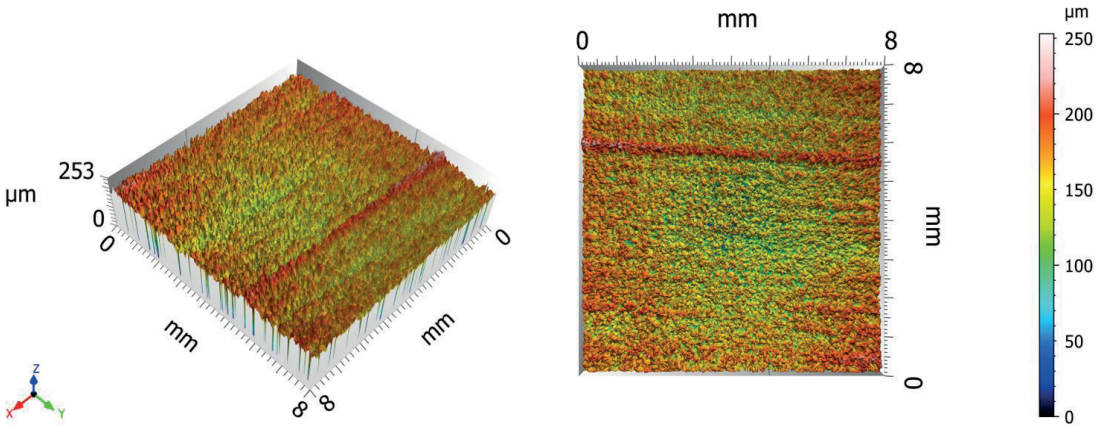

Figure 14 *Primary surface PA12 - Smooth - Selective laser sintering (SLS)*

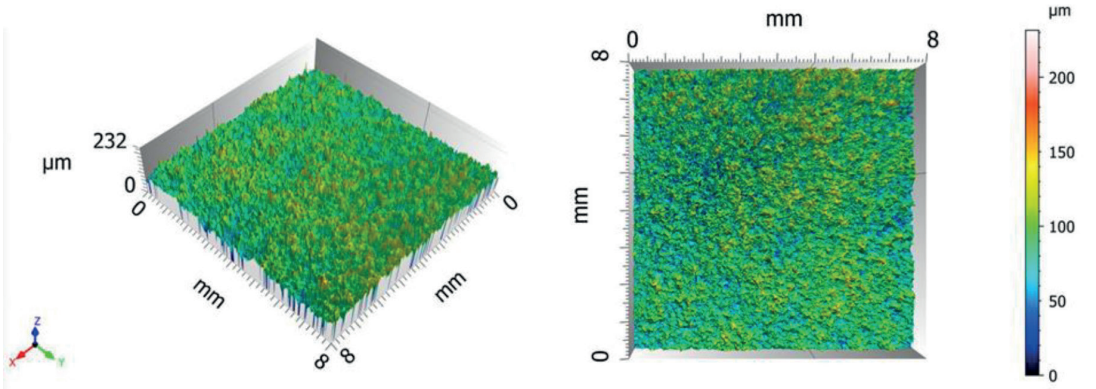

Figure 15 *Primary surface PA12 - PA 2 200 - Selective Laser Sintering (SLS)*

and left-hand sides. However, one valve is visible on the back side of the protective half-face mask (Figure 13). The front round valve exhales consumed air. Both inside valves use musk rubber, ensuring air penetration into and out of the chambers. The outer cover is equipped by a groove for a silicone gasket, which is visible on the back side of the outer surface of the mask.

3.2 Observation of the surface topography of PA12 with Alicona infinite Focus G5

The last stage of experimental research was focused on the samples' surface topography investigation. The 3D graphs show the primary surface of samples in perfect natural resolution and clarity. The display of colors is authentic and at a high micro level. The results of investigation follow ISO 16610 - 61 standards. Additionally, the roughness profile is shown in a 2D diagram with a complete RA surface roughness analysis. Figure 14 shows the primary surface of sample AM - No.1 (PA12 - Smooth) at 100 times magnification. The unevenness of the primary surface ranged from 350 to 100 µm.

Figure 15 presents the primary surface of sample AM - No.2, made of powder material PA12 - PA 2 200 at 100 times magnification. The sample showed more pores and minor irregularities in the surface structure. In addition, the unevenness of the primary surface ranged from 100 to 240 µm. The second sample, AM - No.2, was printed by selective laser sintering technology on the printer EOS Formiga P100.

The last sample, AM - No.3, was prepared by additive Multi-Jet Fusion (MJF) technology. At 100 - fold magnification regularly repeating waves are seen on the structure of the surface that arise after applying the powder material (Figure 16). The unevenness of the primary surface ranges from 120 to 180 µm.

The authors of [39] presented research on the surface roughness profile for both parallel and perpendicular orientations of 3D-printed polymers. They concluded that the similar direction shows a consistent periodicity for the surface topography with peak height. However, at perpendicular orientation, the profile shows different peak height values for the scan lengths with a reasonably consistent peak periodicity between the consecutive peaks [39]. The authors of [40] presented the surface roughness of the manufactured parts of the Lisa 3D printer using the Focus Variation (FV) technology. The authors described the experimental investigation of the surface roughness of three samples from PA12. The experimental investigation occurred

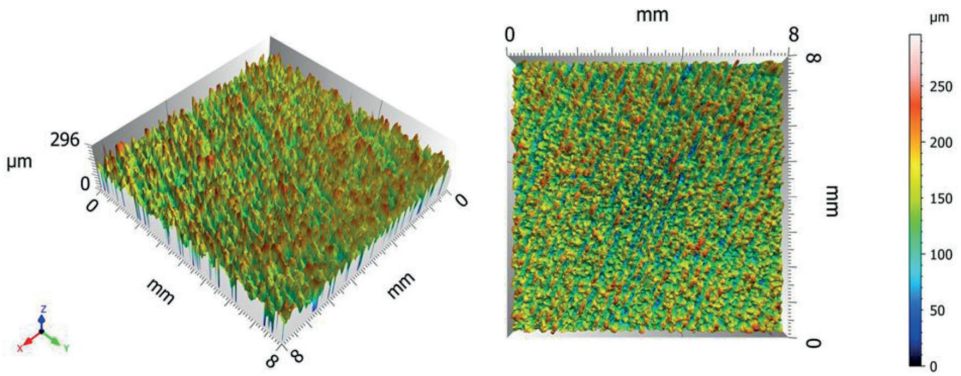

Figure 16 *Primary surface PA12 - MJF - Multi - Jet Fusion (MJF)*

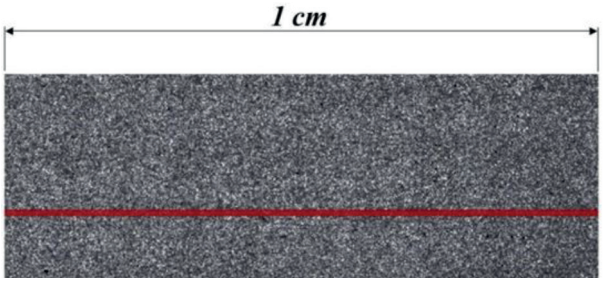

Figure 17 *PA12 Smooth - 2D surface roughness measurement path*

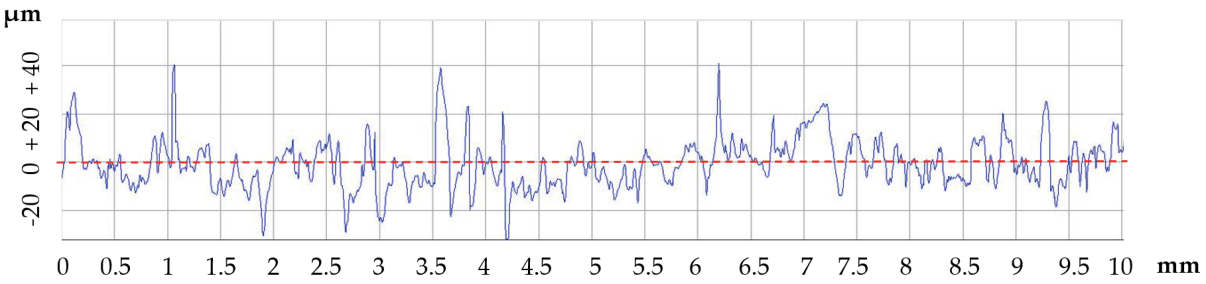

Figure 18 *Diagram of PA12 Smooth profile roughness measurement - Sinterit Lisa*

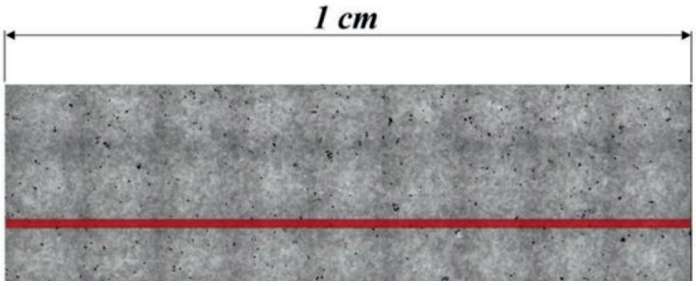

Figure 19 *PA12 Smooth - 2D surface roughness measurement path*

in the certified measurement laboratory, where they investigated the 2D, as well as the 3D surface roughness of the three samples above. The measurement of surface roughness took place with the help of the Alicona Infinite Focus G5 device. The measuring device used an optical sensor IF Sensor C100 G1 to extract the primary surface. During the experimental investigation of the 2D roughness on the sample's surface, 50 roughness profiles per 1 cm length were pulled. The diagrams show the graphic course of roughness results with the worst surface parameters in terms of surface functionality. The red line on each sample (Figures 17-21) represents 1 cm of the length and location of the 2D roughness measurement. During the test, the parameters of the 2D surface roughness (Figures 18-22) were measured. These parameters were the average roughness of the profile (Ra), root mean square roughness (R_q), the mean height of the roughness profile from peak to valley (Rz), maximum roughness profile valley height (R_v) and roughness profile distortion (R_{sk}).

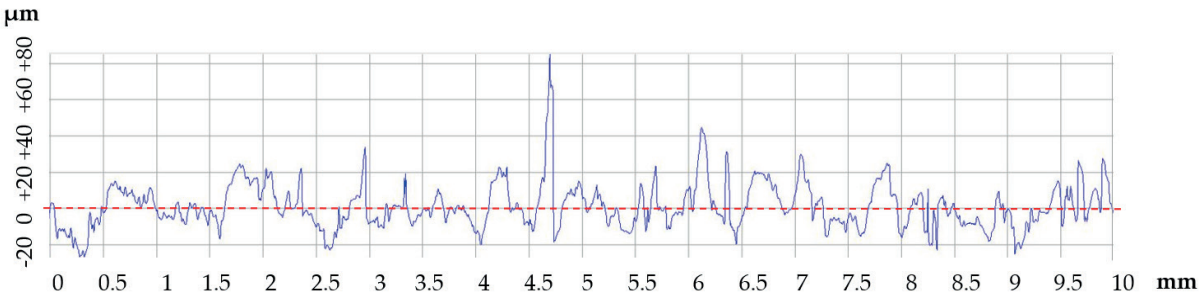

Figure 20 *Diagram of PA 2 200 profile roughness measurement - EOS Formiga*

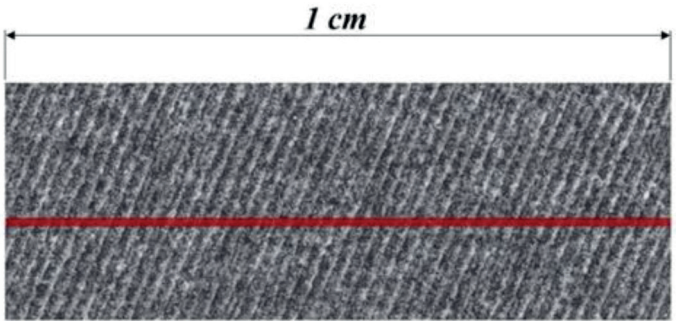

Figure 21 *PA12 Smooth - 2D surface roughness measurement path*

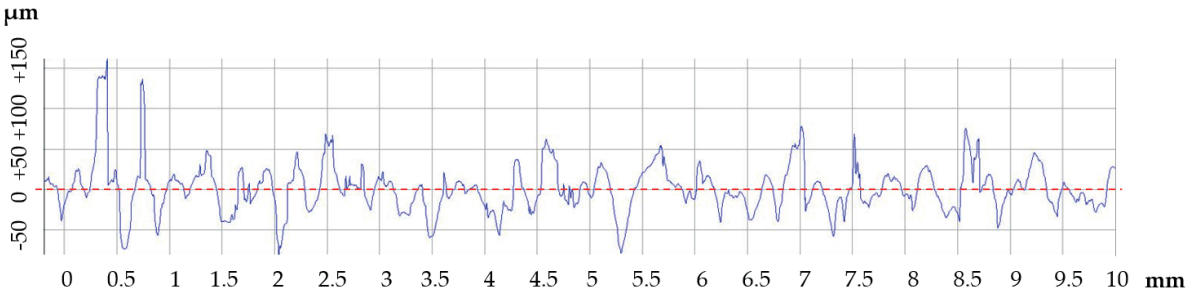

Figure 22 *Diagram measuring the roughness of the PA12 profile - MJF - HP Jet Fusion 3D 4200*

Table 2 *2D surface roughness parameters of all samples*

Samples	R_a (µm)	R_q (µm)	R_z (µm)	R_v (µm)	R_{sk} (µm)	R_v/R_z (µm)
AM - No.1	7.656	10.498	59.421	32.194	0.959	0.541
AM - No.2	9.185	12.499	66.363	28.714	1.430	0.432
AM - No.3	21.200	30.045	157.093	81.992	1.245	0.521

The R_v/R_z ratio is the most important, indicating whether depressions or elevations predominate on the sample's surface. If depressions prevail, cracks may appear in the structure of the polyamide sample. However, in the case of cyclic stress, the split can occur after some time. Bacteria and viruses can accumulate in cracks, which is undesirable for protective half-face masks with a UV-C light source. The acceptable value of the R_v/R_z ratio is in the interval from 0 to 0.55. Ultimately, this finding stems from the long-term research experience of researchers. The results of all investigated parameters are given in Table 2.

From the measured results it is clear that the R_{sk} parameter came out in positive numbers for on all the examined samples. That means that protrusions are predominantly present the surface of each sample. However, when the value R_{sk} of is negative, the sample's surface is dominated by holes. The R_v/R_z ratio is at the limit of the permissible value of 0.55 for all the samples. The 3D surface roughness was investigated in the last phase of the experiment. When evaluating the surface's topography, the nesting index is fixed to 8 mm. In addition, the evaluation was to use the Gaussian filter. The first sample represents the 3D surface of sample AM - No. 1 (Figure 23). The second sample represents the 3D surface of sample AM - No. 2 (Figure 24).

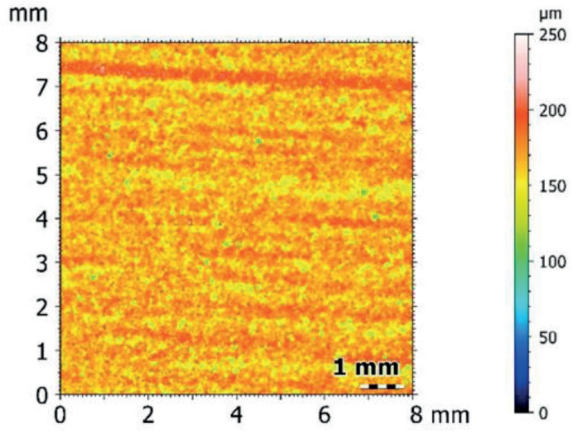

Figure 23 *The 3D roughness PA12 – Smooth*

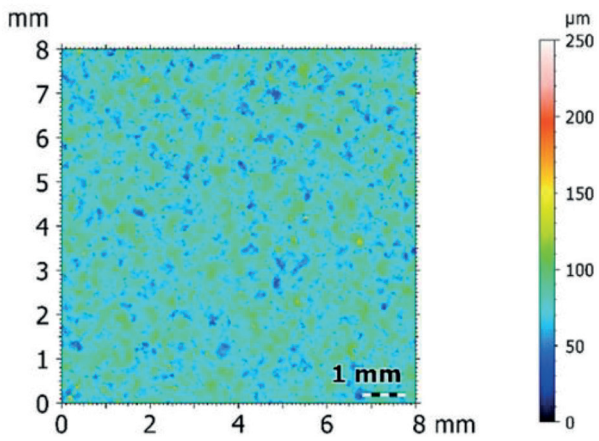

Figure 24 *The 3D surface roughness PA12 – 2200*

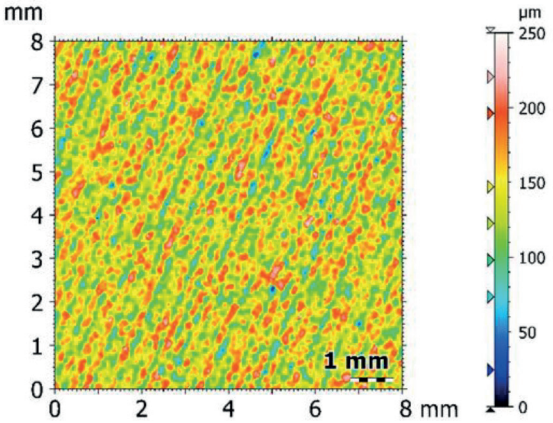

Figure 25 *The 3D surface roughness of PA12 – MJF*

The last sample represents the 3D surface of sample AM - No. 3. The sample is printed-out from PA12 - MJF powder material (Figure 25). During the measurement of 3D roughness, a Gaussian filter (FALG) was applied by the ISO 16610 - 61 standard on all the samples.

4 Discussions

Manuscript [41] listed that the global pandemic that has affected humanity has contributed to the breakdown of traditional supply chains responsible for providing personal protective equipment for health and social staffers.

The researchers' strategy was to mitigate the impact of infectious diseases on the world's population. The researchers of this experimental study decided to contribute with their prototyping experience and proposed a protective UV-C half-face mask.

The protective half-face mask can be printed out on a 3D printer that works with SLM or MJF technology, based on a digital parametric model, in any corner of the world, where the technical means are available. The main idea of this project was to immediately use the created digital mask data. Another part of the research and development was preparing a chamber for disinfecting the inhaled air with a source of UV-C light and preparing the section for breathing disinfected air. Some publications [42-43] state that the ideal wavelength band of UV-C light for the air disinfection, which does not harm human health is the band of wavelengths from 220 to 222 nm. In addition, several publications mention that UV-C light with wavelength band UV from 220 to 222 nm should not produce ozone (O_3) and using UV with said wavelength is biocompatible. Therefore, this claim will continue to be explored and verified. However, the authors of [43] state that further evaluation and testing of the safety and efficacy of the band of wavelengths from 220 to 222 nm UV-C light is needed. Therefore, the research will be extended to clinical evaluation and testing of the wavelength band UV from 220 to 222 nm in the future and its impact on the human health in prolonged use. The project will also focus on other additive technologies and materials suitable for such protective masks. Ultimately, additive technology allows production of parts with complex

designs, with certain limitations depending on the specific additive technology [44-45]. Several researchers dealt with polyamide materials listed in this manuscript within development. The researchers also focus on UV-C portable disinfection boxes for small objects, such as a set of keys, a mobile phone, etc. A team of researchers is also considering developing a device for disinfecting factories' production areas by using a UV-C module mounted on an automated guided vehicle (AGV) cover of the body.

5 Conclusions

The developers used the advantages of the 3D scanning while developing the protective UV-C half-face mask, since in development of a protective half-face mask technology of non-contact and non - destructive 3D laser scanning, details of a human head was needed. As already mentioned at the beginning of the experimental study, as a part of the development of the prototype of the protective UV-C half-face mask, three samples were prepared, which consisted of the PA 12 powder material. However, the final sintering of the PA12 powder material took place on the three 3D printers with different sintering technologies. At the first glance, the difference in the surface structure is easily visible in all samples. It is essential to mention that any additive technology influences the surface roughness of components with PA12 in a certain way. The right choice of a suitable PA12 powder material for a protective half mask is also necessary due to the roughness and porosity of the PA12 material. The research also showed significant differences in surface porosity in all the investigated samples. The first sample, AM - No.1, produced by selective laser sintering of PA12 - Smooth powder material, is biocompatible. Sample AM - No.1 has a smooth surface and is pleasant to the touch. The surface 2D roughness results are the proof and the 3D diagram (Figure 18) proves it, as well. This sample has the minimum number of pores in the structure surface. The second sample of AM - No.2, produced by the EOS Formiga P100 printer, has visible pores in its surface structure that, when enlarged, resembled a sieve. Evidence can be black dots in the 2D diagram (Figure 20), which present holes. The blue to black spots are visible on the chart of the 3D roughness surface of the second sample. Chemical surface protections for technical plastics from practice are known. However, applying a chemical surface treatment to the printed parts of the PA12 material and thus filling a large number of pores is impossible since this protective half-mask is for biocompatible use. The EOS Formiga P100 printer works with selective laser sintering (SLS) technology, similar to the SINTERIT Lisa printer. It is essential to note that the authors of [46] stated that PA 2 200 is biocompatible.

In the case of MJF technology, the sample surface quality (AM - No.3) is, at the first glance, reasonable, it has fewer pores and no additional surface treatment is required. However, the sample made by Multi-Jet Fusion (MJF) technology showed the highest surface roughness value of all three examined samples. The texture in place of the sample's surface resembled a wave shape and rougher. Compared to all the analyzed samples, the last piece, AM - No.3, has a distinct surface structure, which can also be seen at the macro level.

The summary of the experimental investigation of the surface roughness:

- Regarding the surface structure of samples and print quality, PA12 smooth or PA12 MJF material is recommended for the protective UV-C half-face mask.
- Roughness of the PA12 Smoot has a value of Ra 7.656 μm.
- Roughness of the PA12 2200 has a value of Ra 9.185 μm.
- Roughness of the PA12 MJF has a value of Ra 21.200 μm.
- Continue clinical research and testing of the mask, especially the impact of UV-C light at a wavelength of 220 *nm* on human health.

The protecting UV-C half-face mask will find application mainly in medical facilities and public service (fire and police forces etc.). The advantage of the protective UV-C half-face mask is the possibility of repeated use. The use time is limited to one battery charge because the battery provides an electricity source for the UV-C led light. The FFP2 protective filter placed into the mask protects human health for more than four hours. The FFP2 filter is also advisable to replace after each use. In conclusion, it is necessary to appreciate that the collaboration between the 3D printing community and the healthcare system has helped in providing innovative solutions to combat the crisis.

Acknowledgment

This article was funded by the University of Zilina project 313011ASY4 "Strategic implementation of additive technologies to strengthen the intervention capacities of emergencies caused by the COVID - 19 pandemic."

Conflicts of interest

The authors declare that they have no known competing financial interests or personal relationships that could have appeared to influence the work reported in this paper.

References

[1] ARMENTANO, I., BARBANERA, M., CAROTA, E., CROGNALE, S., MARCONI, M., ROSSI, S., RUBINO, G., SCUNGIO, M., TABORRI, J., CALABRO, G. Polymer materials for respiratory protection: processing, end use and testing methods. *ACS Applied Polymer Materials* [online]. 2011, **3**(2), p. 531-548. eISSN 2637-6105. Available from: https://doi.org/10.1021/acsapm.0c01151

[2] WESEMANN, C., PIERALLI, S., FRETWURST, T., NOLD, J., NELSON, K., SCHMELZEISEN, R., HELLWIG, E., SPIES, B. CH. 2 3-D printed protective equipment during COVID-19 pandemic. *Materials* [online]. 2020, **13**(8), 1997. eISSN 1996-1944. Available from: https://doi.org/10.3390/ma13081997

[3] ZUNIGA, J. M., CORTES, A. The role of additive manufacturing and antimicrobial polymers in the COVID-19 pandemic. *Expert Review of Medical Devices* [online]. 2020, **17**(6), p. 477-481. ISSN 1743-4440, eISSN 1745-2422. Available from: https://doi.org/10.1080/17434440.2020.1756771

[4] COOK, T. M. Personal protective equipment during the coronavirus disease (COVID) 2019 pandemic - a narrative review. *Anaesthesia* [online]. 2020, **75**(7), p. 920-927. eISSN 1365-2044. Available from: https://doi.org/10.1111/anae.15071

[5] NOURAZARAN, M., YOUSEFI, R., MOOSAVI-MOVAHEDI, A. A. Effects of vitamin D in fighting COVID-19 disease. *Iranian Journal of Nutrition Sciences and Food Technology* [online]. 2022, **16**(4), p. 121-130. ISSN 1735-7756, eISSN 2252-0694. Available from: http://nsft.sbmu.ac.ir/article-1-3294-en.html

[6] VARANGES, V., CAGLAR, B., LEBAUPIN, Y., BATT, T., WEIDONG, H., WANG, J., ROSSI, R. M., RICHNER, G., DELALOYE, J.-R., MICHAUD, V. On the durability of surgical masks after simulated handling and wear. *Scientific Report s*[online]. 2022, **12**(1), 4938. eISSN 2045-2322. Available from: https://doi.org/10.1038/s41598-022-09068-1

[7] US Department of Labor [online] [accessed 2021-02-01]. Available from: https://www.osha.gov/news/newsreleases/trade/08032021

[8] ZHUANG, Z. Head-and-face anthropometric survey of U.S. respirator users [online]. Final report. Available from: https://nap.nationalacademies.org/resource/11815/Anthrotech_report.pdf

[9] ZHUANG, Z., BRADTMILLER, B. Head-and-face anthropometric survey of U.S. respirator users. *Journal of Occupational and Environmental Hygiene* [online]. 2005 **2**(11), p. 567-576. ISSN 1545-9624, eISSN 1545-9632. Available from: https://doi.org/10.1080/15459620500324727

[10] SWENNEN, GWEN, R. J., LIES, P., HAERS, P. E. Custom-made 3D-printed face masks in case of pandemic crisis situations with a lack of commercially available FFP2/3 masks. *International Journal of Oral and Maxillofacial Surgery* [online]. 2020, **49**(5), p. 673-677. ISSN 0901-5027, eISSN 1399-0020. Available from: https://doi.org/10.1016/j.ijom.2020.03.015

[11] PIOMBINO, P., COMMITTERI, U., NORINO, G., VAIRA, L. A., TROISE, S., MAGLITTO, F., MARINIELLO, D., DE RIU, G., CALIFANO, L. Facing covid-19 pandemic: development of custom-made face mask with rapid prototyping system. *Journal of Infection in Developing Countries* [online]. 2021, **15**(1), p. 51-57. ISSN 972-2680. Available from: https://doi.org/10.3855/jidc.13384

[12] PRABHU, R., BERTHEL, J. T., MASIA, J. S., MEISEL, N. A., SIMPSON, T. W. Rapid response! Investigating the effects of problem definition on the characteristics of additively manufactured solutions for COVID-19. *Journal of Mechanical Design Transactions of the ASME* [online]. 2022, **144**(5), 054502. ISSN 1050-0472, eISSN 1528-9001. Available from: https://doi.org/10.1115/1.4052970

[13] KOHAR, R., MADAJ, R., SASIK, R., GAJDAC, I. Rapid prototyping technologies/Rapid prototyping technologie (in Slovak). 1. ed. Zilina, Slovakia: EDIS ZU, 2018. ISBN 978-80-554-1519-2.

[14] KOHAR, R., STOPKA, M., WEIS, P., SPISAK, P., STEININGER, J. Modular 3D printer concept. *IOP Conference Series: Materials Science and Engineering* [online] 2018, **393**, 012092. ISSN 1757-8981, eISSN 1757-899X. Available from: https://doi.org/10.1088/1757-899X/393/1/012092

[15] MEHRPOUYA, M., TUMA, D., VANEKER, T., AFRASIABI, M., BAMBACH, M. AND GIBSON, I. Multimaterial powder bed fusion techniques. *Rapid Prototyping Journal* [online]. 2022, **28**(11), p. 1-19. eISSN 1355-2546. Available from: https://doi.org/10.1108/RPJ-01-2022-0014

[16] WOHLERS, T., CAFFREY, T. Wohlers report 2014: 3D printing and additive manufacturing state of the industry annual worldwide progress report. Fort Collins, Col.: Wohlers Associates, 2014.

[17] BATTEGAZZORE, D., CRAVERO, F., BERNAGOZZI, G., FRACHE, A. Designing a 3D printable polypropylene-based material from after use recycled disposable masks. *Materials Today Communications* [online]. 2022, **32**, 103997. eISSN 2352-4928. Available from: https://doi.org/10.1016/j.mtcomm.2022.103997

[18] ABDELMOMEN, M., DENGIZ, F.O., TAMRE, M. Survey on 3D technologies: case study on 3D scanning processing and printing with a model. In: International Conference on Research and Education in Mechatronics REM: proceedings [online]. 2020. ISBN 978-1-7281-6225-6, eISBN 978-1-7281-6224-9. Available from: https://doi.org/10.1109/REM49740.2020.9313881

[19] GOLOVIN, M. A, MARUSIN, N. V., GOLUBEVA, Y. B. Use of 3D printing in the orthopedic prosthetics industry. *Biomedical Engineering*, **52**(2), 2018, p. 100-105. ISSN 0006-3398, eISSN 1573-8256. Available from: https://doi.org/10.1007/s10527-018-9792-1

[20] ZHANG, L., YICK, K. L., LI, P. L., YIP, J., NG, S. P. Foot deformation analysis with different load-bearing conditions to enhance diabetic footwear designs. *PloS ONE* [online]. 2022, **17**(3), e0264233. eISSN 1932-6203. Available from: https://doi.org/10.1371/journal.pone.0264233

[21] KARTINI, W., IKHSAN, M., ISMAIL, R., JAMARI, J., BAYUSENO, A. P. Use of 3D scanner and photogrammetry method for scanning foot deformities: CAD data analysis of morphology and shape of geometry. *ARPN Journal of Engineering and Applied Sciences*. 2020, **15**(13), p. 1419-1425. ISSN 1819-6608.

[22] NULTY, A. B. A comparison of full arch trueness and precision of nine intra - oral digital scanners and four lab digital scanners. *Destiny Journal* [online]. 2021, **9**(7), 75. eISSN 2304-6767. Available from: https://doi.org/10.3390/dj9070075

[23] TAPPA, K., JAMMALAMADAKA, U. Novel biomaterials used in medical 3D printing techniques. *Journal of Functional Biomaterials* [online]. 2018, **9**(1), 17. eISSN 2079-4983. Available from: https://doi.org/10.3390/jfb9010017

[24] MUSSI, E., SERVI, M., VOLPE, Y., FACCHINI, F. A simple interactive tool for the CAD modelling of surgical guides for autologous ear reconstruction. *Computer-Aided Design and Applications* [online]. 2023 **20**(1), p. 109-118. ISSN 1686-4360. Available from: https://doi.org/10.14733/cadaps.2023.109-118

[25] KHYATI, D., ZAHERI, M., GOMES, G. V. Superhydrophilic 3D-printed scaffolds using conjugated bioresorbable nanocomposites for enhanced bone regeneration. *Chemical Engineering Journal* [online]. 2022, **445**, 136639. ISSN 1385-8947, eISSN 1873-3212. Available from: https://doi.org/10.1016/j.cej.2022.136639

[26] HABIB, A. A. I., SHEIKH, N. A. 3D printing review in numerous applications for dentistry. *Journal of The Institution of Engineers (India): Series C* [online]. 2022, **103**(4), p. 991-1000. ISSN 2250-0545, eISSN 2250-0553. Available from: https://doi.org/10.1007/s40032-022-00810-2

[27] CRISTACHE, C. M., GROSU, R. A. C., CRISTACHE, G., DIDILESCU, A. C., TOTU, E. E. Additive manufacturing and synthetic polymers for bone reconstruction in the maxillofacial region. *Plastic materials / Materiale Plastice* [online]. 2018, **55**, p. 555-562. ISSN 0025-5289, eISSN 2668-8220. Available from: https://doi.org/10.37358/mp.18.4.5073

[28] TREBUNA, P., TROJAN, J., MIZERAK, M., KLIMENT, M. 3D scanning - Technology and Reconstruction/3D skenovanie - technologia a rekonstrukcia (in Slovak). In: 23th International Scientific Conference Trends and Innovative Approaches in Business Processes: proceedings. Vol. 21. 2018. ISBN 978-80-553-3210-9.

[29] KHRIES, H. M. Photogrammetry versus 3D scanner: producing 3D models of museums' artifacts. *Collection and Curation* [online]. 2021, **40**(4), p. 153-157. ISSN 2514-9326. Available from: https://doi.org/10.1108/CC-06-2020-0021

[30] KUS, A. Implementation of 3D optical scanning technology for automotive applications. *Sensors* [online]. 2009, **9**(3), p. 1967-1979. eISSN 1424-8220. Available from: https://doi.org/10.3390/s90301967

[31] Sinterit Lisa user manual - Sinterit Sp.z o.o. [online] [accessed 2021-02-01]. Available from: https://sinterit.com/wp-content/uploads/2021/12/LISA-1.5_full-user-manual_1.5.pdf

[32] MAZZOLI, A. Selective laser sintering in biomedical engineering. *Medical and Biological Engineering and Computing* [online]. 2013, **51**(3), p. 245-256. ISSN 0140-0118, eISSN 1741-0444. Available from: https://link.springer.com/article/10.1007/s11517-012-1001-x

[33] CHAVEZ, L. A., IBAVE, P., HASSAN, M. S., HALL-SANCHEZ, S. E., BILLAH, K. M. M., LEYVA, A., MARQUEZ, C., ESPALIN, D., TORRES, S., ROBISON, T., LIN, Y. Low - temperature selective laser sintering 3D printing of PEEK - nylon blends: impact of thermal post-processing on mechanical properties and thermal stability. *Journal of Applied Polymer Science* [online]. 2022, **139**(23), 52290. eISSN 1097-4628. Available from: https://doi.org/10.1002/app.52290

[34] Lisa SLS 3D printer - Sinterit Sp.z o.o. [online] [accessed 2021-02-01]. Available from: https://sinterit.com/3dprinters/lisa/

[35] HP Multi Jet Fusion technology - HP Development Company [online] [accessed 2023-01-15]. Available from: https://h20195.www2.hp.com/v2/GetDocument.aspx?docname=4AA5-5472ENW

[36] LA FE-PERDOMO, I., RAMOS-GREZ, J. A., BERUVIDES, G., MUJICA, R. A. Selective laser melting: lessons from medical devices industry and other applications. *Rapid Prototyping Journal* [online]. 2021, **27**(10), p.1801-1830. ISSN 1355-2546. Available from: https://doi.org/10.1108/RPJ-07-2020-0151

[37] RAZAVIYE, M. K., TAFTI, R. A., KHAJEHMOHAMMADI, M. An investigation on mechanical properties of PA12 parts produced by a SLS 3D printer: An experimental approach. *CIRP Journal of Manufacturing Science and Technology* [online]. 2022, **38**, p. 760-768. ISSN 1755-5817, eISSN 1878-0016. Available from: https://doi.org/10.1016/j.cirpj.2022.06.016

[38] MADAJ, R., KOHAR, R. Additive Technologies/Aditivne technologie (in Slovak). 1 ed. Zilina, Slovakia: EDIS ZU, 2020. ISBN 978-80-554-1685-4.

[39] DANGNAN, F., ESPEJO, C., LISKIEWICZ, T., GESTER, M., NEVILLE, A. Friction and wear of additive manufactured polymers in dry contact. *Journal of Manufacturing Processes* [online]. 2020, **59**, p. 238-247. ISSN 1526-6125, eISSN 2212-4616. Available from: https://doi.org/10.1016/j.jmapro.2020.09.051

[40] PETZOLD, S., KLETT, J., SCHAUER, A., OSSWALD, T. A. Surface roughness of polyamide 12 parts manufactured using selective laser sintering. *Polymer Testing* [online]. 2019, **80**, 106094. ISSN 0142-9418, eISSN 1873-2348. Available from: https://doi.org/10.1016/j.polymertesting.2019.106094

[41] IBRAHIM, N., JOVIC, T., JESSOP, Z. M., WHITAKER, I. S. Innovation in a time of crisis: a systematic review of three - dimensional printing in the COVID-19 pandemic. *3D Printing and Additive Manufacturing* [online]. 2021, **8**(3), p. 201-215. ISSN 2329-7662, eISSN 2329-7670. Available from: https://doi.org/10.1089/3dp.2020.0258

[42] FUKUI, T., NIIKURA, T., ODA, T., KUMABE, Y., OHASHI, H., SASAKI, M., IGARASHI, T., KUNISADA, M., YAMANO, N., OE, K., MATSUMOTO, T., MATSUSHITA, T., HAYASHI, S., NISHIGORI, CH., KURODA, R. Exploratory clinical trial on the safety and bactericidal effect of 222-nm ultraviolet C irradiation in healthy humans. *PloS ONE* [online]. 2020, **15**(8), e0235948. eISSN 1932-6203. Available from: https://doi.org/10.1371/journal.pone.0235948

[43] KITAGAWA, H., NOMURA, T., NAZMUL, T., OMORI, K., SHIGEMOTO, N., SAKAGUCHI, T., OHGE, H. Effectiveness of 222-nm ultraviolet light on disinfecting SARS-CoV-2 surface contamination. *American Journal of Infection Control* [online]. 2021, **49**(3), p. 299-301. ISSN 0196-6553, eISSN 1527-3296. Available from: https://doi.org/10.1016/j.ajic.2020.08.022

[44] NAJMON, J. C., RAEISI, S., TOVAR, A. 2-Review of additive manufacturing technologies and applications in the aerospace industry. In: *Additive Manufacturing for the Aerospace Industry* [online]. FROES, F., BOYER, R. (Eds.). Elsevier Inc. All, 2019. ISBN 978-0-12-814062-8, p. 7-31. Available from: https://doi.org/10.1016/B978-0-12-814062-8.00002-9

[45] LUPONE, F., PADOVANO, E., CASAMENTO, F., BADINI, C. Process phenomena and material properties in selective laser sintering of polymers: a review. *Materials* [online]. 2022, **15**(1), 183. eISSN 1996-1944. Available from: https://doi.org/10.3390/ma15010183

[46] STOIA, D. I., VIGARU, C., OPRIS, C., VASILESCU, M. Properties and medical applications of biocompatible polyamide in additive manufacturing. *Plastic materials / Materiale Plastice* [online]. 2021, **58**(1), p. 113-120. ISSN 0025-5289, eISSN 2668-8220. Available from: https://doi.org/10.37358/MP.21.1.5451

AUTOMATED ROAD MILLING CUTTER FOR REPAIR OF THE ROAD SURFACES WITH VARIABLE TRACKAGE

Nurbol Kamzanov[1], Marzhana Amanova[2], Aigyl Baikenzheyeva[3], Guldariya Naimanova[3], Rustem Kozbagarov[3,*]

[1]Satbayev University, Almaty, Republic of Kazakhstan
[2]Kazakh University of Transport Communications, Almaty, Republic of Kazakhstan
[3]Academy of Logistics and Transport, Almaty, Republic of Kazakhstan

*E-mail of corresponding author: ryctem_1968@mail.ru

Nurbol Kamzanov 0000-0002-2420-8362,
Aigyl Baikenzheyeva 0000-0002-6013-2086,
Rustem Kozbagarov 0000-0002-7258-0775
Marzhana Amanova 0000-0002-8894-5257,
Guldariya Naimanova 0000-0003-4619-7243,

Resume
The article presents a method of experimental research and created stand with metrological equip-ment that allows to simulate the complex process of milling asphalt concrete samples by force and coordinate closure. As a result of the research, regression equations describing the milling parame-ters of asphalt concrete samples, were obtained. It is established that during the transition from the power (elastic) closure of the technological system to the rigid (coordinate) one, milling errors de-crease by up to 15 % and their spread is up to 30 %. The developed method for restoring the road surface can be applied in practice not only within Kazakhstan, but outside the country, as well.

Article info
Received 15 December 2022
Accepted 2 March 2023
Online 30 March 2023

Keywords:
road milling cutter
asphalt concrete pavement
pit repair
cutting element
highway
working body
track

Available online: https://doi.org/10.26552/com.C.2023.039

ISSN 1335-4205 (print version)
ISSN 2585-7878 (online version)

1 Introduction

In the Republic of Kazakhstan, the Law "On Technical Regulation" was adopted, which established that the technical regulation is carried out in accordance with the principles of: application of uniform rules for establishing requirements for products, production processes, operation; unity of rules and methods of research (testing) and measurements during the mandatory conformity assessment procedures. According to this Law, in the current market conditions, the requirements for the parameters of work should mainly be regulated in contracts, mandatory requirements - in national standards.

Over the past 30 years, the equipment has been modified and it is proposed to use new equipment already. These are graders with an automated "Profile" system, self-propelled rollers with a wide range of speed and vibrations, powerful domestic and imported milling cutters, recyclers, automated modern asphalt pavers, asphalt concrete mix loaders, etc. [1-5]. New materials and technologies have appeared with new possibilities for mixing uniformity, laying, with automation of modes. Accordingly, the work requirements and tolerances should be revised, justified and supplemented directly based on conducting the full-scale experimental work on road sections with a secured level of quality of work.

During operation, the road is subjected to various kinds of transport and weather-climatic factors. The very first and most unprotected element experiencing such effects is the asphalt concrete pavement. Practice has established that the main reason that has the greatest influence on the decrease in the quality of the roadway is called excess weight, the flow of cars that form rut, as well as the stressed-deformed state and service life of asphalt concrete pavements of highways depend on increased summer temperatures [6-8].

Wheel formation on roads is one of the main reasons leading to an increase in the degree of risk of road accidents, reduces the comfort and economic efficiency of using roads. The gauge bulges reach 170 mm in height and up to 350 mm in width [9].

Over the past more than twenty years, the road equipment has been modified. Accordingly, the requirements to the road pavement profiling technology, including milling, should be revised, substantiated and supplemented.

The creation of automated road cutters made it possible to significantly easier and more efficiently implement the operations of milling tracks and their spikes as a part of measures to repair roads and ensure road safety [10].

Therefore, the topic of improving the methods of coordinate closure of automated cutters for the repair of track formation of road surfaces is relevant and, therefore, the problem of increasing the efficiency of repair of road surfaces based on the use of coordinate closure of automated road cutters, is urgent.

2 Materials and methods

The long-term urban development plans are inextricably linked with an increase in the pace of construction of residential complexes, individual housing and other socially significant facilities. In development of urban areas, a special role is played by solving a complex of issues on their improvement for comfortable living of the population. At the same time, one of the important tasks is improvement of the sidewalks, courtyard roads and playgrounds, as well as squares, alleys and park areas, require a large number of a wide range of road construction materials.

Currently, concrete pavers of various configurations and asphalt concrete are widely used to solve these problems. However, as practice shows, during the operation of these roads, their destruction is often observed. The fact is that the concrete paving stones are necessarily exposed to the actions of sulphate salts of acids and alkalis, since they are necessarily present in the composition of the soils of the surface being laid and are additionally exposed to the actions of chemical reagents coming from the external environment (rains, car oils, groundwater etc.). Under the influence of these chemicals, concrete pavers and products made on the basis of cement binders are corroded, as a result of which they eventually collapse.

Based on the analysis of the layouts of the existing automated road cutters, the dominant factors determining the change in the mutual position of the working elements of the machine and the road surface in the process of milling the road surface with a variable gauge are determined, which causes a decrease in the evenness of the profiled surface of the road surface [9,11].

As a result of studies, it has been found that the problems of controlling the track milling and its overheads on existing road milling machines come from a lack of feedback, therefore, it is possible to build an adaptive road surface milling system provided that the milling system is supplemented with feedback sensors and appropriate software.

The proposed principle of operation of the software complex of computational modeling makes it possible to determine the recommended height of the removed ramp allowance for the initial conditions of the steady-state mode. Based on that, the numerical modeling of the milling process was carried out.

The possibilities of using the contact sensors are considered, converters of movements into electrical signals, which are usually inductive.

The solution of this problem was proposed to be carried out by changing the structures of the control systems and laws of control of the road milling machines working bodies, as an automated road technological manipulator with several degrees of mobility of a working body - a milling tool operating in generalized technological coordinates for repair of the road surfaces with variable rut and due to the transition from elastic (power) to the rigid (positional or coordinate), as well as the combined closure of the technological system for milling the track and its legs.

At the same time, the need to switch from an elastic (power) closure of the position control circuit to a rigid (coordinate) closure of the track milling process scheme and its overheads is justified, which allows reducing, not only the current average error (deviations from the required level) of milling, but their spread (standard deviation), as well.

3 Results and discussions

At present, when carrying out the repair work to eliminate ruts on road surfaces, the technology of milling outbursts has been used as a temporary measure. When milling outbursts (influx), the required coefficient of adhesion and a smooth surface of the road surface are provided. The problem of precise milling of swells, side bumps next to the track is solved. The milling technology of the track itself does not change [6,9].

Usually, the track is filled with a mixture for patching (cationic emulsion with fine crushed stone, fraction size 5 to 10 mm) or milled to a given depth without requiring accuracy and filled with asphalt concrete mixture followed by compaction. Precise milling is necessary to ensure evenness and ensure road safety. The milling error should not exceed 1 to 3 mm/m.

During the milling, the relative position of the axis of rotation of the milling cutter changes relative to the chassis of the road milling cutter and, accordingly, the road surface, vertical corrective movement is carried out [11-13]. The distance from the cutting line to the axis of rotation of the cutter will be called the level of dimensional adjustment, i.e. during the milling, corrective variable movements are carried out for the vertical position of the cutter.

The cutting line lies at the level of the initial surface of the road surface outside the area, in order to avoid the risk of road traffic accidents (accidents) and to meet the technical requirements of the track repair project. The influx is a mass of asphalt concrete mixture squeezed out of the track to the right or to the left, with different dimensional and mechanical characteristics (height, width, density, shape, strength, presence of cracks, staining, porosity). We will assume that the front and rear wheels of the milling cutter travel on a flat section of road outside the track. The new road construction machines use computer control with drives and working bodies. In addition, additional control circuits can be made independently of the main computer, based on a microcontroller or an industrial computer. The control of the vertical displacement drive will be carried out by adding up the signals coming from the main computer and from the compensation circuit for the deviation of the milling dimensions.

The milling cutter is usually of a Wirtgen (FRG) type design it is recommended to use the free-layout teeth of the milling cutter in the mounting housing to reduce diffusion wear. The freely rotating cutting element is constantly shifted by the heated contact point to the side, outside the contact zone, so the milling cutter section has time to cool down. Therefore, there is no molecular diffusion exchange and the usual mechanical wear is significant for rigid tools are significant.

New road machines use computer control of drives and working organs. In addition, additional control circuits can be implemented independently of the main computer based on the microcontroller or industrial computer. The vertical drive will be controlled by summing the signals from the host computer and the milling size deviation compensation circuit.

A contactless laser sensor is used, the base length is 250 mm, with an error of 0.5 mm of the BOSCH type, which is a housing with an optical eye of the receiving and transmitting system, there is also a microprocessor and an output to computer equipment. The control system sets the setting for the signal received from the sensor, the difference from which this signal gives deviations in the milling dimensions. The feedback control is used with help of correction variables for turning the level of dimensional adjustment of the milling cutter. In fact, it is proposed to switch from kinematic closure by force to kinematic closure by coordinate (displacement or increments of the movements of the milling cutter), because it allows to fully realize the capabilities of the numerical control system of the road milling cutter.

This makes it possible to reduce, not only the current average milling deviation, but their spread, as well (the standard deviation, the square of which is the variance). The task of ensuring only evenness is solved, the task of ensuring the coefficient of adhesion is not set and is not discussed. For traditional constructions of the road milling cutter, power take-off from the main engine or the use of an additional engine is characteristic. In manual control, feedback is implemented through the adaptation of the driver to changing environmental conditions. Previously, kinematic force closure was actually used (by hydro, pneumatic suppression power take-off or by power take-off through auxiliary elements). In fact, this method of controlling the road milling cutter allowed only to prevent or reduce the initial deviation of the treated surface of the road surface during milling. If the size of the allowance and its influx density became larger, then the milling cutter experienced additional vertical loads and additionally deviated upwards from the cutting line, which resulted in deviations in dimensions of the milled surface of the road surface, which led to an increase in the risk of an accident. Changes in the size of these surges can be 10 to 170 mm and will affect the road repair site by 5 to 10 times. Accordingly, the additional vertical component of the cutting force changes at times, caused by a change in the dimensional mechanical parameters of the influx. Therefore, the task arises of compensating for undesirable additional vertical movements of the milling cutter and controlling the level of the milling cutter adjustment in real time.

It is used to set a digital model of the road surface. As an initial information for determining the level of dimensionality of the milling cutter setting, existing milling cutter layouts assume the operation of the milling cutter cutting elements in the milling cutter coordination system, if the interaction occurs through the milling cutter and wheels or, more importantly, through the milling cutter and rollers rolling on the road surface outside the track. In fact, the second method allows milling in the coordinate system of the road surface and without elastic elements in the form of wheels. From the road milling cutters there is only a power take-off. However, this does not allow compensating for the wear of the cutting elements of the cutter, errors in adjustment, temperature deformations. Therefore, the scanning systems determine the digital model of the road surface outside the track and calculate the trajectory of the cutting lines. With respect to this virtual line, automatic or virtual adjustments of tool departures are made so that the tool vertices lie on this calculation line. The adjustment can be done manually.

Previously, the control was carried out according to the instantaneous height - the average value of deviation of the milling dimensions and now we are additionally engaged in reducing the spread of the deviation of the milled surface. For the first time, the precision control of milling of specific elements of the highway is applied - eliminating the influx from the side of the track, the principle of controlling the road milling cutter by feedback is used.

Non-mechanical kinematic connections are widely used in automated road milling cutters. For example, by wires or radio signals. Previously, gears were used. As a rule, new types of drive can work with different types of kinematic closures. For example, by speed, by increment of movements, by moment, by power

Figure 1 *Procedure for measuring deformations of an asphalt concrete coating sample using a universal magnetic measuring head*

Figure 2 *Measurement of vibroacoustic vibrations during the cutting using a vibration measuring system*

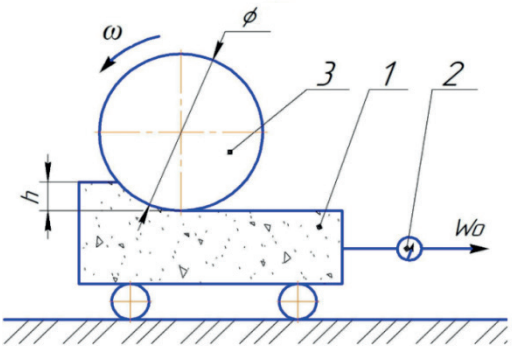

Figure 3*Diagram of the experimental stand for determining the main milling parameters: 1- trolley with a sample of asphalt concrete, 2 - diamond disc, 3 - dynamometer*

(electricity sold). In the work, the control for the increment of movements is selected as the main one. In the non-mechanical kinematic connections, the control principle is important. Control is considered by feedback and by perturbations. The feedback control is selected, which consists in measuring the output parameter, determining the milling deviation, multiplying by the adjustment coefficient and implementing this correcting the variable increment through the vertical displacement drive (correcting variable increment of displacement) of the milling cutter. Comparative simulation tests of cutting asphalt concrete samples with elastic and coordinate closure were carried out. In their formulation, implementation and processing of the results, well-developed and modern methods of experimental research were used. Specifically, the experimental research methodology was developed by Kochetkov [9, 14].

The experimental stand was implemented based on the vertical milling machine in the laboratory of metal-cutting machines. By readjusting it, the axis of rotation of the cutting tool was installed in a horizontal position. As a model of a milling cutter, standard disc cutters with a diameter of 110 and 230 mm (metal-cutting tools) were selected. Photos of the developed stand are shown in Figures 1 and 2.

Figure 1 shows the procedure for measuring deformations of an asphalt concrete coating sample using a universal magnetic measuring head. Figure 2 shows the measurement of vibroacoustic vibrations during cutting using a vibration measuring system. Two series of experiments with elastic and rigid closure were carried out. In the first case, a rubber sheet of a thickness of 5 mm was placed between the magnetic clamping device and the milling machine table. In the second case, the magnetic clamping device was rigidly attached to the milling machine table. A disc milling cutter and a sample of asphalt concrete with an uneven surface were selected. Example, at the real time of the deviation of the milling size consisted of 10 mm, multiply it by the adjustment factor equal to - 0.5, get -5 mm - the value of the variable correction increments and add it to the existing level of dimensional adjustment of the cutter.

This compensates for random changes in the dimensional mechanical parameters of the gauge influx, it also compensates for pressure changes in pneumatic tires, for wear of cutting elements, thermal temperature deformations of the working body and the road milling cutters themselves and compensates for changes in the mass characteristics of the milling cutter. The determined (linear) and periodic (correlating) component of the

Table 1 *Plan and results of experiments*

No.	Plan in natural variables		Feed force W_o (kN)	Residual deformations	
	h (mm)	V (m/s)		rigid fastening	fastening through an elastic element
1	10	0.03	3.8	1.8	1.6
2	60	0.03	20.6	2.8	2.4
3	10	0.05	4.2	2.0	1.7
4	60	0.05	22.7	2.1	1.5
5	7.68	0.04	2.6	1.7	2.4
6	77.68	0.04	26.2	2.8	4.6
7	35	0.023	11.2	2.1	3.0
8	35	0.047	13.1	2.2	3.1
9	35	0.04	11.7	2.6	3.1
10-13	35	0.04	12.0	2.7	3.3

milling deviation sequence is actually compensated. The random component cannot be controlled.

Comparative simulation tests of the cutting asphalt concrete samples with elastic and coordinate closure were carried out. A methodology for study of the main parameters of milling has been developed. The research was aimed at determining the relationship between the milling depth (h) and the disk feed rate (V) on the feed resistance (Wo). The experiments were carried out on a specially made stand (Figure 3).

The rotation frequency of the disk was taken as a constant in the experiments, which provided a linear cutting speed of up to 50 m/s. At the same time, the feed rate of the diamond disc varied from 1.8 m/min to 3 m/min and the milling depth h - from 10 to 60 mm. The experiments were carried out with 3-fold repetition, in accordance with the developed plan of the factor experiment presented in Table 1 with the results of the experiments.

The scientific result is registering the fact of an increase in the spread of residual cutting deformations (errors) in comparison of rigid and elastic force closures [9, 14-15]. After the processing of the experimental results, mathematical dependences were obtained (the feed effort of the W_o on the milling depth h and the feed speed V)

$$W_O = 0.35h + 0.1h \cdot B\,. \tag{1}$$

Based on this dependence, the average value of the milling resistance was determined, q_o as

$$q_O = W_O/h \cdot B\,, \tag{2}$$

where B is the milling width. The q_o values are 60 to 80 kPa and can be used to determine the drive power N

$$N = 0.5 \cdot q_O \cdot h \cdot B \cdot D \cdot \omega\,, \tag{3}$$

where D - is the diameter of the disk, ω - is the angular velocity of rotation of the disk.

The experimental stand is implemented based on the horizontal milling machine 6M82G. At the same time, the task was to reproduce the process of interaction between the milling tools and asphalt concrete as close as possible to the real one. As a model of the drum of the road milling cutter, a prefabricated milling cutter with a ratio of diameter and width similar to the working bodies of existing machines was chosen. The milling cutter was assembled from a typical metal-cutting tool, taking into account the peculiarities of asphalt concrete processing, discs with a large tooth were selected to reproduce the effect of dyeing (breaking out) and not cutting the sample.

Two series of experiments with elastic and rigid closure were carried out. Milling was carried out towards the treated surface (against the feed). Two modes were investigated: - with an elastic element (rubber base with a thickness of 20 mm) (Figure 4 a, b) - simulation of milling by force closure. The sample was fixed on a specially designed experimental table mounted on the frame through an elastic element. In this case, there was an increased spread of deviations of milling parameters and an increase in the average height of the profile of the milled surface - in the case when the sample with asphalt concrete was fixed rigidly (Figure 4 c, d) - imitation of coordinate closure, a decrease in deviation of the milling dimensions was observed, according to approximate estimates, by 2 times. This confirms the effectiveness of the transition from force closure to coordinate closure or displacement control. Photos of part of the experiments are shown in Figure 4.

Outside of the experimental plan, the milling of an asphalt concrete sample was carried out by force closure using springs of variable stiffness as elastic elements, simulating different stiffness of the milling cutter - tool-coating system. The observation showed that the effect of the rigidity of the milling cutter - tool-coating system on the deviation of the milling profile is not linear and

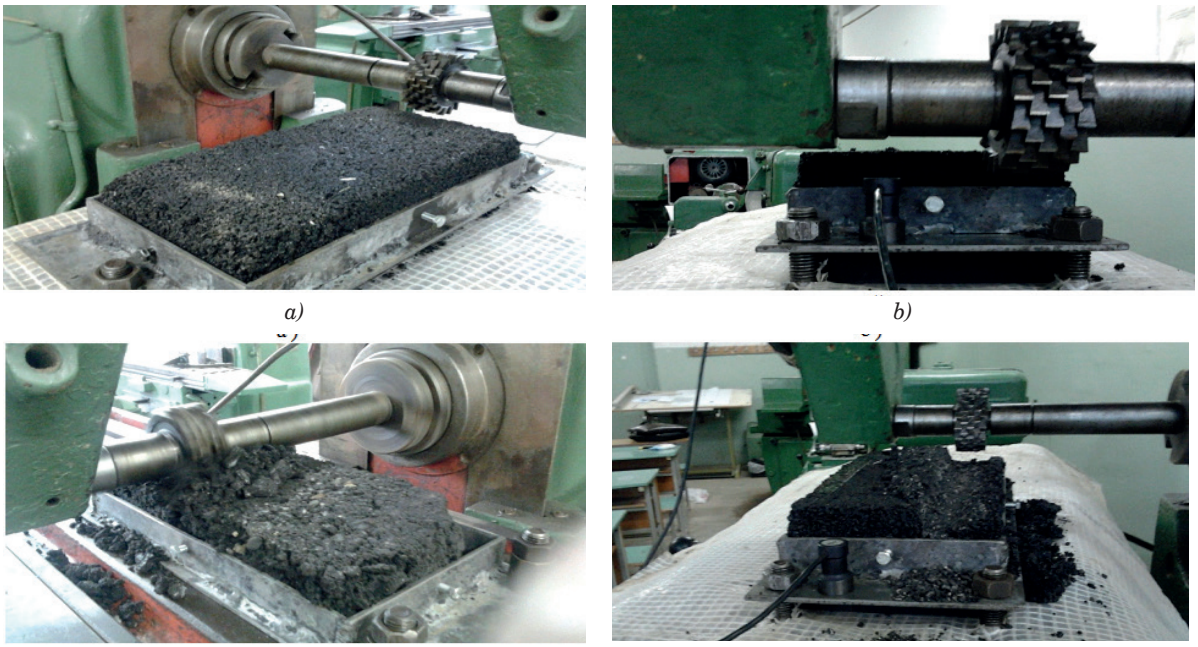

a) *b)*

c) *d)*

Figure 4 *Experiment on simulation milling of asphalt concrete samples: a)with elastic element (rubber base 20 mm thick); b) simulation of milling by power closure; c) the sample with asphalt concrete was fixed rigidly; d) imitation of coordinate closure*

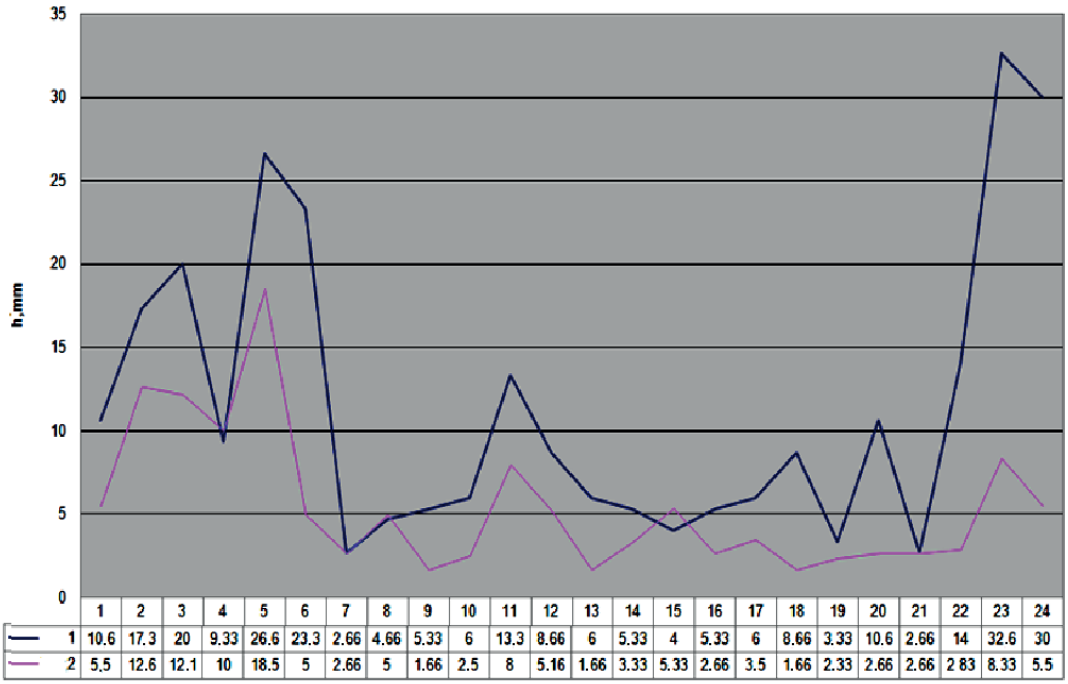

	1	2	3	4	5	6	7	8	9	10	11	12	13	14	15	16	17	18	19	20	21	22	23	24
1	10.6	17.3	20	9.33	26.6	23.3	2.66	4.66	5.33	6	13.3	8.66	6	5.33	4	5.33	6	8.66	3.33	10.6	2.66	14	32.6	30
2	5.5	12.6	12.1	10	18.5	5	2.66	5	1.66	2.5	8	5.16	1.66	3.33	5.33	2.66	3.5	1.66	2.33	2.66	2.66	2 83	8.33	5.5

Figure 5 *Comparison of results of the road surface milling with use of the road cutters: - elastic closure, - rigid closure*

increases abruptly with a decrease in the rigidity of the system (an increase in its elasticity).

It is possible to use the developed algorithms of adaptive sign and proportional adjustments. As a result of modeling based on the initial sample, a decrease in the average value of the milled surface of the protrusions by 20 % was obtained when using sign pulsating adjustments with a variable pulse. Comparison of the results of milling asphalt concrete pavement with use of the road cutters for elastic (power) and rigid (coordinate) closure is shown in Figure 5.

The technological scheme of milling of the first track of the road surface has been developed, the effectiveness of the rigid (coordinate) closure of the technological scheme of milling in comparison to the elastic (force) method has been confirmed.

Practical results of the study of methods of automated road milling control were obtained. It is obtained that during the motion control (coordinate closure) there is a decrease in the residual deformation spread compared to the elastic closure control.

The use of results of this work would allow for more efficient work on construction, repair and maintenance of highways, to ensure the required transport and operational characteristics, the safety of highways and road safety.

4 Conclusions

Based on the analysis of the layouts of existing automated road cutters, the dominant factors determining the change in the relative position of the working bodies of the machine and the road surface, during the milling of the road surface with variable track height are determined, which causes a decrease in the evenness of the profiled surface of the road surface.

The concept of presenting a road milling cutter as an automated road transport and technological manipulator that corrects the level of dimensional adjustment by vertical movements of the working body is proposed, based on of which a new design of an automated road milling cutter, for repairing road surfaces with variable trackage with the possibility of adjusting the working body in height, has been developed.

The feasibility of the transition from elastic (force) closure to rigid (coordinate-kinematic) closure of the track milling process scheme has been substantiated and proved, which allows not only to reduce the current average deviations of the height of the milled surfaces, but their variations from the average, as well.

The transition to coordinate and kinematic closure makes it easier, both from the point of view of building a drive system and from the point of view of programming processes, to implement the process of operation of automated road cutters.

Grants and funding

The authors received no financial support for the research, authorship and/or publication of this article.

Conflicts of interest

The authors declare that they have no known competing financial interests or personal relationships that could have appeared to influence the work reported in this paper.

References

[1] FEDOROV, D. I. *Working bodies of earth-moving machines*. Moscow: Mechanical Engineering, 1977. ISBN 5-217-00490-8.

[2] DOVGYALO, V. A., BOCHKAREV, D. I. *Road construction machines. Part I: Machines for earthworks.* Gomel: Belarusian state University of Transport, 2010. ISBN 978-985-468-741-4.

[3] DOVGYALO, V.A., BOCHKAREV, D.I. *Road construction machines. Part II. Machines for the construction and repair of road surfaces.* Gomel: Belarusian state University of Transport, 2018. ISBN 978-5-7996-2386-9.

[4] VOLKOV, D. P., KRIKUN, V. Y., TOTOLIN, P. E., GAEVSKAYA, K. S. *Earthwork machines.* Moscow: Mechanical Engineering, 1992. ISBN 5-217-01973-5.

[5] SHERBAKOV, A. P., PUSHKAREV, A. E., MAKSIMOV, S. E. Replacement working body material as a way to increase reliability of road construction machines. *The Russian Automobile and Highway Industry Journal* [online]. 2021, **18**(6), p. 646-661. ISSN 2658-5626. Available from: https://doi.org/10.26518/2071-7296-2021-18-6-646-661

[6] BURGONUTDINOV, A. M. *Machines for the construction, repair and maintenance of highways. Part 3: Machinery and equipment for the repair and maintenance of road.* Perm: Perm National Research Polytechnic University, 2011. ISBN 978-5-398-00900-2.

[7] JIANG, Z. Damage mechanism of asphalt concrete pavement under different immersion environments. *Wireless Communications and Mobile Computing* [online]. 2022, **2022**(5), p. 1-7. ISNN 1530-8677. Available from: https://doi.org/10.1155/2022/6061004

[8] LUKASHUK, O. A., KOMISSAROV, A. P., LETNEV, K. YU. *Machines for soil development. Design and calculation*. Ekaterinburg: Ural University Publishing House, 2018. ISBN 978-5-7996-2386-9.

[9] KOZBAGAROV, R. A., KAMZANOV, N. S., AKHMETOVA, S. D., ZHUSSUPOV, K. A., DAINOVA, Z. K. Improving the methods of milling gauge on highways. *News of the National Academy of Sciences of the Republic of Kazakhstan, Series of Geology and Technical Sciences* [online]. 2021, **3**(447), p. 87-93. ISSN 2518-170X. Available from: https://doi.org/10.32014/2021.2518-170X.67

[10] ILGE, I. Model of selection of a road miller. *Bulletin of Kharkov National Automobile and Highway University* [online]. 2021, **1**(92), p. 103-108. ISBN 2219-5548. Available from: https://doi.org/10.30977/BUL.2219-5548.2021.92.0.103

[11] KOZBAGAROV, R. A., ZHUSSUPOV, K. A., KALIYEV, Y. B., YESSENGALIYEV, M. N., KOCHETKOV, A. V. Determination of energy consumption of high-speed rock digging. *News of the National Academy of Sciences of the Republic of Kazakhstan, Series of Geology and Technical Sciences* [online]. 2021, **6**(450), p. 85-92. ISSN 2518-170X. Available from: https://doi.org/10.32014/2021.2518-170X.123

[12] KOZBAGAROV, R. A., SHALBAYEV, K. K., ZHIYENKOZHAYEV, M. S., KAMZANOV, N. S., NAIMANOVA, G. T. Design of cutting elements of reusable motor graders in mining. *News of the National Academy of Sciences of the Republic of Kazakhstan, Series of Geology and Technical Sciences* [online]. 2022, **3**(453), p. 128-141. ISSN 2518-170X. Available from: https://doi.org/10.32014/2022.2518-170X.185

[13] KOZBAGAROV, R., AMANOVA, M., KAMZANOV, N., BIMAGAMBETOVA, L., IMANGALIYEVA A. Investigation of wear of cutting part of polygonal knife car graders in different ground conditions. *Communications - Scientific letters of the University of Zilina* [online]. 2022, **24**(4), p. D229-D238. ISSN 2585-7878 [online]. Available from: https://doi.org/10.26552/com.C.2022.4.D229-D238

[14] ZAKHAROV, O. V, KOCHETKOV, A. V. Minimization of the systematic error in centerless measurement of the roundness of parts. *Measurement Techniques* [online]. 2016, **589**(12), p. 1317-1321. ISSN1573-8906. Available from: https://doi.org/10.1007/s11018-016-0892-6

[15] BALOVNEV, V. I. *Modeling of interaction processes with the environment of working bodies of road construction machines*. Moscow: Higher School, 1981, ISBN 5-217-02343-0.

UNIVERSITY
OF ŽILINA

1953 70 2023

In its over 70 years of successful existence, the University of Žilina (UNIZA) has become one of the top universities in Slovakia.

The mission of UNIZA is to develop education on the basis of science, research and art activities within national and democratic traditions, to develop harmonic personality, knowledge, the good and creativity of a man and to contribute to the advancement of education, science, and culture for the welfare of the whole society.

Professional profile of UNIZA is unique and includes transport (road, railway, water, air), transport and postal services, communications, civil engineering construction, electrical engineering, telecommunications, informatics, information and communication technologies, management and marketing, mechanical engineering, materials and technologies, robotics, machinery design, energies, civil engineering, crisis and security management, civil security, fire protection, forensic engineering, applied mathematics, teacher training, library and information sciences, social pedagogy and high mountain biology. Results of science and research activities of the University have an important influence not only on the educational activities but also on the development of international cooperation or interconnection with practice.

UNIVERSITY PARTS
7 faculties
9 research and educational institutes and centres
3 specialized professional and training workplaces
3 information workplaces
1 economic and administrative department
4 dedicated facilities

EDUCATION
7 faculties:
8 000 students
more than 88 000 graduates
172 study programmes

SCIENCE AND RESEARCH
699 creative workers
785 000 hours, annual research capacity
190 domestic scientific projects
45 foreign projects
30 scientific and technical journals
50 scientific and professional events per year

INTERNATIONAL COOPERATION
The University of Žilina in Žilina has almost 50 valid university-wide bilateral agreements, and cooperates with foreign universities in the EU, Asia, America and Africa. It cooperates on foreign non-research projects and has concluded more than 300 agreements in the ERASMUS + programme.

UNIVERSITY OF ŽILINA
Science & Research Department

Univerzitná 8215/1,
010 26 Žilina,
Slovakia

Ing. Janka Macurová
tel.: +421 41 513 5143
e-mail: janka.macurova@uniza.sk

INCREASE OF THE AUTOMOTIVE POWER TRANSISTOR MODULES MANUFACTURE RELIABILITY USING AI DETECTING SYSTEM FOR SOLDERING SPLASHES

Dušan Koniar[1], Peter Klčo[1], Libor Hargaš[1], Marek Chnápko[2], Katarína Pocisková Dimová[2], Vladimír Kindl[3,*]

[1]Department of Mechatronics and Electronics, Faculty of Electrical Engineering and Information Technologies, University of Zilina, Zilina, Slovakia
[2]Semikron, s.r.o., Vrbove, Slovakia
[3]Department of Power Electronics and Machines, Faculty of Electrical Engineering, University of West Bohemia, Pilsen, Czech Republic

*E-mail of corresponding author: vkindl@fel.zcu.cz

Dušan Koniar 0000-0003-3029-3193, Peter Klčo 0000-0001-5386-2243,
Libor Hargaš 0000-0001-8716-0944, Vladimír Kindl 0000-0003-2378-8059

Resume
This study discusses the automated visual inspection of electronic boards used in the mass production of power electronics equipment. Soldering splashes, produced during the necessary manufacturing stages, can affect the hybrid power semiconductor modules' quality, specifications and lifespan. Splashes from soldering may appear in some electronic boards areas when they may cause decreasing of quality of these boards and need to be removed. Image analysis algorithms are used to search for such areas. The automated inspection is based on neural network YOLO. The images of electronic boards, acquired by authors in SEMIKRON Slovakia company, were used as training, testing and validation dataset for the YOLO network. The custom recording system was designed to acquire those images. The implementation of this method may increase the object search success and then thereby increase the overall quality of module production.

Article info
Received 5 December 2022
Accepted 25 January 2023
Online 1 March 2023

Keywords:
transistor
module
solder
splash

Available online: https://doi.org/10.26552/com.C.2023.032

ISSN 1335-4205 (print version)
ISSN 2585-7878 (online version)

1 Introduction

The first IGBT based standard module appeared in 1989. Today the construction is still closely related to the original set-up. One or more ceramic plates DCBs (Direct Copper Bond) are soldered onto a copper base plate, which also serves as the mounting surface to the heatsink. They consist of a thin insulating substrate made of Al_2O_3, Si_3N_4 or AlN and copper with variable thickness coated on both sides.

Soldered to the top of the DCBs are the bottom sides of the chips (IGBTs: collectors, diodes: usually cathodes). The chip tops sides (IGBTs: gate and emitter, diodes: anode) are contacted by parallel Al or Cu bond wires to corresponding pads on the DCB substrate. Either soldered, or ultrasonic welded, directly onto these pads, are the module terminals. There are more soldered, ultrasonic welded or bonded connections to the terminals mechanically fixed in the module housing (Figure 1).

The continuous development of the construction and connection technology of power modules is driven by the cost measures in production and processing of the modules on the one hand and ever-increasing demands on the module properties on the other.

This involves the best possible dissipation of the heat loss in the semiconductors to the cooling, both statically, as well as for the short-term loads. Power modules can be utilized very effectively with efficient cooling, which is a “must” for the high power and lowest possible semiconductor cost. Thus, the permissible temperatures of the IGBT and diode chips are increased from one chip generation to the next. However, high chip operating temperatures and efficient heat dissipation tighten the requirements for temperature and power cycling capability of the module designs. This requires

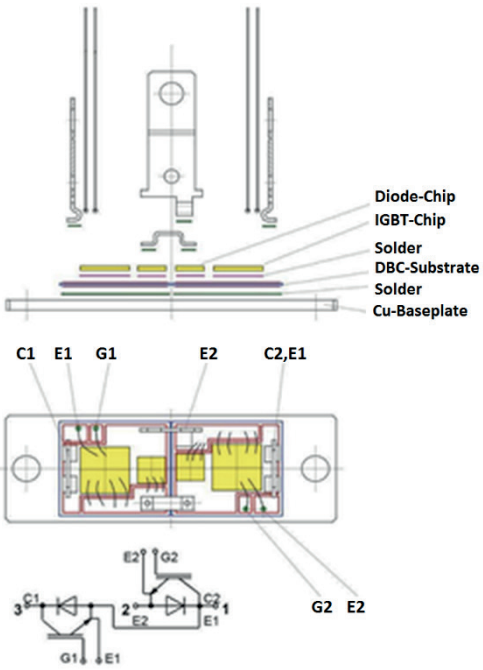

Figure 1 *Basic concept of soldered module*

continuous development of the construction and connection technologies.

One of the most important processes in power modules production is soldering (Figure 2). Soldering is currently one of the basic methods of connecting circuit elements. When soldering power modules, it is necessary to ensure a perfect connection of individual components with the baseplate. In practice, it sometimes happens that during the soldering of individual elements there is an imperfect connection of components or splashes are formed. Detection of soldering splashes is important for increasing the quality and reliability of power electronic modules and it is important from the economical point of view, as well: most of detected soldering splashes can be removed and electronic board of expensive module can be used again.

Industrial manufacturing processes are supervised by the visual inspection systems, to identify possible defects. To increase reliability, reduce the number of defects (higher identification rate) and decrease the time required for this procedure, progressive detection algorithms and visual systems are being developed within last years. Last decade, the computer vision tasks for specific objects detection are based on neural networks (especially convolutional neural networks - CNN). There are some works comparing the modern CNNs and conventional classifiers (such as Support Vector Machine - SVM) used in algorithms for searching specific objects in images. Ren et al. [1] concluded that selected CNN obtained better results for identification of given object as method based on SVM. Multilayer feedforward neural networks can be computationally demanding due to high number of weight parameters. The neuronal representation of spatial information can be another bottleneck for flattened layers [2]. Due to significant expansion and massive implementation of CNNs to many image identification tasks, it exists several CNN architectures and their derivatives. The YOLO architectures, which were used for our application, are discussed in the following. The research shown their applicability to inspect the electronic boards (PCBs) for different types of defects. The YOLO model (You Only Look Once) belongs to deep neural networks designed by Joseph Redmon as one step process classification algorithm. The input image is divided into a grid SxS. The YOLO network can detect multiple bounding boxes in single grid cell. In comparison to other deep neural networks, the YOLO's detection speed is relatively high. The YOLO can classify multiple categories simultaneously [3]. The final stage of model classification results in localization of bounding box and type of category identification [4]. In our case there is only one object category - soldering splash. The YOLO classification model is considered as one of the most successful modifications of Convolutional neural networks [5]. Adibhatla et al. proposed deep learning model based on Tiny-YOLOv2 architecture for PCB quality inspection. Their dataset consisted of 11000 images (420x420 pixels) obtained from the automated optical inspection (AOI) machine. The model achieved 98% accuracy for batch size 32. The YOLO model can have lower recall or increased localization errors than the Fast R-CNN network model [2]. The YOLO architecture can be preferred due to tradeoff between detection accuracy and speed. The authors consider template-matching and image subtraction as traditional methods for the PCB defect detection [6-8]. Liao et al. used improved YOLOv4 algorithm for detection of 6

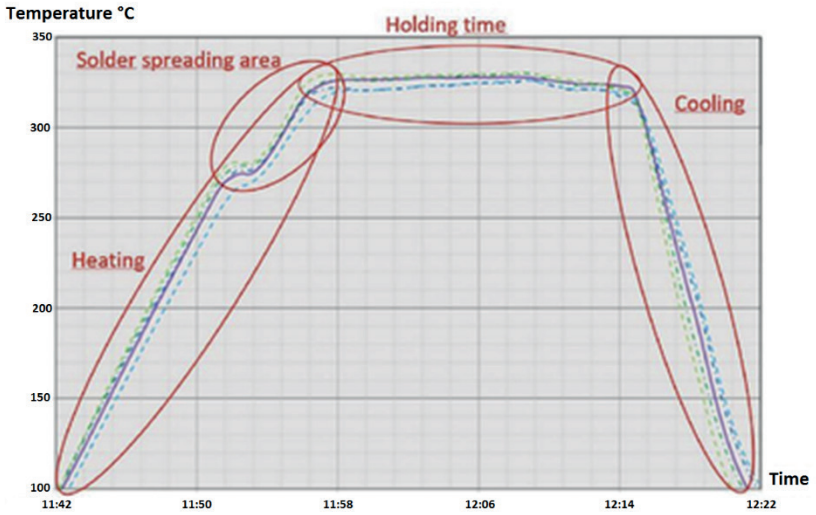

Figure 2 *Timeline of automated soldering procedure*

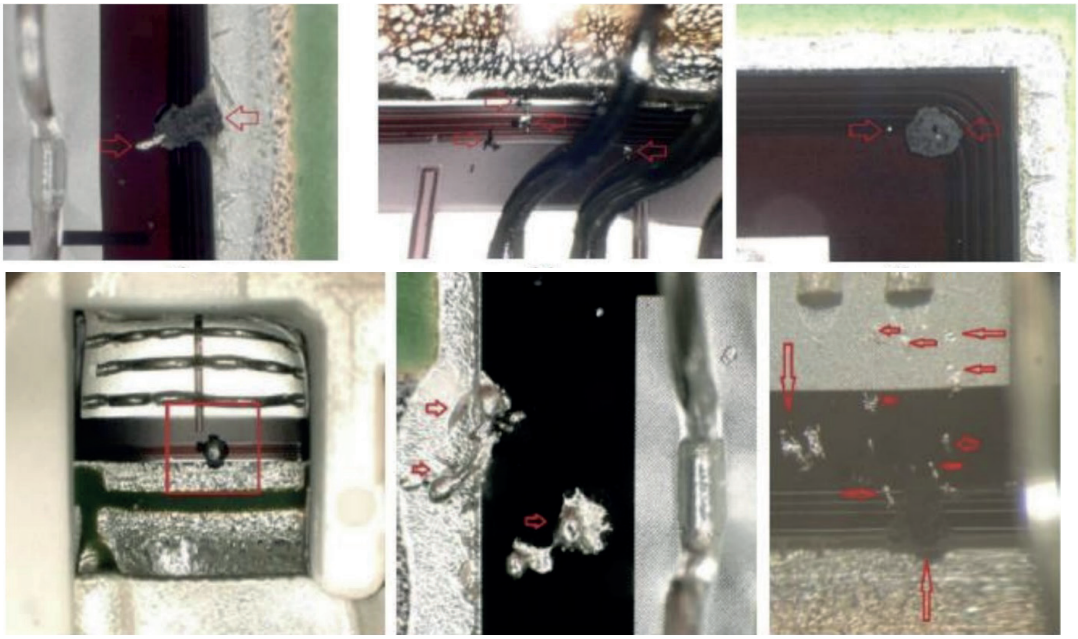

Figure 3 *Typical examples of soldering splashes in inspected images*

different PCB surface defects - scratch, clutter, broken line, hole loss, line repair damage and over oil-filling. The original dataset consisted of 2008 PCB defect images. The data augmentation was performed and number of images increased to 19029. Originally 12-megapixel images were resized to 416 x 416 pixels and labelled with LabelImg program. The neural network model with 39.5 million of weight coefficients achieved high performance with 98.6 % mean average precision score (mAP) [9].

2 Soldering process characteristics

In production soldering process, exist three procedures:

- One-step soldering process: whole power module with chips and terminals (power terminals and signal terminals) is assembled in soldering mask and soldered together by the preform solder.
- Two-step soldering process: power module is assembled in two steps, the 1st step consists of silicone chips soldering by the solder paste, the 2nd step consists of preform soldering from power hybrid to baseplate and terminals (main power terminals and auxiliary/signal terminals).
- The second soldering process: used for power modules with high void ratio under the DCB or chips. This process is introduced for decreasing the scrap ratio after the soldering process and eliminate unwanted voids.

Solder under the chips consists of solder and flux (solder paste). Solder under the DCB is without flux (preform solder used for Semitrans10, SEMiX Press-fit). In two-step soldering process (or second soldering

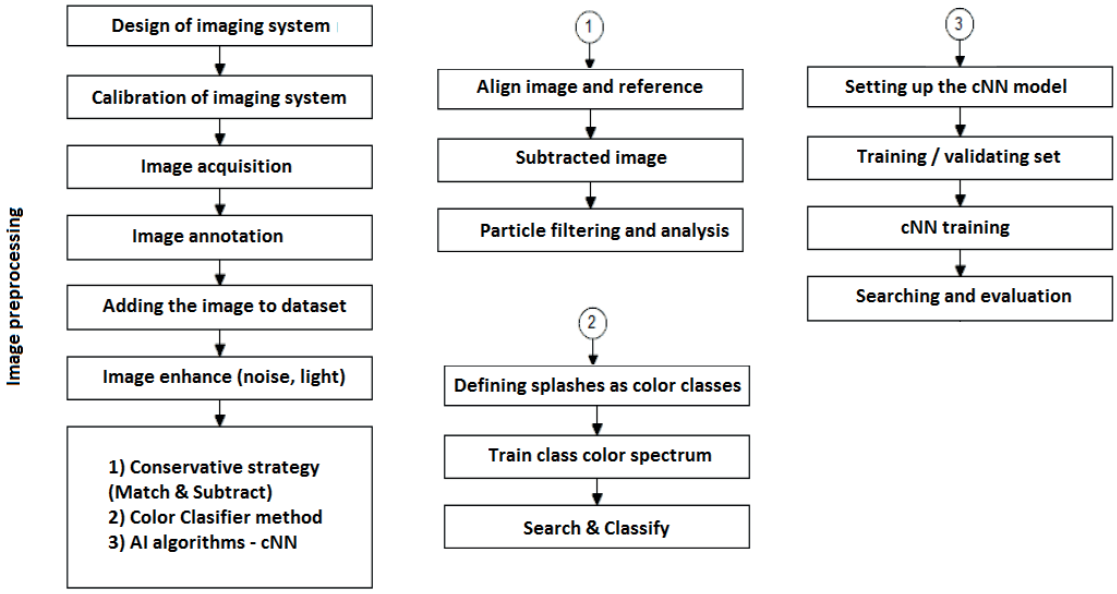

Figure 4 *Image acquisition, preparation of image dataset and 3 image analysis concepts*

process) during the soldering (or re-soldering) of power hybrids (PH) to the baseplate the solder under the chips is melted again. Flux is flowing out from the solder to the chips' edges. If there is some restriction or resistance to the flux movement, it can cause increase of internal mechanical forces and solder splashes. Solder splashes can be found on more than one production line and for different solder alloys and for different soldering equipment (Centrotherm oven or Pink oven) (Figure 3). It can be found for all the power hybrids and chips dimensions.

In production there are restricted areas, directly defined in product drawings (power hybrid drawing, module drawing, etc.), where solder splashes cannot be found. If the solder splashes are in the restricted area it is necessary to clean these areas. Proposed operations for cleaning, actually used and tested, are milling (used in production) or ultrasonic washing (actually tested for various products).

- Solder splashes most often cause problems with micro welding, bonding and ultrasonic welding. Bigger solder splashes can cause micro welding and bonding head damage.
- Additional problem, caused by solder splashes, is when they are located on Data Matric Code (DMX) position. This can cause damage of the DMX code and restrict or wipe out traceability in production process.
- Another effect is for position of solder splashes on power hybrid (PH) where it can cause damage on chip passivation, decreasing of minimal electrical distances, decreasing the module lifetime etc. This causes decreasing of power module reliability and quality.
- Solder splashes located on baseplate will directly influence thermal characteristics of the power module, increase in thermal resistance, as well as increase in thermal paste thickness and cooling in target customer application.

3 Proposal for imaging system and preprocessing of image information

When designing the chain of acquisition and preprocessing of image information, it is important to precisely plan individual steps in advance, so that the final result meets all the requirements. Since we are working with LabVIEW software, the following steps will also be closely related to its use. To obtain a data source of images, it is necessary to prepare the equipment for scanning, which consists of a stand, provision of constant light, auxiliary template reference white color, dark uniform background, defective VPM with containing object of interest, industrial camera from the company Basler type: ace acA4600-10uc together with C125-1218-5M 12 mm lens and processing software, marking area of interest and storing image information in the necessary data form.

The entire creation process is shown in Figure 4. How the system is set up depends on imaging environment and the type of analysis and processing to be performed. The imaging system should produce images of sufficient quality so the required information can be extracted.

3.1 Sensing chain

Sensing chain is processing several steps from sensed information:

- Design of sensing apparatus

Table 1 *Parameters of sensing apparatus - Basler camera*

Parameter	Specification
Video output	USB 3.0
Manufacturer	Basler
Type of sensor	Progressive Scan CMOS
Format of camera sensor	1 / 2.3”
Pixels	4.6 x 3.3
Sensing area (mm)	6.45 x 4.6
Depth of pixel	12 bit
Resolution (megapixels)	15.10

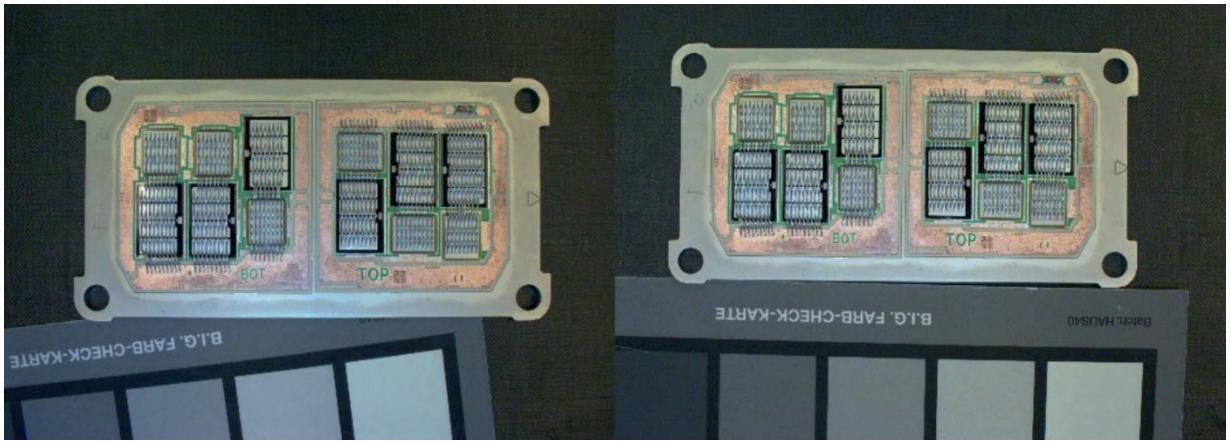

Figure 5 *Comparison of images for 8 mm focal length (left) and 12 mm focal length (right)*

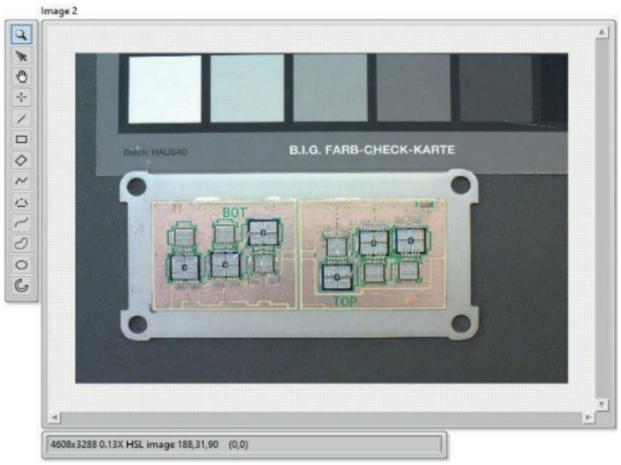

Figure 6 *Preprocessed image after the noise filtration and color balancing (normalization)*

- Pre-processing and storage of sensed information
- Detection and acquisition of position of object of interest
- Camera Basler, type: ace acA4600-10uc with C125-1218-5M 12 mm objective was used as a sensing apparatus. Main parameters are listed in Table 1.

Lenses with a focal length of 8 mm and 12 mm were used in the design of the sensing apparatus. The difference between images with 8 mm focal length and 12 mm focal length is shown in Figure 5.

Pylon Viewer is a software tool, which was used for storage of image information. It has high compatibility with camera and enables automatic modification of the image, what improves white color correction requirements. Stored image is converted to .bmp format, while the object of interest is defined by the technology engineer. The next step is then gaining the coordinates of the objects of interest. Since the deep learning algorithms have been analyzed in this study as well, a set of databases of power module images was developed (approximately 200 recorded modules).

Preprocessing of image information is realized with the use of LabVIEW environment, using NI-IMAQ and Vision Development libraries. The principle of

the sequential loading of images algorithm consists in incrementing the input - the value of the number in the for loop, which is added to the string and thereby creates the whole string path to the new image frame. Images are saved in bmp format with names from 0000 to 0197. The white balance algorithm is based on dividing the image into 3 basic components: red, green and blue, to compare the area of interest and thus our reference white color, the value of which should be 255 points. Reference values of 255 points are divided with the mean value of the given colors. After getting new colors that will be added to the original ones obtained, the image is recomposed using the field-to-image transfer function and their subsequent replacement into the original image (Figure 6).

4 Image database design

To realize the detection algorithms, it is required to modify acquired images by crop and mask tasks, i.e. unnecessary areas, which can influence detection of the objects of interest, are eliminated (Figure 7).

Masking is similar to image straightening on the coordinates of comparison of the extreme point patterns and by calculating their distances, the algorithm can automatically adjust dimensions and placement masking for each frame separately, using the reference percentage value. Once the necessary straightening and masking coordinates are obtained, they can be implemented into a color image, since we have been working in the gray-tone area so far for more accuracy comparing endpoint patterns. The resulting image can be cropped using coordinates and saved to a new file with a new name, making the data source ready for the phase practical implementation of algorithms for detection of objects of interests.

There are several ways how to identify and detect specific objects among which the used algorithms are described later. Algorithms are then utilized for advanced intelligence algorithms for neural networking and predictions of soldering splash detection.

4.1 Global thresholding

A global thresholding technique is one that uses a single threshold value for the whole picture. By correctly setting the colors, red, green and blue, in the form of RGB or hue, saturation and lightness in the form of HSL, the object can be extracted from the background by a simple operation that compares the image values with a threshold value T. Pixels subject and background have gray levels grouped into two dominant modes. One obvious way to extract an object from the background is to choose a threshold T, which separates these modes. Thresholding results in a binary image where pixels with a value intensity of 1 correspond to objects, while pixels with a value of 0 correspond to the background.

As can be seen in Figure 8 it is possible to utilize

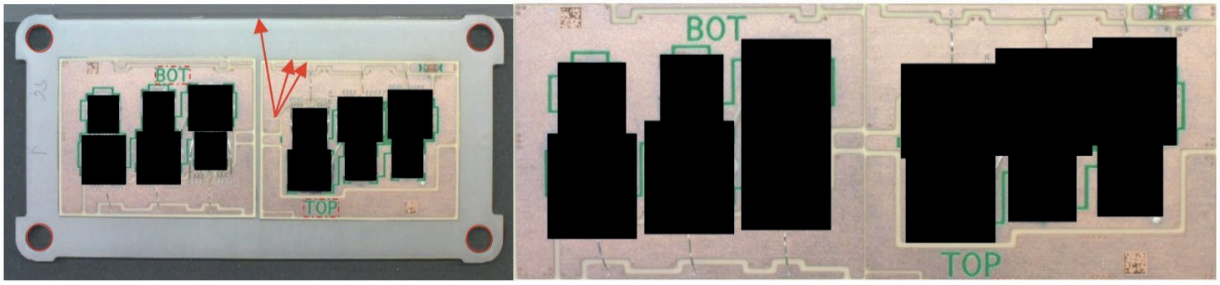

Figure 7 *Comparison of original and modified image with crop and masking algorithms*

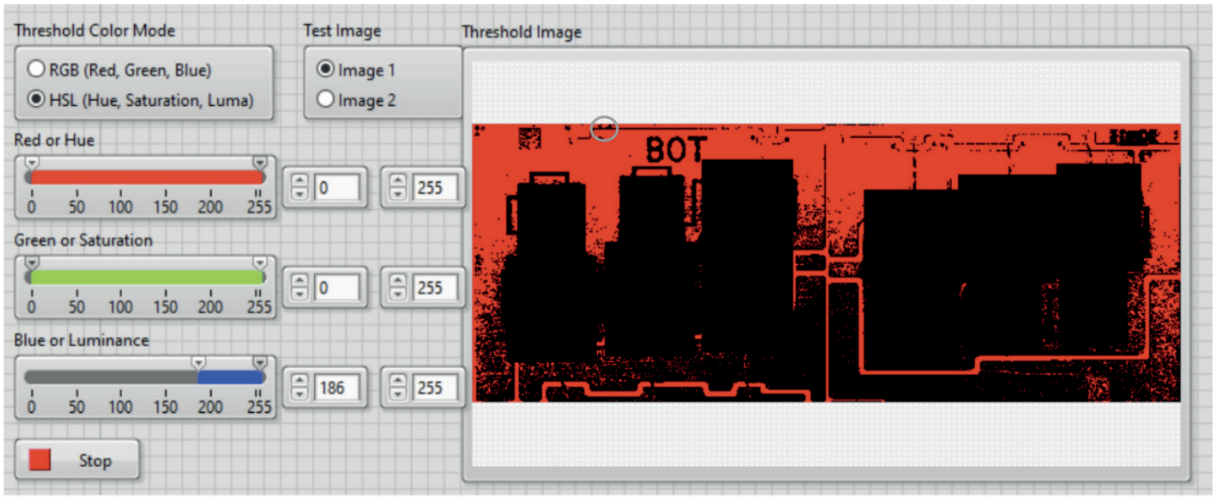

Figure 8 *Example of global thresholding and decomposition into object and background*

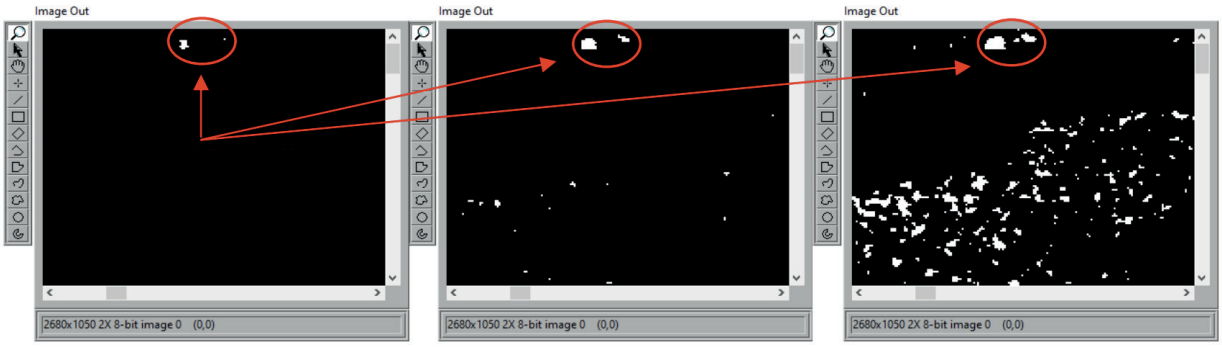

a) *b)* *c)*

Figure 9 *Manual thresholding a) 250 threshold b) 240 threshold c) 230 threshold*

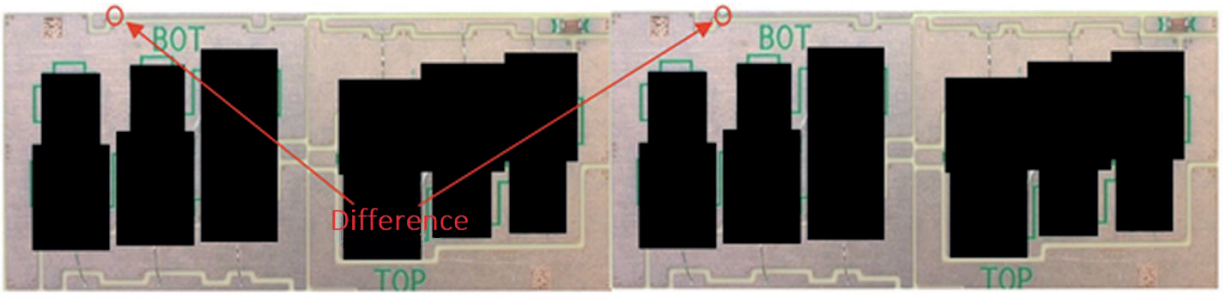

Figure 10 *Comparison of the samples for image difference operation*

the global thresholding to separate the light component from the dark one and thus the solder spatter is in the foreground with a value of 1 and the dark part that surrounds the splash has a value of 0. The disadvantage of the method is that it divides components only in 2 parts, if there is a small difference between the object of interest and the environment, components merge.

4.2 Manual thresholding

Assertion on dependence on the uniformity of lighting is resulted on Figure 9. For clear and relatively large solder joints splashes, it is possible to record their occurrence and thereby separate them from the rest of the image. However if those sprinkles are located in the upper part, where the luminosity is, in our case, the sharpest, it is difficult to separate them from the environment at lower threshold values, what prevents the detection of faulty elements in the image.

When detecting faults on others images, there was a problem not only in uneven lighting but in the variety of colors, size and color difference of the solder splash, as well, whether as a result of the melt or splash location on the power semiconductor module.

4.3 Image difference operation

It works on a pixel-by-pixel basis of reading two images. The important part is so that the images are symmetrical “pixel by pixel” to ensure the expression

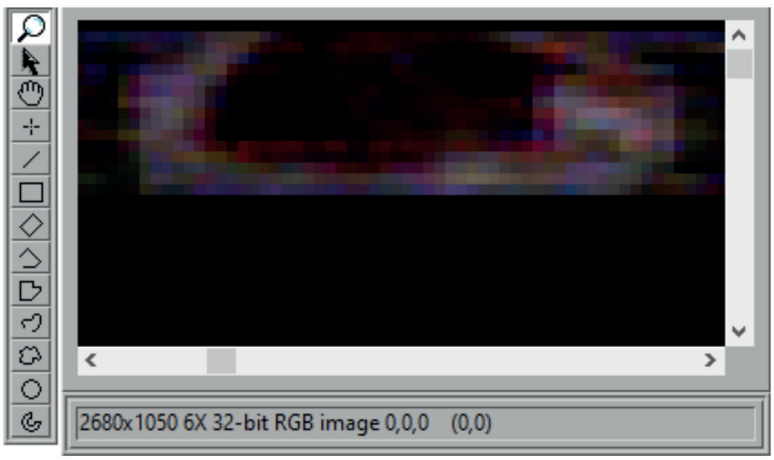

Figure 11 *Result of image difference operation*

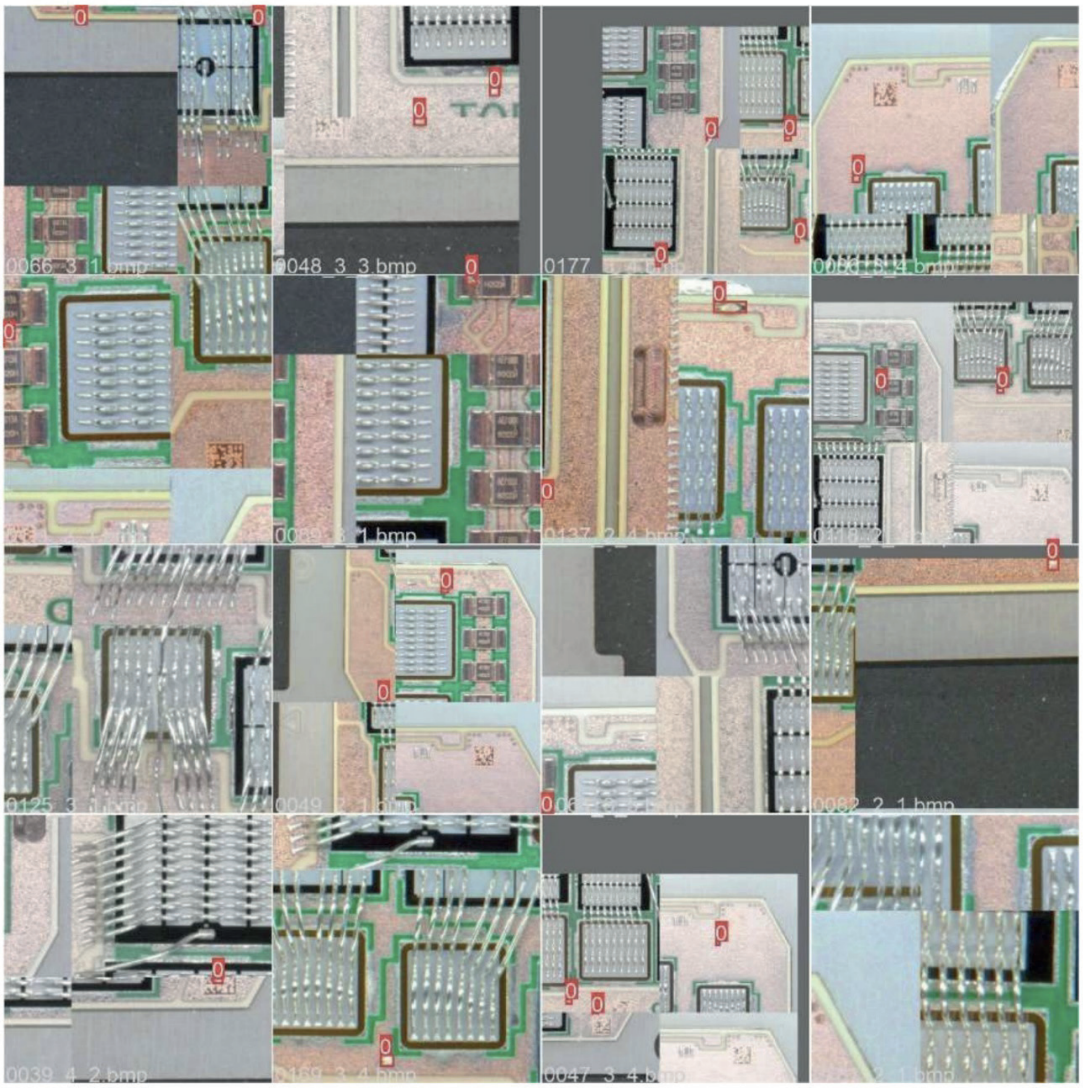

Figure 12 *Example of dataset of images from neural network training*

Table 2 *Model parameters*

Method	Setting
Initial learning rate	0.0001
Optimizer	Adam
Batch	16
Epochs	1000
Image HSV value augmentation	0.0
Patience	300
Image resolution	640

of object difference and to have the same dimensions. The basis is the correct preparation of the data source, which was secured using the multiple coordinates of edge detectors, by coincidence selected patterns, rotation of the image and adding masking. Initially, modified image, with separated solder splash, was used together with the original image (Figure 10). This created an identical match with the difference of the currently searched defect.

Figure 11 shows an enlarged single bright point, which is the soldering splash, whose data information remained after reading the frames. When trying to read two different modules in the picture, it is possible to see the deviations that are caused by different installation of elements on power module, surface changes, material changes and moving the x and y axes. Despite the imperfect match of the two images, it is possible to recognize the object of interest on the image.

5 Neural network training and proposal for AI detection algorithms

Within the proposed system, we decided to use the last versions of the YOLO model, i.e. YOLO v5. It is the most advanced version of this classification algorithm and Python software support is useful in scientific research area. The YOLOv5 medium model was chosen as compromise between the detection speed and accuracy. After the neural network model selection, the training process must be provided. Training process requires a huge dataset of samples. There are many official datasets for various image classification problems, but for detecting the soldering splashes we had to create our own dataset.

After the neural network model selection, the training process must be provided. Training process requires a huge dataset of samples. There are many official datasets for various image classification problems, but for detecting soldering splashes we had to create our own dataset (Figure 12).

As we declared in the previous section, each image in the acquired dataset was annotated by SEMIKRON Company specialist with LabelImg tool dedicated for YOLO. We defined just one class - soldering splash. The original resolution of PCB images was 4608x3288 pixels. The complete dataset actually consists of 231 images and there are 350 soldering splash objects annotated.

Nvidia GTX 1070 with 8 GB of memory was used as a GPU to speed up the training of YOLO model parameters. It was necessary to install the PyTorch, CUDA and OpenCV software libraries. The YOLOv5 neural network model could not be trained on the original image resolution due to the high-resolution quality of the input images and the huge video memory requirements [10]. In order to create 640x640 pixels images, the PCB images were tiled using the YOLO image tiling algorithm [11]. The original resolution of the object was preferred since soldering splashes are rather small-scale objects. The training, validation and testing sets were randomly assigned the following ratios: 70 % - 20 % - 10 % of the input dataset.

The YOLOv5 model was initially trained using the initialization parameters' default values. In a computer simulation experiment, these parameters were modified to determine the ideal starting point for the neural network training. The values of the YOLOv5 model's configurable parameters that produced the best classification performance are shown in Table 2. This configuration was used ten times to replicate the model learning.

Precision was 92.7 %, recall was 87.9 % and the

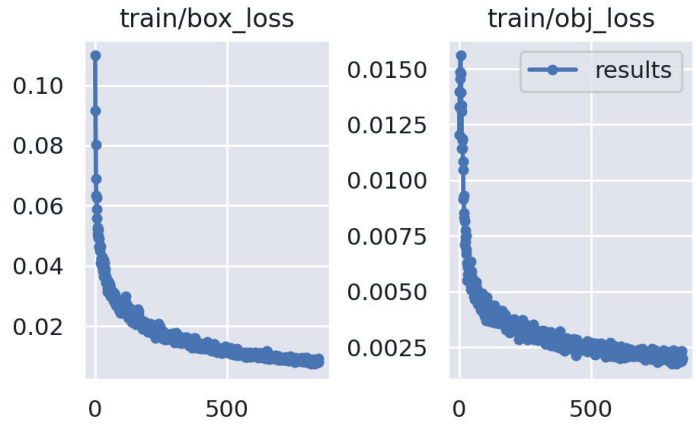

Figure 13 *Plots of objectness and box loss over the training epochs for training set*

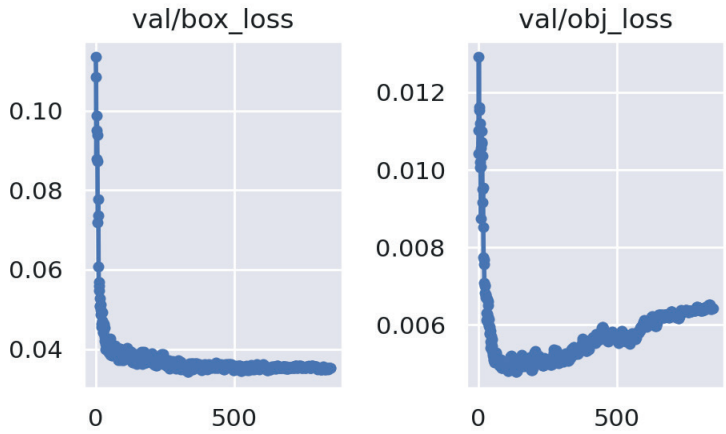

Figure 14 *Plots of objectness and box loss over the training epochs for validation set*

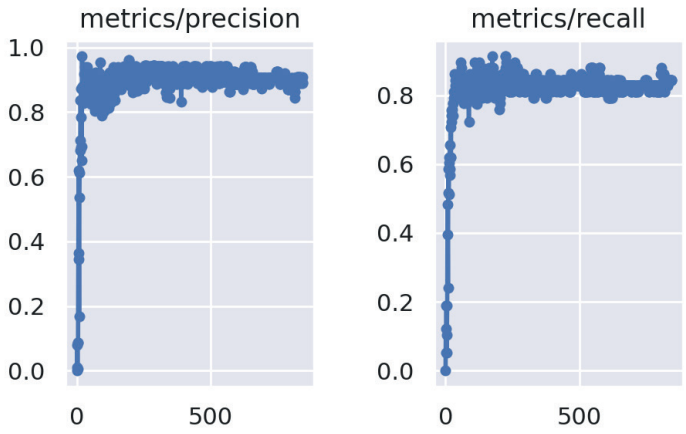

Figure 15 *Plots of precision and recall over the training epochs for training set*

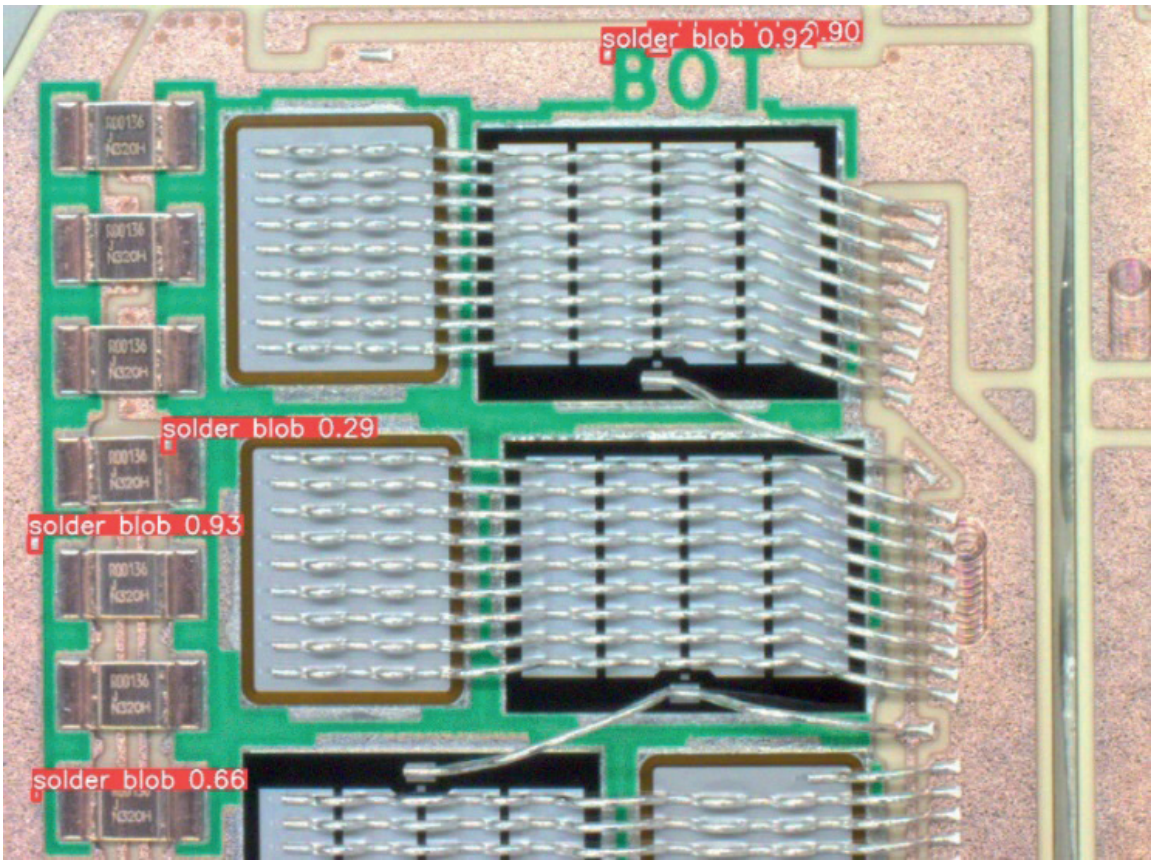

Figure 16 *Example of detected soldering splashes with YOLOv5 model, the solder splashes detected by the computer are marked by red rectangles, numbers indicate confidence score*

mean average precision score (mAP) was 90.6% with these model parameters. Model correctness is described by the mean average precision parameter; a higher value denotes a more accurate neural network model. The following formulas were used to calculate the metrics:

$$Presicion = \frac{True\ Positive}{True\ Positive + False\ positive}, \tag{1}$$

$$Recal = \frac{True\ Positive}{True\ Positive + False\ Negative}. \tag{2}$$

Precision score is represented by Equation (1), where the true positives refer to soldering splashes that were accurately detected, but false positives relate to image areas that were incorrectly identified as soldering splashes. The recall score is represented by Equation (2), where false negatives are related to undetected solder splash items and the remaining terms are the same as those in Equation (1).

Figures 13, 14 and 15 display the pertinent metrics. The training process revealed a declining trend for the training set's normalized box loss score over the epochs (Figure 13). The box loss function shows how well the predicted bounding box encloses an object and

how precisely the algorithm can find the object's center (soldering splash). A measure of the likelihood that an object exists in a suggested region of interest is called the objectness loss (obj loss) (ROI) [12].

The normalized box loss score trend over the training epochs is shown in Figure 14. The box loss also decreased in the training and validation sets over the training phase. This suggests that the YOLOv5 model has strong generalizability potential in terms of pinpointing soldering splash centers. After 100 epochs, the objectness loss in the validation set showed an upward trend, therefore the training was cut short.

Throughout the training, the precision and recall scores were steadily dropping. The recall score could rise if there are more photographs in the collection. The precision and recall score are shown to grow over the training epochs in Figure 15. The trained model was very accurate at identifying the soldering blobs.

Even soldering droplets with small areas were successfully recognized by the specially trained YOLOv5 model (Figure 16). These outcomes were related to the direct application of the YOLOv5 medium model. No image manipulations or alterations were used. The input photos contain several items with similar color and texture to soldering splashes, which can impair classification ability.

6 Discussion and conclusion

Although the YOLOv5 algorithm is not a novel technique, in this article we show the use of machine learning-based object detection in an original dataset of particular PCBs. The study demonstrates that the YOLOv5 algorithm was successfully employed for item recognition, including people, cars, animals and more. This algorithm's use for tiny items, such as soldering droplets, is innovative in the field.

Due to the scarcity of official photos of that kind, we first constructed an annotated dataset of PCBs (including 4 categories of boards).

The trained neural network model achieved precision of 92.7%. Considering the relatively tiny training set and small region of detected objects, these results can be deemed satisfactory. Additionally, several items in the PCB photos, particularly wires and connections, had color or texture characteristics that were similar to soldering splashes.

Using the alternative classification model RetinaNet might improve classification performance. A larger dataset and improved spatial resolution for the PCB photos both have the potential to improve the classification accuracy. Further study will be conducted on this.

Acknowledgment

The results presented in this paper were supported by grant No. APVV 20-0500 - Research of methodologies to increase the quality and lifetime of hybrid power semiconductor modules. This research has also been supported by the Ministry of Education, Youth and Sports of the Czech Republic under the project OP VVV Electrical Engineering Technologies with High-Level of Embedded Intelligence CZ.02.1.01/0.0/0.0/18_069/0009 855. Authors want to thank all SEMIKRON Slovakia company staff for cooperation.

Conflicts of interest

The authors declare that they have no known competing financial interests or personal relationships that could have appeared to influence the work reported in this paper.

References

[1] REN, Z., FANG, F., YAN, N., WU, Y. State of the art in defect detection based on machine vision. *International Journal of Precision Engineering and Manufacturing-Green Technology* [online]. 2022, **9**, p. 661-691. ISSN 2288-6206, eISSN 2198-0810. Available from: https://doi.org/10.1007/s40684-021-00343-6

[2] ADIBHATLA, V. A., CHIH, H. C., HSU, C. C., CHENG, J., ABBOD, M. F., SHIEH, J. S. Defect detection in printed circuit boards using you-only-look-once convolutional neural networks. *Electronics* [online]. 2020, **9**(9), 1547. eISSN 2079-9292. Available from: https://doi.org/10.3390/electronics9091547

[3] REDMON, J., DIVVALA, S., GIRSHICK, R., FARHADI, A. You only look once: unified, real-time object detection. In: IEEE Conference on Computer Vision and Pattern Recognition: proceedings [online]. IEEE. 2016. eISSN 1063-6919, p. 779-788. Available from: https://doi.org/10.1109/CVPR.2016.91

[4] HUANG, Y. Q., ZHENG, J. C., SUN, S. D., YANG, C. F., LIU, J. Optimized YOLOv3 algorithm and its application in traffic flow detections. *Applied Sciences* [online]. 2020, **10**(9), 3079. eISSN 2076-3417. Available from: https://doi.org/10.3390/app10093079

[5] HUANG, R., GU, J., SUN, X., HOU, Y., UDDIN, S. A rapid recognition method for electronic components based on the improved YOLO-V3 network. *Electronics* [online]. 2019, **8**(8), 825. eISSN 2079-9292. Available from: https://doi.org/10.3390/electronics8080825

[6] MALGE, P. S. PCB defect detection, classification and localization using mathematical morphology and image processing tools. *International Journal of Computer Applications* [online]. 2014, **87**, p. 40-45. ISSN 0975-8887. Available from: https://doi.org/10.5120/15240-3782

[7] TAKADA, Y., SHIINA, T., USAMI, H., IWAHORI, Y. Defect detection and classification of electronic circuit boards using keypoint extraction and CNN features. In: 9th International Conferences on Pervasive Patterns and Applications Defect PATTERNS 2017: proceedings. 2017. ISBN 978-1-61208-534-0, p. 113-116.

[8] ANITHA, D. B., MAHESH, R. A survey on defect detection in bare PCB and assembled PCB using image processing techniques. In: 2017 International Conference on Wireless Communications, Signal Processing and Networking WiSPNET: proceedings [online]. IEEE. 2017. ISBN 978-1-5090-4443-6, eISBN 978-1-5090-4442-9, p. 39-43. Available from: https://doi.org/10.1109/WiSPNET.2017.8299715

[9] LIAO, X., LV, S., LI, D., LUO, Y., ZHU, Z., JIANG, C. YOLOv4-MN3 for PCB surface defect detection. *Applied Sciences* [online]. 2021, **11**(24), 11701. eISSN 2076-3417. Available from: https://doi.org/10.3390/app112411701

[10] MASTERS, D., LUSCHI, C. Revisiting small batch training for deep neural networks. *ArXiv* [online]. 2018, 1804.07612. eISSN 2331-8422. Available from: https://doi.org/10.48550/arXiv.1804.07612

[11] YOLO dataset tiling script [online]. Available from: https://github.com/slanj/yolo-tiling

[12] Manish Chablani: YOLO - you only look once, real time object detection explained [online]. Available from: https://towardsdatascience.com/yolo-you-only-look-once-real-time-object-detection-explained-492dc9230006

Dear colleague,

We would like to send you a copy of the journal Communications - Scientific Letters of the University of Zilina.

Journal Communications - Scientific Letters of the University of Zilina are a well-established open-access scientific journal aimed primarily at the topics connected with the field of transport. The main transport-related areas covered include Civil engineering, Electrical engineering, Management and informatics, Mechanical engineering, Operation and economics, Safety and security, Travel and tourism studies. The full list of main topics and subtopics is available at: *https://komunikacie.uniza.sk/artkey/inf-990000-0500_Topical-areas.php*

Journal Communications - Scientific Letters of the University of Zilina is currently indexed and accepted by CEEOL, Crossref (DOI), DOAJ, EBSCO Host, Electronic Journals Library (EZB), ERIH Plus, Google Scholar, Index Copernicus International Journals Master list, iThenticate, JournalGuide, Jouroscope, Norwegian Register for Scientific Journals Series and Publishers, ROAD, ScienceGate, SCImago Journal & Country Rank, SciRev, SCOPUS, WorldCat (OCLC).

Journal Communications - Scientific Letters of the University of Zilina is preserved in CLOCKSS and Portico to guarantee long-term digital preservation and is archived in the national deposit digitalne pramene.

Authors can share their experiences with publishing in our journal on SciRev.

Journal Communications - Scientific Letters of the University of Zilina is under evaluation for inclusion to Web of Science database.

I would like to invite authors to submit their papers for consideration. We have an open-access policy and there are **no publication, processing or other fees** charged for published papers. Our journal operates a standard single-anonymised review procedure, the successful completion of which is a prerequisite for paper publication.

The journal is issued four times a year (in January, in April, in July and in October).

I would also like to offer you the opportunity of using already published articles from past issues as source of information for your research and publication activities. All papers are available at our webpage: http://komunikacie.uniza.sk, where you can browse through the individual volumes. Our journal offers access to its contents in the open access system on the principles of the license **Creative Commons (CC BY 4.0)**.

For any questions regarding the journal Communications - Scientific Letters of the University of Zilina please contact us at: *komunikacie@uniza.sk*

We look forward to future cooperation.

Sincerely

Branislav Hadzima
editor-in-chief

IMPROVEMENT PRIORITIZATION IN BIKE LANE ATTRIBUTES BASED ON THE VIEW OF DIFFERENT GENDER AND AGE CYCLIST GROUPS (CASE STUDY: QAZVIN CITY, IRAN)

Shima Zarabadipour[1], Ehsan Ramezani-Khansari[2,*], Alireza Abdolrazaghi[3]

[1]Deputy of Transportation and Traffic Municipality, Qazvin, Iran
[2]Imam Khomeini International University, Qazvin, Iran
[3]Faculty of Engineering, Imam Khomeini International University, Qazvin, Iran

*E-mail of corresponding author: E.R.khansari@aut.ac.ir, E.R.Khansari@gmail.com

Ehsan Ramezani-Khansari 0000-0001-9642-6134, Alireza Abdolrazaghi 0000-0002-2912-7692

Resume

A survey of cyclists in the city of Qazvin, Iran, was conducted by focusing on improving the bike lane attributes (increasing width, increasing attractiveness or appeal of the bike lane (painting, planting …), improving pavement conditions, improving sight distance and removing obstacles in the bike lane). It was seen that there was no difference between age groups. Two important priorities for the men group were increasing the lane width and improving the sight distance, while the women considered improving the pavement conditions and the appeal of the bike lanes. Increasing the lane width and improving the pavement conditions for the recreational group and increasing the lane width and improving the sight distance for the non-recreational group were the most important improvements. It can be said that increasing the width of the bike lane was the most important factor for almost all groups.

Article info

Received 10 September 2022
Accepted 2 February 2023
Online 8 March 2023

Keywords:

bike lane
gender
age
cycling purpose
transportation infrastructure

Available online: https://doi.org/10.26552/com.C.2023.031

ISSN 1335-4205 (print version)
ISSN 2585-7878 (online version)

1 Introduction

Many countries have tried to encourage people to use bicycles more, but despite the support for public transportation and bicycles, their use is low. Research in some developing countries in 2009 showed that 84% of city trips had been made by private car [1]. For example, while in Curitiba (Brazil), only 11 and 17% of the adult population uses a bicycle for commuting and leisure, respectively [2], in countries with high income, these values were higher (26% for leisure and 41% for commuting) [3-4].

Although increasing the proportion of cycling in trips faces many obstacles, it is one of the best ways for sustainable transportation and development. Therefore, it is necessary to put some improvements into practice to encourage the use of public transportation and bicycles for those who go from home to work, school and shopping every day [3, 5]. There are many surveys and studies about barriers that may hinder the use of bicycles for commuting. The most common barriers reported in the previous articles are lack of adequate infrastructure (bike lanes), lack of safety, lack of company and climate [6-7].

De Sousa Suely et al. conducted a survey of 380 college students in three Brazilian cities, [8]. Their questionnaire was based on the theory of planned behavior and included: cycling infrastructure, lack of safety, distance to be traveled, physical fitness, slopes and climate. They found a lack of dedicated cycling infrastructure. De Camargo et al. [9] recruited 84 adults of both sexes and characteristics related to cycling (commute, leisure time users and activists) in focus groups interviews. The most-reported barrier was lack of safety, followed by lack of bike lanes. Parkin et al. [10] applied UK 2001 census data with logistic regression for cycle choice. They found that hilliness was the most important factor that had affected the proportion that cycles to work. The following three factors were physical conditions of the highway, rainfall and temperature. Garrard et al. used the census of cyclists observed at 15 locations of Melbourne, Australia's central business district (CBD). They found that the most important facilitator for female commuter cyclists was maximum

separation from motorized traffic [11]. "Barriers" are the factors that by their negative effects on cyclists (or a group of cyclists) hinder cycling and "facilitators" are those that by their positive effects, encourage cycling [12].

Segadilha and Sanches [13] compared the shortest path between orientation and destination (by using geographical information system (GIS)) and chosen path (by using global positioning system (GPS) data) for the cyclist in Brazil. They examined which factors caused them to choose a longer route. They demonstrated that the speed and volume of motorized traffic and the pavement quality were top factors that affected the cyclists. In contrast to Segadilha and Sanches, Harvey et al. found that cyclists became more comfortable with cycling in heavy conditions and did not affect their chosen route [14]. Dill and Voros studied a set of factors that could affect bicycle demand in Portland, Oregon region of the USA. They observed that the availability of bike lanes and higher levels of street connectivity has led to an increase in using a bicycle [15]. Surveys and examinations demonstrated that travel time could strongly influence bicycle route choice [16-17].

Jain and Tiwari [18] surveyed bicyclists in Pune, India. The bicyclists interacted with pedestrians better than the vehicles. A parked vehicle was considered more dangerous during the parking maneuver. The used questions include a set of factors such as on-street parking, pedestrians as barriers, pavement quality, road width, the density of land use and slope. Another study by Krizek [19] confirmed the results of Jain and Tiwari [18]. Majumdar et al. [20] examined a set of attributes affecting bicycle route choice, including the presence of the motorized vehicle on road or traffic volume, road width, on-street parking, route visibility, etc. They found road width as the most important attribute.

Basu and Vasudevan [21], conducted a questionnaire survey in four major Indian cities. to rank some bicycle friendly infrastructures and policies. Dedicated bicycle lane was found to be the most preferred bicycle friendly infrastructure and whereas facility to carry bicycle on public transportation was found to be the least preferred one.

On the one hand, the share of cycling in Iranian cities is very low, for example, the share of cycling in the city of Tehran [22], Ahvaz [23] and Mashhad [24] are 1%, 2% and 1.5%, respectively. On the other hand, the share of women is less than men. For instance, the share of women cycling is 25% of the total number of cyclists in the city of Tehran [25]. Of course, it has been seen that women less cycle for non-recreational purposes in developing countries with low bicycle transport mode share [10-11].

Cycling facilities and infrastructure in developing countries, such as Iran, are not suitable enough and the budget needed to improve them is limited. Therefore, it should be examined how any improvement in the attributes of infrastructure and bike lanes affects the demographic groups of cyclists and encourages them. As the municipality has tried to build the all possible bicycle lane in the city, it is practically not possible to increase the length of these facilities easily. On the other hand, the municipality is trying to increase the quality and willingness of people to use the existing bike lanes.

Many previous studies have used aggregate data to analyze, but in this research, the survey of different groups of cyclists has been examined separately. First, the data were categorized according to age and gender and then the priorities of different groups for improvement in the attributes of bike lanes were compared to each other. The research methodology has been described in the next section. The data collection is introduced in the third section. The fourth section has been devoted to statistical analysis and comparison of different groups of cyclists. The results have been discussed in the fifth section. Finally, the sixth section has summarized and concluded the research.

2 Methodology

In this research, the options for improving the bike lanes conditions have been prioritized based on the opinions of cyclists. It should be mentioned that bike lane means a segregated path or track for the bicycles. It can be on the street or on the sidewalk. It depends on the transverse profile of the road. Questionnaires have been completed by interview. The demographic composition of people in a city can be different, so the investigation aimed to examine priorities for improving the conditions of bike lanes for different user groups.

The questionnaires were divided according to age (over and under 40 years old) and gender (male and female). Respondents were given five options to improve the conditions of the bike lanes, which they should choose the importance of each option based on the Likert scale (between 1 and 5). Using statistical tests, the priority of bike lanes improvement options for each group of users was examined. Then, the differences of opinions in different groups have been studied. The questions were prepared based on the opinions of traffic engineers at the Qazvin department of transportation. In other words, the experts considered these options the most important options for improving bike lanes among some options.

Questions about the bike lane were: increasing width, increasing attractiveness or appeal of the bike lane (such as painting, planting), improving pavement conditions, improving sight distance and removing obstacles in the bike lane. The questionnaire also included other questions, such as demographic characteristics and the goal(s) of cycling. At the end of the analysis, options were arranged based on different groups of cyclists based on the results.

Table 1 *Distribution of respondents*

Variable	Mean	SE Mean	St Dev	Minimum	Q1	Median	Q3	Maximum
Age	38.498	0.861	15.435	13.00	27.000	36.00	51.50	80.00
Gender	0.804	0.022	0.3978	0.000	1.0000	1.00	1.00	1.00

To compare opinions between different groups, statistical methods should be used, the most important and well-known of which is ANOVA. This method can only prove the existence of differences. So, Tukey's method is used to compare groups individually and rank them.

3 Data collection

The paper targets bicycle lane improvement options, so respondents should be bike users and familiar with bike lanes. Here, bicycle users were defined as cyclists who use bicycles at least once a week. Total of 457 Questionnaires were collected from people on the street, from which 321 were riding a bicycle. Cochran's formula was used to estimate enough number of questionnaires. Considering the population of about 400,000 people in Qazvin city and the error level of 5 %, at least 384 data are required and more than this amount have been collected here. The survey was conducted during different days of a week.

There are many studies that have used Global Positioning System (GPS) data to investigate the behavior of cyclists [26-28]. Although those data have uncertainty, they can continuously provide a wide range of information to the researcher. In this research, survey and questionnaire methods were used because the paper aimed to investigate the opinions and feelings of cyclists about bicycle lane attributes. The GPS data cannot help here, because by using the GPS data, it is possible to find out whether a cyclist has used a path or not, but it is not possible to extract her/his satisfaction and opinions. Table 1 shows the distribution of respondents.

The age range of the respondents was between 13 and 80 years with an average of 38 years. Only 3 % of the participants were over 65 years old, so respondents within the age range of middle-aged adults and old adults were categorized as the elder group (age > 40). In other words, two age groups were defined, which were young (age < 40) and elder (age > 40).

The survey of cyclists using bike lanes was conducted on the main central business district (CBD). Qazvin city is one of the small cities in Iran. Most land uses and population in Qazvin are centralized, so most bike lanes are also located in CBD. The total length of bicycle infrastructure in Qazvin is about 10 km.

The participants were asked what is the main purpose of their trips by bicycle. Non-recreational purposes included commuting to work, school, or university, while recreational cycling included exercising, just enjoying cycling (riding around), or shopping. Shopping was also considered a recreational destination, because in shopping trips, unlike business trips (such as getting to work, university or school), the user is not under pressure and is not done regularly. The respondents could state recreational, non-recreational or both as the purpose of cycling.

The existence of a multimodal system like bike-and-ride is necessary to encourage people to use bicycles. The goal of this paper was not studying the factors that can influence using a bicycle, but to measure the satisfaction of cyclists with bicycle facilities (bicycle lane). In other words, considering the existing limitations in the expansion of cycling facilities in a small and dense city like Qazvin, the goal is to improve the existing facilities based on the opinion of users [29-31].

4 Analysis

This section statistically analyzes the survey of bike lane users according to age and gender groups to prioritize improvement options, then uses other data in the questionnaire.

4.1 Male cyclists

First, the men's group was studied and then the women's group. Tables 2 and 3 represent the result of the men's survey.

Test results ANOVA One-way showed a significant difference between men in terms of priority of options (P-Value = 0.013). To determine the priority of options Tukey test was applied. From the point of view of male cyclists, the most important improvement was increasing the width of the bike lane, followed by sight distance and pavement conditions.

4.2 Female cyclists

The analysis process for men was also applied to the group of women. ANOVA One-way results are shown in Table 4. If the confidence interval is chosen 90 %, there would be a difference between the women's group (P-Value = 0.071). Then, Tukey test was used to rank the improvements, which showed that the improvement of pavement conditions was the most important, followed by bike lane appeal and increasing the width of the bike lane (Table 5).

Table 6 compares the survey results of female

Table 2 *ANOVA of men's priorities*

Source	DF	Adj SS	Adj MS	F-Value	P-Value
Factor	4	19.14	4.785	3.22	0.013
Error	615	915.01	1.488		
Total	619	934.15			

Table 3 *Ranking of men's priorities*

Factor	N	Mean	Grouping	
Bike_lane_width	124	3.4919	A	
Sight_distance	124	3.3306	A	B
Bike_lane_pavement_conditions	124	3.282	A	B
Bike_lane_obstacles	124	3.258	A	B
Bike_lane_appeal	124	2.952		B

Means that do not share a letter are significantly different.

Table 4 *ANOVA of women's priorities*

Source	DF	Adj SS	Adj MS	F-Value	P-Value
Factor	4	10.43	2.606	1.61	0.071
Error	310	501.43	1.618		
Total	314	511.85			

Table 5 *Ranking of women's priorities*

Factor	N	Mean	Grouping
Bike_lane_pavement_conditions	63	3.317	A
Bike_lane_appeal	63	3.238	A
Bike_lane_width	63	3.206	A B
Sight_distance	63	3.143	B
Bike_lane_obstacles	63	2.794	B

Means that do not share a letter are significantly different.

Table 6 *Comparison between women and men's priorities*

Priority	Male	Female
1	Bike_lane_width	Bike_lane_pavement_conditions
2	Sight_distance	Bike_lane_appeal
3	Bike_lane_pavement_conditions	Bike_lane_width
4	Bike_lane_obstacles	Sight_distance
5	Bike_lane_appeal	Bike_lane_obstacles

and male cyclists. It can be seen that there would be differences, which are more examined in following sections.

4.3 Young cyclists

The survey of young cyclists (age < 40) has been assessed by One-way ANOVA. Table 7 shows that by considering a 95% confidence interval, there was a significant difference within the young group (P-Value = 0.035). Tukey test (Table 8) demonstrated that increasing the width of the bike lane and improving the sight distance have the highest priority for this group.

4.4 Elder cyclists

By considering 95% confidence, it can be seen that there was a difference within the elder group (P-value = 0.015). In the elder group, such as the young group, increasing the lane width and improving the sight distance had the priority. The results are shown in Tables 9 and 10.

Table 11 compares the priorities for young and older cyclists. In general, it can be said that the priorities of

Table 7 *ANOVA of young cyclists` priorities*

Source	DF	Adj SS	Adj MS	F-Value	P-Value
Factor	4	15.71	3.928	2.60	0.035
Error	775	1170.67	1.511		
Total	779	1186.38			

Table 8 *Ranking of young cyclists` priorities*

Factor	N	Mean	Grouping	
Bike_lane_width	156	3.4615	A	
Sight_distance	156	3.3333	A	B
Bike_lane_pavement_conditions	156	3.2821	A	B
Bike_lane_obstacles	156	3.256	A	B
Bike_lane_appeal	156	3.026		B

Means that do not share a letter are significantly different.

Table 9 *ANOVA of older cyclists` priorities*

Source	DF	Adj SS	Adj MS	F-Value	P-Value
Factor	4	18.59	4.647	3.12	0.015
Error	820	1221.60	1.490		
Total	824	1240.19			

Table 10 *Ranking of older cyclists` priorities*

Factor	N	Mean	Grouping
Bike_lane_width	165	3.4242	A
Sight_distance	165	3.3273	A B
Bike_lane_obstacles	165	3.097	A B
Bike_lane_pavement_conditions	165	3.0727	B
Bike_lane_appeal	165	3.0606	B

Means that do not share a letter are significantly different.

Table 11 *Comparison between young and older` priorities*

Priority	Young	Elder
1	Bike_lane_width	Bike_lane_width
2	Sight_distance	Sight_distance
3	Bike_lane_pavement_conditions	Bike_lane_obstacles
4	Bike_lane_obstacles	Bike_lane_pavement_conditions
5	Bike_lane_appeal	Bike_lane_appeal

both groups were similar. It should be noted that since the number of men who participated in the survey was significantly larger than women, the priorities of both young and older groups were more like men's opinions.

The analysis showed that the priorities for improving the bike lanes were different within gender and age groups. For further examination, the survey data were categorized based on the purpose of cycling. As has been mentioned, the questionnaire also included the purpose of cycling. Two general purposes of recreation and non-recreational were considered.

Table 12 shows the distribution of purpose of using the bicycle for different age and gender groups.

It can be seen that men used bicycles for non-recreational purposes more than women. There is no significant difference between young groups and older groups in this regard. This can be due to the equal distribution of men and women in all age groups. In general, the survey indicated that most of the cyclists in the city of Qazvin are cycling for recreational purposes.

It can be said that the reason for the meager share of the bicycle in Qazvin is that bicycle is not yet recognized as a mode of transportation and is often used

Table 12 *Distribution of data based on cycling purpose*

	Gender		Age	
	Male	Female	Young	Elder
Recreation	63	80.5	70	68.7
Work	37	19.5	30	31.3

Table 13 *ANOVA of recreational cyclists` priorities*

Source	DF	Adj SS	Adj MS	F-Value	P-Value
Factor	4	20.12	5.029	3.64	0.006
Error	1160	1600.68	1.380		
Total	1164	1620.79			

Table 14 *Ranking of recreational cyclists` priorities*

Factor	N	Mean	Grouping	
Bike_lane_width	233	3.4421	A	
Bike_lane_pavement_conditions	233	3.3176	A	B
Bike_lane_appeal	233	3.2833	A	B
Bike_lane_obstacles	233	3.1717	A	B
Sight_distance	233	3.0558		B

Means that do not share a letter are significantly different.

Table 15 *ANOVA of non-recreational cyclists` priorities*

Source	DF	Adj SS	Adj MS	F-Value	P-Value
Factor	4	42.13	10.532	6.09	0.000
Error	490	846.93	1.728		
Total	494	889.06			

Table 16 *Ranking of non-recreational cyclists' priorities*

Factor	N	Mean	Grouping	
Bike_lane_width	99	3.434	A	
Sight_distance	99	3.404	A	
Bike_lane_obstacles	99	3.394	A	
Bike_lane_pavement_conditions	99	2.859		B
Bike_lane_appeal	99	2.778		B

Means that do not share a letter are significantly different.

for recreational purposes. It was assessed whether there is a difference between the priorities of cyclists based on the purpose of cycling.

4.5 Recreational cyclists

Tables 13 and 14 show the result of the survey of recreational cyclists. It can be seen that there was a difference within recreational cyclists by considering a 95% confidence interval (P-value = 0.006). Three top improvements were as follows: increasing the lane width, improving pavement conditions and improving the appeal of the bike lanes.

4.6 Non-recreational cyclists

As recreational users, it can be seen that there was a significant difference within non-recreational cyclists for the bike lane. The first three priorities were increasing the lane width, improving the sight distance and removing the obstacles in the bike lane (Table 15 and 16).

Given the above results, it can be said that the priorities of cyclists were different according to the cycling purpose. Table 17 compares the choices of recreational and non-recreational cyclists.

Table 17 *Comparison between recreational and non-recreational cyclists` priorities*

Priority	Recreational	Non-recreational
1	Bike_lane_width	Bike_lane_width
2	Bike_lane_pavement_conditions	Sight_distance
3	Bike_lane_appeal	Bike_lane_obstacles
4	Bike_lane_obstacles	Bike_lane_pavement_conditions
5	Sight_distance	Bike_lane_appeal

Table 18 *The priorities of different groups*

Priority	Male	Female	Elder	Young	Non-recreational	Recreational
1	width	Pavement_ conditions	width	width	width	width
2	Sight distance	appeal	Sight_ distance	Sight_ distance	Sight_ distance	pavement_ conditions
3	pavement_ conditions	width	obstacles	pavement_ conditions	obstacles	appeal
4	obstacles	Sight_ distance	pavement _conditions	obstacles	pavement_ conditions	obstacles
5	appeal	obstacles	appeal	appeal	appeal	Sight_ distance

Table 19 *Descriptive statistics of data*

Overall priority	Variable	Sum	Mean	Variance	Min	Max
1	Bike_lane_width	8	1.333	0.667	1	3
2	Sight_distance	17	2.833	1.767	2	5
2	Bike_lane_pavement_conditions	17	2.833	1.367	1	4
3	Bike_lane_obstacles	23	3.833	0.567	3	5
4	Bike_lane_appeal	25	4.167	1.767	2	5

5 Results and discussion

The priorities of different groups are summarized in Table 18 so that the data can be better analyzed. The table shows that the priorities of different groups were different for improving the bike lane attribute. Now it should be examined what were the general opinions of the participants.

Previously, the opinions of different groups were compared using statistical methods, but here those opinions are summarized. The third column in table 1 is the sum of the values of the first column of Table 2, so that it can be find out which attribute has a higher priority for improvement in general. For example, the bicycle lane width attribute has a priority value of 1 in all groups, except for the female group, whose priority is 3. So, its total or sum priority is 8. So, the lower the value of the total priority, the more important it is. Table 1 is sorted by sum column value.

The values of Table 19 are depicted in Figure 1. The lower the value distribution and the smaller the values, the higher their priority.

Lane width has been given the highest priority because it can be considered one of the most important safety and comfort factors for cyclists. According to the field survey, most of the lanes in Qazvin have a width of 1.5 meters or less and on the other hand and many of them are as two-way bike lane, which leads to safety and maneuver problems in peak hours. It is noteworthy that the priority difference of this attribute, compared to the next attribute(s), is very high and it shows that the inappropriate lane width was the main problem for cyclists to use the bike lane. It can be seen in Figure 1 that in other attributes there is a dispersion of opinions between different groups, but regarding the width of the bicycle path, the dispersion is very small and almost all groups agree on its priority.

Sight Distance and pavement conditions were the next priorities. Pavement conditions and appropriate sight distance help cyclists to travel safely and at their desired speed on the bike lane. In other words, the unproper pavement conditions makes it more difficult to move faster and also the unproper sight distance makes it unsafe to move faster.

Obstacles on the bike lane are the next priority. Perhaps it was expected that this attribute would have a higher priority because the presence of an obstacle in the bike lane greatly disrupts the movement and greatly

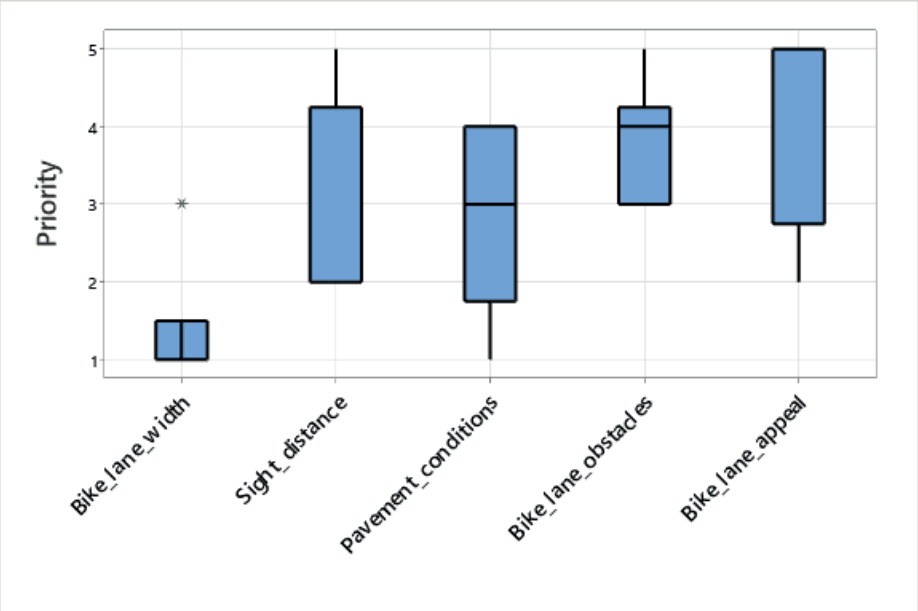

Figure 1 *Boxplots of priority data*

reduces the quality and safety of the bike lane. But in the city of Qazvin, most of the bicycle lanes are completely separated from the traffic flow by using physical barriers and the interference of parked cars or other obstacles with cyclists is little. Therefore, this attribute was not so important according to the respondents. Improving the appearance of bike lanes has been the last priority. This is to be expected because the priority of cyclists has been to use the bike lane safely and at a suitable speed.

In the following, the findings in this research are compared with similar researches.

There are many researches about the factors affecting the willingness to use bicycle. For example, one of these studied factors is environmental conditions [10, 14]. Another factor is the existence of a bicycle lanes, which has received a lot of attention and researchers have found that the absence of a bicycle lane reduces the willingness to use a bicycle.

In the CBD of small and dense cities, the possibility of building bicycle lanes is limited and bicycle lanes cannot be developed easily to encourage more people to use a bicycle. Therefore, the focus should be on increasing the quality of the existing bike lanes. Very few researchers have studied the opinions of cyclists regarding bike lane attributes.

Jane and Tiwari [18] and Krizek [19] found that the most important factors affecting the bike lane are obstacles and pavement quality. Here, pavement conditions have taken the second place and have been very important from the point of view of cyclists. However, obstacles had lower priority because as explained, the entry of cars into the bicycle lane was limited. Majumdar [32] examined three factors, including route visibility, obstacles and lane width and found that the lane width was the most important attribute, which is similar to the results of this research.

6 Conclusions

The proportion of bicycles in the transportation of developing countries, such as Iran, is very low and should be helped to increase by improving infrastructure. One of the most important infrastructures is bike lanes. Given the limitation of financial resources, it is necessary to consider which attributes of bike lanes are more important to improve from the cyclists' point of view. Priorities for improving attributes of bike lanes can vary for different groups of cyclists. Therefore, a survey of cyclists in the city of Qazvin was conducted.

Questions about the bike lane were: increasing width, increasing attractiveness or appeal of the bike lane (such as painting, planting), improving pavement conditions, improving sight distance and removing obstacles in the bike lane. It was seen that there was no difference between the priorities of different age groups and their most important priorities were increasing the lane width and improving the sight distance. Two important priorities for the men group were increasing the lane width and improving the sight distance, while the women considered the improvement of the pavement conditions and the appeal of the bike lanes more important. Increasing the lane width and improving the pavement conditions for the recreational group and increasing the lane width and improving the sight distance for the non-recreational group were the most important improvements in the attribute of the bike lanes.

Generally speaking, it can be said that increasing the width of the bike lane has been the most important factor for almost all the groups and should be a priority because it would increase both comfort and safety. It was seen that in the city of Qazvin, the bicycle was mostly used for recreational purposes and has not yet been

accepted as a mode of transportation. Therefore, more attention should be paid to safety of the bike lane to increase the tendency to use the bicycle.

Grants and funding

The authors received no financial support for the research, authorship and/or publication of this article.

Conflicts of interest

The authors declare that they have no known competing financial interests or personal relationships that could have appeared to influence the work reported in this paper.

References

[1] STEWART, O. T., MOUDON, A. V. Using the built environment to oversample walk, transit and bicycle travel. *Transportation Research Part D: Transport and Environment* [online]. 2014, **32**, p. 15-23. ISSN 2058-8305A, eISSN 2058-8313. Available from: https://doi.org/10.1016/j.trd.2014.06.012

[2] KIENTEKA, M., REIS, R. S., RECH, C. R. Personal and behavioral factors associated with bicycling in adults from Curitiba, Parana State, Brazil. *Reports in Public Health / Cadernos de Saude Publica* [online]. 2014, **30**(1), p. 79-87. ISSN 0102-311X, eISSN 1678-4464. Available from: https://doi.org/10.1590/0102-311x00041613

[3] ENGBERS, L. H., HENDRIKSEN, I. J. M. Characteristics of a population of commuter cyclists in the Netherlands: perceived barriers and facilitators in the personal, social and physical environment. *International Journal of Behavioral Nutrition and Physical Activity* [online]. 2010, **7**, 89. ISSN 1479-5868. Available from: https://doi.org/10.1186/1479-5868-7-89

[4] TITZE, S., GILES-CORTI, B., KNUIMAN, M. W., PIKORA, T. J., TIMPERIO, A., BULL, F. C., VAN NIEL, K. Associations between intrapersonal and neighborhood environmental characteristics and cycling for transport and recreation in adults: baseline results from the RESIDE study. *Journal of Physical Activity and Health* [online]. 2010, **7**(4), p. 423-431. ISSN 1543-3080, eISSN 1543-5474. Available from: https://doi.org/10.1123/jpah.7.4.423

[5] BROWN, L. R. *Plan B 3.0: mobilizing to save civilization* (substantially revised). New York: WW Norton and Company, 2008. ISBN 978-0393330878.

[6] EVENSON, K. R., AYTUR, S. A., SATINSKY, S. B., RODRIGUEZ, D. A. Barriers to municipal planning for pedestrians and bicyclists in North Carolina. *North Carolina Medical Journal*. 2011, **72**(2), p. 89-97. ISSN 0029-2559, eISSN 2379-4313.

[7] FORMAN, H., KERR, J., NORMAN, G. J., SAELENS, B. E., DURANT, N. H., HARRIS, S. K., SALLIS, J. F. Reliability and validity of destination-specific barriers to walking and cycling for youth. *Preventive Medicine* [online]. 2008, **46**(4), p. 311-316. ISSN 0091-7435, eISSN 1096-0260. Available from: https://doi.org/10.1016/j.ypmed.2007.12.006

[8] DE SOUSA, A. A., SANCHES, S. P., FERREIRA, M. A. G. Perception of barriers for the use of bicycles. *Procedia - Social and Behavioral Sciences* [online]. 2014, **160**, p. 304-313. ISSN 1877-0428. Available from: https://doi.org/10.1016/j.sbspro.2014.12.142

[9] CAMARGO, E., FERMINO, R., ANEZ, C., REIS, R. Barriers and facilitators to bicycle use for transport and leisure among adults. *Brazilian Journal of Physical Activity and Health / Revista Brasileira de Atividade Fisica e Saude* [online]. 2014, **19**(2), 256. ISSN 2317-1634. Available from: https://doi.org/10.12820/rbafs.v.19n2p256

[10] PARKIN, J., WARDMAN, M., PAGE, M. Estimation of the determinants of bicycle mode share for the journey to work using census data. *Transportation* [online]. 2008, **35**(1), p. 93-109. ISSN 0049-4488, eISSN 1572-9435. Available from: https://doi.org/10.1007/s11116-007-9137-5

[11] GARRARD, J., ROSE, G., LO, S. K. Promoting transportation cycling for women: The role of bicycle infrastructure. *Preventive Medicine* [online]. 2008, **46**(1), p. 55-59. ISSN 0091-7435, eISSN 1096-0260. Available from: https://doi.org/10.1016/j.ypmed.2007.07.010

[12] SALLIS, J. F., OWEN, N. *Physical activity and behavioral medicine* [online]. SAGE publications, 1999. ISBN 9780803959965, eISBN 9781452233765. Available from: https://dx.doi.org/10.4135/9781452233765

[13] PEREIRA SEGADILHA, A. B., DA PENHA SANCHES, S. Analysis of bicycle commuter routes using GPSs and GIS. *Procedia - Social and Behavioral Sciences* [online]. 2014, **162**, p. 198-207. ISSN 1877-0428. Available from: https://doi.org/10.1016/j.sbspro.2014.12.200

[14] HARVEY, F., KRIZEK, K. J., COLLINS, R. Using GPS data to assess bicycle commuter route choice. In: Transportation Research Board 87th Annual Meeting: proceedings. 2008.

[15] DILL, J., VOROS, K. Factors affecting bicycling demand: Initial survey findings from the Portland, Oregon, region. *Transportation Research Record: Journal of the Transportation Research Board* [online]. 2007, **2031**, p. 9-17. ISSN 0361-1981, eISSN 2169-4052. Available from: https://doi.org/10.3141/2031-02

[16] SENER, I. N., ELURU, N., BHAT, C. R. An analysis of bicycle route choice preferences in Texas, US. *Transportation* [online]. 2009, **36**(5), p. 511-539. ISSN 0049-4488, eISSN 1572-9435. Available from: https://doi.org/10.1007/s11116-009-9201-4

[17] STINSON, M. A., BHAT, C. R. Frequency of bicycle commuting: Internet-based survey analysis. *Transportation Research Record: Journal of the Transportation Research Board* [online]. 2004, **1878**, p. 122-130. ISSN 0361-1981, eISSN 2169-4052. Available from: https://doi.org/10.3141/1878-15

[18] JAIN, H., TIWARI, G. Discrete route choice model for bicyclists in Pune, India. *Urban Transport Journal*. 2010, **9**(2), p. 1-12.

[19] KRIZEK, K. J. Two approaches to valuing some of bicycle facilities' presumed benefits. *Journal of the American Planning Association* [online]. 2006, **72**(3), p. 309-320. ISSN 0194-4363, eISSN 1939-0130. Available from: https://doi.org/10.1080/01944360608976753

[20] MAJUMDAR, B. B., MITRA, S., PAREEKH, P. Methodological framework to obtain key factors influencing choice of bicycle as a mode. *Transportation Research Record: Journal of the Transportation Research Board* [online]. 2015, **2512**, p. 110-121. ISSN 0361-1981, eISSN 2169-4052. Available from: https://doi.org/10.3141/2512-13

[21] BASU, S., VASUDEVAN, V. Effect of bicycle friendly roadway infrastructure on bicycling activities in urban India. *Procedia - Social and Behavioral Science* [online]. 2013, **104**, p. 1139-1148. ISSN 1877-0428. Available from: https://doi.org/10.1016/j.sbspro.2013.11.210

[22] MOSTOFI, H., MASOUMI, H., DIENEL, H. L. The association between the regular use of ICT based mobility services and the bicycle mode choice in Tehran and Cairo. *International Journal of Environmental Research and Public Health* [online]. 2020, **17**(23), p. 1-20. eISSN 1660-4601. Available from: https://doi.org/10.3390/ijerph17238767

[23] SHAFIEE NIKOO, H., SERTIYAK, S. Investigating the implementation of bicycle transportation system and its impact on environmental indicators and reducing pollutant emissions. Case study: City of Ahvaz. In: 2nd National Conference on Applied Researches in Civil Engineering, Architecture and Urban Planning: proceedings (in Persian). 2014.

[24] POOYA, Y., AYOUBINEJAD, J. Problems of Mashhad bicycle transportation system (case study of Vakil Boulevard) and providing solutions for its improvement and development. In: The 1st International Congress on Specialized Researches in Science, Engineering: proceedings (in Persian). 2017.

[25] A story of cycling in the streets of Tehran - Khabar Online (in Persian) [online] [accessed 2021-06-09]. Available from: https://www.khabaronline.ir/news/1523354

[26] POLIZIANI, C., RUPI, F., SCHWEIZER, J., POSTORINO, M. N., NOCERA, S. Modeling cyclist behavior using entropy and GPS data. *International Journal of Sustainable Transportation* [online]. 2022, latest articles, p. 1-10. ISSN 1556-8318, eISSN 1556-8334. Available from: https://doi.org/10.1080/15568318.2022.2079446

[27] SCHWANEN, T. Uncertainty in contextual effects on mobility: an exploration of causality. *Annals of the American Association of Geographers* [online]. 2018, **108**(6), p. 1506-1512. ISSN 2469-4452, eISSN 2469-4460. Available from: https://doi.org/10.1080/24694452.2018.1456313

[28] SHAHEEN, S. A., GUZMAN, S., ZHANG, H. Bike sharing in Europe, the Americas and Asia: past, present and future. *Transportation Research Record: Journal of the Transportation Research Board* [online]. 2010, **2143**(1), p. 159-167. ISSN 0361-1981, eISSN 2169-4052. Available from: https://doi.org/10.3141/2143

[29] BIEHL, A., STATHOPOULOS, A. Investigating the interconnectedness of active transportation and public transit usage as a primer for mobility-as-a-service adoption and deployment. *Journal of Transport and Health* [online]. 2020, **18**, 100897. ISSN 2214-1405, eISSN 2214-1413. Available from: https://doi.org/10.1016/j.jth.2020.100897

[30] BRUZZONE, F., SCORRANO, M., NOCERA, S. The combination of e-bike-sharing and demand-responsive transport systems in rural areas: a case study of Velenje. *Research in Transportation Business and Management* [online]. 2021, **40**, 100570. ISSN 2210-5395, eISSN 2210-5409. Available from: https://doi.org/10.1016/j.rtbm.2020.100570

[31] MARTENS, K. The bicycle as a feedering mode: experiences from three European countries. *Transportation Research Part D: Transport and Environment* [online]. 2004, **9**(4), p. 281-294. ISSN 2058-8305A, eISSN 2058-8313. Available from: https://doi.org/10.2495/TDI-V1-N1-92-102

[32] MAJUMDAR, B. B., MITRA, S., PAREEKH, P. Methodological framework to obtain key factors influencing choice of bicycle as a mode. *Transportation Research Record: Journal of the Transportation Research Board* [online]. 2015, **2512**, p. 110-121. ISSN 0361-1981, eISSN 2169-4052. Available from: https://doi.org/10.3141/2512-13

MONITORING OF SHALLOW-GROOVED TRAMWAY CROSSINGS

Magdalena Křečková*, Hana Krejčiříková

Faculty of Civil Engineering, CTU in Prague, Prague, Czech Republic

*E-mail of corresponding author: magdalena.kreckova@fsv.cvut.cz

Magdalena Křečková 0000-0003-0734-4159, Hana Krejčiříková 0000-0002-6989-7763

Resume

The article presents selected results and the sequencing of research into the project "Long-Term Monitoring of Rail Structures in Tramway Crossings with a Focus on Shallow-Grooved Crossings Aimed at the Optimization of their Maintenance and Noise Reduction", which was running with support from the Technology Agency of the Czech Republic within the Zeta Project (project registration No. TJ04000257) in 2020-2022. The project was elaborated jointly with the Prazska strojirna a.s. Company in cooperation with the Prague Public Transit Company (hereinafter PPTC). The project's objective was to optimize the maintenance of tramway tracks with a focus on shallow-grooved crossings in rail structures taking into account the noise emission levels during the life cycle of these crossings.

Article info

Received 6 November 2022
Accepted 2 February 2023
Online 31 March 2023

Keywords:

rail structure
deep-grooved crossing
shallow-grooved crossing
wear
noise emission level

Available online: https://doi.org/10.26552/com.C.2023.033

ISSN 1335-4205 (print version)
ISSN 2585-7878 (online version)

1 Introduction

The rail structures installed in tramway crossings are part of tramway tracks loaded by the passage of the tram cars. To a lesser extent, they are also loaded by the passage of road vehicles, which, however, impact more significantly mainly on the track geometry parameters rather than the rail wear. The loading causes the wear of rails and flangeways, as well as the deformation of flangeway bottoms - resulting in the deformation of the prescribed flangeway shape. What seems problematic is, above all, the rail head wear and the lateral rail head loss at the crossings and entering rails, which are directly connected to the crossings. The resulting wear and deformations are affected by the crossing's geometry. The lateral rail head loss is mostly manifested in the branching-off direction, while the rail head wear in the straight direction. Although the rail wear phenomenon in rail structures with shallow-grooved crossings is relatively predictable, the rail profile development over time and the growth of the above deformations have not been validated yet [1-2].

Excessive flangeway wear is connected with the rail head loss in the crossing. It changes the contact area at the wheel-rail interface. Such wear levels also instigate the wheel wear, which is obviously undesirable in traffic operation. Therefore, the flangeway profile is always repaired by welding on new material into the flangeway space after reaching an unacceptable wear level, i.e. the flangeway shape is reprofiled.

The increasing wear of shallow-grooved crossings is associated with development of the noise emission level. The noise emission level changes during the crossing's life cycle - the noise emission around the track grows with the increasing wear of the crossing. The noise emission level is affected not only by the wear, but by the maintenance of shallow-grooved crossings, as well. The crossings are maintained by welding on the missing material and its successive grinding. It has been empirically found and confirmed by measurements that noise emission levels increase (by roughly 4 dB) after the crossing has been welded. Due to traffic, the added material is rolled over and the noise emission level is subsequently stabilized at a lower level again. Like in the above case, it still holds true here that no continuous measurements have been performed so far to match the rail condition with the noise emission arising during the passage of a tram car over the crossing. Nor has the moment been identified when the noise emission is reduced due to the added material rolling over after the crossing was welded [3].

Up to now, the decision about the repair of a shallow-

grooved crossing has been made and the interval between individual repairs identified empirically, based on the experience of track administrators. The optimization of the maintenance planning of the rail structures, the grinding plans, flangeway reprofiling and other works on rail structures, should lead to reduced cost and labour requirements. The maintenance planning should be optimized respecting the development of deformations based on the passing loads taking into account the development of the noise emission level. Preventive maintenance campaigns are presumed as well [4].

The stimulus for research into the above issues was made by PPTC during 2019. Nevertheless, as these issues are relatively complex and very extensive to grasp, the project was only oriented towards a part of the whole related field with a focus on shallow-grooved crossings, encompassing just a small range of monitored structures and relationships.

2 Definition of terms

In order to describe the project and the phenomena mentioned in more detail, it is necessary to define the terms used and outline the local specifications of the tram operation within which the project was designed.

Shallow-grooved crossing (crossing with a shallow flangeway) - a crossing with a reduced flangeway depth so that the wheel flange deliberately travels on the flangeway bottom for some time during the wheel passage over the crossing [5-7].

Deep-grooved crossing (crossing with a deep flangeway) - a crossing with such a depth of the flangeway that the wheel rolls on the running surface and there is no contact between the wheel flange and the flangeway bottom of the crossing during the wheel passage over the crossing [5-7].

Entering rail - a rail manufactured in the same shape as the corresponding grooved rail, but without the rolled flangeway, which is subsequently milled according to the required geometry [8-10].

Individual tramway networks within the Czech Republic differ in the wheel profile geometry. Therefore, the flangeway depth for a shallow- or deep-grooved crossing has not been precisely defined. The project focused on the tramway traffic operation within PPTC where the shallow-grooved crossings have a flangeway depth of 14 mm. The flangeway width affecting the crossing's geometry depends on the flangeway geometry (straight track x curve). The flangeway in a straight track is 27 mm wide and the flangeway in a curve is 29 mm wide (measured 9 mm below the top of the rail). The crossing is connected to connecting grooved rails with a depth of 39 mm. The height difference is compensated by a 1500 mm long flangeway entering piece. The PPTC network uses the wheel running profile with a width of 86 mm [5].

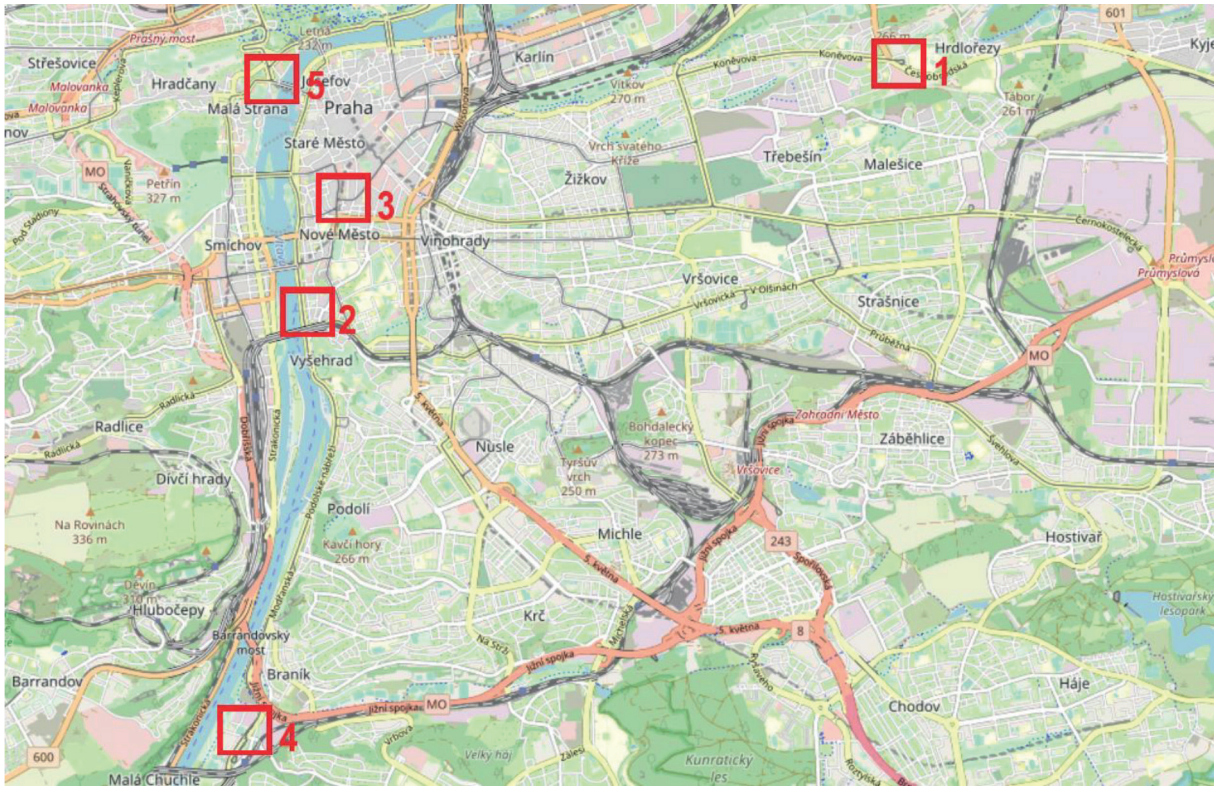

Figure 1 *Map of Prague with marked localities monitored within the project: 1 - Spojovaci Terminus; 2 - Rasin Embankment - Svobodova Street junction; 3 - Lazarska - Spalena Street junction; 4 - Junction point to Branik Terminus; 5 - Klarov - Letenska Street junction*

3 Project sequencing

The project was elaborated within the PPTC tramway track network from 07/2020 to 06/2022. It was a direct follow-up to the previous pilot academic measurements initiated by the PPTC. The project can be divided into 3 research phases.

In the first project phase, the localities, or rail structures and crossings, respectively, were selected to be continuously and systematically monitored during the project. A total of 5 crossings within the PPTC network were selected, situated in the localities marked on the map below (Figure 1):

- Spojovaci Terminus, specifically the 2nd crossing of the take-off turnout - "Spojovaci" Locality;
- Rasin Embankment - Svobodova Street junction, specifically the crossing in the direction from the centre, to Modrany in the straight direction, or to Albertov in the branching-off direction - "Vyton" Locality;
- Lazarska - Spalena Street junction, specifically the crossing in the direction from Narodni Avenue to Vodickova Street - "Lazarska" Locality;
- Junction point to Branik Terminus, specifically the crossing in the R04 high-speed turnout - "Branik" Locality;
- Klarov - Letenska Street junction, specifically the crossing in the direction from Staromestska to Malostranska Metro Station - "Klarov" Locality.

The crossings in the "Vyton" area and the Spojovaci Terminus had already been monitored prior to the start of the project, from 2019. During that time, the above localities underwent reconstruction and new crossings were installed in the track structures. It was, therefore, possible to monitor the crossings starting from their new, factory condition. The crossings in those localities were monitored systematically over a long time interval - for more than 3 years. This approach is not a common practice in the maintenance of track structures and crossings. It allowed the comparison of the deformation development of a new and repaired (welded) crossing.

The monitoring of the wear and development of individual deformations was carried out using the Contour II measuring instrument (see below). Based on the experience of the PPTC staff, the measurements were carried out at an interval of once a month. After the installation of the structures, or after the flangeway shape reprofiling respectively, the interval was shorter - once every 14 days.

Furthermore, preventive welding of the crossing in the "Vyton" Locality took place during this project phase. This allowed the comparison of the wear and deformations of a new, factory-provided crossing with the crossing welded during the traffic operation. At the same time, the effect of the crossing welding on the noise emission level was observed.

The second project phase involved systematic evaluations of all the measured data and searching for relevant correlations of individual parameters. In particular, these were the correlations enabling the prediction of the crossing's condition - "passing load - rail wear" and "time from repair - rail wear". The noise emission levels of tram car passing over the crossings were continuously measured in two localities: in Branik and Vyton. Both localities had been chosen with regard to possibilities of the noise measurement offered by the spatial layout of the localities, the traffic load of the localities, especially by non-rail traffic and with regard to the noise of the surrounding environment.

In the third project phase, the measured data were evaluated, involving both the data related to the wear and deformations of the crossings and the data related to the noise emissions. During this period, the noise load was matched with the wear development pattern of the crossings and the wear development pattern was correlated with the loading of individual structures.

4 Measurement - contour II

Under Regulation No. 177/1995 Coll. of the Ministry of Transport, regular inspections and measurements of railway structures are performed to ensure the operability of tramway tracks. Regular inspections of tramway turnouts in traffic rails are performed on a daily basis. At the same time, tracks are patrolled every two weeks. Based on the recommendation of track supervisors, control measurements of designated sections are made with various instruments (Krab measuring trolley, Contour II.). The measurements within the project were performed with the Contour II measuring instrument (shown in Figure 2) [11-13].

The Contour II measuring instrument is used for checking the PPTC rail wear. It is usually used to check the wear in curves and to check the correct welding of entering rails of shallow-grooved crossings. The instrument measures by means of a red dot laser beam, which is dispersed over the rail and is also imaged by a camera.

The measurement with the Contour II measuring instrument can be divided into 2 types - continuous measurement and spot measurement. Spot measurement reads individual rail transverse profiles, which are defined by the user. Continuous recording captures transverse rail profiles in 3.84 mm or 5.75 mm increments - as selected by the user. The distance between individual points of the transverse profile is 0.13 mm for both continuous and spot recording. The transverse profile width sensed by the instrument is 150-200 mm [1].

The measured data were evaluated in the Contour Eval III programme. Excel was used for the subsequent data comparison to model 2D transverse profiles. The Contour II measuring instrument does not allow

Figure 2 *Contour II measuring instrument*

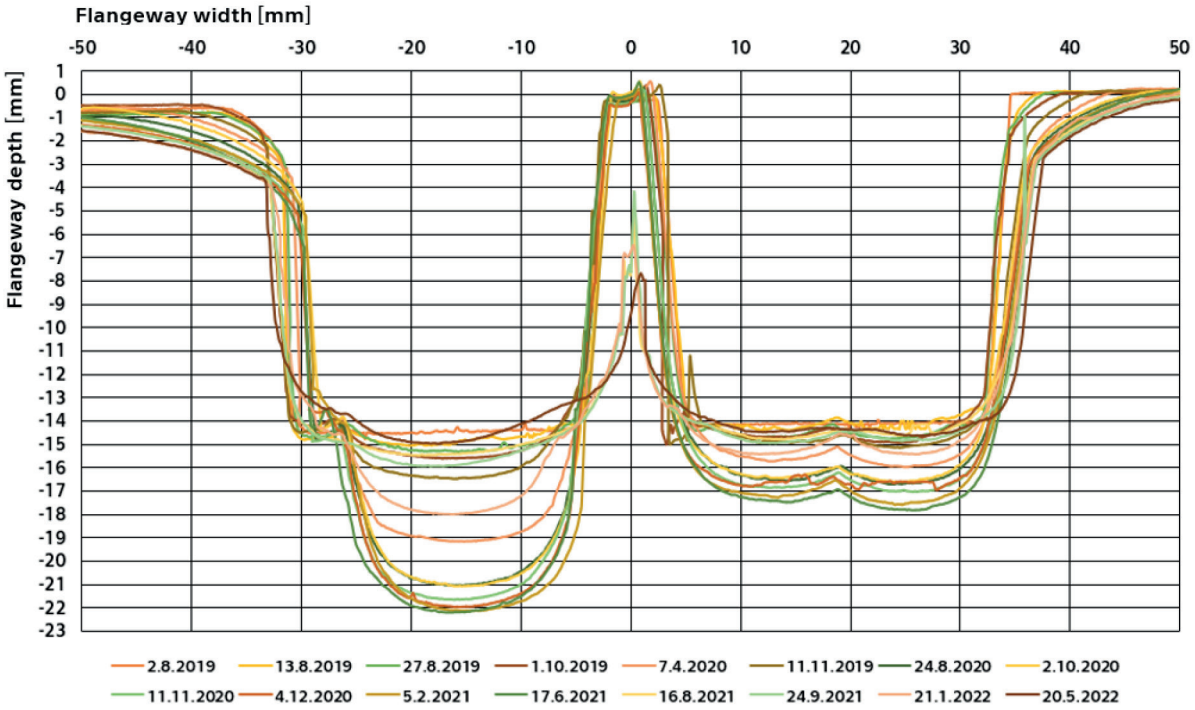

Figure 3 *Example of an evaluated profile of the exit nose of a crossing from the rail structure situated at the Rasin Embankment - Svobodova Street junction (Vyton Locality)*

creation of a 3D model as it does not record the track geometry. Using the profiles processed in this way, the development of the wear and deformations over time can be observed (as shown in Figure 3 for illustration). Subsequently, these data can be related to the noise emission level and to the passing load, as well.

5 Shallow-grooved crossing: wear and deformation

Crossings with shallow or deep flangeways can be used in tramway structures. Individual operated networks differ in the wheel profile geometry. For this reason, the flangeway depth for shallow-grooved or deep-grooved crossings has not been precisely defined [1, 6].

The use of shallow-grooved or deep-grooved crossings depends, above all, on the wheel profile geometry and the crossing angle of individual rail structures. Therefore, the regulations for the use of shallow-grooved crossings differ for individual networks operated within the Czech Republic. The project is focused on the monitoring of shallow-grooved crossings within the PPTC tramway network, where the wheel profile with a width of 86 mm and a critical crossing angle for the deep-grooved crossing of roughly 12° are used (for a wheel with a width of 100 mm this angle is 16°) [5, 7-9].

Tramway crossings are subjected to wear due to traffic - the flangeways get deeper and wider. The wear of the crossing depends, above all, on the passing load. Thus, a shallow-grooved crossing becomes a deep-grooved one over time. At this point, its maintenance and the flangeway reprofiling are carried out. This is achieved by adding new material into the flangeway by welding. The wear of the crossing is also characterized by deformations of the flangeway bottom. The resulting deformations are mainly dependent on the crossing's geometry. The flangeway in a straight direction is mainly characterized by the flangeway deepening and by the rounding of its edges. The flangeway in a branching-off direction (flangeway in a curve) is deepened due to traffic and a longitudinal edge is formed at the flangeway bottom due to the passage of the wheel flange dividing the flangeway into two parts - the so-called double flangeway is formed. Characteristic defects include the break-off of the crossing's take-off nose.

6 Selected results

The wear and deformation development pattern at the crossing in the "Vyton" Locality has been chosen as an example (as shown in Figure 5). In particular, the figure displays the profile in the middle of the crossing where the flangeways in the crossing intersect. For better illustration, a photo with a marked monitored profile is added (Figure 4).

A total of 18 measurements were carried out in the "Vyton" Locality during the project. The results of all the measurements were correlated in one diagram, which shows the time-related development pattern of the wear and deformations, starting from the installation of a new crossing in the structure, including the crossing's flangeway welding (Figure 5).

Figure 5 clearly shows that a vertical flangeway wear from a depth of 14 mm to a flangeway depth of 21.6 mm occurred from the installation of a new crossing (curve of 2.8.2019) to the condition before the crossing maintenance by welding on new material (curve of 17.6.2021). Successively, the flangeway bottom was welded (curve of 30.7.2021) and the flangeway depth was 15 mm. For illustration, see the diagram presenting the respective selected values, Figure 6.

From the above results, it can be concluded that the vertical wear of the crossing over a period of 22 months (from 2.8.2019 to 17.6.2021) was 7.6 mm. On closer examination of the measured results (as seen in Figure 5), it is evident that the wear is slower at the beginning of the crossing's life cycle. Subsequently, the flangeway is deepened more dramatically to a value of approximately 20.5 mm, at which the wear development pattern slows down again. The stabilization of the wear at the end of one life cycle of the crossing (before the flangeway bottom of the crossing is welded) is caused by a change in the contact interfaces between the wheel and the crossing. At the beginning of the life cycle, the crossing is travelled over by the wheel flange. However, the deepening of the flangeway results in the wheel being guided over the crossing on the wheel running surface. Subsequently, the lateral wear, in particular, increases and the vertical wear gradually stabilizes. At this point, the crossing is welded, as the shallow-grooved crossing has become a deep-grooved one, to which the crossing's geometry is not adapted.

In cooperation with PPTC, passing loads were monitored and load counts were carried out on the monitored rail structures. Or, the numbers of passages of individual types of tram cars and trains were monitored, respectively. For the "Vyton" Locality, a total of 850,000 units passed during the period of interest

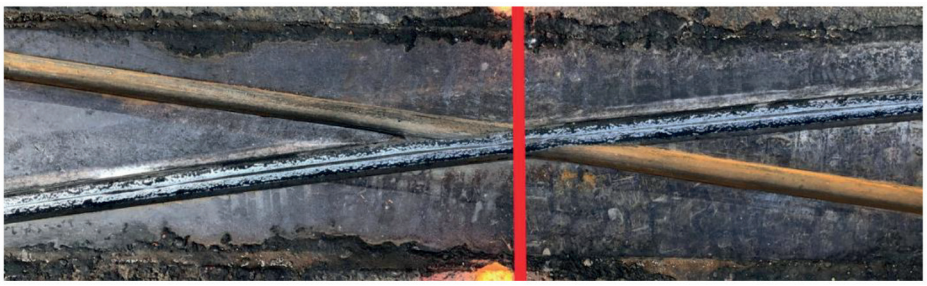

Figure 4 *Marked (with a red line) monitored transverse profile of the crossing presented in the article for illustration*

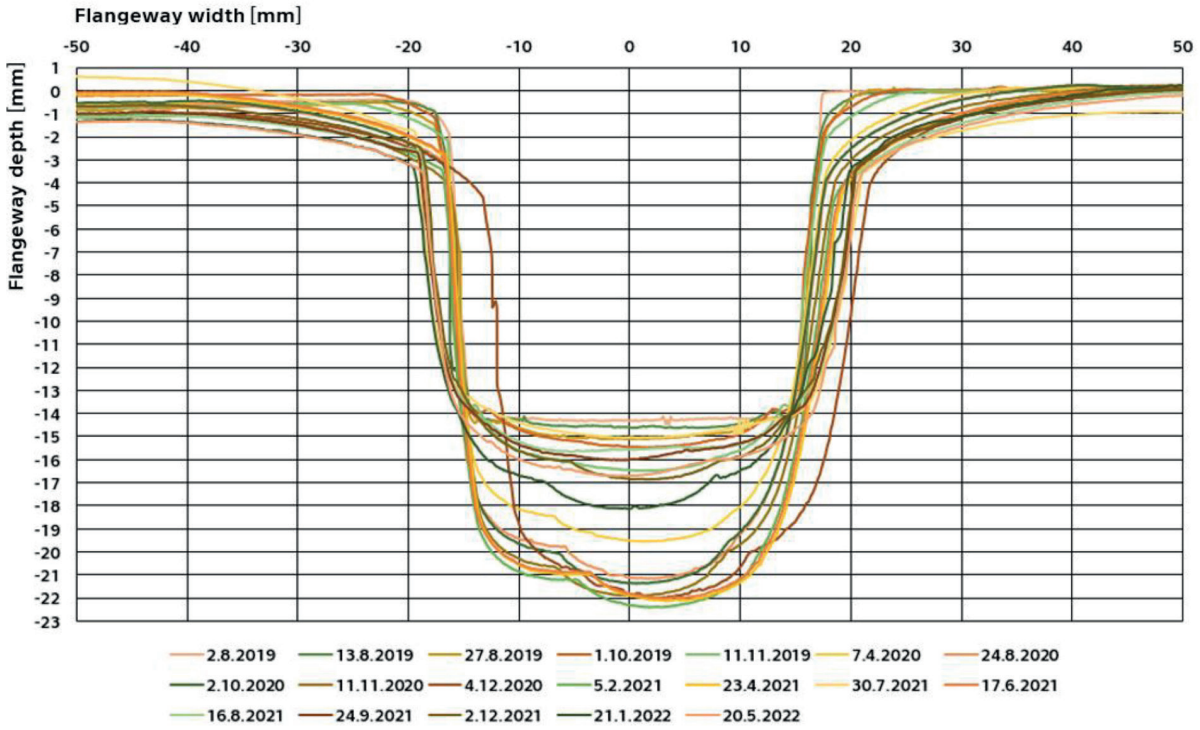

Figure 5 *Wear and deformation development pattern of the centre of the crossing in the "Vyton" Locality*

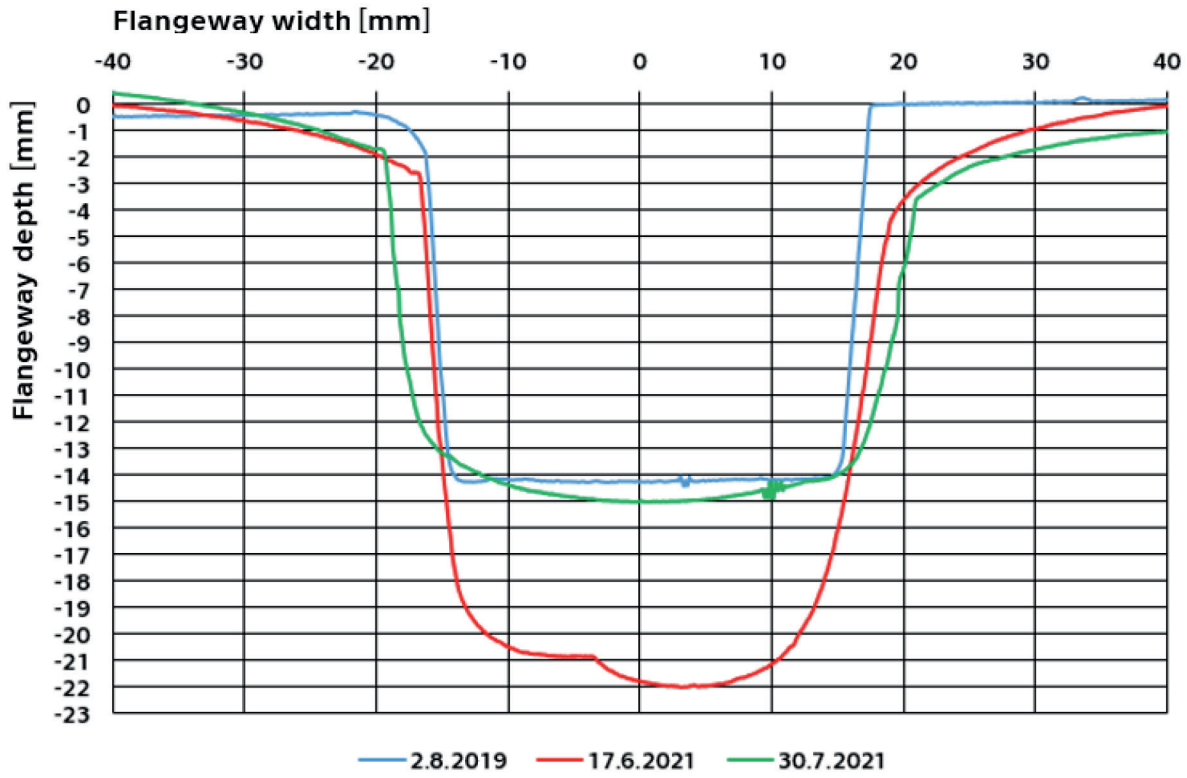

Figure 6 *Selected data from measurements in the "Vyton" Locality.*

from August 2019 to June 2021, which represents the passage of approximately 5,600,000 individual axles (combinations of four-, six- and eight-axle cars and trains) and corresponds to a passing load of 40 million tons. This load had caused a wear of 7.6 mm on the crossing. Subsequently, new material was welded into the crossing.

The new material welding (see Figure 7) to the

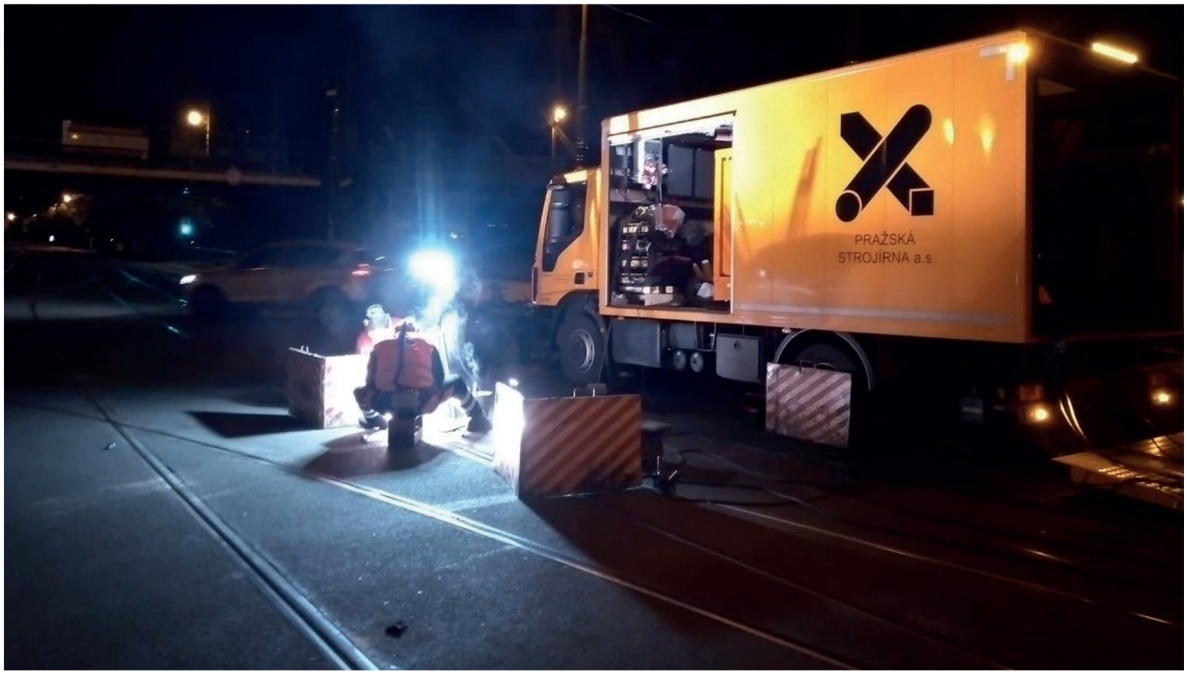

Figure 7 *Illustration of welding the flangeway bottom of a shallow-grooved crossing in the "Vyton" Locality. The welding was done with the Weltrode 40 electrode*

bottom of the flangeway takes place during the night operation without a traffic closure. For this reason, the welding is not as precise as factory welding. Even so, there is an effort to weld the material to a depth of approximately 14 mm. Consequently, the depth of a factory-made flangeway (flangeway depth of 14 mm) differs from the depth of the flangeway of a welded crossing (flangeway depth of 15 mm) - this is visible in Figure 6. After the welding on new material, the crossing is finished by grinding and individual weld beads are "smoothened".

7 Conclusions

The so-called shallow-grooved crossings undergo vertical flangeway wear during their life cycle. The crossings that were designed as shallow-grooved (travelled on the flangeway bottom) gradually change their profile due to the contact with the wheel and become deep-grooved ones (travelled on the top surface of the crossing). To return the crossing to the original condition, new material must be added by welding it into the flangeway. Excessive wear of the crossings and their flangeways causes a change in the contact interfaces with the wheel. This causes a shift in the contact area between the wheel and the rail, a phenomenon undesirable in traffic conditions as it causes faster wheel wear.

The wear development pattern of crossing depends primarily on the geometry parameters of the crossing (curve radius) and the passing load. The monitored structure experienced a flangeway deepening to the wear limit value (wear at which a shallow-grooved crossing becomes a deep-grooved one) in about 2 years, after approximately 850,000 units had passed over it. Subsequently, the maintenance and reprofiling of the crossing's flangeways was scheduled. By going through this procedure, the crossing enters the second phase of its life cycle, when the whole process is repeated.

The monitoring campaign confirmed the assumptions that the straight flangeways are worn out and deepened in one concentrated track of the passing vehicle wheel flanges, while the curved flangeways are worn out and deepened in two parallel tracks. The wear rate (material loss) corresponds to the passing load - the number of vehicles.

Grants and funding

This research was funded by the project "Long-Term Monitoring of Rail Structures in Tramway Crossings with a Focus on Shallow-Grooved Crossings Aimed at the Optimization of their Maintenance and Noise Reduction", which was running with support from the Technology Agency of the Czech Republic within the Zeta Project (project registration No. TJ04000257) in 2020-2022.

Conflicts of interest

The authors declare that they have no known competing financial interests or personal relationships that could have appeared to influence the work reported in this paper.

References

[1] ZELENKA, J., KOHOUT, M. Rail-wheel Interaction in conditions of tram operation / Vztah kolo-kolejnice v podminkach tramvajoveho provozu (in Czech). In: 46. Meeting of Tram Expert Group: proceedings. Association of Public Transit Company, Czech Republic. 2012.

[2] SVOBODOVA, A. Rail materials and profiles in rail Transportation / Materialy a tvary kolejnic v kolejove doprave (in Czech) [online]. Bachelor's thesis. Brno: VUT v Brne, Faculty of Mechanical Engineering, 2019. Available from: https://www.vut.cz/www_base/zav_prace_soubor_verejne.php?file_id=193175

[3] BRET, O. Acoustic analysis of tram passage over a switch with shallow crossing / Akusticka analyza prujezdu tramvaji pres kolejovou konstrukci odboceni se srdcovkou s melkym zlabkem (in Czech). In: Juniorstavinternational Scientific Conference of Civil Engineering for PH.D. Students: proceedings. 2021.

[4] SCHNEIDEROVA-HERALOVA, R., MESTANOVA, D., TOMEK, A., HROMADA, E., VITASEK, S. Crossing and life cycle cost / Vyhybka a naklady zivotniho cyklu (in Czech) [online]. Certified methodology of Ministry of Transportation, Czech Republic, 2017. Available from: https://www.mdcr.cz/getattachment/Dokumenty/Veda-a-vyzkum/Certifikovane-metodiky/Metodicky-postup-ve-forme-prirucky-pro-navrhovani/34METODICKY-POSTUP-CESTI-VYHYBKA-V-LCC.pdf.aspx

[5] KRECKOVA, M. Monitoring of selected tramway crossing / Monitoring vybranych tramvajovych srdcovek (in Czech). Bachelor's thesis. Prague: CTU in Prague, Faculty of Civil Engineering, 2020.

[6] BRET, O., KRECKOVA, M. Long-term monitoring of the condition of tramway crossing and the development of their degradation / Dlouhodoby monitoring stavu tramvajovych srdcovek a vyvoj jejich opotrebeni (in Czech). In: Seminar organized by VOS a SPS Decin: proceedings. 2022. ISBN 978-80-905733-8-3, p. 66-72.

[7] IZER, J., ZELENKA, J. Contact geometry characteristics / Charakteristiky kontaktni geometrie (in Czech). *Scientifics Papers of the University of Pardubice. Series B, The Jan Perner Transport Faculty*. 1996, **2**, p. 39-62. ISSN 1211-6610.

[8] PENC, M. Project of rail-wheel interaction / Projekt kolo-kolejnice (in Czech). Prague: Prague Public Transit Company, 2009.

[9] SUROVSKY, J. Rail-wheel interacion of tram / Vztah kolo-kolejnice u tramvaji (in Czech). Prague: Prague Public Transit Company, 2009.

[10] MARUNA, Z. Principles of motion along a rail / Zaklady pohybu po koleji (in Czech). *Scientifics Papers of the University of Pardubice. Series B, The Jan Perner Transport Faculty*. 1996, **2**, p. 23-38. ISSN 1211-6610.

[11] Decree no. 177/1995 Coll., issuing the railway construction and technical rules / Vyhlaska c. 177/1995 Sb. Ministerstva dopravy (in Czech). Ministry of Transportation, Czech Republic, 1995. Version of 1.4.2018.

[12] Transport and signal regulation for tram D1/2 / Dopravni a navestni predpis pro tramvaje D1/2 (in Czech). Internal regulation. 3. novelization edition. Prague: Prague Public Transit Company, 2012.

[13] IZVOLT, L., SESTAKOVA, J., SMALO, M., GOCALOVA, Z. Monitoring of the track geometry quality around the portals of new tunnel construction Turecky vrch - preliminary results. *Communications - Scientific letters of the University of Zilina* [online]. 2014, **16**(4), p. 9-20. ISSN 1335-4205, eISSN 2585-7878. Available from: https://doi.org/10.26552/com.C.2014.4.9-20

EXPERIMENTAL INVESTIGATION AND THEORETICAL BACKGROUND OF THE OPTIMAL CONTROL OF THE CONCRETE MIXTURE FORMING

Pavlo Pshinko[1], Tatyana Dekhta[2], Olena Hromova[3,*], Oksana Steinbrech[2]

[1]Director General of Institute Dniprogiprotrans TDV, Dnipro, Ukraine
[2]Prydniprovska State Academy of Civil Engineering and Architecture, Dnipro, Ukraine
[3]Ukrainian State University of Science and Technology, Dnipro, Ukraine

*E-mail of corresponding author: eleanagromova@gmail.com

Pavlo Pshinko 0000-0003-4187-5340,
Olena Hromova 0000-0002-5149-4165,
Tatyana Dekhta 0000-0001-5023-3070,
Oksana Steinbrech 0000-0001-7742-2445

Resume

Concrete belongs to the most used building materials, applied in almost all types of constructions (civil, industrial, road, hydraulic, subway constructions, etc.). Currently, the most common is the vibration method of molding concrete and reinforced concrete products.

However, the issues of choosing a rational mode for compacting concrete mixtures, its effect on density and, accordingly, strength, water resistance, frost resistance and deformation properties of concrete, remain insufficiently studied. The best results are obtained by using the optimal frequentative vibratory influence method. In this case, concrete strength is increased by 25-30 % in comparison to the factor of concrete compacted by traditional method.

Article info

Received 11 August 2022
Accepted 7 February 2023
Online 27 March 2023

Keywords:

the intensity of vibrations
the optimal control of forming
the inertial current of energy

Available online: https://doi.org/10.26552/com.C.2023.034

ISSN 1335-4205 (print version)
ISSN 2585-7878 (online version)

1 Introduction

For the construction industry, the development and improvement of methods of compaction of concrete mixtures in forming of the reinforced concrete products is one of the leading areas in the concrete technology. At the forming stage, the necessary concrete structure is created, its required density, homogeneity and, accordingly, the quality of the product have to be secured. Therefore, we have modernized and substantiated the optimal mode of compaction of concrete mixtures during the products' forming. This would make it possible to significantly reduce the duration of the products' forming and the consumption of the energy can be reduced too. Such implementations are one of the actual solutions in concrete technology at the companies of the construction industry.

Achievements in theoretical physics and analytical mechanics were used to develop the foundations of the theory of optimal control of the process of vibration compaction of concrete mixture [1-4].

Some researchers represent the concrete mixture as a system of aggregate particles connected by elastic or elastic-plastic connections [5]. The role of such connections is assigned to the layers of cement paste. It is assumed that each particle of a certain mass, connected by an elastic connection, must have some frequency of natural vibrations and vibration will be the most effective when the period of the vibrator's perturbing force coincides with the period of natural vibrations of the aggregate particles, i.e. at resonance. It has been proven that a low vibrations frequency is necessary for the resonance of large aggregate particles and a higher frequency for the small ones. Since the aggregate particles, of different sizes, weights and shapes, are usually present in the concrete mixture, the multifrequency vibrations should be the most effective [5].

One of the main parameters of compaction of concrete mixtures is the optimal duration of compaction, after which the density and strength of concrete are practically not increasing. For durations of compactions below this value, the mixture would be uncompacted and the strength and other properties of concrete would not be fully utilized. The same degree of compaction can be achieved with different combinations of intensity

and duration of vibrations. As the intensity increases, the time required for compaction of the mixture decreases and vice versa. The increased duration of the compaction does not provide a noticeable improvement of strength and other properties of concrete. Such a measure is ineffective and sometimes even harmful (overconsumption of energy, unproductive use of equipment, longer exposure to noise) [3, 5-6].

Currently, the vibrations are the most common method of compaction of concrete products. However, despite the available developments in this field, the issues of choosing a rational mode of compaction of concrete mixtures, its effect on density and, accordingly, strength, waterproofing, frost resistance and deformable properties of concrete remain insufficiently studied [5].

2 Experimental material and methods

The paper aimed at developing the scientific and technical principles of optimal management of the reinforced concrete products' forming process by the vibrating method. This would significantly improve the quality of reinforced concrete (in terms of strength, waterproofing, frost resistance, deformation indicators, etc.).

Portland cement M400, 20-40 mm fraction gravel and the fine Dnieper sand (Mkr = 1.2-1.3) were used in the research.

The composition of the concrete was characterized by the ratio of components Cement: Sand: Crushed stone: Water = 1:1.63:3.68:0.59 (C:S:C:W = 1:1.63:3.68:0.59; (C = 357 kg/m^3, S = 582 kg/m^3, C = 1314 kg/m^3, W = 210 l/m^3)), the mobility of the concrete mixture - the slump of a standard cone of 30 - 40 mm (S1 = 30 - 40 mm), concrete class B 15 (C12/15).

For compaction of concrete mixtures when forming samples of 100 × 100 × 100 mm, a laboratory vibrating table VT-1 was used (oscillation frequency 2860 cycles/min, amplitude under load - 0.35 mm).

3 Research methodology

Vibrations compaction of concrete mixtures with a constant intensity of vibrations (at a constant energy flow) results in voids (jamming of aggregates and especially crushed stone or gravel). This significantly reduces the sealing efficiency. To increase the efficiency of compaction, it is suggested to apply optimal management of the forming process, which includes multiple vibrations actions. This would contribute to the destruction of voids, as well as directed capillaries, which are formed as a result of air removal, redistribution of cement paste and soluble component. The technology of manufacturing reinforced concrete products by the optimal molding control allows to significantly increase the physical and mechanical properties of concrete and reduce their cost.

Compaction of concrete mixtures by the vibrations method can be carried out under different modes (the intensity value, its change over time, the duration of compaction, etc.), however, after the end of the process, a concrete mixture of different densities will be obtained [5-6]. The task is to develop and theoretically justify such a mode of vibrations compaction, in which compaction of the concrete mixture (achieving the minimum possible volume) would take place in the shortest time.

Significant factors, characterizing the quality and speed of compaction of the concrete mixture, are the change in the volume of the compacted mixture and the speed of removal of the air phase. Therefore, using the terms «theory of optimal control», the phase plane is defined by the coordinate X_1^y - the volume of the compacted concrete mixture and the coordinate X_2^y - the rate of air removal during vibrations compaction, water removal during vibrovacuum, centrifugation, etc. The origin of the coordinates will be characterized by the minimum possible volume of the compacted mixture and the removal rate of the air and liquid phase, which is equal to zero. Admissible control has the following components: pressure in the concrete mixture without vibrations, during the vacuuming etc. and pressure in the concrete mixture during the vibrations compaction, vibrations vacuuming etc.

The phase state of the concrete mixture (terms of "theory of optimal control") at the initial moment of time $(X_1^y(t_0), X_2^y(t_0))$ and the control function $\overline{P}(t)$ uniquely determine the phase trajectory of the state of the concrete mixture during the compaction. Based on this, a dependence was obtained, which gives the optimal control in terms of speed, which turns out to be piecewise-continuous (relay) - it changes periodically [7-8]. The number of switches (or control stability intervals) for the linear systems is always normal and depends on the control field, initial and final conditions. We have proven that the optimal control of the forming is carried out by rational regulation of the pressure inside the compacting concrete mixture [7, 9-10]:

$$\overline{P_a}(t) = K^Y(t)sign\psi(t) = K^Y(t)sign\psi(c_1 - c_2 t), \quad (1)$$

where:

P_a - pressure in the concrete mixture (active pressure);

ψ - amount of movement (impulse of the system);

t - compaction time;

c_1, c_2 - constant integrations;

K^Y - coefficient depending on the type of compacted mixture.

Taking into account the obtained results of theoretical studies, as well as developments [8], a structural diagram of the concrete mixture vibrations compaction control with feedback was developed (Figure 1).

Thus, the optimal forming control is carried out by the rational pressure regulation inside the concrete mixture compacted by the vibrations method by means

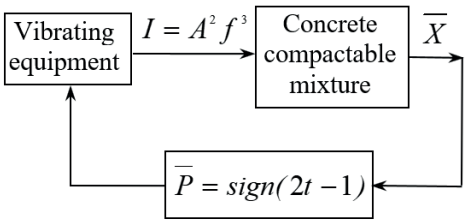

Figure 1 *Block diagram of the concrete mixture vibrations compaction control with feedback, where: I - is the intensity of compaction, A - is the vibrations amplitude of the vibrations device, f - is the vibrations frequency of the vibrations device*

Table 1 *Density and strength of concrete depending on the method of vibrations*

Type of sealing	Duration of operation of the included vibrating table (s)	The average density of concrete, ρ_0 (kg/m^3)	Concrete strength limit, f^{28}_{6} (MPa)
Without inertial intensity flow (energy flow)	20	2343	19.5
With inertial intensity flow (energy flow)	10	2357	21.2
Without inertial intensity flow (energy flow)	30	2357	19.2
With inertial intensity flow (energy flow)	20	2263	20.9
Without inertial intensity flow (energy flow)	40	2352	19.1
With inertial intensity flow (energy flow)	30	2360	22.2

of multiple vibrational influences (multiple intensity pulses).

With this mode of compaction, the inertial intensity flow (inertial energy flow) will significantly affect the quality of compaction of the concrete mixture. To reveal its role, two batches of samples were formed using different methods of vibrations.

4 Results and discussion

The first batch of samples was formed without an inertial intensity flow (energy flow), the duration of forming was 20, 30 and 40 s, respectively. In this case, the form with the concrete mixture was installed on the vibrating table, the vibrating table was turned on and after the set time, the form was removed from the vibrating table without turning it off.

The second batch - taking into account the inertial energy flow: the duration of the vibrations effect in this case was only 10, 20 and 30 s - here the form with the concrete mixture was installed on the vibrating table, the vibrating table was turned on and turned off after a certain period of time, the form was removed only after a complete stop of the vibrating table The density of concrete at the age of one day and the strength limit after 28 days were determined (Table 1, Figure 2).

The results of the research show that the inertial energy flow has an important impact on both the density and strength of concrete, as well as on the forming duration, which is significantly increased if this flow is excluded from the technological process of compaction of the concrete mixtures. It should be noted that with the help of an additional inertial intensity flow (energy flow), it is possible to increase the concrete strength by 10-15 %, relative to the strength of concrete compacted by the standard molding method. Repeated use (application) of the inertial energy flow can significantly improve the quality of concrete compaction.

In the course of research, a comparative assessment of various modes of vibrations compaction of concrete mixtures was carried out. Materials used for production of the concrete mixtures were the same as in previous studies.

Optimal control of the forming process of concrete and reinforced concrete products is an inertial energy flow under vibrations. That is, the general cycle of product molding is divided into several segments: when the concrete is exposed to vibrations and when the vibrations are interrupted. The time interval between the vibrations impact was 2-3 s and duration of vibrations (with optimal control) was 6-18 s. The entire cycle of compaction of the concrete mixture is 30 s.

Molded samples were hardened under the normal conditions. At the age of 28 days, the density and compressive strength of concrete were determined. The results of the research are given in Table 2, which confirmed the conclusions obtained during the theoretical development of optimal forming control [8]. A comparative assessment of various methods and regimes of the concrete mixtures compaction showed that the best results were obtained by applying the optimal control, which uses the mode with multiple vibrations effects. In this case, the greatest increase in concrete strength was achieved in comparison to the indicators of the concrete compacted by the traditional method.

Since the frost resistance is one of the most important properties of concrete for determining its durability, we have carried out research on the frost resistance of concrete compacted with the commonly used method of vibrations compaction and optimal management

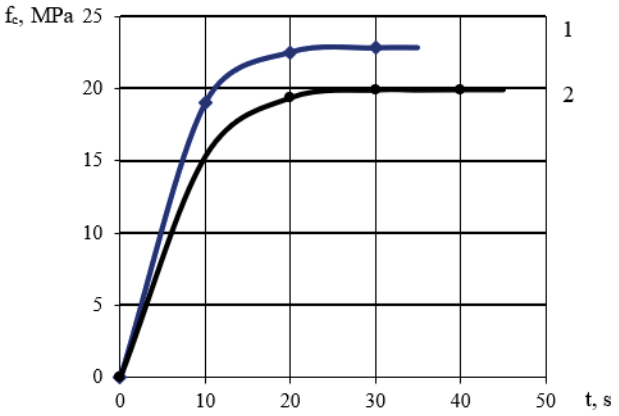

Figure 2 *Influence of the method of vibration exposure during the molding of products on the strength characteristics of concrete: 1 - with inertia energy flow; 2 - without inertial energy flow*

Table 2 *Density and strength of concrete depending on the compaction mode*

Type of sealing	Vibro-sealing at the maximum possible intensity		Concrete density mixture, ρ_0 (kg/m^3)	Strength of concrete, f^{28}_c (MPa)
	Duration of vibrations actions (s)	Number of vibrations		
Existing method of vibrations compaction (at constant intensity)	30	1	2384	19.4
The proposed method of vibrations compaction (with multiple vibrations)	13	2	2466	23.0
	8	3	2505	25.8
	6	4	2507	25.9

according to standard DSTU B.V.2.7-47-96. A freezer was used to test for frost equipment. The tests were carried out at a temperature of -50^0 C. Duration of the test cycle in the freezer was 2.5 hours. The main samples are tested for strength 2 hours after being removed from the freezer. In the experimental studies, used concrete mixes and concretes, as well as the materials for their preparation, were the same as in the previous experiments.

The degree of the frost resistance was judged by changes in sample weight and compressive strength after 50, 100, 150 and 200 freezing cycles.

The results of the research are shown in Figures 3 and 4. During the period of testing for the frost resistance (273 days), the control samples that were stored in water hardened, increased their mass and strength. At the same time, the largest increase in mass (3.5 %) and strength (10 MPa) was observed in samples of concrete compacted at a constant intensity of vibrations.

Samples of concrete compacted with optimal control of forming showed a smaller increase in mass due to lower water absorption (within 2 %), the increase in strength was 9 MPa on average

Samples subjected to freeze-thaw cycles within 100 cycles increased mass and strength with greater intensity than the control ones. The strength of samples molded by vibration in the usual mode (at constant intensity), after 200 cycles, decreased by 16% compared to control samples.

After 200 cycles the compressive strength of the concrete compacted by the optimal control of the compaction (with repeated vibrations effects) was almost at the same level as that of the control samples (the decrease was only 5-6.5 %).

The research results show that concrete compacted under optimal control of forming has higher frost resistance compared to concrete compacted under constant vibrations intensity. The results of our studies of the main properties of concrete, compacted by different modes of vibrations, have shown that in addition to the increased frost resistance, the optimal control of forming also significantly increased the water resistance of concrete (by 1.3-1.6 times) and on the other hand, it significantly reduced the value of capillary moistening and water absorption, as well as deformation, shrinkage and swelling.

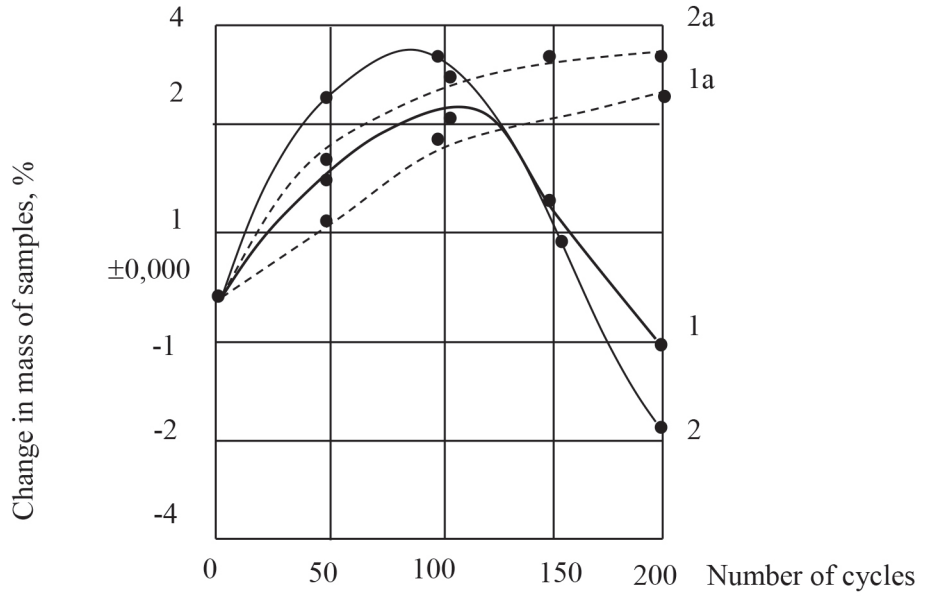

Figure 3 *The mass of concrete samples depending on the duration of hardening, the number of freezing and thawing cycles: 1 - for samples formed with optimal control and freezing-thawing; 1a - the same, for control samples; 2 - for samples molded according to the traditional mode (with constant vibrations intensity) and subjected to freezing-thawing; 2a - the same, for control samples*

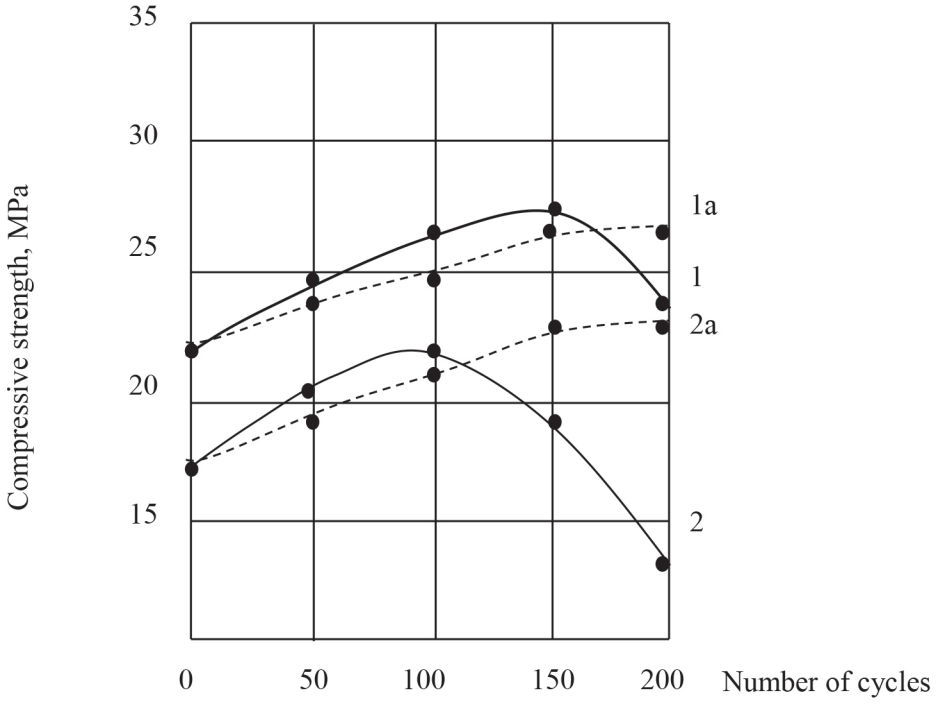

Figure 4 *Compressive strength of concrete samples depending on the duration of hardening, the number of freezing and thawing cycles: 1 - for samples formed with optimal control and freezing-thawing; 1a - the same, for control samples; 2 - for samples molded according to the traditional mode (with constant vibrations intensity) and subjected to freezing-thawing; 2a - the same, for control samples*

5 Conclusions

Experimental research has confirmed the conclusions obtained during the theoretical considerations, regarding the improvement of the compaction mode of concrete mixtures:

- A comparative assessment of different methods and regimes of compaction showed that the better results were obtained by application of the optimal control of forming, i.e. when using the mode with multiple vibrations effects. In that case, the increase in strength of concrete was 25-30 %, compared to the indicators of concrete compacted by the traditional method;
- When obtaining the full-strength concretes, it is possible to reduce the cement consumption. At the same time, the duration of forming is significantly reduced and the proposed forming method does not require additional capital costs for implementation - it requires just the standard mechanical equipment widely used in the construction industry.

Grants and funding

The authors received no financial support for the research, authorship and/or publication of this article.

Conflicts of interest

The authors declare that they have no known competing financial interests or personal relationships that could have appeared to influence the work reported in this paper.

References

[1] STOROZHUK, N., DEKHTA, T. On the inertial energy flow with optimal control of the formation of reinforced concrete structures. *Bulletin of the Prydniprovska State Academy of Civil Engineering and Architecture*. 2003, 1, p. 24-31. ISSN 2312-2676.

[2] STOROZHUK, N., DEKHTA, T. *Optimal control of the compaction of concrete mixtures in the production of reinforced concrete*. Monograph. Dnepropetrovsk: Thresholds, 2012. ISBN 978-617-518-197-3.

[3] STOROZHUK, N., DEKHTA, T. Optimal control of compaction of concrete mixtures by vibration method and its features. *Bulletin of the Bulletin of the Prydniprovska State Academy of Civil Engineering and Architecture* [online]. 2018, 4, p. 56-64, ISSN 2312-2676. Available from: https://doi.org/10.30838/J.BPSACEA.2312.231018.56.311

[4] PSHINKO O., KRASNYUK A., HROMOVA O., Theoretical study of the conditions of combined action of materials of old and new concrete in the repair and restoration of the structures of transport facilities. In: 23-nd International Scientific Conference Transport Means 2019: Sustainability: Research and Solutions: proceedings. Part I. 2019. ISSN 1822-296X, eISSN 2351-7034, p. 508-513.

[5] DEKHTA T. Optimal control molding in technology concrete structures. *Promising Scientific Researches of Eurasian Scholars.* 2021, 8, p. 8-11. ISSN 2709-183X

[6] PSHINKO O., HROMOVA O., RUDENKO D., Study of rheological properties of modified concrete mixtures at vibration. *Material Science Forum*. 2019, 968, p. 96-106. ISSN 1662-9752. Available from: https://doi.org/10.4028/www.scientific.net/MSF.968.96

[7] STOROZHUK, N. *Vibrovacuumization of concrete mixtures and properties of vacuum concrete*. Dnepropetrovsk: Thresholds, 2008. ISBN 978-966-525-966-4.

[8] STOROZHUK, N., DEKHTA, T. The problem of optimal control of the compaction of concrete mixtures. *Bulletin of the Prydniprovska State Academy of Life and Architecture*. 2001, 1, p. 46-53. ISSN 2312-2676.

[9] STOROZHUK, N. On the issue of compaction of concrete mixtures by vibro-vacuum. *Izvestiya VUZov. Construction and Architecture*. 1976, 2, p. 110-115.

[10] STOROZHUK, N. Investigation of a new method of compaction of concrete mixtures under the action of vacuum. *Izvestiya VUZov. Construction and Architecture*. 1982, 11, p. 67-71.

DEVELOPING PEDESTRIAN FATALITY PREDICTION MODELS USING HISTORICAL CRASH DATA: APPLICATION OF BINARY LOGISTIC REGRESSION AND BOOSTED TREE MECHANISM

Malaya Mohanty[1,*], Bitati Sarkar[2], Piotr Gorzelańczyk[3], Rachita Panda[1], Srinivasa Rao Gandupalli[4], Ampereza Ankunda[1]

[1]School of Civil Engineering, KIIT Deemed to be University, Bhubaneswar, India
[2]Department of Civil Engineering, National Institute of Technology, Silchar, India
[3]Department of Engineering, Stanislaw Staszic University of Applied Sciences, Pila, Poland
[4]GITAM School of Technology, GITAM Deemed to be University, Visakhapatnam, India

*E-mail of corresponding author: malaya.mohantyfce@kiit.ac.in

Malaya Mohanty 0000-0002-6116-782X, Piotr Gorzelańczyk 0000-0001-9662-400X,
Srinivasa Rao Gandupalli 0000-0002-4937-2652

Resume

Pedestrian fatality rate plays a key role in examining effectiveness of the road safety. The present study attempts to examine the effect of various categories of accused vehicles and the average 85th percentile speed at accident location on the pedestrian crash fatality. The study also attempts to develop pedestrian crash severity models using the binary logistic regression and boosted trees technique. Historical crash data, along with the video recording technique at accident sites, have been utilized for the present study. From regression equations, it is observed that when the heavy vehicle (HV) hits a pedestrian as compared to two-wheeler (2W), the average chance of death increases 2.44 times. According to the Boosted tree model, the contribution of speed is 60 %, whereas the contribution of category of accused vehicle is 40 % for pedestrian fatality prediction. The study should help in planning better strategies like all red time at intersections or pedestrian foot over bridge at critical locations.

Article info

Received 25 November 2022
Accepted 28 February 2023
Online 21 March 2023

Keywords:

Pedestrian fatalities
vehicle category
85th percentile speed
binary logistic model
boosted tree model

Available online: https://doi.org/10.26552/com.C.2023.036

ISSN 1335-4205 (print version)
ISSN 2585-7878 (online version)

1 Introduction

Pedestrians form an integral part of every roadway environment. The conflict between pedestrians and vehicles is a vital factor to examine the efficiency of the roadway traffic [1]. World Health Organisation (WHO) [2] has reported that more than 1.3 million deaths occur every year around the world, due to the road crashes. Among them, 54 % of the global road accidental deaths comprise of pedestrians, cyclists, and motor cyclists with pedestrians outnumbering the other two categories [3]. Further, 93 % of fatalities due to road crashes occur in low-and middle-income countries even though they comprise only 60 % of the total number of vehicles in the world [2]. In a developing country like India, more than 150,000 people die in road crashes every year [3]. Although the number of persons killed in road crashes have slightly declined in 2019 (-0.2 % as compared to 2018), however, the share of pedestrian deaths has shown increasing trend. Despite the pedestrians being involved in 14 % of total road accidents in the country, their share in total deaths is alarming at 17 % [3], suggesting that the fatality rate in road accidents involving pedestrians is very high. The cases of hit and run has also increased over the years [3], which concludes pedestrians being the worst sufferers in the road accidents. All these numbers press for an imperative need to study and examine the pedestrian safety on roads.

Many studies have been conducted over the years to assess pedestrian safety, as well as the overall safety on roads. While earlier studies [1, 4-5] focused mainly on studying the pedestrian behaviour from recorded videos with relation to the accepted gaps and vehicles dynamics, recent studies [6-10] are focused on development of mathematical models like MLR, Logit and Probit models, etc. to predict different characteristics of both the vehicle and a pedestrian during the conflict situation. Most of these models and simulations-based analysis are based

on the data collected from the field through recorded videos, historical crash data, or questionnaire-based surveys. Few other researchers [7, 11] have also examined the pedestrian safety based on various surrogate safety measures (SSM), like Post encroachment time (PET), Time to vehicle (TTV), Deceleration time (DT), Time to accidents (TTA), etc. Similarly, few researchers [12-13] have also utilized decision trees, like CART, Random Forest, Boosted Trees, or ANN, to model the safety of vehicles and pedestrians on road. Hu and Cai (2022) [14] reported that the logistic model is first applied for relationship explanation, and then the machine learning classifiers like ANN or Fuzzy are applied for prediction modeling. Tamakloe et al. (2022) [15] opined that logistic regression helps in identifying the individual effect of factors affecting crash severity. According to Pande et al. (2010) [16], various decision trees, like CART and boosted trees, make it easier to interpret the results unlike the ANN. The CART and boosted trees also remove the problems of multicollinearity.

Although the usage of SSMs have grown popularity in last few years due to its ability to predict crashes without occurrence of the incident [17-18], still the analysis of historical reported road crashes is common due to its proof of occurrence. Moreover, with historical data, varied geometrical and driver behavior along with vehicle flow data can be considered. Safety assessment of road networks and heterogenous traffic conditions of developing countries like India have historically relied on police-reported crash data [19-20]. According to [19], the fatal crashes should be assessed in detail for developing countries like India, to understand what factors contributes to fatal crashes. Past studies reveal that the role of accused vehicles/perpetrators have not been probed much to inspect their effects on pedestrian deaths. Few studies have undertaken the effect of motorcycles and heavy vehicles [20-21] on all the road crashes. However, their effect on pedestrian deaths was not in focus much.

In the present study, historical crash data have been utilized to assess the role of accused vehicles on pedestrian deaths. Along with the historical crash data, field studies are conducted at accident locations to gather speed data, which is also used as a factor to analyze the pedestrian fatalities. Thereafter, pedestrian severity prediction model has been developed by using logistic regression and boosted tree. The developed severity prediction models can help to understand the pedestrian fatalities better and help in framing better strategies for reducing the death rate during their crashes.

2 Data collection and methodology

Data collection is a significant aspect for attaining the objectives of the present study since better prediction models can be developed with a greater number of data points. In order to pursue the study, historical road crash data has been collected from Visakhapatnam, an emerging smart city in India. A total of 2425 road crash data have been analyzed, out of which 789 crashes involved pedestrians. All these crashes have occurred in 2019. The data were extracted on spreadsheets and analyzed using the MINITAB and JMP SAS software for correlations and development of models. Since the study deals with examining the role of accused vehicle, all the road crash incidents where victims were pedestrian, the details regarding the accused vehicle category and the outcome of the crash (injury or death), are noted. Further, field studies using video recording technique have been conducted at the accident locations to collect the 85th percentile speed for the road stretch where the accident occurred. It was observed that there was no major difference between the 85th percentile speeds collected on different days at those locations for various time periods. In addition, since this research has been ongoing for a longer time period of more than 2 years, it was seen that the 85th percentile speed also remained statistically similar in different years, too. Therefore, the 85th percentile speed data used to understand the effect of operating speed on pedestrian fatality is not much different to the 85th percentile speed on the day of the road accident at that location. Figure 1 displays the camera setup to collect speed data at various locations. In order to collect the speed data, 2 lines are marked 20 m apart at certain road sections near busy streets or accident blackspots. A camera is placed at the locations strategically so that it can cover a view of 20 meters. The data are collected during both the peak and off-peak periods. Next, the recorded videos are played on monitor to extract time data of various vehicles while crossing these 20 m interval lines, which in turn is used for extraction of speed data. Further, based on the time during which the road crash has occurred, the 85th percentile speed during that time interval is extracted and used in the study.

All the above-mentioned factors have been considered and correlated with pedestrian fatality to identify causative factors for pedestrian deaths and develop pedestrian fatality prediction models.

3 Results and discussions

The road crash data used for the study had 2425 reported crashes, which included all kinds of vehicles. It was observed that out of 2425 road crashes, pedestrians were the victim in 789 instances (32.5 %). Similarly, although 550 of the total 2425 crashes were fatal (22.7 %), the fatality percentage when pedestrians are victim is 35.1 % (277 out of 789 crashes). The preliminary data itself shows two major points. Firstly, how rampant is the pedestrian hit road crashes when compared to other vehicles on the road, and secondly, how the fatality rate escalates when pedestrians are hit on roads. The section has been divided into two major parts:

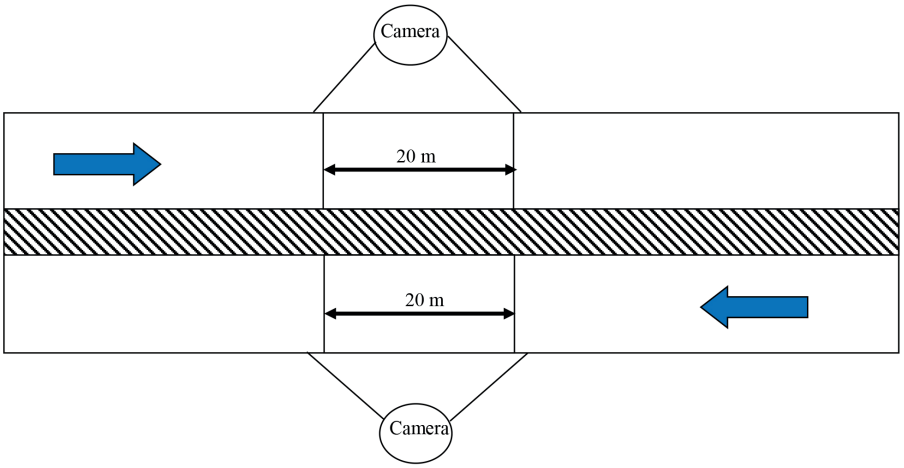

Figure 1 *Camera setup for the field data collection*

Table 1 *Pedestrian fatality rate based on various category of perpetrators*

Accused vehicle/Perpetrator	Number of crashes	Number of fatal crashes	Proportion of fatal crashes
2W	326	81	24.85
3W	51	18	35.29
4W	234	94	40.17
HV	178	84	47.19
Total number of crashes involving pedestrians	789	277	35.11

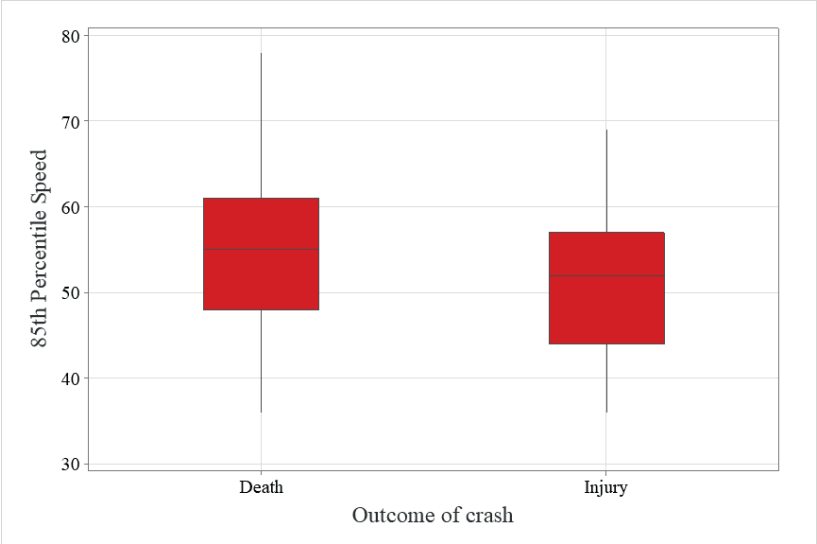

Figure 2 *Boxplot for assessing the impact of 85th percentile speed on pedestrian fatalities*

1. Relationship of accused vehicle category and speed with pedestrian fatality and
2. Development of pedestrian severity prediction models.

3.1 Relationship of accused vehicle category and speed with pedestrian fatality

The major category of vehicles, which hit pedestrians on roads are the Two-wheelers (2W), Three-wheelers (3W), cars, SUVs, jeeps, etc. (4W), and heavy vehicles (HV). Table 1 represents the number of accidents with each accused vehicle category and the percentage of fatal crashes with each category as perpetrator.

Results from Table 1 clearly show the effect of each category as perpetrator, while hitting a pedestrian. The effect of HV and 4W are particularly concerning, since the fatality rate increases to 40 and 47 %, respectively, as compared to the total average fatality rate of pedestrians (35.11 %), which itself is a high severity rate. In addition to the category of perpetrators, the operating speed (85th percentile speed at accident location is considered) has also been analyzed to study its effect on pedestrian

Table 2 *Odd's ratio for independent predictors*

Level A	Level B	Odds Ratio	95% CI
Accused category			
3W	2W	1.411	(0.7376, 2.6993)
4W	2W	1.737	(1.1892, 2.5360)
HV	2W	2.441	(1.6320, 3.6500)
4W	3W	1.231	(0.6401, 2.3665)
HV	3W	1.730	(0.8863, 3.3759)
HV	4W	1.405	(0.9308, 2.1221)
85th percentile speed		1.073	(1.053 to 1.093

NB - Odds ratio for level A relative to level B

fatality rate. A box plot (as shown in Figure 2) is plotted to understand the effect of 85th percentile speed on pedestrian fatality rate. Figure 2 clearly presents that with increase in 85th percentile speed, the pedestrian fatality rate also increases. The average 85th percentile speed when road accidents, involving pedestrians lead to fatalities, is observed to be 56.4 km/h, whereas the same average 85th percentile speed reduces to 50.9 km/h when only injuries are sustained by pedestrians. 2 sample t-test is also conducted, which shows that the mean 85th percentile speeds resulting in pedestrian injury and fatalities are significantly different from each other ($p < 0.05$) at 5% significance level. Next, pedestrian severity prediction modelling is conducted by two techniques - (a) Binary logistic model, and (b) Boosted tree model.

3.2 Development of pedestrian severity prediction models

In the present study, the preliminary analyses revealed clear relationship to be existing among pedestrian fatality, category of accused vehicle, and 85th percentile speed. Two techniques have been utilized - (a) Binary logistic, and (b) Boosted tree to developed predictive models.

3.3 Binary logistic model

Being a nominal variable with death/fatality and injury as two outputs, at first a binary logistic regression is carried out to predict the severity of pedestrian hit crashes. The general equation of logistic regression, to calculate the probability of fatality/deaths of pedestrians, is provided in Equation (1). P(fatality) refers to probability of pedestrian fatality in the case of a crash event. Equations (2) to (5) present the Y' functions for each category of accused vehicle.

$$P(\textit{fatality}) = \left[\exp(Y')/(1+\exp(Y'))\right], \quad (1)$$

$$Y'_{2W} = -4.779 + 0.0702 * 85\textit{th per.speed}\,, \quad (2)$$

$$Y'_{3W} = -4.435 + 0.0702 * 85\textit{th per.speed}\,, \quad (3)$$

$$Y'_{4W} = -4.227 + 0.0702 * 85\textit{th per.speed}\,, \quad (4)$$

$$Y'_{HW} = -3.887 + 0.0702 * 85\textit{th per.speed}\,. \quad (5)$$

Equations clearly depict that the HV shall give higher probability of pedestrian fatalities, as compared to other categories since the constant term is lowest here with a negative sign. Hence, the least number will be subtracted from the other term (85th per. speed*0.0702) in the equation. That term is same for all equations. Therefore, the Y' for HV shall be highest and therefore the probability of fatality for same 85th percentile speed. The proposed model predicts the outcome of 67.2% of the pedestrian crashes correctly with correct prediction for 88% of injuries and only 35% of deaths. However, the accuracy of predicting fatalities can be increased by decreasing the cut-off value for deciding fatality/injuries. Default settings suggest that if the pedestrian fatality is predicted to be more than 0.5, then the regression predicts the outcome as deaths, else injuries. However, the actual fatality rate of pedestrian as per the recorded crash data used for the study is 35.1%. This suggests that if the predicted probability for death is more than 35.1%, it is more likely to result in death of a pedestrian, since it is more than total average. If the cut-off value is decreased from 0.5 to 0.35, the prediction of accuracy for pedestrian deaths increases to 60% and for injuries, decrease to 65%. The equations (Equations (2) to (5)) reveal the higher effect of HV, which was eminent from the crash data too. However, more precise comparison can be made from the odd's ratio obtained from the logistic regression. Table 2 provides the odd's ratio table obtained for the proposed model.

The odd's ratio suggests the increase or decrease of fatality rate for each accused vehicle as compared to other vehicles, considering the 85th percentile speeds. For instance, it is observed that the HV when hits a pedestrian, as compared to the 2W, the average chance of death increases 2.44 times ranges from 1.63 times to 3.65 times. Similarly, when 4W hits a pedestrian the average probability of fatality increases 1.737 (1.189 to 2.536) times as compared to when a 2W

hits a pedestrian. Similarly, 1 km/h increase in 85th percentile speed increases the probability of pedestrian deaths by 1.073 times. Although the results of logistic model provide reasonable estimates of pedestrian crash outcomes, the predictions have not been very accurate. The odd's ratio, on the other hand provides important results regarding pedestrian fatalities, which is useful for development and execution of proper strategies to reduce the pedestrian accident-related deaths. The composition of traffic along with the 85th percentile speeds, at any vulnerable location, can be utilized to assess the threat to pedestrians. Next, decision tree namely, the boosted tree, was used for developing the prediction models due to its higher level of accuracy in predicting the outcome [16, 22].

3.4 Boosted tree model

Boosted tree is a type of decision tree, which uses boosting algorithm at every step to improve the accuracy of prediction of a required outcome. The boosted tree model is a more modern, versatile, and powerful predictive tool for developing the prediction models. In the present study, the model is developed using JMP SAS. The model predicts 95% of injuries and 71% of

Layer	Split	Label	Estimate
1	1	85th percentile speed<69	0.0230073206
1	2	85th percentile speed<70	-0.141280978
1	3	85th percentile speed<76	-0.789928889
1	4	85th percentile speed>=76	-0.789928889
2	1	85th percentile speed<69	0.0204074934
2	2	85th percentile speed<70	-0.125316242
2	3	85th percentile speed<72	-0.679900345
2	4	85th percentile speed>=72	-0.680794883
3	1	Accused Vehicle(3W, 4W, HV)	0.0059343076
3	2	85th percentile speed<44	0.2696723715
3	3	85th percentile speed>=44	0.1014870345
3	4	85th percentile speed>=53	-0.0327151
4	1	85th percentile speed<69	0.0160494116
4	2	85th percentile speed<70	-0.1074587
4	3	85th percentile speed<72	-0.625550795
4	4	85th percentile speed>=72	-0.626690869
5	1	Accused Vehicle(3W, 4W, HV)	0.0034501505
5	2	85th percentile speed<43	0.6235797646
5	3	85th percentile speed>=43	0.0944578748
5	4	85th percentile speed>=53	-0.025769774
6	1	85th percentile speed<69	0.0118506542
6	2	Accused Vehicle(2W)	-0.033801144
6	3	85th percentile speed<70	-0.177177805
6	4	85th percentile speed>=70	-0.59805459
7	1	Accused Vehicle(3W, 4W, HV)	-0.019553723
7	2	85th percentile speed<44	0.1976984364
7	3	85th percentile speed>=44	0.0761925523
7	4	85th percentile speed>=53	0.0012379576

Figure 3 *Sample tree details at each layer*

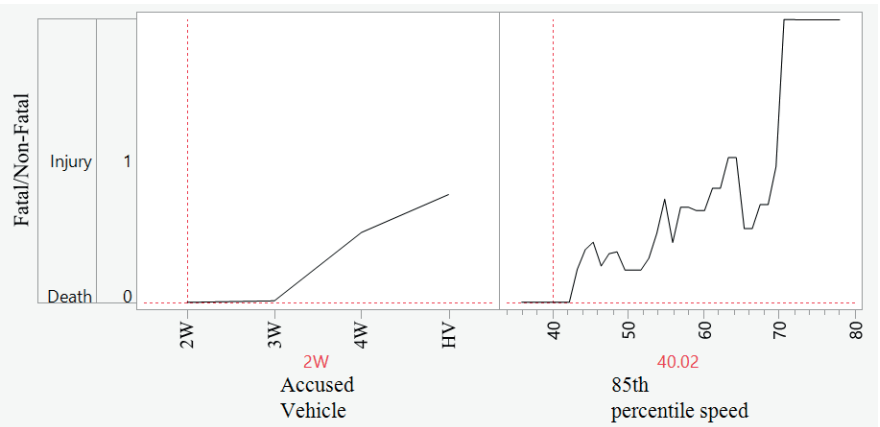

Figure 4 *Prediction profiler for boosted tree method - prediction profiler when the speed is 40 km/h*

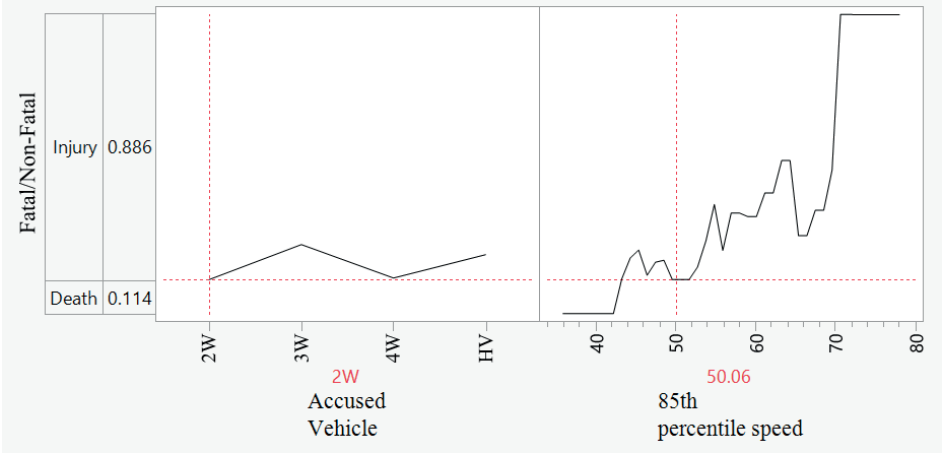

Figure 5 *Prediction profiler for boosted tree method - prediction profiler when the speed is 50 km/h*

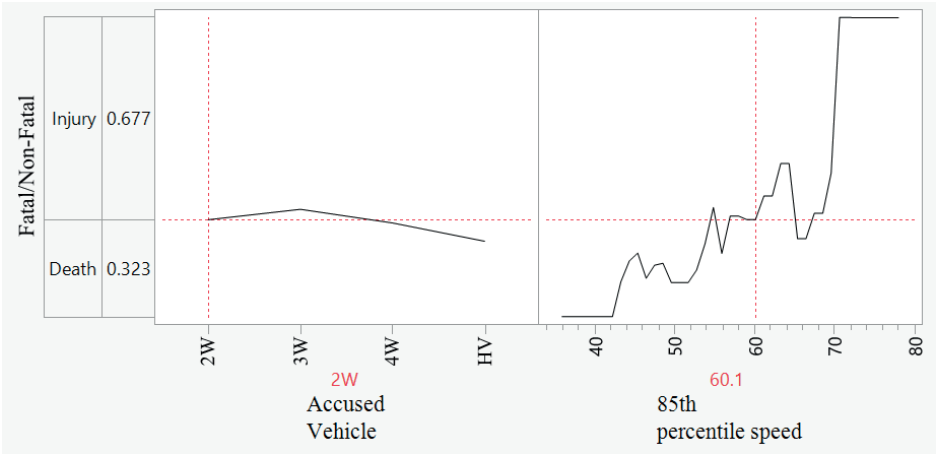

Figure 6 *Prediction profiler for boosted tree method - prediction profiler when the speed is 60 km/h*

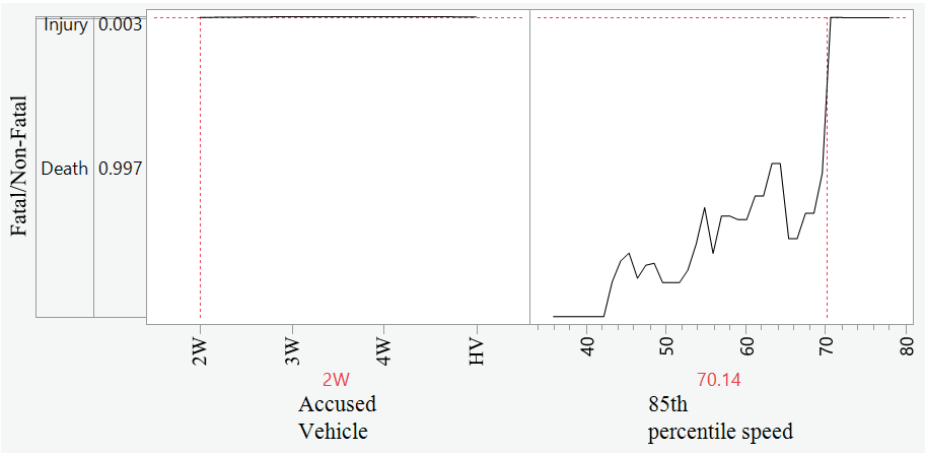

Figure 7 *Prediction profiler for boosted tree method - prediction profiler when the speed is 70 km/h*

deaths correctly. As mentioned earlier, 789 pedestrian involved incidents have been used for study, which implies that the model uses 789 layers of trees to develop the prediction model. At each layer, 3 splits have been modelled, based on data and the developed algorithm changes the estimated percentage of pedestrian fatality and makes it better. The algorithm that works at the backend of the boosted tree is highly dependent on number of data points. With increase in data points, the accuracy of prediction will increase, since that many number of trees shall be used to develop the prediction model. The sample labels of algorithm at each layer and resulting changes in predicted probabilities (tree details) are provided in Figure 3. As can be seen from Figure 3, for each layer, 3 splits or 3 conditions are being developed. For instance, in the first layer, first split describes that when 85th percentile speed decreases below 69 km/h, the probability of fatality decreases by 0.02 times. The

second split denotes that when the speed is less than 70 km/h, the probability of pedestrian fatality reduces by 0.14 times. The third split describes when the speed is less than 76 km/h, the death probability decreases by 0.79 times. The reference level for the algorithm is considered as 100% probability of pedestrian deaths. Figures 4-7 present the prediction profilers for the two independent variables and their effects on pedestrian fatality. Since the plots dynamically changes with change in accused category and 85th percentile speed, therefore, 4 cases are presented in Figures 4-7, viz. the probability of deaths for all category of accused vehicles when speed increases by 10 km/h (40, 50, 60, and 70 km/h). As can be seen, when 4W and HV are hitting a pedestrian while travelling at 40 km/h, the probability of death is around 0.4-0.5. However, of a 2W or 3W hits a pedestrian while travelling at 40 km/h, the probability of death is much smaller. With increase in speed, the probability increases for each category of vehicles. At 70 km/h (Figure 7), the probability of pedestrian fatality is 0.997, irrespective of category of vehicles.

Boosted tree's prediction accuracy is high and can be increased if more data is fed into the algorithm. Prediction profiler is handy to understand the microscopic effect of each variable on pedestrian fatality. In achieving these higher levels of prediction accuracy, speed has 60% contribution, while category of accused vehicle has 40% contribution.

4 Conclusions and recommendations

The present study focuses on examining the role of accused vehicle category and 85th percentile speed of vehicles on pedestrian fatalities. To attain the objective, historical crash data along with the field study (for collecting 85th percentile speed data) have been used. Out of 2425 reported crashes, 789 incidents involved pedestrians. The average fatality rate for pedestrians is found to be 35.1%, which is much more than when other vehicles are hit (22.7 %). The category of perpetrators was classified into the 2W, 3W, 4W and HV. It was found that proportion of pedestrian fatal crashes increases when the HV is the accused vehicle. Along with category, 85th percentile speed has also been utilized in the study. It is observed that the average 85th percentile speed is 56.4 km/h and 50.9 km/h for pedestrian fatalities and injuries respectively. Then, the 2 sample t-test also shows that the mean 85th percentile speeds resulting in pedestrian injury and fatalities are significantly different from each other ($p < 0.05$) at 5% significance level.

After identification of clear relationship to be existing among pedestrian fatality, category of accused vehicle, and 85th percentile speed, pedestrian crash severity model is developed using binary logistic regression and boosted tree model. The binary logistic regression clearly depicts the higher effect of the HV of pedestrian fatalities, as compared to other categories. Besides the category, the specific regression equations, odd's ratio, helps in understanding as how each category impacts pedestrian fatalities as compared to other categories. For instance, from the odd's ratio table is observed that chance of pedestrian crashes increases 2.44 times when the HV hits a pedestrian as compared to the 2W. Similarly, when the 4W hits a pedestrian as compared to the 3W, the probability of death increases 1.23 times. Similarly, 1 km/h increase in the 85th percentile speed, increases the probability of pedestrian deaths by 1.073 times. Next boosted tree model is developed, whose accuracy of predicting injury correctly is 95% and deaths is 71%. The boosted tree employs 3 splits, based on data of each layer, to improve the accuracy denoting that more the data points, the better shall be the accuracy of the developed model. Dynamic prediction profilers, utilizing the change in accused category and the 85th percentile speed, are very helpful to understand the pedestrian fatality rates microscopically. For instance, the probability of pedestrian fatality is almost 0 for the 2W and 3W, when the speed is 40 km/h with around 0.4 for the 4W and HV. At 70 km/h the probability of pedestrian fatality is 0.997, irrespective of category of vehicles. Boosted tree's model is developed with 60% contribution of speed and 40% contribution of category of the accused vehicle. The model identifies that for a speed of around 40 km/h to 50 km/h, the pedestrian crash with the 2W and 3W have very less chance of fatality; whereas the higher speeds increase the probability of fatalities exponentially.

The predicted models can be used to predict the road crashes with great accuracy. The results of the present study should be useful for analyzing the pedestrian safety on any road. Utilizing the composition of a vehicle and the average 85th percentile speed, at any traffic facility, the probability of pedestrian fatality can be obtained using the boosted trees model. Based on the obtained pedestrian fatality probabilities, different strategies, like all red time at intersections or pedestrian foot over bridge at mid-block sections, can be planned and executed to reduce the pedestrian crashes and deaths.

Acknowledgement

The authors would like to thank the Traffic Police Authorities, Visakhapatnam City, Andhra Pradesh, India for providing the dataset used in this study. All opinions and results are those of the authors.

Conflicts of interest

The authors declare that they have no known competing financial interests or personal relationships that could have appeared to influence the work reported in this paper.

References

[1] GUANGXIN, L., KEPING, L. Pedestrian's psychology on gap selecting when crossing street. In: 2nd International Conference on Transportation Engineering ICTE 2009: proceedings [online]. ASCE. 2009. ISBN 9780784410394, p. 2138-2144. Available from: https://doi.org/10.1061/41039(345)354

[2] Road traffic injuries - WHO [online]. 2021. Available from: https://www.who.int/news-room/fact-sheets/detail/road-traffic-injuries/

[3] Road accidents in India - MORTH [online]. 2019. Available from: https://morth.nic.in/sites/default/files/RA_Uploading.pdf

[4] AL-AZZAWI, M., RAESIDE, R. Modeling pedestrian walking speeds on sidewalks. *Journal of Urban Planning and Development* [online]. 2007, **133**(3), p. 211-219. ISSN 0733-9488, eISSN 1943-5444. Available from: https://doi.org/10.1061/(ASCE)0733-9488(2007)133:3(211)

[5] RASTOGI, R., THANIARASU, I., CHANDRA, S. Design implications of walking speed for pedestrian facilities. *Journal of Transportation Engineering* [online]. 2011, **137**(10), p. 687-696. ISSN 2473-2907, eISSN 2473-2907. Available from: https://doi.org/10.1061/(ASCE)TE.1943-5436.0000251

[6] MUKHERJEE, D., MITRA, S. A comparative study of safe and unsafe signalized intersections from the viewpoint of pedestrian behavior and perception. *Accident Analysis and Prevention* [online]. 2019, **132**, 105218. ISSN 0001-4575, eISSN 1879-2057. Available from: https://doi.org/10.1016/j.aap.2019.06.010

[7] CHAUDHARI, A., GORE, N., ARKATKAR, S., JOSHI, G., PULUGURTHA, S. Exploring pedestrian surrogate safety measures by road geometry at midblock crosswalks: a perspective under mixed traffic conditions. *IATSS Research* [online]. 2021, **45**(1), p. 87-101. ISSN 0386-1112, eISSN 0386-1112. Available from: https://doi.org/10.1016/j.iatssr.2020.06.001

[8] KIM, D. The transportation safety of elderly pedestrians: Modeling contributing factors to elderly pedestrian collisions. *Accident Analysis and Prevention* [online]. 2019, **131**, p. 268-274. ISSN 0001-4575, eISSN 1879-2057. Available from: https://doi.org/10.1016/j.aap.2019.07.009

[9] MOHANTY, M., PANDA, R., GANDUPALLI, S. R., ARYA, R. R., LENKA, S. K. Factors propelling fatalities during road crashes: a detailed investigation and modelling of historical crash data with field studies. Heliyon [online]. 2022, 8(11), e11531. eISSN 2405-8440. Available from: https://doi.org/10.1016/j.heliyon.2022.e11531

[10] MOHANTY, M., PANDA, R., GANDUPALLI, S. R., SONOWAL, D., MUSKAN, M., CHAKRABORTY, R., DANGETI, M. R. Development of crash prediction models by assessing the role of perpetrators and victims: a comparison of ANN and logistic model using historical crash data. *International Journal of Injury Control and Safety Promotion* [online]. 2022, latest articles, p. 1-17, Available from: https://doi.org/10.1080/17457300.2022.2089899

[11] KUMAR, K. P., KUMAR, M. U., SEKHAR, V. C., KRISHNA, P. R. Analysis of pedestrian deaths in road traffic accidents-an autopsy based study in Visakhapatnam. *East African Scholars Journal of Medical Sciences* [online]. 2019, **2**(2), p. 74-79. ISSN 2617-4421, eISSN 2617-7188. Available from: https://doi.org/10.36349/easms.2019.v02i02.006

[12] LEE, C., LI, X. Predicting driver injury severity in single-vehicle and two-vehicle crashes with boosted regression trees. *Transportation Research Record* [online]. 2015, **2514**(1), p. 138-148. ISSN 0361-1981, eISSN 2169-4052. Available from: https://doi.org/10.3141/2514-15

[13] ABDEL-ATY, M., ABDELWAHAB, H. Analysis and prediction of traffic fatalities resulting from angle collisions including the effect of vehicles' configuration and compatibility. *Accident Analysis and Prevention* [online]. 2004, **36**(3), p. 457-469. ISSN 0001-4575, eISSN 1879-2057. Available from: https://doi.org/10.1016/S0001-4575(03)00041-1

[14] HU, M., CAI, W. Analysis of lifeboat embarkation efficiency for cruise passengers under multiple scenarios. *Scientific Programming* [online]. 2022, **2022**, 5491621. ISSN 1058-9244, eISSN 1875-919X. Available from: https://doi.org/10.1155/2022/5491621

[15] TAMAKLOE, R., DAS, S., AIDOO, E. N., PARK, D. Factors affecting motorcycle crash casualty severity at signalized and non-signalized intersections in Ghana: insights from a data mining and binary logit regression approach. *Accident Analysis and Prevention* [online]. 2022, **165**, 106517. ISSN 0001-4575, eISSN 1879-2057. Available from: https://doi.org/10.1016/j.aap.2021.106517

[16] PANDE, A., ABDEL-ATY, M., DAS, A. A classification tree-based modeling approach for segment related crashes on multilane highways. *Journal of Safety Research* [online]. 2010, **41**(5), p. 391-397. ISSN 0022-4375, eISSN 1879-1247. Available from: https://doi.org/10.1016/j.jsr.2010.06.004

[17] MOHANTY, M., PANDA, B., DEY, P. P. Quantification of surrogate safety measure to predict severity of road crashes at median openings. *IATSS Research* [online]. 2021, **45**(1), p. 153-159. ISSN 0386-1112, eISSN 0386-1112. Available from: https://doi.org/10.1016/j.iatssr.2020.07.003

[18] WANG, J., MA, J., LIN, P., SARVI, M., LI, R. Pedestrian single file movement on stairway: Investigating the impact of stair configuration on pedestrian ascent and descent fundamental diagram. *Safety Science* [online]. 2021, **143**, 105409. ISSN 0925-7535, eISSN 1879-1042. Available from: https://doi.org/10.1016/j.ssci.2021.105409

[19] VEDAGIRI, P., PRAGNA, T. Evaluation of traffic safety at unsignalized intersection under mixed traffic conditions. In: Transportation Research Board 92nd Annual Meeting: proceedings. 2013. 13-4000.

[20] PUTHAN, P., LUBBE, N., SHAIKH, J., SUI, B., DAVIDSSON, J. Defining crash configurations for powered two-wheelers: comparing ISO 13232 to recent in-depth crash data from Germany, India and China. *Accident Analysis and Prevention* [online]. 2021, **151**, 105957. ISSN 0001-4575, eISSN 1879-2057. Available from: https://doi.org/10.1016/j.aap.2020.105957

[21] ANDERSON, J., HERNANDEZ, S. Heavy-vehicle crash rate analysis: comparison of heterogeneity methods using Idaho crash data. *Transportation Research Record* [online]. 2017, **2637**(1), p. 56-66. ISSN 0361-1981, eISSN 2169-4052. Available from: https://doi.org/10.3141/2637-07

[22] PAN, Y., CHEN, S., QIAO, F., UKKUSURI, S. V., TANG, K. Estimation of real-driving emissions for buses fueled with liquefied natural gas based on gradient boosted regression trees. *Science of the Total Environment* [online]. 2019, **660**, p. 741-750. ISSN 0048-9697, eISSN 1879-1026. Available from: https://doi.org/10.1016/j.scitotenv.2019.01.054

komunikácie
COMMUNICATIONS

VEDECKÉ LISTY ŽILINSKEJ UNIVERZITY
SCIENTIFIC LETTERS OF THE UNIVERSITY OF ŽILINA

ISSN (print version): 1335-4205

ISSN (online version): 2585-7878

is indexed / abstracted / accepted in

- CEEOL
- CLOCKSS
- Crossref (DOI)
- digitálne pramene
- DOAJ
- EBSCO Host
- Electronic Journals Library (EZB)
- ERIH Plus
- Google Scholar
- Index Copernicus International Journals Master list
- iThenticate
- JournalGuide
- Jouroscope
- Norwegian Register for Scientific Journals Series and Publishers
- Portico
- ROAD
- ScienceGate
- SCImago Journal & Country Rank
- SciRev
- SCOPUS
- WorldCat (OCLC)

Journal Komunikácie - vedecké listy Žilinskej univerzity v Žiline / Communications - Scientific Letters of the University of Žilina is under evaluation for inclusion to **Web of Science** database.

ANALYSIS OF TERRAIN MODELLING METHODS IN THE COASTAL ZONE

Oktawia Lewicka

Department of Geodesy and Oceanography, Gdynia Maritime University, Gdynia, Poland and Marine Technology Ltd., Gdynia, Poland

E-mail of corresponding author: o.lewicka@wn.umg.edu.pl, o.lewicka@marinetechnology.pl

Oktawia Lewicka 0000-0002-0382-2793

Resume

Geospatial data are increasingly used to model the terrain in the coastal zone, in particular in shallow waterbodies (with a depth of up to 1 m). In order to generate a terrain relief, it is important to choose a method for its modelling that will allow it to be accurately projected. Therefore, the aim of this publication is to analyze the terrain modelling methods in the coastal zone. For the purposes of the research, five most popular methods for terrain modelling were described: Inverse Distance Weighted (IDW), Modified Shepard's Method (MSM), Natural Neighbor Interpolation (NNI), kriging and spline. Each of the methods has been described in a uniform way in terms of: the essence of its operation, mathematical expression and application examples. The advantages and disadvantages of each of the methods for terrain modelling are also discussed. It should be stated that the choice of the method for the terrain modelling of a shallow waterbody is not unambiguous, as it depends on the type of data recorded during bathymetric and photogrammetric measurements.

Article info

Received 29 December 2022
Accepted 28 February 2023
Online 6 April 2023

Keywords:

terrain modelling
coastal zone
inverse distance weighted (IDW)
modified shepard's method (MSM)
natural neighbor interpolation (NNI)
kriging
spline

Available online: https://doi.org/10.26552/com.C.2023.041

ISSN 1335-4205 (print version)
ISSN 2585-7878 (online version)

1 Introduction

Geodetic and hydrographic measurements are increasingly carried out by Unmanned Aerial Vehicles (UAV), Unmanned Surface Vehicles (USV) or Terrestrial Laser Scanners (TLS) [1-3]. The use of these modern methods in coastal zone measurements enables the acquisition of high-quality bathymetric data. However, these data do not cover the total area of the seabed [4]. For this reason, data interpolation methods, which create Digital Terrestrial Models (DTM), are used [5]. Hence, it is important to know that the creating of a DTM is a multi-stage process (Figure 1).

Creation of a DTM requires prior data collection. In addition to the above-mentioned measurement equipment, the following measurement methods are used to obtain the land surface geospatial data:

- Direct field measurements - they consist of the position survey or height of objects in the field. Currently, modern electronic total stations and Global Positioning System (GPS) receivers are used for direct measurements. The data obtained by the direct method are characterized by high accuracy. However, a direct field survey is time-consuming and thus provides small amount of data [6-8];
- Photogrammetric measurements - a measurement method consisting in recreating a ray going from the camera lens to the select point using a camera. Surveys provide information about the shape of the object and its position in relation to other objects in space [9]. UAVs equipped with cameras are increasingly used to take photogrammetric images. Moreover, photogrammetric data can be derived from aerial or satellite images [10-11];
- Bathymetric measurements - they consist of obtaining the processed data on the depth distribution in a waterbody. Bathymetric measurements are usually performed using a Single Beam Echo Sounder (SBES) or a MultiBeam Echo Sounder (MBES). A limitation of the measurement method using a SBES is the lack of depth data between profiles [12-13];
- Map vectorization - consists of converting the raster data into vector data. Map vectorization can

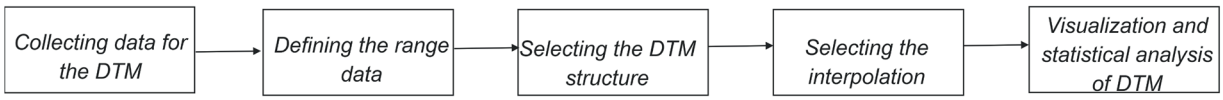

Figure 1 *A diagram showing the stages in creating a DTM*

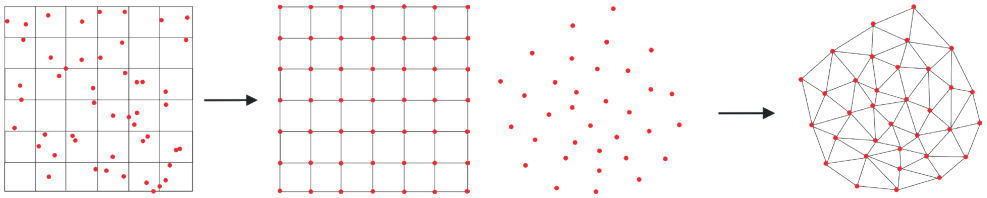

(a) *(b)*

Figure 2 *A diagram showing the structure of a GRID (**a**) and a TIN (**b**)*

be performed using the Geographic Information System (GIS) software, e.g. ArcGIS, GeoMedia or QGIS. The data acquired by this method are affected by errors associated with coordinate transformation [14-15];

- Laser scanning measurements - surveys in which the system measures the distance and the angle between the instrument and the surface being measured [16]. Laser scanning surveys can be performed using either Airborne Lidar Bathymetry (ALB) or Terrestrial Laser Scanning (TLS). Data obtained from the laser scanning are characterized by high accuracy [17-18];
- Interferometric Synthetic Aperture Radar (InSAR) - a method that measures the spatial extent and magnitude of surface deformation. It is a remote sensing method that uses the phase difference between the two complex radar SAR observations of the same area, taken from slightly different sensor positions [19-20].

The next stage in creating the model is to define the data range. An important aspect of data preparation is their density and distribution. Therefore, it is to be expected that data distributed unevenly due to interpolation will create a DTM that will not faithfully reproduce the surface.

Subsequently, the method of DTM representation, i.e. the structure of the model, is determined. The following ways of representing a DTM are distinguished [21]:

- A regular square grid (GRID) (Figure 2a) - a form of DTM representation, in the shape of a squares grid that covers an area evenly. The GRID models are created through interpolation, i.e. estimating an unknown value based on known values and specific interpolation methods. Next, the GRID nodes are created, which form a structure of regular rectangles (usually squares) with a determined resolution;
- Triangulated Irregular Network (TIN) (Figure 2b) - a form of DTM representation, in the shape of an irregular network of triangles. The TIN structure is formed by adjacent triangles whose vertices are located at the real measurement points. These points should be relatively evenly distributed for a network comprising triangles with similar shapes to be created. Where a surface is covered with measurement points unevenly (in a dispersed or linear manner), elongated triangles with no regular shapes will be formed.

After choosing the DTM representation structure, the data interpolation method needs to be selected, which is the most important stage in creating a digital terrain model. As regards the interpolation methods, the two main groups of spatial models can be distinguished:

- Deterministic models - values are determined based on the distance or area function. The deterministic models include, among others the Inverse Distance Weighted (IDW), polynomial and spline [22];
- Statistical models - values are determined based on the probability theory. The statistical methods include kriging and regression models.

The final stage of work is the visualization of the DTM. Additionally, it is recommended that an assessment of accuracy of the generated models be conducted using typical accuracy measures [23]: Root Mean Square Error (RMSE) [24], Mean Absolute Error (MAE) [25] and the coefficient of determination (R^2).

The terrain modelling methods have found applications in many scientific fields. In geology, the interpolation methods are used, e.g. to model geological [26] and geomorphological processes [1], as well as geological structures [27]. It is also worth noting the fact that the interpolation methods can be used to create Electronic Navigational Charts (ENC), which contain a detailed description of hydrographic structures and waterbody depths. In addition, they are the basic source of information in marine navigation [28].

However, a DTM has a particular application in the coastal zone. A model generated in this area enables the study of oceanographic phenomena and processes, as well as modelling of coastline changes. Nevertheless, it poses a research problem of selecting the most accurate method for modelling the surface in the coastal zone.

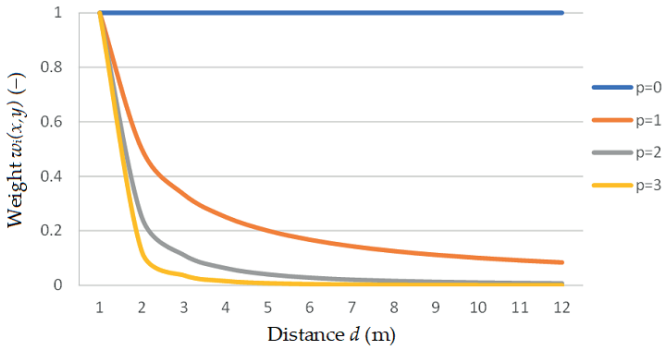

Figure 3 *A diagram showing the relationship between the weight $w_i(x,y)$ with the exponent p and the distance d*

Therefore, it was decided to characterize popular data interpolation methods.

The paper consists of three sections. The first section (Introduction) provides a detailed description of the stages in creating a DTM. The second section (Interpolation methods) presents five most popular methods for terrain modelling: IDW, Modified Shepard's Method (MSM), Natural Neighbor Interpolation (NNI), kriging and spline. Each of the methods has been described in a uniform way in terms of: the essence of its operation, mathematical expression and application examples. The publication concludes with Conclusions, which sum up the methods described.

2 Interpolation methods

2.1 IDW

The most commonly used deterministic model in spatial interpolation is the IDW method, which involves the estimation of the value being interpolated by calculating a weighted average from the values located at a specific distance from the point being interpolated [29].

The height value of the interpolated point by the IDW method can be calculated using the following formula [30]:

$$z_{IDW}(x,y) = \frac{\sum_{i}^{n} w_i(x,y) \cdot z_i}{\sum_{i}^{n} w_i(x,y)}, \tag{1}$$

where:
$z_{IDW}(x,y)$ - height value of the interpolated (unknown) point by the IDW method (m);
x, y - easting and northing of the interpolated (unknown) point (m);
n - number of interpolating (known) points (-);
i - numbering representing successive interpolating (known) points (-);
$w_i\ (x,y)$ - weight value of the i-th point in the IDW method (-);
z_i - height value of the i-th point (m).

However, the weight values are inversely proportional to the distance between the interpolated (unknown) point and the interpolating (known) point [31]:

$$w_i(x,y) = \frac{1}{[d_i(x,y)]^p}, \tag{2}$$

where:
p - exponent (-);
$d_i(x,y)$ - actual distance between the interpolated (unknown) point and the i-th point, defined as follows (m):

$$d_i(x,y) = \sqrt{(\Delta x_i)^2 + (\Delta y_i)^2} = \sqrt{(x - x_i)^2 + (y - y_i)^2} \tag{3}$$

where:
x_i, y_i - easting and northing of the i-th point (m).

A factor affecting the shape of the surface being modelled is dependent on the value of the exponent p. Application of the exponent p as the weight function is referred to in the literature as the Inverse Distance to a Power (IDP) method [32-33]. Usually, a basic exponent value of p = 2 or p = 3 is applied. However, application of these exponents does not always result in representation of the actual surface. Based on the weight function, it can be concluded that it decreases with an increase in distance. An increased exponent results in the weight decreasing its value (Figure 3) [34].

Another parameter that has an effect on the surface mapping is the smoothing parameter. The modified IDW method, to include the smoothing parameter, is as follows [35]:

$$z'_{IDW}(x,y) = \frac{\sum_{i}^{n} \frac{1}{[d_i(x,y) + \sigma]^p} \cdot z_i}{\sum_{i}^{n} \frac{1}{[d_i(x,y) + \sigma]^p}}, \tag{4}$$

where:
σ - smoothing parameter (m).

A high value of the smoothing parameter σ results in the target interpolating value having less influence on the interpolated value. Moreover, in order to smooth

the modelled surface, independent smoothing methods are used [36].

The next additional parameter in the modified IDW method is the effective distance. It is used when the phenomenon of anisotropy is considered in the data interpolation procedure. This phenomenon involves a change in properties of an object depending on the direction of observation of a particular feature. This means that values of the interpolating data change depending on the direction under consideration [37].

In the modified IDW method, which considers the phenomenon of anisotropy, the actual distance is replaced by the effective distance [38]. The modified IDW method can be written using Equation (4). However, the distance between the measurement point and the interpolated point has the following form [35, 39]:

$$d_i'(x,y) = \sqrt{\begin{matrix} A_{xx}\cdot(\Delta x_1)^2 + A_{xy}\cdot\Delta x_i\cdot\Delta y_i + \\ + A_{yy}\cdot(\Delta y_i)^2 \end{matrix}}, \tag{5}$$

where:
$d_i'(x,y)$ - effective distance between the interpolated (unknown) point and the i-th point (m).

The unknown parameters in the formula for the effective distance are determined as follows [35, 39]:

$$A_{xx} = \sin^2(\theta) + \frac{\cos^2(\theta)}{\rho^2}, \tag{6}$$

$$A_{xy} = 2\cdot\left[\frac{\sin(\theta)\cdot\cos(\theta)}{\rho^2} - \sin(\theta)\cdot\cos(\theta)\right], \tag{7}$$

$$A_{yy} = \frac{\sin^2(\theta)}{\rho} + \cos^2(\theta), \tag{8}$$

where:
θ - anisotropy angle (°);
ρ - anisotropy ratio (-).

It should be noted that an anisotropy ratio value smaller than 2 has no significant impact on interpolation, while a ratio value greater than 4 has such an impact.

The IDW method, along with its numerous modifications, is the most commonly used method for modelling phenomena and surfaces. It has found application in many areas of scientific research, particularly in the coastal zone modelling. An example is a study presented in [31], which created a DTM of the coastal zone by the IDW method. Moreover, the generated models enabled a geospatial analysis of the tombolo phenomenon in a waterbody adjacent to the beach in the city of Sopot. It should be noted that the IDW method was applied without using additional parameters, such as the anisotropy, exponent and smoothing. On the other hand, the depth data were derived from the SBES and the data from ENC cells were used.

Another example of the IDW application is described in a publication by Maleika [36]. The method was tested on data from an MBES, and its parameters were modified in terms of accuracy. A research problem in this study was the density of the data being entered into the IDW method, as having too many measurement points during the interpolation increases the model error and significantly increases the computation time. Therefore, based on different modifications of the IDW method, it was determined that the best results were obtained for 5-8 measurement points located within a radius of 0.6 m. Based on a study by Maleika [36], it should be concluded that the IDW method enables the modification of parameters, which translates into the method fitting to obtain the best results. The next example of the IDW application is presented in an article by Lubczonek et al. [1]. It is noteworthy that the IDW method was applied to data derived from an UAV and an USV. The integration of the data derived from these two systems enabled creation of a model of a bathymetric surface extending to the coastline.

2.2 MSM

The MSM method is another modification of the IDW method. It appears in the literature as an independent numerical method, which is why it was decided to characterize it in a separate subsection. The method was developed to reduce the expressive local values, which result in the so-called bull's-eye or the butterfly shape. The MSM method was developed by Shepard in 1968 [40] and implemented in studies by Franke and Nielson [41], Renka [42] and Basso et al. [43].

The MSM function has the following equation [42-44]:

$$z_{MSM}(x,y) = \frac{\sum_i^n w_i'(x,y)\cdot Q_i(x,y)}{\sum_i^n w_i'(x,y)}, \tag{9}$$

where:
$z_{MSM}(x,y)$ - height value of the interpolated point by the MSM method (m);
$w_i'(x,y)$ - weight value of the i-th point in the MSM method (-);
$Q_i(x,y)$ - bivariate quadratic function of the i-th point (-).

The bivariate quadratic function is the second-degree polynomial with one or more variables, which is calculated by the least squares method for the selected reference points [45]:

$$\begin{matrix} Q_i(x,y) = a\cdot(x-x_i) + b\cdot(y-y_i) + c\cdot(x-x_i)^2 + \\ + d\cdot(y-y_i)^2 + e\cdot(x-x_i)\cdot(y-y_i) + f, \end{matrix} \tag{10}$$

where:
a, b, c, d, e - numerical coefficients (-);
f - constant of the quadratic function (-).

The polynomial function $Q_i(x,y)$ describes a quadratic surface [46], which is a conic section. Depending on the coefficients a, b, c, d, e and f, the conic section is a circle, ellipse, hyperbola, parabola, point or two straight lines.

It should be noted that the second-degree polynomial $Q_i(x,y)$ is solved by the least squares method [47]. The use of this method allows the data to be fitted to the conic section. The least squares method is used to determine a conic section for which the sum of squared errors will be the smallest, and thus the sum of distances of all points from the conic section will be minimum.

The weight function, as suggested by Franke and Nielson [41], has the following form:

$$w_i'(x,y) = \left[\frac{(R_w - d_i(x,y))_+}{R_w \cdot d_i(x,y)}\right]^2 \text{ for } (R_w - d_i(x,y))_+ = \begin{cases} R_w - d_i(x,y) & if \quad d_i(x,y) < R_w \\ 0 & if \quad d_i(x,y) \geq R_w \end{cases}, \tag{11}$$

where:
R_w - radius of influence around the i-th point (m).

In the modified IDW method with the radius parameter, in the weight function [48], the radius value determines the decrease in the weight with an increasing radius R_w. The radius R_w, exactly like the exponent used in the IDW method, enables the smoothing of the modelled surface. Moreover, an accurate representation of the surface is obtained for the coefficient R_w equal to the distance from the furthest interpolating point [34].

Derivation of the second-degree equation to the IDW results in an unrealistic landform on the edges. This is due to the merging of extreme points on the interpolated area edges that does not refer to the overall variability trend. Consequently, the MSM method smooths surfaces, thus eliminating outliers.

The MSM method was compared to the IDW method in [44]. The methods were applied to a small data set. The input data for the models included the permeability, porosity and thickness of the Neogene hydrocarbon sandstone reservoirs in northern Croatia. The cross-validation results proved that the MSM method could be recommended for geological mapping of the Neogene deposits. Moreover, the MSM method eliminated all unwanted geological features in the model.

2.3 NNI

The simplest approach to interpolation was applied in the NNI method. This method was introduced for the first time by Sibson [49] as a weighted average weighted interpolation method. Additionally, research concerning the structure and properties of the method are described in studies by Farin [50] and Piper [51].

The height value of the interpolated point by the NNI method can be calculated using the following formula [52]:

$$z_{NNI}(x,y) = \sum_j^m w_j(x,y) \cdot z_j\,, \tag{12}$$

where:
$z_{NNI}(x,y)$ - height value of the interpolated (unknown) point by the NNI method (m);
m - number of neighboring points (-);
j - numbering representing successive neighboring points (-);
$w_j(x,y)$ - weight value of the j-th point in the NNI method (-);
z_j - height value of the j-th point (m).

The weight value according to Sibson [49, 53] is the quotient of the stolen area of the j-th Voronoi cell [54] for the whole area of the new Voronoi cell [55]:

$$w_j(x,y) = \frac{S_j}{S}\,, \tag{13}$$

where:
S_j - stolen area of the j-th Voronoi cell (m²);
S - whole area of the new Voronoi cell (m²).

Using the previous Equations (12) and (13), the following equation was obtained:

$$z_{NNI}(x,y) = \sum_j^m \frac{S_j}{S} \cdot z_j\,. \tag{14}$$

It should be noted that the Voronoi diagram method [56] consists in a creation of irregular polygons based on the analyzed points and then entering of the corresponding point value into each polygon. In the literature, this method is also referred to as Thiessen diagrams or polygons. This is due to the fact that the article published in 1911 by an American meteorologist Alfred H. Thiessen proposed a method for determining the average amount of precipitation over the study area [57-58]. This method used the same polygons for the calculations as Voronoi diagram method.

The procedure for constructing the Voronoi diagram consists of the following stages (Figure 4) [59]:

A. Selection of measurement points for the construction the Voronoi diagram;

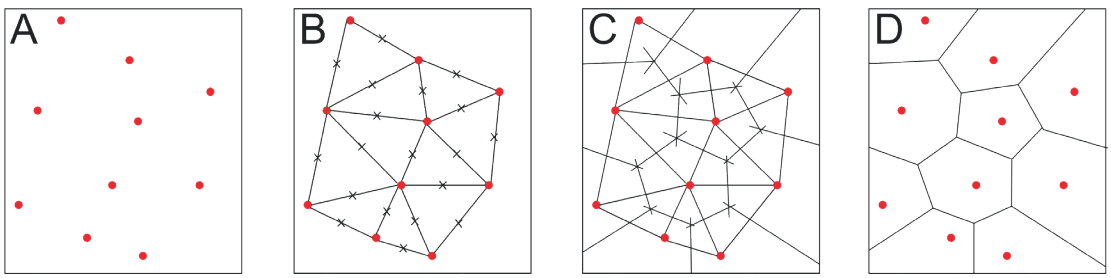

Figure 4 *The process of creating the Voronoi diagram [59]*

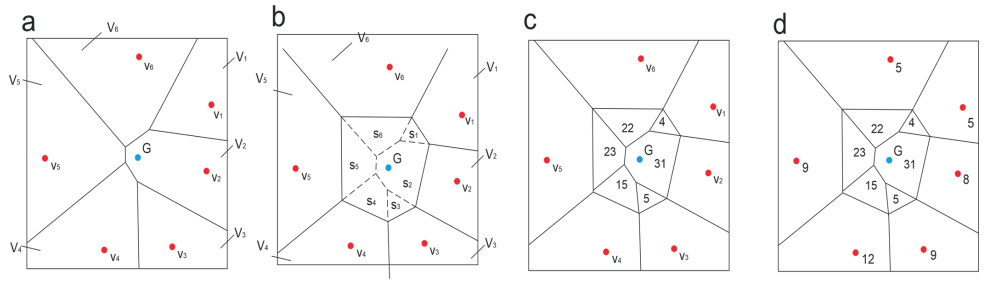

Figure 5 *A diagram showing the constructions and calculations for the NNI method based on the example from [60]*

B. Determination of sections between the most closely located points;
C. Drawing perpendicular bisectors for each section;
D. Connecting each of the points where the three bisectors intersect.

On the other hand, the diagram of the interpolation procedure by the NNI method is as follows (Figure 5):

a. Creation of the Voronoi diagram for all the measurement points;
b. Creation of the Voronoi diagram for the point G being interpolated;
c. Determination of the proportion of particular polygons S_1, S_2, S_3, S_4, S_5, S_6 for the polygon G;
d. Calculation of the height value for the point G by the NNI method using Equation (13).

Based on the presented diagrams and equations, it can be concluded that this is a not very complicated method, which means that it can be easily implemented. Moreover, the method is mainly based on forming of a network of triangles by the Voronoi method, which is created locally in relation to the interpolating point. Unlike the other methods, the NNI method has no global data structure and only uses the data which are adjacent to the interpolated value. Therefore, the NNI method can be used for unevenly distributed data. This is confirmed by research conducted in [61]. The NNI method has proven to be more accurate than the IDW, kriging or spline methods.

2.4 Kriging

Geostatistical methods are based on finding a function which determines the similarity of points based on the mutual relationships occurring between them. One such method is kriging. This method was originally developed by Krige [62] for the purposes of a Master's degree thesis, in which he tried to estimate the most likely distribution of gold based on samples from a few boreholes. On the other hand, the theoretical foundations of this method were published by Matheron [63]. Nevertheless, it is Danie Gerhardus Krige who is considered the forerunner of the method.

The function interpolating by the kriging method has the form of the following equation [64]:

$$z_{KR}(x,y) = \sum_{i}^{n} w_i''(x,y) \cdot z_i \,, \tag{15}$$

where:
$z_{KR}(x,y)$ - height value of the interpolated point by the kriging method (m);
$w_i''(x,y)$ - weight value of the i-th point in the kriging method (-).

The kriging method consists of two stages. The first stage is to determine the spatial relationship between these data. In order to describe the spatial variability of the data, the kriging method usually uses half of the variogram, i.e. the so-called semivariogram, which is a graph showing the semivariance values as a function of distance. Therefore, before creating a semivariogram, semivariances need to be calculated for the interpolating points.

Semivariance is a measure that enables determination of the spatial autocorrelation, found in a particular set, i.e. the relationship between the values of a single feature that changes with the distance. This is half of the mean square of the difference between the values of the examined variable at two locations distant by the vector h [65]:

$$\gamma^*(h) = \frac{1}{2 \cdot N(h)} \sum_{i=1}^{N(h)} [z(x_i) - z(x_i + h)]^2 \,, \tag{16}$$

where:
$\gamma^*(h)$ - semivariance value calculated for distance h (m²);
$N(h)$ - number of paired data at a distance of h (-);
$z(x_i)$, $z(x_i+h)$ - height values at a particular location (m);
h - 3D Euclidean distance between the two interpolating points (m).

Once the semivariance has been calculated, the experimental semivariogram can be plotted (Figure 6) to represent the interpolating data on the semivariance graph as a function of distance.

A theoretical semivariogram must then be fitted to the experimental semivariogram (Figure 6) in such a manner that it best represents the empirical model. It should be noted that the best results of the interpolated values depend on the establishment of a correct semivariogram. Selected theoretical semivariogram models are described below and presented in Figure 7.

The spherical model has the form of [67]:

$$\gamma(h) = \begin{cases} C_0 + C_1 \cdot \left[\frac{3}{2} \cdot \left(\frac{h}{g} \right) - \frac{1}{2} \cdot \left(\frac{h}{g} \right)^3 \right] & h \le g \\ C_0 + C_1 & h > g \end{cases}, \tag{17}$$

Gaussian model [65]:

$$\gamma(h) = C_0 + C_1 \cdot \left[1 - e^{\left(\frac{-3 \cdot h^2}{g^2}\right)}\right], \quad (18)$$

while the linear model [65]:

$$\gamma(h) = C_0 + C_1 \cdot \left(\frac{h}{g}\right), \quad (19)$$

where:
$\gamma(h)$ - theoretical semivariogram model for distance h (m^2);

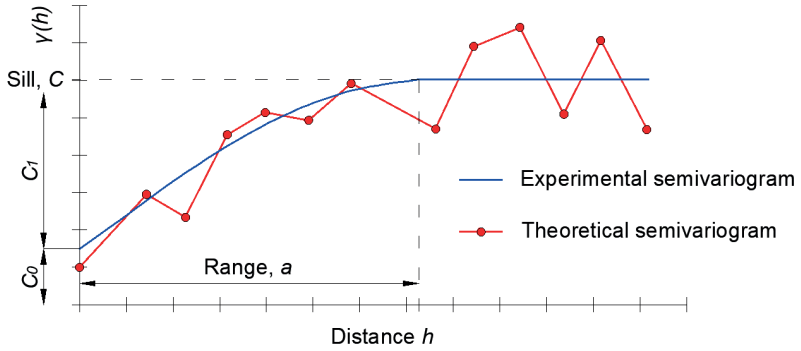

Figure 6 *A graph showing the experimental semivariogram along with the fitted theoretical semivariogram [66]*

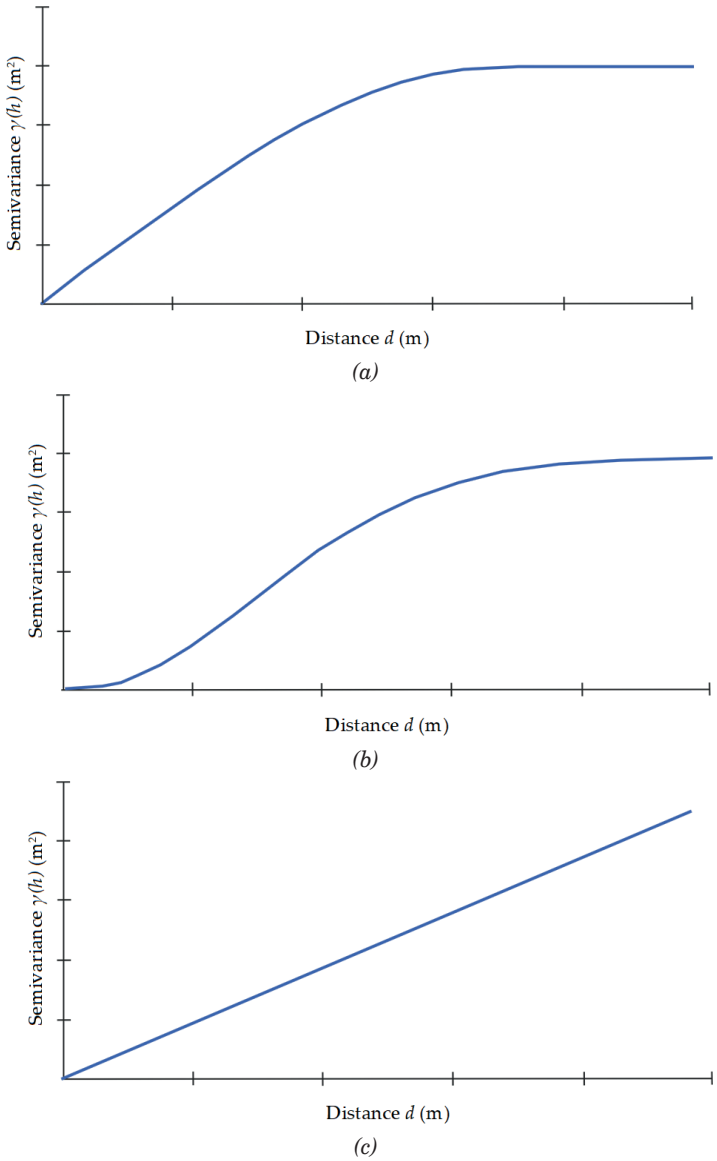

Figure 7 *Examples of the commonly used theoretical semivariogram models: spherical (**a**), Gaussian (**b**) and linear (**c**) [65]*

C_0, C_1 - nugget (unaccountable) and stochastic (accountable) variance (m²);
g - range of influence (m).

The second stage of the work concerns the calculation of the weights $w_i''(x,y)$. Based on the conducted analyses of the other interpolation methods, it must be concluded that the interpolation formula of the kriging method is similar to the IDW formula. Their similarity is due to the fact that the values assigned to the nearest point being interpolated are weighted. However, not only that the weights (referred to as kriging coefficients) are based on the distance between points, but on their spatial distribution, as well. These are determined from a set of equations resulting from the condition of minimizing error variance. This error (referred to as the kriging variance) is defined at measurement points as the difference between the interpolated value and the measurement value [68]:

$$\begin{bmatrix} \gamma(h_{11}) & \gamma(h_{12}) & \vdots & \gamma(h_{1n}) & 1 \\ \gamma(h_{21}) & \gamma(h_{22}) & \vdots & \gamma(h_{2n}) & 1 \\ \cdots & \cdots & \vdots & \cdots & \cdots \\ \gamma(h_{n1}) & \gamma(h_{n2}) & \vdots & \gamma(h_{nn}) & 1 \\ 1 & 1 & \vdots & 1 & 0 \end{bmatrix} \cdot \begin{bmatrix} w_1''(x,y) \\ w_2''(x,y) \\ \vdots \\ w_n''(x,y) \\ \lambda \end{bmatrix} = \begin{bmatrix} \gamma(h_1) \\ \gamma(h_2) \\ \vdots \\ \gamma(h_n) \\ 1 \end{bmatrix}, \quad (20)$$

where:
$\gamma(h_{ik})$ - semivariance between successive points i and k (m²);
$\gamma(h_i)$ - semivariance between the interpolated (unknown) point and the i-th point (m²);
λ - Lagrange multiplier (-).

Only after calculating the weights $w_i''(x,y)$ can one proceed to determine the values for the points being interpolated using Equation (15).

The kriging is among the most commonly used methods for interpolating geological parameters [69-71]. Geological measurements involve drilling the boreholes, as well as sampling soil and water at several locations. In most cases of interpolation methods, the generated model is inaccurate due to the small amount of data. Nevertheless, the kriging method is more effective for a smaller number of measurement points. This is primarily due to the possibility of the interpolation error in the model. However, it should be noted that in this method, not only that the results are determined by the number of measurement points but by the experimental semivariogram parameters and the mathematical model fitting, as well.

Moreover, this method is among the most accurate methods for creating a DTM [72-73]. This is evidenced by a study conducted by [74], who performed interpolation of the data derived from a SBES using different methods. The most accurate digital terrain model was obtained for the radial basis function and kriging methods.

2.5 Spline

Spline functions are an interpolation method used when the input data are diverse in terms of a particular feature. A DTM generated using spline functions is devoid of outliers. This results from the interpolation technique, which involves fitting the polynomial segment to the measurement data. The polynomials are created separately for each interval between the two successive points [75]. A fitted curve is continuous and smooth, i.e. it has a derivative at each point, which means that the slope of a curve on either side of the joining of two polynomials is the same.

Depending on the interpolation conditions and polynomial equations, there are various types of spline functions. However, the most well-known and common is the cubic spline interpolation [76-77]. A cubic spline is the function, which is a third-degree polynomial for each interval [78]:

$$f(x) = f_i(x) = A_i \cdot (x - x_1)^3 + B_i \cdot (x - x_i)^2 + \\ + C_i \cdot (x - x_i) + D_i \quad \text{for} \quad x_i \le x \le x_{i+1} \quad \text{and} \quad (21) \\ i \in \{0, \ldots, n-1\},$$

where:
$f(x)$ - cubic spline (-);
A_i, B_i, C_i, D_i - numerical coefficients of the i-th point (-).

A special case of the cubic spline is the so-called natural spline, which, additionally, satisfies the following condition:

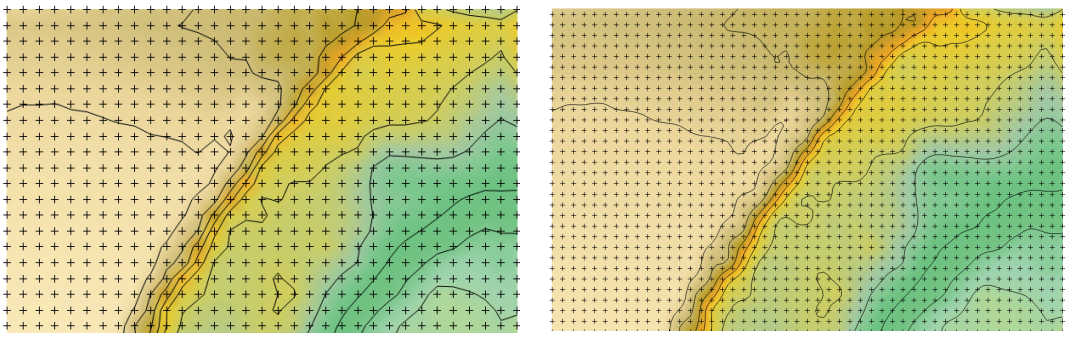

(a) *(b)*

Figure 8 *Isolines, the original surface (**a**) and its image after the spline smoothing (**b**)*

Table 1 *Summary of advantages and disadvantages of selected terrain modelling methods*

Terrain modelling method	Advantages	Disadvantages
IDW	Short computation time	It generates the so-called bull's-eye, i.e. concentric contours around measurement points
MSM	It receives similar results to those of the IDW but does not tend to generate the so-called bull's eye	Terrain deformations are formed
NNI	It receives good results for unevenly distributed data	It does not extrapolate the terrain relief
Kriging	It receives the best, non-affected linear estimations	Semivariogram modelling problem occurs
Spline	It forms a smooth surface	It is not suitable for points located close to each other and having different values

$$f''(x_0) = f''(x_n) = 0\,, \tag{22}$$

where:
$f''(x_0)$, $f''(x_n)$ - second derivatives of the cubic spline (-).

The literature and terrain modelling programs [79-80] mention the so-called smoothing spline. This method is based on the same definition of a spline function as that in Equation (21). The only modification is the values of the nodes. Each point (x_i, y_i) is replaced with a node (x_i, D_i).

Spline smoothing is a method applied when a map in the form of curves includes contours and surfaces refracted at different angles. The method application increases the model grid density, which results in the smoothing of the sharp refract of the isolines, thus minimizing the surface curvature. As a result, the interpolated surface is smooth (Figure 8).

The spline method was applied to interpolate the sea surface temperature in the southern part of the Indian Ocean [81]. Moreover, the model generated by the spline method was compared to the models interpolated by the IDW, NNI and kriging methods. Based on the conducted analyses, all of the methods were found to have similar RMSE values. North and Livingstone [82] compared the two methods that rely on the fitting of a polynomial to data. The two-point linear interpolation and cubic spline interpolation were applied to interpolate water column profiles in a lake. The results of the study showed that both methods are suitable for interpolating the incomplete input data.

3 Conclusions

In the coastal zone monitoring studies, optoelectronic and hydroacoustic methods are used [83]. However, these methods do not ensure the coverage with data of the entire coastal zone. Therefore, the terrain modelling methods are used [84]. Moreover, the land surface modelling in the coastal zone deserves particular attention, as the accurately mapped surface in this area is a part of coastal monitoring.

This study provides an overview of the most important terrain modelling methods. In the future, these methods will be applied to the real data derived from the coastal zone. Therefore, before proceeding to the data processing stage, it was decided to describe the selected interpolation methods, important in terms of the coastal zone modelling, using equations. Moreover, examples of the use of methods were provided in various areas, e.g. geology and meteorology. Table 1 presents advantages and disadvantages of selected terrain modelling methods.

It should be noted that the general characteristics of the methods provide no information on the fit between the terrain modelling method and the phenomenon [85-87]. This is due to the fact that each phenomenon being interpolated is characterized by different spatial distribution of measurement points, resulting from the data acquisition method applied. Therefore, the statistical analyses should be carried out for characteristic data in the selected area.

Acknowledgement

This research was funded by the National Centre for Research and Development in Poland, grant number LIDER/10/0030/L-11/19/NCBR/2020. Moreover, this research was funded from the statutory activities of Gdynia Maritime University, grant number WN/PI/2023/03.

Conflicts of interest

The authors declare that they have no known competing financial interests or personal relationships that could have appeared to influence the work reported in this paper.

References

[1] LUBCZONEK, J., KAZIMIERSKI, W., ZANIEWICZ, G., LACKA, M. Methodology for combining data acquired by unmanned surface and aerial vehicles to create digital bathymetric models in shallow and ultra-shallow waters. *Remote Sensing* [online]. 2021, **14**(1), 105. eISSN 2072-4292. Available from: https://doi.org/10.3390/rs14010105

[2] SPECHT, C., LEWICKA, O., SPECHT, M., DABROWSKI, P., BURDZIAKOWSKI, P. Methodology for carrying out measurements of the tombolo geomorphic landform using unmanned aerial and surface vehicles near Sopot Pier, Poland. *Journal of Marine Science and Engineering* [online]. 2020, **8**(6), 384. eISSN 2077-1312. Available from: https://doi.org/10.3390/jmse8060384

[3] STATECZNY, A., WLODARCZYK-SIELICKA, M., GRONSKA, D., MOTYL, W. Multibeam echosounder and LiDAR in process of 360-degree numerical map production for restricted waters with HydroDron. In: 2018 Baltic Geodetic Congress Geomatics 2018: proceedings. 2018.

[4] SPECHT, M., STATECZNY, A., SPECHT, C., WIDZGOWSKI, S., LEWICKA, O., WISNIEWSKA, M. Concept of an innovative autonomous unmanned system for bathymetric monitoring of shallow waterbodies (INNOBAT system). *Energies* [online]. 2021, **14**(17), 5370. eISSN 1996-1073. Available from: https://doi.org/10.3390/en14175370

[5] LI, J., HEAP, A. D. Spatial interpolation methods applied in the environmental sciences: a review. *Environmental Modelling and Software* [online]. 2014, **53**, p. 173-189. ISSN 1364-8152, eISSN 1873-6726. Available from: https://doi.org/10.1016/j.envsoft.2013.12.008

[6] SPECHT, C., SPECHT, M., DABROWSKI, P. Comparative analysis of active geodetic networks in Poland. In: 17th International Multidisciplinary Scientific GeoConference SGEM 2017: proceedings [online]. 2017. ISBN 978-619-7408-02-7, ISSN 1314-2704, p. 163-176. Available from: https://doi.org/10.5593/sgem2017/22/S09.021

[7] SPECHT, C., SZOT, T., DABROWSKI, P., SPECHT, M. Testing GNSS receiver accuracy in Samsung Galaxy series mobile phones at a sports stadium. *Measurement Science and Technology* [online]. 2020, **31**, 064006. ISSN 0957-0233, eISSN 1361-6501. Available from: https://doi.org/10.1088/1361-6501/ab75b2

[8] SPECHT, C., WEINTRIT, A., SPECHT, M. A history of maritime radio-navigation positioning systems used in Poland. *The Journal of Navigation* [online]. 2016, **69**(3), p. 468-480. ISSN 0373-4633, eISSN 1469-7785. Available from: https://doi.org/10.1017/S0373463315000879

[9] HELLWICH, O. Photogrammetric methods. In: *Encyclopedia of GIS* [online]. SHEKHAR, S., XIONG, H., ZHOU, X. (Eds.). Cham, Switzerland: Springer Cham, 2017. ISBN 978-3-319-17884-4, eISBN 978-3-319-17885-1, p. 1574-1580. Available from: https://doi.org/10.1007/978-3-319-17885-1

[10] BURDZIAKOWSKI, P., BOBKOWSKA, K. UAV photogrammetry under poor lighting conditions - accuracy considerations. *Sensors* [online]. 2021, **21**(10), 3531. eISSN 1424-8220. Available from: https://doi.org/10.3390/s21103531

[11] WANG, X., LIU, Y., LING, F., LIU, Y., FANG, F. Spatio-temporal change detection of Ningbo coastline using Landsat time-series images during 1976-2015. *ISPRS International Journal of Geo-Information* [online]. 2017, **6**(3), 68. eISSN 2220-9964. Available from: https://doi.org/10.3390/ijgi6030068

[12] NIKOLAKOPOULOS, K. G., LAMPROPOULOU, P., FAKIRIS, E., SARDELIANOS, D., PAPATHEODOROU, G. Synergistic use of UAV and USV data and petrographic analyses for the investigation of beach rock formations: a case study from Syros Island, Aegean Sea, Greece. *Minerals* [online]. 2018, **8**(11), 534. eISSN 2075-163X. Available from: https://doi.org/10.3390/min8110534

[13] SPECHT, M., SPECHT, C., MINDYKOWSKI, J., DABROWSKI, P., MASNICKI, R., MAKAR, A. Geospatial modeling of the tombolo phenomenon in Sopot using integrated geodetic and hydrographic measurement methods. *Remote Sensing* [online]. 2020, **12**(4), 737. eISSN 2072-4292. Available from: https://doi.org/10.3390/rs12040737

[14] DOUCETTE, P., AGOURIS, P., MUSAVI, M., STEFANIDIS, A. Road center line vectorization by self-organized mapping. *International Archives of Photogrammetry and Remote Sensing*. 2000, **XXXIII**(B3), p. 246-253. ISSN 1682-1750.

[15] WANG, C., HUANG, K., SHI, W. An accurate and efficient quaternion-based visualization approach to 2D/3D vector data for the mobile augmented reality map. *ISPRS International Journal of Geo-Information* [online]. 2022, **11**(7), 383. eISSN 2220-9964. Available from: https://doi.org/10.3390/ijgi11070383

[16] WILLIAMS, R., BRASINGTON, J., VERICAT, D., HICKS, M., LABROSSE, F., NEAL, M. Chapter twenty - monitoring braided river change using terrestrial laser scanning and optical bathymetric mapping. *Developments in Earth Surface Processes* [online]. 2011, **15**, p. 507-532. ISSN 0928-2025, eISSN 2213-588X. Available from: https://doi.org/10.1016/B978-0-444-53446-0.00020-3

[17] MARCHEL, L., NAUS, K., SPECHT, M. Optimisation of the position of navigational aids for the purposes of SLAM technology for accuracy of vessel positioning. *The Journal of Navigation* [online]. 2020, **73**(2), p. 282-295.

ISSN 0373-4633, eISSN 1469-7785. Available from: https://doi.org/10.1017/S0373463319000584
[18] SAYLAM, K., BROWN, R. A., HUPP, J. R. Assessment of depth and turbidity with airborne Lidar bathymetry and multiband satellite imagery in shallow water bodies of the Alaskan North Slope. *International Journal of Applied Earth Observation and Geoinformation* [online]. 2017, **58**, p. 191-200. ISSN 1569-8432, eISSN 1872-826X. Available from: https://doi.org/10.1016/j.jag.2017.02.012
[19] KETELAAR, V. B. H. (Gini). *Satellite radar interferometry* [online]. Dordrecht, Netherlands: Springer Dordrecht, 2009. ISBN 978-90-481-8125-4, eISBN 978-1-4020-9428-6. Available from: https://doi.org/10.1007/978-1-4020-9428-6
[20] SOLTANIEH, A., MACCIOTTA, R. Updated understanding of the Ripley landslide kinematics using satellite InSAR. *Geosciences* [online]. 2022, **12**(8), 298. eISSN 2076-3263. Available from: https://doi.org/10.3390/geosciences12080298
[21] VAN KREVELD, M. Digital elevation models and TIN algorithms. In: *Algorithmic foundations of geographic information systems* [online]. VAN KREVELD, M., NIEVERGELT, J., ROOS, T., WIDMAYER, P. (Eds.). Vol. 1340. Berlin, Heidelberg, Germany: Springer Berlin, Heidelberg, 1997. ISBN 978-3-540-63818-6, eISBN 978-3-540-69653-7, p. 37-78. Available from: https://doi.org/10.1007/3-540-63818-0_3
[22] MENG, Q., LIU, Z., BORDERS, B. E. Assessment of regression kriging for spatial interpolation - comparisons of seven GIS interpolation methods. *Cartography and Geographic Information Science* [online]. 2013, **40**(1), p. 28-39. ISSN 1523-040, eISSN 1545-0465. Available from: https://doi.org/10.1080/15230406.2013.762138
[23] GENCHI, S. A., VITALE, A. J., PERILLO, G. M. E., SEITZ, C., DELRIEUX, C. A. Mapping topobathymetry in a shallow tidal environment using low-cost technology. *Remote Sensing* [online]. 2020, **12**(9), 1394. eISSN 2072-4292. Available from: https://doi.org/10.3390/rs12091394
[24] PHAM, H. A new criterion for model selection. *Mathematics* [online]. 2019, **7**(12), 1215. eISSN 2227-7390. Available from: https://doi.org/10.3390/math7121215
[25] WILLMOTT, C. J., MATSUURA, K. Advantages of the mean absolute error (MAE) over the root mean square error (RMSE) in assessing average model performance. *Climate Research* [online]. 2005, **30**(1), p. 79-82. ISSN 0936-577X, eISSN 1616-1572. Available from: http://dx.doi.org/10.3354/cr030079
[26] CORTI, G., RANALLI, G., SOKOUTIS, D. Quantitative modelling of geological processes. *Tectonophysics* [online]. 2010, **484**(1-4), p. 1-3. ISSN 0040-1951, eISSN 1879-3266. Available from: https://doi.org/10.1016/j.tecto.2009.09.004
[27] TEOFILO, G., GIOIA, D., SPALLUTO, L. Integrated geomorphological and geospatial analysis for mapping fluvial landforms in Murge Basse Karst of Apulia (Southern Italy). *Geosciences* [online]. 2019, **9**(10), 418. eISSN 2076-3263. Available from: https://doi.org/10.3390/geosciences9100418
[28] LUBCZONEK, J., TROJANOWSKI, J., WLODARCZYK-SIELICKA, M. Application of threedimensional navigational information in electronic chart for inland shipping (in Polish). *Archives of Photogrammetry, Cartography and Remote Sensing*. 2012, **23**, p. 261-269. eISSN 2391-9477.
[29] LU, G. Y., WONG, D. W. An adaptive inverse-distance weighting spatial interpolation technique. *Computers and Geosciences* [online]. 2008, **34**(9), p. 1044-1055. ISSN 0098-3004, eISSN 1873-7803. Available from: https://doi.org/10.1016/j.cageo.2007.07.010
[30] LI, Z., WANG, K., MA, H., WU, Y. An adjusted inverse distance weighted spatial interpolation method. In: 3rd International Conference on Communications, Information Management and Network Security CIMNS 2018: proceedings [online]. 2018. ISSN 2352-538X. Available from: https://doi.org/10.2991/cimns-18.2018.29
[31] MAKAR, A., SPECHT, C., SPECHT, M., DABROWSKI, P., BURDZIAKOWSKI, P., LEWICKA, O. Seabed topography changes in the Sopot pier zone in 2010-2018 influenced by tombolo phenomenon. *Sensors* [online]. 2020, **20**(21), 6061. eISSN 1424-8220. Available from: https://doi.org/10.3390/s20216061
[32] BARTIER, P. M., KELLER, C. P. Multivariate interpolation to incorporate thematic surface data using inverse distance weighting (IDW). *Computers and Geosciences* [online]. 1996, **22**(7), p. 795-799. ISSN 0098-3004, eISSN 1873-7803. Available from: https://doi.org/10.1016/0098-3004(96)00021-0
[33] DAVIS, J. C. *Statistics and data analysis in geology*. 3. ed. Hoboken, NJ, USA: John Wiley & Sons, Inc., 2002. ISBN 978-0-471-17275-8.
[34] STATECZNY, A. *Comparative navigation methods* (in Polish). Gdansk, Poland: Gdansk Scientific Society, 2004. ISBN 83-87359-88-2.
[35] TOMCZAK, M. Spatial interpolation and its uncertainty using automated anisotropic inverse distance weighting (IDW) - cross-validation/jackknife approach. *Journal of Geographic Information and Decision Analysis*. 1998, **2**(2), p. 18-30. ISSN 1480-8943.
[36] MALEIKA, W. Inverse distance weighting method optimization in the process of digital terrain model creation based on data collected from a multibeam echosounder. *Applied Geomatics* [online]. 2020, **12**, p. 397-407. ISSN 1866-9298, eISSN 1866-928X. Available from: https://doi.org/10.1007/s12518-020-00307-6

[37] GOLDSZTEJN, P., SKRZYPEK, G. Applications of numeric interpolation methods to the geological surface mapping using irregularly spaced data (in Polish). *Polish Geological Review*. 2004, **52**, p. 233-236. ISSN 0033-2151.

[38] Surfer® user's guide - Golden software LLC [online] [accessed 2023-03-16]. Available from: https://downloads.goldensoftware.com/guides/Surfer20UserGuide.pdf

[39] PHOTHONG, T., DUMRONGCHAI, P., SIRIMONTREE, S., WITCHAYANGKOON, B. Spatial interpolation of unconfined compressive strength for soft Bangkok clay via random technique and modified inverse distance weight method. *International Transaction Journal of Engineering, Management, and Applied Sciences and Technologies* [online]. 2017, **8**(1), 13-22. ISSN 2228-9860, eISSN 1906-9642. Available from: http://TUENGR.COM/V08/013.pdf

[40] SHEPARD, D. A Two-dimensional interpolation for irregularly-spaced data. In: 23rd Association for Computing Machinery National Conference ACM 1968: proceedings [online]. 1968. p. 517-524. Available from: https://doi.org/10.1145/800186.810616

[41] FRANKE, R., NIELSON, G. Smooth interpolation of large sets of scattered data. *International Journal for Numerical Methods in Engineering* [online]. 1980, **15**(10), p. 1691-1704. eISSN 1097-0207. Available from: https://doi.org/10.1002/nme.1620151110

[42] RENKA, R. J. Multivariate interpolation of large sets of scattered data. *ACM Transactions on Mathematical Software* [online]. 1988, **14**(2), p. 139-148. ISSN 0098-3500, eISSN 1557-7295. Available from: https://doi.org/10.1145/45054.45055

[43] BASSO, K., DE AVILA ZINGANO, P. R., DAL SASSO FREITAS, C. M. Interpolation of scattered data: investigating alternatives for the modified Shepard method. In: 12th Brazilian Symposium on Computer Graphics and Image Processing: proceedings. 1999.

[44] MALVIC, T., IVSINOVIC, J., VELIC, J., SREMAC, J., BARUDZIJA, U. Application of the Modified Shepard's Method (MSM): a case study with the interpolation of neogene reservoir variables in Northern Croatia. *Stats* [online]. 2020, **3**(1), p. 68-83. eISSN 2571-905X. Available from: https://doi.org/10.3390/stats3010007

[45] JANKOVIC, V. Quadratic functions in several variables. *The Teaching of Mathematics* [online]. 2005, **VIII**(2), p. 53-60. ISSN 1451-4966, eISSN 2406-1077.

[46] ZEVENBERGEN, L. W., THORNE, C. R. Quantitative analysis of land surface topography. *Earth Surface Processes and Landforms* [online]. 1987, **12**(1), p. 47-56. eISSN 1096-9837. Available from: https://doi.org/10.1002/esp.3290120107

[47] SALKIND, N. *Encyclopedia of measurement and statistics* [online]. Vol. 2. Thousand Oaks, CA, USA: Sage Publications, 2007. ISBN 9781412916110, eISBN 9781412952644. Available from: https://doi.org/10.4135/9781412952644

[48] FRANKE, R. Scattered data interpolation: tests of some methods. *Mathematics of Computation* [online]. 1982, **38**(157), p. 181-200. ISSN 0025-5718. Available from: https://hdl.handle.net/10945/40152

[49] SIBSON, R. A Brief description of natural neighbor interpolation. In: *Interpreting multivariate data*. BARNETT, V. (Ed.). Hoboken, NJ, USA: John Wiley and Sons, Inc., 1981. ISBN 978-0471280392, p. 21-36.

[50] FARIN, G. Surfaces over Dirichlet tessellations. *Computer Aided Geometric Design* [online]. 1990, **7**(1-4), p. 281-292. ISSN 0167-8396, eISSN 1879-2332. Available from: https://doi.org/10.1016/0167-8396(90)90036-Q

[51] PIPER, B. Properties of local coordinates based on Dirichlet tessellations. In: *Geometric modelling*. FARIN, G., NOLTEMEIER, H., HAGEN, H., KNODEL, W. (Eds.). Vol. 8. Vienna, Austria: Springer Vienna, 1993. ISBN 3-211-83603-9, p. 227-239.

[52] CUETO, E., SUKUMAR, N., CALVO, B., MARTINEZ, M. A., CEGONINO, J., DOBLARE, M. Overview and recent advances in natural neighbour Galerkin methods. *Archives of Computational Methods in Engineering* [online]. 2003, **10**(4), p. 307-384. ISSN 1134-3060, eISSN 1886-1784. Available from: https://doi.org/10.1007/BF02736253

[53] SIBSON, R. A Vector identity for the Dirichlet tessellation. *Mathematical Proceedings of the Cambridge Philosophical Society* [online]. 1980, **87**(1), p. 151-155. ISSN 0305-0041, eISSN 1469-8064. Available from: https://doi.org/10.1017/S0305004100056589

[54] TAMASSIA, R. Introduction to Voronoi diagrams [online] [accessed 2023-03-16]. Available from: https://cs.brown.edu/courses/cs252/misc/resources/lectures/pdf/notes09.pdf

[55] LEDOUX, H., GOLD, C. An efficient natural neighbour interpolation algorithm for geoscientific modelling. In: *Developments in spatial data handling*. FISHER, P. F. (Ed.). Berlin, Heidelberg, Germany: Springer Berlin, Heidelberg, 2005. ISBN 978-3-540-22610-9, eISBN 978-3-540-26772-0, p. 97-108. Available from: https://doi.org/10.1007/3-540-26772-7_8

[56] VORONOI, G. A New A new applications of the continuous parameters in the theory of quadratic forms. First memoir. On some properties of the perfect positive quadratic forms (in English) *Journal for Pure and Applied Mathematics*. 1908, **134**, p. 97-178. ISSN 0075-4102, eISSN 1435-5345.

[57] THIESSEN, A. H. Precipitation averages for large areas. *Monthly Weather Review* [online]. 1911, **39**(7), p. 1082-1084. ISSN 0027-0644, elSSN 1520-0493. Available from: http://dx.doi.org/10.1175/1520-0493(1911)39<1082b:PAFLA>2.0.CO;2

[58] SCHUMANN, A. H. Thiessen polygon. In: *Hydrology and lakes. Encyclopedia of earth science*. HERSCHY, R. W., FAIRBRIDGE, R. W. (Eds.). Dordrecht, Netherlands: Springer Dordrecht, 1998. ISBN 9780412740602, p. 648-649.

[59] ANGELUCCI, G., MOLLAIOLI, F. Voronoi-like grid systems for tall buildings. *Frontiers in Built Environment* [online]. 2018, **4**, 78. eISSN 2297-3362. Available from: https://doi.org/10.3389/fbuil.2018.00078

[60] NONOGAKI, S., MASUMOTO, S., NEMOTO, T., NAKAZAWA, T. Voxel modeling of geotechnical characteristics in an urban area by natural neighbor interpolation using a large number of borehole logs. *Earth Science Informatics* [online]. 2021, **14**, p. 871-882. ISSN 1865-0473, eISSN 1865-0481. Available from: https://doi.org/10.1007/s12145-021-00600-x

[61] COLEMAN, J. B., YAO, X., JORDAN, T. R., MADDEN, M. Holes in the ocean: filling voids in bathymetric Lidar data. *Computers and Geosciences* [online]. 2011, **37**(4), p. 474-484. ISSN 0098-3004, eISSN 1873-7803. Available from: https://doi.org/10.1016/j.cageo.2010.11.008

[62] KLEIJNEN, J. P. C. Kriging metamodeling in simulation: a review. *European Journal of Operational Research* [online]. 2009, **192**(3), p. 707-716. ISSN 0377-2217, eISSN 0377-2217. Available from: https://doi.org/10.1016/j.ejor.2007.10.013

[63] MATHERON, G. Principles of geostatistics. *Economic Geology* [online]. 1963, **58**(8), p. 1246-1266. ISSN 0361-0128, eISSN 1554-0774. Available from: http://dx.doi.org/10.2113/gsecongeo.58.8.1246

[64] FANCHI, J. R. Chapter 2 - Geological modeling. In: *Principles of applied reservoir simulation*. FANCHI, J. R. (Ed.). 4. ed. Houston, TX, USA: Gulf Professional Publishing, 2018. ISBN 9780128155639, eISBN 9780128155646, p. 9-33.

[65] MERT, B. A., DAG, A. A Computer program for practical semivariogram modeling and ordinary kriging: a case study of porosity distribution in an oil field. *Open Geosciences* [online]. 2017, **9**(1), p. 663-674. ISSN 2391-5447. Available from: https://doi.org/10.1515/geo-2017-0050

[66] WONG, A. H., KWON, T. J. Advances in regression kriging-based methods for estimating statewide winter weather collisions: an empirical investigation. *Future Transportation* [online]. 2021, **1**(3), p. 570-589. eISSN 2673-7590. Available from: https://doi.org/10.3390/futuretransp1030030

[67] MONTES, F., HERNANDEZ, M. J., CANELLAS, I. A Geostatistical approach to cork production sampling estimation in Quercus Suber Forests. *Canadian Journal of Forest Research*. 2013, **35**(12), p. 2787-2796. ISSN 0045-5067.

[68] JOURNEL, A. G., HUIJBREGTS, CH. J. *Mining geostatistics*. London, UK: Academic Press, 1978. ISBN 0123910501.

[69] CHE, D., JIA, Q. Three-dimensional geological modeling of coal seams using weighted kriging method and multi-source data. *IEEE Access* [online]. 2019, **7**, p. 118037-118045. eISSN 2169-3536. Available from: https://doi.org/10.1109/ACCESS.2019.2936811

[70] DAI, H., REN, L., WANG, M., XUE, H. Water distribution extracted from mining subsidence area using kriging interpolation algorithm. *Transactions of Nonferrous Metals Society of China* [online]. 2011, **21**(s3), s723-s726. ISSN 1003-6326, eISSN 2210-3384. Available from: https://doi.org/10.1016/S1003-6326(12)61669-0

[71] MALVIC, T., IVSINOVIC, J., VELIC, J., RAJIC, R. Kriging with a small number of data points supported by jack-knifing, a case study in the Sava Depression (Northern Croatia). *Geosciences* [online]. 2019, **9**(1), 36. eISSN 2076-3263. Available from: https://doi.org/10.3390/geosciences9010036

[72] VAN BEERS, W. C. M., KLEIJNEN, J. P. C. Kriging for interpolation in random simulation. *Journal of the Operational Research Society* [online]. 2003, **54**(3), p. 255-262. ISSN 0160-5682, eISSN 1476-9360. Available from: https://doi.org/10.1057/palgrave.jors.2601492

[73] WOJCIECH, M. Kriging method optimization for the process of DTM creation based on huge data sets obtained from MBESs. *Geosciences* [online]. 2018, **8**(12), 433. eISSN 2076-3263. Available from: https://doi.org/10.3390/geosciences8120433

[74] PARENTE, C., VALLARIO, A. Interpolation of single beam echo sounder data for 3D bathymetric model. *International Journal of Advanced Computer Science and Applications (IJACSA)* [online]. 2019, **10**(10), p. 6-13. ISSN 2158-107X, eISSN 2156-5570. Available from: https://doi.org/10.14569/IJACSA.2019.0101002

[75] LAM, N. S.-N. Spatial interpolation methods: a review. *The American Cartographer* [online]. 1983, **10**(2), p. 129-150. ISSN 1523-0406, eISSN 1545-0465. Available from: https://doi.org/10.1559/152304083783914958

[76] CHAPRA, S. C., CANALE, R. P. *Numerical methods for engineers*. 6. ed. New York, NY, USA: McGraw Hill, 2009. ISBN 978-0-07-340106-5.

[77] BURDEN, R. L., FAIRES, J. D. *Numerical analysis*. 9. ed. Boston, MA, USA: Brooks/Cole Publishing Company, 2010. ISBN 978-0-538-73351-9.

[78] DIAZ-ARAUJO, M., MEDINA, A., CISNEROS-MAGANA, R., RAMIREZ, A. Periodic steady state assessment of microgrids with photovoltaic generation using limit cycle extrapolation and cubic splines. *Energies* [online]. 2018, **11**(8), 2096. eISSN 1996-1073. Available from: https://doi.org/10.3390/en11082096

[79] Surfer help - Grid spline smooth [online] [accessed 2023-03-16]. Available from: https://surferhelp.goldensoftware.com/gridmenu/idm_splinesmooth.htm

[80] WANG, Y. *Smoothing splines: methods and applications* [online]. 1. ed. London, UK: Chapman and Hall/CRC, 2011. eISBN 9780429146923. Available from: https://doi.org/10.1201/b10954

[81] KUSUMA, D., MURDIMANTO, A., SUKRESNO, B., JATISWORO, D. Comparison of interpolation methods for sea surface temperature data. *JFMR (Journal of Fisheries and Marine Research)* [online]. 2018, **2**(2), p. 103-115. eISSN 2581-0294. Available from: https://doi.org/10.21776/ub.jfmr.2018.002.02.7

[82] NORTH, R. P., LIVINGSTONE, D. M. Comparison of linear and cubic spline methods of interpolating lake water column profiles: interpolation of lake profiles. *Limnology and Oceanography: Methods* [online]. 2013, **11**(4), p. 213-224. eISSN 1541-5856. Available from: https://doi.org/10.4319/lom.2013.11.213

[83] LEWICKA, O., SPECHT, M., STATECZNY, A., SPECHT, C., BRCIC, D., JUGOVIC, A., WIDZGOWSKI, S., WISNIEWSKA, M. Analysis of GNSS, hydroacoustic and optoelectronic data integration methods used in hydrography. *Sensors* [online]. 2021, **21**(23), 7831. eISSN 1424-8220. Available from: https://doi.org/10.3390/s21237831

[84] KARAKI, A. A., BIBULI, M., CACCIA, M., FERRANDO, I., GAGLIOLO, S., ODETTI, A., SGUERSO, D. Multi-platforms and multi-sensors integrated survey for the submerged and emerged areas. *Journal of Marine Science and Engineering* [online]. 2022, **10**(6), 753. eISSN 2077-1312. Available from: https://doi.org/10.3390/jmse10060753

[85] STATECZNY, A. The neural method of sea bottom shape modelling for the spatial maritime information system. In: *Maritime engineering and ports II*. BREBBIA, C.A., OLIVELLA, J. (Eds.). Vol. 51. Southampton, UK: WIT Press, 2000. ISBN 1-85312-829-5, p. 251-259.

[86] WLODARCZYK-SIELICKA, M., STATECZNY, A. Fragmentation of hydrographic big data into subsets during reduction process. In: Baltic Geodetic Congress 2017 BGC 2017: proceedings [online]. IEEE. 2017. ISBN 978-1-5090-6041-2, eISBN 978-1-5090-6040-5. Available from: https://doi.org/10.1109/BGC.Geomatics.2017.67

[87] WLODARCZYK-SIELICKA, M., STATECZNY, A., LUBCZONEK, J. The reduction method of bathymetric datasets that preserves true geodata. *Remote Sensing* [online]. 2019, **11**(13), 1610. eISSN 2072-4292. Available from: https://doi.org/10.3390/rs11131610


1953
70
2023
ŽILINSKÁ UNIVERZITA V ŽILINE
BioTechUSA
SOM VEDEC
PYTAJTE SA MA
NOC
drobtak
Stavebná fakulta
BA BB
E 499062

ROAD ACCIDENT ANALYSIS AND SAFETY AUDIT: A CASE STUDY OF MDR 132

Amir Ali Khan, Sabir*, Sachin Dass, Gyanendra Singh, Saurabh Jaglan

Deenbandhu Chhotu Ram University of Science and Technology, Murthal, India

*E-mail of corresponding author: sabirkhan490@gmail.com

Amir Ali Khan 0000-0002-3309-9831,
Gyanendra Singh 0000-0002-0050-719X,
Sachin Dass 0000-0003-1015-4807,
Saurabh Jaglan 0000-0001-8719-4677

Resume

Road accident and road safety are the key global concerns and problem for emerging nations like India. It has been attempted to examine the accidents that happened on Major District Road (MDR) 132 (Nuh to Hodal), India in the last five years. The primary objective of this study was to perform the Road Safety Audit for identification of accident-prone areas based on Accident Severity Index (ASI) and provide some improvement measures in order to lower the frequency and severity of accidents. Identified accident prone locations (blackspots) were ranked according to the ASI index. The distribution of accidents based on various parameters were also discussed. Site visit of critical sections of the road to observe road deficiencies were made and safety recommendations, along with the risk associated with them and priority as per IRC: SP: 88-2019, were suggested.

Article info

Received 26 September 2022
Accepted 17 January 2023
Online 7 February 2023

Keywords:

accident prone location
accident severity index (ASI)
road safety audit
severity
nature of accident

Available online: https://doi.org/10.26552/com.C.2023.026

ISSN 1335-4205 (print version)
ISSN 2585-7878 (online version)

1 Introduction

In developing nations, there is a severe problem with traffic accidents. In spite of this, several groups are working to mitigate the impact of these tragedies. The results of the efforts show that while accident-related mortality declined by 0.20 %, the number of road accident instances in India was reduced by 3.86 % in 2019 compared to the previous year. This study tries to identify the many causes of traffic accidents and offers suggestions for future accident prevention based on the RSA conducted on the stretch under study.

The stretch used in this investigation was chosen on MDR-132 between Nuh and Hodal, Haryana. From 2017 to 2021, the FIR records from Haryana's official website have been gathered (up to July). The FIR report includes the time, date, day, month and year, as well as the number of injuries, including fatalities, serious and minor wounds and property damage. It also includes some information about the accident's location and the nature of its causes. To ascertain the criticality of the linkages and stretches, the data has been collated and several parameters have been examined. With this study, key junctions, times, types of vehicles etc. are discovered, and the findings are shown in charts.

2 Literature review

Haque et al. (2022) identified blackspots on NH 76 using accident severity index approach. Corrective safety measures to improve identified blackspots were presented in [1]. Minor road junctions of Nuh were analyzed for safety aspects by Asruddin et al. (2022). The FIR accident data from various police stations were collected and analyzed to identify accident prone locations and then safety measures to correct the road features were given in the study [2]. Mir et al. (2022) performed a case study of J&K (Jammu and Kashmir) for accident analysis and presented accident data in terms of month, year, cause of accidents, location of accidents etc. [3]. Khan et al. (2022) compiled and analyzed the FIR data of accidents occurred in three years on the study stretch and concluded that over-speeding is the main reason causing majority of accidents [4]. E-rickshaws are responsible for many minor accidents especially on city roads. Khan and Singh (2021) developed passenger car unit of e-rickshaw so that designated facilities can be provided for e-rickshaws while planning and designing to ensure safety of e-rickshaws and to avoid safety concerns related to e-rickshaw [5]. In their research, Elena et al. (2018) suggested forecasting techniques for

accidents involving vehicles in the Driver-Vehicle-Road-Environment (DVRE) system. A study of effectiveness of the recommended action to increase the traffic safety was conducted using the approach, which allowed for the measurement of the influence on the accident rate [6]. The road safety scenario of the rural roads was studied by Naveen et al. (2017). This article examines variables that influence the safety of rural road and perform road safety audit. The study was based on two different sections of the road. Finally, this project intends to address the issues that arise throughout the rural road implementation process and presents remedies to assist the work of the road safety audit [7]. Tawar and Dass (2017) identified the black spots on NH 65 and analyze the safety measures on the selected section of 19.5 km of NH 65. Safety measures based on the RSA conducted on selected stretch were also presented in [8]. Borole et al. (2017) conducted research on traffic crashes on NH 6 and found that during the last few years, there has been an increase in the number of traffic crashes in Jalgaon. Geospatial data was used to identify crash locations, as well as to examine the pattern of traffic crashes in Jalgaon [9]. Kaur et al. (2017) estimated the severity of accidents on State highways and other district roads. By evaluating the accident severity based on the kind of accident and location of accident using the R tool, this study focused on forecasting the occurrence of accidents on roads. The frequency of traffic crashes on roads was evaluated using the correlation analysis and exploratory visualization approaches, pointing out the traffic collision data on roadways. Finally, a system for analyzing the road traffic accidents has been developed. Improvement in the level and scope of the road traffic safety management can be effectively implemented using this methodology. The current study modeled accident and incident data acquired from traffic data and data pertaining to the construction industry [10]. Singh et al. (2016) predicted the accidents using the M5 tree model and binomial regression model on rural road sections of Haryana state. Data on accidents were obtained from police records. Field studies were used to gather data on geometry, traffic and environment parameters. By separating roadways into parts with specific uniform geometric properties, 222 data points were acquired. It was concluded that minor highway accesses must be properly constructed and managed, service roads must be made functional and speed dispersion must be reduced to improve the highway safety in India [11]. The NH-55 was analyzed for road accidents by Dehury et al. (2013) and a predictive model was proposed to reduce road accidents on the selected stretch. The study depicted that major cases of fatalities involve trucks in road accidents. This study adopted the method of regressions for predicting the future accident growths [12]. The majority of accidents, according to research by Ganveer and Tiwari (2005), involve persons between the ages of 18 and 37. Because of this, the nation is being hurt twice. Risk-taking behaviors among children may be a contributing factor to the greater accident rate in these age groups [13]. The accident scenario of Patna was analyzed by Singh and Misra (2004) and found that pedestrian fatalities were exceptionally high as a portion of all traffic deaths where public transportation facility is not provided properly. It was also found that the new bypass road on NH-38 was determined to be the most accident hotspot in the town [14].

3 Data collection and data analysis

The research was done on MDR132 from Nuh to Hodal. The study stretch was covering Nuh Bypass, Adbar, Raipuri, Ujina, Chilawali, Bibipur, Thekra Mode, Bhimsika, Malai, Uttawar, Maluka Mode, Mithaka, Kot, Pahari Mode, Bahin, Nangal Jat, Sunder Nagar, Sondh and Hodal village. Accident data were collected from the official website of Haryana police stations, as shown in Table 1. On this route, 63 accidents occurred in 2017, 43 accidents occurred in 2018, 44 accidents occurred in 2019, 36 accidents occurred in 2020 and 23 accidents have occurred until July in 2021.

3.1 Month-wise distribution of accidents

As observed in Figure 1, accident severity follows a complex pattern with the month of occurrence. The figure suggests that month of January followed by August and December are the most unsafe in terms of number of injured persons and their severity levels. The month of May is the month in which the least accidents occurred.

Table 1 *Total accidents recorded on MDR132 from Nuh to Hodal*

Year	Location (Nuh to Hodal)	Total Accidents	Fatalities
2017	MDR-132	62	34
2018	MDR-132	43	27
2019	MDR-132	44	24
2020	MDR-132	36	16
2021 (till July)	MDR-132	23	8
Total		208	109

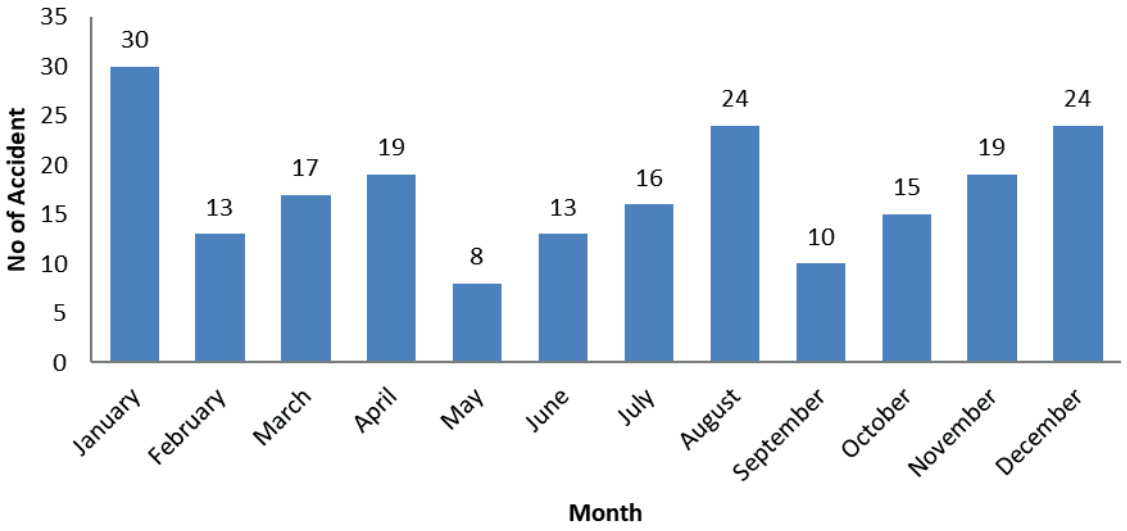

Figure 1 *Classification of the accident according to month*

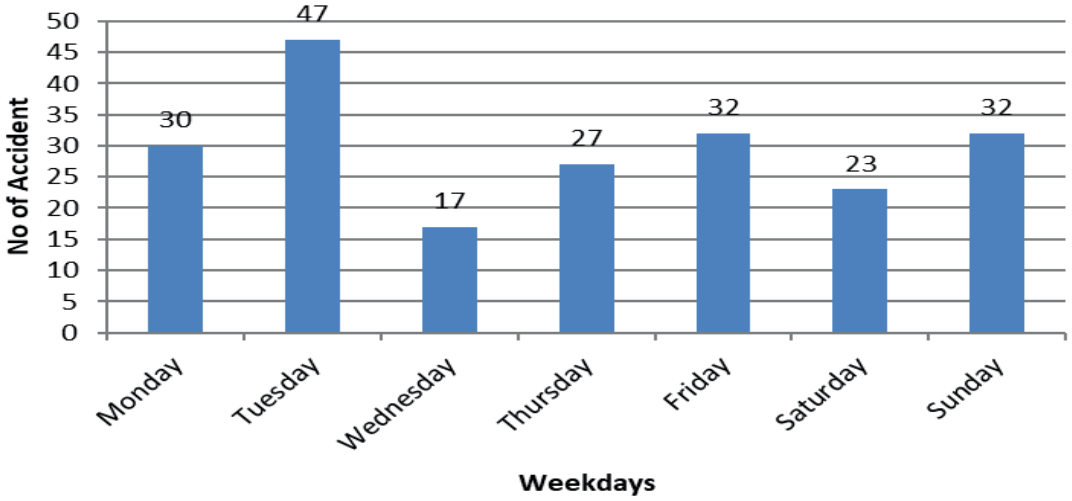

Figure 2 *Classification of accidents according to day of the week*

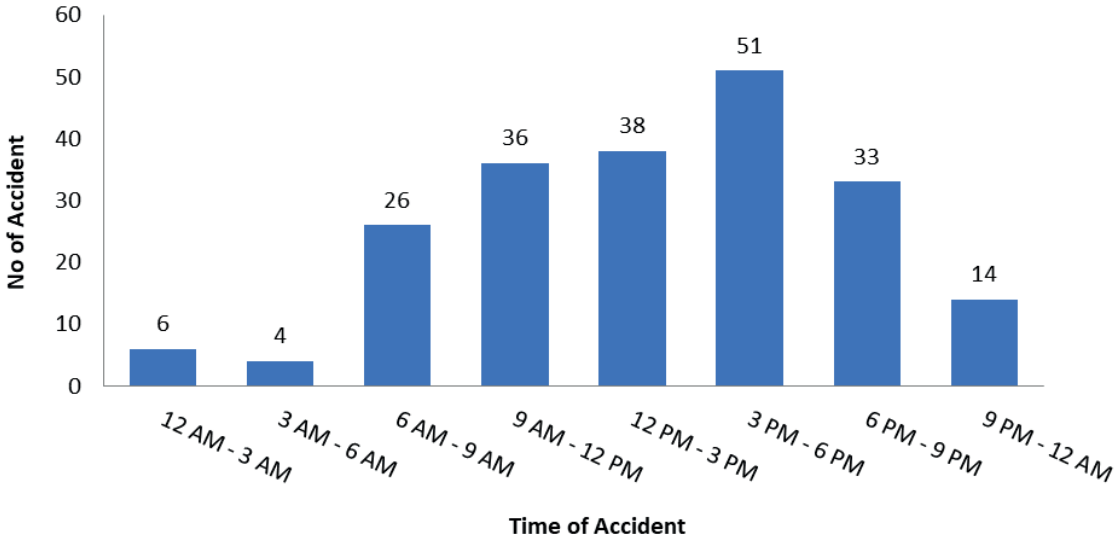

Figure 3 *Time-wise distribution of accidents*

3.2 Day wise distribution of accidents

Figure 2 shows variation of accident severity according to the day of a week. The figure clearly indicates that more severe injuries are taking place on Tuesdays and then Fridays and Sundays. The basic reason behind the observation was that both days are close to weekends when more people travel from and to their homes (extended families) to their workplace. People also break traffic rules due to congestion and hurry, which further leads to higher number of accidents.

The least accident occurred on Wednesday or Saturday as shown in Figure 2.

3.3 Distribution of accidents according to time of occurrence

Figure 3 shows pattern of accident severity according to the time of day. The figure indicates that more severe accidents occurred between 3 PM and 6 PM and then between 12 AM and 3 PM, while during the time between 3 AM and 6 AM least accidents occurred.

Figure 4 presents the combined graph showing the relation between the number of accidents and time, day and month.

3.4 Distribution of accidents according to the nature of accident

According to an FIR assessment of the previous five years, the head-on collision accidents accounted for 65 accidents, rear end collision accidents accounted for 50 accidents and skidding was the cause of just one accident as per records in FIRs (see Figure 5).

3.5 Distribution of accidents according to geometric design of the road

According to statistics from the past five years' FIR reports, there were more accidents on the straight section of the road (68 % of all incidents), followed by 11 % on the stretch's curve, while there were less accidents at the X- and Y-junctions, as shown in Figure 6. Around 75 % of the study stretch is straight, which

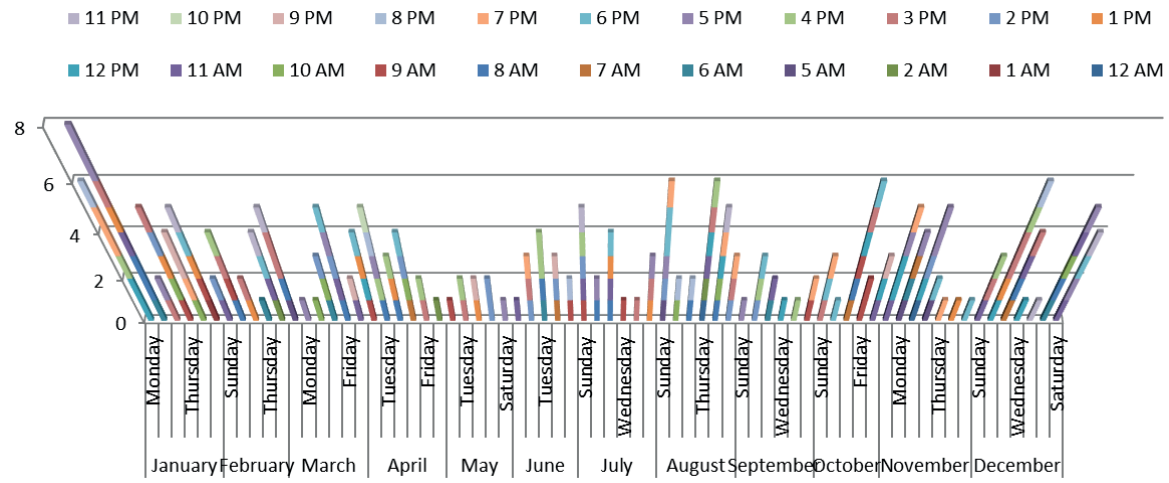

Figure 4 *Distribution of accidents according to time, day and month*

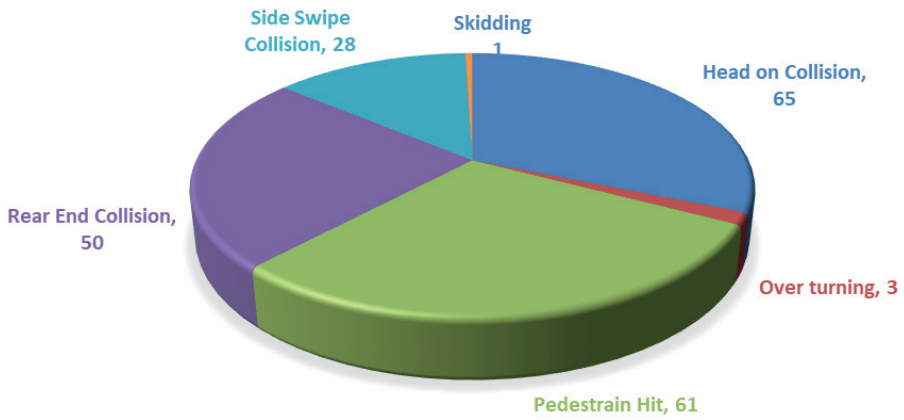

Figure 5 *Distribution of accidents according to their nature*

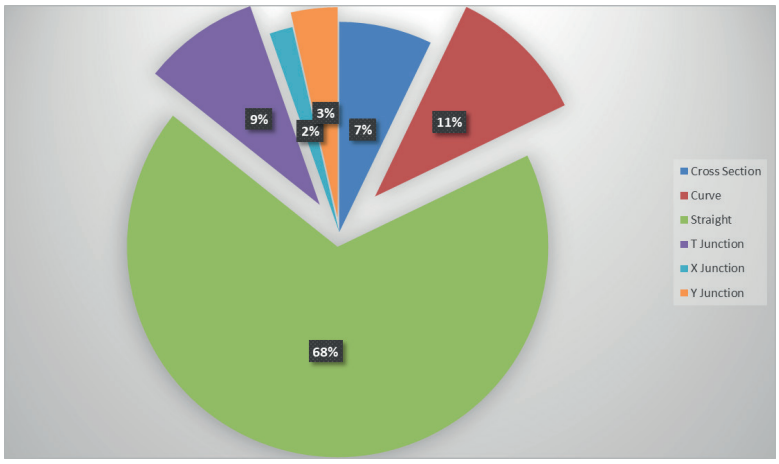

Figure 6 *Distribution of accidents according to the geometric design of the road*

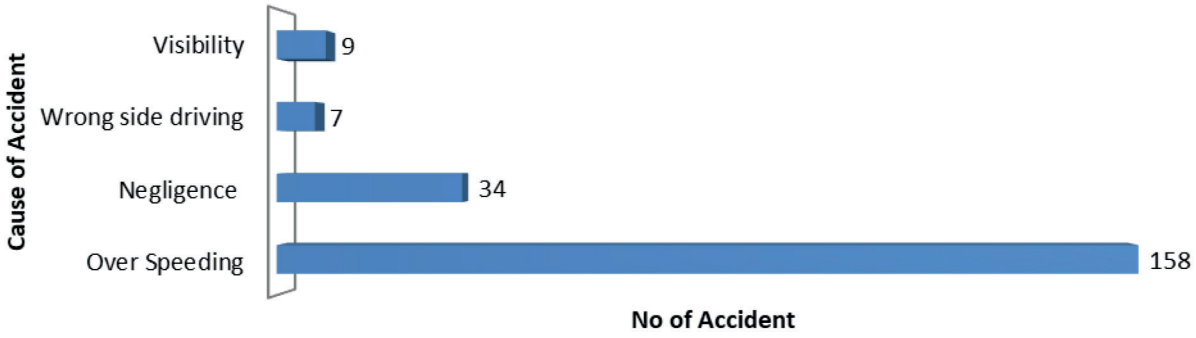

Figure 7 *Cause wise distribution of accidents*

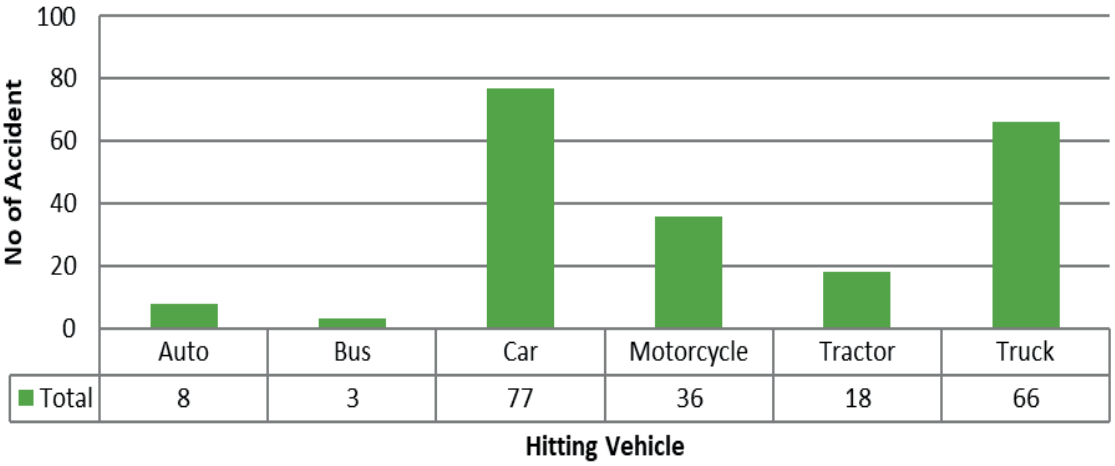

Figure 8 *Distribution of accidents according to the hitting vehicle*

is why 68 % of accidents have occurred on the straight sections. This stretch lacks traffic control devices.

3.6 Distribution of accidents according to the cause of an accident

According to the number, speeding contributed to 158 accidents. On this route, excessive speeding is the leading cause of collisions, followed by carelessness on the part of other drivers. While the FIR data of the previous five years, as shown in Figure 7, indicates that the least accidents were caused by the wrong-side driving and visibility. Heavy vehicles like truck and tractor ply significantly in numbers without following the rules and regulations. There is the absence of speed control devices like speed hump, rumble strips on this stretch and there is no enforcement there. To reduce the number of accidents and to minimize the impact of accidents, it is recommended to install speed limit sign boards, speed hump and rumble strips at the locations where accidents frequently occur. It is also recommended to maintain

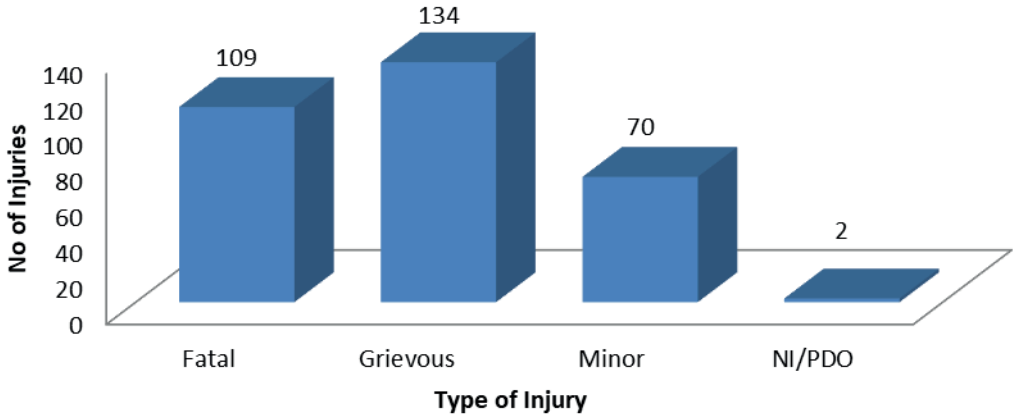

Figure 9 *Distribution of accidents as per the type of injury*

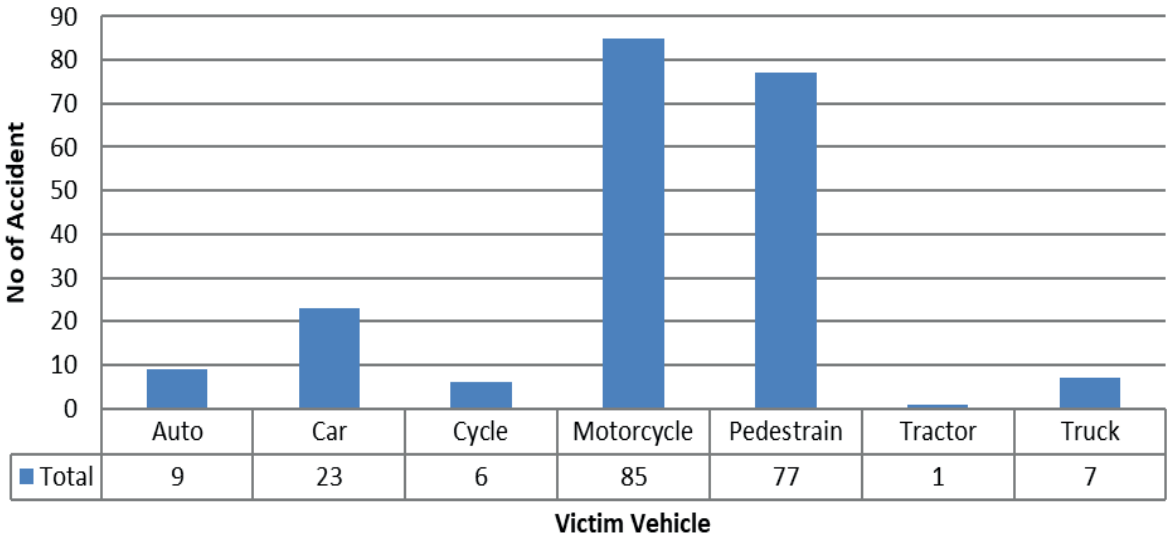

Figure 10 *Distribution of accidents as per types of victim's vehicle*

proper enforcement and to educate the people about the road safety and the negative impacts of speeding.

3.7 Distribution of accidents according to the hitting vehicle

It was discovered that most collisions involved cars. As seen in Figure 8, those vehicles account for 77 of the 208 incidents reported by FIR, followed by trucks, while buses and three-wheelers are less commonly involved in road accidents.

3.8 Distribution of accidents according to the type of injury

From Figure 9, it can be stated that the share of grievous injuries is more as compared to other types of injuries followed by the fatalities while no injury share is the least. The fact that the majority of situations were resolved without being reported may be the cause of the low rate of reported incidents in police records.

3.9 Distribution of accidents according to type of victim's vehicle

Motorcycles, followed by pedestrians, were the most common victims of the accidents that happened on this route during the research period. Figure 10 demonstrates that incidents involving tractors and bicycles are less common.

3.10 Distribution of accidents according to location wise

From the Figure 11, identified accident prone locations are Uttawar Chowk, Jaisinghpur junction,

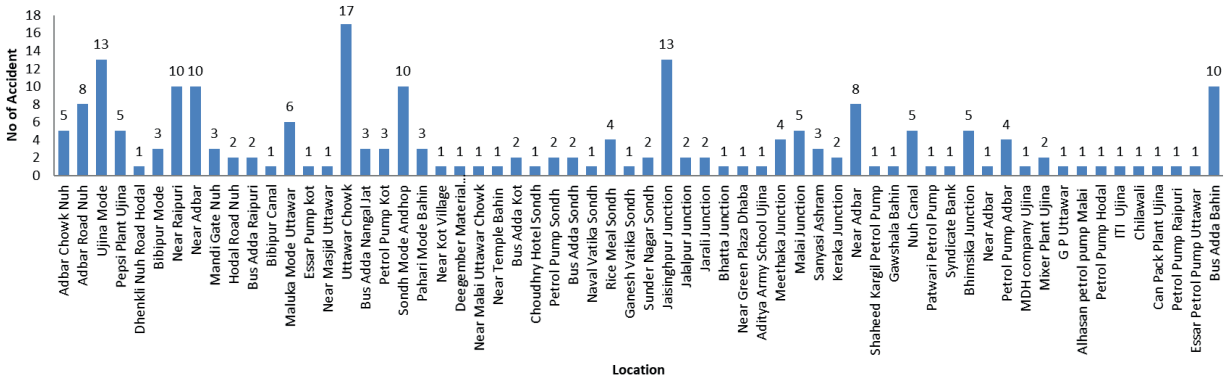

Figure 11 *Identified accident prone locations*

Ujina Mode, Bus Adda Bahin etc. Total of 17 accidents occurred at Uttawar Chowk, then 13 at Jaisinghpur junction and Ujina Mode.

4 Identification of black spots

Blackspot locations can be identified by various methods. Accident severity index (ASI) and MoRTH method are the most widely used methods.

According to the Popli Sudarshan K. study titled "Black Spot Management," Equation (1) is utilized to determine ASI [15].

$$ASI = (Nf * Wf) + (Ng * Wg), \quad (1)$$

where:
Nf = Number of fatal accidents at the spot
Wf = Weightage assigned to the fatal accident is 7
Ng = Number of grievous accidents
Wg =Weightage assigned to grievous is 3.

Note: When conducting a safety audit of NHAI PPP projects, the values Wf = 7 and Wg = 3 were recently adopted for determination of the black spots

Table 2 *List of identified Blackspots in the study area*

S. No	Location	Number of affected persons				Average	Standard Deviation	Threshold Value	ASI
		Fatal	Grievous	Minor	Non-Injured				
1	Adbar Road Nuh	1	2	3	0				13
2	Pepsi Plant Ujina	2	2	3	0				20
3	Maluka Mode Uttawar	2	0	0	0				14
4	Uttawar Chowk	2	0	0	0				14
5	Sunder Nagar Sondh	3	0	3	0				21
6	Bus Adda Raipuri	2	1	0	0				17
7	Sondh Mode Andhop	2	0	0	0				14
8	Bus Adda Bahin	2	0	0	0				14
9	Bus Adda Nangal Jat	2	0	0	0				14
10	Bhatta Junction	2	0	0	0	5.70	4.17	11.95	14
11	Aditya Army School Ujina	2	0	0	0				14
12	Maluka Mode Uttawar	2	0	0	0				14
13	Sondh Mode Andhop	2	0	0	0				14
14	Near Adbar	1	2	0	0				13
15	Jaisinghpur Junction	3	0	0	0				21
16	Near Adbar	3	0	0	0				21
17	Rice Meal Sondh	2	0	0	0				14
18	Petrol Pump Kot	2	0	0	0				14
19	Near Adbar	2	0	1	0				14

Table 3 *Ranking of blackspots*

Rank	ASI	Location
1	21	Sunder Nagar Sondh Jaisinghpur Junction Near Adbar
2	20	Pepsi Plant Ujina
3	17	Bus Adda Raipuri Maluka Mode Uttawar Uttawar Chowk Sondh Mode Andhop Bus Adda Bahin Bus Adda Nangal Jat Bhatta Junction Aditya Army School Ujina
4	14	Maluka Mode Uttawar Sondh Mode Andhop Rice Meal Sondh Petrol Pump Kot Near Adbar Adbar Road Nuh
5	13	Near Adbar

Table 4 *Locations' specific safety observations and recommendations*

Image	Observations	Recommendation	Risk and Priority
	• Pavement edge marking missing. • Speed breaker and its marking missing at entry of junction • Speed breaker sign missing on the entry of junction. • Information Sign Missing in all directions.	• Pavement edge marking should be provided towards both edges. • Provide speed breaker sign board before intersection in all the incoming directions to alert the drivers • Provide light reflecting tape/paint on all such poles. • Provision of cat eyes at the entry of junction on both carriageways. • Provide information sign in all directions to guide the road user.	Risk: High Priority: Highly desirable
	• Pavement edge marking missing. • Electrical poles laying on main carriage way obstructing the traffic without marking.	• Road marking should be painted properly on the road. • The electric pole should be removed from the carriageway to avoid safety hazards. At least the retro-reflective tape should be pasted on both sides of the pole.	Risk: High Priority: Highly desirable

and the findings were quite good. Minor and non-injury accidents are sometimes considered and given a weight of 1. However, since they are typically not reported in India, they may not be considered when determining the "black spots".

5 Black spot recognition

According to MoRTH, "a Road Accident Blackspot is a stretch of National Highway of around 500 meters in length where either 5 road accidents (including fatalities/grievous injuries) occurred in the previous three calendar years, or 10 fatalities occurred in the previous three calendar years." The Hazardous Spots are ranked using the ASI and SD (standard deviation). Dangerous regions, known as "Black Spots", have an ASI higher than the TH (threshold value). Following formulas are used to calculate threshold value TH [16]:

$$\text{TH value} = \text{Avg of ASI} + 1.5 * \text{SD}, \tag{2}$$

$$\text{TH value} = \bar{\text{V}} + 1.5\sqrt{\frac{\Sigma(\text{V} - \bar{\text{V}})^2}{(\text{N} - 1)}}, \tag{3}$$

where, $\text{V} = \text{V}_1, \text{V}_2, \ldots \text{V}_n$ is the ASI values of locations 1, 2…. N, respectively; $\bar{V}$ is the average ASI value and N is the total number of ASI values.

$$\bar{\text{V}} = \frac{\text{V}_1 + \text{V}_2 + \cdots + \text{V}_n}{\text{N}}. \tag{4}$$

As seen in Table 2, the black spots are mentioned from all accident-prone areas in the study where the ASI estimates are higher than the threshold value. Out of many locations where accidents occurred, 19 locations were identified as potential black spots using ASI, according to the data provided from January 2017 to July 2021, as shown in Table 2.

Table 5 *Locations' specific safety observations and recommendations*

Image	Observations	Recommendation	Risk and Priority
	• Road marking/Speed breaker marking is missing, which can cause visibility problems for road users at night-time as it can lead to the road crashes.	• Provide speed breaker along with the sign board before the intersection to alert the drivers. • Pavement edge marking should be provided.	Risk: High Priority: Highly desirable
	• The shoulders are covered under vegetation.	• The tree branches have come on the carriageway at very low height require pruning along with removal of weeds/ plants from roadside.	Risk: Medium Priority: Desirable
	• The information and direction signages are not provided	• To warn residents of habitation, a standard village signboard should be installed (as per IRC-67,99). • Speed Limit signboard should be provided.	Risk: High Priority: Highly Desirable

6 Ranking of black spots

Black spots are ranked according to the accident severity index of the location. Ranks of the black spots of the study location are shown in Table 3. Locations under rank 1 type are the most severe in terms of accidents and hence priority should be given to such locations. "Adbar road nuh" is the least severe accident blackspot.

7 Safety observations and adequate recommendations

Location specific safety observations and recommendations along with priority as observed from the Road Safety Audit during the field visit are shown in Tables 4 to 7. Identified blackspots were audited to identify the potential safety concerns and to suggest the corrective measures to improve those locations. The risk, along with the priority, is also given in Tables 4 to 7. The road safety manual IRC: SP:88-2019 was used for the road safety auditing. The format and content of Tables 4-7 is in accordance with IRC: SP:88-2019.

8 Discussion and conclusions

The road safety audit and accident analysis are carried out to identify the probable cause of accidents and to identify the accident-prone locations. In this study, accident study was carried out on a 67 km stretch of MDR - 132 from Nuh to Hodal. The FIR data of the last five years from the year 2017 to the year 2021 (July) were

Table 6 *Locations' specific safety observations and recommendations*

Image	Observations	Recommendation	Risk and Priority
	• Road side green areas and trees abutting are not properly maintained. • Retro-reflective tape is missing on the electric pole.	• Formation land along with footpath should be free from vegetation/ weeds. • Retro-reflective tape should be provided on both sides of the electric poles placed close to the carriageway as per IRC-35	Risk: High Priority: Highly desirable
	• Truck drivers are parking their trucks in no parking zone approx. 1 km near Ujina mixture plant.	• Unauthorized parking on the carriageway must be removed	Risk: Medium Priority: Desirable
	• Speed hump is not visible. It can lead to road crashes.	• All marking should be reinstalled and maintained properly and kept clean of dust at all times for the proper visibility.	Risk: High Priority: Highly desirable

Table 7 *Locations' specific safety observations and recommendations*

Image	Observations	Recommendation	Risk and Priority
	• Text is missing on Signboard	• Text on signboard should be placed as per IRC-67-2012.	Risk: Medium Priority: Desirable
	• Uncontrolled Junction: Due to the traffic entering and leaving and heavy pedestrians crossing, this is a safety hazard. • Signboards and speed humps are missing.	• The junction should be improved as per IRC SP 73-2015 standard. • Provide speed breaker along with sign board before the intersection to alert the drivers. •	Risk: Very High Priority: Essential

collected from the Haryana police website. Distribution of accidents, according to various parameters, like month, time, year, vehicle involved, location, cause of accidents etc. were classified after interpretation of FIR data. The main interpretations of accidental the FIR data are as follows:

1. In the month of January and December, more accidents occurred. Probable reasons might be foggy conditions during the winter season.
2. Head-on collision (65 accidents) was found as contributing type of accidents for this stretch due to undivided nature of road and lack of enforcements.
3. Out of 208 accidents, 158 accidents are due to speeding according to the collected FIR data. Flow of truck is significant in this stretch and many accidents occurred due to negligence and speeding of trucks. Motorcyclists too ply with over speed in this stretch. In 84 accidents, truck and tractor combined were hitting vehicles.

Accident prone locations (blackspot) were identified using the accident severity index method in which accident severity index of locations where accidents occurred were calculated along with the threshold value for these locations. Any location having higher ASI value than the threshold value is termed as blackspot. A total of 19 such locations were identified and those locations were ranked accordingly. Those 19 locations were audited to find out safety concerns and to provide safety measures with the help of road safety manual IRC: SP:88-2019. The main observations with the suggestive measures are as follows:

1. The major victims of the accidents were seen to be motorcyclists and pedestrians (Vulnerable Road Users) (VRU), while cars and trucks were observed as the main hitting vehicles causing accidents. Monotony of drivers should be broken on longer sections having considerable VRU movements. Separation of the VRU from vehicular traffic with adequate pedestrian facilities on service roads

ensures less chances of pedestrian from entering the carriageway as mentioned in IRC 103:2012.
2. All informatory signage, road marking, hazard marking must be provided as per IRC 67-2012 & IRC 35.
3. Provide proper signboards, retro reflective markings on all the fixed obstructions and cat eyes as edge marking and central line for the night vision.
4. Remove all unauthorized hoardings from lighting and electricity poles.
5. The unauthorized encroachments in the form of street vending, parking and material storage must be removed.
6. Regular cleansing and removal of debris and aggregates from carriageway is a must.
7. Trees and bushes on the edge of road and median obstructing the carriageway should be trimmed regularly on all roads.

These safety measures are location specific and can be applied for the roads having similar safety issues across India.

Grants and funding

The authors received no financial support for the research, authorship and/or publication of this article.

Conflicts of interest

The authors declare that they have no known competing financial interests or personal relationships that could have appeared to influence the work reported in this paper.

References

[1] HAQUE, M. I., KHAN, A. A., SINGH, G., DASS, S., JAGLAN, S. Accident analysis and road safety audit: a case study on NH-76. *IOP Conference Series: Earth and Environmental Science* [online]. 2022, **1086**, 012025. ISSN 1755-1307, eISSN 1755-1315. Available from: https://doi.org/10.1088/1755-1315/1086/1/012025

[2] ASRUDDIN, M., KHAN, A. A., SINGH, G., DASS, S., JAGLAN, S. Safety aspects of minor road junctions on MDR 132-Nuh to Hodal. *IOP Conference Series: Earth and Environmental Science* [online]. 2022, **1086**, 012030. ISSN 1755-1307, eISSN 1755-1315. Available from: https://doi.org/10.1088/1755-1315/1086/1/012030

[3] MIR, I. A., KHAN, A. A., DASS, S., SINGH, G., JAGLAN, S. Accident analysis: a case study of J&K. *NeuroQuantology* [online]. 2022, **20**(9), p. 480-486. ISSN 1303-5150. Available from: https://doi.org/10.14704/nq.2022.20.9.NQ440050

[4] KHAN, A. A., MUNDAY, A., BHORIA, R., YOGESH., TARUN., KHUSHBOO., PREETI. Compilation and analysis of accidental FIR data. *International Advanced Research Journal in Science, Engineering and Technology* [online]. 2022, **9**, 9629. ISSN 2394-1588, eISSN 2393-8021, Available from: https://doi.org/10.17148/IARJSET.2022.9629

[5] KHAN, A. A., SINGH, G. Development of PCU value of e-rickshaw on urban roads. In: *Advances in Water Resources and Transportation Engineering* [online]. Lecture Notes in Civil Engineering. Vol. 149. MEHTA, Y. A., CARNACINA, I., KUMAR, D. N., RAO, K. R., KUMARI, M. (Eds.). Singapore: Springer, 2021. ISBN 978-981-16-1302-9, eISBN 978-981-16-1303-6, p. 123-138. Available from: https://doi.org/10.1007/978-981-16-1303-6_10

[6] KURAKINA, E., EVTIUKOV, S., RAJCZYK, J. Forecasting of road accident in the DVRE system. *Transportation Research Procedia* [online]. 2018. **36,** p. 380-385. ISSN 2352-1457, eISSN 2352-1465. Available from: https://doi.org/10.1016/j.trpro.2018.12.111

[7] NAVEEN, N., RAJESH, M., SRINIVAS, M., FASIODDIN, M. Road safety audit of a rural road. *International Journal of Civil Engineering and Technology (IJCIET)*. 2017, **8**(4), p. 752-761. ISSN 0976-6308, eISSN 0976-6316.

[8] TAWAR, S., DASS, S. Identification of accident black spots on NH-65 (Chaudhriwas, Hisar to Hisar city). *International Research Journal of Engineering and Technology*. 2017, **4**(2), p. 848-852. ISSN 2395-0072, eISSN 2395-0056.

[9] BOROLE, D., MALI, J. R., PATIL, V., PACHPOLE, K., PANDHARE, B., BOROLE, R. Studies on road accidents on national highway No. 6. *International Journal of Advance Research, Ideas and Innovations in Technology (IJARIIT)*. 2017, **3**(2), p. 926-930. ISSN 2454-132X.

[10] KAUR, G., KAUR, H. Prediction of the cause of accident and accident prone location on roads using data mining techniques. In: 2017 8th International Conference on Computing, Communication and Networking Technologies (ICCCNT): proceedings [online]. IEEE. 2017. ISBN 978-1-5090-3039-2, eISBN 978-1-5090-3038-5, p. 1-7. Available from: https://doi.org/10.1109/ICCCNT.2017.8204001

[11] SINGH, G., SACHDEVA, S. N., PAL, M. M5 model tree based predictive modeling of road accidents on non-urban sections of highways in India. *Accident Analysis and Prevention* [online]. 2016, **96**, p. 108-117. ISSN 0001-4575, eISSN 1879-2057. Available from: https://doi.org/10.1016/j.aap.2016.08.004

[12] DEHURY, A. N., PATNAIK, A. K., DAS, A. K., CHATTRAJ, U., BHUYAN, P., PANDA, M. Accident analysis and modelling on NH-55 (India). *International Journal of Engineering Innovations*. 2013, **2**(7), p. 80-85. ISSN 2319-6491, eISSN 2278-7461.
[13] GANVEER, G. B., TIWARI, R. R. Injury pattern among non-fatal road traffic accident cases: a cross-sectional study in Central India. *Indian Journal of Medical Sciences*. 2005, **59**(1), p. 9-12. ISSN 0019-5359, eISSN 1998-3654.
[14] SINGH, S. K., MISRA, A. Road accident analysis: a case study of Patna City. *Urban Transport Journal* [online]. 2004, **2**(2), p. 60-75. Available from: https://ssrn.com/abstract=570441
[15] Official website of Public Works Department, Uttar Pradesh [online]. Available from: http://uppwd.gov.in/site/writereaddata/siteContent/20190424201227766620.pdf
[16] Section 1: Introduction - ERNET [online]. Available from: http://tripp.iitd.ernet.in/assets/publication/blackspot_literature.pdf

ASSESSING THE IMPACT OF TRUCKING INFRASTRUCTURE ON FREIGHT EFFICIENCY AND SAFETY

Piotr Gorzelańczyk*, Jakub Czech, Jolanta Olechnowicz

Stanislaw Staszic State University of Applied Sciences in Pila, Pila, Poland

*E-mail of corresponding author: piotr.gorzelanczyk@ans.pila.pl

Piotr Gorzelańczyk 0000-0001-9662-400X, Jolanta Olechnowicz 0000-0002-4610-8995

Resume

The change in people's lifestyles, their desire or compulsion to move constantly and the development of technology, have forced development of communications, which has led, among other things, to an intensive increase in traffic. For this reason, the purpose of the article is to identify the main causes of traffic delays and the factors affecting the sense of safety on the road. It is followed by the analytical part, which presents the effect of a survey conducted on a group of 401 respondents. The respondents' answers show that the most common causes of road accidents and collisions are: failure to adjust the speed to road conditions (89 %), failure to give priority (84 %), which is in line with the 2019 police report. The results show a clear difference between Western Europe and Eastern Europe.

Article info

Received 20 October 2022
Accepted 19 January 2023
Online 22 February 2023

Keywords:

road infrastructure
Poland
Europe
road safety
road transport

Available online: https://doi.org/10.26552/com.C.2023.029

ISSN 1335-4205 (print version)
ISSN 2585-7878 (online version)

1 Introduction

Year after year, people are changing their lifestyles. This is due, among other things, to the need for constant movement and the development of technology. This leads to the increased development of communications and an intense increase in traffic.

As we read in the article by Hoy, women's motivating factors for travel are shopping, accompanying others, including children to school and with administrative errands. It should also be noted that "motivations to travel are not fixed, but depend on specific life situations and change with the stages of a person's life, [1]. The key stages affecting travel behaviour are: becoming employed, having children and retiring." The article also notes that men are more likely to use cars and women are more likely to use public transportation. In the article below, women make up 18% of respondents and men 82%.

Road safety is worth leaning into. However, as the author Racynska-Bulawa noticed, increasing the road safety requires intervention in many aspects of public policy [2]. The road safety policy directions for 2011-2020, set by the European Commission, clearly indicate that a forward-looking road safety policy should be taken into account in other EU policy areas, while at the same time such a policy should take into account the objectives of other policy areas. Road safety is closely linked to policies on energy, environment, employment, education, youth, public health, research, innovation and technology, justice, insurance, trade and foreign affairs, among others.

Among the factors that have a decisive impact on the road safety (human-road-vehicle as a causal factor in accidents), the first place is definitely occupied by humans. It is the behaviour of particular groups of road users, in general, that affects the occurrence of traffic accidents - argue author of [3]. When driving on the road, certain rules and regulations must be observed [4]. Improving road safety is influenced by many elements, related not only to the promotion of correct driver behaviour [5-7], but to the proper organization of traffic and the proper technical condition of roads and vehicles, as well, [8-11]. Training and examinations for future drivers should also be considered. The road safety is a scientific field that includes the above-mentioned aspects, as well as issues related to traffic supervision, emergency medical services and transport psychology [12]. The problem of using the road as a means of transportation in terms of safety is discussed in [13-23].

The European Commission's efforts to further improve the road safety are based on the adopted long-term EU goal of achieving zero fatalities and serious injuries in the road transport by 2050, i.e. "Vision

Zero" and "Safe System." Published on the European Commission's website, the document sets the goal of to reduce road fatalities and serious injuries by 50 % by 2030 compared to 2020 [24]

2 Research

2.1 Purpose and methodology of the survey

The survey was conducted in late 2021 and early 2022 among residents of Poland. The collection of respondents' opinions needed for the survey was carried out through two research methods: an online survey and through direct collection of information. The survey was posted on forums, related to transportation, on social media and among friends. The survey was fully anonymous, contained 12 questions and consisted of three parts: a brief driver metric, questions about drivers' feelings about the road safety and an assessment of infrastructure in European countries.

The main purpose of the survey was to find out the opinions of the road transport users on road safety and the causes of traffic delays and to compare European countries in terms of infrastructure. The countries that were pitted against each other in the survey are: Poland, Austria, Belgium, Czech Republic, France, Germany, Hungary, Lithuania, the Netherlands, Romania, Slovakia, Spain and the United Kingdom. Those countries were selected based on a report by OCRK (the National Center for Driver Accountability), which indicates to which countries Polish drivers travel the most often [25]. The survey includes mainly adult respondents with a driver's license, although this is not a prerequisite. One of the main goals was also to acquire at least 350 responses, including the opinions of at least

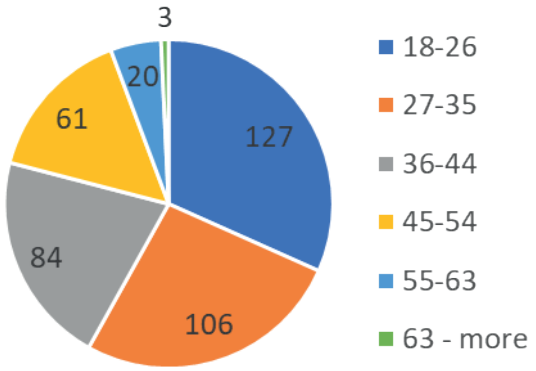

Figure 1 *Age of respondents*

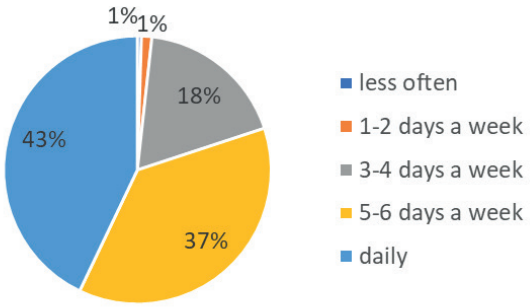

Figure 4 *Frequency of vehicle use per week by respondents*

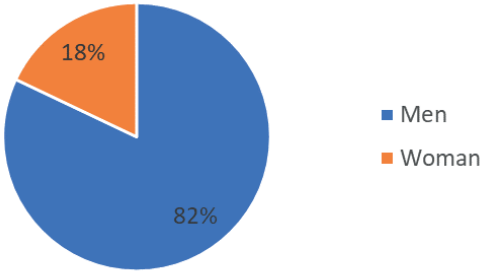

Figure 2 *Gender of respondents*

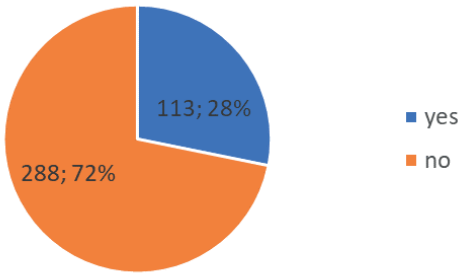

Figure 5 *Number of professional drivers*

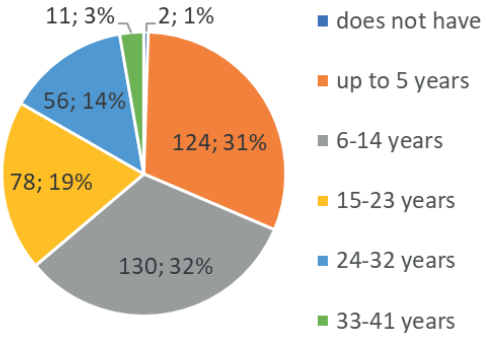

Figure 3 *Length of time respondents have held a driver's license*

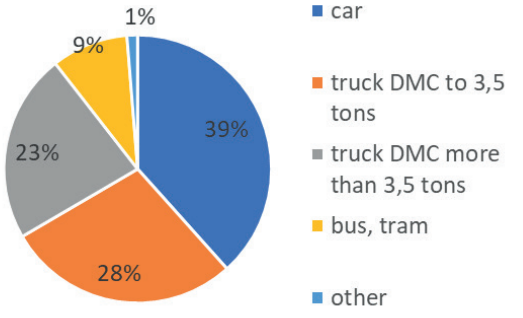

Figure 6 *The mode of transportation most frequently used by respondents*

100 professional drivers. The next step in implementing the survey was to calculate the research sample. For Poland (population 38151 thousand), assuming a confidence level of 95% and a maximum error of 5%, the required number of survey respondents was 384. The survey was completed by 401 respondents.

Respondents' responses were also analysed for metric questions, namely. Gender, age, seniority of driver's license, professional driver, frequency of use of transportation and mode of transportation. In addition, two analyses (by gender and age) were considered in the context of the Chi-square statistics. This statistical test is used to make hypotheses for random variables. One can test, whether the variables are related to each other by the common pattern of the results obtained. If the theoretical Chi-square was less than the calculated one, then there is a significant relationship between the variables. The formula for the chi square test of concordance has the following form [25]:

$$x^2 = \sum_r^{i=1} \frac{(f_i - np_i)^2}{np_i}, \quad (1)$$

where: χ2 - Chi-square test,
f_i - the number of observed values from a given interval,
np_i - number of units (n) that should be in a given interval (expected values of the intervals).

2.2 Results

The survey was completed by 401 respondents in different age ranges: 18-26, 27-35, 36-44, 45-53, 54-62, 63-71. Above the age of 71 there were no respondents. The largest group of respondents was in the 18-26 age range (32 %), followed by 27-35 (26 %), 36-44 (21 %), 45-53 (15 %), 54-62 (5%) and 63-71 (1 %). Efforts were made to have respondents in each age range, which presented some difficulty especially in the 54-62 (5%) and 63-71 (1%) age ranges (Figure 1). Women accounted for 18% of the respondents and men 82%. (Figure 2).

Next, the question asked was how long they have held their driver's license. The largest range is those who have had a driver's license for 6 to 14 years (32 %), followed by up to 5 years (31 %), 15-23 (19 %), 24-32 (14 %), 33-41 (3%) and over 42 years (1 %). Two people did not have a driver's license (Figure 3).

In the next question, respondents were asked to specify the frequency of use of transportation. By far the largest number of respondents use means of transportation daily and 5-6 times a week, 43% and 37% respectively. This was followed by 3-4 times a week (18 %), 1-2 times a week (1%) and less often (1%) (Figure 4).

The fifth question concerned the breakdown of professional drivers. A professional driver is a person who has an entry in the driving license document with code 95 and a valid certificate of professional qualification. This includes driving license categories C, C+E, D [26]. Among the respondents, there were 113 professional drivers (28 %). This result was achieved mainly by posting the survey on groups, forums specifically related to this profession, as well as through their own acquaintances (Figure 5).

In the sixth question, respondents were asked to indicate which mode of transportation they use the most often. Respondents most often use cars (3 9%), followed by vans, trucks up to 3.5 tons (2 8%), trucks over 3.5 tons (23 %), bus, streetcar (9%) and others (Figure 6).

Analysis of responses by gender. The first question concerned the age of the respondents. Here we can see a significant difference between some age ranges. From the Chi-square test with a significance of 0.05, one can conclude that the variables are not independent, as x^2 is 41.80 and the theoretical x^2 is 11.07. The next question shows the respondents' answers regarding the time of holding a driver's license. The Chi-square test with a significance of 0.05 shows that there is a relationship between gender and the time of holding a driver's license, as x2 is 34.55 and x^2 theoretical is 11.07.

The third question concerns the frequency of use of means of transportation. The answers showed that respondents most often use means of transportation 5-6 times a week and daily. The number of degrees of freedom was 4 that is, the critical value of the Chi-square test is 9.488. The result of the Chi-square test was 17.73, this means that the results are statistically significant for a significance level of p = 0.05.

Question four asks whether the respondent is a professional driver. The number of degrees of freedom is 1, so the critical value of the Chi-square test is 3.841. The result of the Chi-square test was 12.287. This means that the results are statistically significant for the significance level of p = 0.05. The fifth question asks what type of transportation respondents use most often (multiple choice). The respondents' answers show that they most often use a personal car (Table 1).

The results of question six show that there is a relationship and this is confirmed by a Chi-square test result of 723.09 with a theoretical 43.77. (Number of free degrees 30). Respondents are most likely to take their driving test just after they turn 18.

The next table shows the respondents' answers on the use of any means of transportation. The Chi-square test with a significance of 0.05 shows that there is a relationship between gender and the time of holding a driver's license, as x^2 is 42.80 and x^2 theoretical is 26.30 (number of degrees of freedom 16). Question eight - where the result of the Chi-square test indicates that there is no correlation between these concepts. The x^2 test result is 6.67, while x^2 theoretical is 11.07 (number of degrees of freedom 5). Another analysis looks at the frequency of transportation use in relation to gender (Table 2).

People in the age range of 18-26, 54-62 and over 62 are less likely to use means of transportation during the week. Item 11 of the table shows that those with a driver's license for up to 5 years, 6-14 years and 15-23

Table 1 *Research results*

Category	Fermale (%)	Male (%)
1. Age		
18-26 years	61.11	25.34
27-35 years	26.39	26.74
36-44 years	8.34	23.1
45-53 years	4.16	17.63
54-62 years	0.00	6.08
63-71 years	0.00	0.91
2. Time to hold a driver‘s license		
I do not own	2.77	0.00
Up to 5 years	52.77	26.13
6-14 years	29.16	33.16
15-23 years	11.1	21.27
24-32 years	4.6	16.1
33-41 years	0.00	2.26
Over 42 years	0.00	1.08
3. Frequency of transport use		
Less often	2.77	0.00
1-2 times a week	4.16	0.6
3-4 times a week	15.3	18.84
5-6 times a week	43.05	45.28
Daily	34.72	52.28
4. Is the respondent a professional driver?		
Yes	11.11	31.91
No	88.88	68.09
5. Type of means of transportation		
Passenger car	79.16	70.51
Light truck with GVW up to 3.5T	8.33	46.8
Vans with a gross vehicle weight of more than 3.5T	9.72	31.3
Bus streetcar	19.44	9.72
Other	2.77	1.82

years are using transportation most frequently. The likely reason for these results is that these people are the most active and travel daily or 5-6 times a week.

Not surprisingly, professional drivers use means of transportation much more often (Table 3).

Of the professional drivers surveyed, 92.93 % are men. This is a very difficult profession, which generally requires leaving home even for several weeks. In recent years, however, more and more female professional drivers can be observed. The largest number of professional drivers is among respondents who have held a driver's license for 6-14 and 15-23 years (item 14). This is due to the fact that professional drivers can become professional drivers after the age of 21 and the fact that it is quite an expensive course. Professional drivers move much more frequently 5-6 days a week and every day. In those who are not professional drivers, the frequency of transportation use is more spread out (item 15) (Table 4).

Since most of the women surveyed are young, they most often hold a driver's license for up to 5 years. As the age of holding a driver's license increases, the prevalence of men in this aspect increases (item 16) (Table 5).

Another part of the questions dealt with drivers' feelings about delays in transportation and road safety. Respondents were asked to select factors related to delays and safety, which were given by the authors of the paper. According to respondents, the most common causes of transportation delays are traffic congestion (82 %) and poor road class (69 %). As other factors, respondents pointed to weather conditions (53 %), the condition of the road surface (39 %), poor information flow between companies (33 %), the quality of rolling stock (30 %), poor company storage facilities (loading,

Table 2 *Research results*

Criterium	Number of responses (%)					
6. Age breakdown of respondents regarding holding a driver‘s license						
Age	18-26	27-35	36-44	45-53	54-62	63-71
Don‘t own	0.24	93	0.00	0.00	0.00	0.00
Up to 5 years	81.25	8.41	3.68	0.00	0.00	0.00
6-14 years	17.96	81.3	7.31	1.63	0.00	0.00
15-23 years	0.00	9.34	75.6	9.83	0.00	0.00
24-32 years	0.00	0.00	13.41	85.24	22.53	0.00
33-41 years	0.00	0.00	0.00	3.27	77.47	0.00
Over 42 years	0.00	0.00	0.00	0.00	0.00	0.00
7. Breakdown of respondents by age versus frequency of transportation use						
Age	18-26	27-35	36-44	45-53	54-62	63-71
Less often	1.56	0.00	0.00	0.00	0.00	0.00
1-2 times a week	2.34	0.93	0.00	1.63	5	33.33
3-4 times a week	22.65	14.01	17.07	13.11	30	33.33
5-6 times a week	40.62	40.18	30.48	32.78	45	0.00
Daily	32.81	44.85	52.43	54.09	20	33.33
8. Responses of respondents by age regarding professional driver						
Age	18-26	27-35	36-44	45-53	54-62	63-71
Yes	20.31	29.9	32.92	31.14	40	33.33
No	79.59	69.1	67.08	68.86	60	66.66
9. Respondents‘ responses by frequency regarding gender						
frequency	less frequently	1-2 per week	3-4 per week	4-5 per week	daily	
Female	100	60	15.06	20.8	14.53	
Male	0.00	40	84.94	79.8	85.47	

Table 3 *Research results*

Criterium	Number of responses (%)				
10. Respondents‘ answers by frequency regarding age					
Frequency	less frequently	1-2 per week	3-4 per week	4-5 per week	daily
18-26	100	50	39.72	34.89	24.41
27-35	0.00	16.66	20.54	28.85	27.9
36-44	0.00	0.00	19.17	16.77	25.00
45-53	0.00	0.00	10.95	13.42	19.18
54-62	0.00	16.66	8.21	6.04	2.32
above 62	0.00	16.66	1.36	0.00	0.58
11. Respondents‘ responses by frequency regarding having a driver‘s license					
Frequency	less frequently	1-2 per week	3-4 per week	4-5 per week	daily
I do not own	50.00	0.00	1.36	0.00	0.00
Up to 5 years	50.00	33.33	21.91	31.2	25.00
6-14 years	0.00	33.33	17.18	30.2	33.13
15-23 years	0.00	0.00	8.21	20.8	22.67
24-32 years	0.00	0.00	6.84	12.75	15.11
33-41 years	0.00	16.66	1.36	5.36	5.23
over 42 years	0.00	16.66	0.00	0.00	0.58
12. Respondents‘ answers by frequency regarding professional driver					
Frequency	less frequently	1-2 per week	3-4 per week	4-5 per week	daily
Yes	0.00	0.00	6.84	27.51	38.95
No	100.00	100.00	93.16	67.49	61.05

Table 4 *Research results*

Criterium	Number of responses (%)	
13. Responses of respondents by professional driver regarding gender		
Professional driver	Yes	No
Female	7.07	22.22
Male	92.93	77.88
14. Responses of respondents by professional driver regarding the length of time they have held a driver‘s license		
Professional driver	Yes	No
I do not own	0.00	0.69
Up to 5 years	12.98	38.19
6-14 years	32.74	32.19
15-23 years	30.08	15.27
24-32 years	17.69	11.8
33-41 years	6.19	1.04
Pow 42	0.88	0.69
15. Respondents‘ answers by professional driver regarding frequency		
Professional driver	Yes	No
less often	0.00	0.69
1-2 per week	0.00	1.73
3-4 per week	4.42	23.61
5-6 per week	36.28	37.5
daily	59.29	36.45

Table 5 *Research results*

Criterium	Number of responses (%)						
16. Responses of respondents by time of holding a driver‘s license regarding gender							
Driving license time	I don‘t have	Up to 5 years	6-14 years	15-23 years	24-32 years	33-41 years	above 42
Female	100.00	30.64	16.15	10.25	5.35	0.00	0.00
Male	0.00	69.36	83.85	89.75	94.65	100.00	100.00

unloading) (29 %), the method of loading and unloading (25 %), a road accident (20 %), vehicle breakdown (17 %) and driver or GPS navigation errors (14 %) (Figure 7).

Another issue concerned respondents' feelings about factors affecting the road safety. According to respondents, the sense of safety on the road is most influenced by driver experience (71 %), followed by driver's rest (65 %), class of the road (highway, expressway) (60 %), psychomotor efficiency (55 %), weather conditions (45 %), technical condition of the vehicle (43 %), adapted traffic volume to the road capacity (26 %), condition of the road surface (25 %), use of road junctions (type WA - completely collision-free junction, where the tracks do not intersect; WB type - partially collision-free, on one road the tracks of some relations intersect) (20 %), proper signage and signalling (19 %), road controls and speed cameras (12 %), road safety barriers (6 %) and proper lighting of roads, tunnels (4 %) (Figure 8).

The respondents' answers show that the most common causes of traffic accidents and collisions are: failure to adjust speed to the road conditions (89 %), failure to give priority (84 %), improper overtaking, turning, turning around, changing lanes, stopping (64 %), failure to maintain a safe distance between vehicles (41 %), failure to give priority at a pedestrian crossing (54 %), improper overtaking (37 %), fatigue, falling asleep (31 %), distraction (ringing phone, smoking, drinking beverages, talking) (16 %), failing to obey other signs and signals (23 %), driving under the influence of alcohol or psychoactive substances (23 %), weather conditions (16 %), crossing the road in a prohibited place by a pedestrian (11 %), driving without the required lighting (10 %), sudden braking (7 %), vehicle breakdown (5 %), psychological stress (distress) (4 %) (Figure 9).

The last part of the survey questions was to rate each European country in terms of the road safety and infrastructure. Drivers had to rate 14 countries, the rating scale was as follows: 1 - terrible, 2 - poor, 3 - average - 4 good and 5 - very good. Questions included an assessment of the feeling of safety on the country's roads, the density of the road network, the density of gas stations, the quality of roads, signage and parking lots (Table 6).

The survey showed the most common causes of

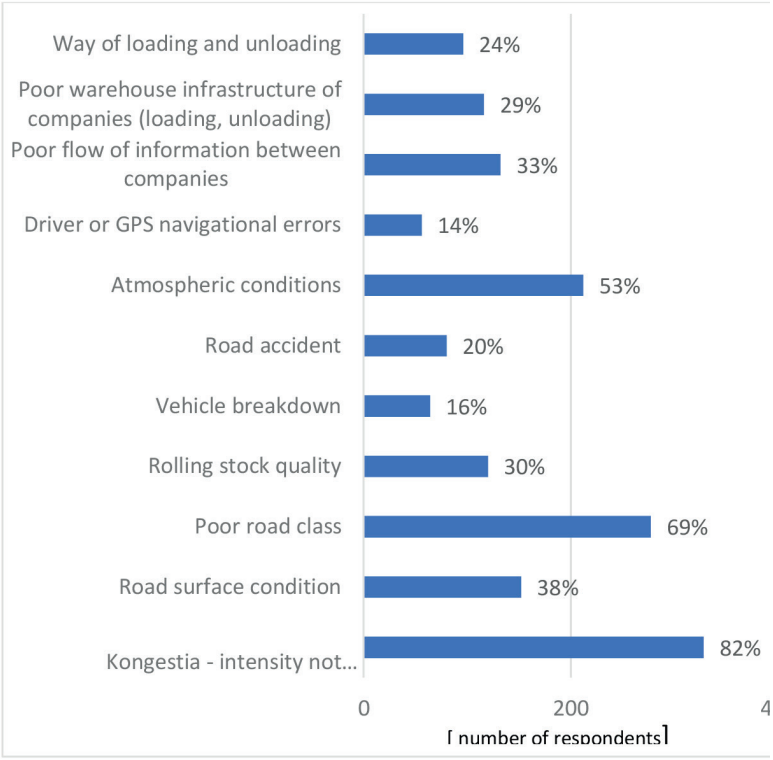

Figure 7 *Factors affecting transportation delays*

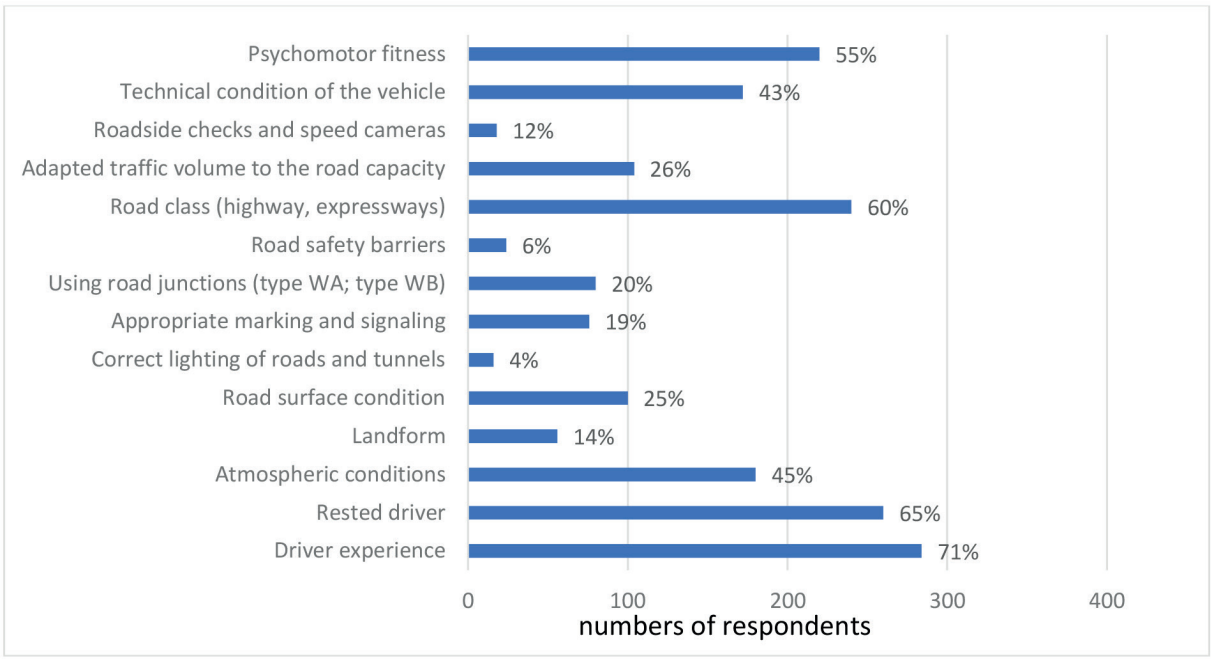

Figure 8 *Factors affecting feelings of safety on the road*

delays in transportation. These include traffic congestion (82%) and poor road class (69 %). These reasons are somewhat interrelated, as it is common for a road in a given location to have insufficient capacity. A high score was given to the factor of weather conditions (53 %). Considering recent years in Europe, weather conditions can be extreme and changeable. In the summer, drivers especially have to contend with hot weather, which causes fatigue and thus reduced concentration. Precipitation can be very intense, due to which the average speed of vehicles decreases. In winter, the main obstacles to transportation are ice and snow. Most of the surveyed people working as drivers marked at least one answer from the following: poor flow of information between companies (33 %), poor storage infrastructure of companies (loading, unloading) (29 %), method of loading and unloading (25 %). From these responses it can be concluded that companies still need

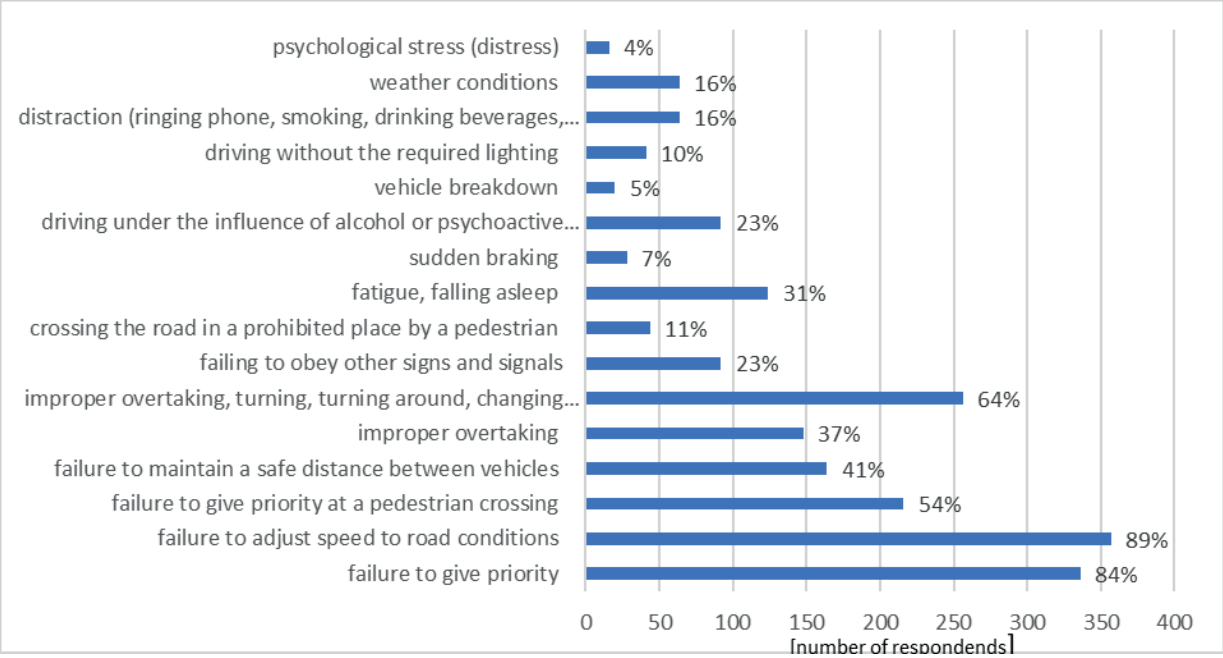

Figure 9 *Most common reasons for accidents, traffic collisions*

Table 6 *Places and ratings of European countries in each statement [27]*

Country	A sense of security	Density of the road network	Fuel station density	Quality of roads - condition of pavement	Signage	Parking lots
Austria	4	4	6	2	3	4
	4.02*	4.07*	3.98*	4.25*	4.05*	3.17*
Belgium	8	2	1	9	7	10
	3.31*	4.5*	4.52*	3.1*	4*	2.91*
Czech Republic	9	10	5	12	10	13
	3.16*	3.53*	4.04*	2.62*	3.6*	2.59*
France	6	5	10	5	5	2
	3.71*	4.01*	3.79*	3.75*	4.08*	3.47*
Spain	5	6	9	4	4	3
	3.77*	3.93*	3.86*	3.91*	4.16*	3.42*
Netherlands	1	1	2	1	2	1
	4.41*	4.59*	4.46*	4.36*	4.64*	3.61*
Lithuania	12	13	13	7	13	12
	2.9*	2.95*	3.18*	3.41*	3.58*	2.65*
Germany	2	3	4	3	1	7
	4.04*	4.22*	4.27*	4.12*	4.35*	3.01*
Poland	13	12	8	10	8	5
	2.88*	3.06*	3.86*	2.85*	3.65*	3.15*
Romania	14	14	14	14	14	14
	2.13*	2.5*	2.83*	2.11*	3.66*	2.24*
Slovakia	7	11	12	13	11	11
	3.5*	3.09*	3.43*	2.51*	3.46*	2.67*
Hungary	10	8	11	11	9	6
	3.09*	3.7*	3.53*	2.66*	3.29*	3.07*
United Kingdom	3	7	7	6	6	8
	4.02*	3.86*	3.92*	3.62*	3.96*	2.96*
Italy	11	9	3	8	12	9
	3.02*	3.68*	4.31*	3.21*	3.71*	2.94*

* evaluation of respondents

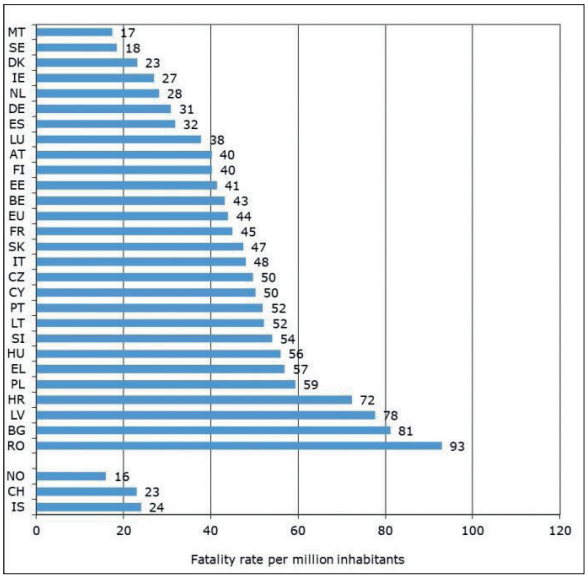

Figure 10 *Number of road fatalities per million inhabitants by country, 2021 [28]*

to improve their work organization, as well as their storage infrastructure.

According to respondents, the feeling of safety on the road is most often influenced by the experience of the driver (71%) - almost 85% of responses to the driver experience factor were given by those who have more than 6 years of driving license. This is followed by driver rest (65 %), class of the road (highway, expressway) (60%) and psychomotor efficiency (55 %), weather conditions (45%) and technical condition of the vehicle (43 %). This shows that drivers' sense of safety is influenced by a number of factors, ranging from the general condition of the driver to road infrastructure and natural phenomena.

Respondents' answers regarding the main causes of traffic collisions and accidents show that the public is knowledgeable on the subject. Comparing the respondents' surveys with the report Road accidents in Poland in 2021, created by the Traffic Bureau of the Police Headquarters, many similar conclusions can be found. Respondents identified as the main factors in traffic collisions and accidents: failure to adjust speed to road conditions (89 %), failure to give priority (84 %), improper passing, turning, turning around, changing lanes, stopping (64 %), failure to maintain a safe distance between vehicles (41 %), failure to give priority at pedestrian crossings and in other circumstances involving pedestrians (54 %), improper overtaking (37%) and fatigue, falling asleep (31%) In the Police report, these factors statistics account for the following number of accidents: failure to adjust speed to road conditions (5,254; 23% of all accidents), failure to give precedence to pedestrians (5,566; 24% of all accidents), improper bypassing, turning, reversing, turning, changing lanes, stopping, stopping (4,185; 18% of all accidents), failure to maintain a safe distance between vehicles (1,607; 7% of all accidents), failure to give priority at pedestrian crossings and in other circumstances involving pedestrians (2,487; 11 %), improper overtaking (1,012; 4%) and fatigue, falling asleep (538; 2 %). Adding up these factors, they caused about 95% of all the traffic collisions and accidents caused by drivers in 2019. This shows that people are aware of what causes lead to incidents on the roads and yet Poland has a very high road fatality rate of 77 people per million. A very positive note is that as many as 23% and 16% got the answers in turn: driving under the influence of alcohol or psychoactive substances and distractions (a ringing phone, smoking, drinking a drink, talking), respectively. In police statistics, these responses do not appear. That is because they are attributed to other factors, such as failure to adjust speed to road conditions or under the term "other." This is because they often appear together. The large number of votes cast by respondents for these factors shows that all the advertising spots and media campaigns work.

3 Assessment of the feeling of security in European countries

Another issue was to assess the state of the feeling of safety in European countries. The averages obtained were compared to the statistics in 2021 of fatal accidents per million inhabitants of a country. The country with the highest average of deaths per million of population is Romania (93), followed by Bulgaria (81), Latvia (78), Croatia (72), Poland (59), Greece (57), Hungary (56), Slovenia (54), Latvia and Portugal (52), Cyprus and Czechia (50), Italy (48), Slovakia (47), France (45), Belgium (43), Estonia (41), Austria and Finland (40), Luxembourg (38), Spain (32), Germany (31), Netherlands

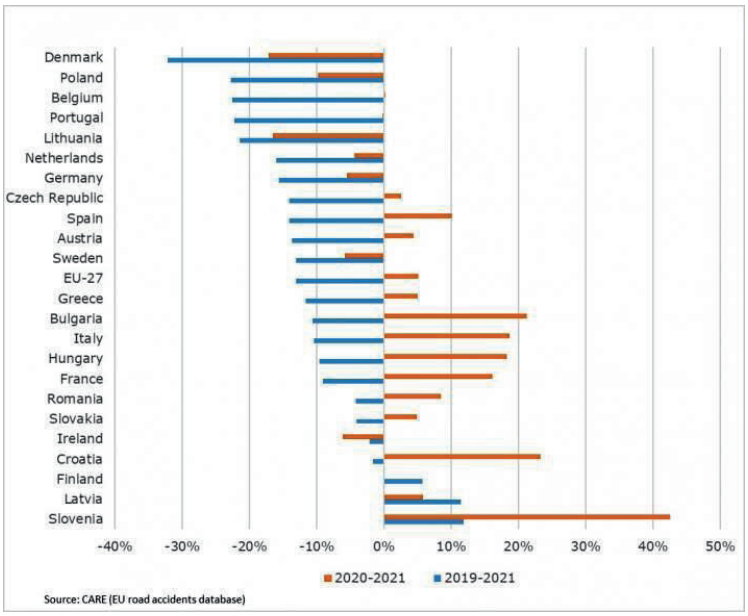

Figure 11 *Short-term trend in the number of road fatalities (2021 compared to 2019 and 2020) [28]*

(28), Ireland (27, Denmark (23), Sweden (18) and Malta (17) (Figure 10).

Comparing 2019 to 2021, it is Slovenia that has the largest increase in road fatalities, up 43%. This represents the largest increase in the EU. The next country is Croatia with an increase of 23%, followed by Bulgaria with an increase of 21%, Italy with an increase of 19%, Hungary with an increase of 18%, France with an increase of 16%, Spain with an increase of 10% and Romania with an increase of 8%. The country with the highest decrease in the number of fatalities per million inhabitants in 2021, compared to 2020, is Denmark 17% - Lithuania 17% decrease. In Poland, the number of fatalities per million inhabitants fell by 23%. Across the EU, there were an average of 44 traffic fatalities per million residents in 2021, up 5% from 2020, but down 13% from 2019, before the pandemic (Figure 11).

4 Summary

The purpose of the above work was to analyse and evaluate the impact of trucking infrastructure on freight efficiency and safety. This allowed to draw relevant conclusions that in the future can improve transport efficiency, safety of drivers and cargo. The conclusions also show the state of infrastructure in Europe and the direction of development of the road infrastructure.

The respondents' answers show that the most common causes of road accidents and collisions are: failure to adjust speed to road conditions (89 %), failure to give priority (84 %), which is in line with the 2019 police report. Countries were compared in terms of: sense of the road safety, density of the road network, density of the gas stations, quality of the road condition, road markings and number of parking lots. The results show a clear difference between Western Europe and Eastern Europe. The best rated country in all the aspects is by far the Netherlands, followed by Germany, Austria, France, the UK, Spain and Belgium. Poland's performance is very average and places it further down the list. The worst country among those compared is Romania, which ranked as the last in all the assessments. The survey confirms that despite the visible progress and huge investments in recent years, Poland still lags behind Western countries. For this reason, the transport infrastructure must continue to be improved.

Grants and funding

The authors received no financial support for the research, authorship and/or publication of this article.

Conflicts of interest

The authors declare that they have no known competing financial interests or personal relationships that could have appeared to influence the work reported in this paper.

References

[1] NOSAL HOY, C. The gender factor in transportation behaviour/Czynnik plci w zachowaniach komunikacyjnych (in Polish). *Urban and Regional Transport/Transport Miejski i Regionalny*. 2018, **5**, p. 5-11. ISSN 1732-5153.

[2] RACZYNSKA-BULAWA, E. Road traffic safety in Europe - EU policy assumptions and evaluation of measures taken from the perspective of statistical data (in Polish). *Buses - Technology, Operation, Transport Systems/Autobusy - Technika, Eksploatacja, Systemy Transportowe*. 2016, **17**(10), p. 8-14. ISSN 1509-5878, eISSN 2450-7725.

[3] PODGORSKA, A., RAJCHEL, J. Legal issues of safety and order in road traffic and road accidents (in Polish). *Roads / Drogownictwo*. 2019, **11**, p. 328-335. ISSN 0012-6357.

[4] CELINSKI, I. Mobile diagnostics of vehicles as a means to examine and define speed limits in a road (in Polish). *Diagnostics / Diagnostyka*. 2017, **18**(1), p. 67-72. eISSN 2449-5220.

[5] TOPOLSEK, D., CVAHTE OJSTERSEK, T. Do drivers behave differently when do you drive a car or a motorcycle? *European Transport/Trasporti Europei*. 2017, **66**, 7. ISSN 1825-3997.

[6] GOLAKIYA, H. D., CHAUHAN, R., DHAMANIY, A. Assessment of safe distance for pedestrians on sections of downtown city blocks with the use of trajectory plots. *European Transport / Trasporti Europei*. 2020, **75**, 2. ISSN 1825-3997.

[7] MOHANTY, M., SAMAL, S. R. The role of young drivers in road accidents: a case study in India. *European Transport/Trasporti Europei*. 2019, **74**, 1. ISSN: 1825-3997.

[8] PRENTKOVSKIS, O., PRENTKOVSKIENE, R., LUKOSEVICIENE, O. Investigation of potential deformations caused by elements of transport and pedestrian traffic restricting the gates during interaction of the motor vehicle with the gate. *Transport* [online]. 2007, **22**(3), p. 229-235. ISSN 1648-4142, eISSN 1648-3480. Available from: https://doi.org/10.1080/16484142.2007.9638130

[9] PRENTKOVSKIS, O., SOKOLOVSKIJ, E., VILIUS, B. Investigating traffic accidents: collision of two motor vehicles. *Transport* [online]. 2010, **25**(2), p. 105-115. ISSN 1648-4142, eISSN 1648-3480. Available from: https://doi.org/10.3846/transport.2010.14

[10] PRENTKOVSKIS, O., BELJATYNSKIJ, A., PRENTKOVSKIENE, R., DYAKOV, I., DABULEVICIENE, L. A study of the deflections of metal road guardrail elements *Transport* [online]. 2009, **24**(3), p. 225-233. ISSN 1648-4142, eISSN 1648-3480. Available from: https://doi.org/10.3846/1648-4142.2009.24.225-233

[11] LUKE, R., HEYNS, G. J. Reduction of risky behaviour of drivers by implementing a driver risk management system *Journal of Transport and Supply Chain Management* [online]. 2014, **8**(1), a146. ISSN 2310-8789, eISSN 1995-5235. Available from: https://doi.org/10.4102/jtscm.v8i1.146

[12] Reflectors for vulnerable road users - Driving school portal (in Polish) [online] [accessed 2022-10-22]. Available from: https://www.portalnaukikuje.pl/aktualnosci/odblaski-dlaniechrononychuczestnikowruchu-road-2152.html

[13] GORZELANCZYK, P., KACZMAREK, L. The influence of modern information systems on the operation of passenger vehicles (in Polish). *Buses - Technology, Operation, Transport Systems/Autobusy - Technika, Eksploatacja, Systemy Transportowe*. 2019, **227**(1-2), p. 211-215. ISSN 1509-5878, eISSN 2450-7725. Available from: https://doi.org/10.24136/atest.2019.038

[14] GORZELANCZYK, P. Expert systems in diagnostics of means of transport (in Polish). *Logistics / Loistyka*. 2012, **3**, p. 661-668. ISSN 1231-5478.

[15] MICHALSKI, R., WIERZBICKI, S. Analysis of the degradation of used vehicles (in Polish). *Maintenance and Reliability/Eksploatacja i Niezawodnosc*. 2008, **1**(37), p. 30-32. ISSN 1507-2711, eISSN 2956-3860.

[16] GOLAKIYA, H. D., CHAUHAN, R., DHAMANIYA, A. Evaluating safe distance for pedestrians on urban midblock sections using trajectory plots. *European Transport/Trasporti Europei.* 2020, **75**, 2. ISSN 1825- 3997.

[17] DELL'ACQUA, G., DE LUCA, M., PRATO, C. G., PRENTKOVSKIS, O., JUNEVICIUS, R. The impact of vehicle movement on exploitation parameters of roads and runways: a short review of the special issue. *Transport* [online]. 2016, **31**(2), p. 127-132. ISSN 1648-4142, eISSN 1648-3480. Available from: https://doi.org/10.3846/16484142.2016.1201912

[18] GORZELANCZYK, P. Study of the tread wear process based on bus tyres operated by PT operator in Pila (in Polish). *Buses - Technology, Operation, Transport Systems / Autobusy - Technika, Eksploatacja, Systemy Transportowe*. 2017, **18**(12), p. 891-896. ISSN 1509-5878, eISSN 2450-7725.

[19] WACHOWIAK, P., GORZELANCZYK, P., KALINA, T. Analysis of the effectiveness of shock absorbers in light of Polish and Slovak regulations (in Polish). *Buses - Technology, Operation, Transport Systems/Autobusy - Technika, Eksploatacja, Systemy Transportowe* [online]. 2018, **19**(6), p. 764-770. ISSN 1509-5878, eISSN 2450-7725. Available from: https://doi.org/10.24136/atest.2018.172

[20] GORZELANCZYK, P., GORNIAK, W. Assessment of the technical condition of forklift tyres used in internal transport by investigating damage and operating conditions. *Engineering Science and Technology/Nauki*

Inzynierskie i Technologie [online]. 2019, **2**(33), p. 44-59. ISSN 2080-5985, eISSN 2449-9773. Available from: https://doi.org/10.15611/nit.2019.2.03

[21] GORZELANCZYK, P., ROCHOWIAK, L. Assessment of the technical condition of tyres used in agricultural and forestry machines. *Engineering Science and Technology / Nauki Inzynierskie i Technologie* [online]. 2019, **2**(33), p. 60-70. ISSN 2080-5985, eISSN 2449-9773. Available from: https://doi.org/10.15611/nit.2019.2.04

[22] GORZELANCZYK, P., PYSZEWSKA, D., KALINA, T., JURKOVIC, M. Analysis of road traffic safety in the area of the district of Pila. *Scientific Journal of the Silesian University of Technology* [online]. 2020, **107**, p. 33-52. ISSN 0209-3324, eISSN 2450-1549. Available from: https://doi.org/10.20858/sjsutst.2020.107.3

[23] Where do Polish truck drivers go and what should they watch out for? (in Polish) [online] [accessed 2022-10-22]. Available from: https://www.ocrk.pl/wp-content/uploads/2019/01/Dok%C4%85d-je%C5%BCd%C5%BC%C4%85-Polscy-kierowcy-ci%C4%99%C5%BCar%C3%B3wek-i-na-co-powinni-uwa%C5%BCa%C4%87-4.09.2018.pdf

[24] Vision Zero [online] [accessed 2022-12-23]. Available from: https://visionzero.global

[25] Chi-square consistency test (in Polish) [online] [accessed 2022-10-22]. Available from: www.naukowiec.org/wzory/statystyka/test-zgodnosci-chi-kwadrat_20.html

[26] How to become a professional driver? (in Polish) [online] [accessed 2022-10-22]. Available from: https://www.prawo-jazdy-360.pl/aktualnosci/jak-zostac-kierowca-zawodowym

[27] Road safety: European Commission rewards effective initiatives and publishes 2020 figures on road fatalities [online] [accessed 2022-10-22]. Available from: https://transport.ec.europa.eu/news/road-safety-european-commission-rewards-effective-initiatives-and-publishes-2020-figures-road-2021-11-18_en

[28] 2021 road safety statistics: what is behind the figures? [online] [accessed 2022-12-23]. Available from: https://transport.ec.europa.eu/2021-road-safety-statistics-what-behind-figures_en

Errata: Communications - Scientific letters of the University of Zilina, 2022, 24(3), p. B228-B238, https://doi.org/10.26552/com.C.2022.3.B228-B238, Prediction of the ultra-large container ships' propulsion power at the initial design stage

Piotr Kamil Korlak

Doctoral School of the Maritime University of Szczecin, Szczecin, Poland

*E-mail of corresponding author: 27901@s.am.szczecin.pl

Piotr Kamil Korlak 0000-0002-4548-4796

Errata
Communications - Scientific letters of the University of Zilina, 2022, 24(3), p. B228-B238, https://doi.org/10.26552/com.C.2022.3.B228-B238, Prediction of the ultra-large container ships' propulsion power at the initial design stage.

Available online: https://doi.org/10.26552/com.C.2023.040

Errata info
Received 30 March 2023
Accepted 30 March 2023
Online 3 April 2023

ISSN 1335-4205 (print version)
ISSN 2585-7878 (online version)

The author has identified incorrect description in his paper [1]. Two significant errors have crept into the description of Table 6 and one of the rows below. The previous Equation (5) should be removed with the addition of the comment "not applicable, the assumed value", as well as the row below the Table 6 providing the incorrect information about the p-value, as shown in the table below. Also, all subsequent equations must be renumbered. However, the highlighted errors did not affect the accuracy of the results presented in a mentioned paper.

The author would like to apologise for any inconvenience caused.

The corrected table and text should read as follows:

Table 6 *Regression analysis results [20]*

Parameter	Symbol	Value	Equation	
Sample size	N	500	$N = n_v \cdot n_c$	(4)
Confidence level	CL	0.95	Not applicable, the assumed value	
Standard deviation	SD	22,046.57 kW	$SD = \sqrt{\frac{\sum_{i=1}^{N}(P_{Bi} - \overline{P_{Bi}})^2}{N-1}}$	(5)
Determination coefficient	R^2	0.9959	$R^2 = 1 - \frac{\sum_{i=1}^{N}(P_{Bi} - \widehat{P_{Bi}})^2}{\sum_{i=1}^{N}(P_{Bi} - \overline{P_{Bi}})^2}$	(6)
Standard error of propulsion power	SE	985.95 kW	$SE = \frac{SD}{\sqrt{N}}$	(7)

where:

n_v = 25 - Total number of points related to sailing speeds between 0 and 24 knots with an interval equal to 1,

n_c = 20 - Total number of ship classes, including a total of 142 ships,

P_{Bi} - Propulsion power, the actual value of the dependent variable, (kW),

$\widehat{P_{Bi}} = P_B$ - Propulsion power, the predicted value of the dependent variable based on the regression model, (kW),

$\overline{P_{Bi}}$ - Propulsion power, the mean value of the actual dependent variable, (kW).

References

[1] KORLAK, P. K. Prediction of the ultra-large container ships' propulsion power at the initial design stage. *Communications - Scientific letters of the University of Zilina* [online]. 2022, **24**(3), p. B228-B238. Available from: https://doi.org/10.26552/com.C.2022.3.B228-B238

UNIVERSITY
OF ŽILINA

1953 70 2023

In its over 70 years of successful existence, the University of Žilina (UNIZA) has become one of the top universities in Slovakia.

Scientific conferences

organized by University of Žilina

38th International Colloquium Advanced Manufacturing and Repair Technologies in Vehicle Industry
Date and venue: May 2023, Budapest (HU)
Contact: lenka.kucharikova@fstroj.uniza.sk

Crisis Situations Solution in Specific Environment
Date and venue: 17. - 18. 5. 2023, Žilina (SK)
Contact: valeria.moricova@uniza.sk
crisis@uniza.sk
Web: https://www.fbi.uniza.sk/stranka/konferencia-2023
https://fbi.uniza.sk/en/aktuality/26th-conference-crisis-situations-solution-in-specific-environment

TRANSCOM 2023
Date and venue: 29. - 31. 5. 2023, Mikulov (CZ)
Contact: transcom@uniza.sk
Web: www.transcom-conference.com

Information and Digital Technologies
Date and venue: 20. – 22. 6. 2023, Žilina (SK)
Contact: elena.zaitseva@fri.uniza.sk
Web: https://idt.fri.uniza.sk/

46. Assets of Workers in the Department of Steel Constructions
Date and venue: June 2023, Žilina (SK)
Contact: jaroslav.odrobinak@uniza.sk

World Multidisciplinary Earth Sciences Symposium 2023 – WMESS
Date and venue: 28. 8. – 1. 9. 2023, Prague (CZ)
Contact: marian.drusa@fstav.uniza.sk

The Machine Learning Summer School @UNIZA
Date and venue: September 2023, Žilina (SK)
Contact: milan.straka@fri.uniza.sk
michal.gregor@uniza.sk
Web: https://mlss.sk/

World Multidisciplinary Civil Engineering-Architecture-Urban Planning Symposium 2023 - WMCAUS
Date and venue: 4. – 8. 9. 2023, Prague (CZ)
Contact: marian.drusa@fstav.uniza.sk

Current Problems of Physics Education and Possible Solutions
Date and venue: 13. – 14. 9. 2023, Zuberec (SK)
Contact: peter.hockicko@uniza.sk

39th DANUBIA – ADRIA Symposium on Advances in Experimental Mechanics 2023
Date and venue: 26. – 29. 9. 2023, Siofok, Balaton (HU)
Contact: frantisek.novy@fstroj.uniza.sk
Web: https://das.tuwien.ac.at

Horizons of Railway Transport 2023
Date and venue: 27. – 28. 9. 2023, Hotel Permon, Podbanské (SK)
Contact: gasparik@uniza.sk

UNIVERSITY OF ŽILINA
Science & Research Department

Univerzitná 8215/1,
010 26 Žilina,
Slovakia

Ing. Janka Macurová
tel.: +421 41 513 5143
e-mail: janka.macurova@uniza.sk

KOMUNIKÁCIE
COMMUNICATIONS

VEDECKÉ LISTY ŽILINSKEJ UNIVERZITY
SCIENTIFIC LETTERS OF THE UNIVERSITY OF ZILINA

VOLUME 25 Number 2

April 2023

Each paper was reviewed by at least two reviewers.
Individual issues of the journal can be found on: http://komunikacie.uniza.sk
The full author quidelines are available at: https://komunikacie.uniza.sk/artkey/inf-990000-0400_Author-guidelines.php
Published quarterly by University of Žilina in EDIS - Publishing House of the University of Žilina.

Communications is currently indexed, abstracted and accepted by CEEOL, CLOCKSS, Crossref (DOI), digitálne pramene, DOAJ, EBSCO Host, Electronic Journals Library (EZB), ERIH Plus, Google Scholar, Index Copernicus International Journals Master list, iThenticate, JournalGuide, Jouroscope, Norwegian Register for Scientific Journals Series and Publishers, Portico, ROAD, ScienceGate, SCImago Journal & Country Rank, SciRev, SCOPUS, WorldCat (OCLC).
Journal Komunikácie - vedecké listy Žilinskej univerzity v Žiline / Communications - Scientific Letters of the University of Žilina is under evaluation for inclusion to Web of Science database.

Contact:
Komunikácie - vedecké listy Žilinskej univerzity v Žiline
Communications - Scientific Letters of the University of Žilina
University of Žilina
Univerzitná 8215/1
010 26 Žilina
Slovakia

E-mail: komunikacie@uniza.sk
Web: https://komunikacie.uniza.sk

ISSN (print version): 1335-4205
ISSN (online version): 2585-7878

Registered No. (print version): EV 3672/09
Registered No. (online version): EV 3/22/EPP
Publisher, owner and distribution:
University of Žilina, Univerzitná 8215/1,
010 26 Žilina, Slovakia

Company identification number IČO: 00 397 563
Frequency of publishing: four times a year
Circulation: 150 printed copies per issue
Print edition price: free of charge

Publishing has been approved by:
Ministry of Culture, Slovak Republic

1953 70 2023
UNIZA

15th International Scientific Conference on Sustainable, Modern and Safe Transport

transcom 2023

Mikulov, Czech Republic
MAY 29 – 31, 2023

TRANSCOM 2023 aims to establish and expand international contacts and cooperation. The main purpose of the conference is to provide Ph.D. students and young scientists with an encouraging and stimulating environment in which they present the results of their research to the scientific community. TRANSCOM has been organised regularly every other year since 1995 by the University of Zilina, Slovakia.

IMPORTANT DATES

- January 31, 2023
  FULL PAPERS SUBMISSION
- March 20, 2023
  NOTIFICATION OF ACCEPTANCE
- April 20, 2023
  CONFERENCE FEE PAYMENT
- May 15, 2023
  CONFERENCE PROGRAMME
- May 29 - 31, 2023
  CONFERENCE

TOPICS

- Operation and Economics in Transport
- Mechanical Engineering in Transport
- Electrical Engineering in Transport
- Civil Engineering in Transport
- Management Science and Informatics in Transport
- Safety and Security Engineering in Transport
- Travel and Tourism Studies in Transport Development

CONTACT

University of Zilina, Department for Science & Research
Univerzitna 8215/1, 010 26 Zilina, Slovakia
e-mail: transcom@uniza.sk
www.transcom-conference.com